



UNIVERSITAT DE
BARCELONA

Design, synthesis and characterisation of photoswitchable allosteric modulators of metabotropic glutamate receptors

Xavier Gómez Santacana

ADVERTIMENT. La consulta d'aquesta tesi queda condicionada a l'acceptació de les següents condicions d'ús: La difusió d'aquesta tesi per mitjà del servei TDX (www.tdx.cat) i a través del Dipòsit Digital de la UB (diposit.ub.edu) ha estat autoritzada pels titulars dels drets de propietat intel·lectual únicament per a usos privats emmarcats en activitats d'investigació i docència. No s'autoritza la seva reproducció amb finalitats de lucre ni la seva difusió i posada a disposició des d'un lloc aliè al servei TDX ni al Dipòsit Digital de la UB. No s'autoritza la presentació del seu contingut en una finestra o marc aliè a TDX o al Dipòsit Digital de la UB (framing). Aquesta reserva de drets afecta tant al resum de presentació de la tesi com als seus continguts. En la utilització o cita de parts de la tesi és obligat indicar el nom de la persona autora.

ADVERTENCIA. La consulta de esta tesis queda condicionada a la aceptación de las siguientes condiciones de uso: La difusión de esta tesis por medio del servicio TDR (www.tdx.cat) y a través del Repositorio Digital de la UB (diposit.ub.edu) ha sido autorizada por los titulares de los derechos de propiedad intelectual únicamente para usos privados enmarcados en actividades de investigación y docencia. No se autoriza su reproducción con finalidades de lucro ni su difusión y puesta a disposición desde un sitio ajeno al servicio TDR o al Repositorio Digital de la UB. No se autoriza la presentación de su contenido en una ventana o marco ajeno a TDR o al Repositorio Digital de la UB (framing). Esta reserva de derechos afecta tanto al resumen de presentación de la tesis como a sus contenidos. En la utilización o cita de partes de la tesis es obligado indicar el nombre de la persona autora.

WARNING. On having consulted this thesis you're accepting the following use conditions: Spreading this thesis by the TDX (www.tdx.cat) service and by the UB Digital Repository (diposit.ub.edu) has been authorized by the titular of the intellectual property rights only for private uses placed in investigation and teaching activities. Reproduction with lucrative aims is not authorized nor its spreading and availability from a site foreign to the TDX service or to the UB Digital Repository. Introducing its content in a window or frame foreign to the TDX service or to the UB Digital Repository is not authorized (framing). Those rights affect to the presentation summary of the thesis as well as to its contents. In the using or citation of parts of the thesis it's obliged to indicate the name of the author.

DESIGN, SYNTHESIS AND CHARACTERISATION OF PHOTOSWITCHABLE ALLOSTERIC MODULATORS OF METABOTROPIC GLUTAMATE RECEPTORS

Tesi doctoral

Memòria presentada per Xavier Gómez Santacana per optar al títol de doctor per la Universitat de Barcelona

Aquesta Tesi ha estat realitzada en el Programa de Doctorat en Química Orgànica de la Universitat de Barcelona, en les instal·lacions del Institut de Química Avançada de Catalunya (IQAC-CSIC)

Doctorant:

Xavier Gómez Santacana

Director:

Dr. Amadeu Llebaria Soldevila

Investigador científic

Departament de Química Biomèdica (IQAC-CSIC)

Codirector:

Dr. Pau Gorostiza Langa

Professor de Recerca ICREA

Institut de Bioenginyeria de Catalunya (IBEC)

Tutor:

Dr. Albert Moyano Baldoire

Catedràtic de Química Orgànica

Departament de Química Orgànica (UB)

Abbreviations

7TM	Transmembrane domain
Å	Angstroms
Abs	Absorbance
AcOH	Acetic acid
AMPA	α -amino-3-hydroxy-5-methyl-4-isoxazolepropionic acid
ANOVA	Analysis of variance
Cat.	Catalytic quantities
CNS:	Central Nervous System
CRD:	Cysteine-rich domain
DAD	Diodes array detector
DCE	1,2-dichloroethane
DCM	Dichloromethane
DIPEA	Diisopropylethylamine
DMF	Dimethyl formamide
DMEM	Dulbecco's modified Eagle's medium
DMSO	Dimethylsulfoxide
EC₅₀	half maximal effective concentration
ECD	Extracellular domain
edAM	Extracellular domain allosteric modulator
Eq:	Equivalents
EtOAc	Ethyl acetate
FRET	Förster resonance energy transfer
FXS	Fragile X syndrome
GPCR	G-Protein coupled receptor
h:	Hours
HATU	1-[Bis(dimethylamino)methylene]-1H-1,2,3-triazolo[4,5-b]pyridinium hexafluorophosphate
HEK293:	Human Embryonic kidney cell line
HPLC	High performance liquid chromatography
HRMS	High resolution mass spectrometry
HTRF	Homogeneous Time Resolved Fluorescence
IC₅₀	half maximal inhibitory concentration
iGluR	Ionotropic glutamate receptor
KA:	Kainate
LED:	Light Emitting Diodes
MeOH	Methanol

MeCN	Acentonitrile
mGlu	metabotropic glutamate
mGluR	metabotropic glutamate receptor
min:	Minutes
mM:	Millimolar
MP	Melting point
ms	Milliseconds
MS	Mass spectrometry
μM	Micromolar
nm	Nanometres
NAM	Negative allosteric modulator
NMDA:	<i>N</i> -methyl-D-Aspartate
NMR	Nuclear magnetic resonance
PAM	Positive allosteric modulator
PBS	Phosphate buffered saline
PD	Parkinson's disease
PDA	Photodiodes detector
PIS	Photoisomerisation score
PNS	Peripheral Nervous System
ppm	Parts per million
PPS	Photoinduced potency shift
PTL	photochromic tethered ligand
quant:	Quantitatively
rt	Room temperature
s	Seconds
SAM	Silent allosteric modulator
SEM	Standard error of the mean
t_{1/2}	Half-life
TEA	Triethylamine
THF	Tetrahydrofurane
TMD	Transmembrane domain
TOF	Time of flight detector
TR-FRET	Time resolved Förster resonance energy transfer
UPLC	Ultrahigh Performance Liquid Chromatography
μs:	Microseconds
UV	Ultra violet
VFT	Venus fly trap domain
Vis	Visible

Table of Contents

General Introduction	3
G-Protein Coupled Receptors (GPCRs)	7
Glutamate and its homonym receptors	19
Control of protein function with light	41
Objectives	57
Results and discussion	61
Chapter 1: alloswitch-1 and optogluram: a proof of concept	65
Chapter 2: alloswitch-1 & optogluram non-photoswitchable bioisosters and the confirmation of the double molecular switch.....	89
Chapter 3: a new series of phenylazopyrines to fine control mGlu5 function with light	95
Chapter 4: The quest of dual mGlu4 PAMs and mGlu5 NAMs: azo- and amide-replacement of 2-BisPEB.....	128
Chapter 5: A more suitable therapeutic approach: cis-on photoswitchable mGlu4 PAMs and mGlu5 NAMs.....	148
Summary of results and conclusions	169
Experimental part	175
Synthetic chemistry.....	179
Photochemical characterisation	227
Pharmacological characterisation	230
Resum en català	243
Bibliographic refernces	305

General Introduction

General Introduction contents

G-Protein Coupled Receptors (GPCRs)	7
Guanine nucleotide-binding proteins (G-Proteins).....	8
Classification of human GPCRs.....	9
<i>Class A GPCRs</i>	10
<i>Class B GPCRs</i>	13
<i>CLASS C GPCRs</i>	14
<i>Class F GPCRs</i>	15
<i>Adhesion Class GPCRs</i>	17
Glutamate and its homonym receptors	19
The ionotropic Glutamate Receptors (iGluRs).....	20
The metabotropic glutamate receptors (mGluRs).....	22
<i>mGluRs topology and mechanisms of activation</i>	22
<i>Classification of the mGluRs, functional anatomy and main biological roles</i>	24
<i>Modification of mGluR function: orthosteric and allosteric ligands</i>	27
<i>Targeting mGlu receptors to treat human disorders</i>	32
Up-to-date mGlu ₄ PAMs and mGlu ₅ NAMs.....	37
<i>mGlu₄ PAMs</i>	37
<i>mGlu₅ NAMs</i>	38
Control of protein function with light	41
Photo-reversible switches.....	42
<i>Retinal</i>	43
<i>Spiropyran</i>	43
<i>Dithienylethene</i>	44
<i>Azobenzene</i>	44
Optopharmacological approaches.....	49
<i>Optogenetics</i>	49
<i>Optogenetic pharmacology</i>	50
<i>Optopharmacology with caged compounds</i>	51
<i>Optopharmacology with photoisomerisable compounds</i>	52

G-Protein Coupled Receptors (GPCRs)

GPCRs are a superfamily of cell surface receptors encoded by about the 800 genes in human, 4% of the human genome¹. GPCRs regulate many physiological processes and are sensitive to a wide variety of endogenous ligands, such as neurotransmitters, peptide and protein hormones, amino acids or lipids². Moreover, chemosensory GPCRs play an important role in sight, smell and taste. That's why the genetic diversification in GPCRs in certain animals is much larger than in humans, since the 800 genes encoding GPCRs for human turn into 1400 for rat³ or the 328 olfactory GPCRs in human turns into 1037 in mouse⁴.

GPCRs have been a hot topic in science for the last years and constitute important targets for pharmaceutical development. In 2012 the Nobel Prize in chemistry was awarded to Brian K. Kobilka and Robert J. Lefkowitz for "studies of G-protein coupled receptors"⁵ and there have been at least seven Nobel Prizes awarded for G-protein-mediated signalling. Despite GPCRs only constitute 4% of the human genome, they are the target of approximately 26% of the drugs currently on the market⁶⁻⁸. Moreover, during the 2010-2013 period, the FDA^a approved 90 new molecular entities. Of these, 17 (19%) targeted GPCRs, which indicate that GPCRs are still a mainstay for new drugs⁷.

Generally, GPCRs have a common topology and signalling mode (*figure 1*). All of them include seven transmembrane alpha helices (TMD domain) with an extracellular *N*-terminal and an intracellular *C*-terminal, and other domains depending on the class and type of GPCRs. As a general rule, GPCRs are activated by extracellular ligands, causing a conformational change of the TMD that makes possible the activation of the heterotrimeric G-protein in the cytosol face. After this activation, the G-protein begins the signalling cascade.

A wide range of ligands, such as, ions, small molecules or proteins, can activate GPCRs. They usually bind in the orthosteric site, which is a pocket located either on extracellular domains or embedded within the transmembrane domain. This binding causes a conformational change of the TMD that permits the activation of a G-protein. These orthosteric ligands can be endogenous (produced by the organism) or exogenous (uptaken substance or drug). Additionally, some GPCRs can incorporate also an allosteric site, where, the orthosteric ligands do not bind, but other substances, like ions, sterols, peptides, proteins or small molecules can bind, causing a change in the normal conformational response of the receptor⁹⁻¹¹ Furthermore, recent advances on crystallography made possible the solution of many crystal structures of

^a Food and Drug Administration (United States)

GPCRs (136 according to Protein Data Bank), which helps the scientific community to understand the structural issues of these proteins and their binding with the corresponding ligands¹². These advances are also of great importance for medicinal chemistry, allowing the design and synthesis of more selective and potent drug-like compounds¹².

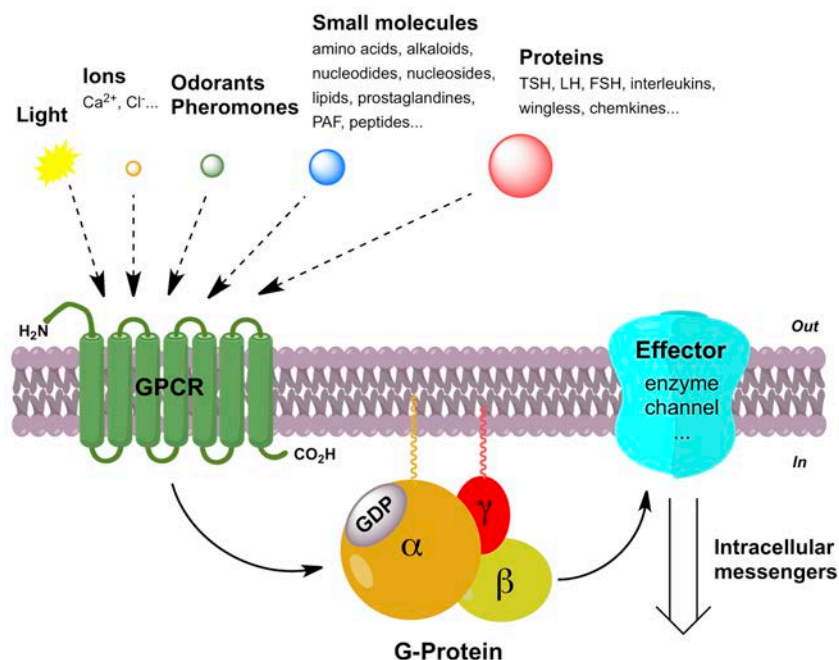


Figure 1: Topology of the GPCR and G-Protein and activation of the signalling cascade (Adapted from Bockaert & Pin¹³)

Guanine nucleotide-binding proteins (G-Proteins)

G proteins are a large family of proteins that act as molecular switches inside the cells and are involved in transmitting signals to the interior of the cells. G proteins bind and catalyse the hydrolysis of guanosine triphosphate (GTP) to guanosine diphosphate (GDP) and those that interact with GPCRs comprise a heterotrimeric complex with three subunits: the largest one G α (45 kDa) where GTP binds, G β (35kDa) and G γ (8kDa). The interaction with the active conformation of the GPCR induces the dissociation G α and G β γ subunits, releasing an active G α subunit that catalyses the exchange GDP \rightarrow GTP. Then the signalling cascade begins with the interaction of the G α or G β γ with the corresponding effectors, which are summarised in *table 1*. Once the reaction is finished, inactive G α is back-associated with G β γ subunit.

Family	Subtype	Action
G _s α	G _s α	Activate adenylyl cyclases, Maxi K channel, Src tyrosine kinases and GTPases
	G _{olf} α	Activate adenylyl cyclases from olfactory sensorial neurons
G _{i/o} α	G _i α, G _o α, G _z α	Inhibit adenylyl cyclases and Ca ²⁺ channels; activates ERK/MAP kinases, K ⁺ channels, GTPase of tubulin, Src tyrosine kinases and GRIN1-mediated activation of Cdc42
	G _t α	Activate cGMP PDE (phosphodiesterase) in the photoreceptors
	G _{gust} α	Activate cGMP PDE in the gustative sensorial neurons
G _q α	G _q α, G ₁₁ α, G ₁₄ α, G ₁₆ α	Activate PLC-β (Phospholipase C-β) isoforms, p63-RhoGEF (guanine nucleotide exchange factor), Bruton's tyrosine kinase and K ⁺ channels
G _{12/13} α	G ₁₂ α, G ₁₃ α	Activate Phospholipase B and Cε, NHE-1, iNOS, E-cadherin-mediated cell adhesion, p115RhoGEF, PDZ-RhoGEF, LARG (Leukaemia-associated RhoGEF), Radixin, PP5 (Protein phosphatase 5), AKAP110-mediated activation of PKA, HSP90
Gβγ	β ₁₋₅ γ ₁₋₁₂	Inhibit adenylyl cyclase I and Ca ²⁺ channels; activate PLC-β isoforms, adenylyl cyclases II, IV, VII, PI-3 kinases, K ⁺ channels, P-Rex1 (guanine nucleotide exchange factor for the small GTPase Rac), GTPase of tubulin, c-Jun N-terminal kinase (JNK) Src kinases, GPRC kinase recruitment to membrane, protein kinase D, Bruton's tyrosine kinase, p114-RhoGEF

Table 1: Summary of the human heterotrimeric G-Protein families and subtypes, with the main functions of each family (adapted from Milligan & Kostenis¹⁴)

Classification of human GPCRs

Human GPCRs were commonly classified in three main classes (1, 2 and 3 or A, B C), plus class F (or Frizzled), taking into consideration phylogeny, ligand features and binding modes¹³. A pure phylogenetic classification, called GRAFS¹ appeared after the sequencing of the human genome. It consisted in three main families: Glutamate, Rhodopsin, Adhesion, Frizzled/Taste2 and Secretin. Nevertheless, IUPHAR^a classifies GPCRs in class A (rhodopsin family), class B (secretin family), class C (glutamate family), class F (frizzled family), adhesion family and other non-classified 7TM proteins¹⁵⁻¹⁷. There also are two more families, D and E, which does not exist in human genome and represent fungal pheromone receptors and cAMP receptors. Furthermore, there are some subfamilies of classes A-F that neither exist in humans, such as family IV in class A (invertebrate opsin receptors) or archaebacterial opsins in class F¹.

^a International Union of Basic and Clinical Pharmacology

Class A GPCRs

Class A GPCRs, or rhodopsin family GPCRs, comprise the largest number of GPCRs, with 719 receptors in the human genome, from which 329 are non-olfactory and 87 are orphan^{a,17}. In the GRAFS classification, the family was divided in four groups: α , β , γ and δ and can be activated by many different molecules, from small molecules to proteins, as well as they can bind many different G-Proteins, depending on the receptor subtype.

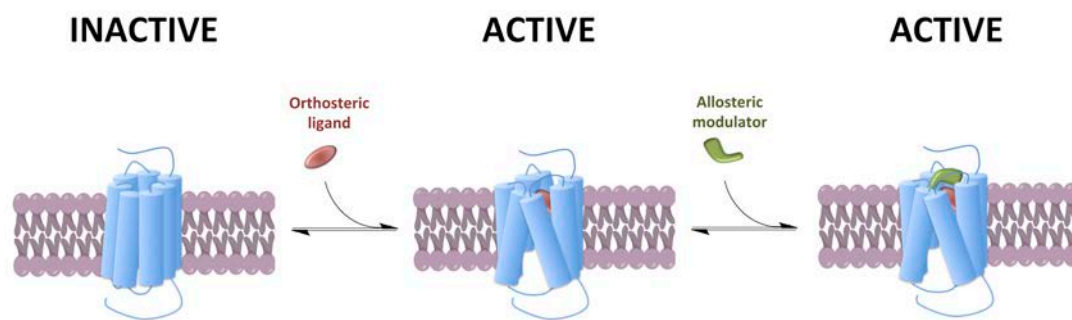
Group	Subgroup	Examples
α (Small molecules)	Prostaglandin	Prostaglandin and orphan receptors
	Amine	Serotonin (HTR/HT), dopamine (DRD/D), muscarinic (CHRM/M), histamine (HRH/H), adrenergic (ADR/ α / β), trace amine (TAR/TA) and orphan receptors.
	Opsin	Rod visual pigments (RHO), cone visual pigments (OPN), peropsin (RRH), encephalopsin (OPN), melanopsin (OPN) and retinal GPCR (RGR)
	Melatonin MECA	Melatonin (MTMR/MT) and orphan receptors Melanocortin (MCR/MC), endothelial differentiation GPCRs or Lysophospholipid (EDGR/LPA/S1P), cannabinoid (CNR/CB), adenosine (ADORA/A) and orphan receptors
β (Peptides)	-	Hypocretin (HCRTR/OX), neuropeptide FF (NPFFR/NPFF), neuropeptide Y (NPYR/Y), tachykinin (TACR//NK), cholecystokinin (CCKAR/CCK), endothelin-related (EDNR/ET), bombesin-like (GRPR/BB ₁ ; NMBR/BB ₂ ; BRS3/BB ₃), neurotensin (NTSR/NTS), growth hormone secretagogue (GHSR), thyrotropin-releasing hormone (TRHR), vasopressin (AVPR/V), gonadotropin-releasing hormone (GNRHR), oxytocin (OXTR) and orphan receptors
γ (Peptides - small proteins)	SOG	Galanin (GALR/GAL), kisspeptin (GPR54), somatostatin (SSTR/SST), neuropeptide B/W (NPBWR), opioid (OPR/ δ , κ , μ , NOP) receptors.
	MCH	Melanin concentrating hormone receptor (MHCR/MHC-R)
	Chemokine	Classic chemokine (CCR, CXCR / CC, CXC), angiotensin (AGTR), Bradykinin (BDKRB/B), chemerin (CMKLR) and orphan receptors
δ (Peptide, small proteins, small molecules)	MAS	MAS1 oncogene (MAS) and MAS-related (MRG, MRGX) receptors
	Glycoprotein	Glycoprotein hormone receptors (FSHR, TSHR, LHCGR) and leucine-rich repeat containing GPCRs (LGR)
	Purinergic	Formyl peptide (FPR), nucleotide (P2RY/P2Y), Lysophosphatidic acid (LPA/LPAR), hydroxycarboxylic acid (HCA/HCAT), succinate (SUCNR), Oxoglutarate (OXGR), free fatty acids (FFAR/FFA) and orphan receptors
	Olfactory	many

Table 2: Summary of the human class A or rhodopsin family GPCRs, with a phylogenetic groups and subgroups classification¹. Find human gene symbol and IUPHAR receptor name in parenthesis¹⁶.

^a An orphan receptor is an apparent receptor that has a similar structure to other identified receptors but whose endogenous ligand has not yet been identified.

Class-A-GPCRs consist of a transmembrane domain (TMD), with seven helices forming a bundle with an eighth helix that runs parallel to the membrane near the C-terminus. A few class-A-GPCRs have large extracellular domains (ECD) at the N-terminus, that bind ligands but, the orthosteric binding of the majority of class A GPCRs is located in extracellular half of the bundle. These receptors can accommodate small molecules, peptides or proteins as ligands, depending on the group or subgroup of receptors (*table 3*). Some small-molecule-binding class A receptors have a vestibule on the extracellular entrance of the binding site, just upper the binding site. This vestibule can act as an allosteric binding site or can accommodate parts of a long orthosteric ligand (figure 2A) due to the large variety of Class-A-GPCRs.

A



B

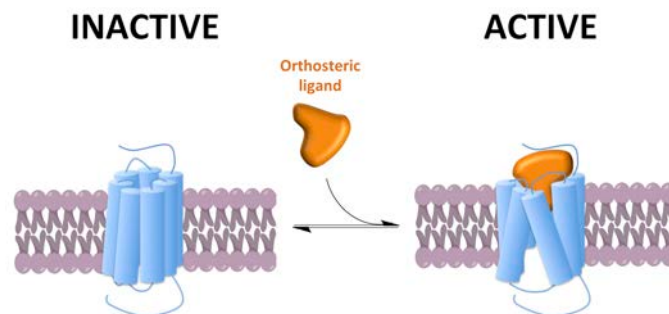


Figure 2: Topology of two class A GPCRs and general binding model: A) model of binding to a Class A GPCR of a small molecule and a possible allosteric modulator in a “vestibule” allosteric pocket. B) Model of binding of a peptide or a small protein to a Class A GPCR.

Class A GPCRs constitute a vast protein family that can bind several G-Proteins, depending on the receptor subtypes and encompasses a wide range of functions, including various autocrine, paracrine, and endocrine processes.

For the last 14 years, especially the last 5 years, many receptor crystal structures have seen the light of day. The first solved class A GPCR crystal structure was bovine rhodopsin in 2000¹⁸. Seven years after β_2 -adrenergic (β_2 -AR) receptor crystal structure was solved in its inactive conformation with the co-crystallization of an antagonist^{19, 20}. From that day many other Class-

A-GPCRs crystal structures were solved, in both active and inactive conformations¹² (table 3), which constitute helpful tools for the rational design of new drugs design.

Group	Receptor (species)	Conformation (years of publication)	
α	β_1A (turkey)	<i>Inactive</i> : 11 crystal structures (2008-2014) <i>Active</i> : 5 crystal structures (2011)	
	β_2A (human)	<i>Inactive</i> : 9 crystal structures (2007-2012) <i>Active</i> : 7 crystal structures (2011)	
	A_{2A} (human)	<i>Inactive</i> : 9 crystal structures (2008-2012) <i>Active</i> : 3 crystal structures (2011)	
	D_3 (human)	<i>Inactive</i> : 1 crystal structure (2010)	
	H_1 (human)	<i>Inactive</i> : 1 crystal structure (2011)	
	M_2 (human)	<i>Inactive</i> : 1 crystal structure (2012) <i>Active</i> : 2 crystal structures (2013)	
	M_3 (human)	<i>Inactive</i> : 1 crystal structure (2012)	
	RHO (bovine)	<i>Inactive</i> : 13 crystal structures (2000-2013) <i>Intermediates</i> : 5 crystal structures (2006-2011) <i>Active</i> : 5 crystal structures (2006-2014)	
	RHO (squid)	<i>Inactive</i> : 2 crystal structures (2008) <i>Intermediates</i> : 3 crystal structures (2011-2015)	
	$S1P_1$ (human)	<i>Inactive</i> : 2 crystal structures (2012)	
	5-HT _{1B} (human)	<i>Active</i> : 2 crystal structures (2013)	
	5-HT _{2B} (human)	<i>Active</i> : 2 crystal structures (2013)	
	β	NTS ₁	<i>Active</i> : 4 crystal structures (2012-2014)
	γ	CXC ₄ (human)	<i>Inactive</i> : 5 crystal structures (2010)
CC ₅ (human)		<i>Inactive</i> : 1 crystal structure (2013)	
δ (mouse)		<i>Inactive</i> : 1 crystal structure (2012)	
δ (human)		<i>Inactive</i> : 1 crystal structure (2013)	
κ (human)		<i>Inactive</i> : 1 crystal structure (2012)	
μ (mouse)		<i>Inactive</i> : 1 crystal structure (2012)	
NOP (human)		<i>Inactive</i> : 1 crystal structure (2012)	
δ	PAR1 (human)	<i>Inactive</i> : 1 crystal structure (2012)	
	P2Y ₁₂	<i>Inactive</i> : 1 crystal structure (2014) <i>Active</i> : 2 crystal structures (2014)	
	FFA ₁	<i>Active</i> : 1 crystal structures (2014)	

Table 3: Current class A GPCR with solved crystal structures

Class B GPCRs

Class B GPCRs, or secretin family GPCRs, comprise 15 receptors¹⁷ with no orphans reported, that are activated by peptide ligands of intermediate size (30-40 amino acids residues), such as hormones, neuropeptides and peptide autocrine factors²¹. They mainly activate G_s , with a lower predominance to G_q and G_i signalling pathways and are involved biological and pathophysiological functions²¹.

They consist of a transmembrane domain (TMD), with seven transmembrane helices forming a bundle. It incorporates in the *N*-terminus a moderately sized extracellular domain (ECD) (100-160 amino acid residues) and tail in the C-terminus. Peptides bind the receptor in a two-domain model as a general mechanism: the C-terminal portion of the peptide binds the ECD and the *N*-terminal portion, the TMD, with a consecutive activation of the receptor and the binding of the corresponding G-protein.

Subgroup	Examples
CRHRs/CALCRLs	Calcitonin (CALCR/CT) and corticotropin-releasing hormone (CRHR/CRH)
PTHRs	Parathyroid hormone receptors (PTHR)
GLPRs/GCGR/GIPR	Gastric inhibitory polypeptide (GIPR/GIP-R), glucagon (GCGR/GL-R) and glucagon-like peptide (GLPR/GLP-R) receptors
Secretin	Secretin (SCTR/SE), growth-hormone-releasing hormone receptor (GHRHR), vasoactive intestinal polypeptide (VIPR/VPAC), Pituitary adenylate cyclase-activating polypeptide type I (ADCTAP1/PAC) receptors

Table 4: Summary of the human class B or secretine family GPCRs, with a phylogenetic subgroups classification¹. Find human gene symbol and IUPHAR receptor name in parenthesis¹⁶

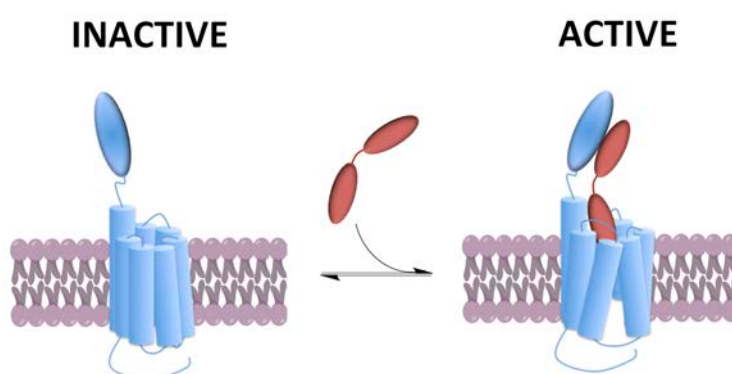


Figure 3: Topology of a class B GPCRs and general binding model of peptide interaction (adapted from Hoare²¹)

Class B GPCRs regulate several biological functions and constitute potential targets for drug discovery. In fact, there are several peptide agonists of Class B GPCRs currently in the market. An example of such may be salmon calcitonin, pramlintide, eduglutide, Lixisenatide or Tesamorelin used to treat osteoporosis, diabetes, hypercalcaemia, Paget's disease or HIV-

associated lipodystrophy. In addition, there are other peptide agonists in clinical phase 2 and 3, with multiple indications, but also monoclonal antibodies and small-molecule drug-like antagonists²².

In 2013, crystal structures of corticotropin-releasing factor type 1 (CRF₁) and glucagon receptor (GL) have been solved, both without ECD and co-crystallised with a non-peptidic antagonist. In both cases the antagonist was found to bind in the cytoplasmic half of the receptor, in a much deeper position compared to the binding site of class A GPCRs. These structures will be a very useful tool for the development of new drug-like compounds but new structures with both TMD and ECD and in active conformation would improve our understanding of the mechanisms of action as well as the design of new agonist small-molecule drugs.

CLASS C GPCRS

Class C GPCRs, or glutamate family GPCRs, comprise 22 receptors¹⁷ with 7 orphans. Small molecules, such as amino acids, or ions, activate these receptors. They can bind several G-protein subtypes, depending on the receptor subtypes and they are mainly expressed in the central nervous system (for GABA-B and mGlu), in the tongue (TAS1) or in multiple tissues (CaS).

Subgroup	Examples
GABA-B	Gamma amino butyric acid B receptors (GABBR/GABA _B)
TAS1/CASR	Taste 1 (TAS1R), calcium sensing receptors (CASR/CaS)
Glutamate	Metabotropic glutamate receptors (GRM/mGlu)
RAIG	Retinoic acid-inducible receptor (RAIG)

Table 5: Summary of the human class C or glutamate family GPCRs, with a phylogenetic subgroups classification¹.
Find human gene symbol and IUPHAR receptor name in parenthesis¹⁶

A common characteristic of class C GPCRs is the obligatory dimerization at the cell surface, either as homodimers (mGlu and CaS) or heterodimers (GABA_B and T1Rs)²³. Each protomer consists in three different domains. Like the rest of GPCRs, they contain a transmembrane domain (TMD) with seven transmembrane alpha helices with the C-terminus in the cytosol side, where the G-protein binds. At the N-terminus, there is a large domain, called “Venus fly trap” (VFT) and it is where the endogenous ligands bind. In all class C GPCRs, except GABA_B receptors, there is also a cysteine-rich domain (CRD) between the TMD and The VFT, which is formed by 70 amino acid residues with 9 cysteines and transduces the signal from the VFT to the TMD²⁴.

Each VFT domain consists in two opposing lobes separated by a cavity where the endogenous ligand is recognised. These two lobes fluctuate between open and close conformations and agonists usually stabilize the closed one, whereas antagonists stabilise the open one^{23, 25}. Since 2000 many crystal structures of class C GPCR dimeric VFTs have been solved, in close an open conformations, which helped to understand the activation of this class of receptors²⁵⁻²⁹.

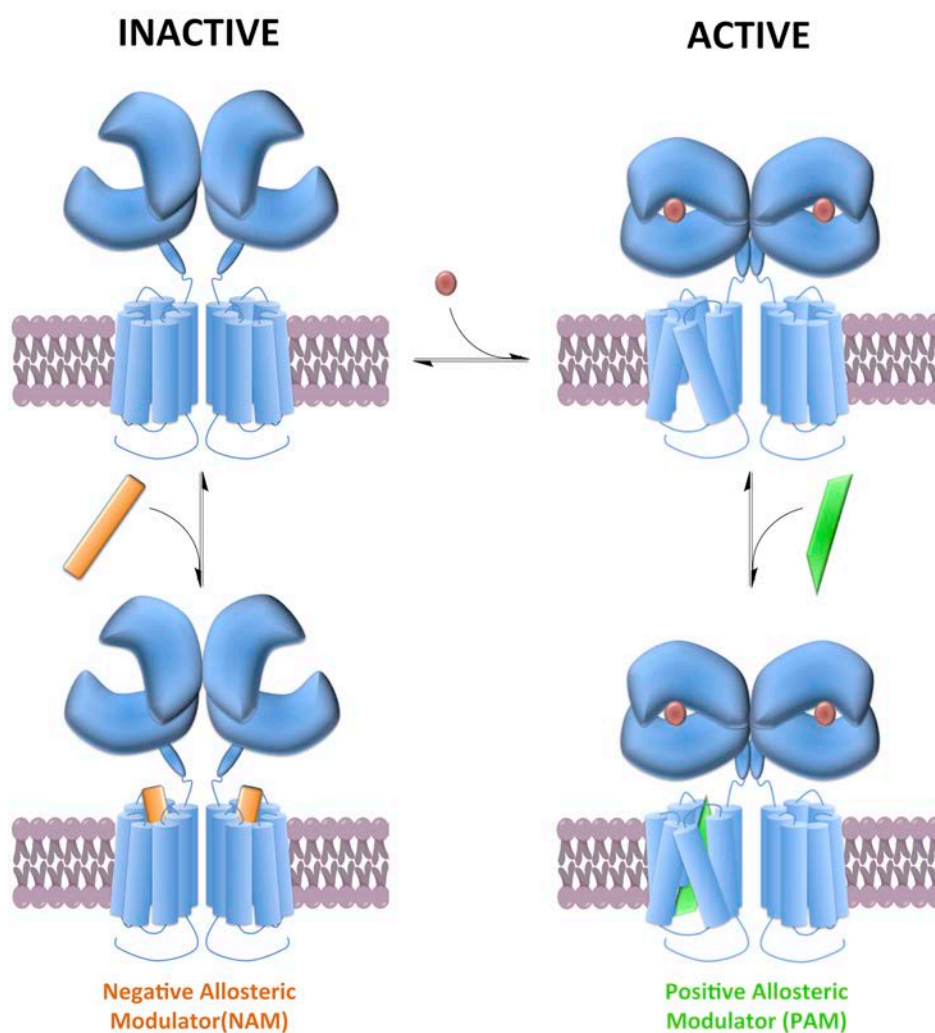


Figure 4: Topology of a class C GPCRs and general binding model of endogenous agonist and allosteric modulators (adapted from Rondard³⁰)^a

Class C GPCRs control a great variety of functions, mainly in the CNS for mGlu and GABA_B, while also CaS control calcium homeostasis by regulating the release of parathyroid hormone (PTH) or T1Rs sense the sweet and umami tastes in the tongue. Due to the importance of class-C-GPCR functions, its druggability is particularly appealing for drug discovery programs, both for new orthosteric ligands and allosteric modulators. In 2014 two crystal structures of TMD of class C GPCRs (mGlu₁ and mGlu₅) were solved in their inactive conformations bound with a

^a Ligands are supersized for a better visualisation of the figure

negative allosteric modulator^{31,32}. These crystal structures showed that the allosteric binding site was positioned a bit deeper than orthosteric site for class A GPCRs, but not as deep as the allosteric site of class B GPCRs. Like for class B GPCRs, these solved crystal structures have increased the understanding of the mechanism of action of these receptors and constitute a new powerful tool for drug discovery to find out new allosteric modulators in a more effective way and with better perspectives.

Class F GPCRs

Class F GPCRs, or frizzled family or frizzled/smoothened GPCRs, comprise 11 receptors, 10 frizzled (FZD) and 1 smoothened (SMO), with no orphans¹⁷. The FZD are activated by lipoglycoproteins of the wingless/int1 (WNT) family, whereas SMO is indirectly activated by the Hedgehog (HH) family of proteins acting on the transmembrane protein patched (PTCHA). According phylogenetic GRAFS classification¹, TAS2 receptors clustered together with the frizzled receptors, despite not having obvious similarities. Nevertheless, IUPHAR classify its 30 subtypes as Class A GPCRs¹⁷.

FZDs have an important role in cellular communication for proper embryonic development, stem cell differentiation, organogenesis and patterning. Also WNT/FZD signalling has a crucial role in the maintenance of tissue homeostasis, regeneration, plasticity and repair³³.

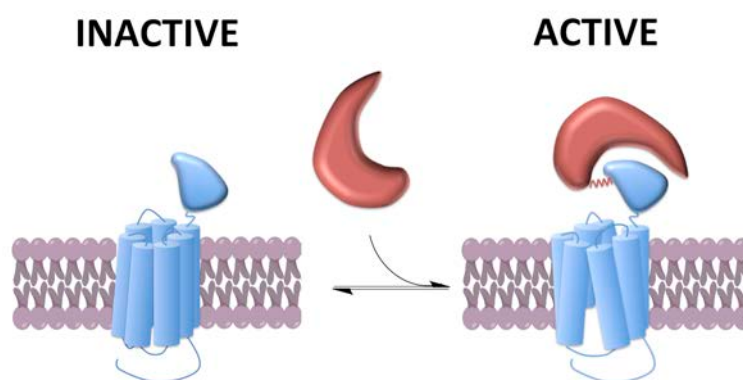


Figure 5: Topology of a class F GPCRs and general binding model of Wnt-protein interaction (adapted from previous publications^{31,34})

The basic mechanisms and associated components of response produced by and activation of Frizzled family GPCRs are poorly understood³³. Like the rest of GPCRs, these receptors include a domain with seven transmembrane helices (TMD) with a C-terminus in the cytosol side, where the G-protein binds, and in the N-terminus have a cysteine rich domain of about 160 amino acids residues, that has been proposed to be the main ligand-binding region of the

receptor, present in frizzled and smoothed receptors. Moreover crystal structure of CRD of FZD₈ bound to XWnt-8 has been solved³⁵.

They mainly bind to G_o-protein and antagonists are especially interesting for treatment of several types of cancer and agonists for regenerative medicine³⁶. Furthermore, five crystal structures of SMO has recently been solved, four of them co-crystallized with an antagonist in the inactive conformation and one co-crystallised with an agonist^{34,37}. These crystal structures probably will offer to the scientific new information of the modulation of the function of class F receptors and their contribution to the suppression of tumour growth and the chemo-resistance of some mutations.

Adhesion Class GPCRs

Adhesion Class, is the second largest family of GPCRS with 33 members and are a very peculiar family of GPCRS, phylogenetically related to Class B GPCRS¹⁷. The majority of them are orphans, and recently only eight of them have been matched with natural ligands³⁸.

Group	Former name	Examples
Latrophilin (L)	I	Latrophilin receptors (LPHN/ADGRL) and 'epidermal growth factor (EGF) latrophilin and seven transmembrane domain-containing protein 1' (ELTD1/ADGRL4)
EGF-TM7 (E)	II	EGF-like module-containing mucin-like hormone receptors-like (EMR/ADGRE) and Cluster of differentiation 97 receptor (CD97/ADGRE5)
A	III	GPR123/ADGRA1, GPR124/ADGRA1 and GPR124/ADGRA1
CELSR (C)	IV	Cadherin EGF LAG seven-pass G-type receptors (CELSR/ADGRC)
D	V	GPR133/ADGRD1 and GPR144/ADGRD2
F	VI	GPR110/ADGRF1, GPR111/ADGRF2, GPR113/ADGRF3, GPR115/ADGRF4 and GPR116/ADGRF5
BAI (B)	VII	Brain-specific angiogenesis inhibitors (BAI, ADGRB)
G	VIII	GPR56/ADGRG1, GPR64/ADGRG2, GPR97/ADGRG3, GPR112/ADGRG4, GPR114/ADGRF5, GPR126/ADGRF6 and GPR128/ADGRG7
V	IX	Very Large GPCR receptor 1 (VLGR1/ADGRV)

Table 6

They contain the typical GPCR transmembrane domain (TMD), with 7 helices and they mostly possess large N- and C-termini. All the family members except ADGRA1 include a GPCR autoproteolysis-inducing domain (GAIN) of approximately 320 residues as the first domain in the N-terminus (*figure 6*). Here is where a cysteine-rich GPCR proteolysis site (GPS) of approximately 50 amino acid residues is located³⁹. On the N-terminus, GAIN domain can be

fused to one or several adhesion-like motifs, such as EGF-like repeats, mucin-like regions or cysteine rich domains, often rich in prolines and glycosylation sites (*figure 6*). These motifs are thought to play a role in cell adhesion¹.

A defining feature of adhesion GPCRs is the highly conserved GPS and GAIN domain and its autoproteolysis. They are the units responsible of the cleavage of the receptor in the GPS, leading to two non-covalently bound subunits: a *N*-terminal-fragment (NTF) and a *C*-terminal fragment (CTF) but they both still keep an association after the cleavage. Moreover, adhesion GPCRs, after the cleavage, display promiscuity in NTF and CTF associations, leading to associations with other family members.

The proposed ligands for few adhesion GPCRs are large macromolecules, either membrane proteins on neighbouring cells or extracellular matrix (ECM) molecules. This also suggests that adhesion GPCRs contribute to cell-cell adhesive interactions and sense changes within the environment and the adjacent cells³⁸. They also can bind different G α -protein subunit, depending on the subtypes, as reported in many recent publications, but they are also capable to activating non-G-protein signalling cascades³⁹. However, the adhesion GPCRs switch between active and inactive conformations is yet not well known due to the lack of known ligands. There are two main hypotheses: 1) A segment of the ECD functions as inverse agonist of the constitutive signalling of the TMD, which is removed upon an agonist binding; 2) A segment of the ECD functions as an agonist and binds the TMD, like other ligands do with the rest of GPCRs³⁹

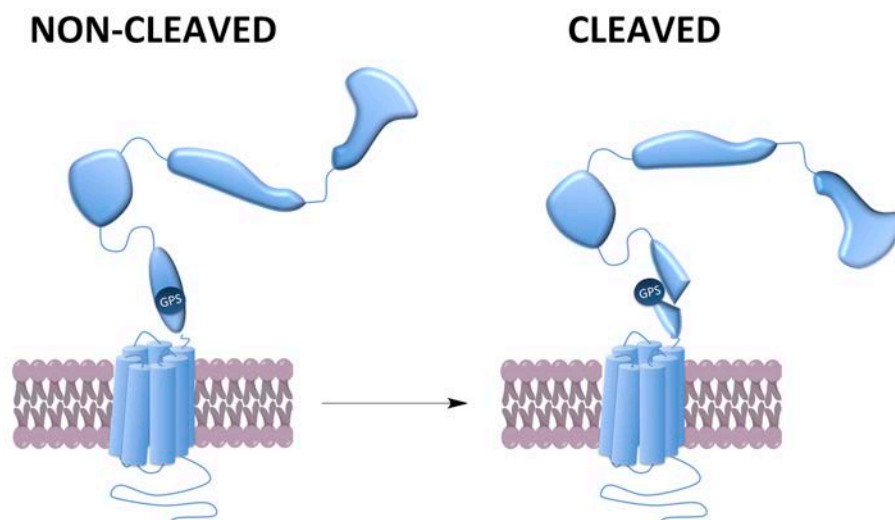


Figure 6: Topology of a theoretical class Adhesion GPCR with GAIN domain and three additional motifs in the ECD and general cleavage model in the GAIN domain (adapted from various publications³⁹)

There are no current drugs or clinical trials acting on adhesion GPCRs. However, there is a considerable interest in the pharmacology of these receptors. They are thought to have important roles in planar cell polarity, in neuronal development, in angiogenesis regulation, in immune cell contact and activation, in stem and lineage markers reproductive tissues and, especially in cancer: in tumour association, metastasis and tumour-specific upregulation³⁸.

Glutamate and its homonym receptors

Glutamic acid or (S)-2-aminopentanedioic acid or glutamate, as the conjugate base, is a non-essential amino acid and its DNA codons for translation are GAA and GGA. The side chain of glutamate corresponds to a propynoic acid with a $pK_a=4.1$, which results in deprotonation at physiologic pH ($pH\approx 7.4$) and, therefore, it is considered a polar amino acid.

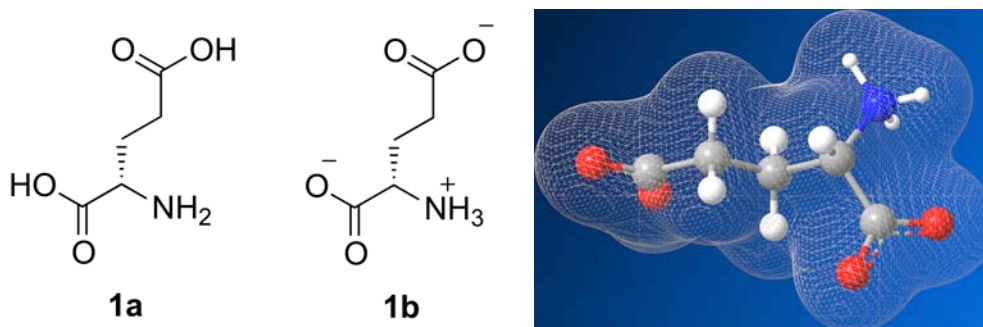


Figure 7: Chemical structure of acid glutamic as a free base **1a**, its corresponding zwitterion form **1b** with the unprotonated chain carboxylic acid (corresponding to physiological pH), and 3D structure in balls with a surface of charge density as a wire mesh.

The biologic functions that involve glutamate are numerous, since it is not only a proteinogenic amino acid. Glutamate is also the responsible of “umami” taste; one of the five basic tastes and it is related to TAS1R1+3 receptor dimer (class C GPCR), which naturally binds glutamate and aspartate as ligands. Glutamate is also the precursor of the synthesis of the inhibitory gamma-aminobutyric acid (GABA) neurotransmitter, in GABA-ergic neurons, through glutamate decarboxylase catalysis and a key compound in cellular metabolism. In addition, glutamate is the major excitatory neurotransmitter in the vertebrate nervous system and its signalling is thus critical for the majority of sensory processing and cognitive function⁴⁰.

In the glutamatergic synapse, glutamate is stored in vesicles in the presynaptic compartments through vesicular glutamate transporters (VGLUT) and, upon calcium influx triggered by action potentials; these vesicles rapidly release the neurotransmitter from the nerve terminal. In addition, glutamate reuptake machinery in both presynaptic terminals and in the adjacent

astrocytes controls glutamate concentration in the synaptic cleft. Once glutamate reaches the postsynaptic terminal of a new cell, in the opposite side of the presynaptic terminal, it activates the machinery of the postsynaptic density (PSD)^a, where glutamate receptors are located, and the signalling cascade continues (*figure 8*).

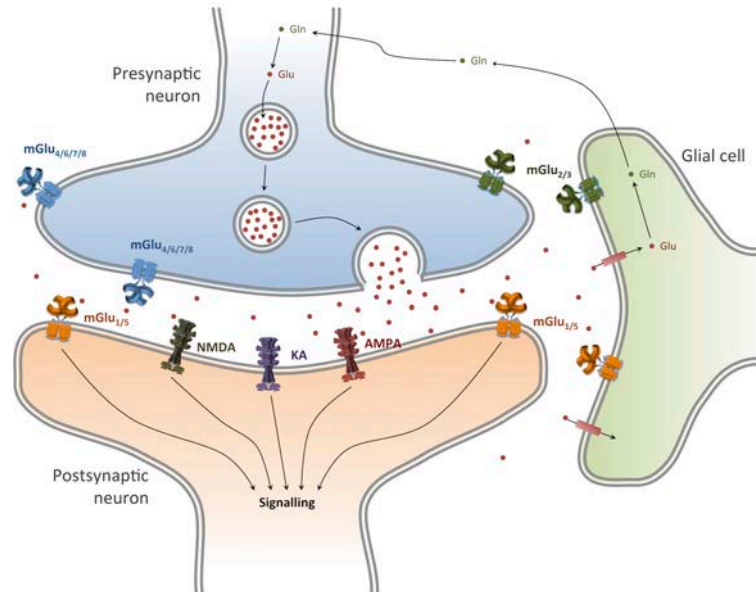


Figure 8: The glutamate synapse. Glutamate (Glu) is accumulated in vesicles in presynaptic terminals through vesicular glutamate receptors (VGLUT). In the synapse these vesicles are fused with the neuron membrane, releasing glutamate. This glutamate then activate iGlu receptors (AMPA, NMDA and KA) and mGlu₁ and mGlu₅, located in the postsynaptic terminal of a new neuron, triggering a signalling cascade. The uptake of glutamate is done by glial cells through glutamate transporters (EAAC), where it is converted to glutamine (Gln) and released to enter again the presynaptic cell, where it is converted to glutamate and stored in glutamate vesicles.

The ionotropic Glutamate Receptors (iGluRs)

Ionotropic glutamate receptors are cationic ligand-gated channels that mediate the excitatory neurotransmission, a transmission crucial for brain development and function. Upon binding, glutamate induces the opening of a cation-selective pore. They are divided in three main subfamilies, named according to the selective synthetic ligand preferred for each subgroup: α -amino-3-hydroxy-5-methyl-4-isoxazolepropionic acid receptor (AMPA), kainate receptor (KA) and *N*-Methyl-D-aspartate receptors (NMDA). There is an additional subfamily, named delta (GluD), which is structurally homologous but not activated by glutamate.

They are all tetrameric protein receptors. Each subunit comprises 4 domains: An *N*-terminal domain (NTD), which regulate the subunit composition and where, for NMDA receptors, some

^a The postsynaptic density (PSD)^a is a network of scaffolding proteins, receptors and signalling molecules, including ionotropic and metabotropic glutamate receptors located in postsynaptic terminals of neurons, in close opposition to the presynaptic active zone.

modulators can bind; a ligand-binding domain (LBD), where glutamate or glycine bind; a transmembrane domain (TMD), which form the channel in the tetrameric disposition, and a C-terminal domain (CTD) where the phosphorylation sites are located and where scaffolding proteins interact.

Family	Gene / Subunit name
AMPA	GRIA1/GluA1, GRIA2/GluA2, GRIA3/GluA3 and GRIA4/GluA4
Kainate	GRIK1/GluK1, GRIK2/GluK2, GRIK3/GluK3, GRIK4/GluK4 and GRIK5/GluK5
NMDA	GRIN1/GluN1, GRIN2/GluN2A, GRIN2B/GluN2B, GRIN2C/GluN2C, GRIN2D/GluN2D, GRIN3A/GluN3A and GRIN3B/GluN3B,
Orphans	GRID1/GluD1, GRID2/GluD2

Table 7: Classification of iGluR with IUPHAR-recommended nomenclature of subunits and human genes⁴¹

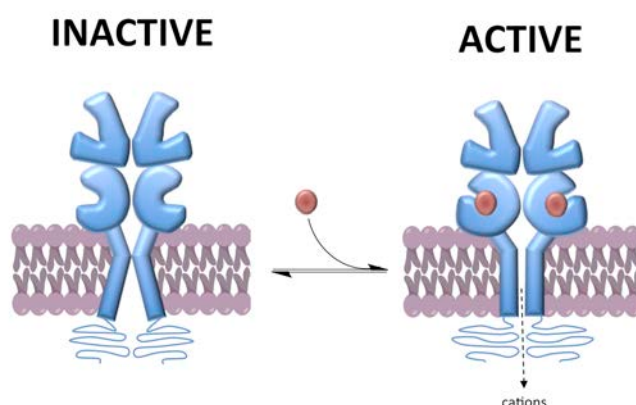


Figure 9: Topology of an iGlu receptor (with two subunits for a proper visualisation, it should be four subunits) and general binding model of glutamate in the LBD with the corresponding opening of the cation channel.

AMPA ionotropic receptors are responsible for an important part of post-synaptic excitatory potential since they are the largest in number and are located at the most active location in the PSD. The channel opens when two of the four binding sites are occupied by an agonist and the current may increase as more binding sites are occupied. Auxiliary proteins (TARPs) may regulate their trafficking⁴² and they are completely permeable to Na⁺ and K⁺ under activation but their permeability to Ca²⁺ depend on the presence of the subunit mGluA2, which makes the channel impermeable to calcium ions. Their high EC₅₀ to glutamate (100-50 μM) evidences that the activation of the receptor only occurs upon synaptic release of glutamate and show fast activation and deactivation rates in addition to both rapid and strong desensitisation⁴³.

Kainate ionotropic receptors have similar properties than AMPA receptors, but they are responsible for a minimal part of the postsynaptic currents. They actually play a neuromodulatory role. A defining difference between AMPA and kainate receptors is that the latter require extracellular Na⁺ and Cl⁻ for their activation and they are also modulated by

auxiliary subunits (Neto proteins). They mediated excitatory postsynaptic currents (EPSCs) and are often much slower than AMPA ones, and this is probably due to the slow deactivation rate of KARs containing the GluK4 or GluK5 subunits properties. Kainate receptors also desensitize faster than AMPA receptors at low agonist concentrations, making kainate receptors insensitive to glutamate spillover from neighbouring synapses^{40,44}.

NMDA ionotropic receptors are heterotetrameric, with two GluN1 subunits and two GluN2 or GluN3 subunits. GluN2 subunits bind glutamate, whereas GluN1 glycine or D-serine, acting as co-agonists. They are a singular type of ion-gated receptor, since they do not only need two different agonists to be activated, but also a strong depolarisation to remove the magnesium ion (Mg^{2+}) that blocks the pore. Their main functions are believed to be regulatory and they are reported to play an important role in controlling synaptic plasticity^a and memory function⁴⁵.

The metabotropic glutamate receptors (mGluRs)

The metabotropic glutamate receptors (mGluRs) belong to class C of G-protein coupled receptors (GPCRs) and are abundant and widely distributed throughout the central and peripheral nervous system (CNS & PNS). They are activated by glutamate and can regulate several neuronal and glial functions. Thus, they have an important role in the neuronal excitability and their synaptic transmission.

mGluRs topology and mechanisms of activation

As class C GPCRs, mGlu receptors are obligatory dimers and each promoter includes three domains: a transmembrane domain (TMD), a cysteine-rich domain (CRD) and the Venus flytrap (VFT) as explained above in class C GPCRs.

The VFT is a large extracellular domain, formed by two lobes defining a cleft where glutamate binds. VFT crystal structures have been solved for mGlu₁ in its open and close conformation with and without glutamate^{26,27}. Later, crystal structures of many others VFT domains of mGlu receptors were solved^{28,29}. These structures strongly support the theory that the two lobes of the shell dynamically open and close in the absence of ligand and, when an agonist binds, the closed conformation is stabilised, since more stable contacts with glutamate were found in the closed conformation than in the open one. Moreover, it has been observed that antagonists prevent the closure of the VFT, while locking the VFT in a closed conformation through a

^a Plasticity is the quality of being easily shaped or molded. In biology the adaptability of an organism to changes in its environment or differences between its various habitats. In neuroscience, synaptic plasticity is the ability of synapses to strengthen or weaken over time, in response to increases or decreases in their activity (New Oxford American dictionary)

disulphide bond leads to a constant activation of the receptor³⁰. The VFTs form stable dimers by means of hydrophobic interactions and a bisulfide bond. Upon activation of the receptor, the dimer experiences a large change in the relative orientation of the VFTs. When VFTs are open, they are in resting conformation and the two VFTs only interact via lobe-I (*figure 10, 1st panel*). However, when one or two lobes are closed, they adopt the active conformation and the interaction of the two VFTs involve lobe II and I (*figure 10, 5th panel*)²³. Intramolecular time-resolved FRET experiments have shown that the rearrangement of the VFT dimer is correlated with the receptor activation in living cells⁴⁶.

The CRD is a domain that links the VFT and the TMD, with 70 amino acid residues, including nine well-conserved cysteines, which afford four intradomain disulphide bridges and the ninth cysteine is linked to the VFT through an additional disulphide bridge²⁹. In the active state, the two CRDs associate and are likely contacting each other²⁴. Its role is reported to be crucial and it is reported that a precise association of the two CRDs is sufficient for full mGluR activation²⁴. Therefore, CRDs may constitute a site of action of molecules that modulate the activity of mGluRs and a possible target for drug discovery²⁴.

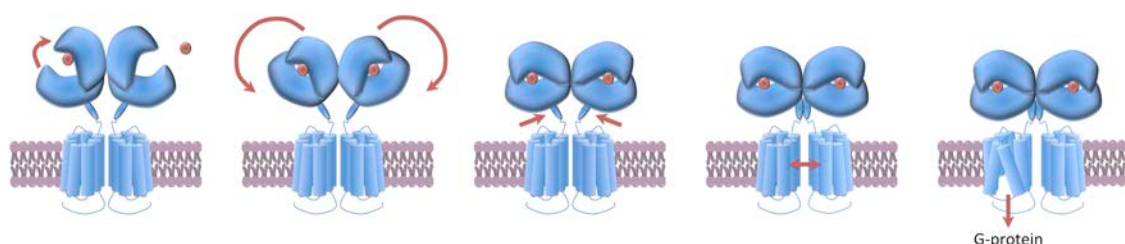


Figure 10: Schematic steps of activation of mGluRs. Adapted from Rondard & Pin⁴⁷.

The TMD, also called 7TM, consists in seven transmembrane helices forming a bundle and it is the responsible for G-protein activation like in the rest of GPCRs. Upon receptor activation, the TMD of only one protomer adopts an active conformation, whereas the other one remains in the resting conformation. That one in the active conformation is responsible of transducing the signal of the activation by glutamate in the VFT to the corresponding G-Protein⁴⁸. In fact, dimerization is needed to activate the receptor with glutamate or an orthosteric ligand, but it is not needed for G-protein coupling, since it is reported that a monomeric subunit or an isolated TMD couples a G-protein upon activation with a positive allosteric modulator (PAM) that binds to an allosteric site in the TMD⁴⁹. Nevertheless, intramolecular time-resolved FRET experiments in dimeric mGluRs in living cells showed that PAMs and NAMs can modulate the activity of the orthosteric agonist and, in many cases, do not show a significant effect if the PAM is applied alone^{46, 50}.

^a Further explained in pages 23-28

The first crystal structures of TMD mGlu₁ and mGlu₅ were recently solved in its inactive conformation^{31, 32, 51}, showing a similar fold to class A GPCRs, despite the low of sequence homology. No crystal structure of an active conformation of an mGlu TMD has been reported to date, but homology models have been reported, showing a similar fold to class A GPCRs with a proposal of the PAM binding sites⁵² and also considerable information about the TMD interface of the mGluRs dimers and its dynamics upon receptor activation⁵⁰.

Figure 10 represents a summary the major steps of activation mechanism explained above, starting from the binding of glutamate or an agonist bind the VFT, which induce its closure and the reorientation of the VFT, followed by the association of CRDs within ~30 ms in total. This intermolecular conformational change is followed by the activation of the TMD of one of the two subunits within ~50 ms, which results in G-protein activation⁵³.

Classification of the mGluRs, functional anatomy and main biological roles

mGluRs comprise 8 different subtypes, classified in three different groups on the bases of similarities in primary sequence, agonist pharmacology, and G-protein effector coupling. Group I subtypes (mGlu₁ and mGlu₅) are mainly presynaptic^a and bind to G_qα subunit, while group II (mGlu₂ and mGlu₃) and group III (mGlu₄, mGlu₆, mGlu₇ and mGlu₈) are mainly postsynaptic^b and bind to G_{i/o}α subunit (*table 8*).

Group	Subtype	Gene	Glu EC ₅₀	Orth. ago	EC ₅₀	G-Prot. (main signalling)
I	mGlu ₁	GRM1	9-13	Quisqualic acid (2)	0.1-1.0	G _q (↑IP ₃ , ↑ intracellular Ca ²⁺ , ↑DAG, PKC activation)
	mGlu ₅	GRM5	3-10		0.03-0.3	
II	mGlu ₂	GRM2	4-20	LY 354740 (3)	0.005	G _{i/o} (↓cAMP, inhibit voltage gated Ca ²⁺ channels, activate K ⁺ channels, activate the MAPK and PtdIns-3-K pathways)
	mGlu ₃	GRM3	4-5		0.0034	
III	mGlu ₄	GRM4	3-20	L-AP4 (4)	0.2-1.2	G _{i/o} (↓cAMP, inhibit voltage gated Ca ²⁺ channels, activate K ⁺ channels, activate the MAPK and PtdIns-3-K pathways)
	mGlu ₇	GRM7	1000		0.9	
	mGlu ₈	GRM8	16		160-500	
	mGlu ₆	GRM6	2.5-11		0.06-0.60	

Table 8: Classification of mGlu receptors in groups, with glutamate potency for every subtype EC₅₀ in μM units⁵⁴, the most common agonists used for each group (*figure 11*), with its potency as EC₅₀ in μM units⁵⁴ with the main corresponding G-protein and the main signalling pathways that they activate⁵⁵.

^a Presynaptic: relating to or denoting a nerve cell that releases a transmitter substance into a synapse during transmission of an impulse (New Oxford American Dictionary).

^b Postsynaptic: located on the distal side of a synapse (Collins English Dictionary)

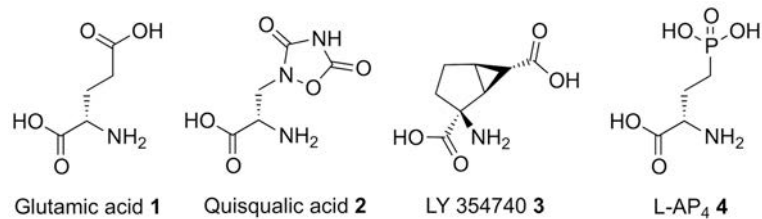


Figure 11: Structure of common group-selective orthosteric agonists and non-selective antagonist LY 341495.

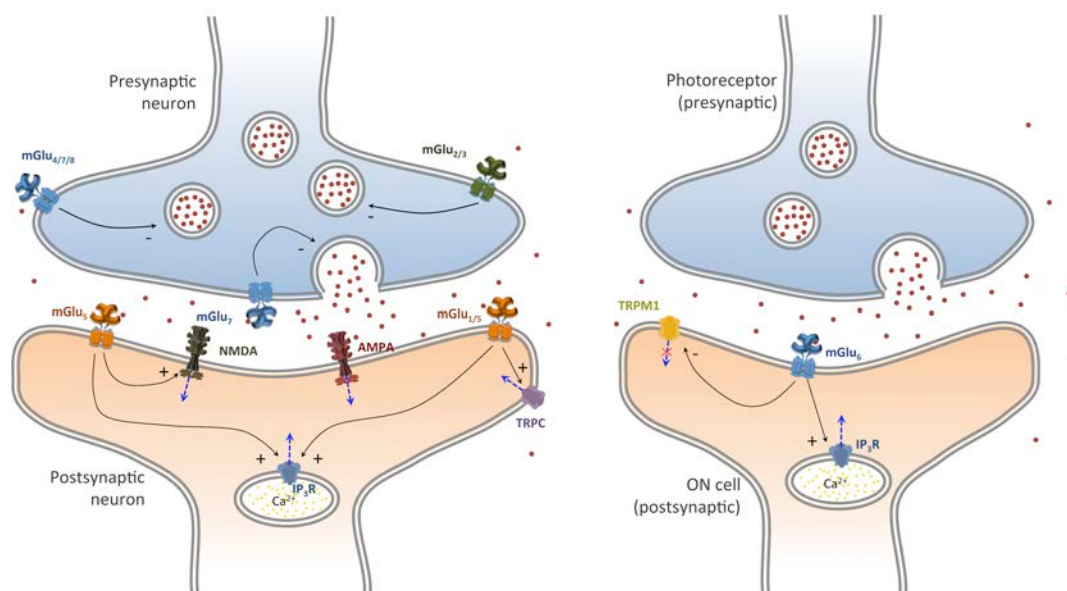


Figure 12: The glutamate synapse for glutamatergic neurons (left) and for photoreceptors/ON cells (right) with a representation of the localisation of the different mGlu subtypes their main functions.

Group I mGluRs^{55, 56}

mGlu₁ and mGlu₅ are extensively expressed in the CNS, in neurons and also in glial cells. They are located predominantly in postsynaptic region, where the receptor appears to be concentrated in perisynaptic^a and extrasynaptic^b areas. Thus, mGlu receptors are recruited by high concentrations of glutamate that escape the clearance mechanisms and spread to the sides of the synaptic cleft. They increase the neuronal excitability and play an important role in neuronal plasticity, partly because of their functional interaction with NMDA receptors. Additionally, when they are found presynaptically they can also modulate neurotransmitter release.

Studies in mGlu₁ knockout^a mice suggested an involvement of mGlu₁ in learning and memory, while mGlu₅ turns out to be more related to cognition, drug addiction, anxiety, chronic pain

^a Perisynaptic corresponds to near the synapse

^b Extrasynaptic corresponds to exterior to a synapse

and obesity. New data also demonstrate that group-I mGlu receptor dysfunction may also contribute generally to the pathophysiology of autism and related disorders⁵⁷.

Group II mGluRs^{55, 56}

mGlu₂ and mGlu₃ are widely distributed in the CNS and also in PNS. Generally they are located presynaptically in neurons, far from the neurotransmitter release zone, where they are activated by an excess of synaptic glutamate or by glutamate released from astrocytes. mGlu₃ can also be found in glial cells and in postsynaptic regions where they induce hyperpolarization.

The major function of these two receptors in presynaptic terminals is to inhibit neurotransmitter release. They have an established role in regulation of synaptic plasticity. Studies in mGlu₂ KO mice, apart from losing mGlu_{2/3} agonists induced effects, they show an enhanced responsiveness to cocaine and alterations in synaptic transmission in several regions of the brain. Regarding mGlu₃ KO mice, they also losing mGlu_{2/3} agonists induced effects and show an increase of hippocampal c-Fos expression.

Group III mGluRs^{55, 56}

Group III mGluRs are widely distributed throughout the CNS in presynaptic regions of neurons, except mGlu₆ which is almost exclusively expressed in retina. Activation of these receptors negatively regulates the neurotransmitter release. Glutamate binds to mGlu₄ and mGlu₈ with a relative high affinity, but displays a very low affinity for mGlu₇ (*table 8*). Moreover, mGlu₇ receptor is localised at the active zones of the synapse. That's why it has been proposed that it has glutamate-overstimulation-preventing role due to its localisation and the high doses of glutamate needed for its activation. mGlu₆receptor, which is involved in visual perception, is expressed postsynaptically in the dendrites of retinal ON bipolar cells and responds to glutamate released from rod and cone photoreceptor cells in the dark.

Experiments with mGlu₄ KO mice showed an association of mGlu₄ with cerebellar synaptic plasticity, learning of complicated motor tasks and spatial memory performance. mGlu₇ has been related with epileptic phenotypes, memory and learning, anxiety and depression. Experiments with mGlu₈ KO mice revealed an association of the receptor with anxiety and weight control. Mice lacking mGlu₆ showed deficits in ON response to light stimulation.

^a A gene knockout (KO) is a genetic technique in which one of an organism's genes is made inoperative.

Modification of mGluR function: orthosteric and allosteric ligands

The classical approaches to modulate the function of mGlu receptors are the use of small-molecule ligands that bind to the receptor, stabilising the active or the inactive conformation. Other approaches are possible, like the use of antibodies, nanobodies or other “bio-tools”, but this goes beyond the scope of the present thesis.

Small-molecule ligands acting on mGluRs can be classified in two main groups: Ligands binding at the VFT, which are usually orthosteric ligands or competitive with glutamate, and ligands binding at the TMD, which are allosteric ligands or non-competitive.

Ligands binding at the VFT

The mGlu receptor's endogenous ligand, glutamate, binds to the VFT cleft. Based on the structure of glutamate and the structural studies on the VFT, many compounds have been designed and screened⁵⁸. They comprise full agonists, partial agonists, antagonists or inverse agonists and they are all competitive with glutamate⁵⁴. However, achieving selectivity for a single mGlu subtype is an arduous task, since glutamate binding site is highly conserved. In the early years, mGlu molecular pharmacology efforts only provided group-selective competitive agonists (*figure 14A*) such as quisqualate for group I (**2**), LY 354740 (**3**) for group II and L-AP4 (**4**) for group III mGlu receptors (*table 8, figure 11*). Besides, antagonists such as LY 341495 were discovered, which is active at the eight mGlu receptors but has a mild selectivity for group II (*figure 13 & 14B*).

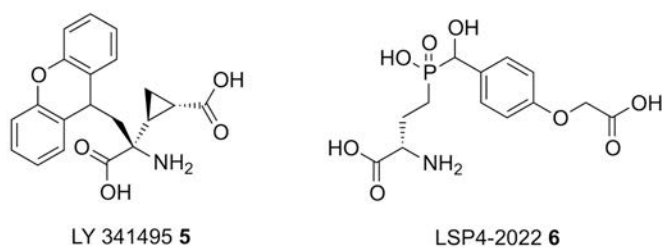


Figure 13: Structures of the orthosteric antagonist LY 341495 and the mGlu₄-selective orthosteric agonist LSP4-2022.

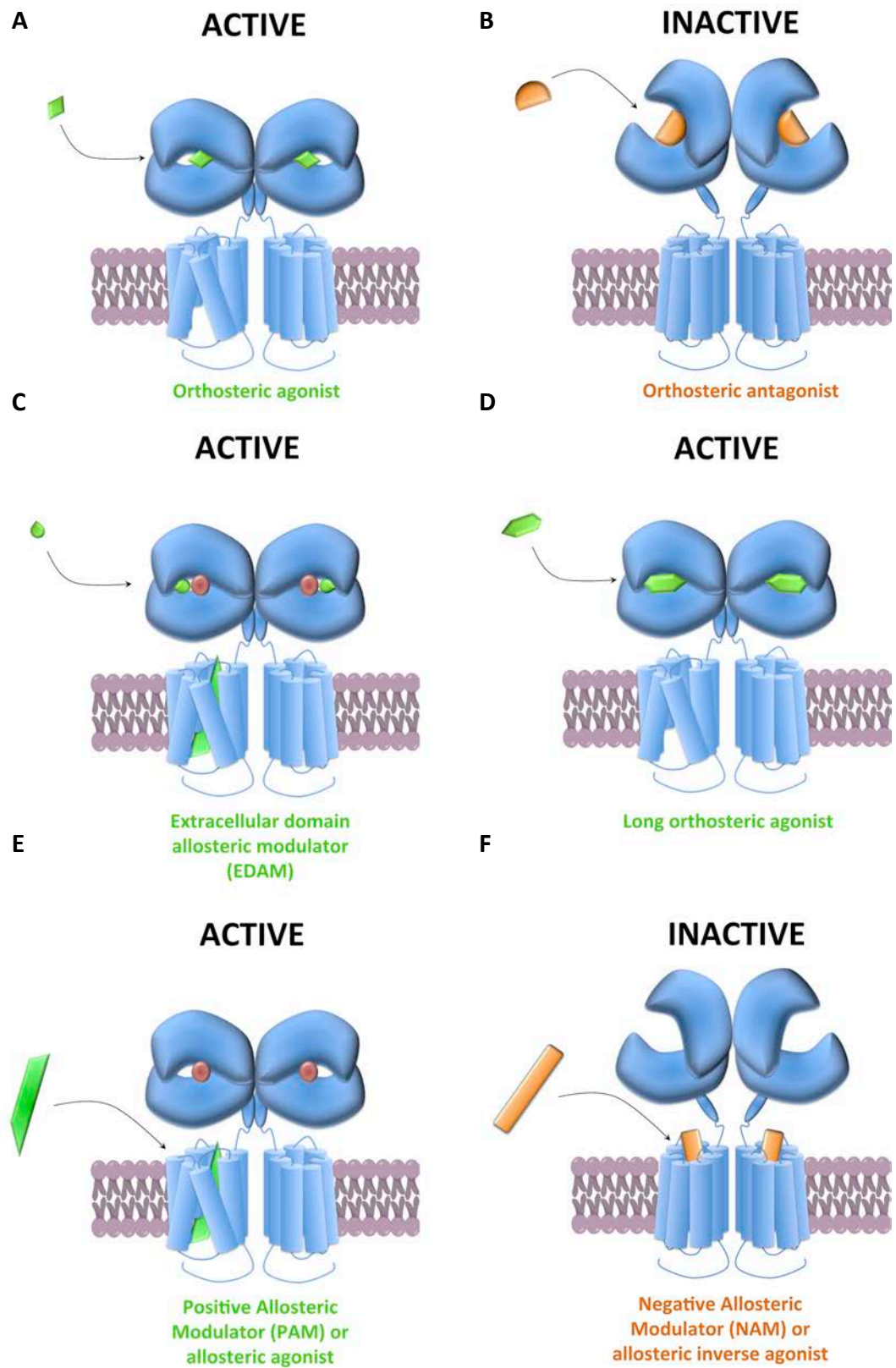


Figure 14: Topology of mGlu receptors and a general binding model of: A) orthosteric agonists, B) orthosteric antagonists, C) extracellular domain allosteric modulators (edAM), D) long orthosteric agonists, E) positive allosteric modulators or allosteric agonists (PAM) and F) negative allosteric modulators or allosteric inverse agonists (adapted from Rondard³⁰ and Kniazeff²³)

More recently new group III agonists with a longer chain have been found, such as LSP4-2022 (**6**)⁵⁹ (*figure 13*), which binds to the glutamate-binding site but also to a close additional pocket. This additional cavity points to a known chloride-binding site (Cl⁻), but the physiologic relevance of this ion on the activity of mGlu receptors was unknown⁶⁰. In fact, very recently, chloride ion was reported to act as a positive allosteric modulator, binding to at least two different sites of the VFT⁶¹. Therefore, this discovery paves the way to find new allosteric modulators that bind to the extracellular domain (edAM) acting on the chloride sites of the VFT (*figure 13C*) or long agonists that binds simultaneously to the orthosteric site and also to the edAM site, such LSP4-2022 (**6**) for mGlu₄. This last approach can lead to potent agonists (*figure 14D*) with an increased selectivity for a subtype taking advantage of the less conserved topography around the allosteric chloride-sites.

Ligands binding at the TMD

Although chloride is reported to allosterically modulate glutamate activity through a binding site located in the VFT, most of mGlu receptor allosteric modulators bind to a pocket located in the TMD, which may confer very different properties to these modulators compared to the ligands that bind to the VFT. They can either enhance (positive allosteric modulators, PAMs, *figure 14E*) or inhibit (negative allosteric modulators, NAMs, *figure 14E*) the receptor activation, modulating the affinity of the orthosteric agonist and affecting the intrinsic efficacy of this agonist to trigger the signalling response⁶². They bind in a similar site than class A ligands, in which NAMs stabilise the inactive conformation of both TMDs and PAMs the active conformation of one TMD. In addition, another type of allosteric modulator exists, which is called silent allosteric modulator (SAM). These allosteric ligands bind to the TMD, but they do not stabilise any single conformation of the receptor, leading to no change of the functionality of the receptor⁶³.

As mentioned before, the TMD is located inside the cellular membrane, and this is possible due to hydrophobic residues that constitute the central part of this domain. Additionally, since class C GPCRs has no endogenous allosteric modulators, the allosteric binding site remained more hydrophobic than class A or B GPCRs. Therefore, the polarity of these allosteric modulators has to be low to afford binding in such a high hydrophobic environment, much lower than orthosteric ligands, which usually are charged amino acid derivatives that bind to the highly hydrophilic VFT. This high lipophilicity may confer to allosteric modulators several advantages and disadvantages compared to orthosteric ligands. For example, the solubility in

water may be low, which is an important drawback that can be compensated with a high potency of the ligand and the usage of lower doses but also the free fraction in plasma may be lower compared to high soluble molecules. Absorption of lipophilic molecules when are orally administered are usually suitable and they tend to pass the blood-brain barrier, whereas for absorption of polar orthosteric ligands, design of pro-drugs is mandatory and they can only cross blood-brain barrier via active amino acid carriers⁵⁸.

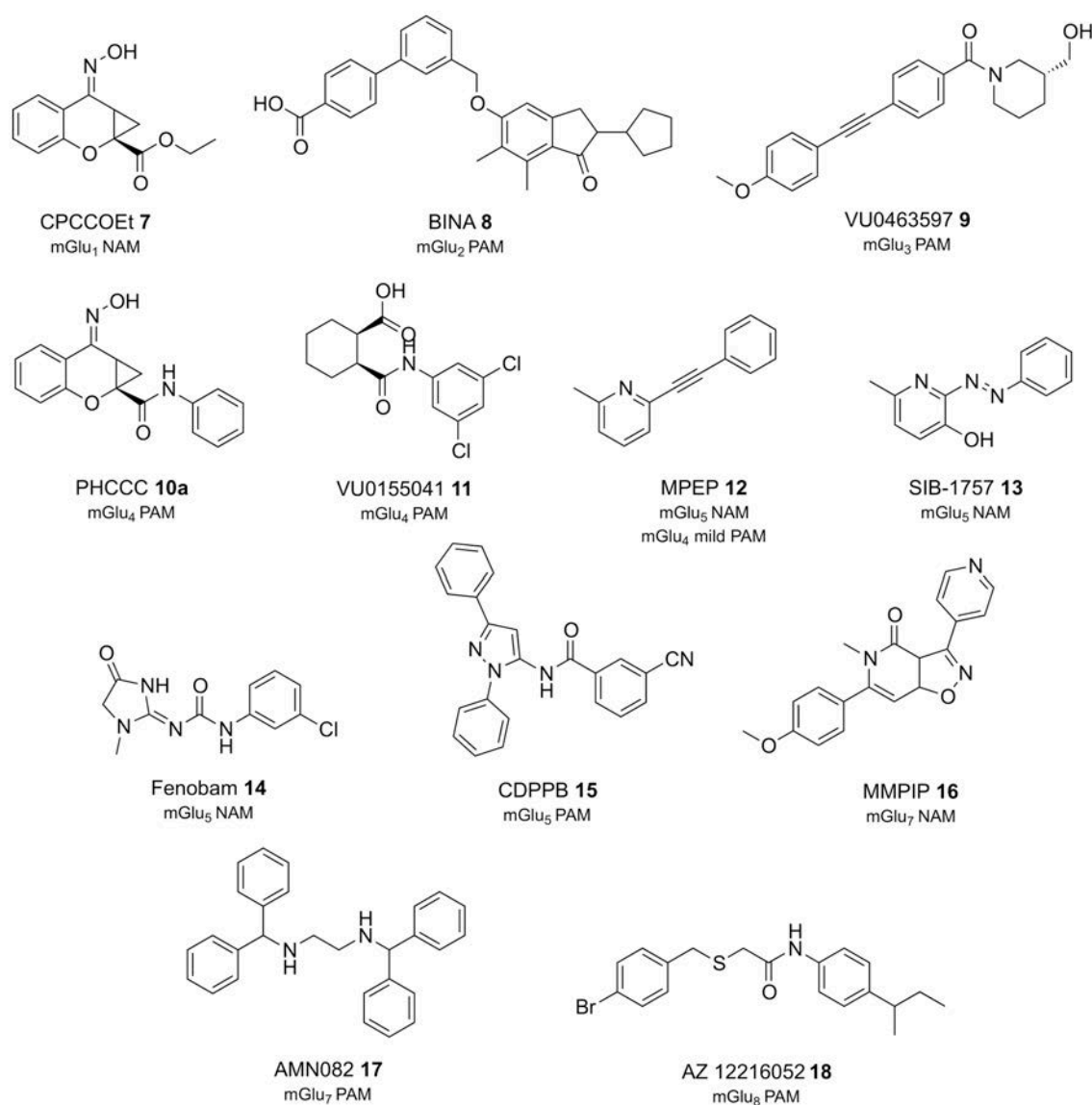


Figure 15: Examples classical allosteric modulators selective for a single mGlu subtype^{56, 64-75}. No examples of mGlu₆ allosteric modulators are shown due to the lack specific pharmacology, since drug discovery programs do not concern its reduced applications.

Apart from that, mGlu allosteric modulators may offer other advantages. For example, molecules binding to the TMD have enhanced possibilities to obtain a proper selectivity across receptor subtypes, due to the lower evolutionary pressure of their binding site in contrast to

the high evolutionary conserved orthosteric binding site in the VFT⁵⁸. Despite the actual possibilities to discover selective-subtype orthosteric agonist through occupation of edAM sites, LSP4-2022 and (S)-DCPG are the only subtype-selective orthosteric ligand acting on mGlu receptors^{59, 76}. Otherwise, literature is plenty of examples of allosteric modulators with high selectivity profiles.

An additional potential advantage is that allosteric modulators that do not display any agonism are completely inactive under absence of orthosteric ligands and they only potentiate or inhibit the response of the receptor in the presence of a released endogenous orthosteric agonist in the synapsis. In contrast, orthosteric agonists and antagonist exert their effect independently of the neurotransmitter release. On the other hand, it is also possible to achieve allosteric partial antagonists, which reduce mGlu response to a new level, but not completely abrogated. Overall, these allosteric modulators offer more of a "fine-tuning" approach, which is believed to confer a better and more controllable therapeutic profile^{10, 63}.

A common phenomenon: molecular switch

Despite the subtype selectivity of an allosteric modulator or the clear role as a PAM, NAM or SAM, very subtle modifications in their chemical structure can induce changes in their pharmacology, binding mode or subtype selectivity. This phenomenon is called "molecular switch" or "chemical switch" and is very commonly found between allosteric modulators in mGlu receptors, but also has been observed for other GPCRs such as muscarinic receptors or for kinase and phospholipase allosteric ligands⁷⁷.

The first example of molecular switch on mGlu receptors is DFB (**19**), which is the first reported mGlu₅ PAM, but the replacement of fluorine substituents led surprisingly to mGlu₅ NAMs and SAMs⁷⁸ (*figure 16*). Other examples can be the ones involving PHCCC (**10**), which is an mGlu₄ PAM and whose structure resembles to CPCCOEt (**7**) despite displaying mGlu₁ NAM activity. However, when fluorine is added in position 4 of the aniline phenyl, it loses the affinity for mGlu₄ to become an mGlu₂ and mGlu₃ SAM and when some small substituents such as chlorine, methyl, or methoxide are added in the same position, they turn out to display mGlu₂ NAM activity and mGlu₃ PAM activity⁷⁹ (*figure 16*). Another molecular example between two subtypes can be the case of VU0092273 (**20**)⁶⁶ or other molecular switch examples, inside the same subtype, selectivity may be the cases of VU0219493 (**21**) and VU0448383 (**22**)⁸⁰ or CPPhENA and CPPENA (**23a-b**)⁸¹.

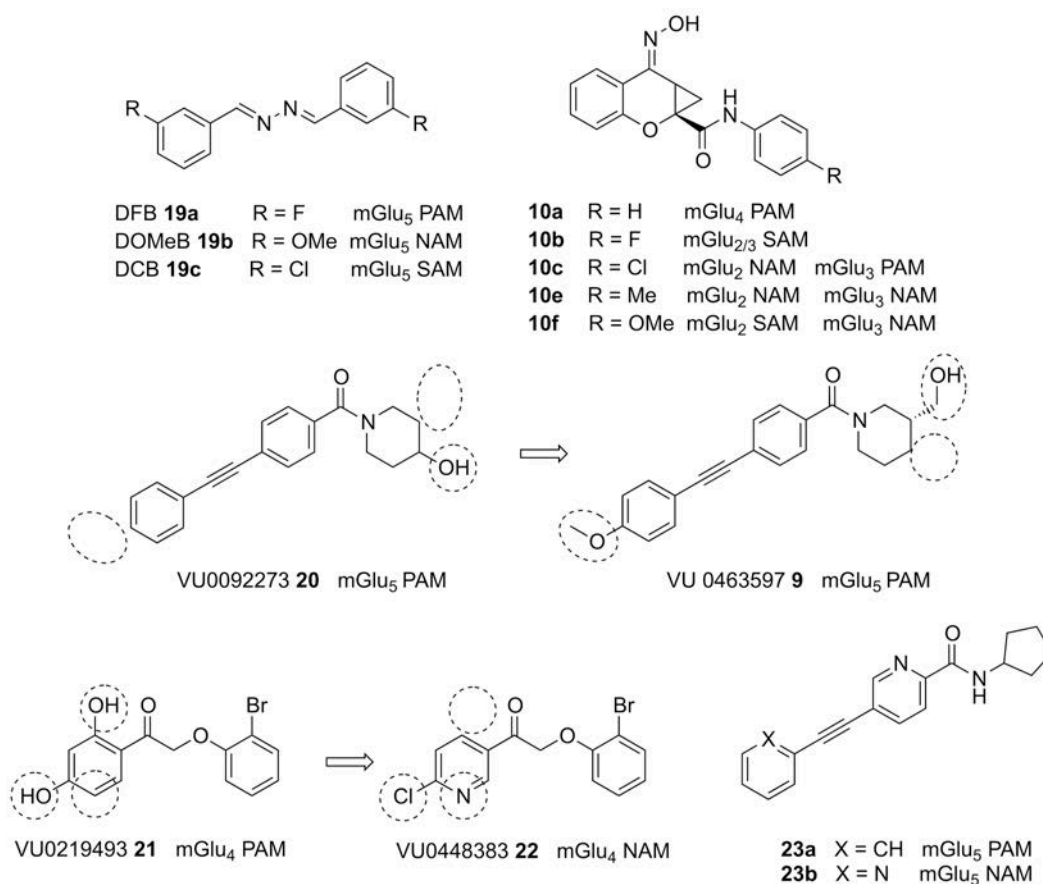


Figure 16: Examples of molecular switches for mGlu receptors allosteric modulators

Targeting mGlu receptors to treat human disorders

As stated above, mGluRs are widely distributed throughout the central and peripheral nervous system and each of the subtypes has singular roles that can be modulated with drug-like agonists, antagonists or allosteric modulators. For that reason mGlu receptors are thought to be excellent therapeutic targets to treat a wide variety of central nervous systems disorders. However, there are still no mGlu ligands in the market. Nonetheless, there is still hope in targeting neurological and psychiatric disorders. Of the eight subtypes, mGlu₅ and mGlu₂ are still the main targets for drug development, but mGlu₄, mGlu₁ and mGlu₃ are also promising targets for drug development. Group III receptors mGlu₆, mGlu₇ and mGlu₈ are clearly undeveloped, although mGlu₇ and mGlu₈ could be proper targets for the treatment of stress-related diseases⁸².

Pain

Chronic pain is a condition that leads to allodynia^a and hyperalgesia^b, affecting seriously the quality of life of more than 19% of adult Europeans, whose treatments do not offer a significant relief. Blocking the increased glutamatergic activity associated to pain may represent a reasonable strategy, but it is necessary to select the adequate targets^{10, 83}. These targets can be different mGlu receptors, since they regulate nociceptive^c processes⁸⁴.

An example of such may be mGlu₁, which is expressed in CNS regions essential to nociceptive processing. Experiments with mGlu₁ knockout mice showed decreased pain sensitivity and administration of selective mGlu₁ NAMs or antagonists were reported to show efficacy in neuropathic pain animal models¹⁰. Another target to treat chronic pain is mGlu₅. In fact, preclinical models of neuropathic pain show analgesic effects with mGlu₅ NAMs. Moreover, inhibition of pain has been clearly demonstrated after mGlu₅ NAM raseglurant (**24**) Phase II trials for migraine, with excellent results but it finally was discontinued for hepatotoxicity issues⁸⁵. Phase I clinical assays have also been performed with fenobam (**14**) has also to treat induced hyperalgesia in healthy volunteers⁸⁶.

Activation of Group II mGlu receptors can also be analgesic. Antinociceptive actions of mGlu_{2/3} agonists have been demonstrated and their systemically injection reduce inflammation induced hypersensitivity to mechanical or thermal stimuli and have analgesic effects in rat models of inflammatory and neuropathic pain. However, the expression of group II mGluRs can be dramatically altered by experience and this can lead to an observed acute tolerance after a chronic treatment^{10, 84}.

Group III mGluRs are also abundant all along the nociceptive pathways, in particular mGlu₄ and mGlu₇. Several animal models demonstrate that mGlu₄ is able to downregulate the abnormal glutamatergic activity seen in pathological pain contexts and consequently reduce the associated hypersensitivity to mechanical stimuli, even with systemic injection of agonists. Moreover, mGlu₄ activation is reported to play a neuroprotective role in inflammation. However, activation of mGlu₇ receptors with the “allosteric agonist” AMN082 (**17**) facilitate inflammatory and neuropathic pain in some animal models, whereas selective activation of mGlu₈ receptors with DCPG produces opposite effects. However, AMN082 has been reported

^a Pain due to a stimulus that does not normally provoke pain (International Association for the Study of Pain <http://www.iasp-pain.org/Taxonomy?navItemNumber=576>)

^b Increased pain from a stimulus that normally provokes pain (International Association for the Study of Pain <http://www.iasp-pain.org/Taxonomy?navItemNumber=576>)

^c Related to the neural process of encoding noxious stimuli (an actually or potentially tissue-damaging event) (International Association for the Study of Pain <http://www.iasp-pain.org/Taxonomy?navItemNumber=576>)

to reveal a rapid metabolism and produce some active metabolites for other targets, probably inducing these unexpected effects⁸⁷. Overall, mGlu₄ and mGlu₈ may be potential targets for developing new analgesics^{10, 55, 83, 84, 88}.

Subtype	MOA*	CNS disease applications
mGlu ₁	PAM	N/A
	NAM	Neuropathic pain, Fragile Syndrome X, Anxiety/stress disorders, addiction
mGlu ₅	PAM	Anxiety disorders, Huntington's disease, schizophrenia, tuberous sclerosis complex
	NAM	Addiction, anxiety, chronic pain, depression, Fragile Syndrome X (autism spectrum disorders), migraine, Parkinson's disease – L-DOPA-induced dyskinesia
mGlu ₂	PAM	Addiction, anxiety disorders, depression, schizophrenia
	NAM	Depression
mGlu ₃	NAM	Depression
mGlu ₄	PAM	Neuropathic pain, neuroinflammation, neuroprotection, Parkinson's disease, schizophrenia.
mGlu ₇	Agonist	Anxiety, depression, Parkinson's disease
	NAM	Anxiety, depression
mGlu ₈	Agonist	Parkinson's disease, anxiety

Table 9: Potential application of mGlu allosteric modulators in CNS diseases (adapted from Nickols¹⁰)

*Mode of Action

Parkinson's disease

Parkinson's disease (PD) is a chronic neurodegenerative disorder with a high incidence in population older than 55 years. The current treatment consisting in dopamine replacement is initially effective, but cause undesired side effects and its efficacy decreases over time as disease progresses. Group III mGlu receptors are expressed presynaptically in at different synapses of a pathway that control motor function, and it is observed glutamatergic overactivity in PD patients that is thought to contribute to the motor dysfunction associated with PD. Therefore Group III mGlu receptor constitute promising drug targets for PD treatment, specially mGlu₄, since L-AP₄ and mGlu₄ PAMs have been found to reverse motor symptoms in rodent models of PD as well as other characteristic symptoms of PD, such as neurodegeneration^{10, 88}.

One of the side effects of current treatments is the progressive development of L-DOPA-induced dyskinesia (LID), which currently can only be treated with weak NMDA antagonist amantadine. However, in experimental animal models, mGlu₅ NAMs have shown activity in reducing both PD motor symptoms and LID. Moreover these drugs also showed

neuroprotective properties in rodents and non-human primates⁸². Mavoglurant (**25**), an mGlu₅ NAM, has shown anti-dyskinetic activity in three initial phase II clinical trials but the drug was inactive in two additional studies, which prompted the discontinuation of the programme. However mGlu₅ NAMs and antagonists are still well considered since other mGlu₅ NAMs showed good profiles in phase II clinical studies⁸².

Fragile X syndrome and autism spectrum disorders

Fragile X syndrome (FXS) is the most common form of human inherited intellectual disability and inherited cause of autism. It is mostly caused by a mutation in the FMR1 gene that results in failure to express the fragile X mental retardation protein (FMRP). FMRP is located in the postsynaptic region of glutamatergic synapses and absence of FMRP expression results in increased constitutive mGlu₅ signalling and subsequent “excessive” mGlu₅-mediated protein synthesis in post-synaptic dendrites with resulting dysregulation of synaptic function. Further studies showed that the constitutive activity of mGlu₅ might be important for FXS. Therefore, inverse agonism shown by mGlu₅ NAMs such as MPEP or fenobam would be beneficial for a chronic treatment of FXS patients¹⁰.

Also mGlu₁ NAMs are reported to have a robust efficacy in FXS animal models and mGlu₅ NAMs was suggested to be useful to treat a broader range of autistic disorders. However, mGlu₅ NAMs were found to exacerbate symptoms of tuberous sclerosis, which were reversed with mGlu₅ PAMs in animal models¹⁰.

Phase II and phase III clinical trials were performed for mGlu₅ NAMs mavoglurant (**25**) and basimglurant (**26**) in FXS patients. Despite the success of preclinical assays, clinical trials have been disappointing and autism development programs have been discontinued⁸².

Additionally, it was recently reported that disrupted μ -opioid receptor signalling is associated with autism spectrum disorders in rodents, and treatment with mGlu₄ PAM VU0155041 (**11**) was more efficient in alleviating behavioural deficits⁸⁹.

Schizophrenia and anxiety disorders

Schizophrenia is a major psychiatric disorder that affects a considerable fraction of the population worldwide. Research suggests that it is based on a hypofunction of NMDA receptors and abnormalities in the functional cross talk between mGlu₂ and 5-HT_{2A}. Group II agonists demonstrate efficacy in preclinical models of psychosis and anxiety and other models related to schizophrenia. In fact a prodrug of the potent mGlu_{2/3} agonist, LY404039 (**27**)

showed very good efficacy in the initial phase II clinical trials, but in the subsequent ones did not, leading to a discontinuation of program^{82, 88}.

Also mGlu₅ PAMs are effective in several animal models of antipsychotic activity, since they are functional partners of NMDA, and are currently tested in phase II clinical trials. Moreover, activation of mGlu₄ with PAMs may also provide an antipsychotic effect and it is also suggested that mGlu₁ receptors are involved in schizophrenia, through a mutation in GRM1 gene that leads to a loss of function of the receptor^{10, 82}.

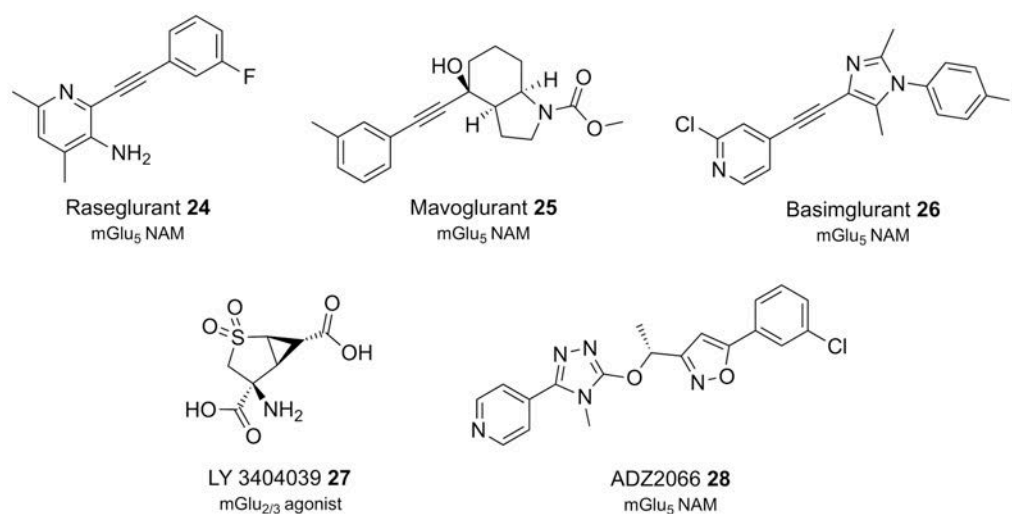


Figure 17: Examples of mGlu ligands tested in clinical trials

Depression

Major depressive disorder (MDD) is very common mental illness that affect between 2% and 16% of the population, depending on the region. Current antidepressants show a poor efficacy in many patients and their onset of action is slow, with the first improvements in mood taking 3–4 weeks to occur.

Ketamine, which is an NMDA antagonist, has shown rapid robust efficacy as antidepressant. Therefore, mGlu₅ NAMs may offer an alternative to ketamine with a safer profile and a lower potential for drug dependence. Currently basimglurant (26) and AZD2066 (28) are under clinical development for depression. Moreover, studies showed that mGlu₂ PAMs display robust antidepressant-like activity in rodents, but other mGlu_{2/3} antagonists displayed antidepressant-like effects also in rodents, which seem to be paradoxical. Clearly, further research is necessary to determine the viability of mGlu_{2/3} PAMs/agonists and/or NAMs in the treatment of depression and it is possible that the use of PAMs or NAMs may depend on the

brain region and state of depression^{10, 82, 88}. Additionally, mGlu₇ NAMs have also shown potential efficacy in animal models for the treatment of anxiety and depression¹⁰.

Drug addiction

Glutamatergic neurotransmission is thought to play a key in both establishment and maintenance of drug addiction. Group I mGlu NAMs constitute potential therapeutic agents for the treatment of addiction. In fact mGlu₅ NAMs and mGlu₁ antagonists show efficacy in rodent models of cocaine addiction. Additionally, mGlu₅ inhibition decreases the rewarding effects of other drugs of abuse such as amphetamine, morphine, and alcohol^{10, 82, 88}.

Experimental evidence also suggests a potential role for mGlu_{2/3} in addictive disorder and it is emerging as a valuable drug target in the treatment of drug dependence. Many mGlu_{2/3} agonists and PAMs reduce drug-seeking behaviours in animal models of self-administration of cocaine, nicotine, methamphetamine and ethanol. Additionally, the mGlu₂ receptor-activating drug, N-acetylcysteine, is now clinically tested for efficacy in cocaine, nicotine, cannabis and methamphetamine addiction^{10, 82, 88}.

Other diseases

Despite the major diseases to be treated by mGlu modulators are explained above, mGlu receptors has been proposed as potential targets for other CNS-related diseases, such as potentiation of mGlu_{2/3} or mGlu₅ NAMs for anxiety, mGlu₅ NAMs for astrocytic disorders, iatrogenic dystonia or gastroesophageal reflux disorder or mGlu₇ or mGlu₈ potentiation for stress and anxiety⁸⁸.

Up-to-date mGlu₄ PAMs and mGlu₅ NAMs

This thesis was conceived in the frame of a neuropathic pain project. Therefore, we centred our efforts in designing and synthesising mGlu₄ PAMs and mGlu₅ NAMs, since they may be potential drugs to treat pain, as mentioned before.

Here we present the up-to-date list of reported mGlu₄ PAMs and mGlu₅ NAMs.

mGlu₄ PAMs

Ten years ago, the role of Group III mGlu receptors was poorly understood due to a lack of specific pharmacology⁸⁴. However, since 2009, many positive allosteric modulators of mGlu₄ have come to light, offering to the scientific community new tools to further study this receptor⁹⁰.

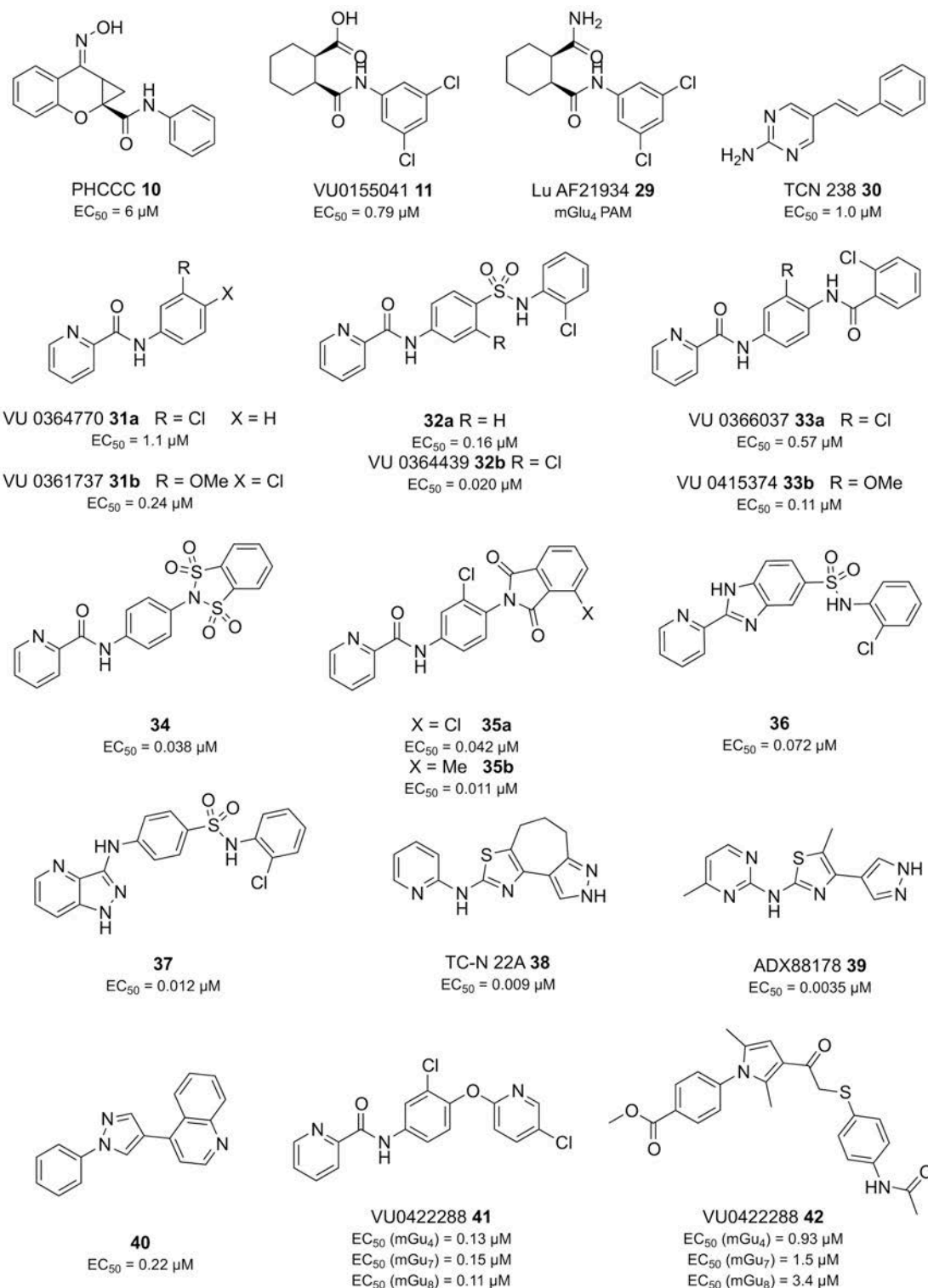


Figure 18: Selection of the most representative mGlu₄ PAMs available in the literature with the corresponding potencies (EC₅₀)

PHCCC (**10**) was the first identified mGlu₄ PAM in 2003 in Vanderbilt University⁶⁷ and five years later they reported on a racemic mixture of VU155041 (**11**) as an improved mGlu₄ PAM⁶⁸. Later our team shown that the activity resided solely with (1*R*, 2*S*) enantiomer⁹¹ and in 2013 the derivative LU AF21934 (**29**) was reported by Lundbeck with an improved potency and better

properties to pass the blood-brain barrier⁹². Boehringer Ingelheim and Evotec also published an mGlu₄ PAM series with TCN238 (**30**) with orally in-vivo activity in rodents⁹³.

Vanderbilt University reported on several mGlu₄ PAMs between the periods 2009-2012. They all had a common chemical structure, based on the *N*-phenyl-picolinamide scaffold with several modifications in position 3 and 4 of the phenyl group. Examples of those compounds can be VU036770 (**31a**)⁹⁴, VU0361737 (**31b**)⁹⁴, VU0364439 (**32b**)⁹⁵, VU0366037 (**33a**)⁹⁶, VU0415374 (**33b**)⁹⁶ or compound **14**⁹⁷. Merck also patented compound **32a**⁹⁸, structurally very related to **32b** with other compounds shown in the same publication⁹⁵, or also compounds **35a** and **35b**⁹⁹. Vanderbilt University patented a related series of compounds where the amide between the pyridine and the phenyl was fused with the phenyl to form a bioisosteric benzoimidazole¹⁰⁰. The most potent compound of the series is compound **36**. In a similar fashion, Merck and Addex also patented a related series with that amide fused with the pyridine an with similar potencies, as shown for compound **37**^{101, 102}.

More recently, other mGlu₄ PAMs with different chemical scaffolds were published. One example is TC-N 22A (**38**), published by Lundbeck¹⁰³, together with a series that were previously patented by Addex¹⁰⁴ and later reported on ADX88178 (**39**), as an mGlu₄ PAM with *in-vivo* activity¹⁰⁵. Another example with a different scaffold is compound **40**, reported by Lundbeck¹⁰⁶. As final examples, Vanderbilt University published two pan-Group III PAMs: VU0422288 (**41**) and VU0155094 (**42**), which have a similar potency in mGlu₄, mGlu₇ and mGlu₈¹⁰⁷.

mGlu₅ NAMs

Due to that mGlu₅ constitute a potential therapeutic target to treat many diseases; many efforts have been done to achieve potent and efficient allosteric modulators, most of them NAMs. Here we mention some examples of the main families of mGlu₅ NAMs to take into account.

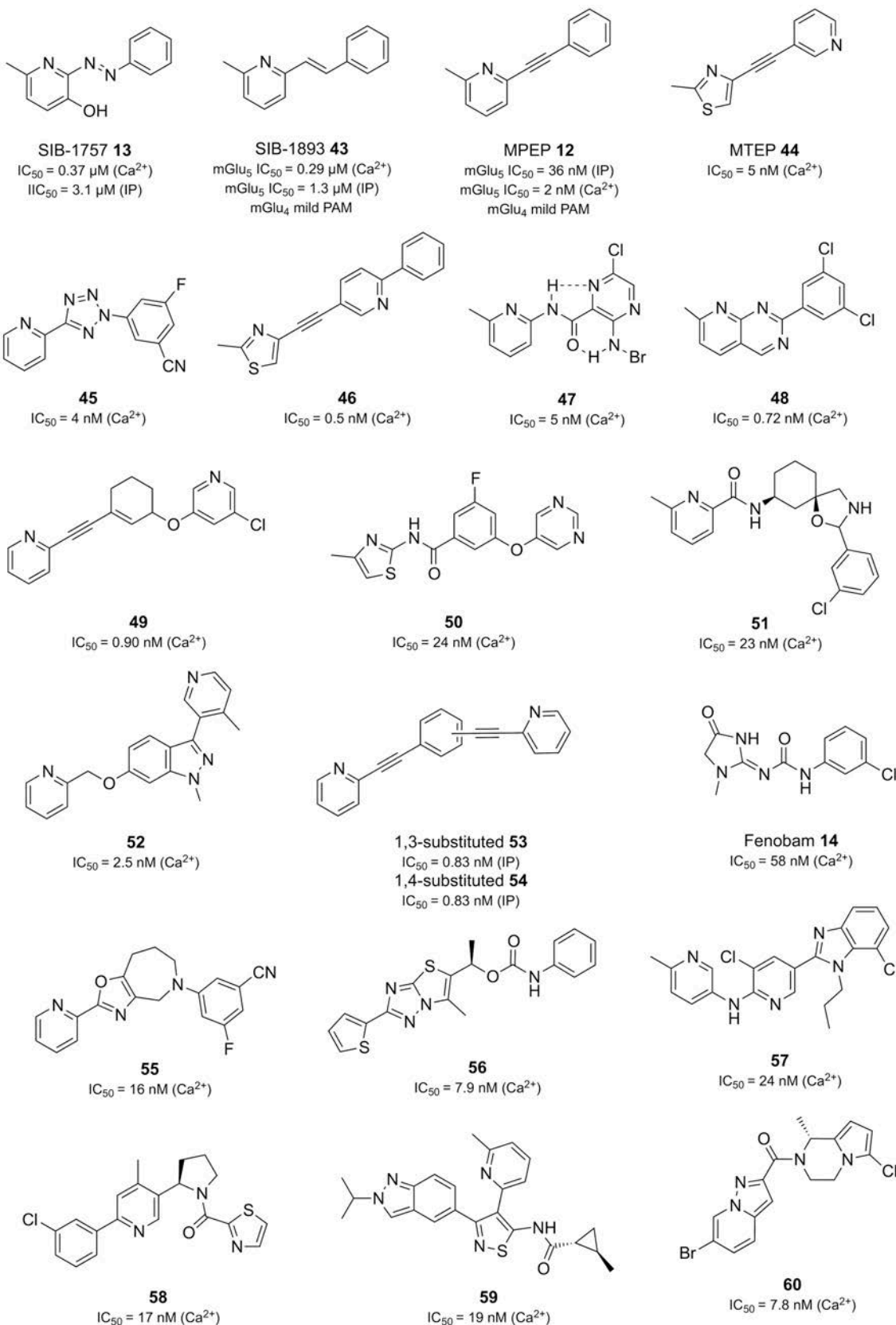


figure 19: Selection of the most representative mGlu₅ NAMs available in the literature with the corresponding potencies (IC₅₀)

The first selective mGlu₅ NAMs that came to light were SIB-1757 (**13**) and SIB-1893 (**49**) in 1999 by SIBIA and Novartis⁷⁵. In the same year the same companies also published MPEP (**11**)⁶⁹, which also show a mild potency in mGlu₄⁷⁰ and is currently the most used standard NAM for mGlu₅. Four years later Merck reported on a series of mGlu₅ NAMs, including MTEP (**44**), a compound structurally related to MPEP with improved *in-vivo* properties. In the next years Merck, Yale University, Vanderbilt University, NIH and Pfizer among others, published several papers with MPEP and MPEP related compounds, with heterocycles, fused rings, rigid amides and methylethers to substitute the ethylene moiety or with an additional ring, usually in position 3 or 4 of the phenyl ring, or even changing the phenyl ring for non-aromatic rings¹⁰⁸⁻¹²⁶. Examples of such may be compound **45-54**.

Other NAMs, with a non-MPEP-related structure have also been tested. The first example to take into consideration may be fenobam (**14**), which was a compound with anxiolytic activity *in vivo*, with an unknown molecular target till it was discovered that it was an mGlu₅ NAM⁷¹ and later several derivatives were also described^{127, 128}. Several pharmaceutical companies have reported on other MPEP-non-related mGlu₅ NAMs, such as Sepracor with compound **55**¹²⁹, GSK with **56**¹³⁰, Novartis with **57**¹³¹, Lundbeck with **58**¹³², Lilly with **59**¹³³ or Merz with **60**¹³⁴.

In addition, as mentioned above, some pharmaceutical companies has developed clinical trials in humans with other mGlu₅ NAMs, such raseglurant (**24**), mavoglurant(**25**), basimglurant (**26**) or ADZ2066 (**28**), developed by Addex, Novartis, Roche and Astrazeneca respectively. All these compounds except **28** also could be considered non-MPEP-related.

Control of protein function with light

Drugs are chemical substances, usually small molecules, which display biological activities by changing in many cases the normal function of proteins, and usually are the active ingredient of medications. Drug discovery is a process by which these new medications are discovered and it is a multidisciplinary process involving different branches of knowledge such as medicine, biotechnology, chemistry and pharmacology, and each one has a crucial role in the overall process.

Pharmacology is the branch knowledge that studies these chemical substances from a biochemical or physiological point of view. For those drugs that change the protein functional activities, pharmacology is the discipline with the responsibility of finding out the interactions of drugs (ligands) and their target proteins, their functional changes and their therapeutic response. However, once the drug is released in the body, through whichever of the possible

routes of administration, the drug is spreading over all over the body and the control of this substance is lost. In a slow and imprecise fashion, they will bind their target protein, wherever it is localised, regardless the kind of cell, tissue or system where they are expressed¹³⁵. In addition, a poor selectivity of these drugs can afford multiple undesirable side effects that can increase the threshold level of toxicity, leading to a decrease of the allowable dose and a partial loss of the drug potential^{136, 137}.

Optopharmacology, also known as photopharmacology, consists in the use of light to regulate the activity of a photosensitive drug at its receptor and combines optics and chemistry to optically control the key proteins function, through photo-reversible switches or photo-cleaving cages, also called photochromic chemical compounds¹³⁵. Light generally does not influence the living system under study and can be used remotely and noninvasively. Light can be manipulated both temporally and spatially with high resolution and should make possible the investigation of fast processes that are confined to specific cellular compartments or specific subsets of cells¹³⁸. Moreover, light can also be regulated in a qualitative and quantitative manner by adjusting the wavelength and the intensity¹³⁷. Therefore, optopharmacology may provide an advantageous and more precise approach to conventional drug therapeutics.

Photo-reversible switches

To achieve a fine reversible control of a protein function with light, it is indispensable to include a light-sensitive moiety formed by a photochromic group covalently linked either to the target protein or to a ligand. If this photochromic group is reversible, it can isomerise under illumination with a single wavelength and promotes a change of geometry, polarity, flexibility or end-to-end distance, which prompts a change of the protein function. Usually, a back-isomerization can be achieved under illumination with a different wavelength with the corresponding recovery of the previous functionality of the target protein.

The most relevant synthetic photo-reversible switches to modulate biological processes, apart from the natural retinal, are dithienylethenes, spiropyranes and azobenzenes (*Table 10*), despite stilbenes, fulgides, hemithioindigos and chromenes have also been reported¹³⁹⁻¹⁴¹.

Switch	Structure and isomerisation	Change
Retinal		Geometry
Spiro-pyran		Polarity and geometry
Dithienyl-ethene		Flexibility
Azo-benzene		Geometry and polarity

Table 10: Most important photoswitches

Retinal

Retinal, also known as Vitamin A aldehyde, is a natural polyene chromophore bound as a Schiff base to opsins, including human rhodopsins, which are class A GPCRs. Human rhodopsins are the responsible for vision, and its back-isomerisation requires several metabolic steps. However, retinal is also bound to light-gated cation channels “channelrhodopsins”, proton pumps “bacteriorhodopsins” or chloride pumps “halorhodopsin” in certain types of archaea or algae. In these last cases, the covalently linked all-*trans*-retinal chromophore of the ChRs absorbs in the visible range (ChR1 around 500 nm and ChR2 around 460 nm). Upon absorption of a photon, all-*trans*-retinal isomerizes to 13-*cis*-retinal, and it thermally relaxes back to all-*trans*-retinal¹⁴¹.

Spiropyran

Spiroprans photoswitch is based on the rupture of the C-O bond under UV light (360-380 nm) to afford a zwitterionic conjugated system (merocyanine form). This isomerization triggers a very large change in the polarity of the molecule (8-15 Debyes) and can be back isomerised both thermally and under illumination with visible light (>460 nm). This switch is particularly useful in order to drive hydrophobic/hydrophilic environmental changes in sensitive proteins to this polarity changes¹³⁹.

Dithienylethene

Dithienylethene (DTE) derivatives are characterised to display a photochromism caused by a reversible photoinduced cyclisation, due to the presence of a hexatriene moiety in the open form. Its open form is characterised to be very flexible and under illumination at 312-360 nm cyclise to afford the rigid close isomer, which can be re-opened with visible light (>420 nm). They are characterised mainly characterised for its absence of thermal relaxation and for their high fatigue resistance and depending on its substitution it is possible to afford complete isomerisations¹³⁹.

Azobenzene

Azobenzene derivatives, including phenylazopyridines and azopyridines, are the most common photoswitches used in biological applications. Its discovery dates back to the mid-XIX century and for many years azo compounds have been an important class of synthetic colouring agents in the dye industry^{139, 142, 143}. Their synthesis is relatively easy¹⁴⁴ and they offer high possibilities of chemical functionalization (up to 10 different points), good photophysical properties with high quantum yields and good rates of isomerisation, a good stability under physiological conditions and a very fast isomerisation rate under illumination, faster than most biological processes¹³⁹.

Azobenzene structure consists of two phenyl rings, joined by a -N=N- group, also called azo-bond or azo-bridge. The *trans*-isomer has a planar geometry with a dihedral angle of 180° and an extended delocalization of the π -electrons over the aromatic rings and the azo-bond and also has a negligible dipolar moment. On the other hand, the *cis*-isomer has a bent geometry, 3 Å shorter than the *trans*-one, with its phenyl rings twisted 55° out of the plane and a dihedral angle of the azo-bond of 11° and a dipolar moment of 3.7 Debye^a. This geometry causes a rupture of the π delocalization on the azo-bond. This rupture can be easily determined by ¹H-NMR of the protons in *ortho* position. For *trans*-azobenzene, these protons are located in a clearly aromatic cone around 7.90 ppm (CDCl₃, 600 MHz)¹⁴⁵, however, for *cis*-azobenzene, the same protons shift to the right till 6.83 ppm (CDCl₃, 600 MHz)¹⁴⁵, a nearly typical chemical shift for aniline (6.70 ppm, CDCl₃, 400 MHz)¹⁴⁶. That points to a rupture of the delocalization of the π -electrons over the -N=N- to afford aniloid electronic properties.

Hartley was the first to report photoisomerisation of azobenzene, after observing a lack of reproducibility in absorbance measurements when a solution of azobenzene was exposed to light¹⁴⁷. The spectra of *trans* and *cis*-azobenzene are distinct but overlapping (*figure 20*). *Trans*-

^a Data measured after DFT minimizations of both isomers with Gaussian 03 (restricted B3LYP, 6-31G)

azobenzene displays a very weak $n\text{-}\pi^*$ band near 440 nm, forbidden by symmetry, and a strong $\pi\text{-}\pi^*$ transition near 320 nm. Alternatively, *cis*-azobenzene shows a stronger $n\text{-}\pi^*$ band also near 440 nm and shorter $\pi\text{-}\pi^*$ bands at 280 nm and 250 nm. The *trans*-isomer of azobenzene is 10-12 kcal/mol more stable than the *cis* one, resulting in a strong predominance of the *trans*-isomer in equilibrium in the dark¹³⁹.

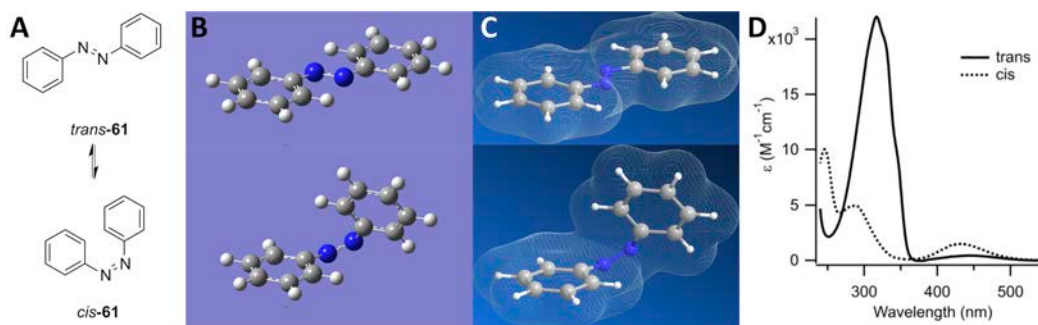


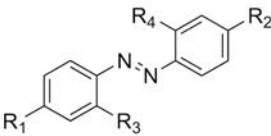
Figure 20: Structure of *trans/cis* isomers and UV-Vis Absorption spectrum. A) 2D structure; B) 3D structure after minimising energy of both isomers with Gaussian 03 (restricted B3LYP, 6-31G); 3D structure with a total electron density surface; D) UV-Vis absorption spectrum of both isomers.

The *cis*-isomer can be obtained under illumination with ultraviolet light (≈ 340 nm), and it is possible to recover the initial state either thermally or by illumination with visible light (>450 nm). The conditions to isomerise from *trans* to *cis* isomer are not suitable for biological applications, since UV light can be harmful for tissues and cells^{148, 149}. Nevertheless, suitable substitutions in the phenyl rings can shift the wavelength to longer biocompatible ranges and, additionally, thermal relaxing time can also be modified¹⁵⁰. A proof of that is the wide variety multiple colour azobenzene dyes present in the literature¹⁵¹, but in most cases the photoisomerisable properties are not described. The most common approaches are azobenzenes, aminoazobenzenes and push-pull azobenzenes, very well reviewed by Bandara¹⁵². However, thermal relaxing properties have also to be taken into account, since azo-hydrazone tautomerism may accelerate the thermal decay of the *cis*-isomers¹⁵³, as well as the polarity of the solvents have a crucial negative influence the relaxation, as it is possible to observe in *table 12*¹⁵⁴.

Azobenzenes family (AB)

The azobenzene family includes all the azobenzenes substituted with electro withdrawing groups (EWG) or mild electron donating groups (EDG), such as alkyl, aryl, halide, carbonyl, carboxylic acid, ester, carboxamide, or even amino and alkoxy in position 3 and also includes azopyridines and phenylazopyridines. In all cases the absorption spectra is similar to the unsubstituted azobenzenes¹⁵⁵. The thermal relaxation time of the *cis*-isomer is generally slow,

but its relaxation times can decrease depending on the number of substituents, as it is possible to observe in table 11. They are used in protein probes or molecular machines where a fast relaxation time is not desired.



Compound 62n

Solvent	ϵ_r	$t_{1/2}$ (min)
Pentane	1.836	255
hexane	1.89	344
1,4-dioxane	2.209	48
CCl4	2.228	293
benzene	2.275	64
Et2O	4.325	45
CHCl3	4.806	3.8
C6H5Cl	5.621	4.2
THF	7.58	1.35
DCM	8.90	0.77
o-C6H4Cl2	9.93	0.99
1,2-DCE	10.36	0.46
Cyclohexanone	18.3	0.083
2-PrOH	19.92	0.084
acetone	20.7	0.072
EtOH	24.55	0.038
MeOH	32.7	0.0135
DMF	36.71	0.0083
DMSO	46.6	0.0023
formamide	111.0	0.00042

Group	Comp.	R ₁	R ₂	R ₃	R ₄	λ_{max} (nm)	$t_{1/2}$ (min)
AB	61	H	H	H	H	315	
	62a	Me	Me	H	H	330	401
	62b	Cl	Cl	H	H	331	431
	62c	NO ₂	H	H	H	330	94
	62d	NO ₂	H	Me		336	60
	62e	NO ₂	NO ₂	H	H	336	29
aAB	62f	OMe	H	H	H	342	357
	62g	OMe	OMe	H	H	353	221
	62h	NMe ₂	H	H	H	390	103
	62i	NMe ₂	Me	H	H	400	70
	62j	NMe ₂	Me	Me	Me	399	24
	62k	NMe ₂	NMe ₂			410	14.8
	62l	NEt ₂	H	H	H	407	70
	62m	NEt ₂	NEt ₂	H	H	431	7.4
ppAz	62n	NMe ₂	NO ₂	H	H	440	1.74
	62o	NMe ₂	NO ₂	Me	H	450	1.00
	62p	NMe ₂	NO ₂	H	Cl	459	0.21

Table 11: (left) Maximum of absorbance corresponding to the π - π^* band, and thermal relaxing half-time life of different azobenzene derivatives with no tautomerisable. Measures of compounds **62a-m** are in cyclohexane at 35 °C and for compounds **62-n-p** in hexane at the same temperature¹⁵⁶⁻¹⁵⁸

Table 12: (right) Thermal relaxing half-life time of *Cis*-**63n** at 25°C in different solvents with distinct polarity (expressed as a dielectric constant ϵ_r)¹⁵⁴

Aminoazobenzenes (aAB)

Aminoazobenzenes family comprise those azobenzenes with one or more 2,4-substitution with amine, methoxy or hydroxyl groups. The electron donating properties of these groups (EDG) shift the π - π^* transition band to higher wavelengths, leading to an overlap with n - π^* transition, and can be increased with additional substituents or depending on its degree of alkylation. *N*-amides, *N*-carbamates and ureas, may also be classified in this group since they also cause a

shift to red of the π - π^* band in compounds of general formula **63** depending on the electron donating properties of each group (figure 21)¹⁵⁹.

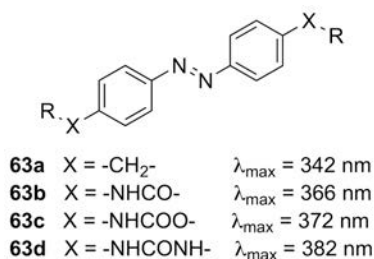


Figure 21: Comparison of the red-shifting effect of π - π^* band of pseudo-amine groups such as amide, carbamate or urea.

Thermal relaxation of the aAB of *cis*-isomers is generally faster than AB, but if *ortho* positions are substituted with bulky substituents can make the relaxation slower due to a stabilisation of the *cis*-isomer¹⁶⁰. Additionally, when amines or hydroxyl groups are not alkylated, thermal relaxation half-life remarkably decrease due to an azo-hydrazone tautomeric equilibrium (figure 22), especially in polar solvents¹⁵³. They are used as industrial dyes, pH and metal indicators, in photoelectric and information storage devices and photoresponsive polymers¹⁵².

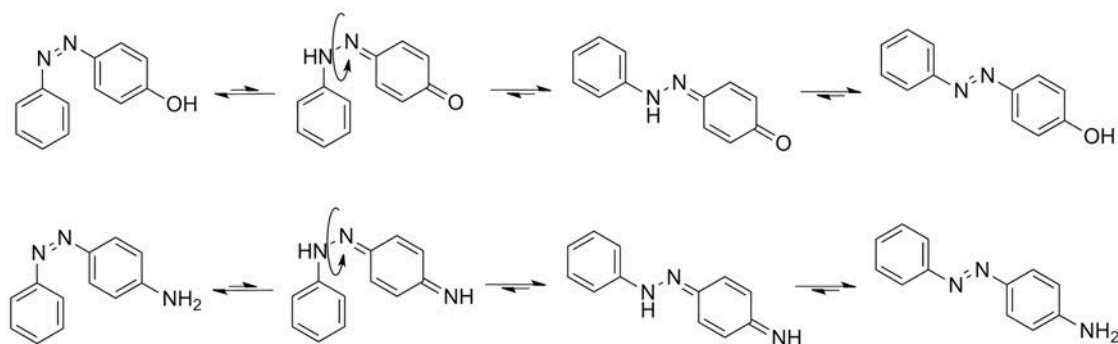


Figure 22: Azo-hydrazone tautomeric equilibrium in non-*N*-substituted aminoazobenzenes or non-*O*-substituted hydroxyazobenzenes

Push-pull azobenzenes (ppAZ)

In push-pull azobenzenes, usually a strong electron donor and a strong electron acceptor occupy the 4 and 4' position of the phenyl rings, but also positions 2 and 2' can display a strong effect. This causes a decrease in the energy of the $\pi\pi^*$ state, leading to a shift of the transition bands to visible ranges. They are also characterised by the extremely fast relaxation of their *cis*-isomers, in the scale from milliseconds to seconds, and, like aAB, depends on the polarity of the solvent (table 12)¹⁵².

The donor acceptor can be also 2- or 4-pyridine, or even 2- or 4-methylpyridinium salt increasing their push-pull effects, and particularly reducing their relaxation half-life time.

Moreover, if the donor or the acceptor allows azo-hydrazone tautomeric equilibrium, this relaxation rate can be radically increased¹⁵³, as *figure 23* shows.

Push-pull azobenzenes are intensively coloured and used as dyes in the industry or as a pH or metal indicators. They are also useful for non-linear optical and photo-refractive materials, optical poling, holographic memory storage devices or as a fast information-transmitting photocromic switches¹⁵³.

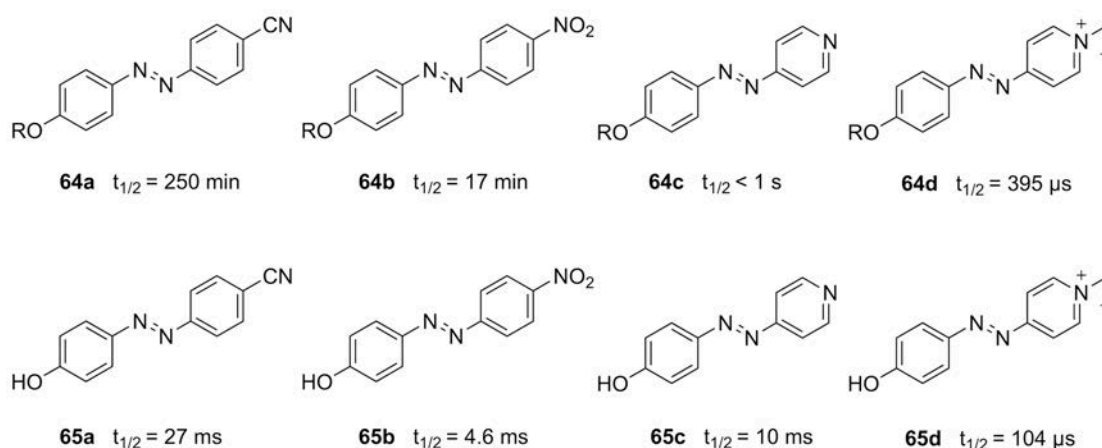


Figure 23: Comparison between electron withdrawing groups and *cis*-isomer relaxation half-life time for push-pull compounds without (**64a-d**) and with azo-hydrazone tautomeric equilibrium (**65a-d**)¹⁵³.

Other azobenzenes (toAB & bAB)

Another type of azobenzenes to be considered is the tetra-*o*-substituted azobenzenes (toAB). These azobenzenes are substituted in position 2, 6, 2' and 6' with groups like methoxy or halides (*figure 24A*) are characterised to red shift the $n-\pi^*$ band of the *trans*-isomer and separate it from the one of the *cis*-isomer. Therefore, isomerisation from the *trans* to the *cis* configuration can be achieved from green to red light illumination, and the back isomerisation with blue light. Additionally, the four *ortho* substituents thermally stabilise the *cis* disposition leading to half-life times from hours to days in aqueous solution^{150, 161}.

Another remarkable type azobenzenes are the bridged azobenzene (bAB) like the one showed in *figure 24B*. This compounds display a "inverse photoisomerisation", since the *cis*-isomer is the thermally more stable. It isomerises from *trans* to *cis* configuration with light between and from 450 to 500 nm and from *cis* to *trans* with light about 370 and 400 nm and the *trans* isomer has a thermal half-life relaxation of 4.5 hours at room temperature¹⁶².

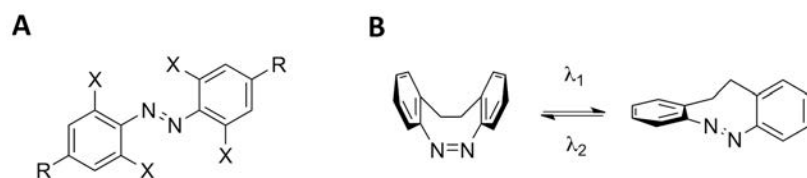


Figure 24: Basic structures of (A) toAB and (B) bAZ

Optopharmacological approaches

The current means most used to control a protein function or a signalling path with light can be divided in 4 approaches: Optogenetics, optogenetic pharmacology, optopharmacology with caged compounds and optopharmacology with photoisomerisable compounds.

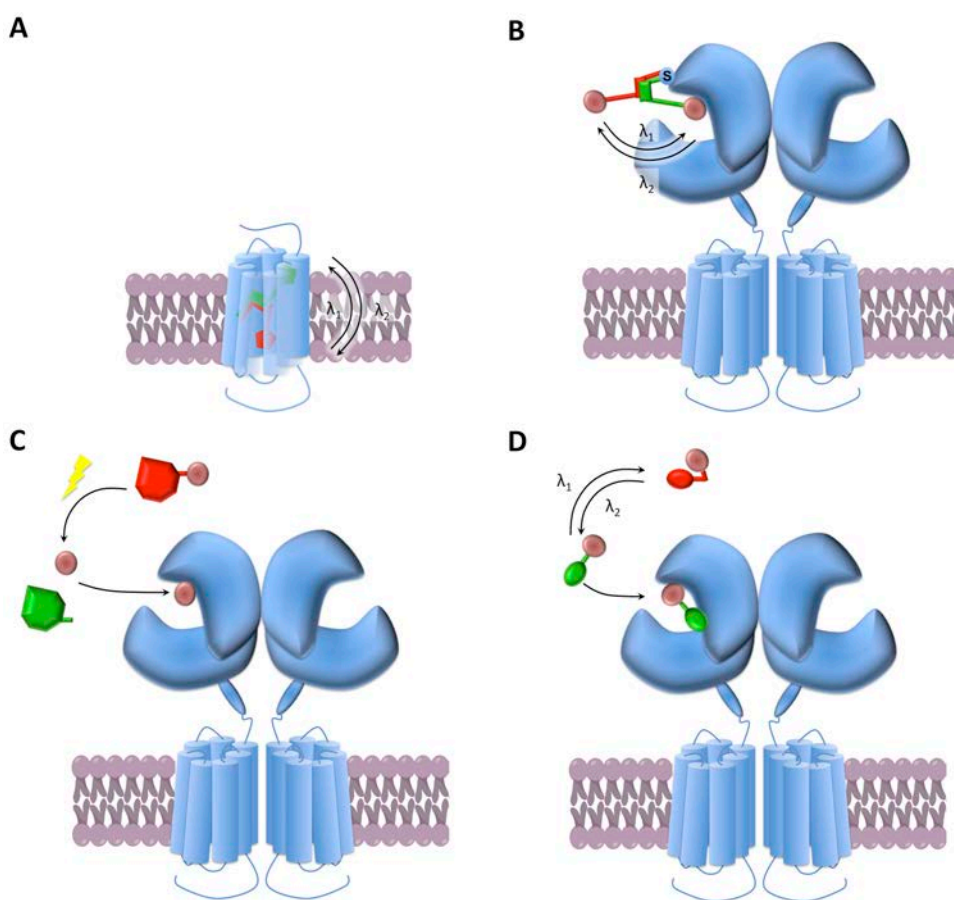


Figure 25: The four main approaches for controlling protein activity with light: (A) Optogenetics, (B) Optogenetic pharmacology; (C) Optopharmacology with caged compounds (D) Optopharmacology with photoisomerisable compounds. Adapted from Kramer¹³⁵.

Optogenetics

Photoisomerisable chromophores can be found in the nature and they switch a protein function by means of light, in a fast and precise manner. An example of such may be retinal in opsin proteins that can regulate the visual transduction (rhodopsin), pump protons as a source

of energy (bacteriopsins), or the trafficking of ions (channelrhodopsins and halorhodopsins)¹⁶³. Several publications stand that these opsins can be genetically transfected in cultured cells, or even *in vivo* and its function can be controlled with light (*figure 25A*)¹⁶⁴⁻¹⁶⁷.

Optogenetic pharmacology

Optogenetic pharmacology is an approach that offers a high precision in terms of triggering a protein response and temporal and spatial use of light, and also includes the cell type specificity that also can be afforded with optogenetics. The most common approach is the use of photoswitchable-tethered ligands (PTLs), which consist in a terminal ligand, which is attached to an intermediate photoswitch, which is also attached in the opposite side to a terminal cysteine-reactive group (*figure 25B*). Therefore, these PTL can be attached by affinity labelling to a cysteine of the surface of the protein, which is usually introduced by mutagenesis at an appropriate location near the binding site, since these residues are not abundant on protein cell surfaces in the reduced form. The ligands of the terminal chain can be agonists, antagonists or blockers and the reactive group can be maleimides, activated carboxylic acids, halides, etc. The length of the chain can be variable, as well as the position of the cysteine, and both can be optimised to reach a *cis* binding PTL or a *trans* binding PTL.

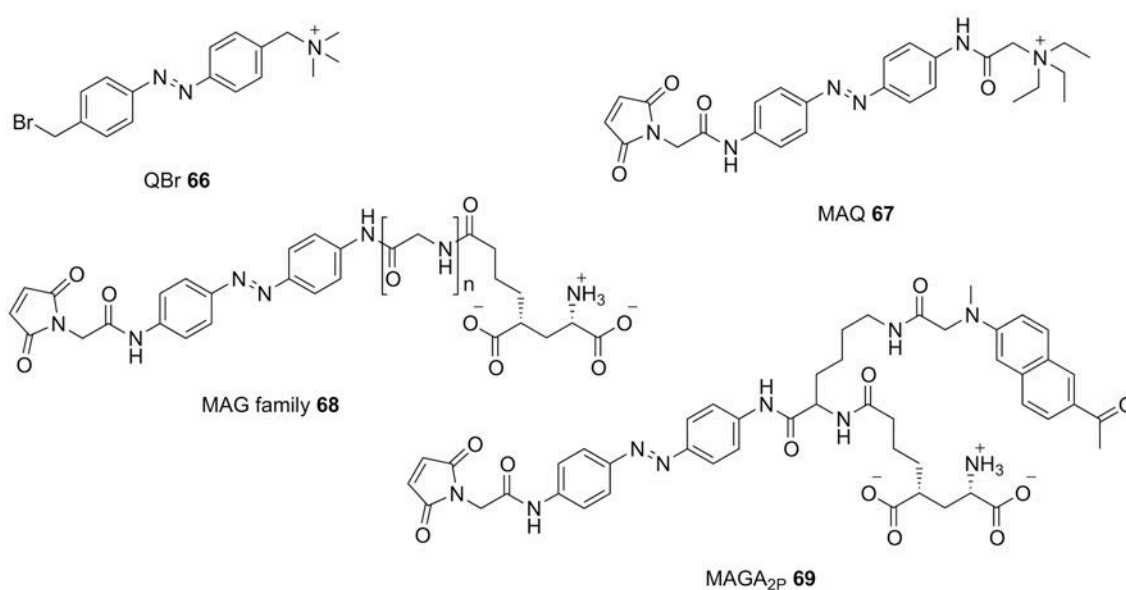


Figure 26: Representative examples of PTL

The first receptors to be engineered with PTLs were nicotinic acetylcholine receptors (nAChR), which natively include a cysteine-rich loop close to the binding site where the PTL (QBr, **66**, *figure 26*) can conjugate. Thus, in *trans*-configuration the agonist binds the active site and in *cis* is not long enough¹⁶⁸. Years after, other PTLs were designed with the corresponding mutations of the target proteins. Examples of such can be MAQ family, as K⁺ channel

blockers¹⁶⁹⁻¹⁷²; MAG family, as GluK2 agonist or mGlu agonists^{173,174}, including MAGA_{2p}, which is photoisomerisable illuminating with infra red with two photon technique¹⁷⁵.

Optopharmacology with caged compounds

Optogenetics and optogenetic pharmacology permit the control protein functions with precision and effectiveness, but genetic modification is needed for both approaches, which exclude them as techniques for human therapeutics. Optopharmacology with caged compounds or with photoisomerisable compounds may constitute a valuable alternative since they do not need the genetic manipulation of the target protein and may keep drug-like properties that can enable them as prospective drugs for human therapeutics.

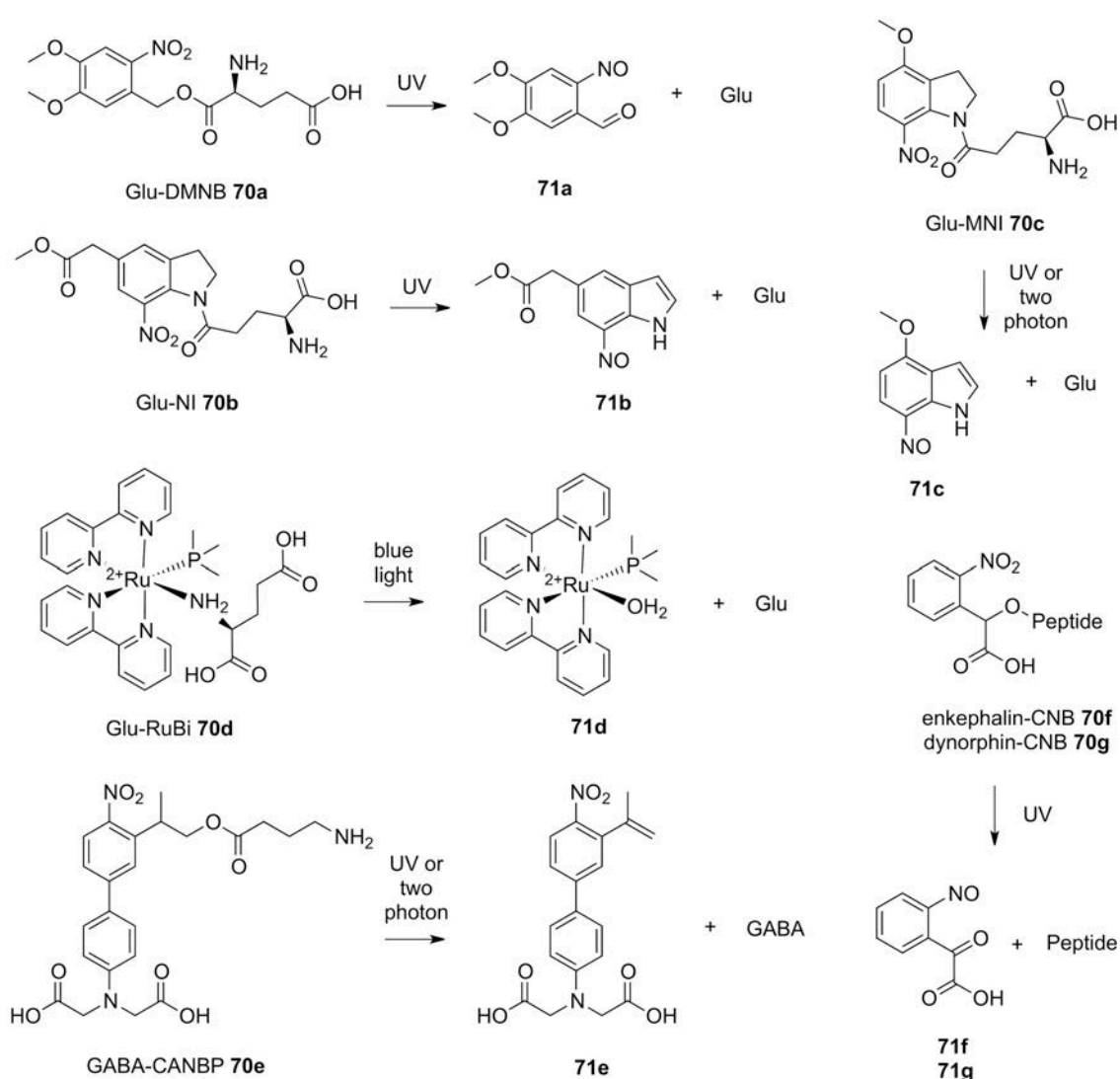


Figure 27: Examples of cages compounds to precise control CNS activity

Caged compounds approach is based on the use of photolabile protecting groups that “cage” bioactive compounds. This cage is based on a protecting group covalently bound to a compound preventing its biological activity; but, under exposure to light, this bond is broken to release the bioactive compound in an irreversible way. This approach permits a spatiotemporal control of the release of the compounds but, once they are released, their control is completely lost as in conventional drugs. Additionally some cage by-products can exert undesired activities or can be toxic (*figure 25C*).

Many different cages can be used and they are very well reviewed by Klán¹⁷⁶ and some cage compounds have been designed for neuronal control. Examples of such may be glutamate with DMNB^{a177}, NI^{b178}, MNI^{c178} or RuBi^{d179} cages; or GABA with NMI¹⁷⁸, RuBi¹⁸⁰ or CANBP^{e181}, or opioid neuropeptides L-enkephalin or dynorphin with CNB^{f182} (*figure 27*).

Optopharmacology with photoisomerisable compounds

Caging systems are irreversible, which leads to a loss of control after its release, and sometimes produce toxic by-products. That is the reason why light control for both activation and inactivation would be an interesting tool. Photoisomerisable ligands may give a solution to this issue as a photoswitch is included inside the ligand scaffold or close to the protein interacting groups in such a way that a large change of the spatial configuration is achieved under illumination with a single wavelength, which can be restored after a second wavelength illumination to recover the initial state (*figure 25D*).

The most common photoswitch used in this approach is azobenzene, which involves two major changes under illumination: a change of the ligand length and a change in the three-dimensional shape, from a straight to a bent geometry. That leads to two different approaches of photoisomerisable ligands: (A) *trans*-on photoisomerisable ligands (*figure 28A*), which bind to the target protein in *trans*-configuration whether in the *cis*-one remain unbound; and (B) *cis*-on photoisomerisable, which undergo in an opposite manner: they bind to the target protein in *cis*-configuration whether in the *trans*-one remain unbound (*figure 28B*).

Both optogenetic pharmacology and optopharmacology enable the control of protein function with light, but one clear advantage of the last one is that can be used without the need of genetic modification. Therefore a therapeutic application of these compounds in humans

^a DMNB: 4,5-dimethoxy-2-nitrobenzyl

^b NI: 7-nitroindolinyl

^c MNI: 4-methoxy-7-nitroindolinyl

^d RuBi: *cis*-[Ru(bpy)₂(PMe₃)X]²⁺, *cis*-bis(2-bipyridine)trimethylphosphine ruthenyl (II)

^e CANBP: 2-(4'-(bis(carboxymethyl)amino)-4-nitro-[1,1'- biphenyl]-3-yl)propan-1-ol

^f CNB: carboxy-2-nitrobenzyl

could be possible. However, the passive diffusion of these compounds supposes a drawback, since they would need to have a high selectivity, which many times result in a gruelling work. Nevertheless, a *cis*-on approach with an inactive *trans*-isomer to the majority of targets would be an optimal approach, since we would be able to activate this ligand in the site of action with a complete spatiotemporal control while it would rest inactive out from the illumination spot.

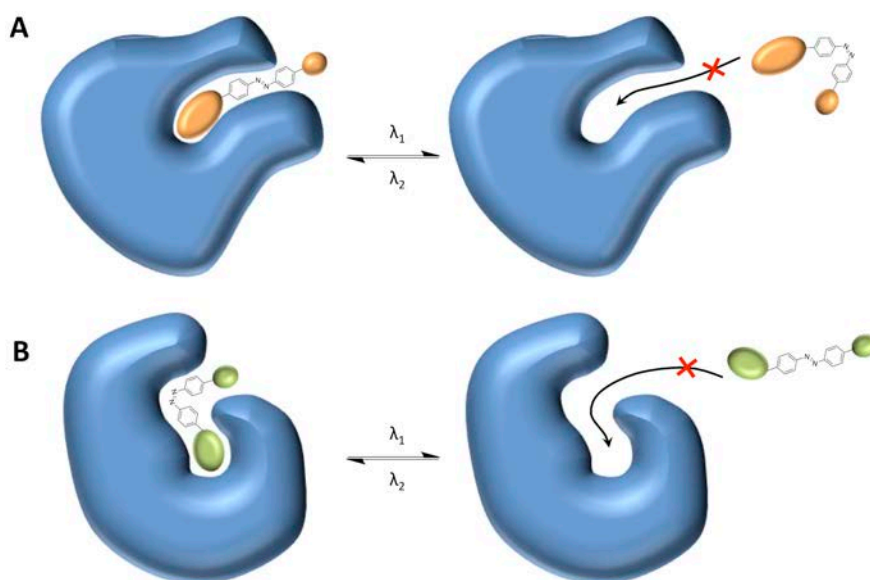


Figure 28: Representation of binding mode of photoisomerisable ligands. (A) *trans*-on approach (B) *cis*-on approach

The first reported photoisomerisable compound with biological activity was bisQ (**72**), which was the non-tethering derivative of QBr (**66**) and in its *trans* disposition opened the pore of nicotinic acetylcholine (nAChR) channels¹⁶⁸. Another classical example is gluazo (**74**), which is a GluK1 agonist in its *trans*-disposition; or the family of MAQ-related potassium ion blockers AAQ, BzAQ, PrAQ, DENAQ, PhENAQ or QAQ (**73a-f**)¹⁸³⁻¹⁸⁶, which have different properties of isomerisation and can block a cationic pore in *trans* or *cis*-disposition depending on the ligand.

Apart from the non-tethered derivatives of the PTLs used in optogenetic pharmacology, previous known drugs or drug-like bioactive compounds have been modified to afford photoswitchable compounds. According to a recent review of Trauner¹⁸⁷ two different approaches are possible: “Azo-extension” and “azologisation”.

On the one hand, azo-extension is obtained extending an azobenzene to a pre-existing aromatic ring of a drug or a known bioactive compound, without abrogating its biological activity. Some of the reported examples are shown in *figure 30*, such as azopropofol (**75b**), an *trans*-on azobenzene derivative of the GABA_A channel potentiator propofol (**75a**)¹⁸⁸, the *cis*-on antibacterial quiniolone-2 (**76b**), derived from ciprofloxacin (**76a**)¹⁸⁹, the also *cis*-on AC4 (**77b**),

derived from the TRPV1 antagonist capsazepin (**77a**)¹⁹⁰, or the μ opioid GPCR agonist fentanyl (**78a**) derivative, photofentanyl (**78b**)¹⁹¹.

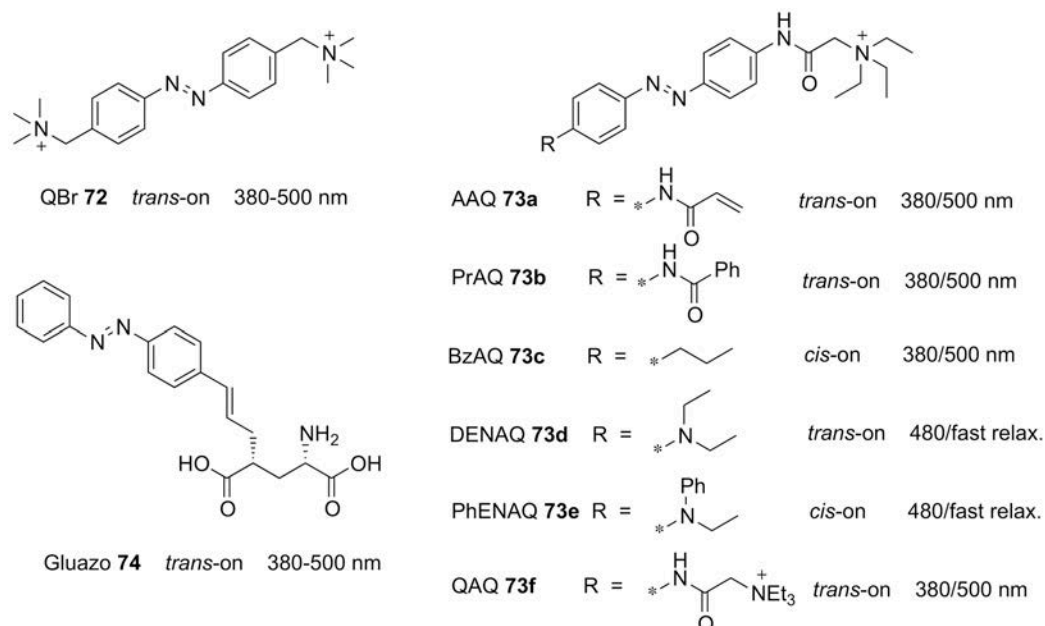


Figure 29: Classical photoisomerisable compounds with activity in the CNS

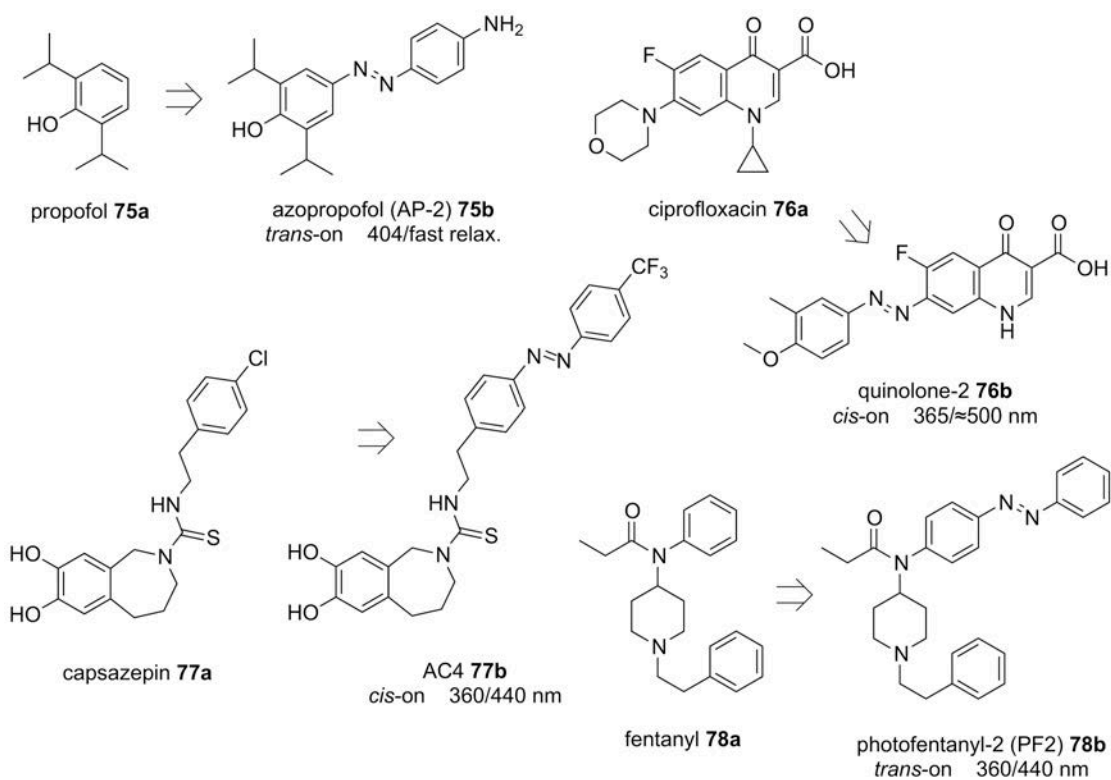


Figure 30: Examples of the azo-extension approach to afford photoisomerisable bioactive compounds

On the other hand, azologisation, or also called *azo-replacement* is based in the substitution of a bridge between two aromatic rings, such as ethylene, amide or methylene ether between

others, with an azo-bond. Several examples can be found in the literature and here we exemplify a small selection (*figure 31*): Fotocaine (**79b**) is a *trans*-on derivative of the local anesthetic fomocaine (**79a**)¹⁹²; JB253 (**80b**), a *cis*-on derivative of glimepiride, an ATP-sensitive K⁺ channels inhibitor¹⁹³; the photoswitchable lipid azCA4 (**81b**), which are derivatives of capsaicin or arvanil lipids and activates TRPV1 channels in its *cis*-configuration¹⁹⁴; and, very recently reported, PST-1 (**82b**), a *cis*-on microtubule inhibitor with antimitotic and proapoptotic properties, derived from combretastatin A-4 (**82a**)¹⁹⁵.

These approaches, especially *cis*-on ones, offer new perspectives to pharmacology, since light provides a fine spatiotemporal control, not achieved with classical pharmacology. This kind of molecules can radically improve the selectivity, not only for one protein subtype, but also for a protein expressed in a single location in the body and whose activity can be suppressed once the therapeutic effect is afforded. Thus, we may be starting to see a light revolution of pharmacology.

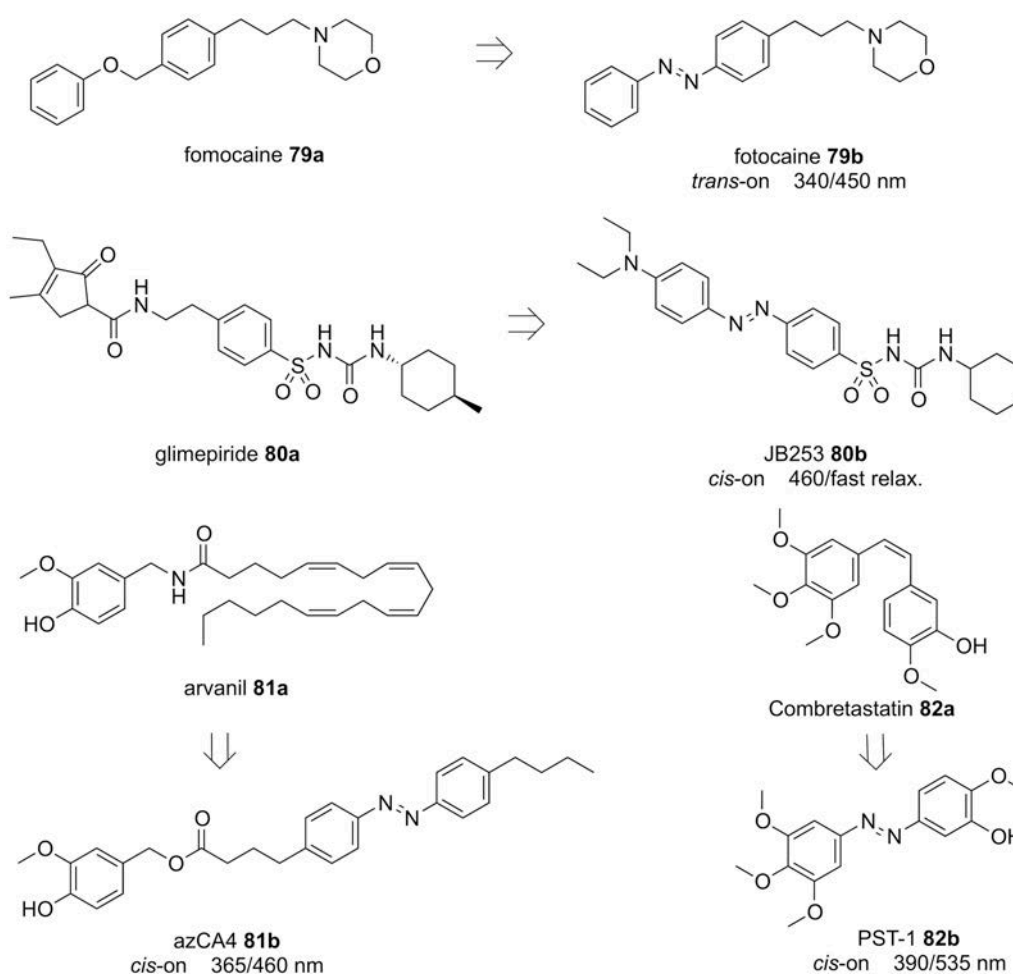


Figure 31: Examples of the azo-isation or azo-replacement approach to afford photoisomerisable bioactive compounds

Objectives

Metabotropic Glutamate receptors (mGluRs) are class C G-Protein Coupled Receptors (GPCRs), which are involved in many neuronal and glial functions. A suitable modulation of their activity can be useful for therapeutically treat many diseases involved in central and peripheral nervous system, including Parkinson disease or neuropathic and inflammatory pain. This modulation can be afforded in a effective way with allosteric modulators, which only exert their activity under receptor activation, constituting a safer and more physiologic approach, compared to orthosteric antagonists and agonists

Classic pharmacology is based in traditional drugs that, once administered, spread all over the body with a completely loss of control and finally reach their target, exerting their therapeutic effect. Optopharmacology with reversible photoisomerisable drugs offers several advantages to classical pharmacology since its activity can be controlled with light. In this case, light offers a control of drug activity in terms of spatiotemporal and also selectivity can be dramatically improved, not only for a single target, but also for a single target expressed in a single location. Overall, this approach offers new perspectives for drug discovery and therapeutics to better control of drug action and to reduce side effects to minimal expression.

According to what stated above the main objectives of the thesis are the following ones:

- 1) Design and synthesise a photoisomerisable allosteric modulator of metabotropic glutamate receptors subtype 4 or 5 (mGlu₄ and mGlu₅), since they are indicated for pain treatment. Our approach is based on existing allosteric modulators like MPEP (**12**), VU036770 (**31a**), VU0415374 (**33b**) or SIB-1893 (**43**), which have a similar modular architecture containing two aromatic groups linked by a two or three-atom bond central unit. These structures will be converted in photoactive ligands through formally introducing the required azo-bond as the central spacer functionality (*trans*-azologisation).
- 2) Photochemical and pharmacological characterisation of the new synthesised compounds, which need to be photoisomerisable, active in mGlu₄ and mGlu₅ and photoisomerisable in a biological environment (cellular culture media, tissues, *in-vivo*,...)
- 3) Design, synthesis and pharmacological characterisation of non-photoisomerisable bioisoster of the previously synthesised photoisomerisable compounds, for example, substituting the azo-bond for an acetylene, which share similar geometric and electronic properties. The aim of this objective is to establish similarities between photoisomerisable and classical ligands, from the point of view of their functionality and to set up new approaches for azologisation.

- 4) Design and synthesise a series of photosomerizable allosteric modulators, derived from the first hits with the development of parallel synthesis. This library has also to be photochemically and pharmacologically characterised, including *in-vivo* studies, and structural-photoisomerisation-activity relationships has to be evaluated, so as to establish optimal chemical structures to afford both outstanding photoisomerisation properties and pharmacological effect is *trans*-disposition.
- 5) Design and synthesise a series of photosomerizable and non-photosomerisable allosteric modulators, comprising common moieties of mGlu₄ positive allosteric modulators (PAM) and mGlu₅ negative allosteric modulators (NAM). The aim of this series is to establish chemical patterns for mGlu₄ PAMs and mGlu₅ NAMs and obtain dual mGlu₄ PAM and mGlu₅ NAM compounds, with photoisomerisable properties or not, which would be of particularly interest for the treatment of neurodegenerative diseases like Parkinson disease or neuropathic or inflammatory pain.
- 6) Design and synthesise a series of photoisomerisable mGlu₄ PAMs and mGlu₅ NAMs, using a *cis*-on approach, in which the *cis*-isomer corresponds to the bioactive disposition. This approach is therapeutically more effective, since the compounds are supposed to be inactive in the thermodynamic equilibrium, but under illumination they isomerises to the active configuration, constituting a precise control of the spot of action of the compound. This series has to be designed through "azo-extension" approach with computational support and the previous knowledge acquired from the other series, has to permit the design of these compounds with a photoisomerisation with blue light.

Results and Discussion

Results and discussion contents

Chapter 1: alloswitch-1 and optogluram: a proof of concept	65
Design of the first series of photoswitchable compounds	65
Synthesis of compounds 33b, 83 and 84.....	66
Photochemical characterization of 83 and 84	68
<i>In-vitro</i> biological evaluation of 83 and 84	73
<i>Preliminary dose-response curves</i>	73
<i>X. Rovira, IGF, Montpellier</i>	73
<i>In-vitro pharmacological characterisation of compound 83: alloswitch-1</i>	74
<i>S. Pittolo, IBEC, Barcelona - IGF, Montpellier</i>	74
<i>In-vitro pharmacological characterisation of compound 84: optogluram</i>	77
<i>In-silico</i> characterisation of 83	79
<i>In-vivo</i> biological evaluation of 83 and 84.....	81
<i>In-vivo pharmacological characterisation of compound 83: alloswitch-1</i>	81
<i>In-vivo pharmacological characterisation of Compound 84: optogluram</i>	85
Conclusions	87
Chapter 2: alloswitch-1 & optogluram non-photoswitchable bioisosters and the confirmation of the double molecular switch	89
Design of alloswitch-1 and optogluram bioisosters.....	89
Synthesis of compounds 99 and 100	90
Pharmacological characterisation of compounds 99 and 100	91
Conclusions	93
Chapter 3: a new series of phenylazopyrines to fine control mGlu₅ function with light	95
Initial considerations and design of a series of phenylazopyridines.....	95
Synthesis	98
Photochemical characterisation of compounds 109-117	101
<i>Photoisomerisation of compounds 109-117 with UV-Vis absorption spectroscopy</i>	104
<i>In-vitro</i> biological evaluation of 109-117	107
<i>Real-time photoswitching in cell assays</i>	117
<i>S. Pittolo, IBEC, Barcelona</i>	117

<i>In-silico</i> characterisation of 110 and 109e,f.....	119
<i>In-vivo</i> biological evaluation of 109-115.....	121
<i>In-vivo zebrafish screening in dark conditions</i>	121
<i>In-vivo zebrafish screening with light</i>	123
Conclusions	127

Chapter 4: The quest of dual mGlu₄ PAMs and mGlu₅ NAMs: azo- and amide-replacement of 2-BisPEB 128

Initial considerations and design of compounds 128-133.....	128
Synthesis of compounds 111c, 115, 128-131, 53, 54	131
Photochemical evaluation of compounds 111c, 115, 128-131, 53, 54	132
<i>In-vitro</i> pharmacological evaluation of compounds 127-133.....	134
<i>Duality mGlu₄ PAM and mGlu₅ NAM: dose-response curves with receptor</i>	134
<i>Selectivity of compounds 111c and 128a</i>	136
<i>An unexpected effect on mGlu₅: Positional isomers lead to different efficacies</i>	140
<i>In-silico</i> characterisation of 110 and 109e,f.....	143
Conclusions	146

Chapter 5: A more suitable therapeutic approach: *cis*-on photoswitchable mGlu₄ PAMs and mGlu₅ NAMs. 148

Design of compounds 140a-141 and 142-144	149
Synthesis of compounds 140a-144	155
Photoisomerisation properties of compounds of 140a-143	157
Pharmacological characterisation of compounds of 140a-143	158
Design and synthesis of compounds 140b-140c.....	162
Photoisomerisation properties of compounds of 140b-c.....	163
Pharmacological characterisation of compounds of 140a-143	165
Conclusions	166

Chapter 1: alloswitch-1 and optogluram: a proof of concept

The first objectives of this thesis were the design and synthesis a photoisomerisable allosteric modulators of metabotropic glutamate receptors subtype 4 or 5 (mGlu₄ and mGlu₅), its photochemical and pharmacological characterisation. In this chapter the experiments and results corresponding to these objectives will be exposed with their corresponding discussion.

Papers related to this chapter:

Silvia Pittolo, Xavier Gómez-Santacana, Kay Eckelt, Xavier Rovira, James Dalton, Cyril Goudet, Jean-Philippe Pin, Artur Llobet, Jesús Giraldo, Amadeu Llebaria and Pau Gorostiza, "An allosteric modulator to control endogenous G protein-coupled receptors with light", *Nature Chemical Biology*, **2014**, 10, 813-815

James A.R. Dalton, Isaias Lans, Xavier Rovira, Fanny Malhaire, Xavier Gómez-Santacana, Silvia Pittolo, Pau Gorostiza, Amadeu Llebaria, Cyril Goudet, Jean-Philippe Pin and Jesús Giraldo, "Shining Light On An mGlu5 Photoswitchable NAM: A Theoretical Perspective", *Current Neuropharmacology*, **2015**, 13, Ahead of print, DOI: 10.2174/1570159X13666150407231417

Currently in preparation of a manuscript

Design of the first series of photoswitchable compounds

At the beginning of the project in which this thesis is embedded, we decided to design a photoisomerisable positive allosteric modulator (PAM) of mGlu₄, through azologisation¹⁸⁷, also called azo-replacement^a, of a previously known mGlu₄ PAM. Therefore, we search in the literature for mGlu₄ PAMs, with aromatic rings with a spacer susceptible to be substituted for an azo-bond (-N=N-).

We find several promising compounds that fulfilled our requirements, but we finally opt for VU0415374 (**33b**)⁹⁶ for three main reasons: (a) it was a very potent mGlu₄ PAM with an EC₅₀ of 99.5 nM and a potentiation over glutamate of 79%⁹⁶; (b) its synthesis apparently was not difficult; and (c) it included two amides flanked by aromatic rings, which were susceptible to be replaced by azo groups. Aromatic amides are characterised to display an unusual rigidity, due to the delocalization of π -electrons over the rings and the amide, giving a planar structure.

^a Azologisation or azo-replacement is based in the substitution of a bridge between to aromatic rings with an azo-bond, see general introduction - Control of protein function with light - Optopharmacological approaches.

This delocalisation is very similar to that on found in azobenzenes. Therefore, we thought that their substitution for azo-bonds would be suitable to afford photoswitchable mGlu₄ PAMs.

Following azo-replacement approach, by replacing the picolinic amide bond in compound **33b** compound **83** is obtained, whereas replacing the 2-chlorophenyl amide bond, compound **84** is afforded (*figure 32*). Applying this approach, and expecting the binding to the *trans*-amide-conformer compound **33b** inside allosteric site of mGlu₄, compounds **83** and **84** should display mGlu₄ PAM activity in its *trans* configuration and, after illumination, the *cis*-isomers should not bind due to the abrupt change of geometrical disposition. That constitutes a *trans*-on approach.

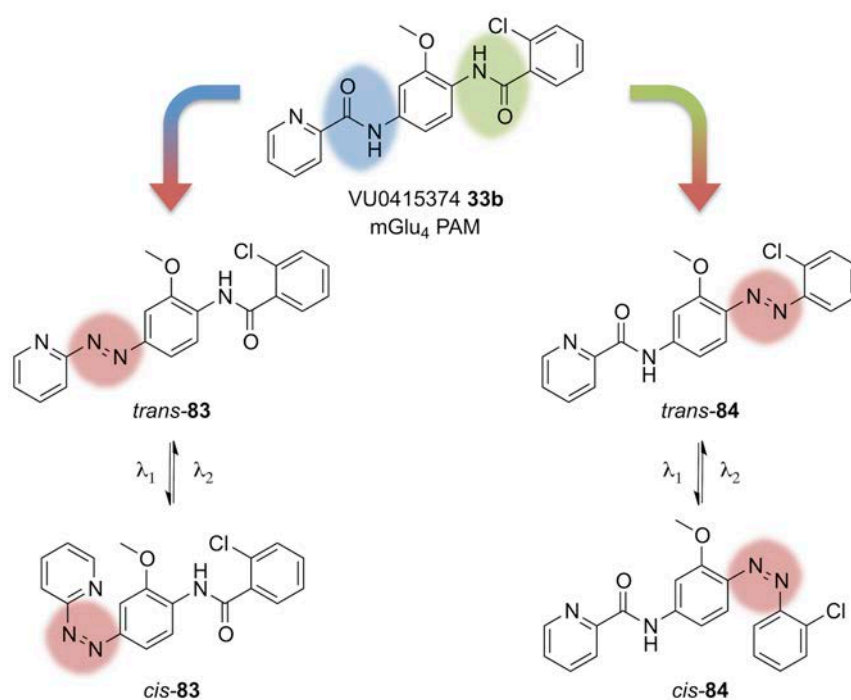
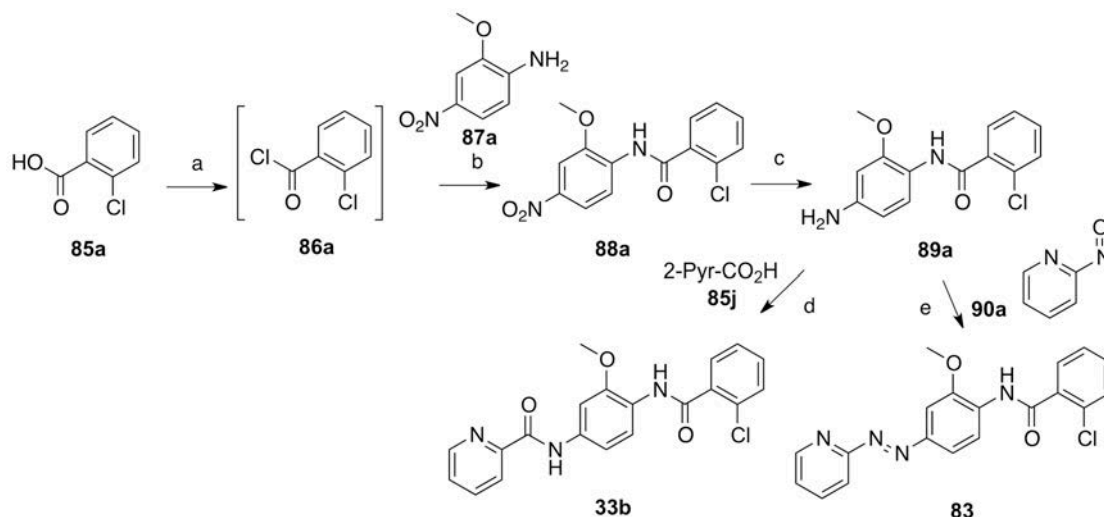


Figure 32: Azo-replacement approaches of VU0415374 (**34b**) to afford theoretically *trans*-on photoisomerisable compounds **83** and **84**.

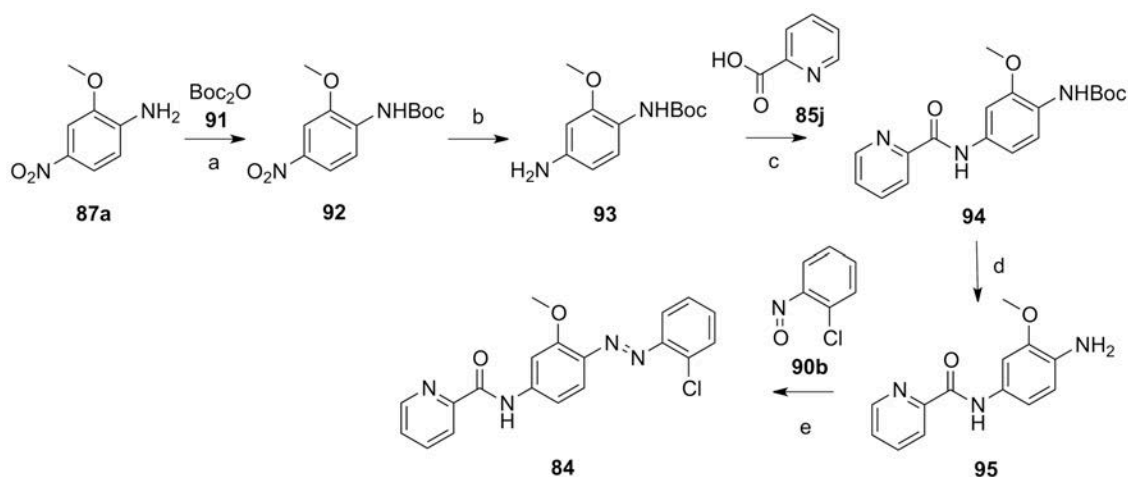
Synthesis of compounds **33b**, **83** and **84**

Compound **33b** was synthesised following a similar procedure to the previously reported⁹⁶, using the aniline **89a** as common intermediate for compound **83**. Both synthetic routes are depicted in *Scheme 1*. The sequence started with the preparation of the corresponding acyl chloride **86a** prepared from 2-chlorobenzoic acid (**85a**) with thionyl chloride (*step a*), which was used to acylate nitroaniline **87a**, with (*step b*), in presence of DIPEA to give **88a** in 99% yield. For the synthesis of **32b**, the reduction on the nitro group has carried out using Sn and aqueous HCl to give key aniline **89a** with a 95% yield. For the synthesis of **83**, the nitro group was hydrogenated with 5% Pt-1% Fe/C catalyst (*Evonik*) to give a quantitative yield of aniline

89a (*step b*). The mGlu₄ PAM VU0415474 (**33b**) was finally obtained by amide coupling of aniline **89a** and picolinic acid (**85j**) with an 80% yield (*step d*). On the other hand, the desired phenylazopyridine **83** was prepared in 81% yield by reacting **89a** with 2-nitrosopyridine **90** in acid media (*step e*).



Scheme 1: Synthesis of compounds **33b** and **83**: (a) SOCl₂, 2h, reflux, quant. (b) DIPEA, DCE, 100°C, 2.5h, 99%; (c) Sn, HCl (aq), THF, reflux, 30 min min, 95%; or H₂ (2 atm), Pt-Fe/C, EtOH, r.t, 15h, quant.; (d) HATU, DIPEA, EtOAc, 40°C, 80%; (e) EtOAc cat., DCM, r.t, 75 hours, 81%.

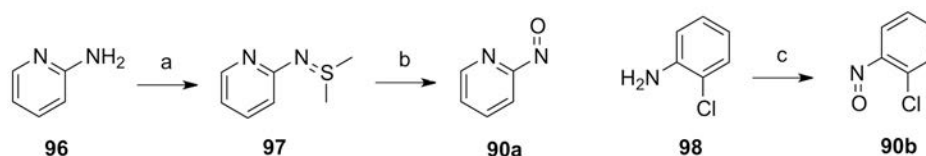


Scheme 2: Synthesis of compound **84**: (a) Boc₂O, DCM, r.t., 48 h, 56% (62% conv.); (b) H₂ (2 atm), Pd/C, EtOH, r.t., 5h, 98%; (c) HATU, DIPEA, EtOH, EtOAc, 40°C, 16 h, 88%; (d) TFA, DMF, r.t., 2h, quant.; (e) AcOH cat., DCM, r.t, 3 d, 75%

Azocompound **84** was prepared following the synthetic strategy shown in *scheme 2*. Protection of the amine group in **87a** with Boc₂O (**91**) in the presence of TEA (*step a*) afforded the nitro compound **92** in 56% yield and 63% conversion. Following reduction, the nitro group yielded aniline **93** with a 98% yield (*step b*). Aniline **93** was acylated with picolinic acid (**86j**) with the coupling agent HATU and DIPEA (*step c*) to afford compound **94** in 88% yield, which was

deprotected under acidic conditions in quantitative yield to **95** (*step d*). Finally, freshly prepared nitroso compound **90b** was used directly in the reaction with aniline **95** under acidic catalysis (*step e*) to afford the desired azobenzene derivative **84** in 75% yield.

2-nitrosopyridine (**90a**) was prepared at multigram scale following a procedure described by Taylor¹⁹⁶. This involves the intermediate sulphimine **97**, which was prepared by chlorination of 2-aminopyridine (**96**), followed by the formation of a sulphonium salt with dimethyl sulphide and consecutively deprotonated with sodium methoxide with in 80% yield. Subsequent oxidation of sulphimine **97** afforded 2-nitrosopyridine with 58% yield. 2-chloro-1-nitrosobenzene (**90b**) was prepared by Oxone oxidation of 2-chloroaniline (**98**) following the procedure described by Priewisch¹⁹⁷.



Scheme 3: Preparation of nitroso compounds **90a** and **90b**: (a) i) NCS, Me₂S, DCM -20°C, 1h, ii) MeONa/MeOH, r.t., 20 min, iii) H₂O, r.t. 2.5h, 80%; (b) i) mCPBA, DCM, 0-5°C, 0.5h, i) Me₂S, 0-5°C 30 min, 58%; (c) Oxone, DCM/H₂O 1:4, r.t., 2h, quant.

Photochemical characterization of **83** and **84**

UV-Vis absorption spectroscopy

To evaluate the photoisomerisation of our azocompounds, we first measured UV-Vis absorption spectrum of a solution 25 μ M in DMSO in dark conditions. Both spectra showed the typical azobenzene π - π^* transition band at 370-390 nm and, therefore, the *Z/E* isomerisation could be achieved under illumination at these range of wavelengths. We did illuminate the same samples two minutes with 380-nm-light and we consecutively collected a new absorption UV-Vis spectrum, with a completely different appearance. Later on we illuminated the samples with 500 nm achieving practically the same UV-Vis absorption spectrum that we obtained in dark conditions (*figure 33A-B*).

Additionally, we determined the optimal isomerisation wavelengths for compound **83**. Thus, we illuminated samples of **83** (25 μ M in a mixture DMSO/PBS 3:1) with different light wavelengths and we next registered the UV-Vis absorption spectrum under each condition. The measure of the height of the band around 380 nm provided a qualitative insight of the amount of *trans*-**83** of the sample. This fact permitted us to generate the plot of the *figure 33C*, where it is shown that the optimal wavelength of illumination to obtain a larger quantity of *cis*-

83 was 390 nm. On the other hand, another sample of **83** was illuminated at 390 nm and immediately illuminated with different light wavelengths, with the corresponding UV-Vis absorption spectrum measured every time. Then, it was possible to determine the optimal wavelength by the measuring the height of the π - π^* band again, showing a larger quantity of *trans*-**83** between 450 and 490 nm (figure 33D).

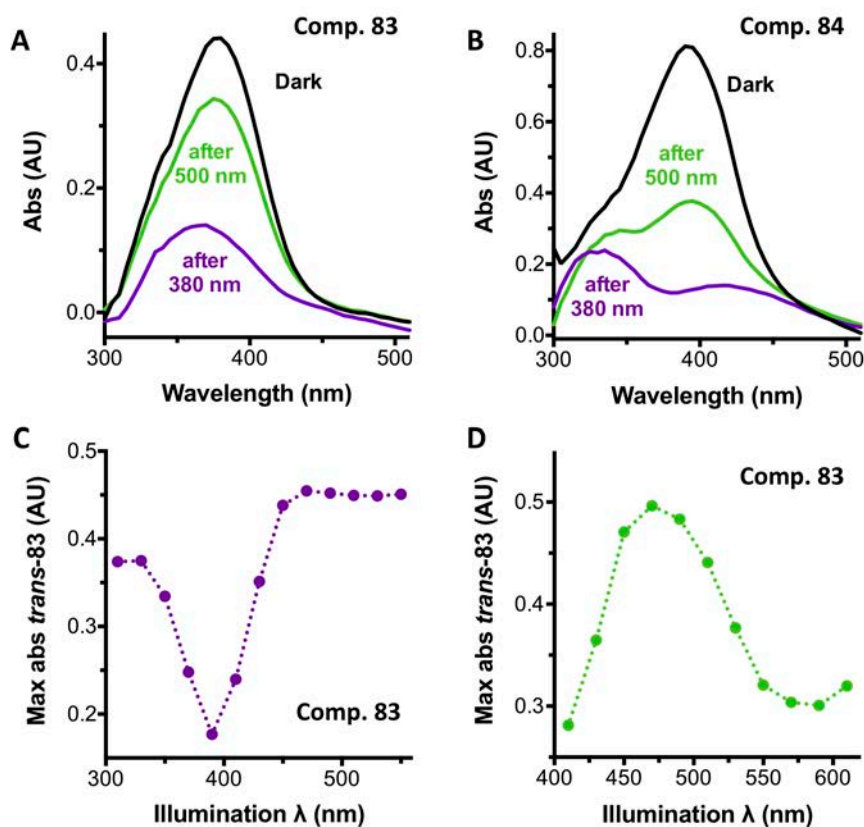


Figure 33: Photochemical properties of compounds **83** and **84** (1): UV-Vis absorption spectra of compounds **83** (A) and **84** (B) in dark conditions (black line), under 380 nm light (violet line) and under 500 nm light (green line). Maximum absorption values of compound **83** (25 μ M in DMSO/PBS 3:1) extracted from UV-VIS absorption spectra measured after illumination of the sample at wavelengths indicated in graphs for *trans*-to-*cis* isomerisation (C) and for *cis*-to-*trans* isomerisation (D).

The photoisomerisation after several photoisomerisation cycles was also determined with a solution in DMSO or in a mixture DMSO/PBS recording the absorbance values after illuminating the samples at 380 nm and 500 nm per cycle. With both compounds there were observed no considerable differences with the absorbance values under green or violet light of the different cycles, showing convincing stability of the photoisomerisation (figure 34AB). The thermal relaxation of the *cis*-isomers in aqueous media was also evaluated, showing a half-life of 80 seconds for *cis*-**83** and of 6.4 minutes for *cis*-**84** (Figure 34 C-D). Those differences in relaxing times are attributable to the chemical structure of their azo-moieties. The

phenylazopyridine **83** includes two different aryl substituents of the azo group: a pyridine with electron withdrawing character (EWG) and a 4-carboxamidophenyl group, with mild electron donating properties (EDG). That all together defines an azocompound with mild push pull properties, which probably are the responsible of this short relaxation half-life^{152, 153}. Concerning compound **84**, its properties were more in accordance to a typical aminoazobenzene family¹⁵², since comprises an azobenzene with an *N*-amide in position 4 and a methoxy group in position 2. The relaxation half-life resulted to be unusually longer probably owing to the presence of two substituents in alpha position respect the azo-bond¹⁶⁰.

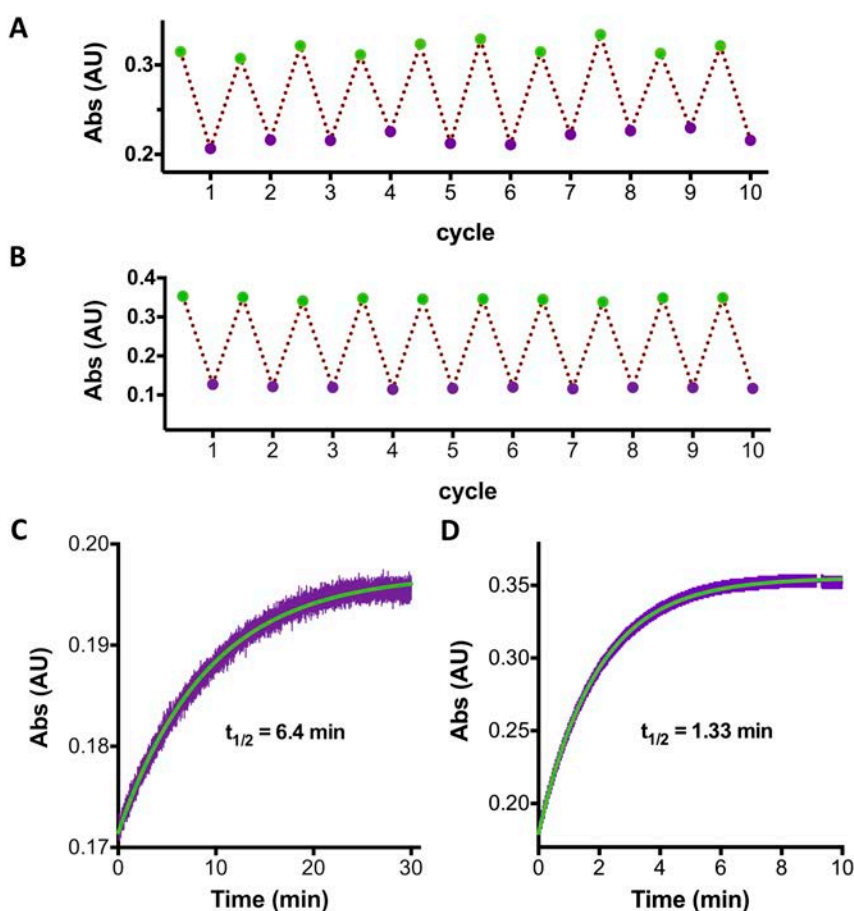


Figure 34: Photochemical properties of compounds **83** and **84** (1): Stability of photoisomerisation of compounds **83** (A) and **84** (B) in a solution 25 μM in DMSO for **83** and 30 μM for in DMSO for **84** after 10 cycles of illumination with light at both 500 nm and 380 nm. Relaxing plot of the *cis*-isomer of compounds **83** (C) and **84** (D) (25 μM in PBS with 1% DMSO for **83** and 30 μM for in PBS with 0.3% DMSO for **84**) after illumination with at and 380 nm.

Despite both compounds showed their π - π^* transition band in a similar area of UV-Vis absorption spectra, several differences in their photoisomerisable properties do exist. Under illumination with 380 nm of wavelength, compound **83** seemed not to reach the maximum photoisomerisation from *trans* to *cis* isomer, since it was possible to observe a remaining small *trans*-isomer π - π^* band. Additionally, we observed that the optimal wavelength for

photoswitching was not 380 nm, but 390 nm, and the fast *cis* isomer relaxation might have influenced to reach a high population of *cis*-isomer at these high concentrations and using a not very intense light source. On the other hand, back isomerisation to *trans*-isomer afforded a very similar close spectrum to that obtained in dark conditions, showing a good isomerisation.

Regarding compound **84**, the illumination at 380 nm induced an abundant population of *cis*-isomer, since the obtained spectra obtained after illuminating at 380 nm displayed a charming *cis* isomer appearance. The fact that the maximum difference of absorption of the *trans*- and *cis* isomers was located in the spectrum around 380 nm and the slower relaxation of the *cis* isomer than that of compound **84**, contributes to achieve a high population of the *cis* isomer under violet illumination. However, when illuminating with 500 nm, the back-isomerisation to *trans*-disposition seemed not to be very efficient, as we could observe the formation of *trans*-isomer π - π^* band but still a part of the *cis* one remained. Nevertheless, considering the possible biological effects, this slower relaxation is not expected to be a problem, since the active *trans*-isomer would be recovered in a relatively short time after the thermal relaxation *cis*-isomer.

Nuclear magnetic resonance (NMR)

An interesting point to take into consideration is the real amount of *cis* and *trans* isomer that is afforded in the photostationary equilibrium under illumination. A reasonable approach previously described¹⁹⁸ is the use of ¹H-NMR under continuous illumination to determine so, since the chemical shifts of *cis* and *trans* configurations of azo-compounds are different and this allow a quantification of the relative amounts of the isomers.

The optimal approach would be to perform this experiment in solution under the same conditions used in biological experiments. However, NMR spectroscopy has some limitations that we have to take in account: solvents need to be deuterated, to not interfere in the proton signals and to adjust the field-frequency lock. Moreover, NMR is a spectroscopic technique with a relatively low sensitivity, which means that we have to use relatively concentrated solutions of the tested compound and accumulate several experiments to obtain a proper signal.

We first tried to perform these experiments with compound **83**. To mimic physiologic conditions we decided to use PBS buffer in deuterium oxide (D₂O) as a solvent. However, the low solubility of the compound was a major drawback, especially with the high concentration needed for this technique. We finally decided to use a mixture of DMSO/PBS solution in D₂O 2:1 to be able to dissolve the compound **83** to obtain a concentration 1 mM, which was

illuminated with 380 nm of wavelength through an optical fibre, which was touching the solution inside the NMR magnet.

Discouragingly, after four acquisitions under 24 minutes of illumination we obtained very low percentage of *cis*-isomer and these results were not qualitatively proportional to those obtained with UV-Vis spectroscopy. A possible explanation for this unusual *cis*-isomer proportion is that the conditions of this experiment are very different to the conditions used for UV-Vis spectroscopy. The sample solution was very concentrated and the intensity of light reaching the solution in our experimental set up was probably not potent enough to compensate the thermal relaxation of the *cis* isomer, which resulted in a very small proportion of *cis*-isomer. Additionally, due to limitations of the technique and the solubility of compound **83**, we were far from the initial idea to mimic biological conditions.

In a last effort, we tried to avoid the difficulties found before by decreasing the concentration of the sample up to 250 μM and using pure DMSO as solvent. Under these conditions, we expected to obtain better isomerisation, since the same intensity of light was supposed to isomerise a higher fraction of *trans*-compound and the absence of water would lower the thermal relaxation rate, helping to accumulate a larger fraction of the *cis*-isomer. Effectively, we obtained a much better isomerisation than with the previous experiment, as it can be observed in *figure 35A*. However, after two hours we had not reached the photostationary equilibrium yet, where the proportion of *cis/trans* isomers is constant.

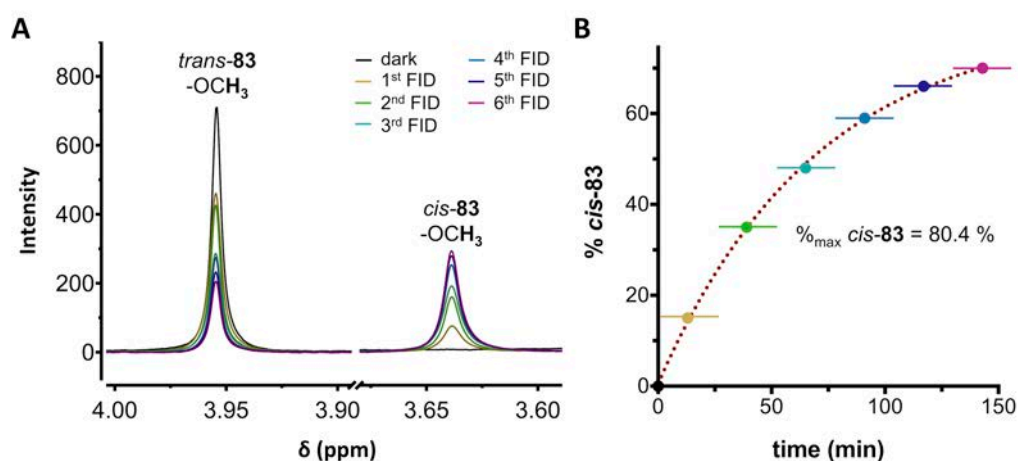


Figure 35: Photoisomerisation assays under ^1H -NMR recording. (A) Fraction of the ^1H NMRs of compound **83** in DMSO corresponding to the methoxy protons of the *trans* and the *cis*-isomer in the dark and after illumination (380 nm) with the corresponding acquisitions every 26 minutes, (B) Plot of the % of *cis-83*, extracted from the integration of methoxy peaks of the ^1H NMR versus time of irradiation. Each point is located in the middle of the corresponding accumulation period of 25 min 41 seconds and they are fitted to an exponential decay function with the corresponding plateau at 80.4%.

Nevertheless, we plotted the percentage of *cis* isomer, extracted from the integration of the methoxy group of compound **83** versus the time of illumination and we fitted an exponential decay function (*figure 35B*), according to a first order equilibrium reaction formula (*experimental part*). The maximum percentage of *cis* that we could obtain in the photostationary equilibrium would be around 80%. Additionally, the use wavelength of 390 nm instead of 380 nm, would lead to a higher percentage of *cis* isomer, as we have already observed with UV-Vis spectroscopy.

Those results are more reliable than the ones obtained previously, but it still constitute an approach far from the UV-Vis spectroscopy conditions, where we had a lower concentration of compound **83** and a direct illumination from a lamp, or much further from a biological environment. Moreover the use of DMSO and the shape of the tube are no advantageous to prompt a rapid diffusion of the recently photoisomerised *cis*-**83**. However, it evidenced that the photoisomerisation occurs without apparent degradation of the azocompounds by just illuminating a sample and, probably, the isomerisation would be more effective by using of lower concentration of the azocompound and a more intense light power.

In-vitro biological evaluation of 83 and 84

Preliminary dose-response curves

X. Rovira, IGF, Montpellier

Compounds **33b**, **83** and **84** were first *in-vitro* evaluated in dark conditions with an inositol phosphate accumulation assay (IP-One) in transfected HEK293 cells with mGlu₄ and G_q-top, which is able to bind all mGlu receptors with a constant concentration of 10 nM of the orthosteric agonist L-AP₄ (**4**). Disappointingly, compound **83** displayed no activity with mGlu₄ and azobenzene **84** was active, but with a lower potency than the diamide **33b**. However, compound **83** is structurally related to MPEP (**12**) or SIB-1757 (**13**) (*figure 36*), since the pyridine-azo-bond-phenyl scaffold is common, or it is structurally and electronically very similar to the pyridine-ethynyl-phenyl scaffold. As MPEP (**12**) and SIB-1757 (**13**) are classical mGlu₅ negative allosteric modulators (NAM)^{69, 75}, it was reasoned that there was a possibility that compound **83** displayed activity on mGlu₅ as a NAM. Therefore **83** and **84** were *in-vitro* evaluated in dark conditions with MPEP (**12**) as control and with the same IP-One assay in mGlu₅ transfected HEK293 cells, which under activation naturally couples to G_q with a constant concentration 300 nM of the orthosteric agonist quisqualate (**2**). From these experiments we discovered that compound **83**, was an excellent mGlu₅ NAM, with potency (IC₅₀) in the

nanomolar range. Due to the excellent properties we gave it the name of alloswitch-1, as the first allosteric modulator able to photoswitch a GPCR function, and we further characterised its activity in mGlu₅ receptor.

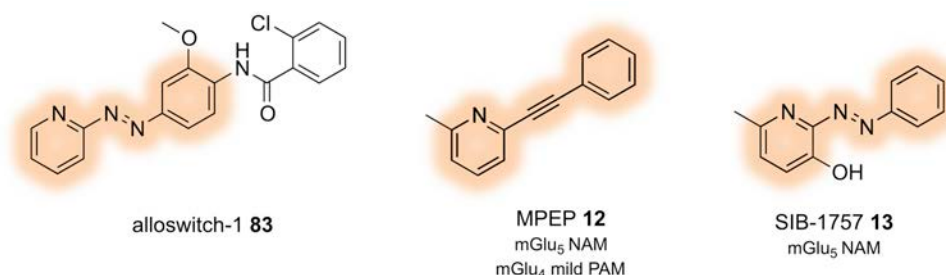


Figure 36: Comparison of the structure of compound **83** with MPEP (**12**) or SIB-1757 (**13**), with a phenylazopyridine in common or a phenylethynylpyridine.

***In-vitro* pharmacological characterisation of compound 83: alloswitch-1**

S. Pittolo, IBEC, Barcelona - IGF, Montpellier

To pharmacologically characterise alloswitch-1 (**83**) and to test whether the photoisomerisation of alloswitch-1 could alter its pharmacological activity, we first performed IP-One assays simultaneously in dark conditions and under illumination with 380 nm of wavelength to generate dose-response curves with the same conditions as mentioned above, in the preliminary IP-One assays with mGlu₅ with a constant concentration of 100 nM of the orthosteric agonist quisqualate (**2**). Those experiments showed a similar potency ($IC_{50}=25\pm 19$ nM) for the non-illuminated curves and the potency for the illuminated ones was 100-fold shifted, achieving a very consistent photoswitch of mGlu₅ activity, not described for a GPCR before.

To give evidence of the reversibility of the mGlu₅ activity photoswitch, we also tested alloswitch-1 (**83**) by monitoring intracellular calcium in real-time individual cell calcium imaging in also HEK293 cells overexpressing mGlu₅ receptor (*figure 37B*). In this experiment, the application of quisqualate in the reading chamber produced intracellular calcium oscillations with a frequency proportional to amount of activated mGlu₅ receptor on the cellular membrane¹⁹⁹. After the following application of alloswitch-1 (**83**), these oscillations were completely inhibited and, under illumination with violet light, the oscillations were recovered, which indicate that mGlu₅ activity was restored. Later on, under illumination with green light, the calcium oscillations were inhibited again, closing a full reversible process that can be repeated several times in a very effective and consistent manner.

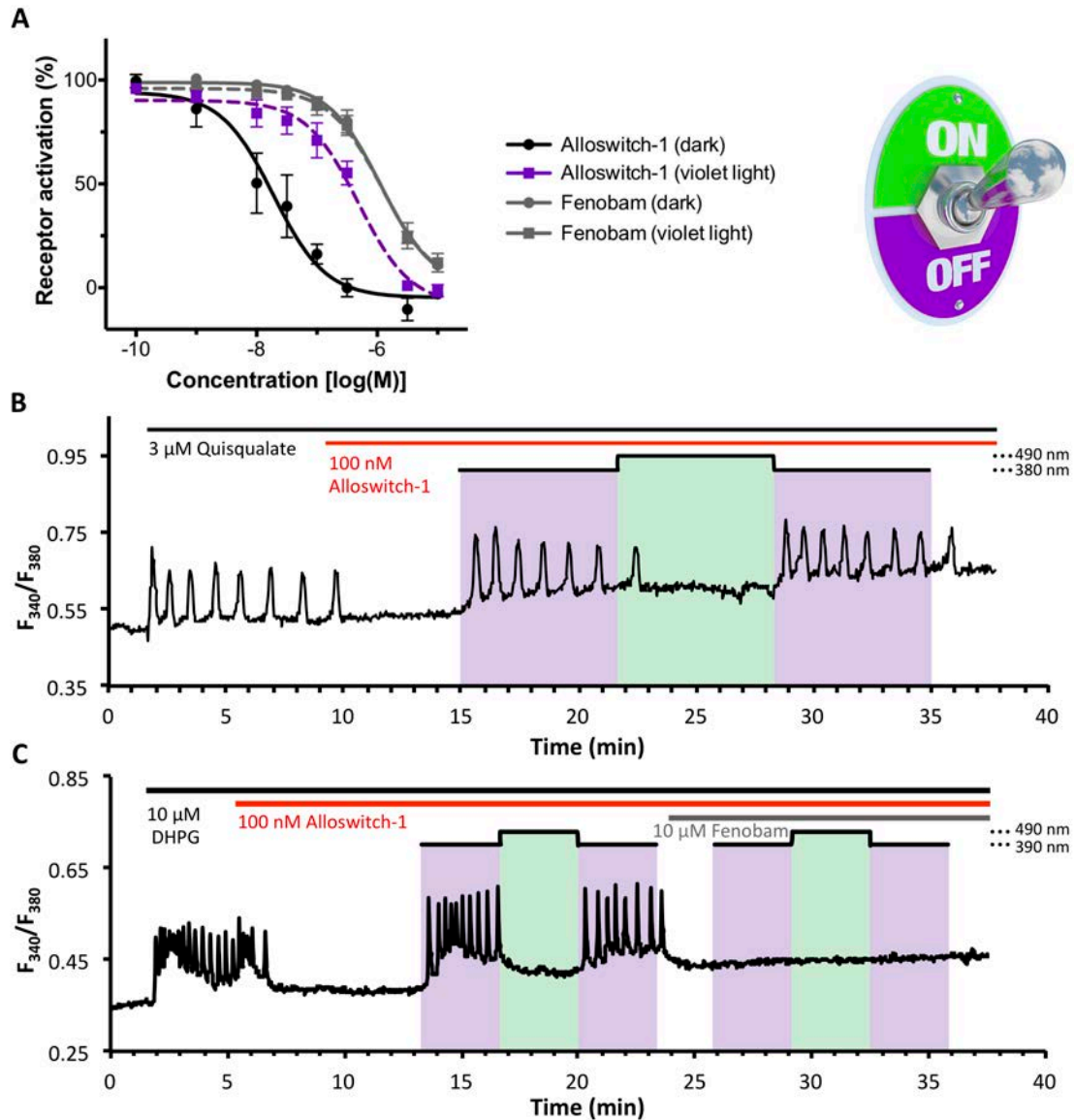


Figure 37: Pharmacological characterisation of alloswitch-1 (**83**). (A) Dose-response curves of alloswitch-1 (**83**) with a constant concentration of quisqualate 100 nM in HEK293 cells over expressing mGlu₅ in different conditions: in dark conditions (rounded spots and black plain line), under illumination at 380 nm of wavelength (square dots and violet dotted line). Fenobam (**14**) was used as an mGlu₅ NAM control (grey lines) in dark conditions (round spots and plain line) and under illumination at 380 nm (square dots and dotted line). (B) Real-time calcium imaging with HEK293 cells overexpressing mGlu₅. Time course of calcium indicator fluorescence ratio (F_{340}/F_{380}) in individual cells treated with agonist (3 μ M quisqualate) and alloswitch-1 (**83**). Boxes indicate violet or green illumination. (C) Real-time calcium imaging with rat cortical astrocytes. Time course of calcium indicator fluorescence ratio (F_{340}/F_{380}) in individual cells treated with agonist (10 μ M DHPG), alloswitch-1 (**83**) and fenobam (**14**). Boxes indicate violet or green illumination.

We also performed a similar assay with rat cortical astrocyte cultures, which natively express mGlu₅ receptor (*figure 37C*). The results were very similar and a posterior fenobam (**14**) application lead to a light-insensitive inhibition of the intracellular calcium oscillations,

indicating that those oscillations were attributable to mGlu₅ receptor and the photoswitching to alloswitch-1 (**83**), which competed with fenobam (**14**) in the mGlu₅ allosteric site. Moreover, a control experiment with vehicle showed no difference in the oscillation frequency between the green and violet illumination cycles (not shown).

Finally, we also studied the selectivity of alloswitch-1 (**83**) over the eight mGlu subtypes at a single dose of 5 μ M of the azo-derivative. We used the IP-One assay in HEK293 cell overexpressing the corresponding receptors with different concentrations of orthosteric agonists (*experimental part*), which were selected depending on the mGlu subtype and the desired effect to measure; either a potentiation (PAM) or an inhibition (NAM) of its activity (*figure 38A and 38B* respectively). The corresponding results showed that alloswitch-1 (**83**) was selective over the eight mGlu subtypes, showing only a clear mGlu₅ NAM activity in mGlu₅ receptor.

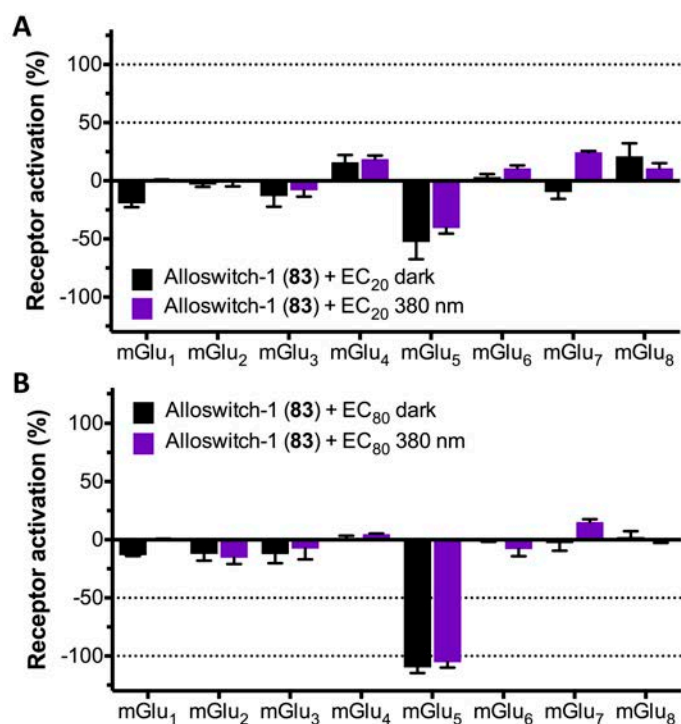


figure 38: Selectivity profile of alloswitch-1 (**83**) among all the mGlu subtypes as PAM (A) and as NAM (B) in dark conditions (black bars) and under 380-nm-illumination (violet bars). Data represent normalized receptor activation for at least 3 independent experiments, done in duplicate, and are represented as mean \pm SEM.

Additionally, an activity study was performed in an external laboratory (*Cerep*, France) involving an *in vitro* radioligand-binding assay on a library of 55 recombinant human GPCRs, ion channels, transporters, and other receptors with 10 μ M of alloswitch-1 (**83**). Compound binding was calculated as a percentage inhibition of the binding of a radioactively labelled ligand specific for each target. Results showed an inhibition or activation higher than 50% were

considered significant and significant inhibition was found for alloswitch-1 (**83**) on 5-HT_{1A}, 5-HT_{2B}, A_{2A}, and A₃ receptors (76.8, 87.5, 61.2, and 69.1% inhibition respectively). Regarding of this lack of selectivity for these few compounds, the observed inhibition was not saturating, which decreased its relevance to a second level. Therefore, we considered the selectivity of alloswitch-1 satisfactory enough to study further its biological activity in *in-vivo* models.

***In-vitro* pharmacological characterisation of compound 84: optogluram**

Compound **84**, despite displaying an mGlu₄ PAM activity with a lower potency compared to VU0415374 (**33b**)⁹⁶ it was also a good candidate to be a suitable photoswitchable positive allosteric modulator for mGlu₄. Therefore, we gave it the name of optogluram and performed further pharmacological characterisation.

In-vitro assays

We first generated dose-response curves with illumination using a IP-One assays simultaneously in dark conditions and under illumination with 380 nm in the same conditions than those used for alloswitch-1 (**83**), but with HEK293 cells overexpressing mGlu₄ and a chimeric G_q protein, which binds all the mGlu receptors and a constant concentration of 3 nM of the group-III-selective agonist L-AP4 (**4**) (*figure 42A*). In dark conditions, we obtained an EC₅₀ of 385±41 nM, much lower than that we obtained from preliminary dose-response curves with no illumination. A possible explanation for this difference in potency values may be the stability of the *cis* isomer in dark conditions if the preliminary are not performed with a suitable protection from the light. Moreover, in UV-Vis spectra, we observed under green light a reduced recovery of the *trans*-isomer, which would mean that visible light partially isomerised some *trans*-optogluram to the *cis* isomer, and the recently isomerised fraction will be relaxed to the *trans*-state thermally.

Additionally, despite the outstanding isomerisation observed from UV-Vis spectra when illuminating at 380 nm, we obtained a photoinduced potency shift^a in cell assay is only of 3.5 fold, lower compared to what we expected. There are two plausible explanations for this issue: a possible PAM activity of the *cis*-isomer with lower potency; or a deficiency of light arriving to the cell environment after crossing the plastic bottom of the plate, which can be partially opaque for 380-nm-light (*experimental part*).

We also studied the selectivity of optogluram (**84**) over the eight mGlu subtypes at a single dose of 30 µM of the azo-derivative and with different concentrations of agonists, depending

^a Photoinduced potency shift corresponds to the ratio of the IC₅₀ in dark conditions and under illumination.

on the mGlu subtype and the desired effect to measure: PAM or NAM activity (figure 39B-C respectively). We used the IP-One assay in HEK293 cell overexpressing the corresponding receptors, like selectivity experiments performed for alloswitch-1 (83). Optogluram (84) was found to be selective among all the mGlu receptors, with the exception of mGlu₆ and mGlu₈, in which some PAM activity was found at 30 μM of compound.

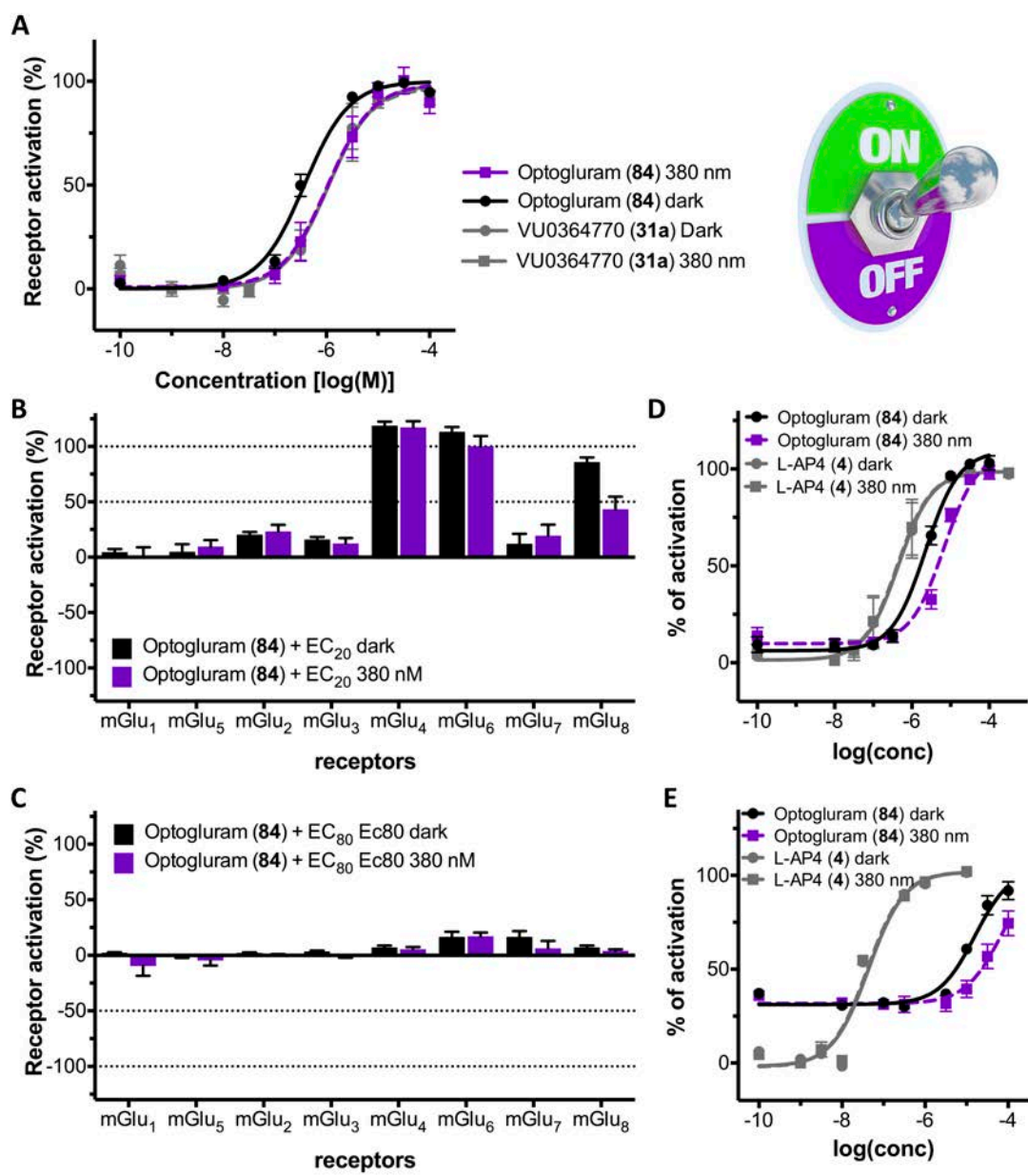


Figure 39: Pharmacological characterisation of optogluram (84). (A) Dose-response curves of optogluram (84) with a constant concentration of L-AP4 (4) 3 nM in HEK293 cells over expressing mGlu₄ in different conditions: in dark conditions (rounded spots and black plain line), under illumination at 390 nm of wavelength (square dots and violet dotted line). VU0364770 (31a) was used as an mGlu₄ PAM control (grey lines) in dark conditions (round spots and plain line) and under illumination at 390 nm (square dots and dotted line). (B) Selectivity profile of optogluram (84) among all the mGlu subtypes as PAM and (C) as NAM in dark conditions (black bars) and under 380-nm-illumination (violet bars). (D) Dose-response curves with of optogluram (84) in dark and 380-nm-illumination in HEK293 cells

overexpressing mGlu₆ or (E) mGlu₈. In both cases a constant concentration of L-AP4 (**4**) 100 nM (D) or 10 nM (E) was used and L-AP4 (**4**) was used as an agonist control. Data represent normalized receptor activation for at least 3 independent experiments, done in duplicate, and are represented as mean ± SEM.

To quantify the potency related to those PAM activities, we generated dose-response curves from data extracted from new IP-One assays with HEK293 cells overexpressing mGlu₆ or mGlu₈ and employing low concentrations of the orthosteric agonist L-AP₄ (**4**). Optogluram resulted to be PAM of each of those receptors with an EC₅₀ = 2.3 μM for mGlu₆ and EC₅₀ = 12.4 μM for mGlu₈ (*figure 39E-F*). Concerning mGlu₈, the potency values were shifted 32-fold, which does not constitute an ideal selectivity, but it is close to the 100-fold threshold, considered for good selectivity. Regarding mGlu₆ potency values shifted only 6-fold, which is far from to the selectivity threshold. However, expression of mGlu₆ is limited to polar cells in retina, whilst mGlu₄ is widely distributed through the CNS. Due to the different location of these receptor subtypes, this lack of selectivity should not be a problem for animal testing, and even for clinical trials. In all the cases this molecule will constitute an excellent starting point for medicinal chemistry optimization of the selectivity among the different mGlu receptor subtypes.

In-silico characterisation of 83

J. A. Dalton, INC-UAB, Bellaterra – Barcelona

In order to investigate *in silico* the NAM functionality in mGlu₅ receptor, the crystal structure (PDB id 4OO9) was re-constructed with MODELLER²⁰⁰ CHIMERA²⁰¹ to afford the groups and amino acids of the wild-type (wt) receptor. As a control, we re-docked the co-crystallized NAM mavoglurant back into the empty allosteric binding pocket of the TM domain using Autodock-4.2²⁰², seeking to reproduce the crystal binding pose (*figure 40A*). In particular, the acetylene bond of mavoglurant traverses a narrow region in the pocket between P655 on TM3 and S809 on TM7, enabling the presence of a co-crystallized water molecule (which forms a three-way H-bonding network with Y659, T781 and S809). We took this result as a validation of our docking protocol, which we then extended to other NAMs.

We therefore docked classic mGlu₅ NAM MPEP (**12**) and the active isomer of alloswitch-1 into mGlu₅ with Autodock-4.2 to compare its binding mode with that of mavoglurant. As a result, MPEP docks in a very similar binding mode to mavoglurant, with its methylated pyridine ring occupying the same position as methylated benzene of mavoglurant (*figure 40B*) in agreement with another recent study²⁰³. Concerning *trans*-alloswitch-1, the orientation of its pyridine ring adopts the same orientation as that one of MPEP, binding deep in the allosteric site. Both

MPEP's acetylene bond and the azo bond and acetylene bond transverses the narrow region at the bottom of the allosteric pocket between P655 on TM3 and S809 and TM7 like mavoglurant. Furthermore, like mavoglurant, S809 on TM7 is observed to make an H-bond with MPEP but, in this case, S809 acts as a proton donor to the nucleophilic nitrogen on the pyridine ring of MPEP. This H-bonding does not affect the rotameric position of the side chain, which remains unchanged with respect to the crystal structure, but involves a rotation of its hydroxyl group. This interaction was not observed for *trans*-alloswitch-1, but MD simulations over 100 ns revealed the formation of this H-bond between *alloswitch-1* and S809, as well as, a stabilisation the co-crystallized water molecule at the bottom of the allosteric pocket³², in the same manner that MPEP does and which is related to NAM functionality.

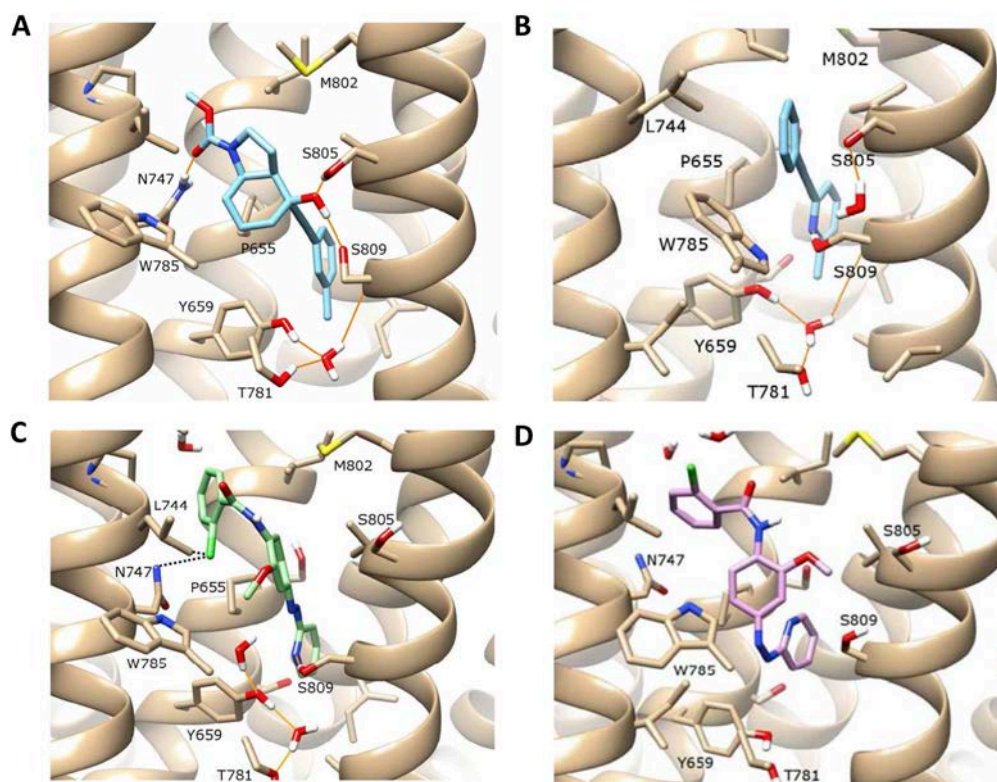


Figure 40: (A) Docking solution of mavoglurant (in blue) (B) Docking solution of MPEP (in blue) after 130 ns of MD simulation. (C) Docking solution of MPEP (in green) after 130 ns of MD simulation. (D) Docking solution of *cis*-alloswitch-1 (in violet) in mGlu₅ (in beige) after 200 ns of MD (0-100 ns in *trans*, 100-200 ns photoexcited in *cis*). All dockings are in the complete wt structure of mGlu₅ (in beige). All protein-ligand H- bonds originally identified in the crystal structure (PDB id: 4O09) were reformed during docking (orange lines, involving residues N747, S805, S809). For visualisation purposes, the backbone of TM6 is not shown, however the side chains of residues W785 and T781 on TM6 are included (in the foreground), with the latter making an H-bond with a co-crystallized water molecule. Regarding helix position, TM5 is foreground left, TM7 is foreground right. In the background, TM4 is left, TM3 is central and TM2 is right.

We next docked the *cis* isomer of alloswitch-1 into the original crystal structure of mGlu₅ with Autodock-4.2. Although the docking score of the top-ranked solution is not as favourable as previously docked *trans* isomers, the non-active *cis*-photoisomer still docks respectably in the allosteric site, suggesting binding to the receptor is possible. However, the binding mode is very different to the previous ones, since the pyridine ring is no longer at the bottom of the cavity like pyridines of alloswitch-1 and MPEP. Additionally, during a 100 ns MD simulation with the azo group maintained in *cis* disposition, the ligand experienced considerable positional fluctuation, moving vertically and rocking in the allosteric pocket, particularly during the first 10 ns of the simulation and the allosteric pocket experiences structural disruption. In particular, the co-crystallized water molecule³² at the bottom of the allosteric pocket was lost during this simulation and not rebound. As such, the water-mediated H-bonding network connecting TM3 (Y659), TM6 (T781) and TM7 (S809) is broken and not re-formed, inducing an unfavourable state. Additionally, in two MD simulations, with alloswitch-1 in *cis*-amide and *trans*-amide conformations respectively, changing the azo from *trans* to *cis* disposition, we obtain practically the same results that those explained above.

Taken together, these results indicate the photoexcited protein-ligand complex is possible and the photoisomerisation of alloswitch-1 might occur inside the allosteric pocket of mGlu₅. However, this isomerisation alters the ligand's binding mode, reduces its binding affinity and stability, and disrupts receptor conformation, particularly with regard to the co-bound water molecule in the allosteric pocket that has been suggested as important for stabilizing the inactive NAM-bound state³², probably leading to an unbinding of the compound.

In-vivo biological evaluation of 83 and 84

In-vivo pharmacological characterisation of compound 83: alloswitch-1

We also tested alloswitch-1 in living animals to evaluate light-dependent behavioural responses. We used three different models, including fish, amphibian and mammals.

Zebrafish locomotion assay

X. Rovira, IGF, Montpellier

In one of these models, the natatorial motility of wild-type TL zebrafish larvae (*danio rerio*, figure 41A) was measured in E3 medium containing vehicle or (**83**) 10 µM alloswitch-1 with two different protocols: first, in dark conditions after application of the compounds and, after that, applying cycles of 1 minute with continuous illumination at 380 nm and 1 minute in dark conditions. The motility of the treated larvae with alloswitch-1 was clearly decreased in dark

conditions with respect to the ones treated with vehicle in the first protocol (*figure 41B*). In the second protocol, the locomotion of the alloswitch-1-treated zebrafish was still inhibited in the dark but, under illumination, those larvae treated with alloswitch-1 not only recovered the level of motility of the non-treated, but also increased its motility. Consecutive dark conditions restored the low-motility level of the treated ones with compound **83** and successive cycles afforded the same results, as shown in *figure 41C*. This model reproduces *in-vivo* the observed behaviour in calcium imaging, since on/off photoswitching of a biological function is clearly controlled with light and in both cases an over-activation of the receptor is achieved after inhibiting it, probably due to a sudden receptor reactivation upon NAM withdrawal with light. In any case, the over-activations observed might be beneficial to obtain a more precise control on the activation or inactivation with light of native mGlu₅ in living systems.

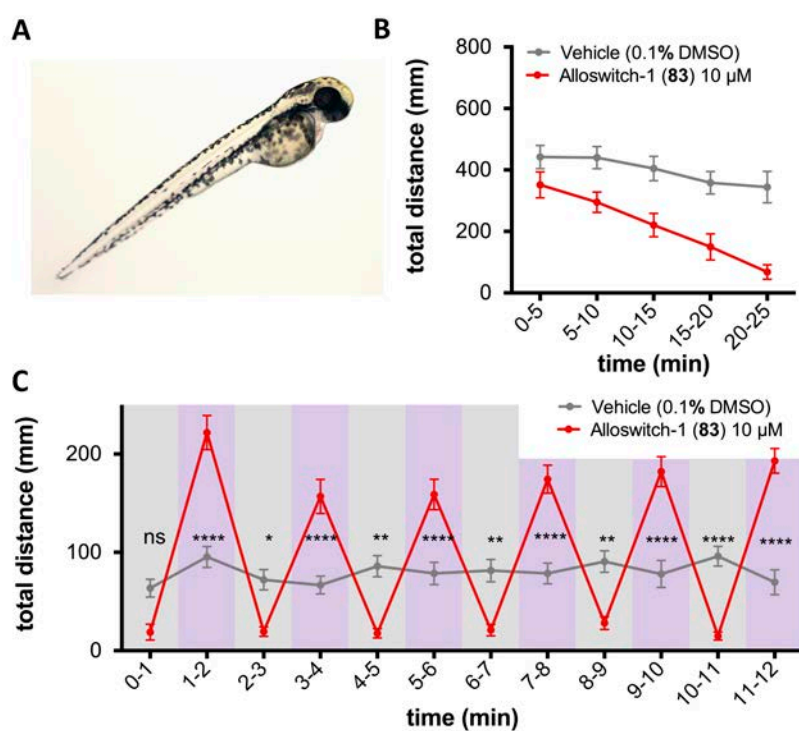


Figure 41: Zebrafish larvae locomotion can be efficiently photocontrolled with alloswitch-1 (**83**). (A) Zebrafish larva. (B) Integration of the total accumulated free-swimming distance in the dark for every 5 minutes after application of 10 μM concentration of the control solutions. Alloswitch-1-treated zebrafish clearly decreased its locomotion respect vehicle-treated ones. (C) Integration of the total accumulated free-swimming distance in the dark for every minute applying cycles of dark conditions/violet illumination every minute to evaluate the effect of light. Alloswitch-1 at 10 μM inhibits animal motility in the dark (grey background), whereas under violet light (violet background) zebrafish larvae treated with alloswitch-1 experience an increase of their normal motility. Values correspond to the mean and the SEM of the behaviour of 17 animals minimum. Statistical comparisons between alloswitch-1 and Vehicle are calculated using analysis of variance: two-way (compound, time) ANOVA with time as repeated measure and including the Šidák correction for multiple testing (* $p < 0.05$, ** $p < 0.01$, *** $p < 0.001$, **** $p < 0.0001$).

Tadpole locomotion assay

K. Eckelt, IBEC, Barcelona

In the second used model, the natatorial behaviour of *Xenopus tropicalis* tadpoles was evaluated in a similar manner than for zebrafish, with 25 μ M of alloswitch-1 (**83**) or the corresponding vehicle in the medium of the tadpoles (figure 42A). In this case, we applied cycles of violet and green light to the animals, obtaining the main difference between treated tadpoles with **83** and control non-treated tadpoles under violet light, where control ones increased dramatically their motility, whereas alloswitch-1 abolished the movement of the treated ones. Under green light illumination, the difference was not significant and was similar to the effect of fenobam (**14**), in the basal level (figure 42B).

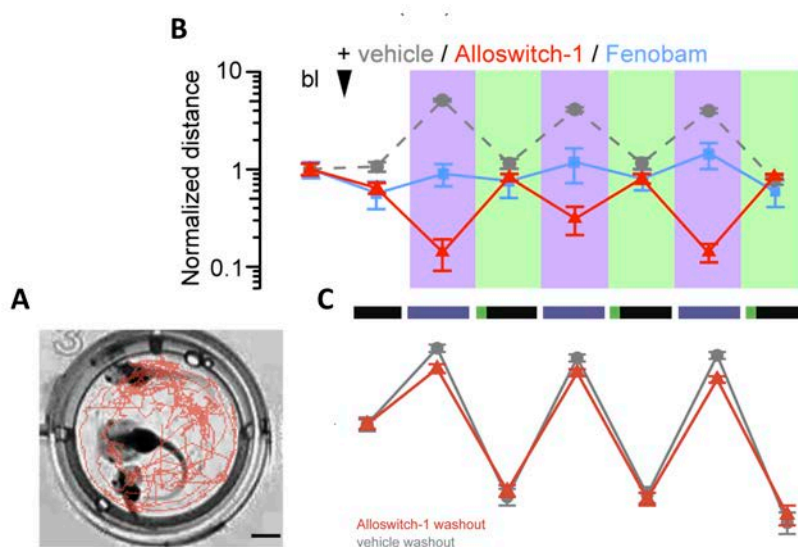


Figure 42: *Xenopus Tropicalis* tadpoles locomotion can be efficiently photocontrolled with alloswitch-1 (**83**). (A) Overlay image showing *Xenopus Tropicalis* tadpoles and their trajectories (red) during behavioural experiment. Scale bar, 5 mm. (B) Quantification of tadpole motility as normalized distance before (basal) and after treatment (arrowhead; 25 μ M alloswitch-1, 100 μ M fenobam (**14**), vehicle; n = 20, 13 and 33 groups, respectively) and in different light conditions after treatment (dark, grey box; violet or green light, coloured boxes). Values represent mean \pm SEM from at least three independent experiments (C) experiment repeated after 24 hours of washout of Alloswitch-1 (25 μ M) or vehicle. Data are represented as mean \pm SEM. Alloswitch-1 washout: red line and triangles, n=12; vehicle washout: grey line and circles, n=12.

However, but the effect under 380-nm-light was clear and reversible upon several cycles. This could be also related to the faster calcium oscillations observed in cultured cells upon sudden unblocking of mGlu₅. Additionally, we repeated the behavioural studies 24 h after washing out alloswitch-1 to determine any possible irreversible effects in the animals (figure 42C). Remarkably, the animals previously treated with alloswitch-1 or those treated with vehicle

showed no behavioural differences and we did not observe any behavioural abnormalities or other signs of toxicity, evidencing that alloswitch-1 is a safe compound for *in-vivo* assays.

Von Frey pain assay in mice

C. Zussy, IGF, Montpellier

The third used model consists in a nociceptive assay based in Von Frey assay in mice²⁰⁴. Thus, an injection of complete Freund's adjuvant (CFA) is applied in the mouse's hind paw to produce an inflammation. Next poking with Von Frey hairs produce the reaction of the animal, in terms of a retractive movement, the elongation of such was measured to evaluate the pain feeling. Alloswitch-1 was directly injected in each of the two amygdalae of the mouse, where mGlu₅ is expressed and which is known to be involved pain sensitivity. These mice, also had an optical fibre in their amygdalae implanted (*figure 43A*), coupled to a source of light that can switch from green light (505 nm) to violet light (385 nm). Injection of 5 μ M of alloswitch-1 (**83**) decreased the pain sensitivity of the mice to the levels of before the inflammation, but upon illumination with violet light, the animals turn out to be sensitive to pain again (*figure 43B*). This effect was reverted with green light and was completely reversible and reproducible upon several cycles with a high statistical significance. However, the over-activations under violet illumination observed in single-cell calcium imaging or in zebrafish locomotion assays were not observed in the present assay. In any case, these results were parallel to cell-based and *in-vivo* with zebrafish and tadpoles, confirming a potent pharmacological effect of alloswitch-1 (**83**) that can be reversibly reverted with light with high precision in living systems.

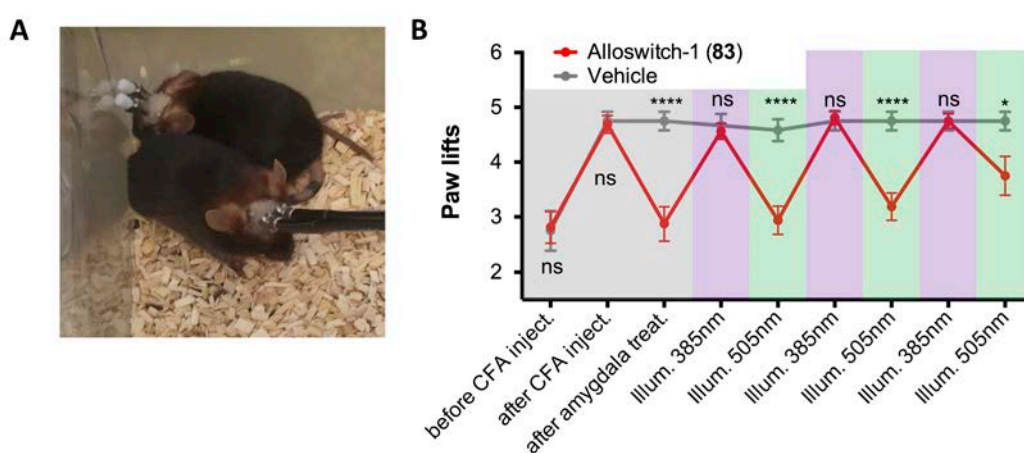


Figure 43: Alloswitch-1 (**83**) efficiently decreased pain sensitivity in an *in-vivo* noxious Von Frey test and enable an on/off control of this sensitivity with light. (A) mice with a cannula and an optic fibre introduced the brain to inject compound **83** and illuminate directly the two amygdalae. (B) Pain sensitivity of the mice when their hind paw was poked with a noxious Von Frey filament before and after inducing inflammation (CFA injection) and after

injection of 5 μM of alloswitch-1 and upon illumination cycles. Statistical comparisons between alloswitch-1 and Vehicle are calculated using analysis of variance: two-way (compound, time) ANOVA with time as repeated measure and including the Šidák correction for multiple testing (* $p < 0.05$, ** $p < 0.01$, *** $p < 0.001$, **** $p < 0.0001$).

***In-vivo* pharmacological characterisation of Compound 84: optogluram**

We also tested optogluram (**84**) in living animals to evaluate light-dependent behavioural responses. We used two of models used for alloswitch-1 (**83**): zebrafish locomotion assay and a pain assay in mammals.

Zebrafish locomotion assay

X. Rovira, IGF, Montpellier

The natatorial motility of wild-type TL zebrafish (*danio rerio*) larvae was measured in a medium with optogluram (**84**) 30 μM in the same conditions than those used for alloswitch-1 (**83**), as preliminary experiments. However, the motility of the treated larvae with optogluram was not decreased in dark conditions with respect to the ones treated with vehicle, as alloswitch-1 did. However, the same treatment with VU0415375 (**32b**) induced an inhibition of zebrafish locomotion. The lack of efficacy of compound **84** might be solved with an increase of dose, since we proved in cell-based assays that compound **32b** is more potent than optogluram (*figure 44B*). In addition, we have to take into account that in this *in-vivo* experiments, the distribution and brain penetration of the two compounds might be different, and these can lead to different behavioural responses.

Nevertheless, we performed the cycles of illumination with the optogluram (**84**) treated larvae. In the first cycles in dark conditions we could not observe an inhibition of the motility of the zebrafish, respect the vehicle-treated ones. However, under violet illumination, these larvae also showed an increase of motility, higher than vehicle treated animals and in some cycles with considerable statistical significance. Successive dark cycles reversibly restored the low-motility level (*figure 44C*). Interestingly, latter dark cycles showed an inhibition of the locomotion of optogluram-treated animals, nor observed before, with considerable statistical significance in 5th dark cycle. As shown in *figure 44C* these effects seem to be related to the vehicle-treated compounds, that cycle-after-cycle increase their locomotion, probably due to a raise of the temperature after the illumination cycles. Otherwise, optogluram treated animals in dark conditions did not show this increase of motility, probably due to the pharmacological effect of *trans*-optogluram. In any case, the preliminary data shown is not sufficient to confirm an *in-vivo* effect of optogluram in zebrafish larvae at 30 μM . More experiments and probably higher doses of optogluram (**84**) will be needed need before drawing conclusions.

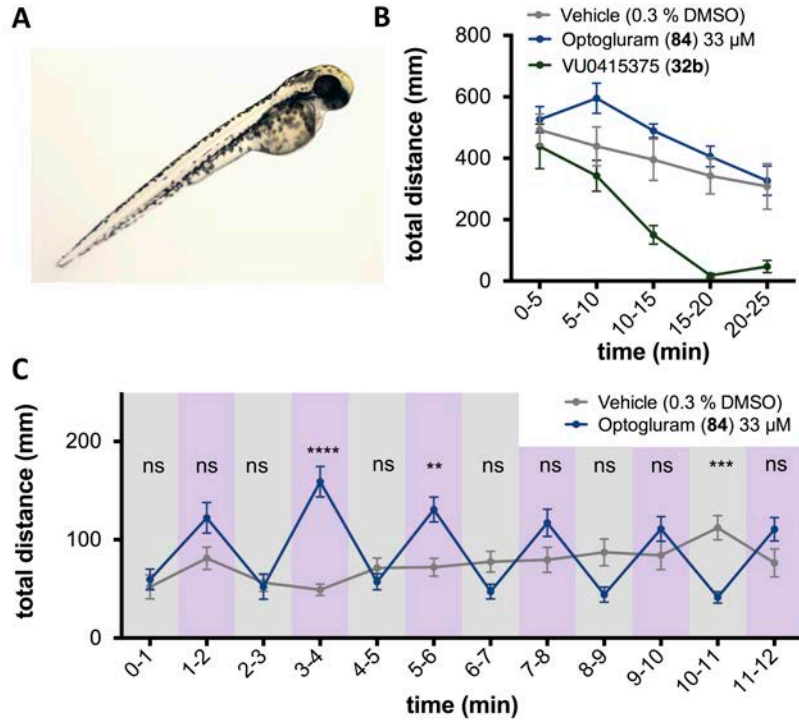


Figure 44: Zebrafish larvae locomotion can be photocontrolled with alloswitch-1 (**84**). (A) Zebrafish larva. (B) Integration of the total accumulated free-swimming distance in the dark for every 5 minutes after application of 30 μM concentration of the control solutions. Optoglutram treated zebrafish did not decrease locomotion respect vehicle-treated ones, but VU041536 did. (C) Integration of the total accumulated free-swimming distance in the dark for every minute applying cycles of dark conditions/violet illumination every minute to evaluate the effect of light. After three dark/light, it can be observed a tendency of inhibition of the motility of optoglutram-treated animals in the dark (grey background), whereas under violet light (violet background) zebrafish larvae treated with optoglutram experience an increase of their normal motility. Values correspond to the mean and the SEM of the behaviour of 6 animals minimum. Statistical comparisons between optoglutram and Vehicle are calculated using analysis of variance: two-way (compound, time) ANOVA with time as repeated measure and including the Šidák correction for multiple testing (* $p < 0.05$, ** $p < 0.01$, *** $p < 0.001$, **** $p < 0.0001$).

Von Frey pain assay in mice

C. Zussy, IGF, Montpellier

This second model used to evaluate optoglutram (**84**) was the same nociceptive assay based in Von Frey assay in mice that we used with alloswitch-1 (**83**)²⁰⁴, consisting in the production of an inflammation in the hind paw of a mice and successive poking produce the reaction of the animal. Like alloswitch-1, optoglutram was directly injected in each of the two amygdalae of the mouse, where mGlu₄ is also expressed and also had implanted an optical fibre in their amygdalae, coupled to the same source of light that can switch from green light (505 nm) to violet light (385 nm). Injection of 30 μM of optoglutram (**84**) decreased the pain sensitivity of the mice to the levels of before the inflammation and upon illumination with violet light, the

animals turn out to be sensitive to pain again, like for alloswitch-1, with no over-activation of the pain sensitivity. This effect was also reverted with green light and was completely reversible and reproducible upon several cycles with high statistical significance, constituting an excellent tool for high-precision control of the pain sensitivity with light. Additionally, as observed for alloswitch-1.

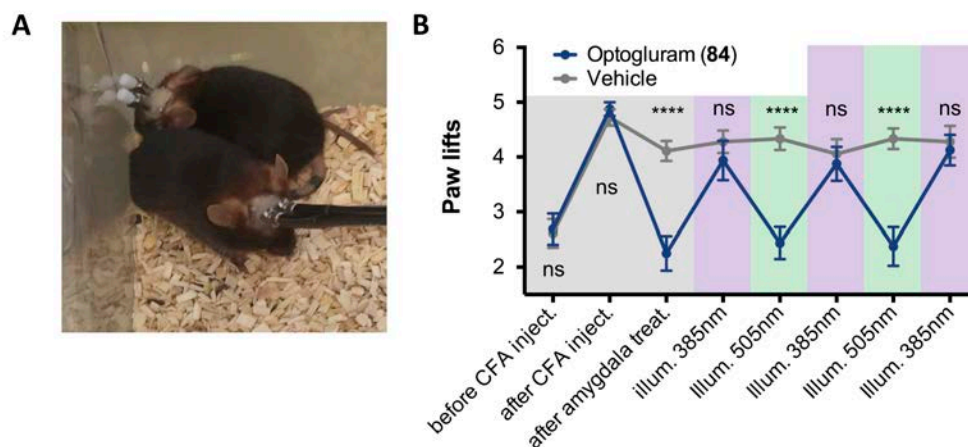


Figure 45: Optogluram (**84**) efficiently decreased pain sensitivity in an *in-vivo* noxious Von Frey test and enable an on/off control of this sensitivity with light. (A) mice with a cannula and an optic fibre introduced the brain to inject compound **84** and illuminate directly the two amygdalae. (B) Pain sensitivity of the mice when their hind paw was poked with a noxious Von Frey filament before and after inducing inflammation (CFA injection) and after injection of 30 μ M of optogluram and upon illumination cycles. Statistical comparisons between optogluram and Vehicle are calculated using analysis of variance: two-way (compound, time) ANOVA with time as repeated measure and including the Šidák correction for multiple testing (* $p < 0.05$, ** $p < 0.01$, *** $p < 0.001$, **** $p < 0.0001$).

Conclusions

The results indicate that used azo-replacement approach was successfully. VU0416374 (**33b**) was an excellent candidate for engineering new mGlu allosteric modulators by replacing an amide with an azo-bond. Additionally, we discovered structural similarities between mGlu₄ PAMs and mGlu₅ NAMs and that azolization might be also successful when replacing acetylenes with azo-bonds.

Alloswitch-1 (**83**) is a potent and selective negative allosteric modulator of mGlu₅ and its activity can be switched on and off by means of different wavelength illumination. It constitutes the first allosteric modulator that bears photoswitchable properties, maintaining its drug-like properties.

Alloswitch-1 (**83**) reversibly photoisomerises in dilution and this is translated in cultured cells to a photoswitch of the functional activity of both transfected and native mGlu₅.

In-silico modelling showed a reasonable binding mode of trans-alloswitch-1 on, in similar poses to other mGlu₅ NAMs and it is possible that the photoisomerisation occurs inside allosteric binding site but affording an unfavourable conformation that might lead to the unbinding of alloswitch-1.

Alloswitch-1 (**83**) enables the control of animal natatorial motility of zebrafish embryo and *Xenopus Tropicalis* tadpoles with light and also control the sensitivity to pain of mice with direct illumination in the amygdala.

Optogluram (**84**) is a positive allosteric modulator of mGlu₄, which activity can also be switched on and off with different wavelengths of light. It also reversibly photoisomerises *in vitro*, it permits the control of animal natatorial motility of zebrafish embryo and also control the sensitivity to pain of mice with direct illumination in the amygdala.

Chapter 2: alloswitch-1 & optogluram non-photoswitchable bioisosters and the confirmation of the double molecular switch

On the first chapter of the present thesis, we showed the design and synthesis two photoisomerisable allosteric modulator of mGlu₄ and mGlu₅ (alloswitch-1 (**83**) and optogluram (**84**)) based on the structure of a known positive allosteric modulator of mGlu₄. In the present chapter, we will present the design, synthesis and characterisation of two non-photoswitchable bioisosteres of alloswitch-1 (**83**) and optogluram (**84**), using a similar design to that described in chapter one, confirming a double molecular switch.

Papers related to this chapter:

Xavier Gómez-Santacana, Xavier Rovira, James A. Dalton, Cyril Goudet, Jean-Pilippe Pin, Pau Gorostiza, Jesús Giraldo and Amadeu Llebaria, "A double effect molecular switch leads to a novel potent negative allosteric modulator of metabotropic glutamate receptor 5", *Medicinal Chemistry Communications*, **2014**, 5, 1548-1554

Design of alloswitch-1 and optogluram bioisosters

In the previous chapter we have described a molecular design approach involving the replacement of the amide bridging the central ring and the pyridine ring of the mGlu₄ PAM VU0415374 (**33b**)⁹⁶ by an azo-bond. The new resulting molecule (alloswitch-1) turned out to be an mGlu₅ NAM. Interestingly, the mGlu₅ NAM SIB-1757 (**13**)² contains the same phenylazopyridine moiety, and other mGlu₅ NAMs contain a structurally similar phenylethynylpyridine, such as MPEP (**12**)^{69, 75} (*figure 36*). The ethynediyl moiety shares with *trans* azo-bond similar geometry, rigidity and electronic delocalisation.

Therefore, the replacement of the amide of VU0415374 (**33b**) or the azo-bond of alloswitch-1 (**83**) for an ethynyl bond would lead to a non-photoswitchable mGlu₅ NAM, which would be also a bioisoster of alloswitch-1 (**83**). Following this theory, if the same procedure is done with inter-phenyl amide of VU0415374 (**33b**) or the azo-bond of optogluram (**84**), we will afford a non-photoswitchable mGlu₄ PAM (*figure 46*).

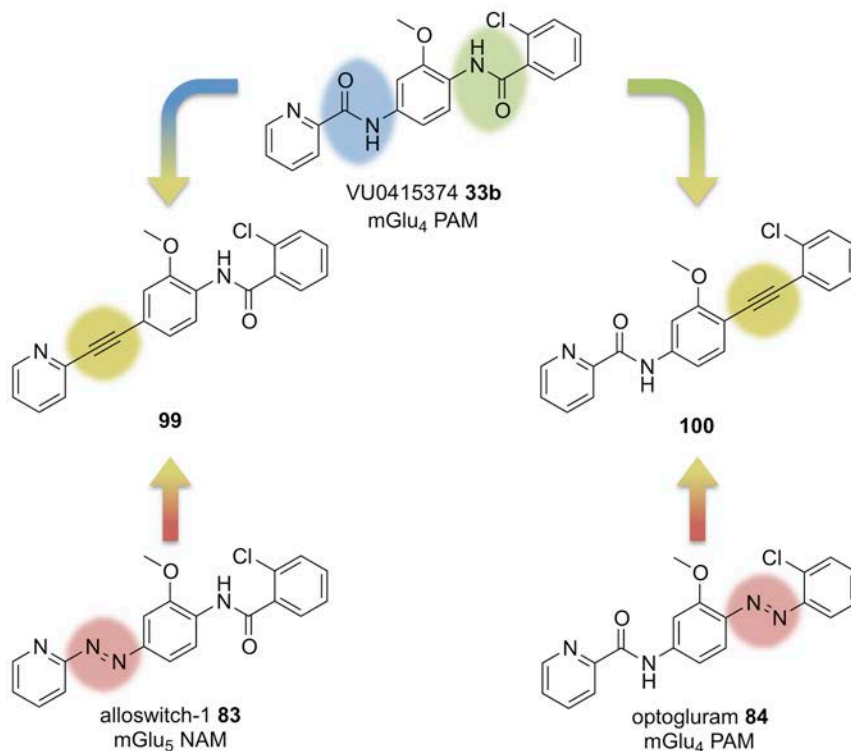
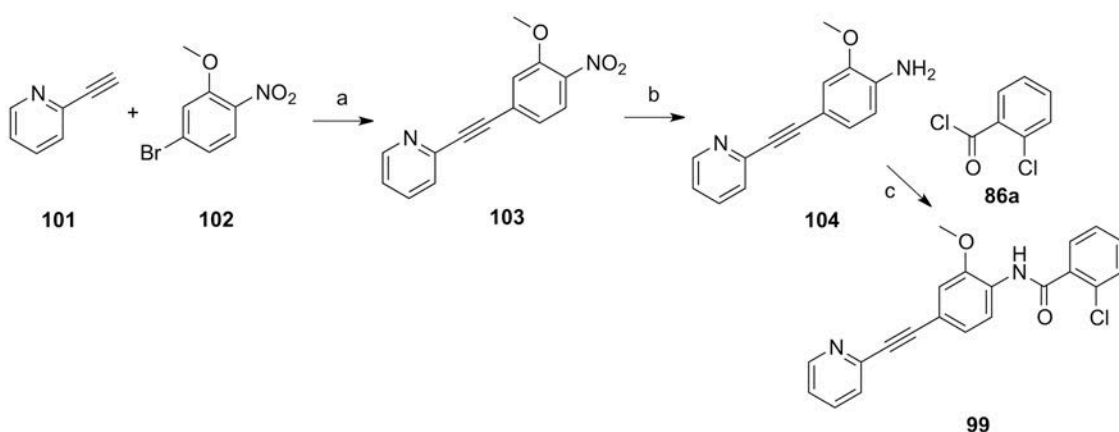


Figure 46: Design of compound **99** and **100**, as bioisosters of VU0415374 (**32b**), alloswitch-1 (**83**) and optogluram (**84**).

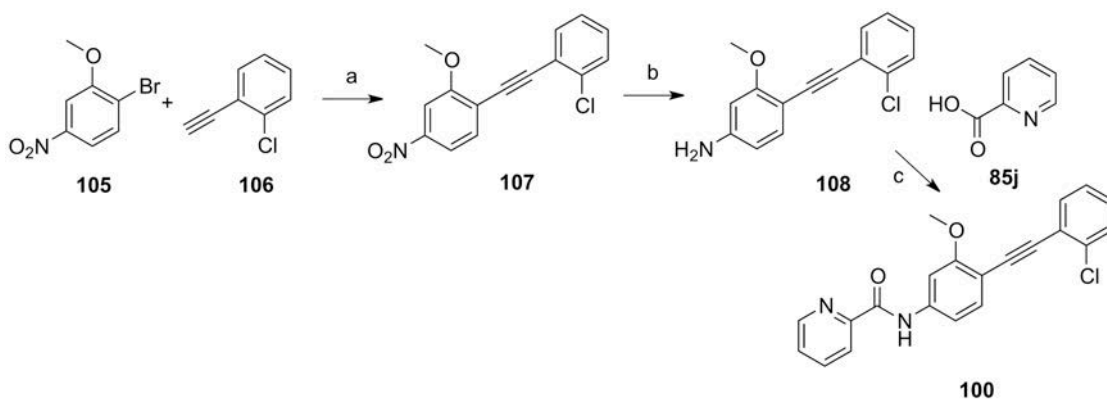
Synthesis of compounds **99** and **100**

Compound **99** was synthesised following the synthetic strategies depicted in *Scheme 3*. First, compound **103** was prepared from 2-ethynylpyridine (**101**) and 5-bromo-2-nitroanisole (**102**) according to *step a*, which consists in the Shonogashira coupling in presence of catalytic copper (I) iodide and bis(triphenylphospine)palladium (II) chloride that gives the diaryl ethyne **103** in 89% yield. This was followed by a selective nitro to amine reduction with the 5%Pt-1%Fe/C catalyst to give aniline **104** accompanied by minor amounts of triple bond reduction side products (<10%) in 89% yield (*step b*). Final compound **99** was obtained by acylation of the ethynyl aniline **104** with freshly prepared 2-chlorobenzoyl chloride (**86a**) and DIPEA in 54% yield (*step c*).

The synthetic preparation of compound **100** is depicted in *Scheme 4*. Compound **107** was prepared from commercially available 2-bromo-5-nitronisole (**105**) and 1-chloro-2-ethynylbenzene (**106**) by Shonogashira coupling in 82% yield (*step a*). The selective hydrogenation of the nitro group with the 5%Pt-1%Fe/C catalyst resulted in amine **108** in excellent yields (*step b*) with minor over-reduction side products (<15%). Finally, the resulting amine **108** was acylated with picolinic acid (**85j**) and the coupling agent HATU/DIPEA to afford the desired compound **100** in 81% yield (*step c*).



Scheme 4: 3 Preparation of **99**. Reagents and conditions: (a) CuI 2.5 %mol, Pd(PPh₃)₂Cl₂ 2.5% mol, TEA, DMF, 50°C, 89%. (b) H₂, Pt-Fe/C cat., EtOH, r.t., 89%. (c) i) 2-chlorobenzoyl chloride, SOCl₂, reflux, 3h, ii) DIPEA, DCE, 90°C, 54%.



Scheme 5: 4 Preparation of **100**. Reagents and conditions: (a) CuI 5 %mol, Pd(PPh₃)₂Cl₂ 5 %mol, TEA, DMF, 50°C, 82%. (b) H₂, Pt-Fe/C cat., EtOH, r.t., 85% (c) picolinic acid, HATU, DIPEA, DMF, 40°C, 81%.

Pharmacological characterisation of compounds **99** and **100**

The functional activity of **33b**, **99** and **100** was determined in parallel in mGlu₄ and mGlu₅ receptors on HEK293 cells overexpressing the corresponding receptor. The three compounds modulated in a dose-dependent manner the activation of mGlu₄ by L-AP₄, and mGlu₅ by quisqualate, when tested in an IP-One assay, like preliminary assays compounds **83** and **84**.

In fact, all three compounds act as PAMs of mGlu₄ with very different potencies. Compound **33b** displayed mGlu₄ PAM activity with nanomolar potency (EC₅₀ = 104 nM), whilst potency of compound **100** decreased to the micromolar range (EC₅₀ = 4 μM) and compound **99** turn out to display a very weak effect. All this indicates that the substitution of amide bonds for ethynyl groups, especially the one between the 2-pyridyl and methoxyphenyl rings, is not favourable for increasing mGlu₄ PAM activity in this family of compounds.

When tested in mGlu₅ assays, **33b** was found to be a low-potency NAM (IC₅₀ = 103 μM) and **100** had no effect, but, **99** was found to be a very potent NAM (IC₅₀ = 24 nM), nearly 4-fold

more potent than related MPEP ($IC_{50} = 89$ nM), which was our mGlu₅ standard NAM. These results indicate that the replacement of the amide between the pyridyl and methoxyphenyl rings in **33b** for an ethynyl group is essential for generating a potent mGlu₅ NAM, whereas substitution of the other amide for an ethynyl group in **100** results in an inactive mGlu₅ compound.

Compound	PAM mGlu ₄		NAM mGlu ₅	
	EC ₅₀ (μM)	SEM	IC ₅₀ (μM)	SEM
33b	0.104	0.017	> 30	
99	> 30		0.024	0.005
100	4.1	0.2	n.a. ^a	
84			0.024	0.019
85	0.39	0.04	n.a. ^a	

Table 13: Potencies of compounds **33b**, **99** and **100** obtained from the dose-response curves (figure 47) in mGlu₄ and mGlu₅. Data shown as mean ± SEM from at least three independent experiments performed in triplicate.

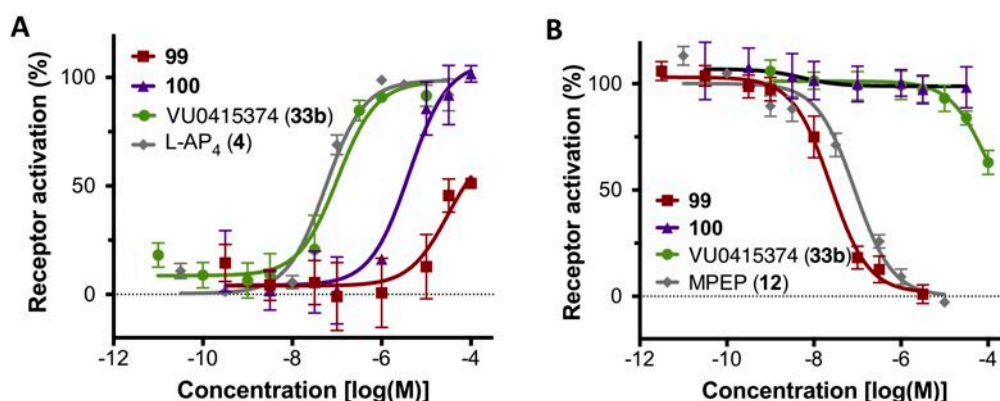


Figure 47: Dose response curves of compounds **33b**, **99** and **100** corresponding to IP-One assay in (A) HEK293 cells overexpressing mGlu₄ with the constant presence of 10 nM of L-AP₄ (4) and (B) cells overexpressing mGlu₅ with the constant presence of 300 nM of quisqualate (2).

As shown in the introduction, molecular switches^b in mGlu receptors are relatively common in the literature and usually strike changes in subtype selectivity or in its pharmacology (PAM, NAM or SAM)^{77, 78, 81}. However, the results obtained, added to the one obtained in *chapter 1*, describe a striking example of a double effect molecular switch in the nanomolar range, where by minimal modifications in the structure of the ligand, prompt a radical change in both pharmacology mode and subtype selectivity. In the present case, a high potency mGlu₄ PAM is

^a Non-active

^b Molecular switch is referred to subtle modifications in the chemical structure of compounds with pharmacological activity that can induce changes in their pharmacology, binding mode or subtype selectivity. See general introduction - glutamate and its homonym receptors - The metabotropic glutamate receptors (mGluRs)

switched to an mGlu₅ NAM. Interestingly, the compounds are active in different receptor subtypes belonging to mGluR groups I and III, which are known to play different roles in synaptic processes.

A related double effect molecular switch can be extracted from the literature, as the amide replacement of the ethynyl moiety in compound **12b**¹²⁷, in addition to the removal of the methyl in the 6-position of the pyridine, leads to the mGlu₄ PAM **31a**⁹⁴. However, this change results in an important drop in compound potency (from an IC₅₀ of 7 nM for **12b** in mGlu₅ 31 to an 1.1 μM EC₅₀ for **31a** in mGlu₄ 32: more than 150-fold), which gives a higher relevance to our findings, as both compounds **33b** and **99**, or even **84**, have strong potencies at nanomolar concentrations. Thus, the high activity of **33b** and **99**, added that of **83** and **84**, suggests a structural similarity between mGlu₄ PAM and mGlu₅ NAM allosteric sites, which are able to selectively recognize compounds differing only in the bridging functionality between two aromatic rings.

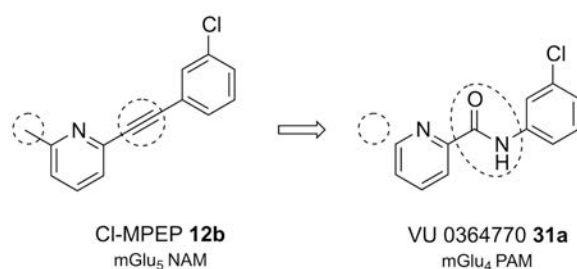


Figure 48: Literature example of double molecular switch between mGlu₅ PAMs and mGlu₄ NAMs present in the literature, but with a high difference in their corresponding potencies.

Conclusions

The results obtained describe the effective an example of a double effect molecular switch in the nanomolar range, where a high potency mGlu₄ PAM is switched to an mGlu₅ NAM by minimal ligand modification, in a very similar manner as we obtained alloswitch-1 (**83**) and optogluram (**84**) in *chapter 1*, but, using an ethynyl-bond instead of a azo-bond. The resulting compounds **99** and **100** are active in different receptor subtypes belonging to mGlu receptors groups I and III, which are known to play completely different roles in synaptic processes, as they activate different signalling pathways.

This molecular switch, altogether with that described in *chapter 1* and that one found in the literature with **12b** and **31a** suggests a structural similarity between mGlu₄ PAM and mGlu₅ NAM allosteric sites, which are able to selectively recognize compounds differing only in the bridging functionality between two aromatic rings.

Moreover, we have proved that azo-replacement of ethynyl between aromatic rings is a powerful approach to afford new azo-compounds with *trans*-on photoswitchable properties, since both moieties share a very similar structural disposition, rigidity and electron density to be recognised by protein targets as bioisosters. Additionally, the pharmacological properties afforded with the ethynyl bioisosters are very similar to the obtained with the *trans*-azo-compounds, especially for compounds **83** and **99** in the mGlu₅-receptor-expressing cells.

The results reported here can be of interest for the pharmacological study of selective modulation of this family of receptors and for establishing the structural determinants of allosteric function in mGlu receptors. These findings constitute a proof of concept for a new strategy in the development of subtype discriminatory mGlu ligands, specifically in the design of new mGlu₄ PAMs from suitable mGlu₅ NAMs, and vice versa. This may be a faster and more effective way to discover pharmaceutically relevant allosteric modulators for mGluR subtypes and to establish the structural features necessary for mGluR subtype selectivity. Additionally, these results also constitute an excellent example of azo-replacement of ethynyl-compounds with very similar functional profile in their *trans*-disposition, which theoretically could be translated to bioactive diarylethynyl compounds with high probabilities of success.

Chapter 3: a new series of phenylazopyrines to fine control mGlu₅ function with light

On the first chapter of the present thesis, we showed the design and synthesis of alloswitch-1 (**83**) as a photoisomerisable allosteric modulator of mGlu₅. In the present chapter, we will present the design, synthesis and characterisation of a small library of phenylazopyridines related to alloswitch-1 (**83**). We will also discuss the different photochemical properties of these compounds, its function in cell assays and its bioactivity *in-vivo* studies.

Papers related to this chapter:

Xavier Gómez-Santacana, Silvia Pittolo, Xavier Rovira, James A. Dalton, Adèle Faucherre, Chris Jopling, Jean-Philippe Pin, Cyril Goudet, Jesús Giraldo, Pau Gorostiza and Amadeu Llebaria, “In-vivo screening with light reveals atypical pharmacological profiles of photoisomerizable phenylazopyridines”, In preparation.

Initial considerations and design of a series of phenylazopyridines

The design of photochromic compounds capable of inducing a pharmacological photoswitch in the activity of a given receptor is not straightforward, since several factors have to be taken into account, which can be summarised in three conditions:

- a) **Biocompatible wavelengths of illumination for photoswitching**, preferably in the visible range, since it is known that UV light can be harmful for cells and tissues. With a harmless wavelength in the visible range, the photoswitchable ligand can be operated during extended periods without toxicity.
- b) **A clear difference on the relative populations of both isomers between the dark and illuminated conditions or under two different conditions of illumination**. This can be afforded by the selection of the optimal illumination wavelengths and a proper relaxation decay of the *cis*-isomer. On the one hand, it is needed a wide difference of absorbance of each of the isomers at illumination wavelength to achieve an effective isomerisation and, on the other hand, relaxation half-lives in the order of several tens of seconds would be also recommendable. In contrast, faster relaxation rates would force to use high-power light intensities to reach a high *cis* population. This irradiation level must be avoided and can be harmful and difficult to be applied in cells or *in-vivo*.

c) **A considerable difference of functional activity of the two photoisomers for the target protein.** One of the isomers must bind to the receptor with a high affinity to be able to induce the desired functional activity but the other one must ideally be completely inactive, giving the expected biological activity for just one of the isomers. The affinity of the inactive isomer is not so important, since compounds with high affinity, can display a very low potency or efficacy or, in the case of allosteric modulators, can show a SAM^a activity. In any case, the importance of the photoswitching resides in the difference of biological activity of the two photoisomers, independently from the binding capability of the inactive isomer. Furthermore, an active and a completely inactive isomer are not imperative, since a sufficiently wide difference in their biological activities is enough to afford a suitable photoswitch for biological applications.

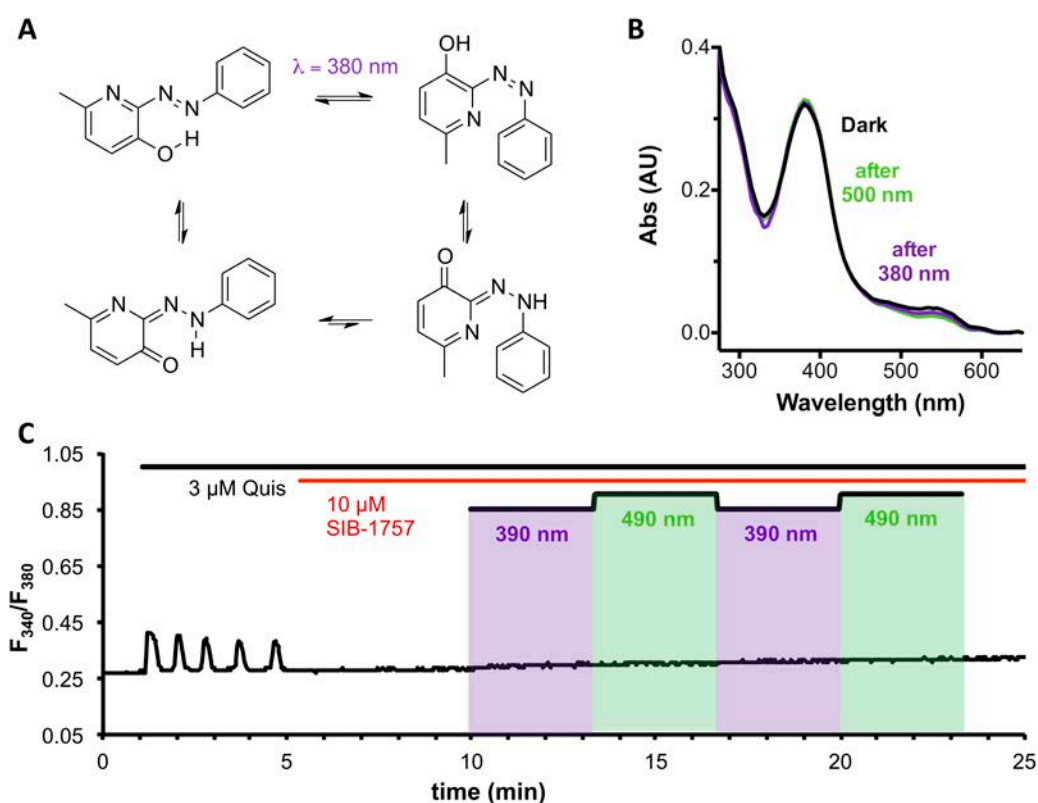


Figure 49: SIB-1757 is not photoswitchable despite being a phenylazopyridine derivative with mGlu₅ NAM activity. (A) Azo-hydrazone equilibrium of SIB-1757 (adapted from Garcia-Amorós¹⁵³). (B) UV-Visible absorption of SIB-1757 (**13**) (25 μM in DMSO) in dark conditions (black line), under 380 nm light (violet line) and under 500 nm light. (C) Real-time calcium imaging with HEK293 overexpressing mGlu₅. Time course of calcium indicator fluorescence ratio (F_{340}/F_{380}) in individual cells treated with agonist (3 μM quisqualate) and SIB-1757 (**13**). Boxes indicate violet or green illumination.

^a SAM: Silent (or neutral) Allosteric Modulator

Alloswitch-1 (**83**) reasonably accomplished these three conditions, and this permitted to observe light-dependent regulation of the receptor activity in cell assays and *in-vivo*, as described in *chapter 1*. In contrast, this does not occur with SIB-1757 (**13**)⁷⁵, which is a phenylazopyryne with mGlu₅ NAM nanomolar potency. However, it is not possible to observe photoisomerisation for this compound (*figure 49B*), probably due to the hydroxyl in *meta*-position that might induce an azo-hydrazone equilibrium, that prompts the rapid isomerisation from *cis*- to *trans*-isomer¹⁵³ (*figure 49A*). Additionally, when we tested SIB-1757 in real-time single-cell calcium imaging, under similar conditions to alloswitch-1 (*chapter-1*), no photoswitching properties in mGlu₅ activity were observed (*figure 49C*).

To create a new library of derivatives of alloswitch-1 (**83**), we decided not to introduce radical changes in the structure of alloswitch-1, but small modifications that could slightly alter the electron density of the azo bond to afford changes on the photoswitching properties or the biological activities. We considered avoiding hydroxyl or aniline substituents, which could induce an azo-hydrazone equilibrium¹⁵³ and the corresponding fast thermal decay of the *cis* isomer, or too electron withdrawing groups, that could shift the π - π^* transition of the *trans*-isomer to the UV region of the spectrum¹⁵⁷. Additionally, the pyridine present in both alloswitch-1 (**83**) and SIB-1757 (**13**) acts as an electron-withdrawing group, therefore, if we added strong electron donating groups (EDG), we could afford a push-pull effect, leading to an undesired strong decrease of the thermal life time of the *cis*-isomer¹⁵³.

Therefore, we decided to maintain the carboxamide bond of alloswitch-1 for most of the compounds of the series. Thus, we decided to investigate the influence of the carboxamide substituents in alloswitch-1 (**83**) and explore the structural determinants for reaching an effective mGlu₅ receptor control with light with phenylazopyridine ligands: we synthesized more bulky derivatives (**109b-c**) than the chlorophenyl of alloswitch-1, other with aliphatic carboxamides (**109d-f**) or with less bulky aromatic carboxamides (**109g-h**) or heterocyclic rings (**109i-l**).

To investigate the effect of the pyridine ring, we replaced it by a phenyl (**110**). We were also interested in the effects of the substitution in the central ring; therefore we changed the position of the methoxy group (**111a**) in the central ring or substituted it for a cyano group (**111b**) or a hydrogen atom (**111c**).

Finally, we explored some changes on the amide group functionality, including imides (**112**, **113**) or a urea (**114**) compound. We also explored the positional isomers **115** and **116** and also synthesized the sulfonamide **117**. All these groups would also confer different electron

densities to the phenylazopyridine moiety, thereby modifying their photoisomerisation properties.

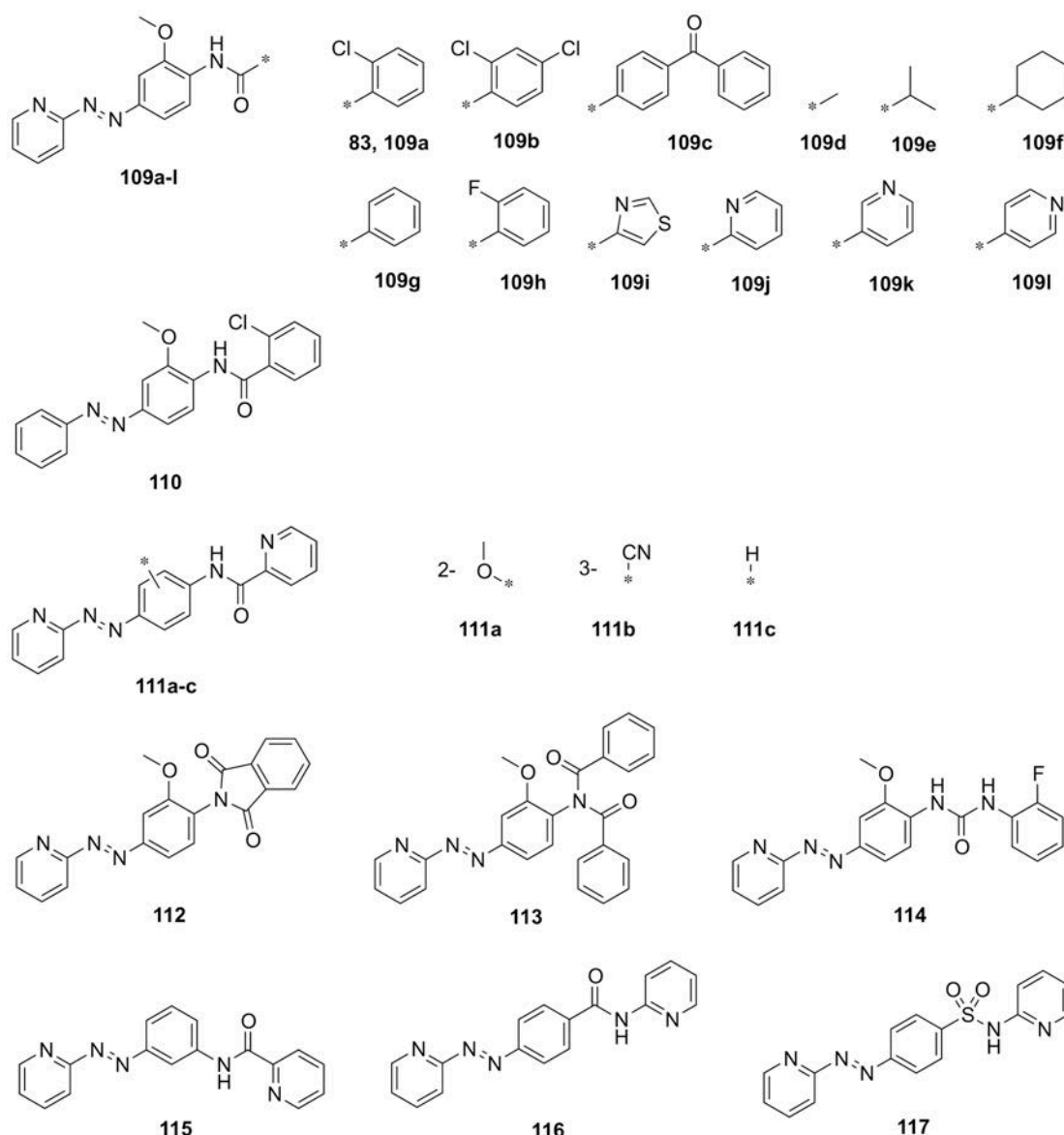
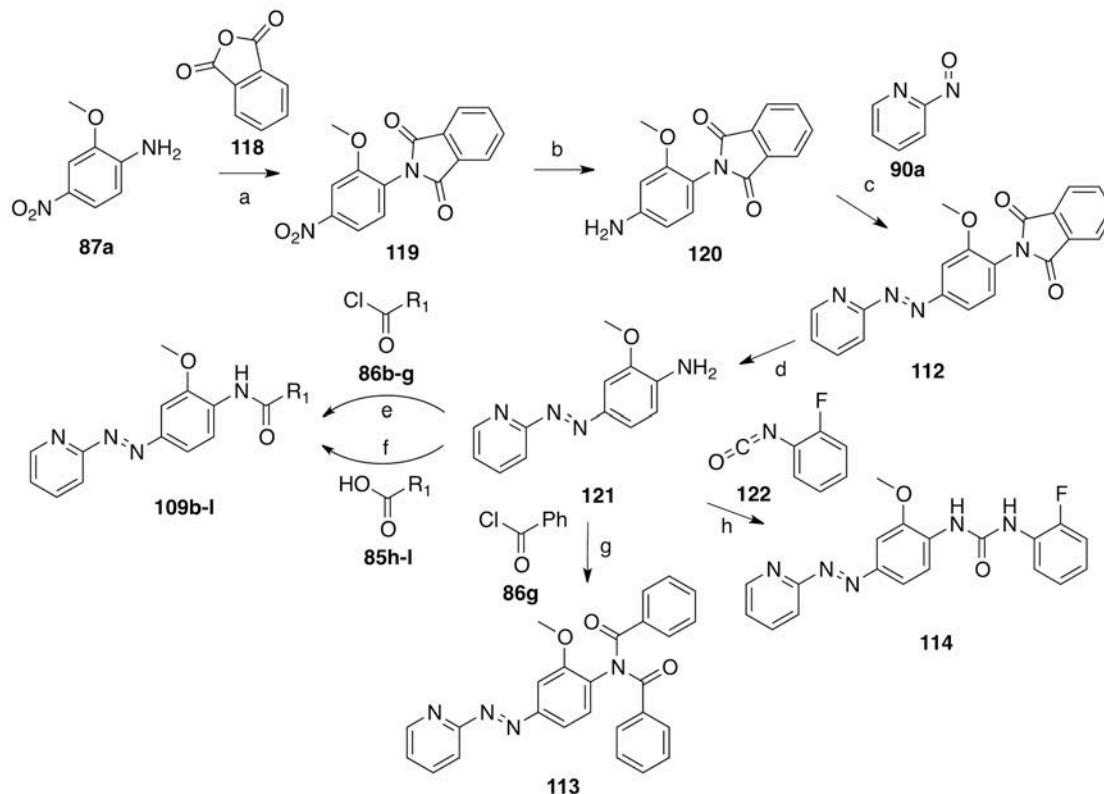


Figure 50: Structures of the compounds constituting a new series of alloswitch-1 analogues (109-117)

Synthesis

Compounds **109b-l** and **113-114** were prepared following the synthetic strategy shown in *Scheme 5*. First, the nitroaniline **87a** was protected to give the phthalimide **119** in 54% yield (*step a*) and the nitro group was hydrogenated to afford aniline **120** in quantitative yield (*step b*). Then, the phenylazopyridine **112** was prepared in 89% yield by reacting in acidic conditions the aniline **120** and the 2-nitrosopyridine **90a**, which was prepared following the synthetic strategies reported by Taylor et al.¹⁹⁶ (*step c*). Phenylazoaniline **121** was obtained from deprotection of the phthalimidoyl group from **112** in 92% yield (*step d*) and used to obtain final phenylazopyridines **119b-l** by reaction with acyl chlorides **86b-c**, previously prepared from

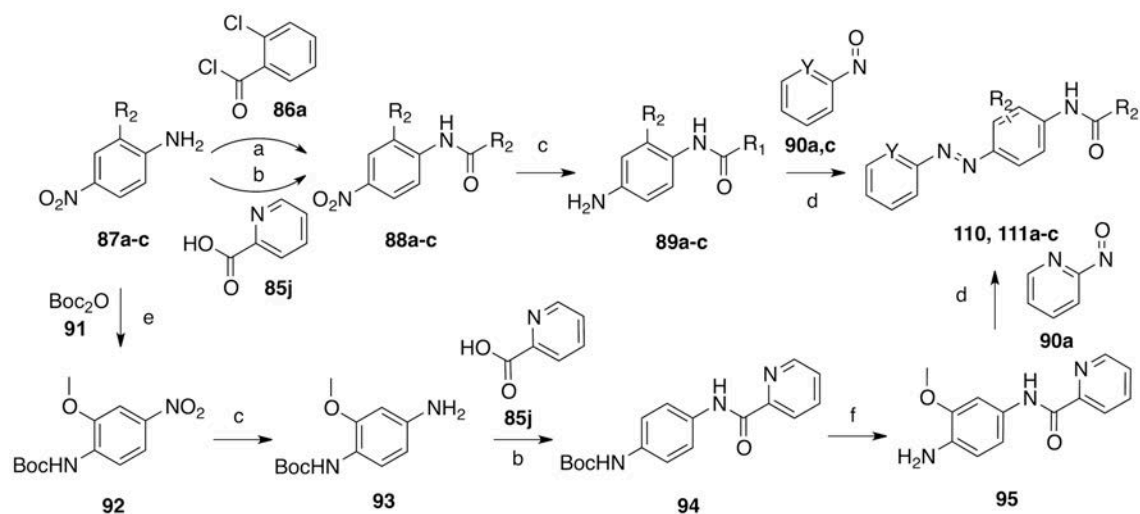
the corresponding carboxylic acid **85b-c**, or a commercially available acyl chloride **85d-g** (step e) or an activated carboxylic acid **85h-l** with HATU (step f). Alternatively, compound **5** was also prepared by reaction of phenylazoaniline **121** with excess of benzoyl chloride **86g** and compound **6** by reaction of phenylazoaniline **121** with isocyanate **122** in good yields (step h).



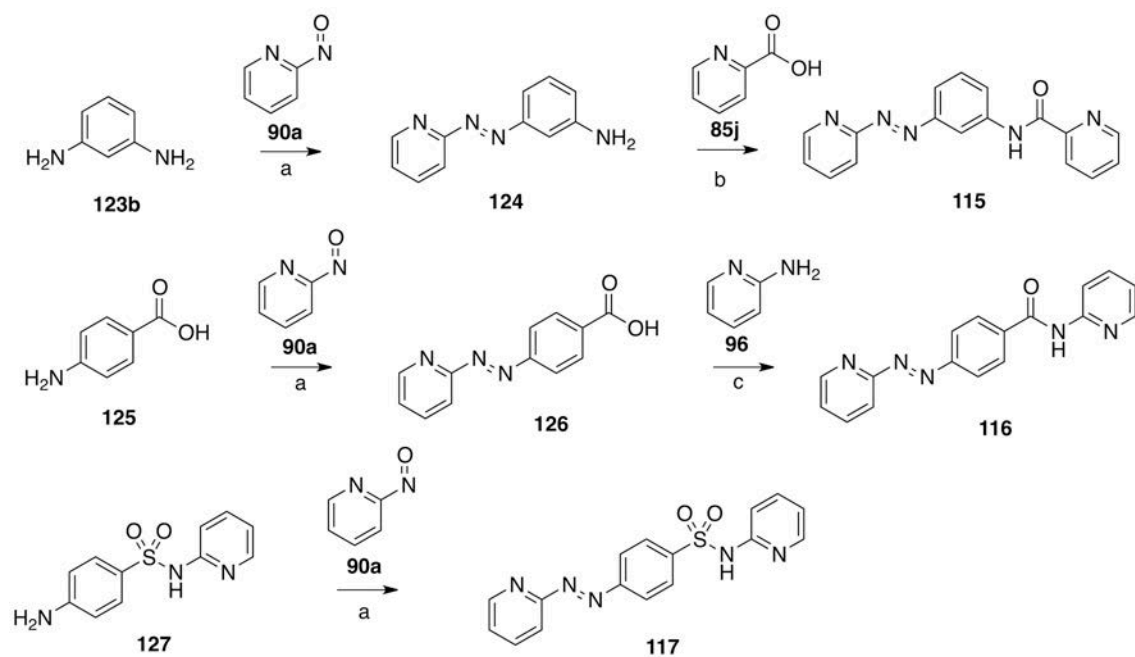
Scheme 6: 5 Synthesis of **109b-l**, **113-114**. Reagents and conditions: (a) AcOH, reflux, 18 hours; 54%; (b) H₂ (2 bar), Pd/C cat., 1-4-dioxane, r.t., 5 h, quant.; (c) AcOH cat., DCM, r.t., 40h, 89%; (d) MeNH₂ 40% (aq.), EtOH, 65°C, 2 h, 92%; (e) DCE, DIPEA, 40°C, 22 h 86-89%; (f) HATU, DIPEA, DMF, 40°C, 22h, 52-93%; (g) DCE, DIPEA, DMAP cat. 40°C, 22h, 89%; (h) DIPEA, THF, 40°C, 22h, 75%.

Compounds **110** and **111a-c** were prepared following the synthetic strategy shown in *Scheme 6*. For compound **110**, steps *a-b* and compounds **88a** and **89a** are described previously in *chapter 1* for the synthesis of **33b** and **83**. Acylation of the nitroaniline **87b-c** with the corresponding activated carboxylic acids **85b-c** afforded compounds **88b-c** in high yields 85-94% (step *b*). Following reduction of the nitro group yielded anilines **89b-c** in also high yields (97%) (step *c*). Finally, the anilines **89a-c** were coupled with the corresponding nitrosoaryl **90a-b** in acidic conditions, which was obtained directly from commercial sources or prepared following the synthetic strategies reported by Taylor et al.¹⁹⁶, to afford the azocompounds **110** or **111b-c** (step *c*) in moderate yields. Compound **111a** was also prepared following the synthetic strategy shown in *Scheme 6* that reproduces the experimental procedure described previously in *chapter 1* for the synthesis of **84**. The final step consists in the coupling of the

aniline **95** with the 2-nitrosopyridine **90a** in acidic conditions to afford phenylazopyridine **111a** in a 68% yield.



Scheme 7: 6 Synthesis of **100**, and **111a-c**. Reagents and conditions: (a) DCE, DIPEA, 100°C, 2.5 h or HATU, DIPEA, DMF or EtOAc, 40°C, 22h (85-99%); (b) H₂ (2 bar), Pt+Fe/C or Pd/C, EtOH/1,4-dioxane r.t. 5 h, 97-100% (c) AcOH cat., DCM, r.t., 20-72h, 47-68%; (d) DCM, r.t., 48 h, 62% conv., 54%; (e) TFA, DCM, r.t., 2h, quant.



Scheme 8: 7 Synthesis of **7-9**. Reagents and conditions: (a) AcOH cat., DCM, r.t., 1-6 days, 27%; (b) HATU, DIPEA, DMF, 40°C, 84%; (c) i) SOCl₂, 75°C, 3.5h, ii) DIPEA; DCE, 90°C, 2h, r.t., 64h, 26%.

Compound **115** was prepared following the synthetic strategy shown *Scheme 7*. Phenylazoaniline **124** was obtained from the coupling of *m*-phenylenediamine **123b** and 2-nitrosoaniline **90a** in acidic conditions in 27% yield. Following acylation with picolinic acid **85j** activated with HATU afforded phenylazopyridine **115** in 84% yield. Compound **116** was

prepared following the synthetic strategy also shown *Scheme 3*. Phenylazopyridinyl carboxylic acid **126** was obtained from reaction of 4-aminobenzoic acid **125** and 2-nitrosoaniline **90a** in acidic conditions in 55% yield. Following formation of the corresponding acyl chloride and reaction with 2-aminopyridine **126** afforded compound **116** in 26% yield. Compound **117** was prepared following the coupling of commercially available sulfapyridine **127** and 2-nitrosoaniline **90a** in acidic conditions in acidic conditions to afford **27** in 90% yield.

Photochemical characterisation of compounds 109-117

UV-Vis absorption spectroscopy of *cis* and *trans* isomer

To biologically apply the isomerisation of azobenzene-like compounds with light, it is important to previously obtain the UV-Vis absorption spectra of both *trans*- and *cis*-isomers. In this way, we can determine the wavelength where the maximum difference of absorption between the *trans* and *cis* isomer is found. This corresponds the optimal wavelength to isomerise from *trans* to *cis* disposition to reach a maximum fraction of *cis* isomer in the photostationary state. On the other hand, the wavelength located at the maximum difference of absorption between the *cis* and the *trans* isomers would be the optimal one for the reverse isomerisation. However, obtaining pure *trans*-isomer and pure *cis*-isomer samples is not evident, since it would require illuminating with a wavelength were *trans* isomer absorbed but *cis* isomer did not and minimising the thermal decay of the *cis* isomer. Therefore, in practice achieving a 100% sample of *cis*-isomer is practically not possible.

Nevertheless, we were able to measure the UV-Vis absorption spectra of both isomers of all the compounds in a mixture of aqueous buffer at pH=7.4 and acetonitrile by HPLC coupled simultaneously to a photodiodes array (PDA) and a mass spectrometer. This technique allowed us to chromatographically separate the two phenylazopyridine-isomers, to measure the UV-Vis absorption spectra of both *cis* and *trans* isomer separately (*figure 51A-C*) and to verify that both peaks had the same molecular ion in their mass spectra. With this technique, we could determine the location of the typical light absorption π - π^* band of the azocompound *trans*-isomer and the n - π^* band of the *cis*-one. The *trans* isomers presented the π - π^* band in the range between 310-400 nm, even though for most of the phenylazopyridine compounds the maximum of the band is around 380 nm (*figure 51C*). The *cis*-isomers displayed the typical n - π^* band with maximum in the range 420-450 nm (*Figure 51D*).

As mentioned above, the situation of these bands depends on the nature of the substituents on the aromatic rings of an azocompound¹⁵². In particular electron-donating properties of substituents of the in position *ortho* or *para* position have an important influence on shift π - π^*

band to higher wavelengths¹⁵². However, in our cases, the 2-pyridine group, which is a π -electron-deficient heterocycle, induce a certain push-pull azobenzene properties, especially in polar solvents^{153, 154}. Then, to achieve a π - π^* band suitable for our interests, mild electron-donating substituents are preferred to shift the wavelength of *trans* isomer maximum absorption (π - π^* transition) to the visible range without inducing an excessive increase of thermal isomerization rate from *cis* to *trans* configurations.

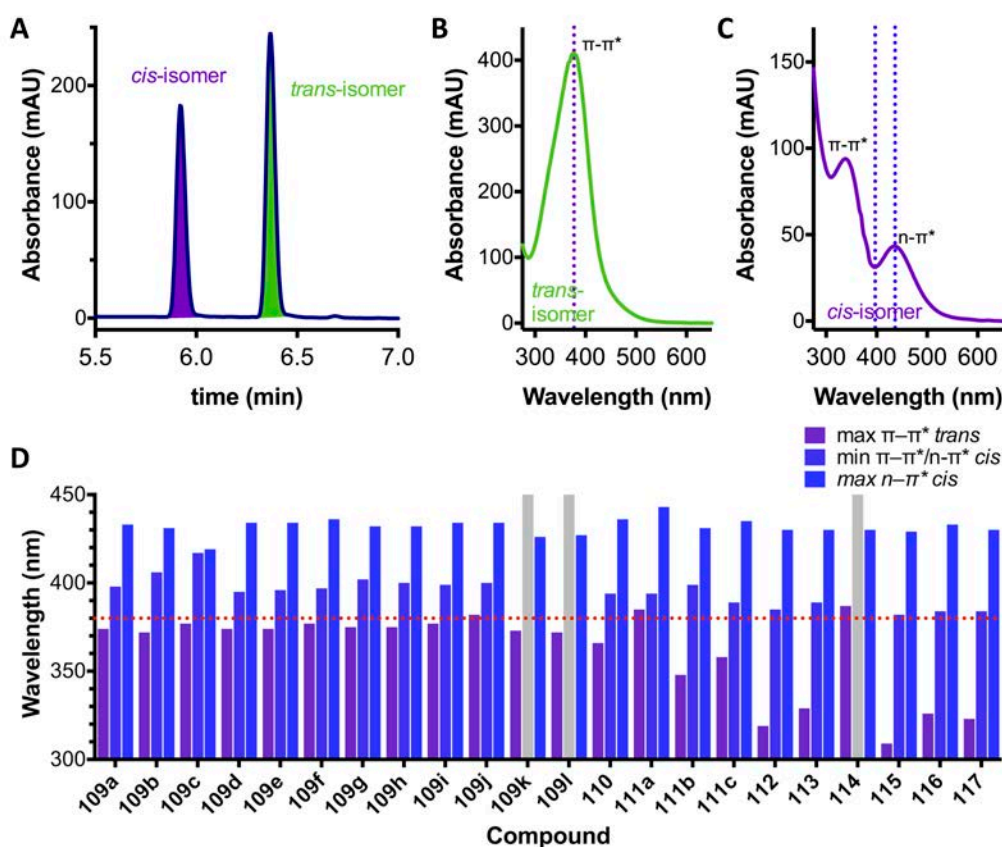


Figure 51: UV-Vis absorption spectra extracted from HPLC-PDA-MS analysis of a mixture of *cis* and *trans* phenylazopyridines. (A) Zoom of the chromatogram of compound **109f** between 5.5 and 7.0 minutes with detection at 254 nm, where *cis* and *trans* isomers are eluted. The first peak correspond to the *cis* isomer, since the mass spectrum corresponds to **109f** and the UV-Vis spectrum corresponds to a *cis*-azobenzene profile, with the typical π - π^* and n - π^* transition bands (C). The second peak corresponds to the *trans* isomer, according to the mass spectrum and the UV-Vis absorption spectrum with only a π - π^* transition band (B). (D) Wavelengths of maximum absorbance of *trans*-isomers π - π^* bands (violet bars), minimum of *cis*-isomers absorption between π - π^* and n - π^* transition bands (purple bars) and wavelengths of maximum of *cis*-isomers n - π^* bands (blue bars). Grey bars correspond to non-measurable absorption minima of *cis*-isomers between π - π^* and n - π^* transition bands. In practically all the compounds, 380 nm (red dotted line) is located between maximum of *trans*-isomers π - π^* bands and, minimum of *cis*-isomers absorption between π - π^* and n - π^* transition bands.

For these reasons the photoswitching properties of alloswitch-1 (**83**) are well suited for biological use, whereas the high electron-withdrawing sulphonamide of compound **117** shifts

the band to energetically higher wavelengths (310 nm), which are not suitable for biological experiments. On the other hand, the urea from compound **114**, more electron-donating than a simple amide, shifts the band to the visible range of the spectrum (387 nm), or even the intermediate **121**, which has a simple amine in that position with stronger electron donating properties that shift the band to blue range of the spectra (417 nm).

Therefore, the electronic properties of substituents in position 2 or 4 have an important influence on shifting π - π^* phenylazopyridine band to higher wavelengths. This phenomenon can be explained as a direct effect of electron richness of the phenylazopyridine moiety given by appropriate substituents; since the stronger electron donors, the higher is the wavelength of maximum absorbance^{156-158, 205}. We proved this hypothesis comparing the wavelength of maximal absorbance (λ) of the phenylazopyridine compounds of the series with the characteristic signal on ¹H-NMR of the proton in position 5 of the pyridine (figure 52A). Its chemical shift (δ) is directly related to the internal induced magnetic field of the atom, which is related to electron density around the nucleus that we are selecting: The lower chemical shift, the higher electron density (due to para-substitution effect, figure 52). Therefore, we observed a strong correlation between lower chemical shift of the mentioned proton, which involves a higher electron density of the azo-bond, and the higher wavelength of maximal absorbance of the compounds (figure 52B) (Pearson correlation coefficient with two tailed P value: $r = -0.76$, $P < 0.0001$).

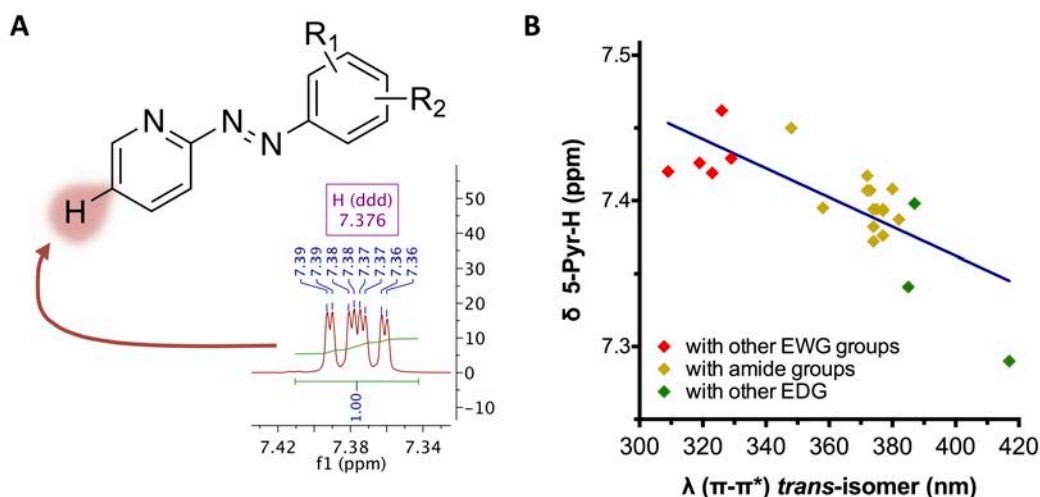


Figure 52: There is a correlation of this shift on the π - π^* band and the electron density of the azo-moiety. (A) Structure of the phenylazopyridines with the fraction of the ¹H-NMR spectra corresponding to the signal of the proton in position 5 of the pyridine. (B) Correlation plot of the chemical shift (δ) of the proton in position 5 of the pyridine and the maximum of *trans*-isomers π - π^* bands ($r = -0.76$, $P < 0.0001$).

Photoisomerisation of compounds 109-117 with UV-Vis absorption spectroscopy

To measure the extent of photoisomerisation, we chose 380 nm as the illuminating wavelength because, for practically all the compounds in the series, it is located between the maximum of absorption of *trans* isomers (π - π^* band) and the minimum located between the π - π^* and n - π^* bands of the *cis* isomers. Therefore, it might be very close to the optimal wavelength to afford to maximize the amount of *cis* compound under illumination. To afford the reverse isomerisation, we chose 500 nm, since it is located closer to the n - π^* transition band of the *cis* isomers but, as thermal relaxation always tends towards *trans*-isomers, we do not need to be so precise as for *trans* to *cis* photoisomerisation.

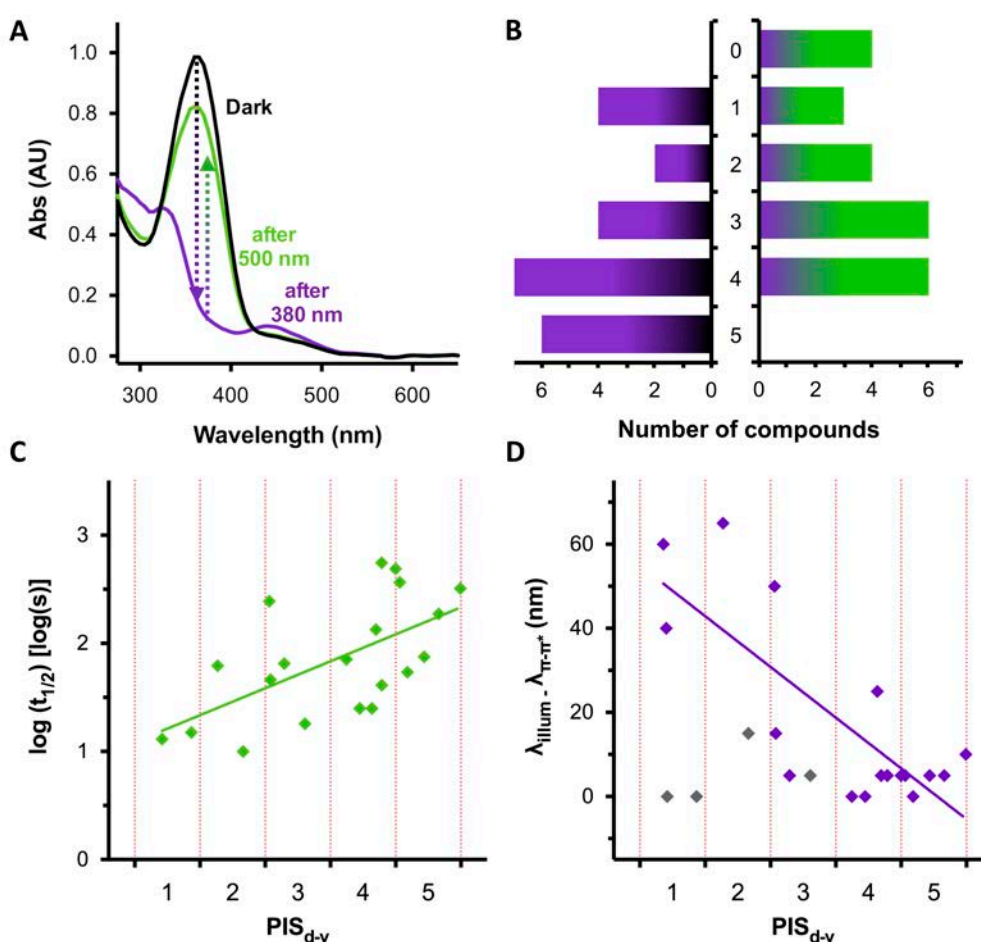


Figure 53: Photoisomerisation of compounds 109-117. (A) UV-Vis absorption spectra of compound 111c in solution 25 μ M in DMSO. The black line corresponds to the spectrum in dark conditions, the violet one corresponds to the spectrum after at 380 nm, and green after the consecutive illumination at 500 nm. Compared to the pure spectra obtained HPLC-PDA-MS (see *annex*), we observe a practical 100% of conversion from *trans* to *cis* isomers and a reasonable back-isomeration from *cis* to *trans* isomer. (B) Compounds with the photoisomerisation score (PIS) under light of 380 nm of wavelength (violet bars) and under light of 500nm of wavelength (green bars). (C) The Pearson correlation coefficient between PIS and *cis* isomer relaxation half-life logarithm was $r = 0.62$ ($P = 0.0039$) and that

for the illuminating λ and the λ of maximum difference of absorbance of the non-illuminated and 380 nm-illuminated spectra was $r = -0.82$ ($P < 0.0001$) if fast relaxing compounds are excluded ($t_{1/2} < 20$ s).

Thus, we measured the UV-Vis absorption spectra of every compound 25 μ M in DMSO in the dark, carefully protecting it from ambient light, and hence we practically only detect the *trans*-isomer. Then we proceeded in a very similar method to that used for compounds **83** and **84** (*chapter 1*): we illuminated the samples with violet light (380 nm) to induce the isomerization from *trans* to *cis* configuration, we collected a new spectra, and after illuminating with green light (500 nm) we collected a new one (*figure 53A*). In consequence, in dark conditions we practically only detected *trans* isomers, while after illuminating with violet light we obtained different amounts of *cis* isomers, depending on each compound. After that, illumination with green light isomerised back a great part of the thermodynamically stable *trans* configuration (*figure 53A*).

With the information obtained from these spectra we proposed a “photoisomerisation score” (PIS) as an index to account for the effectiveness of the photoswitch. PIS is calculated from the data obtained from the UV-Vis absorption spectra as a normalized quotient of maximum difference of absorbance of the dark conditions and the corresponding absorbance at 380nm with the maximum of the dark. It results in an adimensional value between 0 and 5 (5-efficient switching, 0-poor switching, see *experimental part*). We calculated the scores for the isomerisation from *trans* to *cis* isomer (from dark conditions with illumination at 380 nm, PIS_{d-v}) and for the reverse isomerisation (from violet illuminated sample with illumination at 500 nm, PIS_{v-g}) (*figure 53B, table 14*). However, the information that gives PIS_{d-v} is of higher value than PIS_{v-g} , since the *trans*-isomer is the thermally stable one and after illumination with green light all the azobenzenes tends to 100% *trans* with time. Most of the compounds obtained in the pphenylazopyridine series have *trans*-to-*cis* photoswitching behaviours similar to alloswitch-1 (**83**), or even better in some cases. The compounds with lower PIS correspond to those that with the maximum of the *trans* isomer more shifted to UV wavelengths or far from the 380 nm (corresponding to the used illumination wavelength), such as compounds **112**, **113**, **115**, **116** and **117**. This was expected due to the gap between the illumination wavelength and their maximum. In contrast, compounds the maximum π - π^* transition band very close to 380 nm, such as **109a**, **109f** or **111a**, display a higher photoisomerisation score. In other cases, like compound **110** or **111c**, despite not having the maximum of absorption so close to 380 nm (366 and 358 nm respectively by HPLC-PDA-MS), the maximal difference of absorption between non-illuminated and illuminated samples is located around 380 nm (375 and 370 nm respectively), which indicates that it is a suitable wavelength to achieve a high separation

between the two states. In fact, all the compounds with a photoisomerisation score of 4 or 5 have maximal absorption differences between 370 and 390 (*annex*).

Compound	$t_{1/2}$ (s)	λ_{illum} (nm)	PIS _{d-v}	PIS _{v-g}
109a	54	380	5	3
109b	25	380	4	3
109c	19	380	3	2
109d	489	380	4	4
109e	556	380	4	3
109f	353	380	5	3
109g	71	380	4	3
109h	65	380	3	2
109i	41	380	4	3
109j	134	380	4	4
109k	15	380	1	1
109l	13	380	1	0
110	187	380	5	4
111a	75	380	5	4
111b	25	380	4	0
111c	322	380	5	4
112	245	380	3	2
113	46	380	3	2
114	10	380	2	1
		400	5	4
115	62	380	2	1
116	-	380	1	0
117	-	380	1	0

Table 14: Photoisomerisation data for compounds **109-117**

Pyridylamides **109k** and **109l** and urea **114** have π - π^* transitions at wavelengths prone to be photoisomerised around 380 nm but they do not show a good PIS. After measuring the thermal relaxation time of the *cis* isomers (table 14, *annex*), we noticed that these three compounds had a half-life of their *cis* isomer lower than 15 seconds, and this could be a possible drawback to be able to observe a suitable isomerisation. Coincidentally, these three compounds presented a very small *cis* isomer peak in the chromatogram of HPLC-PDA-MS

(*annex*) and its low proportion did not allow the correct measure of the minimum between the π - π^* and the n - π^* transition bands, or maybe the electronic properties of this compounds do not allow a well-defined separation of the π - π^* and the n - π^* transition bands, leading to a poor isomerisation and fast relaxing rate. Additionally, the urea **114** had the maximum of absorbance of the *trans*-isomer over the 380 nm in the UV-Vis spectra extracted from the HPLC-PDA-MS and at 395 nm when spectrophotometrically measured in DMSO. Therefore, we attempted to induce a better photoisomerisation with 400-nm-illumination. With the new conditions, we increased the PIS from 2 to 5, achieving an excellent photoisomerisation in a completely visible wavelength despite the fast relaxation of the *cis*-isomer.

Finally, we compared the values of photoisomerisation score (PIS_{d-v}) and the thermal relaxation rate (as logarithm of the half-life of the *cis*-isomer) and we found a significant correlation (Pearson coefficient $r = 0.62$, $P = 0.0039$, *figure 53C*), which indicates that the photoswitching effectiveness directly depends on the thermal relaxation time of the *cis*-isomer. In addition, we plot the PIS_{d-v} of all the compounds against the wavelength of maximum difference of absorbance of the non-illuminated and 380nm-illuminated spectra, we find a strong correlation (Pearson coefficient $r = -0.80$, $P < 0.0001$) if we exclude fast relaxing compounds ($t_{1/2} < 20s$) (*figure 53D*).

In summary, we have shown that alloswitch-1 (**83**) was fulfilling reasonably the photoisomerisation conditions for control of mGlu₅ with light in living systems, since the light wavelength for its photoisomerization is in the edge of the visible range, which is less harmful than UV wavelengths and its thermal relaxation is slow enough to avoid using too potent light intensities to obtain a high *cis* isomer fraction. Moreover, we found that many other compounds of the series have very similar properties or, in the case of **109f**, **110**, **111a**, **111c** or **114** even better, which make these compounds also suitable for photoswitching applications. However, not every phenylazopyridine meets the photoswitching conditions, since compounds like **115**, **116**, or **117** require UV wavelengths to isomerize or compounds **109k**, **109l** or SIB-1757 (**13**) have too short relaxation time of the *cis*-isomer that limit their use in biological studies.

In-vitro biological evaluation of 109-117

Single dose screenings

To evaluate the pharmacological activity of all the phenylazopyridines of the series we first screened them in HEK293 cells transiently transfected with rat mGlu₅ using an inositol phosphate (IP) accumulation assay based in homogeneous time-resolved fluorescence (HTRF)

assays (*experimental part*). We measured the antagonistic functionality to the orthosteric agonist quisqualate (**2**) at a initial single dose of 30 μM . Gratifyingly, most of the compounds within the series turned out to respond with a very similar efficacy as the mGlu₅ NAM reference standard fenobam (**14**) or MPEP (**12**), except compound **117**, which resulted inactive, and compounds **110**, **111a** and **116**, that seem to display a partial efficacy (*figure 54*).

Additionally, these compounds were also screened in mGlu₄ HEK296 transfected cells, using the same assay, showing a general potentiation of the orthosteric agonist L-AP₄ (**4**) but we observed only saturation for compound **111a**, which has a clear structural resemblance to optogluram **84** (*chapter 1*). Concerning the rest of compounds, only **119f-g**, **110**, **111c** or **112** have a partial efficacy. However the relevance of this effect is low, since very high compound concentrations would be needed to achieve an effective saturation of the receptor response and thus achieve a considerable functional activity.

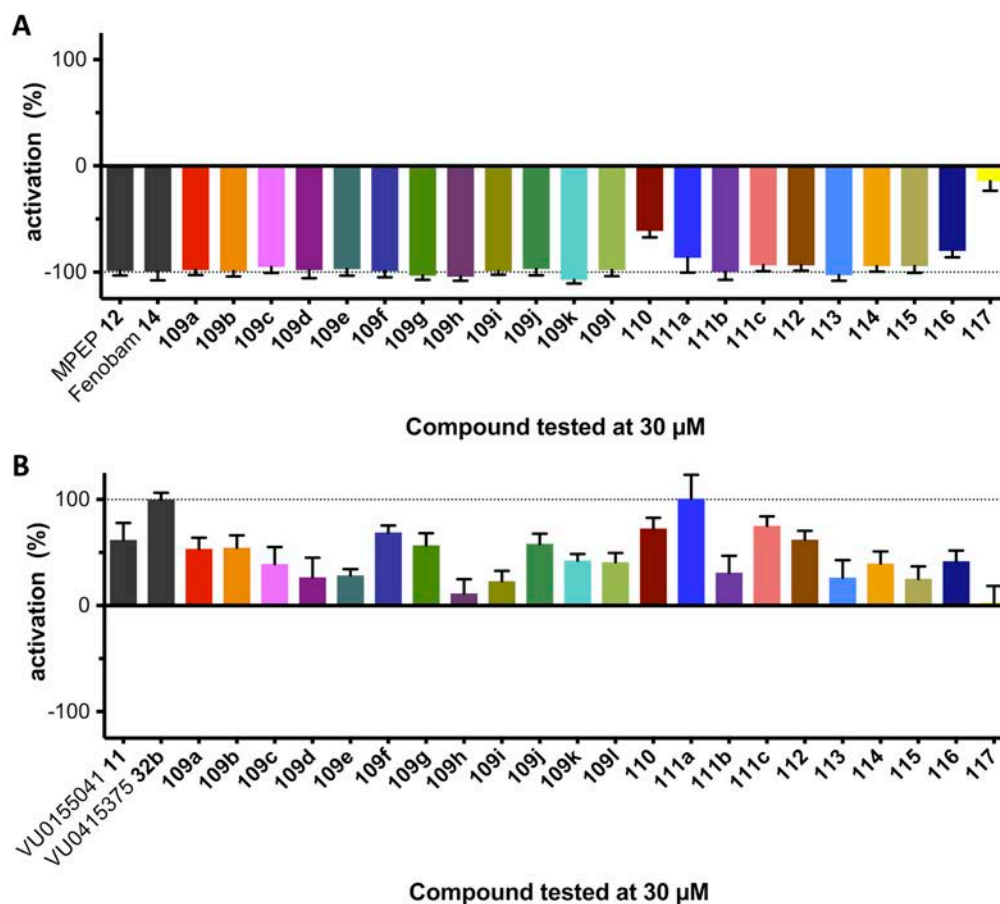


Figure 54: Screening of compounds **109-117** in mGlu₅ and mGlu₄. (A) Assay performed in mGlu₅ transiently transfected HEK293 cells with 30 nM of Quisqualate and 30 μM of each compound. (B) Assay performed in mGlu₄ transiently transfected HEK293 cells with 50 nM of L-AP₄ and 30 μM of each compound.

Dose-response curves (I) in mGlu₅: A plastic answer for biphasic curves?

As single dose assays revealed an inverse agonism of practically all the series, we needed to generate dose-response curves for all the compounds of the series, with the exception of compound **117**, which clearly show a lack of activity in the preliminary screening assay. We used a similar methodology to that used for the pharmacological characterisation of alloswitch-1 (**83**), employing the IP accumulation assay based in HTRF in dark conditions and with 380-nm-illumination simultaneously.

We obtained different types of dose-response curves that could be summarised in two main behaviours:

- A) **Regular one-phase dose-response curves** with a shift to the right on the dose-response curve obtained from the illuminated samples (increase on IC₅₀ values), as we have seen for the rest of compounds. Examples of those are compounds **109c**, **109d**, **109e**, **109g**, **109h**, **109k**, **109l**, **110**, **111c**, **113**, **115** and **116** (figure 55AB).
- B) **Biphasic dose-response curves** with two clear phases and a shift affecting the efficacy obtained from the illuminated samples. Examples of those are compounds **109b**, **109f**, **109h**, **109i**, **109j**, **111b**, **113** and **114** (figure 55CD).

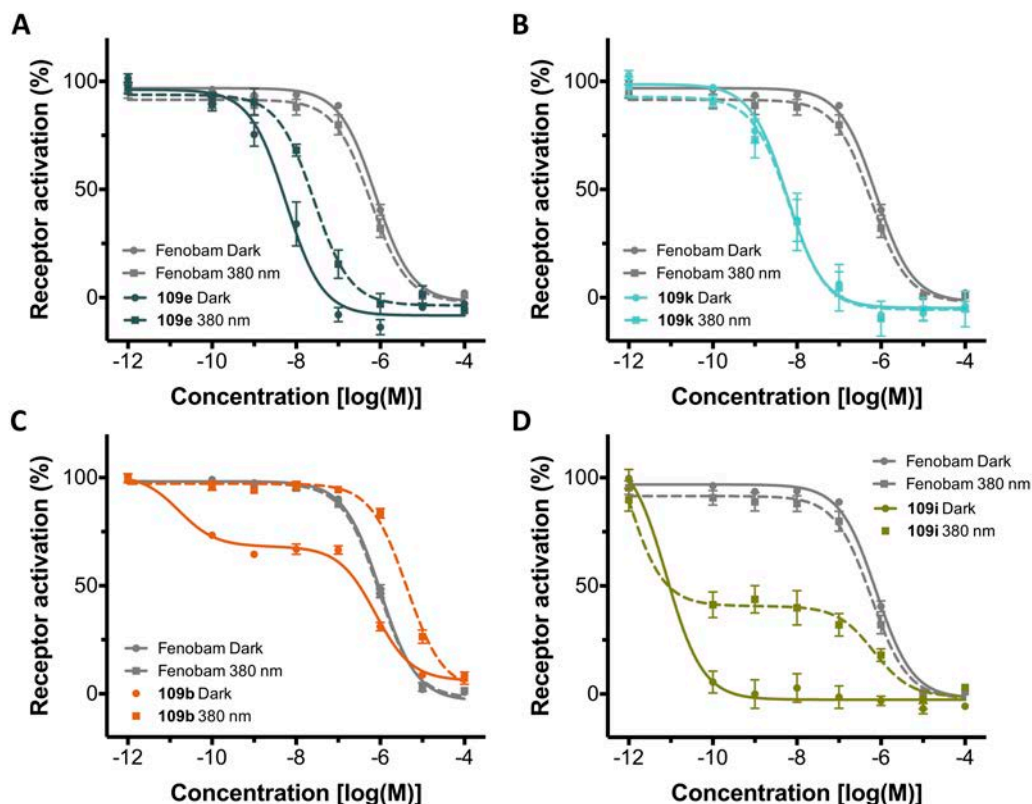


Figure 55: Dose-response curves using the classical protocol with IP-One assay on HEK cells overexpressing mGlu₅ receptor with a 100 nM constant concentration of quisqualate (**2**). Flat lines correspond to the samples incubated in

dark conditions and dotted lines to the samples under 380-nm-illumination. Each point corresponds to the mean of a minimum of two independent replicates with the corresponding SEM as error bars. We obtained monophasic curves with compounds **109e** (A) and **109k** (B) with a photoinduced shift on the potency (IC_{50}) for **109e** and a negligible photoswitch for **109k**. Compounds **109b** (C) and **109i** (D) produced biphasic curves with an additional photoinduced shift on the efficacy. Additionally, compound **109i** (D) constantly inhibited mGlu₅ response in practically all the doses and did not complete the dose-response curve in the picomolar range.

These biphasic curves obtained are not common in mGlu receptors pharmacology, or even in GPCR pharmacology. There are some examples in the literature, where the two phases are related to different binding states or a biased signalling²⁰⁶⁻²⁰⁸ but it is not a common behaviour of mGlu NAMs. Additionally some of those compounds such as **109h** or **109i** saturate the inhibition of the receptor at concentrations in the subnanomolar range, and no completion of the curve was observed even at lower picomolar concentrations. That made these curves not reliable and we had to look for explanations for these unusual results.

Two common properties of these compounds is the intense orange colour of their solutions and their high lipophilicity that can be troublesome when working with aqueous solvents. During the execution of these experiments, we could observe the end of the pipette tips red-dyed during and after the dilution procedure, probably due to an adherence of these apolar phenylazopyridines on the “lipophilic” plastic tips (*experimental part*). Then, we hypothesized that these plastic tips could release small amounts of the retained compounds in every well that may induce a second phase in the dose-response curve at very low “theoretical” concentrations due to this non-desired excess of compound.

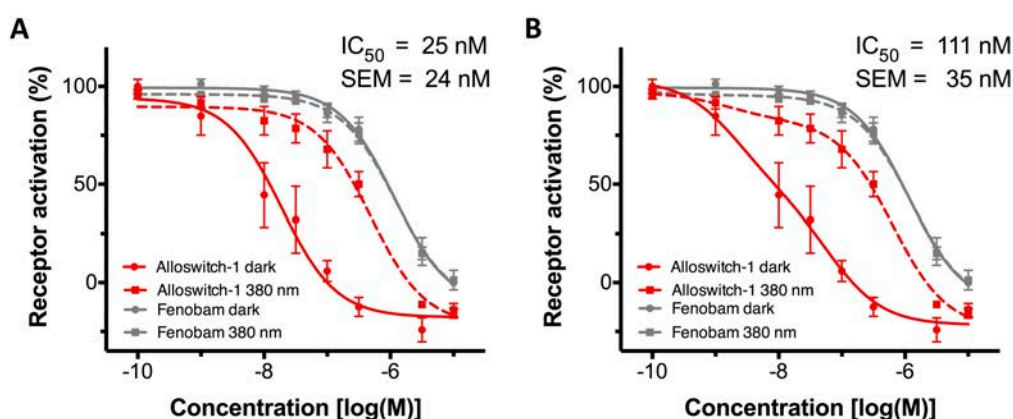


Figure 56: Comparison of dose-response curve of alloswitch-1 (83) from *chapter 1* with a monophasic curve (A) or biphasic curve (B). Each point of the curves are the mean of three independent replicates and the error bars are corresponding SEM. Potency (expressed as IC_{50} s) corresponds to the mean of IC_{50} obtained after fitting a monophasic curve (for A) or a biphasic curve (for B) of each of the independent replicates with the corresponding SEM calculated for the same replicates.

We did not observe this behaviour at final dose-response curve in alloswitch-1 (**83**) in *chapter 1*, but the fitting improved with a biphasic curve, especially for one of the independent replicates (not shown). This was reflected on the final mean and SEM of the replicates fitted with a biphasic curve: we obtained a slight loss of potency in the first phase ($IC_{50} = 111$ nM) but we achieved a better SEM when it is compared to the mean (*figure 56*). Therefore, alloswitch-1 (**84**) shares also the “biphasic” properties with the series of phenylazopyridines, but with a milder effect than other members of the series.

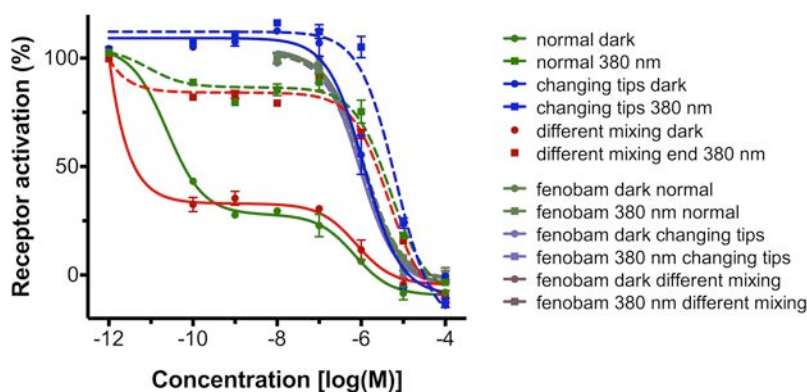


Figure 57: Comparison of different protocols with IP-One assay on HEK cells overexpressing mGlu₅ receptor with a constant concentration of quisqualate (**2**) 100 nM. Flat lines correspond to the samples incubated in dark conditions and dotted lines to the samples under 380-nm-illumination. “Changing tips” protocol provided a monophasic dose-response curve with a photoinduced shift on the potency, whereas the other protocols provided biphasic curves with their photoinduced shift also affecting their efficacy.

Compound	Conditions	Dark IC_{50} (μ M) (1 st phase)	380 nm IC_{50} (μ M) (1 st phase)	PPS
114	Normal	0.69	4.95	7.16
	Different mixing	0.76	4.43	5.81
	Changing tips	1.17	6.51	5.58
Fenobam (14)	Normal	1.16	1.20	1.04
	Different mixing	1.12	0.91	0.82
	Changing tips	0.90	0.99	1.10

Table 15: Comparison of potencies (IC_{50}) of compound **114** extracted from dose-response curves shown in *figure 5*. The obtained IC_{50} from the first phase do not change excessively to that obtained with the “changing tips” protocol, as well as the photoinduced shift on the IC_{50} .

To prove this theory, we generated three dose-response curves in the dark with the corresponding three ones under violet illumination of compound **114** and fenobam as a control mGlu₅ NAM, using the same IP accumulation assay. With that experiment we tested

three different conditions: The normal conditions tested to date, a change of mixing the dilutions before the incubation of the cells, and a change of the plastic tips on the preparation of each dilution (*experimental part, figure 57*).

From the results obtained, we could conclude that there is no substantial change on the potency or the efficacy of fenobam in any of the tested conditions, since we obtained a normal monophasic curve in all the experimental conditions. Concerning compound **114**, the manner of mixing the dilutions did not affect to the shape and the location of the IC_{50} s: we got practically the same biphasic curve than using the normal protocol. In contrast, when we changed the tips while preparing the dilutions, we got a completely different dose-response curve: monophasic and with a shift on the potency for the curve of violet-shined samples (*figure 57, table 15*).

These results confirm the theory that the compounds were sticking at the end of the plastic tips, and small amounts were released in each of the wells used to prepare the dilutions and that could explain the unusual biphasic curves obtained. Therefore, one of the observed phases corresponded to the real IC_{50} corresponding to the compound, and the second one (on the more diluted ranges) would correspond to a “diluting rate” of the adhered compound to the pipette tip. Changing the tips in each dilution avoided this problem, but also led us to discard the tip-adhered amount of product in every dilution and this could affect the determined potency with these new protocols, slightly decreasing the potency (increasing IC_{50} values). Additionally, to evaluate the effectiveness of the photoswitch in the conditions of the assay, we introduced the term “photoinduced potency shift” (PPS) as the ratio of the IC_{50} in dark conditions and under illumination. The photoinduced potency shift of the “changing tips” protocol decreased when compared to the other protocols, but not excessively (*table 15*). In any case, we decided to test all the compounds again with this new protocol to obtain more reliable and consistent results and to establish a robust comparison of the compound series, since they would share the same pharmacological profile.

Dose-response curves (II) in mGlu₅: New protocol and comparison with the previous one

We generated new dose responses using the new protocol, in which we changed the tips for all the dilutions. With this new protocol we obtained monophasic curves with photoinduced shifts only affecting the potency of the compounds (PPS) (*figure 58*). We generally observed slightly lower potencies (higher IC_{50}), compared to the first phase IC_{50} s obtained with the classical protocol under both dark conditions and under violet illumination. In any case, we used the new values to draw conclusions, as the results are more robust.

Compounds	Illumination wavelength	Classical protocol			New protocol		
		IC ₅₀ (nM)	SEM (nM)	PPS	IC ₅₀ (nM)	SEM (nM)	PPS
109a	380 nm	111	35	6.0	297	77	5.1
109b	380 nm	987	128	6.6	904	82	7.1
109c	380 nm	1577	324	1.7	1884	44	1.7
109d	380 nm	96	7	3.6	183	36	3.7
109e	380 nm	7.6	2.9	4.0	30	4	3.7
109f	380 nm	0.25	0.07	24.3	76	12	4.8
109g	380 nm	49	1	7.2	180	28	4.1
109h	380 nm	1187	63	1.2	308	43	4.1
109i	380 nm	187	98	2.3	328	18	2.5
109j	380 nm	439	305	1.7	309	5	2.9
109k	380 nm	9.7	4.4	1.1	356	57	1.3
109l	380 nm	172	82	1.0	1025	257	1.2
110	380 nm	8760	3678	13.0	4667	392	2.5
111a	380 nm	28239	5419	high	31661	3601	>13
111b	380 nm	1205	290	4.5	2002	334	3.6
111c	380 nm	2264	291	high	3209	269	>13
112	380 nm	1413	149	5.2	2496	32	3.2
113	380 nm	1254	1005	2.2	1477	265	3.3
114	380 nm	1816	157	3.5	1204	220	4.4
	400 nm	n.t.*			2184	663	12.3
115	380 nm	5379	969	1.8	14029	1826	1.5
116	380 nm	4894	1687	5.4	7785	640	2.1
Fenobam (14)	380 nm	901	89	1.0	1603	269	0.9

Table 16: Comparison of IC₅₀ and photoinduced potency shift (PPS) obtained from dose-response curves from IP accumulation assays using the classic protocol and the new protocol with illumination (minimum 3 independent replicates). *n.t. non tested,

Concerning the new dose-response curves, the obtained IC₅₀ were in the range from low nanomolar ($9.0 \leq \text{pIC}_{50} < 6.0$) to micromolar ($6.0 \leq \text{pIC}_{50} < 3.0$) (table 16, figure 58), including aliphatic carboxamides such as **109e** and **109f** with a low nanomolar IC₅₀ (nearly 10 and 4-fold more potent than alloswitch-1 (**83/109a**) or 50 and 20-fold than the mGlu₅ NAM standard

Fenobam (**14**)). Some other compounds were found to display a similar potency to alloswitch-1 (**83**), such as **109d**, **109g**, **109h**, **109i**, **109j** or **109k**, whereas some other ones displayed micromolar IC₅₀s, such as **109b**, **109c**, **109l**, **111b**, **111c**, **112**, **113**, **114**, and some other lower potencies (**111a**, **110** and **116**). It is also remarkable the case of compound **110**, which is not a phenylazopyridine since it includes a classical azobenzene in its scaffold. Despite its micromolar potency, it only partially inhibits the response of mGlu₅ (*annex*). A plausible explanation for this different behaviour may be a different binding mode to the receptor, which would avoid the inverse agonist activity found for most of the phenylazopyridines to perform a partial antagonistic effect. In effect, molecular dockings of compounds **110**, **109e** and **109f** in the crystal structure of mGlu₅³² showed different binding modes of compounds **110** compared to **109e** and **109f** or the one previously described of alloswitch-1 (**109a**) in *chapter 1*. These differences did not point to affect their affinity but could affect the functionality of mGlu₅ receptor. (see *docking of compounds 110, 109e and 109f* section).

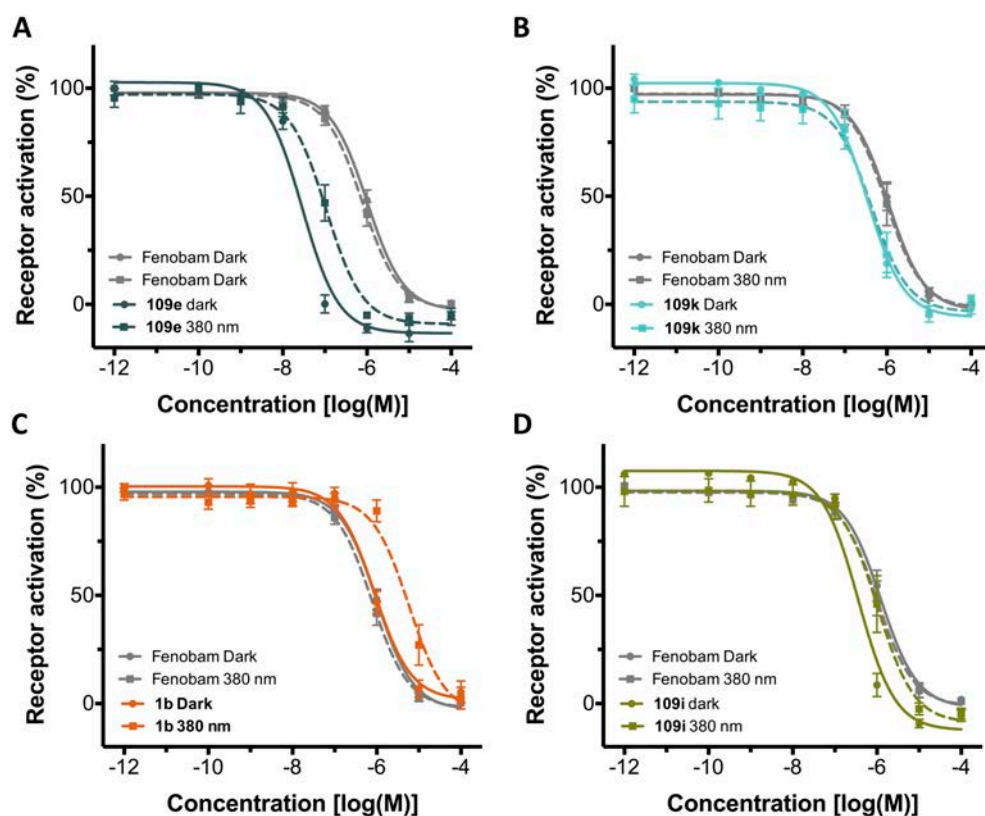


Figure 58: Dose-response curves using the new “changing tips” protocol with IP-One assay on HEK cells overexpressing mGlu₅ receptor with a constant concentration of quisqualate (**2**) 100 nM. Flat lines correspond to the samples incubated in dark conditions and dotted lines to the samples under 380-nm-illumination. Each point corresponds to the mean of a minimum of three independent replicates with the corresponding SEM as error bars. We obtained monophasic curves all compounds with a photoinduced potency shift on the potency, including **109b** (C) and **109i** (D).

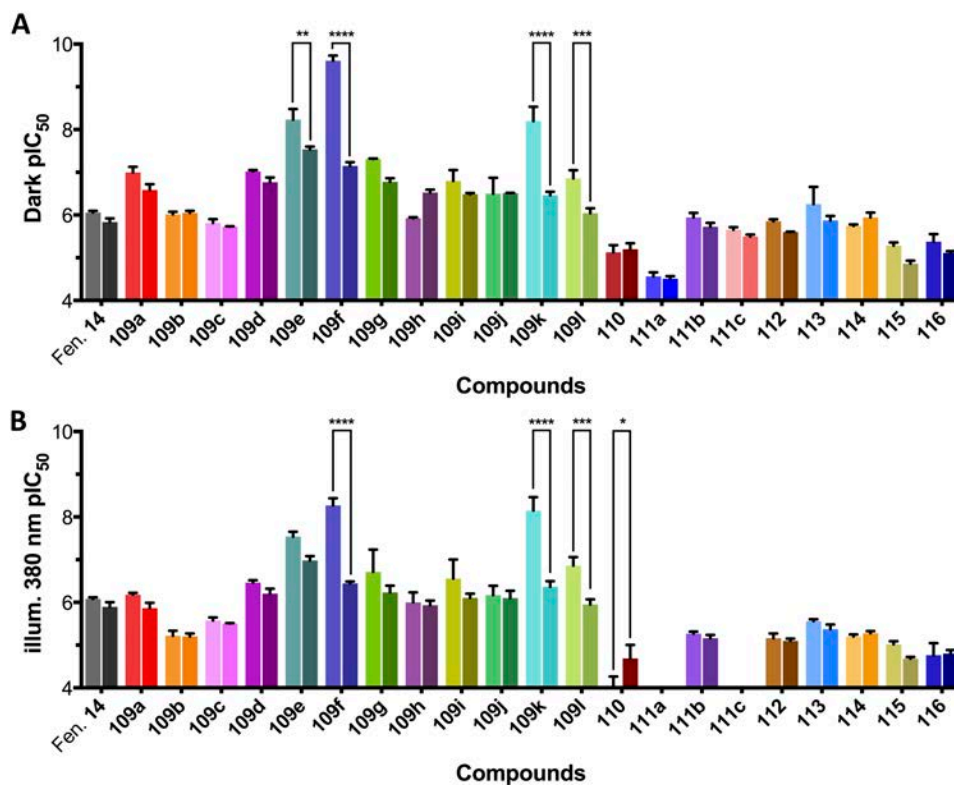


Figure 59: Potency of the compounds of the series (as pIC₅₀) extracted from dose-response curves in dark conditions (A) and under violet illumination (B) using IP-One assay with the classic protocol (pastel colours) and the new “changing tips” protocol (bright colours). Generally the new protocol provide lower potencies but analysis of variance calculation (two-way (compound, condition) ANOVA with condition as repeated measure and including the Šidák correction for multiple testing; *p<0.05, ** p<0.01, ***p<0.001, **** p<0.0001) only showed significant differences with compounds **109e**, **109f**, **109k**, **109l** and **110**.

Concerning the photoswitching properties, we obtained a wide variety of photoinduced potency shifts (PPSs) (*table 16, figure 59A*), which clearly do not depend on the potency of each compound (*figure 60B*, Pearson coefficient $r = -0.28$, $P = 0.2024$), but have a significant correlation with the photoisomerisation score), extracted from the UV-Vis absorption spectra (*figure 60C*, Pearson coefficient: $r = 0.77$, $P < 0.0001$ excluding the partial antagonists or $r = 0.70$ ($P = 0.0003$ including the totality of compounds)). This would indicate that the functional photoswitching of the receptor in living cells is very similar to that observed in solution for the isolated compounds, which validates the central hypothesis of optopharmacology for this family of compounds.

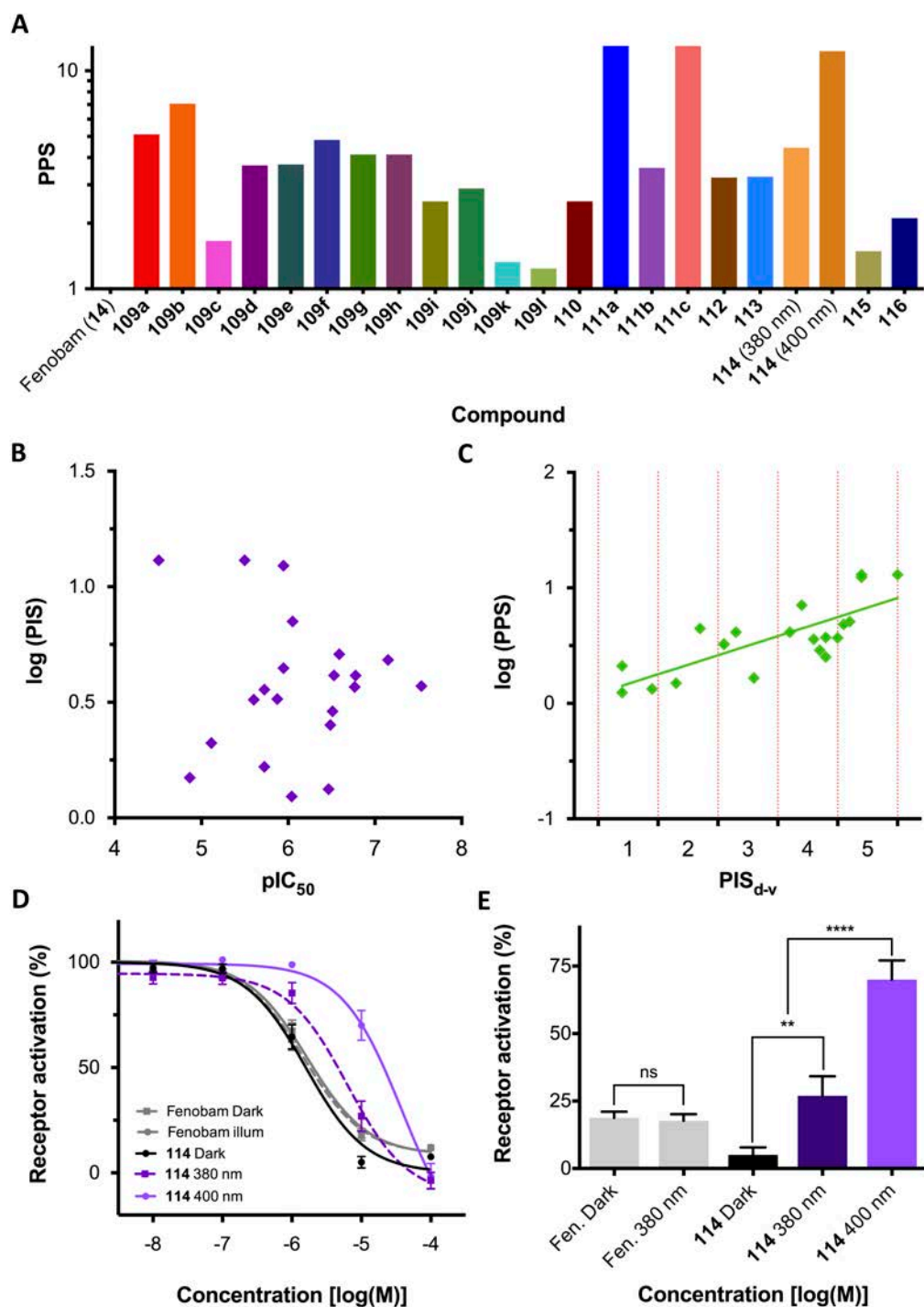


Figure 60: Photoswitching properties in mGlu₅ cell assays. (A) photoinduced potency shift (PPS) of every compound extracted from the corresponding dose-response curves in mGlu₅ using the new protocol. Photoinduced potency shift does not correlate with the potency (B) but strongly correlates with the photoisomerisation score (C) showed in the last section (Pearson coefficient $r = 0.76$, $P < 0.0001$). (D) Dose response-curves using the new protocol with IP-One assay on HEK293 cells overexpressing mGlu₅ receptor with a constant concentration of quisqualate (**2**) 100 nM. Black lines correspond to the samples incubated in dark conditions, dark violet to the samples under 380-nm-illumination and light violet to the samples under 400-nm-illumination. Each point corresponds to the mean of a minimum of three independent replicates with the corresponding SEM as error bars. (E) Percentage of activation of the mGlu₅ with 10 μ M of compound **6** and 100 nM of quisqualate. Analysis of variance (one-way ANOVA with Šidák

correction for multiple comparisons; ** $p < 0.01$, **** $p < 0.0001$) showed significant differences between dark bar and 380-nm values, and also of 400 nm values with both dark and 380-nm values.

Even though **109e** and **109f** share high structural resemblance and similar potencies as NAMs of mGlu₅, they display different receptor photoswitching capacities (PPS(**109e**) = 3.7 and PPS(**109f**) = 4.8). This defines compound **109f** as a stronger candidate to control mGlu₅ activity with light. In addition, we can find other interesting compounds, with IC₅₀ in the micromolar range, but with very high PPS, such as compounds **109b**, **111c** or **114**. Specifically, compound **114** exhibited a very interesting PPS (12.3) when it was illuminated at 400 nm, much better than in those observed at 380 nm (PPS=4.4) (*figure 60D*). Again, these results are consistent with the previous photoisomerisation experiments, which indicated a wavelength dependence of compound **113**, also observed in the receptor cellular assay. Additionally, this effect can be easily identified at a single 10 μ M of **114** in the same cell assay (*figure 60E*). In the dark, cells incubated with **114** showed practically complete inhibition and those illuminated at 380-nm-light still retained 75% inhibition of the mGlu₅ activity, indicating a high remaining antagonist effect for **114** at this wavelength. However, when 400-nm-light was applied, the inhibition was reduced to 25%, showing a lower antagonistic effect, which is compatible with the expected higher fraction of the inactive *cis* isomer at this wavelength. Interestingly, this illustrates again the parallelism between photoisomerisation of the isolated compound and its effects on mGlu₅ receptors in cells. Moreover, this opens the possibility of inducing wavelength-dependent effects to fine-control the activity of the receptor with light, which in conventional pharmacology would require applying different concentrations of ligand.

Real-time photoswitching in cell assays

S. Pittolo, IBEC, Barcelona

We next evaluated the possible application of the observed photoswitching to a reversible real-time control of mGlu₅ receptor. Hence, we selected the most representative phenylazopyridine compounds and tested their effects by time course of intracellular calcium in individual HEK293 cells overexpressing mGlu₅ receptor. In the dark, all the compounds antagonised the calcium oscillations evoked by the activation of mGlu₅ by quisqualate (*figure 61A*). After a period in the dark, illumination with 380-nm-light induced the photoisomerisation of the phenylazopyridines and re-established the calcium oscillations observed in response to the orthosteric agonist, in some cases with an increase of calcium oscillation frequency (*figure 61A*), which suggests an over-activation or an increase of the expression mGlu₅ active receptors¹⁹⁹. This effect was reversed by illumination with green light

and could be repeated over several light cycles for all the compounds, demonstrating a fully reversible photoswitch in cellular medium as well as a fine control of the biological activity with light (*figure 61AC*).

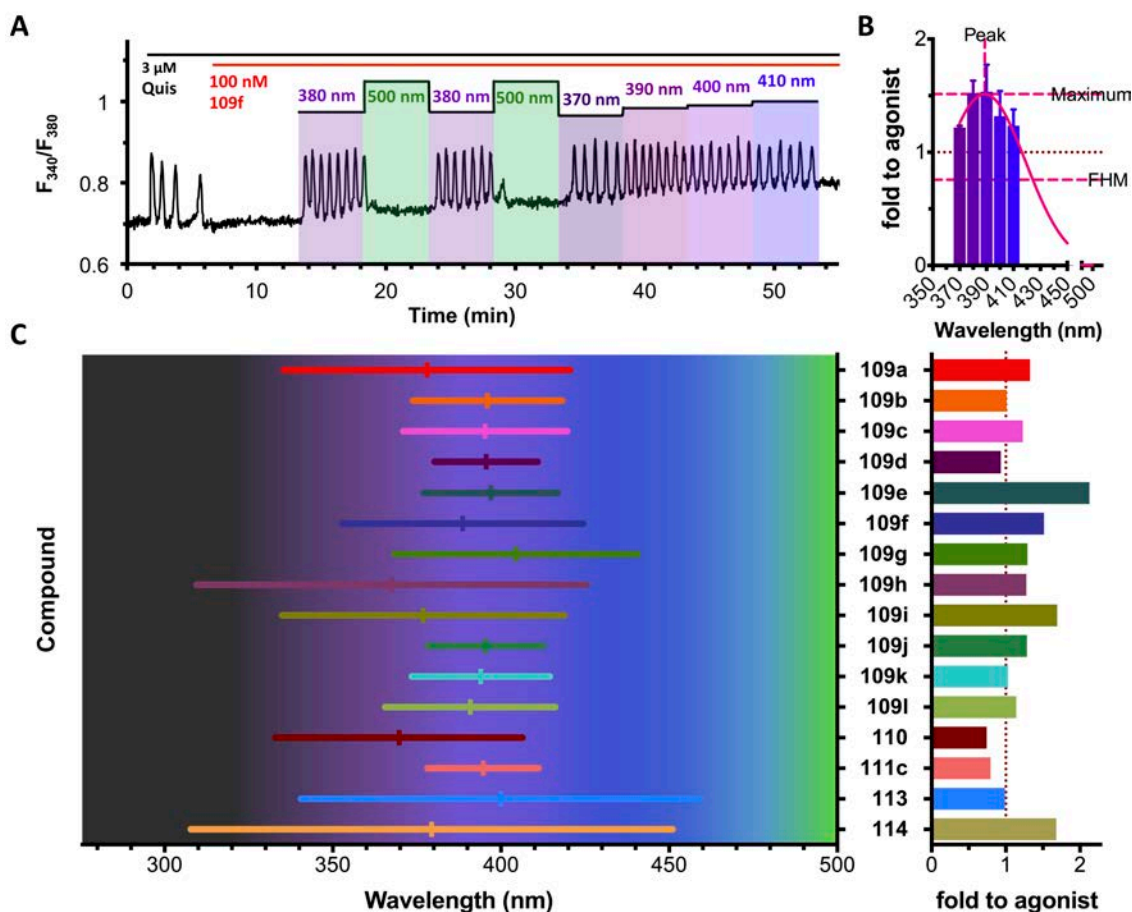


Figure 61: Calcium imaging in individual cell of compounds **109f**. (A) Fluorescence ratio (F_{340}/F_{380}) over time of calcium indicator Fura-2 loaded in mGlu5-expressing HEK293 cells. Application of quisqualate $3 \mu\text{M}$ (black line) activated mGlu5, $1 \mu\text{M}$ of compound **109f** (red lines), and with different illumination wavelengths (six, ranging between 370 and 500 nm) indicated by colour boxes and corresponding numbers above. (B) Quantification of the light-induced receptor activity in the presence of **109f** at indicated illumination wavelengths. Data are presented as mean \pm SEM of the normalized calcium oscillation frequency (oscillations per minute normalised to the initial response to the agonist). Peak, half width at half maximum (FHM) and maximum (Max) values were inferred by fitting a Gaussian function (magenta curve) to the data shown in *panel C*. Summary of wavelength-activity relationship in single-cell experiments for a selection of compounds. In the left graph, the centre of the bars indicate the illumination wavelength (Peak) at which the maximum light-induced receptor activity is obtained for the compounds, whereas bars represent the range of wavelengths at which the light-induced activity is equal to half the maximum response or more (fraction half maximum, FHM). The maximum amplitude of the light-induced receptor activity is reported in the graph on the right, and expressed as times the response to agonist of the naïve receptors. These three parameters (peak, FHM, and maximum) describe the Gaussian fitting performed for all compounds on the original data from single-cell experiments, as shown for compounds **109f** in *panel B*.

After violet-green light cycles, we additionally illuminated the cells with several wavelengths around 380 nm to identify the best wavelength for restoring mGlu₅ activity (*figure 61A*). The oscillatory frequencies for each illumination period were normalized to the response to the agonist alone, plotted versus the wavelength used for illumination and fitted to a Gaussian curve (*figure 61B* and *annex*). This scanning allowed inducing different oscillatory frequencies in the same cell by simply illuminating at different wavelengths and also demonstrated that these phenylazopyridines not only are able to block and release mGlu₅ receptor signalling with green and violet illumination wavelengths, but can also tune its activity by selecting the appropriate wavelengths between 500 and 380. Thus, with these compounds we are able to fine-tune in “real-time” the activity of mGlu₅ receptor by a suitable election of the wavelength of illumination. Moreover, every compound of the series presents a particular and different behaviour (*figure 60C*). For example, compound **109e**, which was found to be the most potent in the IP accumulation assay, is the most effective in the inducing an over-activation under violet illumination (>2 fold to agonist activation, whereas compound **111c** only recovered the response to quisqualate alone (*figure 61C*). The spectral range to achieve this activation also depends on the compound: there are compounds with a wavelength narrow range, such as **109d** or **111c**, whereas others have wider wavelength ranges, such as **113** or **114**.

A similar control of the frequency of mGlu₅ calcium oscillations was previously reported applying different doses conventional mGlu₅ NAMs¹⁹⁹ in cultured cells, but an in-vivo approach of this is unfeasible due to unmanageable drug distribution and metabolism processes. Instead, the use of photoswitchable NAMs offers several advantages over the classical approaches: A single dose can be used since the effective dose can be adjusted illuminating with a specific wavelength and this can be dynamically adjusted over time. This allows a precise control and an exact adjustment of the extent of the desired pharmacological effect, with a high spatiotemporal precision during the time of exposition.

***In-silico* characterisation of 110 and 109e,f**

J. A. Dalton, INC-UAB, Bellaterra

In order to investigate the mGlu₅ NAM functionality of these series of compounds *in silico*, we used the mGlu₅ crystal structure (PDB id 4O09), in a similar procedure to that used in *chapter 1*. Therefore, we docked compounds **109a** (**83**), **109e**, **109f** and **110** with AutoDock4.2²⁰² and the protein-ligand complex was subjected to energy minimization in the Amber14 force-field. We selected these compounds to be compared with presented dockings of compound **83** in *chapter 1*, since **109e** and **109f** are the most potent in IP accumulation

assays and **110** is the only one that do not constitute a phenylazopyridine derivative and show a partial antagonistic effect in IP accumulation assays, which could be associated to a different binding mode in the allosteric pocket.

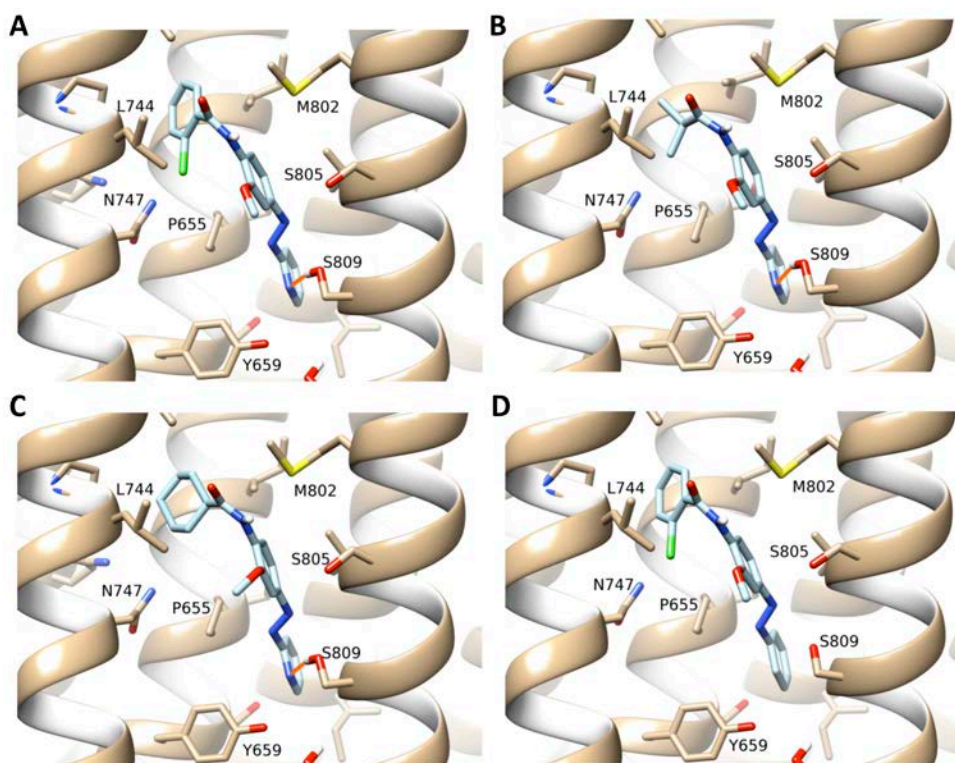


figure 62: Dockings of four compounds: **109a** (A), **109e** (B), **109f** (C) and **110** (D), (in light blue) into the crystal structure of the TM domain of mGlu₅ (in beige, PDB id 4009, including co-crystallized water molecule) using AutoDock4.2. All docked structures were energy-minimized with CHIMERA in the AMBER14 force field. Predicted protein-ligand H-bonds are shown as orange lines. Receptor orientation: TM6 not shown, TM5 front-left, TM7 front-right, TM3 central, TM4 back-left, TM2 back-right.

These computational experiments revealed that compounds **109a**, **109e** and **109f** form a protein-ligand H-bond between the pyridine ring nitrogen and S809 on TM7 of mGlu₅ receptor (PDB id 4009). Obviously, this interaction is not observed with compound **110**, since it has a phenyl ring instead of the pyridine ring (*figure 61*). The predicted docking scores are observed to be equivalent among all ligands, except **109e**, which is less favourable, likely due to its slightly smaller size. This suggests that the pyridine ring does not affect ligand affinity *per se* but does directly affect receptor functional activity. It is theoretically possible that S809 is an allosteric toggle switch for NAM effectivity by H-bonding the allosteric ligands or may simply help to stabilise the NAM-bound receptor state. In more general terms, ligand H-bonding to S809 appears to be necessary for NAM activity, which can either be mediated by a pyridine ring or another ligand substituent, such as the hydroxyl group of mavoglurant in the mGlu₅ crystal structure (PDB id 4009) where an H-bond is made with S809 (and also with adjacent

S805)^{32, 203}. Therefore, the lack of ligand H-bonding to S809 for compound **110** might be the responsible of its different pharmacological properties, previously observed in the IP accumulation assays.

***In-vivo* biological evaluation of 109-115**

***In-vivo* zebrafish screening in dark conditions**

We finally selected the phenylazopyridines with a suitable efficacy in IP accumulation assays and we tested them zebrafish-larvae behavioural assays. Therefore, at this point we discarded compounds **110**, **116** for their lack of efficacy and **118** for its poor activity in mGlu₅ receptor cell assays.

First, the activity of the all compounds was evaluated by monitoring zebrafish locomotion in the dark conditions. Thus, after 10 µM administration of each compound in the swimming medium, we recorded their track during 30 minutes and the free-swimming distance of every animal was integrated every 5 minutes (*figure 63A, annex I*). Under these conditions, the reference NAM fenobam (**14**), used in previous experiments, showed lower but not significant difference with the vehicle, probably due to its relatively low potency and the limited dose used. Thus, we tested 2-BisPEB (**53**), which is a very potent non-photoswitchable NAM of mGlu₅^{124, 209} and shares some structural similarities to our phenylazopyridines, including two phenylethynylpyridine systems and three conjugated aromatic rings. Therefore, 2-BisPEB (**53**) was expected to show similar *in-vivo* absorption and distribution properties compared to the members of our series. Indeed, 2-BisPEB (**53**) significantly inhibited the zebrafish motility, becoming an excellent reference compound. After 20 minutes the compound was exerting its effect in a regular and continuous mode, since the recorded behaviour of the fish was stabilized. This can be indicative of a proper absorption of the compound on animal tissues, indicating a plausible effect on mGlu₅ receptors *in vivo*.

We next screened the phenylazopyridines of our series, and they induced inhibition of the zebrafish motility with different extents, except compounds **114** and **115**, which induced a slight increase in the animal motility (*figure 63B*), compared to the vehicle effect. The reasons for this abnormal behaviour are presently unknown. In general, we observed that 25 minutes after the compound administration, the animal behaviour was stable and hence we assumed that the compounds had been absorbed, well distributed and induced their pharmacological effect. Therefore, we used the cycle of 25-30 minutes to evaluate the *in-vivo* pharmacological effect on every compound (*figure 63C*).

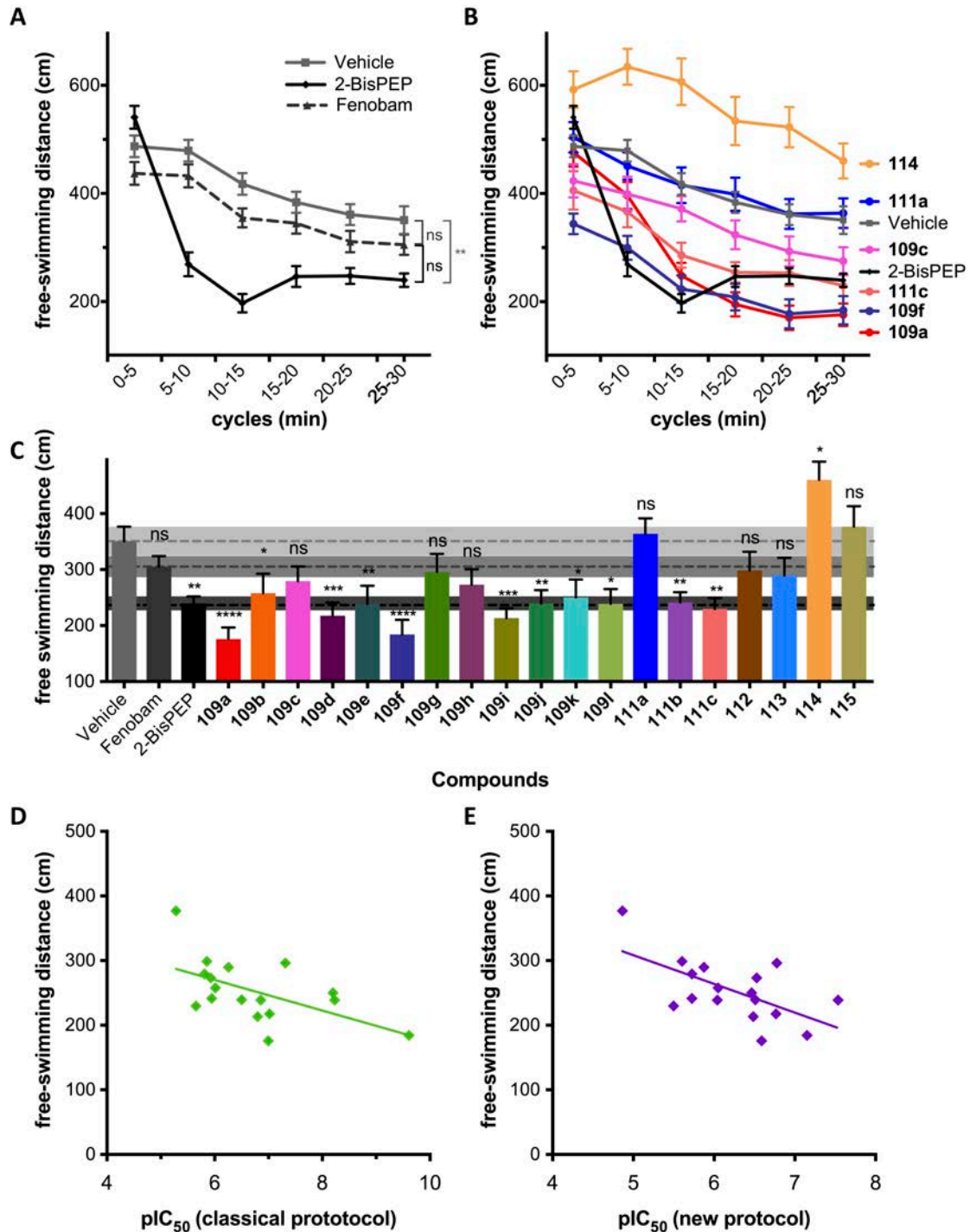


Figure 63: *In-vivo* screening with 7-day-old zebrafish larvae in dark conditions. (A,B) Integration of the total accumulated free-swimming distance for every 5 minutes after application of 10 μ M concentration of the control solutions (A) or different compounds (B). Values correspond to the mean and the SEM of the behaviour of 30 animals minimum. Analysis of variance (two-way (compound, time) ANOVA with time as repeated measure and including the Šidák correction for multiple testing; * $p < 0.05$, ** $p < 0.01$, *** $p < 0.001$, **** $p < 0.0001$) showed significant differences of some compounds response with vehicle response (only shown the cycle 25-30 min). Fenobam (14) did not show a significant effect when compared to vehicle, but 2-BisPEP (53) did. (C) Integration of the total accumulated free swimming distance during 5 minutes 25 minutes after the administration of compounds 109a-l, 111b,c and 112-115 extracted from panel A plots and annex-I. Values correspond to the mean and the SEM

of the behaviour of 30 animals minimum. (D,E) Total accumulated free-swimming distance considerably correlates with the potency obtained IP-One assays, especially when the last protocol was used (D) (Pearson coefficient $r = 0.62$, $P = 0.0084$).

Remarkably, the extent of the inhibition of the animal motility for most of the compounds was comparable to the compound potencies in cell-based assays. Only compounds **109e**, **109g** and **109h**, which in spite of displaying nanomolar potency in IP accumulation assays, inhibited zebrafish motility with a lower efficacy than expected. Indeed, the pharmacological potency (pIC_{50}) and the inhibition of the zebrafish motility (free-swimming distance) are correlated. For the IC_{50} s extracted with the new protocol, the Pearson correlation coefficient was $r = -0.62$ ($P = 0.0084$), excluding non-inhibiting compound **114**. If the non-expected behaviours of **109e** and **109g-h** are also excluded, Pearson correlation coefficient results in $r = -0.82$ ($P = 0.0003$) (*figure 63D*).

***In-vivo* zebrafish screening with light**

To evaluate the physiological photoswitching properties *in-vivo* we performed a new assay with the same animals right after the experiments in dark conditions. During this second experiment, the animal motility was tracked again with an integration of the free-swimming distance every 60 s. We applied six repetitive light cycles consisting in one minute in dark conditions and one minute under illumination with violet light ($\lambda = 380$ nm). Between the violet illumination and the dark conditions, the fish were also illuminated 5 seconds with visible light to accelerate the relaxation from *cis* to *trans* configuration of the phenylazopyridines. All violet light periods prompted an increment of the motility of all the zebrafish tested, including vehicle and 2-BisPEB-treated ones. However, 2-BisPEB-treated animals displayed a sustained inhibition of their motility compared to the vehicle treated animals independently of the light conditions (*figure 64A and annex*).

In general for all the phenylazopyridines of the series, the inhibitory effect in dark conditions disappeared after shining 380-nm-light, and was recovered in the following dark cycle, defining a fully reversible process (*figure 64BC*), even for compound **114**, which induced an increase of the zebrafish motility in the previous experiment. Indeed, compound **114**, after one cycle of illumination, inhibited the animal motility very efficiently in dark conditions, like 2-BisPEB did, and with successive cycles afforded an on/off photoswitching of the animal motility (*figure 64D*). With the information that we dispose we cannot give any explanation of this change of activity before and after applying light cycles.

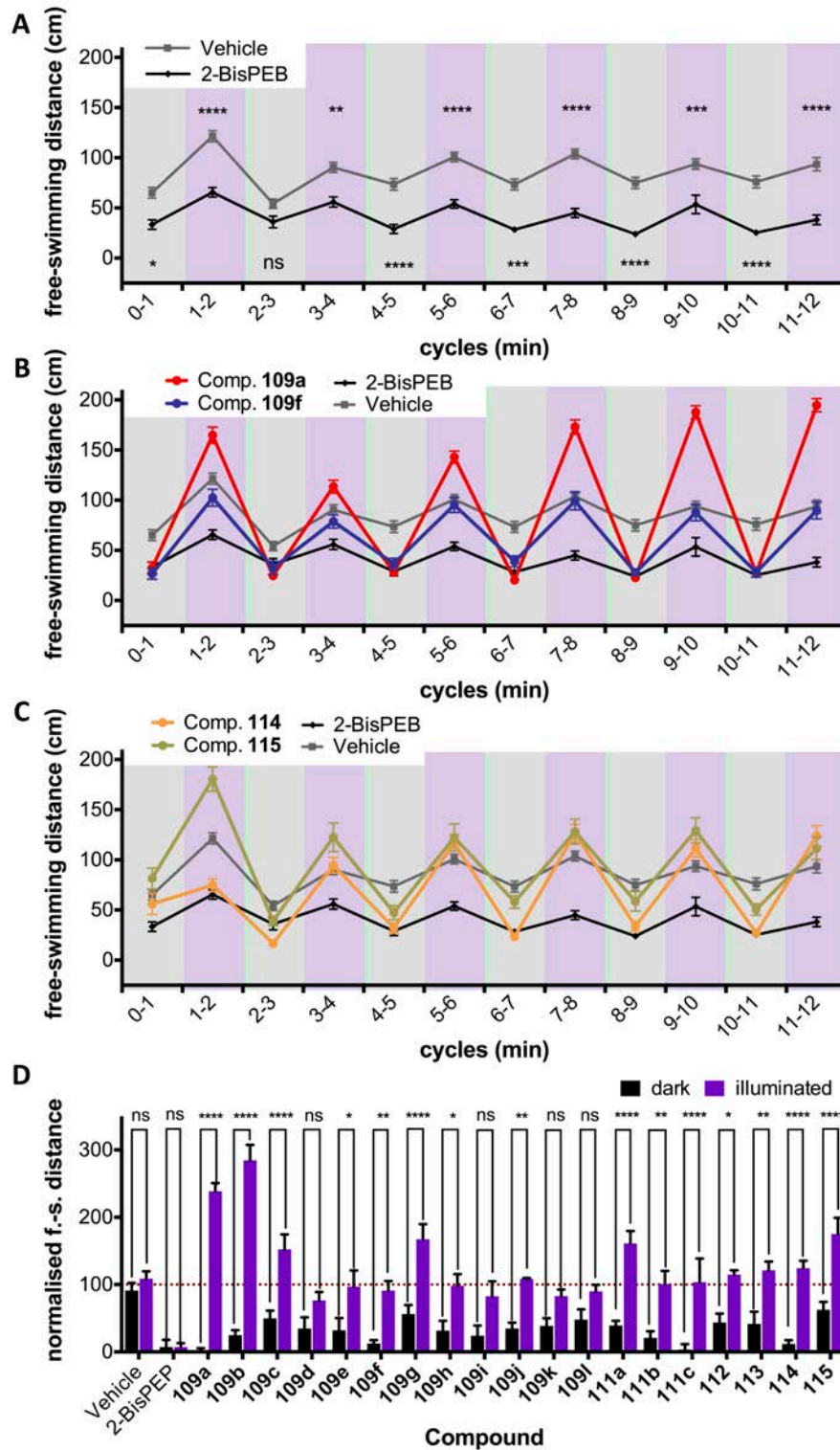


Figure 64: *In-vivo* screening in zebrafish 7-day-old zebrafish larvae with light. (A-C) Integration of the total accumulated free-swimming distance for every minute. We repetitively applied the following light cycle: 1 min in dark conditions and 1 minute with violet illumination. Between both conditions we shined the animals 5 seconds with white light. Analysis of variance: two-way (compound, time) ANOVA with time as repeated measure and including the Šidák correction for multiple testing (* $p < 0.05$, ** $p < 0.01$, *** $p < 0.001$, **** $p < 0.0001$). Vehicle and 2-BisPEB showed significant differences (A) and compound **109a** and **109f** at a concentration 10 μM inhibited animal motility similarly to 2-BisPEB in the dark conditions (grey background), whereas under violet light (violet

background), fish treated with **109f** recovered a normal behaviour and those treated with **109a** experience an increase of their normal motility (B). Animals treated with compound **114** after 1 light cycle displayed a similar behaviour to compound **109f**, and compound **115**, despite not inhibiting significantly the motility in dark conditions, under violet light show an over-activation of the animal motility (C). Values correspond to the mean and the SEM of the behaviour of 24 animals minimum (A-C). (D) *In-vivo* photoswitching efficacy of compounds **109a-l**, **111b,c** and **112-115** with the corresponding variance analysis. Each bar corresponds to the mean and SEM of the sum of the free-swimming distances in dark conditions and under violet illumination points for each experiment (6 animals per experiment, 4 experiments) subtracting the corresponding effect of 2-BisPEB (**53**) and normalizing the distances by the lower effect and vehicle effect to minimize the effect of the light not corresponding to the effect of the administered compounds. Analysis of variance: two-way (compound, light conditions) ANOVA with light conditions as repeated measure and including the Šidák correction for multiple testing (* $p < 0.05$, ** $p < 0.01$, *** $p < 0.001$, **** $p < 0.0001$).

However, we found two different behaviours under 380-nm-illumination:

- a) A group of compounds causing a motility in line to the vehicle-treated fish
- b) A group of compounds inducing an over-activation of the motility of the animals, exceeding the levels displayed by vehicle-treated fish.

Compounds **109a** and **109f** constitute a representative example of each behaviour respectively (*figure 64B*), while in dark conditions they equivalently inhibit the animal motility with a high efficacy.

This *in-vivo* over-activation under violet illumination after dark periods, which could be related to the over-activation observed in real-time cell assays, was evident for compounds **109b**, **109c**, **109g** and **115**, and a milder effect was found for compounds **112**, **113** and **114** (*Annex, figure 64CD*). All these phenylazopyridine derivatives comprise a set of compounds with very different potencies, from low nanomolar ranges to micromolar IC_{50} s in IP accumulation assays. Structurally all have three aromatic rings with a phenyl group in one edge with certain electron-density. In contrast, the group of compounds that did not induce this over-activation, either do not have this third aromatic ring or, if present, its electron density is low due to the presence of electron-withdrawing groups, like fluorine, or they have pyridines, which are intrinsically electron poor. Compound **115** constitutes a particular case, since it also induces over-activations under illumination and includes a 2-pyridylcarboxamide ring as the third aromatic ring. However, it is the only compound with 1,3 substitution in the central ring, that have a minimal influence on the π electron density of the azo-bond. Intriguingly, not all the compounds that induce this over-activation do it in real-time cell assays. For example, compounds **109e**, **109f** and **109i** with a higher over-activation effect in cell-based assays, did not induce a measurable over-activation in animal motility. In contrast, **109b**, unable to

produce the receptor over-activations in cell-based assays, induced the highest over-activation *in-vivo*. This may be due to differences in these two assays, which use different illumination protocols and test mammalian and zebrafish mGlu₅ receptors respectively, whose functionalities can differ considerably. In any case, this atypical effect could only be detected with photoswitchable compounds and will be subject of future studies to be able to give molecular explanations. Other reasons cannot be excluded at this point, including effects on other receptors, influences on receptor recycling processes or any other effect.

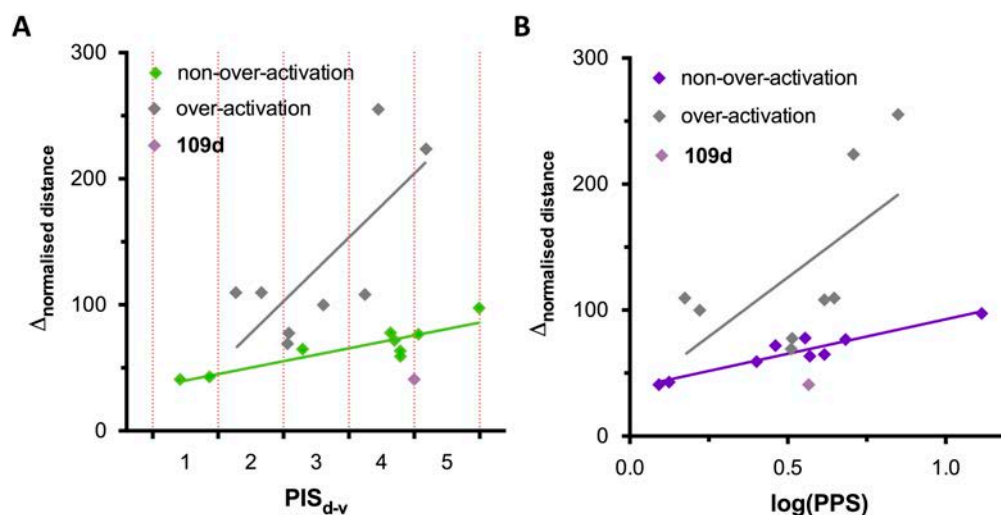


Figure 65: Difference of the normalised free-swimming distance of the non-over-activating phenylazopyridines correlates with both photoisomerisation score (PIS_{d-v}) (“Photoisomerisation of compounds” section) and photoinduced potency shift (PPS) (“Dose-response curves (II)” section). In contrast over-activating compounds show a lower correlation.

Regarding the *in-vivo* photoswitching properties of these phenylazopyridines, all them induce a light-dependent regulation of zebrafish motility (figure 64D) with different extents. The compounds that promoted an over-activation of the animal motility under violet light show higher significances in their photoswitching. Even so, differences for the rest of compounds were still significant, except for compound **109d**, whose *in-vivo* activity was abnormally weak, and **109k** and **109l**, which performed poor photoswitching in the cell assays and in solution probably as a consequence of their limited intrinsic photoisomerisation capacity. In fact, if the compounds with over-activation behaviour are not taken into account, the difference between the violet and dark values of each compound in figure 64D correlate with photoisomerisation score (PIS) (Pearson coefficient $r = 0.70$, $P = 0.025$) and with photoinduced potency shift (PPS) logarithm (Pearson coefficient $r = 0.83$, $P = 0.0031$) (figure 65). If compound **109d** is neither considered due to its low-efficacy response, the Pearson correlation with PIS coefficient rises to $r = 0.89$ ($P = 0.0014$) and to $r = 0.95$ ($P = 0.0001$) with PPS logarithm (figure 65). In contrast, the

compounds inducing an over-activation show lower correlation with the data obtained from *in-vitro* experiments (*figure 65*). All these results show a high robustness of our photoisomerisable compounds throughout different assays, from compounds in solution to cell-based *in-vitro* assays and *in-vivo* behavioural experiments.

Conclusions

We synthesized a series of photoswitchable mGlu₅ NAMs based on phenylazopyridine scaffold, with a robust SAR, with almost all the *trans* isomers active on mGlu₅ in cell-based assays and a half of them significantly inhibiting zebrafish motility at 10 μM of concentration.

We obtained variable photoisomerisation properties, attributable to different structural properties, and their translation to *in-vitro* and *in-vivo* assays was successful, since very few compounds lost its photoswitching properties in any of the different assays in spite of the increasing complexity of the biological tests. From these compounds, we obtained excellent photoswitching behaviour in all the assays performed with compounds **109a**, **109f**, **109i**, **109j**, **111c**, as well as **114**, which resulted in a more powerful photoswitching when illuminating with blue-shifted wavelengths.

We showed *in-silico* that the binding modes of these series of compounds is the mGlu₅ allosteric site is very similar to that one of alloswitch-1 (**83**) (*chapter 1*), and the different pharmacological profile of compound **110** observed in cell-based assays might be explained as a result a different binding mode in the allosteric site of transmembrane domain of the receptor.

The phenylazopyridine series allowed us to define a way to achieve a fine control of mGlu₅ receptor activity by tuning the wavelength of illumination between 360 and 500 nm and, depending on the compound used, we were able to control an over-activation of the receptor. This functional over-activation was also detected *in-vivo* after treating zebrafish larvae with some specific compounds, but not with others. The reasons for this light- dependent atypical effect could be linked to the potentiation of calcium responses in single cell assays and require further investigation. Photoswitchable ligands reveal new paradigms on the ligand-induced protein responses with potential to add a new modulatory dimension to drug therapeutics.

Chapter 4: The quest of dual mGlu₄ PAMs and mGlu₅ NAMs: azo- and amide-replacement of 2-BisPEB

On the first chapter of the present thesis, we showed the design and synthesis two photoisomerisable allosteric modulator of mGlu₄ and mGlu₅ (alloswitch-1 (**83**) and optogluram (**84**)), whose structure was very similar. In the second chapter we presented a very robust bioisosterism between mGlu₅ NAMs with acetylene and *trans*-azo bonds and in the third chapter we presented a series of compounds as mainly mGlu₅ NAMs, but with some individual acting as mGlu₄ PAM.

In the present chapter, we will describe the design, synthesis and characterisation of a new series of compounds, based on simple structures, in part related to alloswitch-1 (**83**) and optogluram (**84**), but more closely related to compound **109j** and **111a**, which differ only in the position of one methoxy group but display very different pharmacological profiles. Overall, the aim of this series is to establish chemical patterns for mGlu₄ PAMs and mGlu₅ NAMs and obtain dual mGlu₄ PAM and mGlu₅ NAM compounds, with photoisomerisable properties or not, which would be of particularly interest for the treatment of neurodegenerative diseases like Parkinson disease^{10, 82, 88} or neuropathic or inflammatory pain^{10, 55, 83-85}.

Papers related to this chapter:

Xavier Gómez-Santacana, James A. Dalton, Xavier Rovira, Cyril Goudet, Jean-Pilippe Pin, Pau Gorostiza, Jesús Giraldo and Amadeu Llebaria, "Positional isomers of azologized negative allosteric modulators induce efficacy changes on mGlu₅ functional response", *ChemMedChem*, **2015**, submitted

Initial considerations and design of compounds 128-133

As we explained in *chapter 1* and *chapter 2*, between mGlu₄ PAM and mGlu₅ NAM allosteric sites may possess a high degree of similarity, since these pockets are able to selectively recognize compounds differing only in the bridging functionality between two aromatic rings. Therefore, it may be plausible to design and synthesises compounds both pharmacological activities: mGlu₄ PAM and mGlu₅ NAM.

An additional example of this duality is the case of compounds **109j** and **111a**, from *chapter 3*. On the one hand, compound **109j** was one of the top mGlu₅ NAMs of the previous series, with nanomolar potency as an mGlu₅ NAM (*figure 66A*) in cell assays and a low efficacy at the screening at 30 μ M as an mGlu₄ PAM (*figure 53*) also in cell assays. On the other hand,

compound **111a**, which only differs from **109j** for the position of the methoxy in the central ring, display a low micromolar potency as a PAM of mGlu₄ (figure 66B) and a negligible activity as an mGlu₅ NAM (IC₅₀ = 32 μM, table 16).

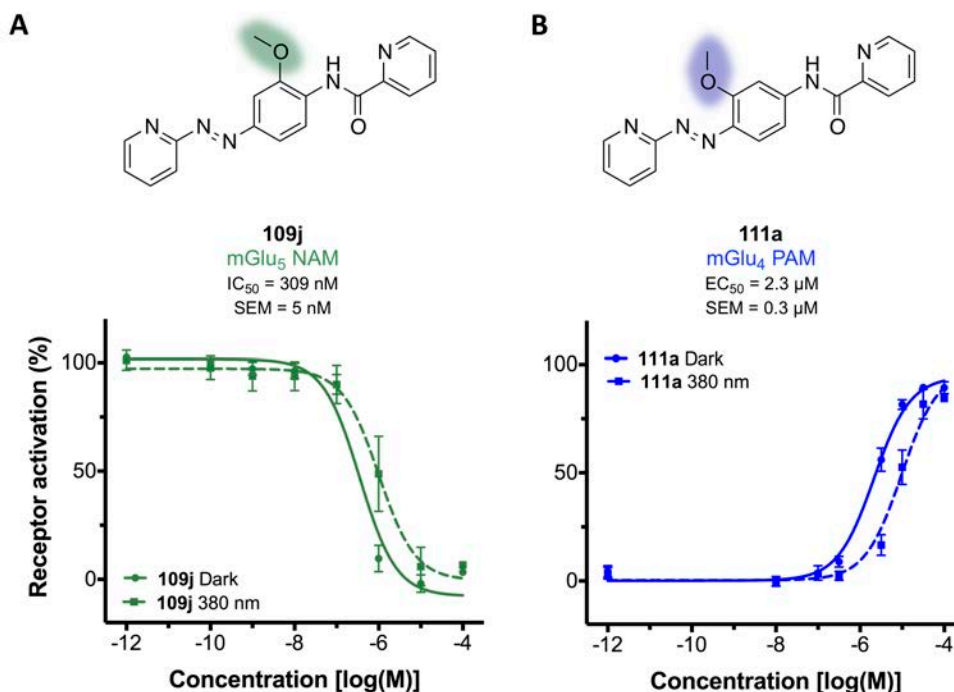


Figure 66: Compounds **109j** and **111a** structurally only differ from the position of the methoxy group, but show different pharmacological profiles: **109j** is an mGlu₅ NAM, whereas **111a** is an mGlu₄ PAM. IC₅₀ and EC₅₀ are the mean of three independent replicates with the corresponding SEM.

Our objective of this chapter was to afford a compound with dual mGlu₄ PAM and mGlu₅ NAM activity. As the only difference between both compounds is the methoxy group position, we considered that removing this group we could obtain one compound with dual mGlu₄ PAM and mGlu₅ NAM activity. We would probably lose potency after this removal, but the synergy of the two effects in the synapse might induce a more powerful biological effect compared to the possible effect of a potent conventional selective mGlu₄ PAM or mGlu₅ NAM.

We had already synthesised this compound (**111c**) in the previous series and it resulted to be a low-micromolar-potency mGlu₅ NAM (IC₅₀ = 3.2 μM) in cell assays, which was acceptable for our purposes. Compound **111c** also displayed a considerable efficacy at the screening at 30 μM as an mGlu₄ PAM, though it was not saturating (figure 54B).

Additionally, since compound **111c** includes a phenylazopyridine, we also considered the possibility to do “invers azo-replacement” (as the inverse process of azologization¹⁸⁷) substituting the azo-bond by an acetylene. In that case, we would achieve a dual non-photoswitchable mGlu₄ PAM and mGlu₅ NAM **128a** (figure 67).

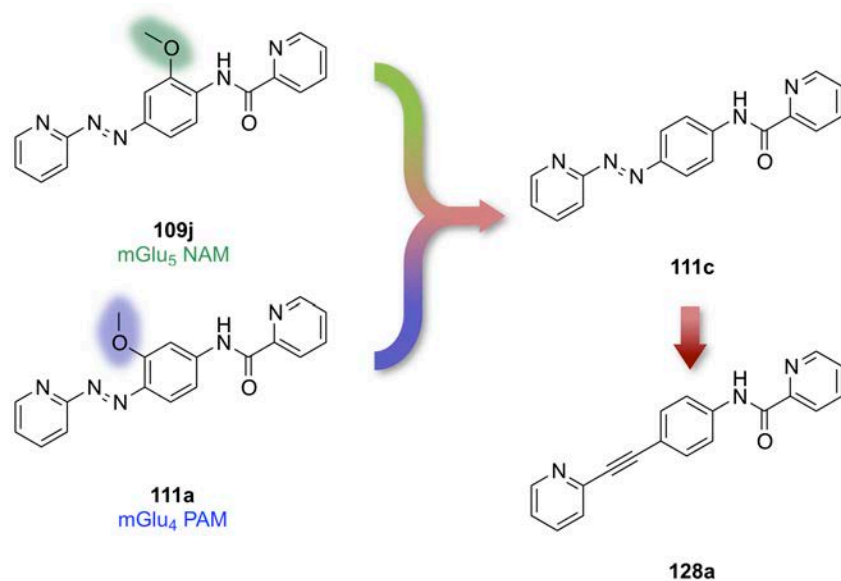


Figure 67: Design of mGlu₄ PAM and mGlu₅ NAM dual compounds. Removal of the methoxy group of compounds **109j** and **111a** lead to compound **111c**, which can display dual mGlu₄ PAM and mGlu₅ NAM activity. “inverse azo-replacement” of compound **111c** would probably lead to the non-photoswitchable mGlu₄ PAM and mGlu₅ NAM

129a.

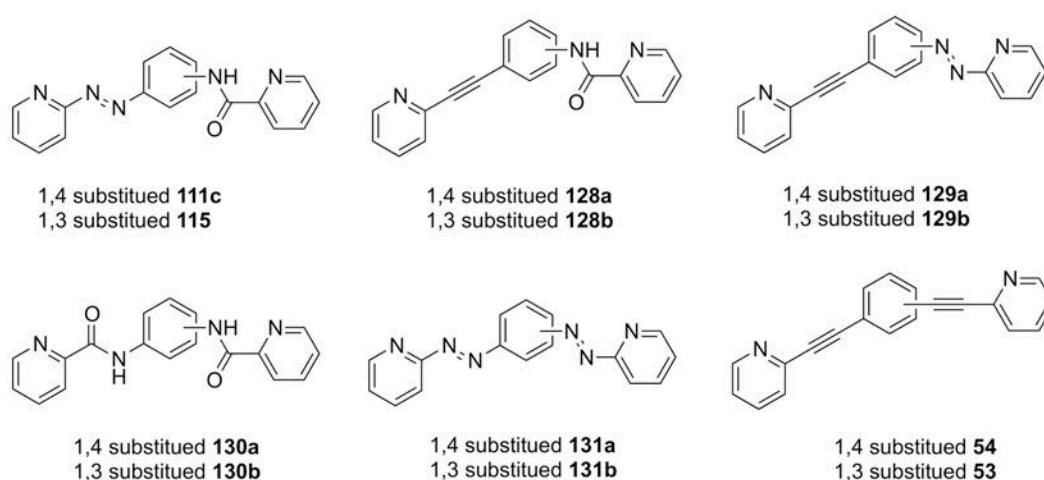
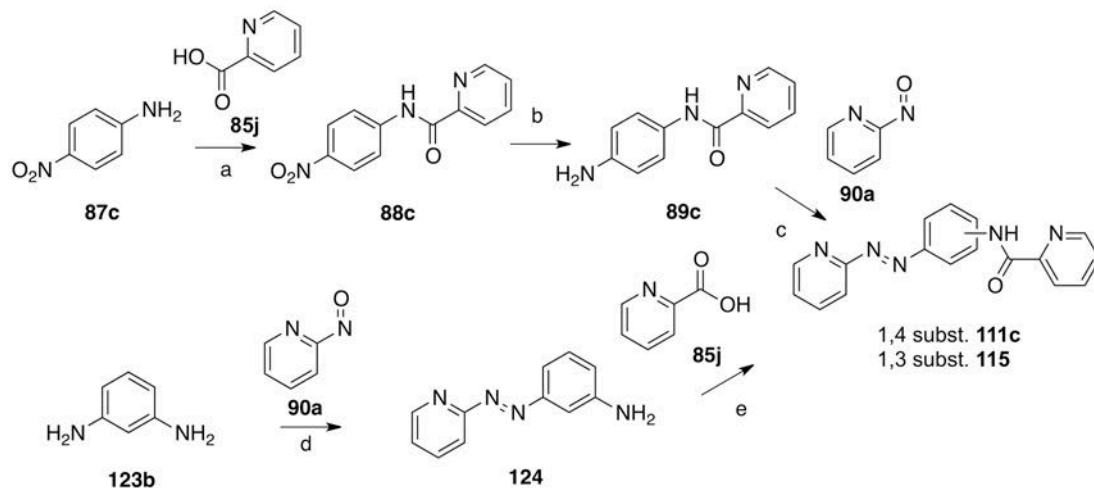


Figure 68: New series of compounds **128-132**

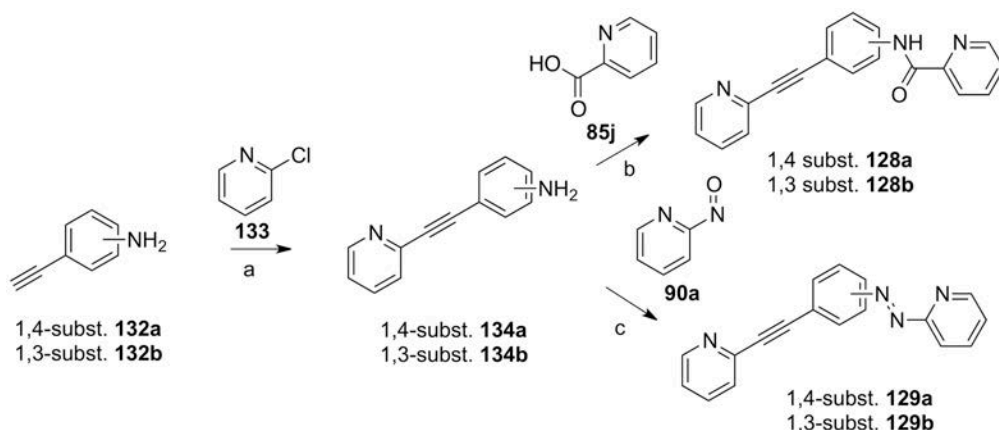
Since **111c** and **128a** comprise a phenyl ring chemically bound in 1,4 position to two 2-pyridines with three possible bridges: azo-bond, acetylene or *N*-amide, we decided to cover all the possible combinations to study how can they affect to the mGlu₅ NAM activity or the mGlu₄ PAM activity. Therefore, apart from **111c** and **128a**, which combine an azo-bond/*N*-amide and acetylene/*N*-amide, we designed compound **129a**, with azo-bond/acetylene and the symmetric bis-*N*-amide **130a**, bis-azo-bond **131a** and the bis-acetylene **54**.

Synthesis of compounds 111c, 115, 128-131, 53, 54

Compounds **111c** and **115** were prepared following the synthetic strategy shown in *Scheme 8*. The synthetic strategies are described in *chapter 3*.



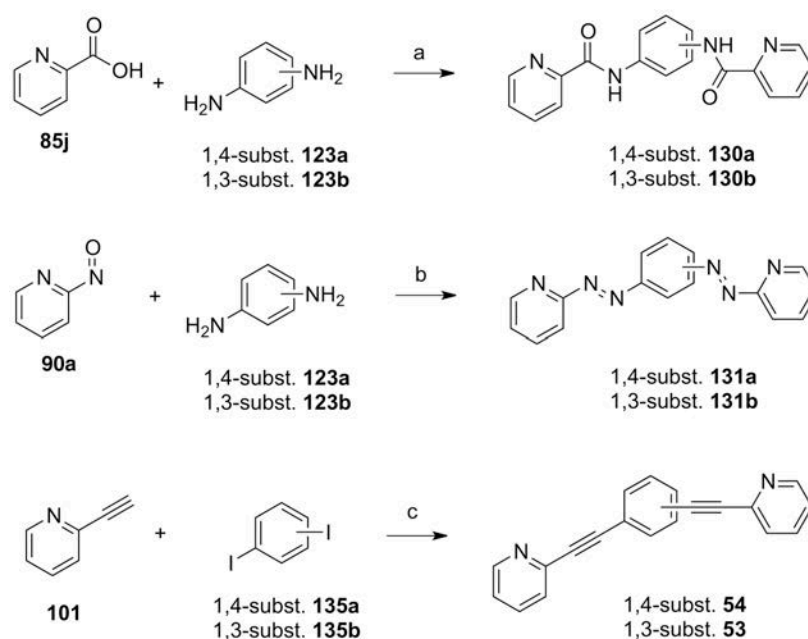
Scheme 9 Synthesis of **111c** and **115**. Reagents and conditions: (a) HATU, DIPEA, DMF, 40°C, 22h (94%); (b) H₂ (2 bar), Pd/C, EtOH/1,4-dioxane r.t. 5 h, 97% (c) AcOH cat., DCM, r.t., 20-72h, 49%;



Scheme 10: 9 Synthesis of **128a-b** and **129a-b**. Reagents and conditions: (a) PdCl₂(PPh₃)₂, CuI, Et₃N, DMF, 60°C (**135a** 23%, **135b** 30%); (b) HATU, DIPEA, DMF, 40°C (**128a** 83%, **128b** 78%); (c) AcOH cat., DCM, r.t., 49% (**129a** 78%, **128b** 76%)

Compounds **128a-b** and **129a-b** were prepared following the synthetic strategy depicted in *Scheme 9*. First, palladium catalysed Sonogashira coupling of ethynylanilines **133a** or **133b** with 2-chloropyridine (**134**) afforded the synthetic intermediates **135a** and **135b** in 23% and 30% yield respectively (*step a*). Following acylation of the aromatic amine of **135a** and **135b** with picolinic acid (**85j**) and HATU/DIEPA gave final compounds **128a** and **128b** in 83% and 78% yield. Additionally, key compounds **129a** and **129b** were also obtained from aniline derivatives **135a** and **135b** with 2-nitrosopyridine (**90a**) with acidic catalysis in 78% and 76% yields.

Symmetric compounds **130-132** were prepared in single step reactions, as depicted in *scheme 10*. Hence, acylation of phenylenediamines **122a** and **122b** with HATU/DIPEA afforded compound **130a** and **130b** with 52% and 81% respectively, and their coupling with 2-nitrosopyridine **90a** gave the azocompounds **131a** and **131b** in 98% and 5% yield each. Finally Sonogashira coupling with diiodobenzenes **136a** and **136b** with 2-ethynylpyridine **101** yielded the previously reported mGlu₅ NAMs **54** and 2-BisPEB (**53**)^{124, 209}.



Scheme 11: 10 Synthesis of **130a-b**, **131a-b**, **54** and **53**. Reagents and conditions: (a) HATU, DIPEA, DMF, 40°C (**130a** 52%, **130b** 81%); (b) AcOH cat., DCM, r.t., 49% (**131a** 98%, **131b** 5%); (c) PdCl₂(PPh₃)₂, CuI, Et₃N, DMF, 60°C (**54** 45%, **53** 87%)

Photochemical evaluation of compounds **111c**, **115**, **128-131**, **53**, **54**

First of all we obtained the UV-Vis absorption spectra of both *trans*- and *cis*-isomers of the azocompounds of the series (**111c**, **115**, **129a-b**, **131a-b**) in a mixture of aqueous buffer at pH=7.4 and acetonitrile by HPLC coupled simultaneously to a photodiodes array (PDA) and a mass spectrometer (*figure 69A-B, annex 1*), as previously done with compounds of *chapter 3*. As for compounds from *chapter 3*, we were again unable to determine the exact composition of *cis*- and *trans*-isomers.

For the *trans* isomers, we observed two groups of azocompounds: those with their central ring with 1,4-substitution (**111c**, **129a** and **131a**), which displayed the band corresponding to the π - π^* transition of the *trans* isomer between 350 and 360 nm; and those with their central ring with 1,3-substitution (**115**, **129b** and **131b**), whose π - π^* transition of the *trans* isomer was located at narrower wavelengths (300-320 nm). This difference may be related to the different

electron delocalisation of the π -electrons of the two groups of compounds, since 1,4-substituted compounds display an extended delocalisation along the three aromatic rings through the corresponding linkers, and for the 1,3-substituted compounds this delocalisation is broken in the central ring, due to the *meta* substitution. In all cases the corresponding *cis* isomers showed the band corresponding to the π - π^* transition at lower wavelengths than the *trans* π - π^* transition, and a weaker additional n - π^* band around 430-440 nm.

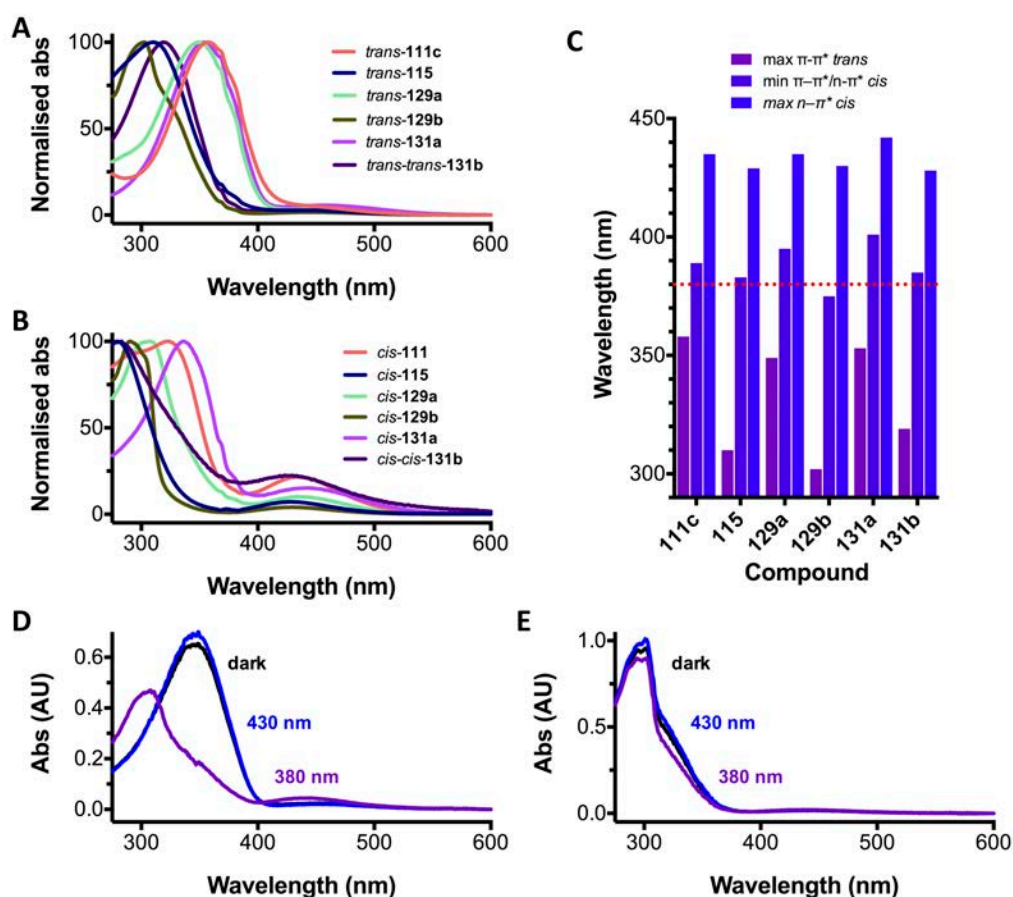


Figure 69: Photochemical and photoisomerisation properties of compounds **111c**, **115**, **129a-b** and **131a-b**. A,B) UV-Vis absorption spectra obtained with HPLC-PDA-MS and normalised to the maximum absorbance in the range between 275 and 650 nm for *trans* (A) and *cis* isomers (B). C) Wavelength of maximum absorbance of the *trans*-isomer (π - π^* transition) (violet bars), minimum of absorbance of the *cis*-isomers (between π - π^* transition and n - π^* transition) (dark violet bars) and wavelength of maximum absorbance of the *cis*-isomer corresponding to the n - π^* transition (blue bars) for compounds **111c**, **115**, **129a-b** and **131a-b**. D,E) UV-Vis absorption spectrum of compound **129a** (D) and **129b** (E) 25 μ M in DMSO in dark conditions (dark line), after illumination at 380 nm (violet line) and after illuminating at 430 nm (blue line).

After that, we searched the optimal wavelength to maximize the amount of *cis* compound under illumination. Theoretically, it is located between the maximum of absorption of *trans*

isomers (π - π^* band) and the minimum located between the π - π^* and n - π^* bands of the *cis* isomers, where a wider difference of absorption between the *cis* and *trans* isomers is found. For 1,4-substituted compounds, this maximum difference is located around 380 nm, as we showed previously in chapter for compound **111c**; and for 1,3-substituted compounds, this wavelength is lower, around 350 nm. However, this wavelength range (\approx 350 nm) is located in the UV range of the spectra and might be harmful for living systems. Therefore, to photoisomerise from *trans* to *cis* configurations, we decided to use 380-nm illumination in both groups of compounds, in order to avoid these non-biocompatible wavelengths. For the reverse isomerisation, we selected 430-nm-wavelength, since all the *cis* isomers bear a band corresponding to the n - π^* transition at around 430 nm, whereas the corresponding *trans* isomers show practically no absorbance at these wavelength range.

Thus, we measured UV-Vis absorption spectra of compounds **111c**, **115**, **129a-b** and **131a-b** in the dark, after violet illumination ($\lambda = 380$ nm) and after blue illumination ($\lambda = 430$ nm) in acetonitrile solution. In the dark we practically detected only *trans*-isomer. We could detect a practically complete photoisomerisation for compound **111c** and **129a** (*figure 69D and annex*). However, for the rest of compounds we could only detect partial photoisomerisation (*figure 69E and annex*). That suggests that lower wavelengths are probably needed to achieve an acceptable photoisomerisation for 1,3-substituted compounds (**115**, **129b** and **131b**). Additionally, the poor photoisomerisation of compounds **115**, **129a**, **131a** and **131b** might be due to an insufficient difference of absorption between the *trans* and *cis* isomers at the wavelength used, as their corresponding *cis* and *trans* isomer spectra found with HPLC-PDA-MS bear a π - π^* band in very close wavelengths (*figure 69A-B and annex*). Overall, this indicates that not all azo-compounds display an adequate photoisomerisation to afford and on/off switching, as we have already showed in the previous chapter.

In-vitro pharmacological evaluation of compounds 127-133

Duality mGlu₄ PAM and mGlu₅ NAM: dose-response curves with receptor

To evaluate the pharmacological profile of this series of compounds we generated dose-response curves with the same IP accumulation assay, used in *chapters 1-3*, with the “changing tips” protocol, described above in *chapter 3* HEK293 cells overexpressing mGlu₄ or overexpressing mGlu₅. Based on the knowledge acquired in previous work, we expected to achieve mGlu₄ PAM activity in compounds comprising the groups pyridine-amide-phenyl, like **111c**, **115**, **128a-b** and **130**. Additionally, compounds including the pyridine-azo-phenyl or pyridine-ethynyl-phenyl groups, such as **111c**, **115**, **128a-b**, **131a-b** and **133a-b**, were expected

to display mGlu₅ NAM activity. Among them, compounds **111c**, **115** and **128a-b**, simultaneously include both moieties, which make them potential candidates for dual pharmacological activity.

We performed the IP accumulation experiments and generated dose-response curves for evaluating mGlu₄ PAM and mGlu₅ NAM activity separately. Our expectations for mGlu₄ receptor were not accomplished, since the only active compounds containing a pyridine-amide-phenyl moiety were **111c** and **128a**, showing low micromolar potencies, altogether with **53** that show a weak mGlu₄ PAM activity (*table 17*). Concerning mGlu₅ receptor, our results show a high promiscuity among the series, with compounds including pyridine-azo-phenyl or pyridine-ethynyl-phenyl moieties, since practically everyone displayed NAM activity, though with different potencies, ranging from high nanomolar to low micromolar IC₅₀s, that will be discussed later in a specific subsection.

Compound	mGlu ₄ PAM			mGlu ₅ NAM		
	EC ₅₀ (μM)	SEM (μM)	PPS	EC ₅₀ (μM)	SEM (μM)	PPS
111c	8.9	1.3	2.8	3.21	0.33	>13
115	>25		-	14.03	2.24	1.5
128a	9.94	3.45		0.84	0.28	
128b	>25			0.84	0.38	
129a	>25		-	3.09	0.27	2.9
129b	>25		-	0.96	0.24	1.2
130a	>25			n.a.		
130b	n.a.			n.a.		
131a	>25		-	6.13	0.16	1.2
131b	n.a.		-	4.92	1.10	2.0
54	>25			1.21	0.46	
53	18.00	2.44		0.43	0.10	
VU0364770	1.17	0.32	1.0			
Fenobam				2.30	0.25	1.0

Table 17: Values extracted from dose-response curves (IP accumulation assays) corresponding to the EC₅₀ as mGlu₄ PAMs and IC₅₀ as mGlu₅ NAMs, as means of minimum three independent replicates with the corresponding standard error of the mean (SEM) and the photoinduced potency shift (PPS), as the quotient of the EC₅₀ or IC₅₀ under illumination and the dark ones for the photoswitchable azo-compounds.

Overall, we obtained two compounds with mGlu₄ PAM and mGlu₅ NAM dual activity with potencies in the micromolar range: **111c**, which is a photoswitchable compound, and **128a**, a

non-photoswitchable compound (*figure 70AB*). Compound **111c**, despite displaying very good photoisomerisation properties in solution, did not perform a comparable photoswitch in mGlu₄ PAM activity, since the corresponding photoinduced potency shift (PPS) is just 2.8 fold (*table 17, figure 70A*). However, as we have already seen in *chapter 3*, this photoinduced potency shift in mGlu₅ NAM activity is very large (PPS > 13). Those differences might be explained taking into account a possible adaptation of the *cis* isomer of **111c** inside the mGlu₄ allosteric pocket in a similar binding mode to the *trans* one, which would lead to functional response for both isomers.

Selectivity of compounds **111c** and **128a**

Once characterised the dual activity of **111c** and **128a**, we next evaluated its activity on the rest of mGlu receptor subtypes to determine the selectivity for these to receptors. Therefore we tested the putative PAM and NAM activities with a single dose of 100 µM in HEK293 cells transiently transfected with the corresponding receptors, in a similar way to that used to characterise the selectivity profile of optoglutram at *chapter 1*.

Unfortunately, we obtained partial effects as a PAM on mGlu₂ and group-III mGlu subtypes (mGlu₆₋₈). However, for compound **111c**, none of the effects in the rest of mGlu subtypes reached the half-effect of mGlu₄ or, for compound **128a**, the undesired effects were situated around the 50% of the effect on mGlu₄.

These selectivity results did not define tool compounds whereby we could test the initial hypothesis on dual mGlu₄ PAM and mGlu₅ NAM molecules. Therefore, we performed new selectivity experiments using lower doses of the tested compounds to evaluate if these undesired effects on other mGlu subtypes were reduced. Thus, we did the same assay with a dose of 30 µM and 10 µM with both **111c** and **128a**, as done before with 100 µM (*figure 71-72*). Disappointingly, this dose decrease did not provide better results, since the non-desired effects were decreased in a similar fashion to the effects on mGlu₄ and mGlu₅, achieving approximately half-effect again, or even higher than half, as can be observed in the graphics of *figure 73*.

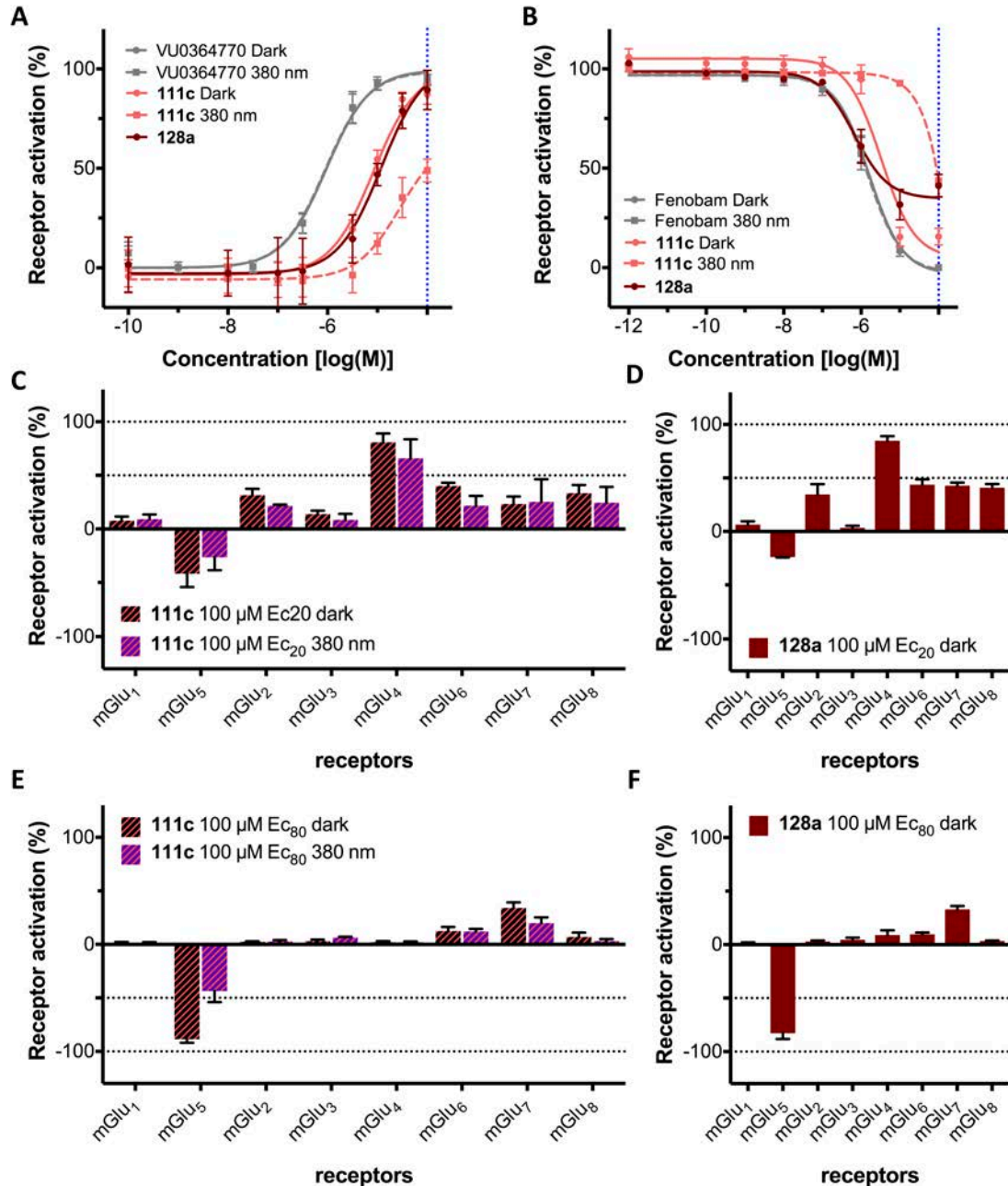


Figure 70: Selectivity of compounds **111c** and **128a** at 100 μ M of concentration using an IP accumulation assay in transiently transfected HEK 293 cells. (A-B) Doses-response curves of compounds **111c** and **128a** in mGlu₄ with a constant concentration of 3 nM of L-AP₄ (A) and in mGlu₄ with a constant concentration of 100 nM of quisqualate. The dose used for selectivity tests (100 μ M) is marked with a blue dotted line. (C-F) Selectivity profiles over the 8 mGlu subtypes of the compound **111c** as a PAM (C) or as a NAM (E) and compound **128a** as a PAM (D) or as a NAM (F) at a concentration of 100 μ M. Values for PAM evaluation are normalised between the EC₂₀ and the saturation of the corresponding orthosteric agonists, and values for NAM evaluation are normalised between the EC₈₀ of the corresponding orthosteric agonists and the saturation of an antagonist. Every point of each graphic corresponds to the mean of a minimum 3 independent experiments with the corresponding SEM as error bars.

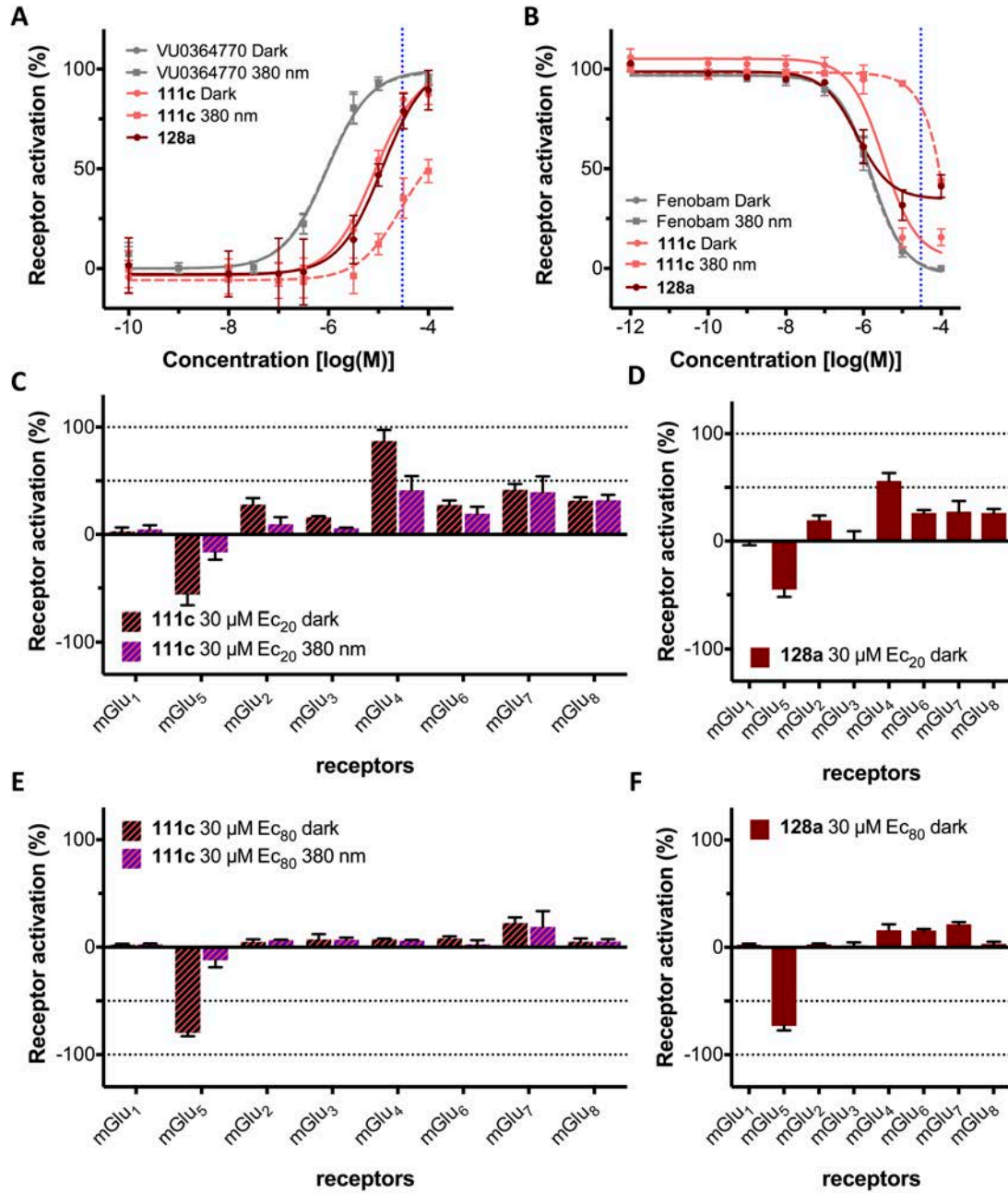


Figure 71: Selectivity of compounds **111c** and **128a** at 30 μM of concentration using an IP accumulation assay in transiently transfected HEK 293 cells. (A-B) Doses-response curves of compounds **111c** and **128a** in mGlu₄ with a constant concentration of 3 nM of L-AP₄ (A) and in mGlu₄ with a constant concentration of 100 nM of quisqualate. The dose used for selectivity tests (30 μM) is marked with a blue dotted line. (C-F) Selectivity profiles over the 8 mGlu subtypes of the compound **111c** as a PAM (C) or as a NAM (E) and compound **115** as a PAM (D) or as a NAM (F) at a concentration of 30 μM . Values for PAM evaluation are normalised between the EC₂₀ and the saturation of the corresponding orthosteric agonists, and values for NAM evaluation are normalised between the EC₈₀ of the corresponding orthosteric agonists and the saturation of an antagonist. Every point of each graphic corresponds to the mean of a minimum 3 independent experiments with the corresponding SEM as error bars.

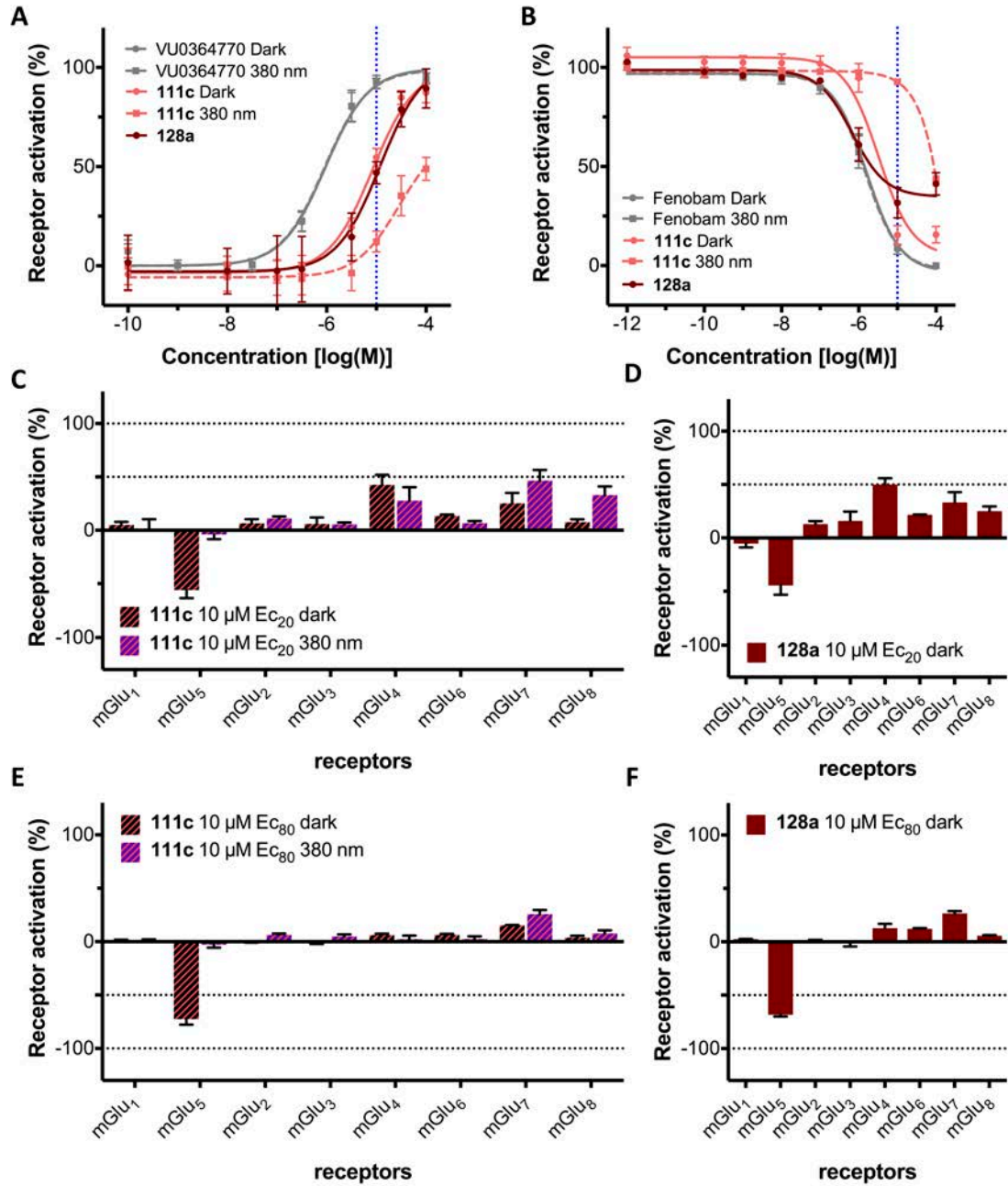


Figure 72: Selectivity of compounds **111c** and **128a** at 30 μM of concentration using an IP accumulation assay in transiently transfected HEK 293 cells. (A-B) Doses-response curves of compounds **111c** and **128a** in mGlu₄ with a constant concentration of 3 nM of L-AP₄ (A) and in mGlu₄ with a constant concentration of 100 nM of quisqualate. The dose used for selectivity tests (30 μM) is marked with a blue dotted line. (C-F) Selectivity profiles over the 8 mGlu subtypes of the compound **111c** as a PAM (C) or as a NAM (E) and compound **115** as a PAM (D) or as a NAM (F) at a concentration of 30 μM. Values for PAM evaluation are normalised between the EC₂₀ and the saturation of the corresponding orthosteric agonists, and values for NAM evaluation are normalised between the EC₈₀ of the corresponding orthosteric agonists and the saturation of an antagonist. Every point of each graphic corresponds to the mean of a minimum 3 independent experiments with the corresponding SEM as error bars.

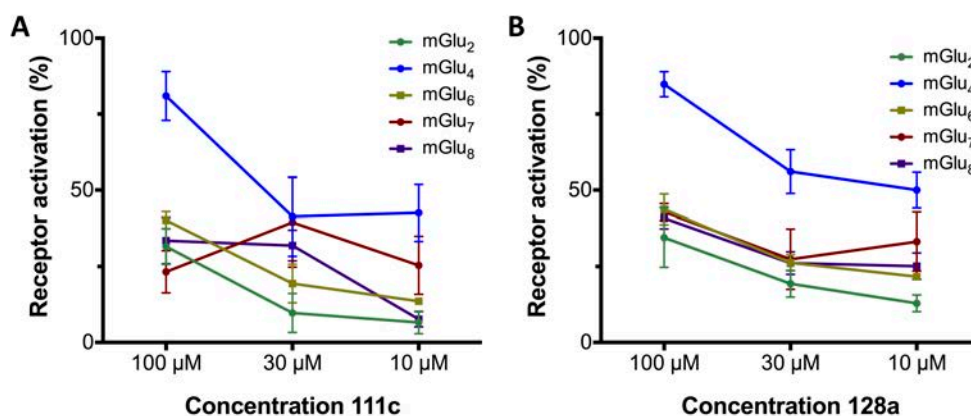


Figure 73: Values extracted from selectivity plots of the effect of compound **111c** (A) and **128a** (B) as PAM different group II and III mGlu subtypes in the three different concentrations tested. Effect on these receptors is approximately half of the effect with mGlu₄ with both compounds, except for mGlu₇ which bears the same effect independently from the concentration used of compounds.

In conclusion, both compounds **111c** and **128a** display dual mGlu₄ PAM and mGlu₅ NAM activities, but its selectivity is not optimal. However, the effects observed in the selectivity experiments would match for a compound with neuroprotective properties, since it is on of the indications of group-II and group-III PAMs⁸². In any case, these two compounds cannot be considered as pure dual compounds, and these results force us to further optimise the activity by better defining the structure-activity relationship of dual compounds. We have to bear in mind that these molecules still constitute very simple structures and many substitutions can be introduced on their scaffolds with a rationally design using computational tools and the knowledge of active compounds in these receptors. Thus, we might achieve new molecules with an increased potency for these two receptors and better selectivity profile. At this point we decided to stop the search for mGlu₄ PAM and mGlu₅ NAM dual compounds and to leave it for future work, while pharmacological assays using simultaneously two selective compounds validate the initial hypothesis of the synergic effect of these mGlu activity modes.

An unexpected effect on mGlu₅: Positional isomers lead to different efficacies

On dose-response curves of *chapter 3* we could detect a slightly lower efficacy of compound **111c** when compared to fenobam, or even lower when compared to other mGlu₅ NAMs of the same series (*annex*). We could not compare it with the effect of its 1,3-substituted isomer (**115**) since its low potency did not allow us to precisely calculate the bottom asymptote of the dose-response curve with the concentrations used (*annex*).

Within this new series, it was possible to clearly notice this difference of efficacy in all the bisosteres of **111c** and **115**. In effect, 1,3-substituted compounds **128b**, **129b** and **131b** were

found to be inverse agonists, in a similar fashion to fenobam or even with a higher efficacy, all together with compound **53** (2-BisPEB) whose pharmacological properties were previously reported^{124, 209}. On the other hand, their 1,4-substituted positional isomers **128a**, **129a**, **131a** and **54** also displayed antagonistic activity in mGlu₅, but with lower efficacy than fenobam, denoting a partial antagonistic efficacy. Moreover, the potency (IC₅₀) of the 1,4-isomers was not significantly altered respect that of the corresponding 1,3-isomers, except for compound **111c**, that shows clearly a better potency than its isomer **115** (table 18, figure 74AB).

Compound	EC ₅₀ (μM)	SEM (μM)	PPS	Efficacy (%)	SEM (%)
111c	3.21	0.33	>13	92	6
115	14.03	2.24	1.5	90	5
128a	0.84	0.28		67	9
128b	0.84	0.38		120	1
129a	3.09	0.27	2.9	35	4
129b	0.96	0.24	1.2	115	4
131a	6.13	0.16	1.2	19	4
131b	4.92	1.10	2.0	114	3
54	1.21	0.46		42	4
53	0.43	0.10		120	1
Fenobam	2.30	0.25	1.0	100	0

Table 18: Values extracted from dose-response curves (IP accumulation assays) corresponding to IC₅₀ as mGlu₅ NAMs, as means of minimum three independent replicates with the corresponding standard error of the mean (SEM), the photoinduced potency shift (PPS), as the quotient of the EC₅₀ or IC₅₀ under illumination and the dark ones for the photoswitchable azo-compounds and the efficacy of inhibition of mGlu₅ activity as means of minimum three independent replicates with the corresponding standard error of the mean (SEM). Efficacy was measured from bottom of the dose-response curve, normalised to the response of fenobam, between 0% and 100%.

The difference of efficacy of these positional isomers, without significantly alter their potency, may be explained as different binding modes in the transmembrane domain. The absence of different functional groups and the structural properties of the azo and ethynyl bonds make the compounds very rigid, either in angular or linear geometries. Additionally the compounds displayed similar potencies, regardless of their angular or linear geometries. To account for the different efficacies, the binding modes of each geometry must be obligatory different, since these molecules do not have the flexibility needed to rearrange their scaffold to be able to bind to the same pocket in the same fashion. Additionally, compounds **111c** and **128a**, which bear a partially flexible amide bridge in their scaffold, show a better efficacy when compared to more rigid **129a**, **131a** and **54**. The highest flexibility would let them to better adapt to the

allosteric site and to reach a better functional pose. Another explanation might be an alteration of the inactive conformation of transmembrane domain when the linear receptors are bound, that partially permits the activation of the G-Protein. In any case, further investigation must be done to explain this different behaviour.

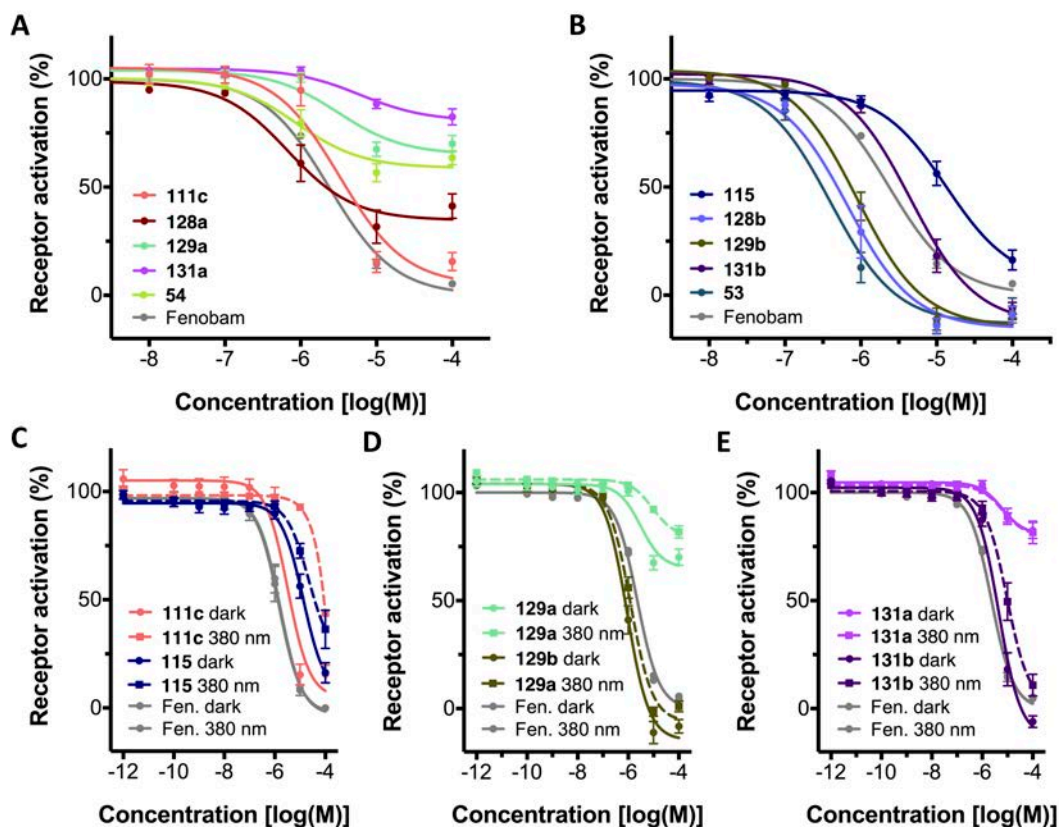


Figure 74: Dose-response curves obtained from IP accumulation assays with HEK293 cells transfected with mGlu₅ receptor. (AB) Zoom on the curves of compounds with 1,4-substitution with partial antagonism (A) and with 1,3-substitution with high-efficacy inverse agonism (B). (C-E) Complete dose-response curves of azo-containing compounds in dark conditions (plain lines) and under illumination at 380 nm of wavelength (dotted lines).

Regarding the potency of these compounds on mGlu₅, all of them retain the NAM activity regardless the inclusion of an ethynyl or azo-bond. However, the acetylenic compounds provide better mGlu₅ NAM properties. For example **53**, with two ethynediyl bridging bonds, present a higher potency than **129b**, which only bears one ethynyl group, and higher than **131b**, which only includes azo-bond bridges. Another example of this behaviour can be observed with **115** and **128b**, which include an amide bridge. Compound **128b** that bears an ethynyl bridge shows a higher potency ($IC_{50} = 0.84 \mu M$) than **111c** ($IC_{50} = 3.21 \mu M$), having an azo-bond bridge. This tendency is similar when comparing the potency of the 1,4-substituted compounds, despite the differences of efficacy observed (table 18, figure 74A).

Regarding the light induced compound responses on mGlu₅ receptor we did not achieve satisfactory results upon illumination at 380 nm. In parallel to the previous photoisomerisation assays, we only detected substantial photoswitching behaviour for compound **111c**, as previously showed in *chapter3*, and **129a**, which was a partial antagonist in its *trans*-isomer that experienced a 3-fold loss on its potency and a loss of 15% in its efficacy (*figure 74CD, table 18*). The photoinduced potency shifts on the dose response curves of the three azo-compounds tested were not sufficiently strong to achieve a proper on/off photoswitching of mGlu₅ response. This can be probably due to an intrinsic molecular lack of photoisomerisation or a possible accommodation of the *cis* isomer in the mGlu₅ allosteric pocket. In any case, as we stated in the previous chapter, not all the bioactive azocompounds have the necessary properties for effective photoswitch receptor activity in cell assays or in-vivo applications.

In-silico characterisation of 110 and 109e,f

J. A. Dalton, INc-UAB, Bellaterra – Barcelona

To explore the possible binding modes linear 1,4-substituted and angular 1,3-substituted compounds of the present series, compounds **129a-b**, **131a-b**, **54** and **53** were docked into the crystal structure of mGlu₅ (PDB id 4009, minus its mavoglurant co-crystallized ligand) using AutoDock4.2, since they are the examples with the most evident differences of efficacy between positional isomers. For each respective docking, the top-ranked (according to AutoDock docking score) complex was subsequently energy-minimized post-docking in the Amber14 force-field to optimize protein-ligand interactions.

From the results shown in *figure 75*, the 1,3-compounds are able to bind at the bottom of the allosteric pocket by accommodating the distinctive angular-shaped binding-site, displaying a similar binding pose to the previously co-crystallized mGlu₅ NAMs: mavoglurant (in PDB id 4009³²) and HTL14242 (in PDB id 5CGD⁵¹). In doing so, each 1,3-compound achieves a favourable docking score (*table 19*), making an H-bond with S809 on TM7 (after energy minimization), and in the case of **129b** and **53**, an additional H-bond with N747 on TM5. However, the 1,4-compounds are unable to bind at the bottom of the allosteric pocket (at least in the mGlu₅ crystal structure of PDB id 4009) as they are unable to accommodate the angular-shaped binding-site. Instead they bind higher in the pocket with a pose similar to that observed with the co-crystallized ligand FITM in the crystal structure of mGlu₁ (PDB id: 4OR2³¹). As a result of this higher binding pose, the 1,4-compounds achieve much less favourable docking scores (*table 19*) and are unable to make an H-bond with S809 on TM7 or any other residue in the allosteric pocket. Although this higher binding pose is apparently

functional in terms of mGlu₁ allostery, it is unlikely to be functional in mGlu₅, as reflected by the poor docking scores observed here (indicating a poor fit), and by experimental data (including current mGlu₅ crystal structures)^{32, 51}, which suggests S809 interaction is critical for correct mGlu₅ NAM functionality²⁰⁹

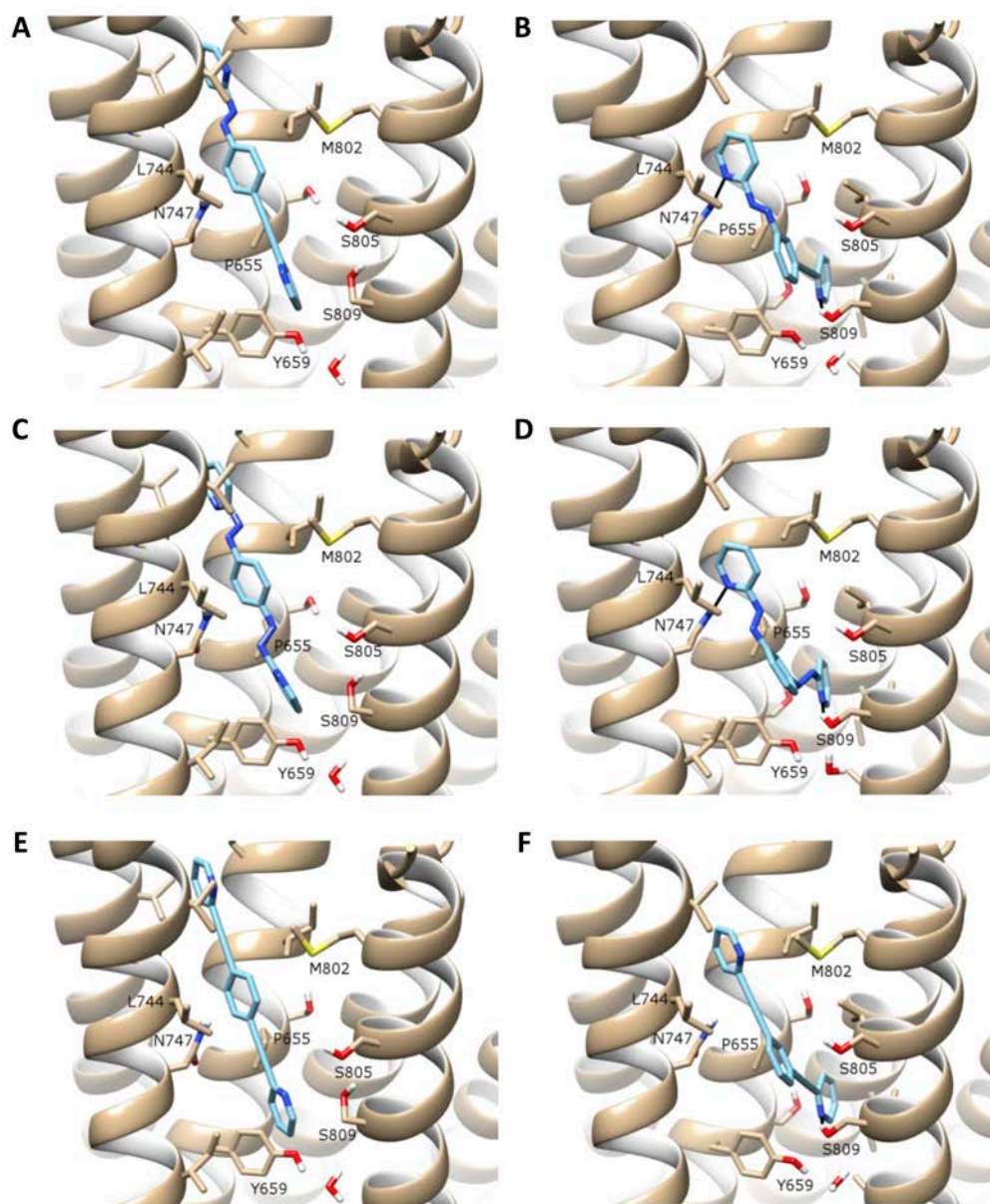


Figure 75: Six compounds docked into crystal structure of mGlu5 (PDB id 4O09) using AutoDock4.2: (A) **129a**, (B) **129b** (C) **131a**, (D) **131b**, (E) **54**, (F) **53**. Ligands are shown in cyan, receptor in beige, protein-ligand H-bonds as black lines. The allosteric binding pocket is shown from the side (TM6 not shown), with TM5 front-left, TM7 front-right, TM3 central, TM4 background-left, TM2 background-right (with chosen residues labelled).

Compound	Docking Score in mGlu ₅ crystal 4009 (Predicted K _i , nM)	Docking Score in alternative mGlu ₅ conformation (Predicted K _i , nM)
129a	0.82	0.41
129b	0.12	-
131a	0.77	0.38
131b	0.14	-
54	9.00	1.00
53	0.44	-

Table 19: Docking scores generated with AutoDock4.2 for six compounds docked into two conformations of mGlu₅ (original crystal structure and a Rosetta-generated alternative). Three linear 1,4-compounds: **129a**, **131a** and **54**, and three angular 1,3-compounds: **129b**, **131b** and **53**

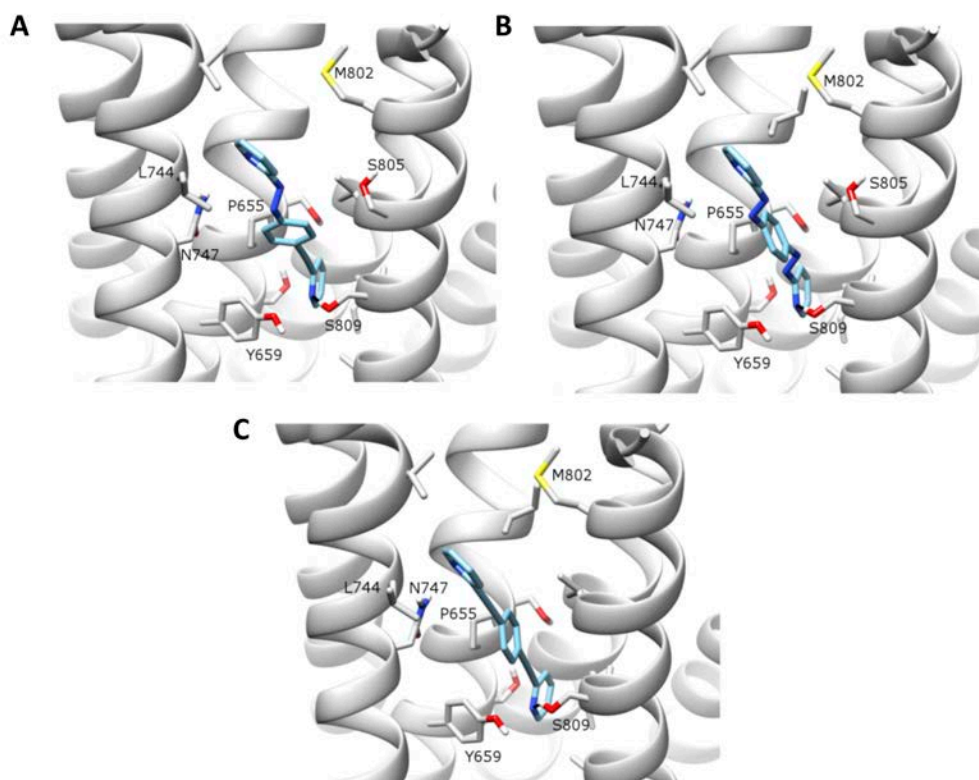


Figure 76: Linear 1,4-compounds: (A) **129a**, (B) **131a**, (C) **54** re-docked into an alternative receptor conformation of mGlu₅, derived from original crystal structure (PDB id 4009). Ligands are shown in cyan, receptor in grey, protein-ligand H-bonds as black lines. The allosteric binding pocket is shown from the side (TM6 not shown), with TM5 front-left, TM7 front-right, TM3 central, TM4 background-left, TM2 background-right (with chosen residues labelled).

In recognition of the fact that GPCRs are flexible dynamic receptors, an alternative conformation of mGlu₅ was utilised to re-dock the 1,4-compounds in an attempt to identify better binding poses at the bottom of the allosteric pocket (more similar in nature to current co-crystallized mGlu₅ NAMs). This alternative receptor conformation was derived from the

original mGlu₅ crystal structure (PDB id 4OO9) through Rosetta relaxation and conformational sampling²¹⁰. This results in a relatively subtle adjustment of side-chain packing between TM6 and TM7 but more significantly, an enlargement and alteration of the binding pocket from an angular shape to a wider linear shape. Using this alternative receptor conformation, the 1,4-compounds instead dock at the bottom of the allosteric pocket, making an H-bond with S809 on TM7 (*figure 76*), the residue designated as important for interaction with mGlu₅ NAMs²⁰⁹, and packing against hydrophobic residues on TM5 (e.g. L744) and TM6. In accordance with this changed binding-mode, the docking scores of the 1,4-compounds are improved compared to the previous dockings in the original crystal structure (PDB id 4OO9) (*table 19*). However, it should be noted that this alternative receptor conformation is perhaps not as readily accessible in energetic terms as the original crystal structure conformation, potentially affecting the actual activity of the 1,4-compounds

Conclusions

We synthesised 12 compounds, based on an phenyl central ring covalently bound to two 2-pyridine units with two different substitution patterns (1,3 and 1,4) and with the combination of three different linkers: amide, azo and ethynyl groups.

We obtained two compounds (**111c** and **128a**) with both mGlu₄ PAM and mGlu₅ NAM activities with similar potencies around the micromolar range. However, their selectivity over mGlu family of receptors was not ideal to constitute effective tool compounds, since they also displayed partial efficacies as mGlu₂, mGlu₆, mGlu₇ and mGlu₈ PAMs. This lack of selectivity limits their possible biological applications only to test a pan-mGlu neuroprotective agent.

Four compounds (**129a-b** and **131a-b**) could be considered azo-replaced¹⁸⁷ derivatives of the mGlu₅ NAMs 1,3-BisPEB and 1,4-BisPEB, by formal replacement of ethynyl groups for azo groups. They maintain very similar pharmacological properties to the previous reported isosteres¹²⁴, including a very similar potency.

Despite the similar potency among the compounds tested in mGlu₅ receptor, we found substantial differences in their antagonistic efficacy on mGlu₅ receptors: compounds with 1,3-substitution displayed an inverse agonist efficacy similar to the reference compound fenobam, whereas compounds with 1,4-substitution displayed partial antagonistic effects.

Computational docking in the mGlu₅ crystal structure³² revealed the angular-shaped 1,3-substituted compounds bind in a very similar pose to the co-crystallised inverse agonist mavoglurant, whereas the linear 1,4-substituted compounds bind in a different pose, unlikely

to be functional and with a concomitantly low docking score. However, an alternative conformation of the mGlu₅ transmembrane domain might adapt to these linear-shaped compounds in a functional-like pose, which may be responsible for the partial antagonism behaviour.

The discovery of a molecular switch from allosteric inverse agonists to partial allosteric antagonists is of high interest, since recent publications have reported the advantageous properties of partial mGlu₅ NAMs^{211, 212}, which might avoid on-target side-effects of mGlu₅ complete blockade by classical allosteric inverse agonists^{213, 214}. Therefore, our approach based on exchanging the substituent position in a rigid mGlu₅ NAM scaffolds to afford a straight-shaped compound may be useful to discover new partial mGlu₅ NAMs with a safer pharmacological profile a better perspectives in the drug discovery trail.

Chapter 5: A more suitable therapeutic approach: *cis*-on photoswitchable mGlu₄ PAMs and mGlu₅ NAMs.

The photoswitchable compounds shown in the first, third and fourth chapters of the present thesis were active compounds in their *trans*-configuration (mGlu₄ PAMs or mGlu₅ NAMs), which is the thermodynamically more stable isomer for azobenzenes with very few and rare exceptions. Upon illumination with violet light, we were able to photoisomerise these compounds leading to a loss of their bioactivity, with variable success and, in some cases, we could induce a light-dependent over-activation of the receptor as a result of the photoisomerization of the compounds.

From the therapeutic point of view, this approach is not the most promising since the switching-off of an already active drug with light with a high spatial and temporal precision has limited therapeutic applications. For example, it could be useful to avoid side effects very localised in a single region of the organism, where the bioactivity of the compound is not recommended or to stop the activity of the compound in a region where the pharmacological effect needs a very short time of exposure. Overall, the major application of the *trans*-on photoswitchable compounds might be the use as tools for further investigate physiological processes with the possibility of on/off switching signalling cascades on purpose, induce over-activation of these cascades or study the unknown effects of intermittent activation by on/off pulses with these modulators.

In any case, all these possible applications do not point to a widespread application to heal patients from a disease. The possibility to achieve inactive photoisomerisable compounds in their thermodynamically stable *trans*-configuration that isomerises to a *cis*-disposition, which might be active, upon illumination, is of high interest for the therapeutic point of view. With these compounds, we would be able to induce a pharmacological effect only in a specific region of the organism with a high-precision spatiotemporal control using light. The thermal relaxation of the *cis* isomers would contribute to the inactivation of the compound while diffusing through the other regions of the organism.

In the present chapter, we will present the rational design, synthesis and characterisation of a new series of photoswitchable compounds using a *cis*-on approach. Our aim is to afford mGlu₄ PAMs and mGlu₅ NAMs that only display pharmacological activity in their *cis* configuration, whilst the *trans* isomer would remain inactive.

Design of compounds 140a-141 and 142-144

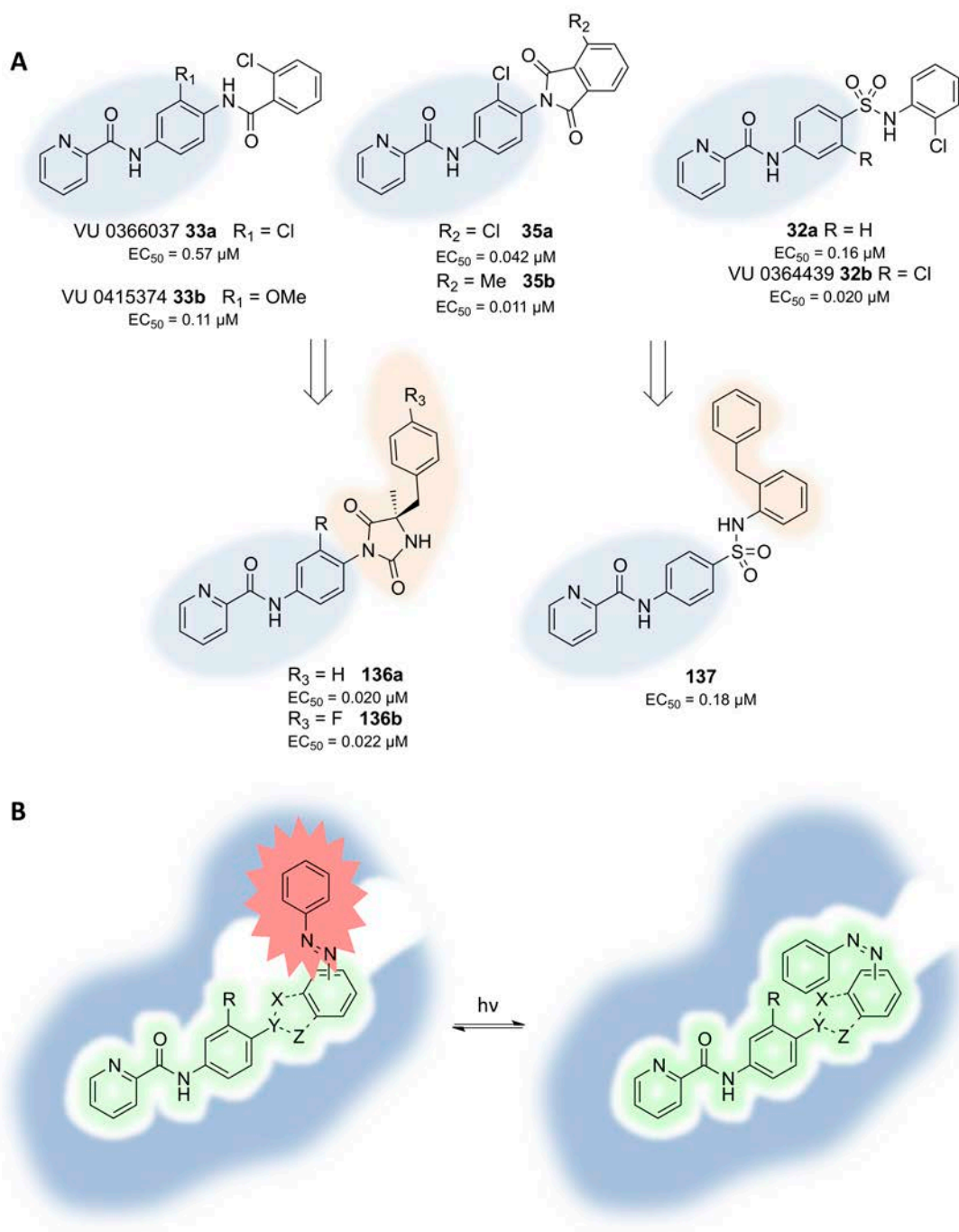


Figure 77: Design of *cis*-on photoswitchable mGlu₄ PAMs. (A) Compounds found in the literature bearing a *N*-phenylpicolinamide^{95-97,99} scaffold. Some of them include a large bent moiety that can be geometrically mimetised by an azobenzene⁹⁸. (B) *Cis*-on design approach for photoswitchable mGlu₄ PAMs with an *N*-phenylpicolinamide and an azobenzene, with the hypothesis of *trans* isomer clashing and the *cis* isomer fitting in the pocket.

Before beginning with experimental protocols we did an exhaustive bibliographic search of mGlu₄ PAMs and mGlu₅ NAMs, focusing on large molecules containing aromatic rings, which would fit in the allosteric binding site with a bent pose. Our aim was to mimic this active bent

position with a *cis*-azo bond in such a way that, upon isomerisation to the *trans* geometry, its straight disposition and higher length did not properly fit into the allosteric pocket, abolishing the effect on the receptor.

When looking for mGlu₄ PAMs, we found *N*-phenylpicolinamide moiety common in several positive modulators, such as VU364439 (**32b**)⁹⁵ or VU0415374 (**33b**)⁹⁶ between others^{90, 97, 99}, or in those that we previously synthesised in *chapter 1* and *3* **85** and **111a** (*figure 77A*). Interestingly, we also found some active larger derivatives, like compound **136a**, **136b**²¹⁵ and **137**⁹⁸ with the same *N*-phenylpicolinamide linked to a large bent moiety susceptible for azo-replacement. Thus, a *cis*-azobenzene in that position could reproduce the effect on binding of the bent diaryl moiety, whereas the corresponding *trans*-isomer would clash to the pocket residues, avoiding its binding or reducing its affinity.

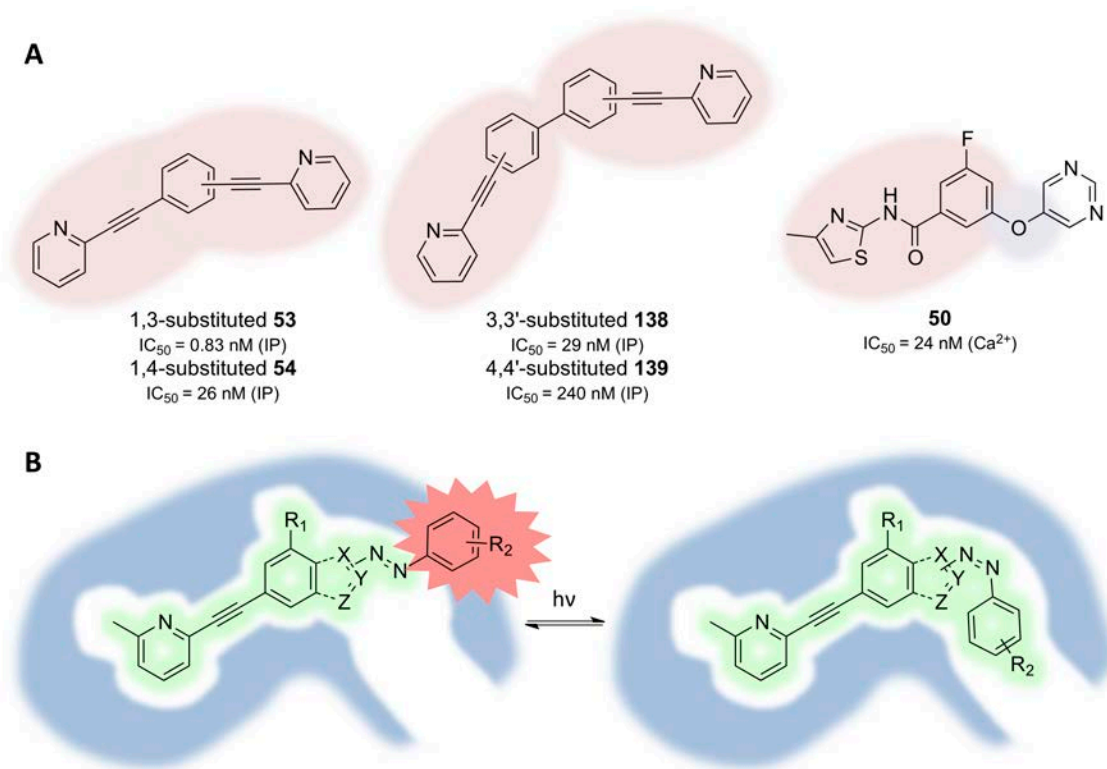


Figure 78: Design of *cis*-on photoswitchable mGlu₅ NAMs. (A) Compounds found in the literature bear 2-pyrindine ethynylphenyl moieties, or other biososters such as methyl pyridines or methyl thiazoles instead of the pyridines or *N*-amides instead of the ethyl bridge¹²³. Generally angular geometries of the compound afford better potencies than linear geometries¹²⁴ (B) *Cis*-on approach for photoswitchable mGlu₅ NAMs with 5-methyl-2-pyrindineethynylphenyl and an azobenzene, with its *trans* isomer clashing and the *cis* isomer fitting.

Concerning mGlu₅ NAMs, a very common moiety in their modulators is an ethynyl bridge, crossing a narrow channel inside the binding pocket³². The triple bond usually bridges a 2-pyridine (or a 5-methyl-2-pyridine) and a phenyl ring, as exemplified in 2-BisPEB (**53**) or MPEP

(**12**)⁶⁹. In some cases this 1,2-ethynediyl group is substituted for an *N*-amide, as in compound **50**¹²³ (*figure 78A*). Additionally, the binding modes of mGlu₅ NAMs seem to be in an angular geometry, as it is clearly shown in mavoglurant bound to mGlu₅ TMD crystal structure³² or as we showed in *chapter 4*. In contrast, the geometrically linear compound binding seems less favourable. The structure-activity correlation for compounds **53**, **54**, **138** and **149** confirmed the hypothesis, showing a shift on the potency between 10 and 30-fold¹²⁴ from angular to linear compounds (*figure 78A*). Thus we designed new photoswitchable compounds bearing the 2-phenylethynylpyridine scaffold with the introduction an additional arylazo group at the phenyl moiety with a linear geometry in *trans* disposition. In that way, this new compound would be unable to bind to the allosteric site in the transmembrane domain. However, upon illumination, the compound could afford an angular geometry that would bind leading to a negative modulation of the receptor activity (*figure 78B*).

In addition to the pyridine-acetylenic compounds, we found another family of compounds, including compound **50**¹²³, that bears the pyridyl-*N*-amide-phenyl moiety and also a diarylether. Diarylethers are considered very interesting to design photoswitchable *cis*-on derivatives, since the angle between aromatic rings, the distance between the aromatic rings and the electronic environment are similar to those of *cis*-azobenzene, and at the same time, show strong differences to a *trans*-azobenzene. Therefore those compounds are considered excellent candidates for azo-replacement to *cis*-on compounds (*figure 78AB*).

Another important aspect that we have to take into account for successful photoswitching is related to the wavelength of illumination and the thermal relaxation half-lives of our new putative photoswitchable *cis*-on compounds. Visible light offers several advantages over azobenzene typical isomerisation wavelengths in the UV range. UV light is harmful for living systems, whereas visible light in moderated intensities is considered innocuous and displays besides a higher penetration in living tissues, especially in red shifted wavelengths. At the moment, the majority azo-compounds described in the thesis need illumination around 380 nm, which is in the edge between violet and UV light. However we can increase this wavelength using electron-donating substituents in *ortho* or *para* position, like dimethylamine or *N*-morpholine. Additionally, we have to bear in mind that using this approach we can achieve push-pull azobenzenes, especially if one of the rings is electron poor and this would lead to short thermal relaxation times of the *cis*-isomers.

In any case, the aim of a *cis*-on approach is to be able to photoisomerise an inactive *trans*-azocompound to obtain an active *cis*-one and produce a pharmacological effect with light in a limited location with spatiotemporal control. If the thermal relaxation of the *cis*-isomer is too

long, the compound may diffuse and activate the target receptor in undesired locations. Therefore, a fast relaxation time may be advantageous, since as soon as the compound diffuses and leak out the spot with illumination, it will back-isomerise to the inactive *trans*-disposition. However, too fast *cis*-isomer-relaxation compounds can limit the *in-vivo* applicability of our compounds, since a very fast thermal relaxation can reduce the photoisomerisation efficacy. Then, to achieve a successful photoisomerisation, we would need a very high intensity of light, which can be harmful for living tissues. Therefore, we need to find proper relaxation rate to achieve an optimum balance between to avoid the diffusion of the active isomer and to avoid the use of to intense light power.

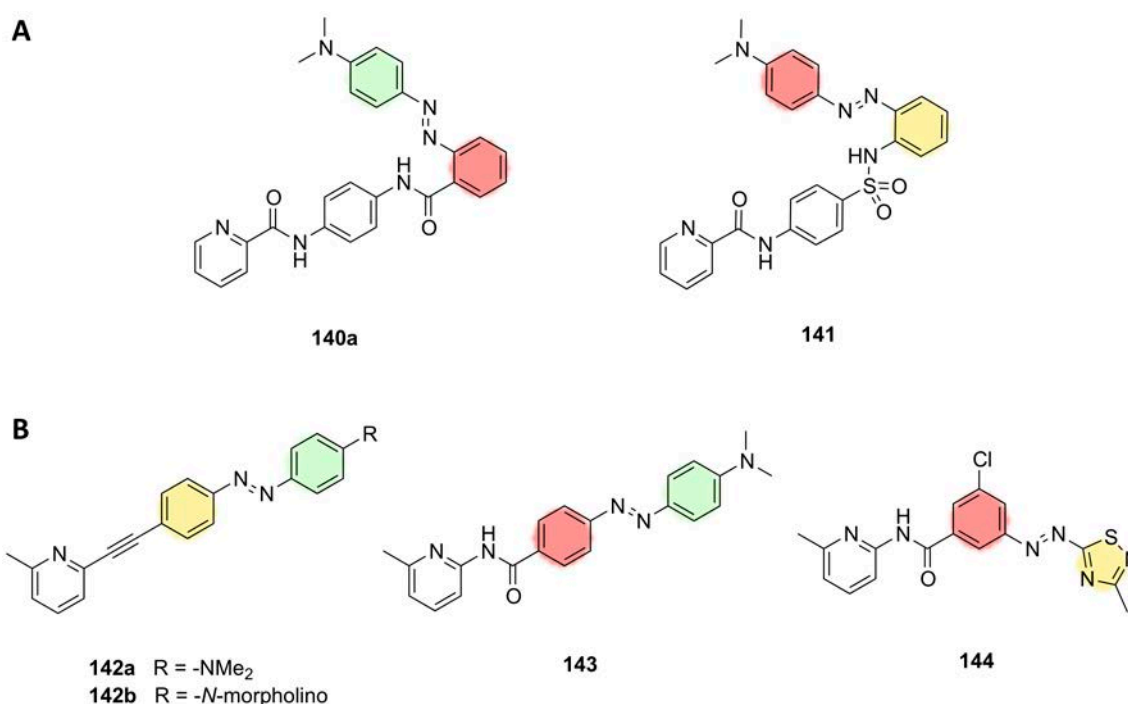


Figure 79: Compounds designed as putative *cis*-on mGlu allosteric modulators. (A) Compounds **140a** and **141** were designed to display *cis*-on mGlu₄ PAM activity. (B) Compounds **142a**, **142b**, **143** and **145** were designed to display *cis*-on mGlu₅ NAM activity. Colour of the aromatic rings of azo moieties represents the electron density of each aromatic ring: green denotes high electron density, yellow medium electron density and red low electron density.

Therefore, compounds **140a** and **143** would display push-pull azobenzene properties.

Taking into account all those points we designed compounds **140a** and **141** as mGlu₄ PAMs (figure 79A). Compound **140a** was based in **33a** and **33b** scaffold, with a simplified central ring (without -Cl or -OMe). Then we introduced the azo-moiety in the third ring, in a similar fashion to the benzyl of compounds **136a** and **136b**. Compound **141** corresponds to the same idea, based on the simplified structure of sulphonamides **32a** and **32b**. At the same time, **141** is also based in the structure of compound **137**, which is still a nanomolar mGlu₄ PAM and includes a benzyl group in the same position of the azobenzene of compound **142**. This implies a high

structural resemblance with the *cis*-isomer. Additionally, compounds **140a** and **141** include an *p*-NMe₂ substitution in the azobenzene, with the aim to increase the electron density of the azobenzene rings and achieve successful isomerisation with visible light (*figure 79A*).

On the other hand, we designed compounds **142a-b**, **143** and **144** as mGlu₅ NAMs. Compounds **142a** and **142b** were based on the straight and kinked geometry of rigid compounds containing the ethynyl pyridine moiety like MPEP or compounds **53**, **54**, **138** and **139**. These two compounds, due to their length and intrinsic rigidity may not bind mGlu₅ allosteric pocket in their *trans* disposition, whilst upon illumination, they may adopt a kinked disposition, able to produce a functional binding. Compound **142a** also include a *p*-NMe₂ substitution, to increase the electron density of the azobenzene. Alternatively, compound **142b** includes an *N*-morpholino moiety, which proportionate a similar electron donating effect and makes the compound even longer. Additionally, the presence of the oxygen atom might increase the solubility of the compound. Compound **143** consist on a derivative of compound **142a**, with an *N*-amide bond instead of the ethynyl bond, which other mGlu₅ NAMs also include (like compound **50**), and the carbonyl of this amide, as a electron withdrawing group, may proportionate a push-pull effect. Finally compound **143** was conceived as a bioisoster of compound **50**, with the azo moiety replacing the oxygen of the diaryl ether present in compound **50** (*figure 79B*)

***In-silico* screening**

Xavier Rovira, IGF-CNRS, Montpellier, and James Dalton, INc-UAB, Bellaterra.

Before proceeding in the synthesis of the new compounds, we performed docking studies both in *cis* and *trans* configuration with all the compounds to check the suitability of the *cis*-on approach in each of the designed molecules. Thus, we docked compounds **140a** and **141** in a homology model of mGlu₄⁵² and compounds **142a-b** and **144** in the crystal structure of mGlu₅ receptor³². Concerning mGlu₄ receptor, compounds **140a** and **141** docked in the *cis* configuration in a very similar pose to other mGlu₄ PAMs in the same model⁵² (*figure 80AB*), whereas in the *trans* configuration the dockings did not result favourable. On the other hand, compounds **142a**, **142b** and **144** in its *cis* configuration showed a well-fitting docking very similar to that of MPEP and Alloswitch-1²¹⁶ (*chapter 1*) and are able to H-bond with S809 on TM7 (*figure 80C-E*), while in its *trans* configuration neither **142a** nor **142b** fit correctly. However, compound **144** in its *trans*-disposition still docs correctly in the receptor model (*figure 80F*).

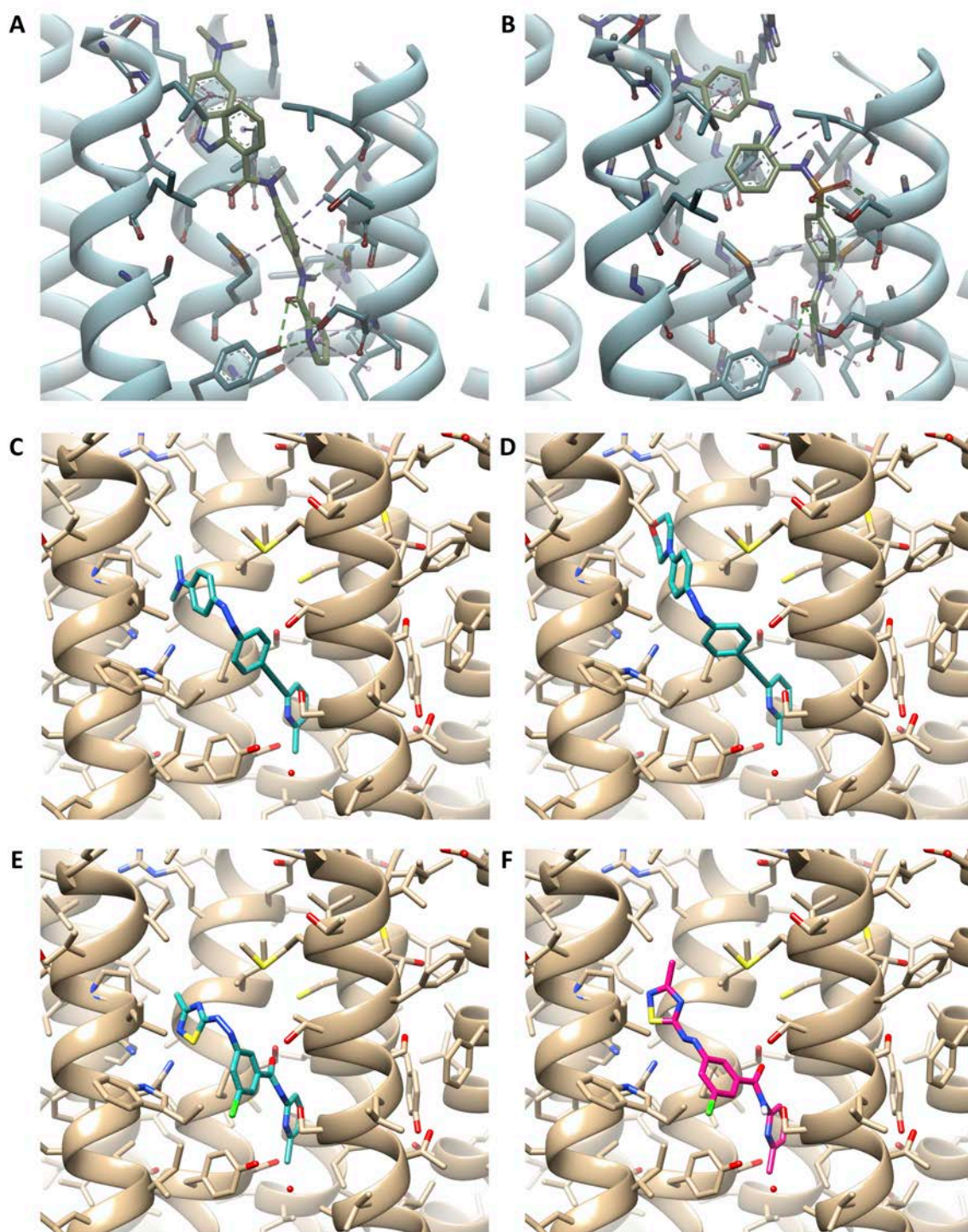
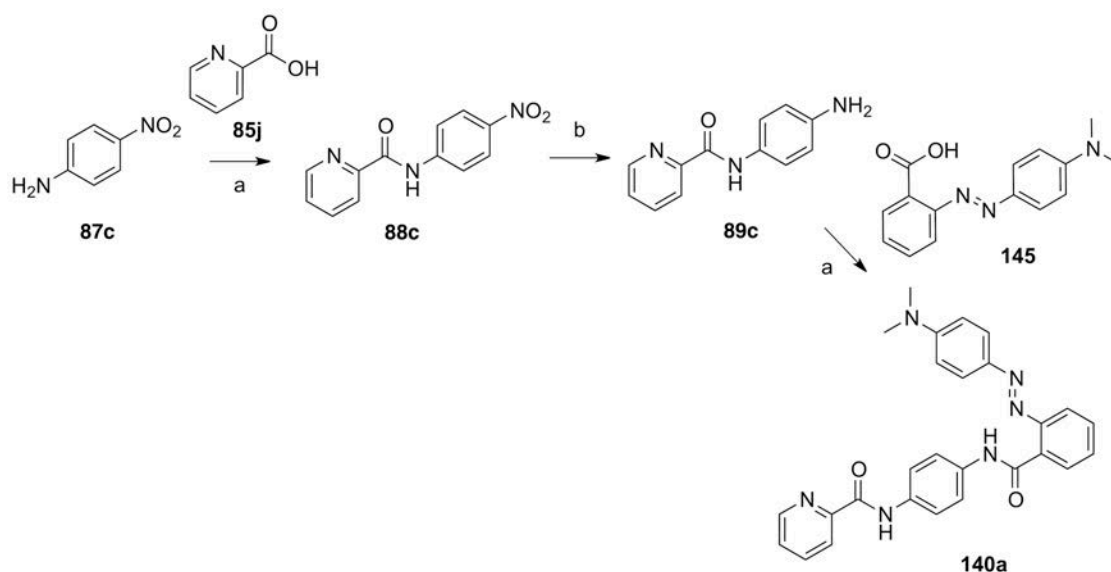


Figure 80: (A,B) Compounds **140s** (A) and **141** (B) docked into a homology model of transmembrane domain of mGlu₄⁵² in its *cis* configuration showing a similar binding modes to other reported mGlu₄ PAMs⁵². Ligands are shown in green, receptor in cyan. The allosteric binding pocket is shown from the side (TM6 not shown), with TM5 front-left, TM7 front-right, TM3 central, TM4 background-left, TM2 background-right (with chosen residues labelled). (C-E) Compounds **142a** (C), **142b**, (D) and **144** (E) in their *cis* configuration and **144** (F) in their *trans* configuration in the crystal structure of mGlu₅ (PDB id 4O09) minus mavoglurant. *Cis* azocompounds are shown in cyan, *trans*-**144** in magenta, receptor in beige. The allosteric binding pocket is shown from the side (TM6 not shown), with TM5 front-left, TM7 front-right, TM3 central, TM4 background-left, TM2 background-right (with chosen residues labelled).

Therefore, we can conclude from these dockings that, for mGlu₄ receptor, compounds **140a** and **141** constitute promising candidates for becoming *cis*-on photoswitchable PAMs and compounds **142a** and **142b** as *cis*-on mGlu₅ NAMs. In contrast, the results of compound **144** seem not to point to a clear-cut effect, as both positional isomers dock in mGlu₅ receptor crystal structure with a similar binding mode, suggesting a comparable affinity of the *cis* and *trans* isomers and an unconvincing projection for photoswitching the corresponding pharmacological activity. Therefore, we decided avoid the synthesis of compound **144**, since its *cis*-on effect is improbable.

Synthesis of compounds 140a-144

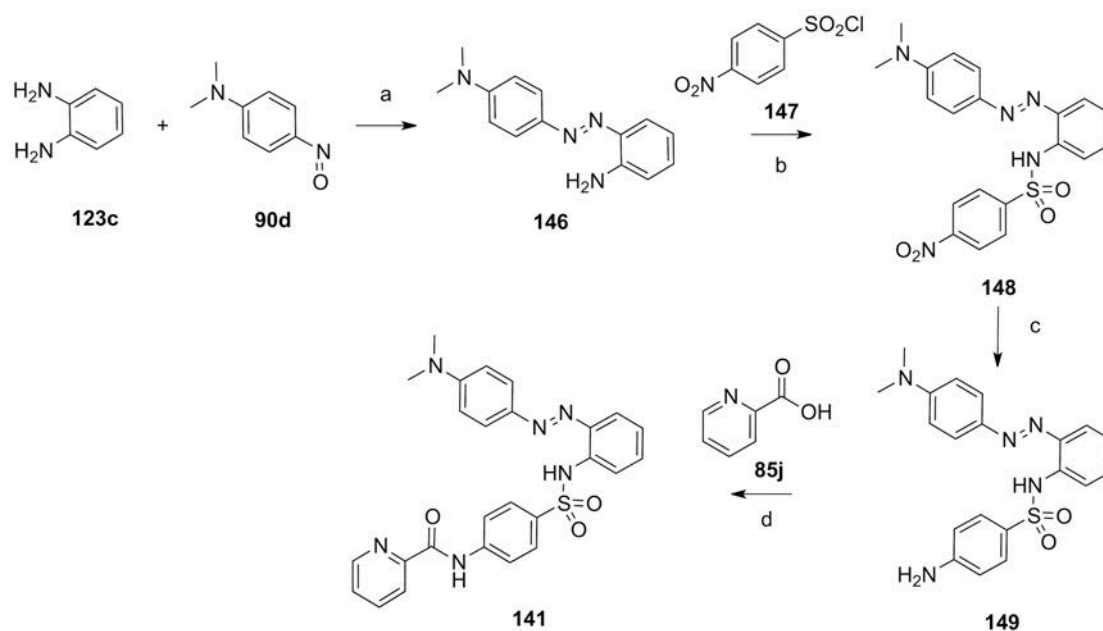
Compound **140a** was prepared following the synthetic strategy shown in *scheme 11*. The first step of acylation of 4-nitroaniline **87c** with picolinic acid (**85j**) and the following reduction of the nitro group of **88c** to give the aniline derivative **89c** (*step b*) was previously described to synthesise compound **111c**. Following step, consisting on acylation of **89c** with methyl red (**145**) activated with HATU/DIPEA afforded final compound **140a** in 49% yield.



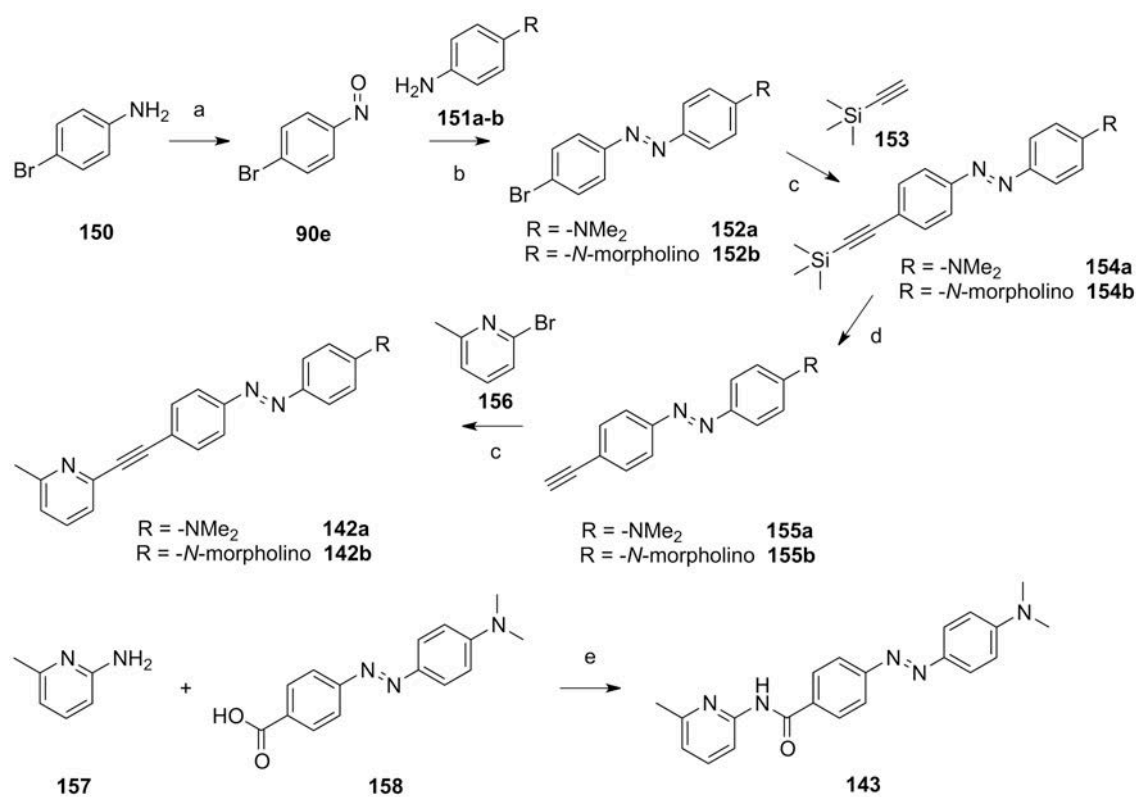
Scheme 12: 11 Synthesis of **140a**. Reagents and conditions: (a) HATU, DIPEA, DMF 40°C, 14-22h, 94%- 49%; (b) H₂ (2 bar), Pd/C, EtOH/1,4-dioxane r.t. 5 h, 97%.

Compound **141** was synthesised following the procedure depicted in *Scheme 12*. Azobenzene **146** was prepared from a reaction in solid phase of *o*-phenylenediamine **123c**, the nitrosoaniline **90d** and potassium hydroxide powder with a 57% yield (*step a*). The sulphonamide **148** was prepared by reaction of the azo-aniline **146** with *p*-nosyl chloride **147** in 72% yield (*step b*) and this was followed by the nitro group reduction with sodium sulphide to give the compound **149** with a 98% yield (*step c*). Finally, Compound **141** was prepared from

the acylation of amine of compound **150** with picolinic acid (**85j**) activated with HATU/DIPEA with a 37% yield (step d).



Scheme 13: 12 Synthesis of **141**. Reagents and conditions: (a) (i) KOH (solvent-free); (ii) toluene 90°C 1h, 57%; (b) pyridine, DCM, r.t., 18h, 72%; (c) NaS·9H₂O, EtOH, reflux, 2h, 98% (d) HATU, DIPEA, DMF, 40°C, 18 h, 37%.



Scheme 14: 13 Synthesis of **142a-b** and **143**. Reagents and conditions: (a) Oxone, DCM/H₂O, 2 h, r.t. 95%; (b) AcOH, DCM, r.t., 60 h, 92%; (c) CuI 7-13% mol, Pd(PPh₃)₂Cl₂ 7-13% mol, TEA, DMF, 50°C, 7.5 h, 16-97%; (e) K₂CO₃, MeOH/THF, 2 h, r.t., 88-95% (f) HATU, DIPEA, DMF, 40°C, 3 d, 61%

Compounds **142a-b** and **143** were synthesised following the procedure depicted in *Scheme 13*. Azobenzene derivatives **152a** and **152b** were prepared from the coupling of the corresponding dimethylamino aniline **151a** or the morpholino aniline **151b** with 4-bromo-nitrosobenzene **90e** (*step b*), previously prepared from the corresponding aniline **150** (*step a*), with high yields (92%, 83%). Following Sonogashira coupling with ethynyltrimethylsilane (**153**) afforded compound **154a** and **154b** with also good yields (97%, 80%) (*step c*) and the removal of the silane was performed with sodium carbonate in MeOH to give the terminal alkynes **155a** and **155b** in high yields (95%, 88%) (*step d*). Finally, compounds **142a** and **142b** were obtained by the Sonogashira coupling of the terminal alkynes **155a** and **155b** with 6-methyl-2-bromopyridine (**156**) with moderate yields (16%, 38%) (*step c*). Compound **143** was synthesised in a single step consisting in the amide formation between 2-amino-6-methyl-pyridine (**157**) and the aminoazobenzene **158** activated with HATU/DIPEA with a 61% yield (*step f*).

Photoisomerisation properties of compounds of 140a-143

UV-Vis absorption spectroscopy

For all the compounds of this series, we first measured the UV-Vis absorption spectra of all the components in a mixture of water with 0.05% of formic acid and acetonitrile with 0.05% of formic acid by HPLC coupled simultaneously to a photodiodes array (PDA) and a mass spectrometer. In contrast to the compounds presented in *chapter 1-4*, these new compounds embody either electron rich azobenzenes or push-pull azobenzenes, which confer a red-shifted wavelength of illumination and fast *cis*-isomer relaxation properties¹⁵⁶⁻¹⁵⁸. Such properties make unable the correct band separation and detection for both *cis* and *trans* isomers. Even though we could perfectly detect the UV-Vis spectrum of all the compounds, showing a common maximum corresponding to the π - π^* transition between 420 and 470 nm.

After that, we tested the photoisomerisation conditions in solution (DMSO, 25 μ M) under different light conditions. To do so, we collected UV-Vis spectra in the dark, and 2 minutes after continuous illumination with 460, 430, 400 or 380 nm wavelengths, registering different UV-Vis spectra, which consisted in a *cis-trans* isomer mixture for each illumination wavelength. The decrease of the height of the π - π^* transition of the *trans*-isomer, denoted a qualitative photoisomerisation rate. For all the compounds we obtained a very similar photoisomerisation properties under illumination with 460 and 430 nm wavelengths, and even 400 nm whereas after illumination with 380-nm-light we recovered a considerable fraction of the *trans* isomer (*figure 81*). Therefore, we were able to use as illuminating wavelengths for cell-based assays

430 or 460 nm, which are in the blue range, or 400 nm, which is in the violet range of the spectrum.

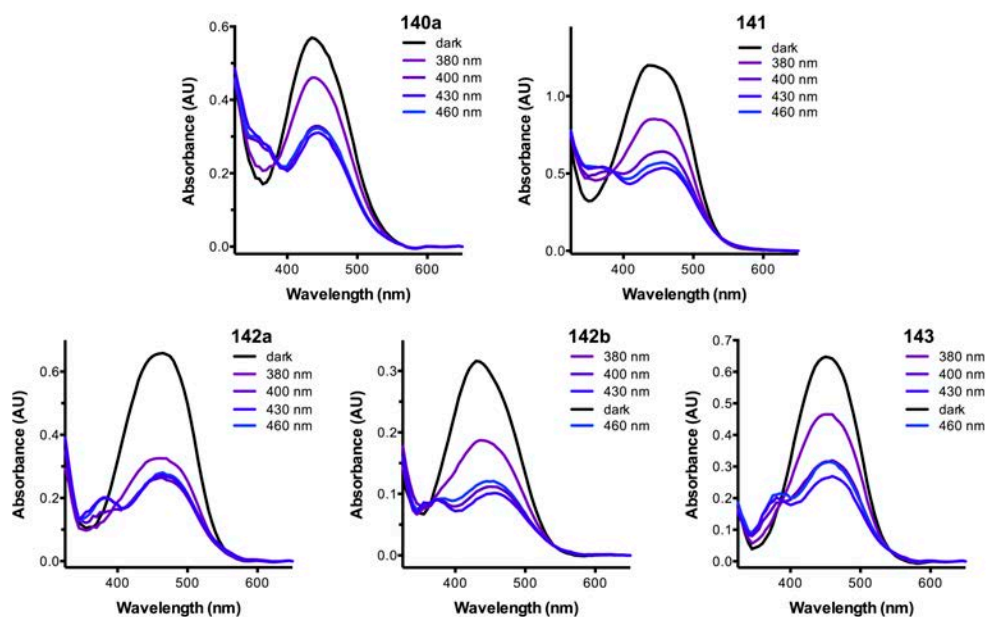


Figure 81: UV-Vis Absorption spectra of compounds **140a**, **141**, **142a-b** and **143** in dark conditions and after illuminating with different wavelengths. Illumination with 400, 430 and 460 nm affords very similar profiles.

Pharmacological characterisation of compounds of 140a-143

Single dose screenings

Joan Font, IGF-CNRS, Montpellier

To evaluate the pharmacological activity of all the putative *cis*-on mGlu₄ PAMs or mGlu₅ NAMs, we first screened the compounds in HEK293 cells transiently transfected with rat mGlu₄ or mGlu₅ using an inositol phosphate (IP) accumulation assay based in homogeneous time-resolved fluorescence (HTRF) assays (*experimental part*). Due to the high promiscuity between of mGlu₄ PAMs and mGlu₅ NAMs, observed in the *chapters 1-4*, we measured their both the PAM and NAM effect in both mGlu₄ and mGlu₅ receptors, independently of the purpose of their design. Additionally every measurement was performed simultaneously in dark conditions and under illumination with blue light ($\lambda = 460$ nm) (*experimental part*). For mGlu₄ we used the orthosteric agonist L-AP₄ (**4**) at a low concentration of 3 nM to measure the PAM effect and 300 nM, as a high concentration, to measure the NAM effect. To measure the modulation of mGlu₅ function we used quisqualate (**2**), as an orthosteric agonist, with a low concentration of 1 nM and a high concentration of 100 nM, to measure PAM and NAM effects, respectively.

Despite the efforts in the design of the compounds, we found no strong effect under illumination with blue light and neither a strong difference of activity between the illuminated samples during their incubation and the corresponding ones in the dark (*figure 82*). The only very weak *cis-on* effects were observed for compounds **140a**, **141** and **143** as mGlu₄ PAMs, with **140a** as the one showing the best *cis-on* effect, but still insufficient (*figure 82A*). Additionally compound **142b** performed some partial PAM effect in mGlu₄ both in the dark and under illumination (*figure 82A*). Therefore we decided to study further this mGlu₄ PAM effect of compounds **140a**, **141**, **142b** and **143**.

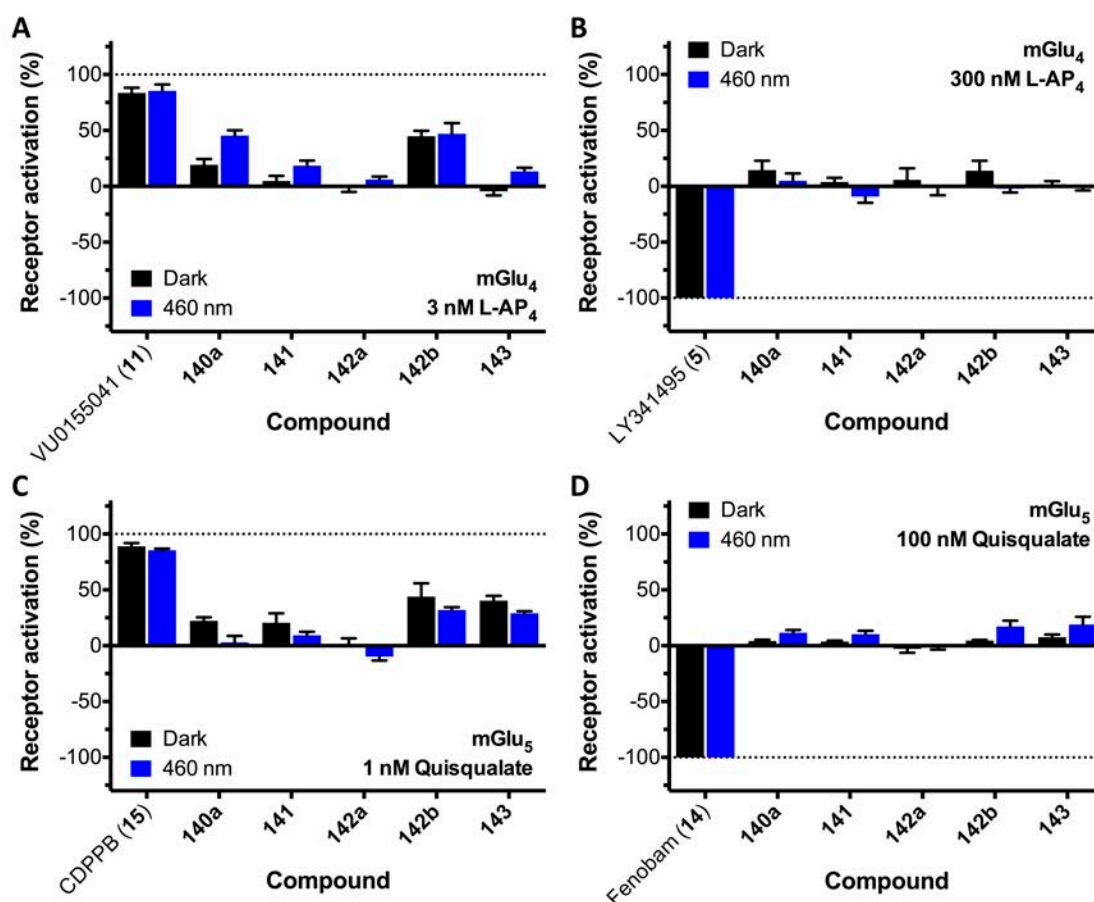


Figure 82: Single-dose screening of compounds **140a**, **141**, **142b** and **143**, as (A) mGlu₄ PAMs, (B) mGlu₄ NAMs, (C) mGlu₅ PAMs and (D) mGlu₅ NAMs. FRET response was normalised to 0%-100% between the effect of the low concentration of agonist (EC_{20}) and the effect of the saturation of agonist for the PAM evaluation. For the NAM evaluation, FRET response was normalised to -100%-0% between the effect of the effect of the saturation of an antagonist and the high concentration of agonist (EC_{80}). Each bar corresponds to the mean of a minimum of two independent replicates with the corresponding SEM as error bars

Dose-response curves

In collaboration with Joan Font, IGF-CNRS Montpellier

To further evaluate the minimal *cis*-on mGlu₄ PAM activity for compounds **140a**, **141**, **142b** and **143** we generated dose-response curves from data obtained with an IP accumulation assay with HEK293 cells transfected with rat mGlu₄ receptor. We used the "changing tips" protocol used in *chapter 3* and *chapter 4*, but with 460 nm as the illuminating wavelength due to the photoisomerisation properties of these compounds, already shown above.

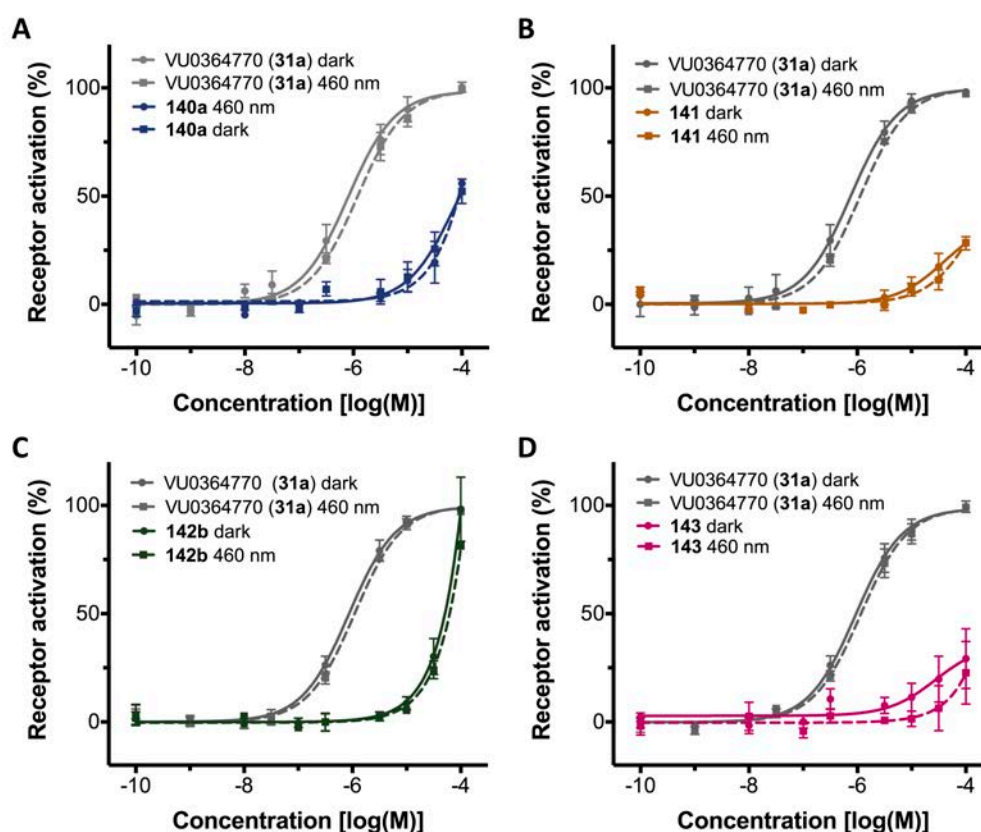


Figure 83: Dose-response curves using "changing tips" protocol with IP-One assay on HEK293 cells overexpressing mGlu₄ receptor with a constant concentration of L-AP₄ (**4**) 3 nM. Flat lines correspond to the samples incubated in dark conditions and dotted lines to the samples under 460-nm-illumination. Each point corresponds to the mean of a minimum of three independent replicates with the corresponding SEM as error bars.

Unfortunately, we could not find any *cis*-on profile in the dose-response curves (*figure 83*) and those results were not in fully agreement with the single-dose profiles, except for compound **142b**, which showed a sharply sloped curve, probably due to non-specific effects, with no difference between the dark and illuminated curves.

In a last attempt to find some conditions for positive results, which could validate our approach and permit us to explore further in this family of compounds, we generated two

additional dose-response curves with compounds **140a** and **141**, which are the ones that show a better *cis-on* effect in the single-dose screening. To generate these curves we used the same IP accumulation assay but using two different protocols: a first one using the protocol without changing the tips for each dilution (the first one used in *chapter 3*, WCT protocol); and a second one with a prolonged incubation time of 60 min, instead of 30 min (LIT protocol) (*experimental part, figure 84*). The aim of these changes in the protocol is to avoid a loss of compound while changing the tips and accumulate a larger amount of IP inside the cells to amplify the FRET response of the assay.

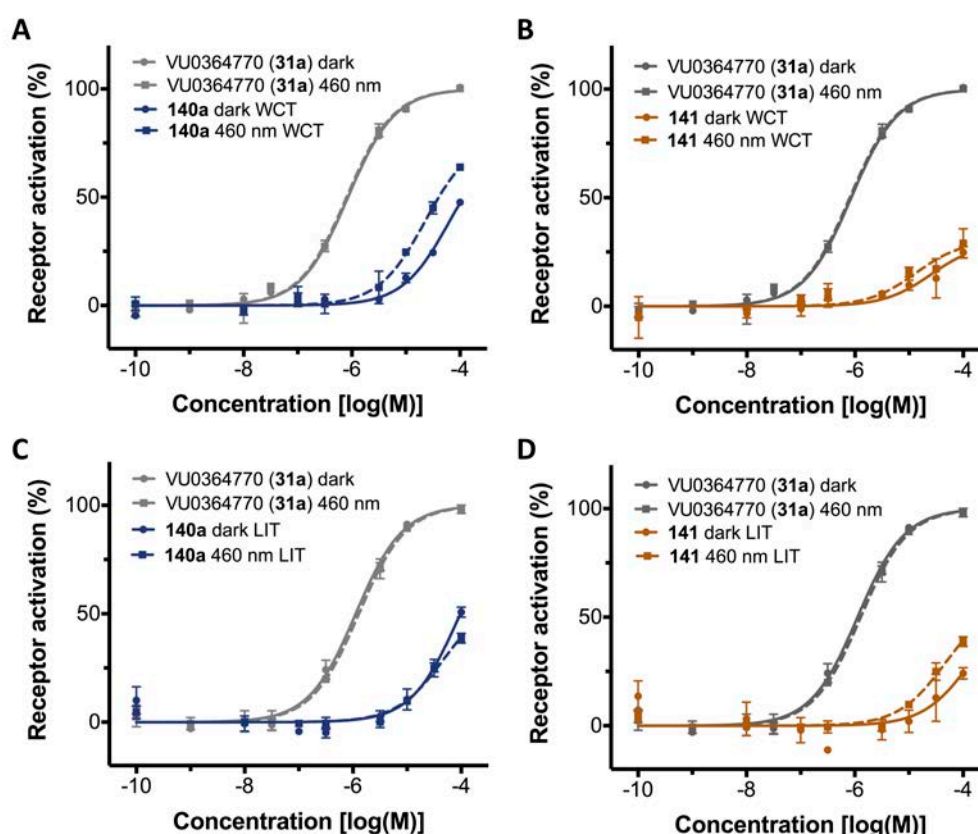


Figure 84: Dose-response curves of compounds **140a** and **141** using “without changing tips” protocol (WCT) (A, B) or “long incubating time” protocol (LIT) (C, D) with IP-One assay on HEK293 cells overexpressing mGlu₄ receptor with a constant concentration of L-AP₄ (**4**) 3 nM. Flat lines correspond to the samples incubated in dark conditions and dotted lines to the samples under 460-nm-illumination. Each point corresponds to the mean of a minimum of three independent replicates with the corresponding SEM as error bars.

Intriguingly, the results obtained changing the protocol conditions were more adequate, since we could detect a shift to the left of the curves corresponding to the 460-nm-illuminating samples in agreement with the single-dose results for compounds **140a** and **141** (shown in *figure 84*, especially **140a** in panel A and **141** in panel D). Despite the minimal *cis-on* effect observed, the response is still insufficient to achieve an appropriate *cis-on* mGlu₄ PAM.

However, these results pave the way for finding out new compounds using the same approach, as compounds **140a** and **141** do not have a strong complexity in their chemical substitution. Therefore, the rational addition substituents in an appropriate position on the chemical scaffold of compounds **140a** and **141**, might lead to new putative *cis*-on mGlu₄ PAMs.

Design and synthesis of compounds 140b-140c

In collaboration with Juan Lorenzo Catena Ruiz, IQAC-CSIC, Barcelona

The mGlu₄ PAM *cis*-on approach used for designing compounds **140a** and **141** was also used to design two new derivatives of compound **140a**, and thus validate the viability of the approach. In the literature we found some compounds with the *N*-phenylpicolinamide moiety with several substitutions in position 3 of the phenyl ring. Among all them, methoxy and chloro-substitutions provided better potencies and efficacies^{94, 96}. Hence, we thought to keep these substitutions in the non-azobenzenic phenyl of **140a** scaffold to improve the compound potency and efficacy as mGlu₄ PAM. Thus we afforded compound **140b**, with a methoxy-substitution and **140c**, with a chloro-substitution (*figure 85*).

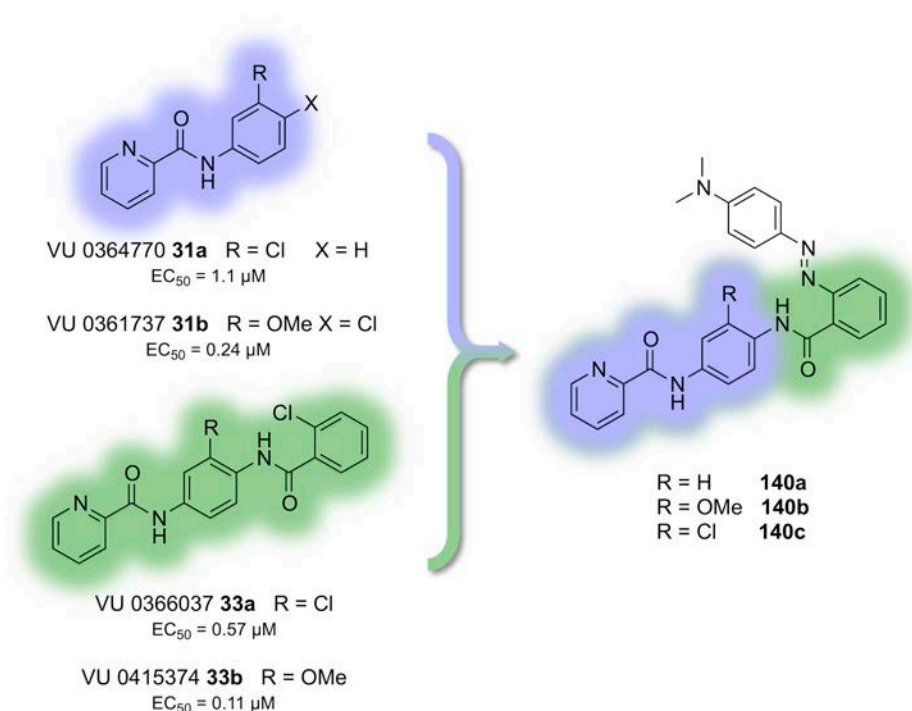
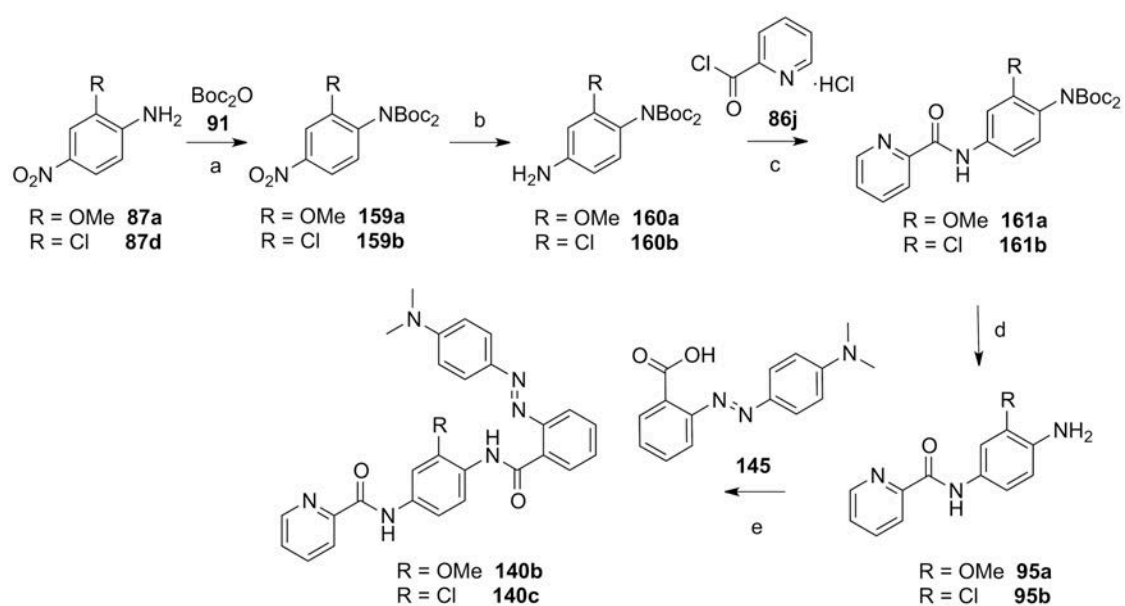


Figure 85: Design of new *cis*-on photoswitchable mGlu₄ PAMs, derived from compound **140a**. Compounds found in the literature that bear *N*-phenylpicolinamide, like **31a-b** and **32a-b**, include a methoxy or chloro substitution in the phenyl ring of the *N*-phenylpicolinamide. Compounds **140b** and **140c** also include methoxy and chloro substitution in the same position, to improve the putative *cis*-on mGlu₄ PAM effect.

Compounds **140b** and **140c** were prepared following the synthetic strategy shown in *scheme 14*. The first step consisted of the protection of the corresponding nitroaniline **87a,d** (*step a*) followed by the hydrogenation of the corresponding nitrocompound **160a-b** to afford anilines **161a-b** (*step b*). Consecutively, the anilines **161a-b** were acylated with picolinoyl chloride hydrochloride (**86j**) to afford the corresponding compounds **161a-b** (*step c*), which were deprotected in acidic media to afford the anilines **95a** and **95b** (*step d*). Finally, compound **140b** and **140c** were obtained from coupling of the corresponding aniline **95a** and **95b** and methyl red (**145**) with HATU/DIPEA with moderate yields (19-28%) (*step e*).



Scheme 15: 14 : a) DMAP cat., THF, r.t., 16 h 82-84%; b) H₂ (2 bar), Pd/C, EtOAc, r.t., 16h 98-100%; c) DIPEA, DCM, 0°C to r.t., 16h, 79-98%; d) HCl 4N in 1,4-dioxane, r.t. 3h 98-100%; e) HATU, DIPEA; DMF, 40 °C, 4d 19-28%

Photoisomerisation properties of compounds of 140b-c

UV-Vis absorption spectroscopy

We measured the UV-Vis absorption spectra of all the compounds in a mixture of water with 0.05% of formic acid and acetonitrile with 0.06% of formic acid by HPLC coupled simultaneously to a photodiodes array (PDA) and a mass spectrometer. As observed for compounds **140a** or **143**, they bear push-pull electronic properties and a maximum of absorption corresponding to the azobenzene π - π^* transition around 470 nm.

After that, we tested the photoisomerisation conditions in solution (DMSO, 25 μ M) under different light conditions (2 minutes after continuous illumination with 500, 460, 430, 430, 400 or 380 nm wavelengths) and we obtained a decrease of the height of the π - π^* transition of the *trans*-isomer achieving different UV-Vis spectra, corresponding to a mixture of *cis-trans*

isomers for each illumination wavelength. We obtained the maximum photoisomerisation rate at 460 and 500 nm illumination, for compound **140b** and at 430 and 460 nm for compound **140c**. In both cases, with 380-nm-light we recovered a fraction of the *trans* isomer (figure 86A). However, we did not obtain the same photoisomerisation quality, compared to the previous *cis*-on candidates, since the decrease on the height of their *trans*-isomer π - π^* band was lower. We thought that a possible explanation for the weaker photoisomerisation could be faster thermal relaxation of the corresponding *cis*-isomer. To confirm that, we tested the relaxation rate of the *cis* isomer of all compounds of the series in DMSO and we obtained a significantly lower half-life for the *cis*-isomers of compounds **140b** and **140c** compared to their parent compound **140a** (table 20, figure 86B). Therefore, we could achieve a more efficient photoisomerisation increasing the light intensity or decreasing the concentration of the compounds.

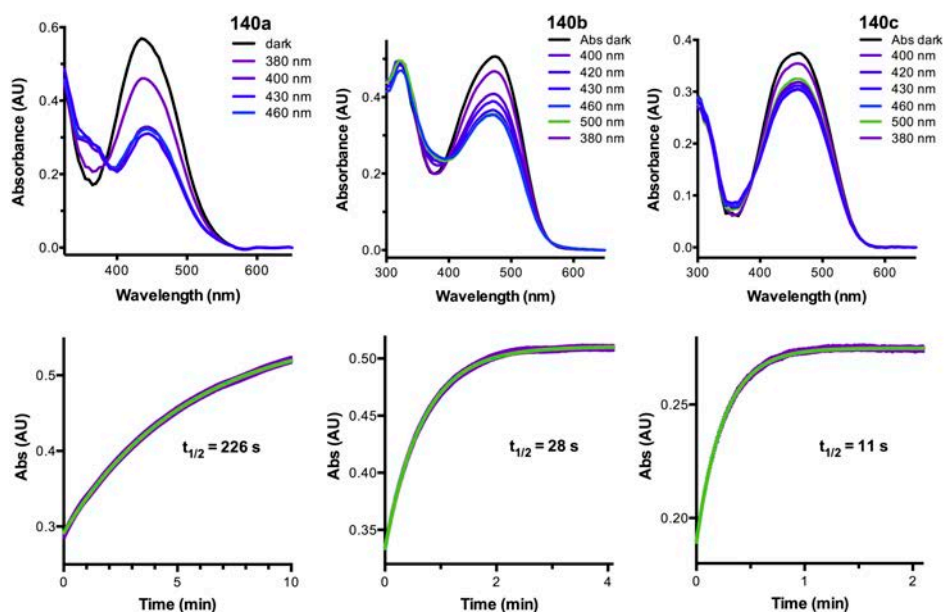


Figure 86: UV-Vis Absorption spectra of compounds **140a-c** in dark conditions and after illuminating with different wavelengths and their corresponding relaxation plot of the *cis*-isomer, showing that the **140b-c**, did not show a proper photoisomerisation due to their fast relaxation of the *cis*-isomer.

Compound	$t_{1/2}$ (s)	EC_{50} (μ M)	$t_{1/2}$ (s)
140a	226	142a	662
140b	28	132b	666
140c	11	143	303
141	277		

Table 20: Relaxation half-life of *cis*-isomers of compounds **140-143** 25 μ M in DMSO

Pharmacological characterisation of compounds of 140a-143

Xavier Rovira – IGF-CNRS Montpellier

To evaluate the possible *cis-on* mGlu₄ PAM activity for compounds **140b** and **140c** we generated dose-response curves extracted from IP accumulation assay with HEK293 cells transfected with rat mGlu₄ receptor used 460 nm as the illuminating wavelength, as done with compounds **140a**, **141**, **142b**.

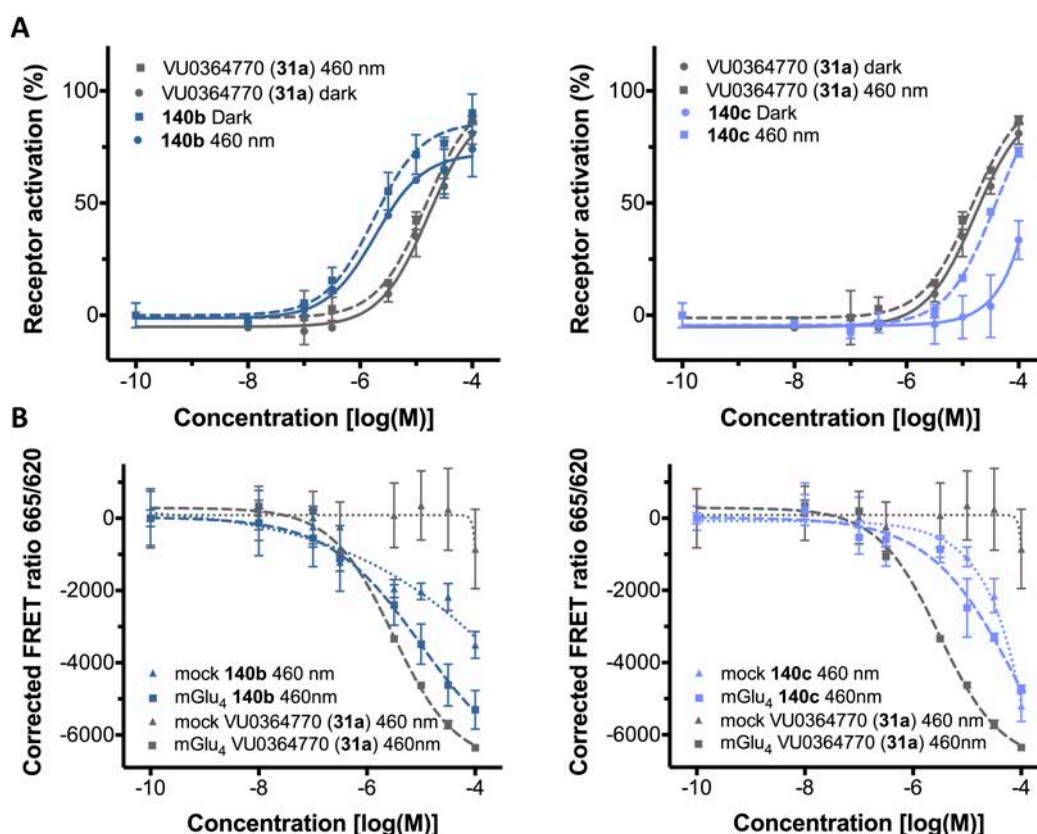


Figure 87: Dose-response curves using “changing tips” protocol with IP-One assay on HEK293 cells with compounds **140b** and **140c** using VU0364770 (**31a**) as a control mGlu₄ PAM (A) HEK293 overexpressed mGlu₄ receptor with a constant concentration of L-AP₄ (**4**) 3 nM. Flat lines correspond to the samples incubated in dark conditions and dotted lines to the samples under 460-nm-illumination. Each point corresponds to the mean of a minimum of three independent replicates with the corresponding SEM as error bars. (B) Large-dotted lines correspond to HEK293 overexpressing mGlu₄ and Small-dotted lines correspond to HEK293 with no expression of mGlu₄ receptor. Both conditions were tested with a constant concentration of L-AP₄ (**4**) 3 nM and under 460-nm-illumination. Each point corresponds to the mean of a minimum of two independent replicates with the corresponding SEM as error bars

The results obtained improved those obtained previously, as we obtained a *cis-on* effect for both compounds. On the one hand, compound **140b** turned out to be an mGlu₄ PAM in dark

conditions with a micromolar potency and when illuminated with blue light displayed a slightly lower IC_{50} , denoting a small increase on the potency, but not sufficient to have a suitable photoswitching of mGlu₄ response (*figure 87A*). On the other hand, compound **140c** showed very weak modulation of mGlu₄ activity in the dark, whereas it showed a considerable effect as mGlu₄ PAM under 460-nm-illumination, with an IC_{50} in the micromolar range (*figure 87A*).

To confirm the results obtained, we finally performed two experiments with compounds **140b** and **140c** to exclude non-specific effects. Thus, we performed an experiment with continuous illumination with 460-nm-light in parallel with HEK293 cells transfected with mGlu₄ receptors and with HEK293 cells with a transfection of an empty DNA plasmid, which did not encode mGlu₄ receptor (mock cells). Disappointingly, both compounds showed an effect in mock cells, similar to that observed in mGlu₄-transfected cells and that was not observed with the mGlu₄ PAM control VU0364770 (**31a**) (*figure 87B*). Moreover, this non-specific effect was more accused for compound **140c**, which was the one with a “higher *cis*-on effect”, indicating that the observed *cis*-on effect is an artefact, which can be the result of a *cis*-on effect induced on unknown endogenous receptors or target proteins constitutively present of HEK293 cells, which are probably involved in IP production.

Conclusions

We designed compounds **140a**, **140b**, **140c** and **141** as candidates to display PAM activity in mGlu₄ receptor in their *cis* configuration, and inactive in their *trans* configuration. This is based in a search for long mGlu₄ PAMs in the literature with a bent disposition to mimic *cis* azobenzene geometry. Therefore, the linear *trans* azo mimetic isomer would be too long to fit in the allosteric binding site of mGlu₄ receptor.

We designed compounds **142a**, **142b**, **143** and **144** as candidates to display NAM activity in mGlu₅ receptor in their *cis* configuration, whereas in their *trans* configuration, they are expected to be inactive. We took advantage of the angular disposition of many mGlu₅ NAMs to design azocompounds that in *trans* disposition adopt a rigid linear non-binding structure and, in *cis* disposition, an angular shape that binds into the mGlu₅ allosteric site. Additionally, **144** was an azo-replaced bioisoter of another reported mGlu₅ NAM with a diarylether.

All the compounds were docked in the models of corresponding transmembrane domains (mGlu₄ homology model and mGlu₅ crystal structure), showing suitable results in their *cis* configuration, except for compound **144** that was docking properly in both *cis* and *trans* configurations.

All the compounds have been designed to display *trans* to *cis* photoswitching in the visible range, with the addition of electron donating substituents. Finally, the obtained optimal wavelengths were located between 430 and 460 nm for all the compounds.

After the corresponding pharmacological evaluation in the dark and under 460-nm illumination, we only found three compounds with some *cis*-on effect: compounds **140a**, **140b** and **140c** as mGlu₄ PAMs. The pharmacological effect found for **140a** was very weak, whereas **140b** and **140c** show better potencies, with **140c** with a considerable *cis*-on effect. However, when compounds **140b** and **140c** were tested in the same assays without mGlu₄ receptor, we obtained similar results. This is interpreted as the *cis*-on activity observed was originated from an unknown activity in HEK293 cells, and therefore this *cis*-on approach failed to give compounds with suitable properties.

Cis-on compounds could to only produce a pharmacological effect in a single region of the organism with a high-precision spatiotemporal control with light with an inactivation after their diffusion throughout the organism. This may avoid numerous drug side effects; especially in drugs that modulate the activity of widely distributed receptors, such as mGlu receptors. That is the reason why this approach is therapeutically the most attractive and more work will be performed in the future towards this goal.

Summary of results and conclusions

The results in *chapter 1* indicate that used azologisation approach was successfully. VU0416374 (**33b**) was an excellent candidate for engineering new mGlu allosteric modulators by replacing an amide with an azo-bond. Additionally, we discovered structural similarities between mGlu₄ PAMs and mGlu₅ NAMs and that azolization might be also successful when replacing acetylenes with azo-bonds.

Alloswitch-1 (**83**) is a potent and selective negative allosteric modulator of mGlu₅ and its activity can be switched on and off by means of different wavelength illumination. It constitutes the first allosteric modulator that bears photoswitchable properties, maintaining its drug-like properties.

Alloswitch-1 (**83**) reversibly photoisomerises in dilution and this is translated in cultured cells to a photoswitch of the functional activity of both transfected and native mGlu₅.

In-silico modelling showed a reasonable binding mode of trans-alloswitch-1 on, in similar poses to other mGlu₅ NAMs and it is possible that the photoisomerisation occurs inside allosteric binding site but affording an unfavourable conformation that might lead to the unbinding of alloswitch-1.

Alloswitch-1 (**83**) enables the control of animal natatorial motility of zebrafish embryo and *Xenopus Tropicalis* tadpoles with light and also controls the sensitivity to pain of mice with direct illumination in the amygdala.

Optogluram (**84**) is a positive allosteric modulator of mGlu₄, which activity can also be switched on and off with different wavelengths of light. It also reversibly photoisomerises *in vitro*, it permits the control of animal natatorial motility of zebrafish embryo and also control the sensitivity to pain of mice with direct illumination in the amygdala.

The results obtained In *chapter 2* describe the effective an example of a double effect molecular switch in the nanomolar range, where a high potency mGlu₄ PAM is switched to an mGlu₅ NAM by minimal ligand modification, in a very similar manner as we obtained alloswitch-1 (**83**) and optogluram (**84**) in *chapter 1*, but, using an ethynyl-bond instead of a azo-bond. The resulting compounds **99** and **100** are active in different receptor subtypes belonging to mGlu receptors groups I and III, which are known to play completely different roles in synaptic processes, as they activate different signalling pathways.

This molecular switch, altogether with that described in *chapter 1* and that one found in the literature with **12b** and **31a** suggests a structural similarity between mGlu₄ PAM and mGlu₅

NAM allosteric sites, which are able to selectively recognize compounds differing only in the bridging functionality between two aromatic rings.

Moreover, we have proved that azologization of ethynyl between aromatic rings is a powerful approach to afford new azo-compounds with *trans*-on photoswitchable properties, since both moieties share a very similar structural disposition, rigidity and electron density to be recognised by protein targets as bioisosters. Additionally, the pharmacological properties afforded with the ethynyl bioisosters are very similar to the obtained with the *trans*-azo-compounds, especially for compounds **83** and **99** in the mGlu₅-receptor-expressing cells.

The results reported here can be of interest for the pharmacological study of selective modulation of this family of receptors and for establishing the structural determinants of allosteric function in mGlu receptors. These findings constitute a proof of concept for a new strategy in the development of subtype discriminatory mGlu ligands, specifically in the design of new mGlu₄ PAMs from suitable mGlu₅ NAMs, and vice versa. This may be a faster and more effective way to discover pharmaceutically relevant allosteric modulators for mGluRs subtypes and to establish the structural features necessary for mGluR subtype selectivity. Additionally, these results also constitute an excellent example of azologization of ethynyl-compounds with very similar functional profile in their *trans*-disposition, which theoretically could be translated to bioactive diarylethynyl compounds with high probabilities of success.

In chapter 3 we showed the synthesis of a series of photoswitchable mGlu₅ NAMs based on phenylazopyridine scaffold, with a robust SAR, with almost all the *trans* isomers active on mGlu₅ in cell-based assays and a half of them significantly inhibiting zebrafish motility at 10 μ M of concentration.

We obtained variable photoisomerisation properties, attributable to different structural properties, and their translation to in-vitro and in-vivo assays was successful, since very few compounds lost its photoswitching properties in any of the different assays in spite of the increasing complexity of the biological tests. From these compounds, we obtained excellent photoswitching behaviour in all the assays performed with compounds **109a**, **109f**, **109i**, **109j**, **111c**, as well as **114**, which resulted in a more powerful photoswitching when illuminating with blue-shifted wavelengths.

We showed *in-silico* that the binding modes of these series of compounds is the mGlu₅ allosteric site is very similar to that one of alloswitch-1 (**83**) (*chapter 1*), and the different pharmacological profile of compound **110** observed in cell-based assays might be explained as

a result a different binding mode in the allosteric site of transmembrane domain of the receptor.

The phenylazopyridine series allowed us to define a way to achieve a fine control of mGlu₅ receptor activity by tuning the wavelength of illumination between 360 and 500 nm and, depending on the compound used, we were able to control an over-activation of the receptor. This functional over-activation was also detected *in-vivo* after treating zebrafish larvae with some specific compounds, but not with others. The reasons for this light- dependent atypical effect could be linked to the potentiation of calcium responses in single cell assays and require further investigation. Photoswitchable ligands reveal new paradigms on the ligand-induced protein responses with potential to add a new modulatory dimension to drug therapeutics.

In chapter 4 we showed the synthesis of 12 compounds, based on an phenyl central ring covalently bound to two 2-pyridine units with two different substitution patterns (1,3 and 1,4) and with the combination of three different linkers: amide, azo and ethynyl groups.

We obtained two compounds (**111c** and **128a**) with both mGlu₄ PAM and mGlu₅ NAM activities with similar potencies around the micromolar range. However, their selectivity over mGlu family of receptors was not ideal to constitute effective tool compounds, since they also displayed partial efficacies as mGlu₂, mGlu₆, mGlu₇ and mGlu₈ PAMs. This lack of selectivity limits their possible biological applications only to test a pan-mGlu neuroprotective agent.

Four compounds (**129a-b** and **131a-b**) could be considered azologized¹⁸⁷ derivatives of the mGlu₅ NAMs 1,3-BisPEB and 1,4-BisPEB, by formal replacement of ethynyl groups for azo groups. They maintain very similar pharmacological properties to the previous reported isosteres¹²⁴, including a very similar potency.

Despite the similar potency among the compounds tested in mGlu₅ receptor, we found substantial differences in their antagonistic efficacy on mGlu₅ receptors: compounds with 1,3-substitution displayed an inverse agonist efficacy similar to the reference compound fenobam, whereas compounds with 1,4-substitution displayed partial antagonistic effects.

Computational docking in the mGlu₅ crystal structure³² revealed the angular-shaped 1,3-substitued compounds bind in a very similar pose to the co-crystallised inverse agonist mavoglurant, whereas the linear 1,4-substitued compounds bind in a different pose, unlikely to be functional and with a concomitantly low docking score. However, an alternative conformation of the mGlu₅ transmembrane domain might adapt to these linear-shaped compounds in a functional-like pose, which may be responsible for the partial antagonism behaviour.

The discovery of a molecular switch from allosteric inverse agonists to partial allosteric antagonists is of high interest, since recent publications have reported the advantageous properties of partial mGlu5 NAMs^{211, 212}, which might avoid on-target side-effects of mGlu5 complete blockade by classical allosteric inverse agonists^{213, 214}. Therefore, our approach based on exchanging the substituent position in a rigid mGlu5 NAM scaffolds to afford a straight-shaped compound may be useful to discover new partial mGlu5 NAMs with a safer pharmacological profile a better perspectives in the drug discovery trail

In *Chapter 5* we showed the design of compounds **140a**, **140b**, **140c** and **141** as candidates to display PAM activity in mGlu₄ receptor in their *cis* configuration, and inactive in their *trans* configuration. This is based in a search for long mGlu₄ PAMs in the literature with a bent disposition to mimic *cis* azobenzene geometry. Therefore, the linear *trans* azo mimetic isomer would be too long to fit in the allosteric binding site of mGlu₄ receptor.

We designed compounds **142a**, **142b**, **143** and **144** as candidates to display NAM activity in mGlu₅ receptor in their *cis* configuration, whereas in their *trans* configuration, they are expected to be inactive. We took advantage of the angular disposition of many mGlu₅ NAMs to design azocompounds that in *trans* disposition adopt a rigid linear non-binding structure and, in *cis* disposition, an angular shape that binds into the mGlu₅ allosteric site. Additionally, **144** was an azologisated bioisoter of another reported mGlu₅ NAM with a diaryether.

All the compounds were docked in the models of corresponding transmembrane domains (mGlu₄ homology model and mGlu₅ crystal structure), showing suitable results in their *cis* configuration, except for compound **144** that was docking properly in both *cis* and *trans* configurations.

All the compounds have been designed to display *trans* to *cis* photoswitching in the visible range, with the addition of electron donating substituents. Finally, the obtained optimal wavelengths were located between 430 and 460 nm for all the compounds.

After the corresponding pharmacological evaluation in the dark and under 460-nm illumination, we only found three compounds with some *cis*-on effect: compounds **140a**, **140b** and **140c** as mGlu₄ PAMs. The pharmacological effect found for **140a** was very weak, whereas **140b** and **140c** show better potencies, with **140c** with a considerable *cis*-on effect. However, when compounds **140b** and **140c** were tested in the same assays without mGlu₄ receptor, we obtained similar results. This is interpreted as the *cis*-on activity observed was originated from an unknown activity in HEK293 cells, and therefore this *cis*-on approach failed to give compounds with suitable properties.

Cis-on compounds could to only produce a pharmacological effect in a single region of the organism with a high-precision spatiotemporal control with light with an inactivation after their diffusion throughout the organism. This may avoid numerous drug side effects; especially in drugs that modulate the activity of widely distributed receptors, such as mGlu receptors. That is the reason why this approach is therapeutically the most attractive and more work will be performed in the future towards this goal.

Experimental part

Experimental part contents

Synthetic chemistry	179
Materials and methods	179
<i>Chemicals and solvents</i>	179
<i>Reaction monitoring</i>	179
<i>Purification of compounds</i>	179
<i>Melting Points</i>	179
<i>Nuclear Magnetic Resonance (NMR)</i>	179
<i>High-Performance Liquid Chromatography</i>	179
Synthetic procedures.....	181
Photochemical characterisation	227
Materials and methods	227
<i>Light source</i>	227
<i>UV-Visible absorption spectra</i>	227
<i>Stability of the photoisomerisation</i>	228
<i>Thermal relaxation of cis isomers</i>	228
<i>Nuclear magnetic resonance (NMR)</i>	229
In-vitro pharmacological characterisation	230
Functional cell-based assays	230
<i>Cell culture and transfection</i>	230
<i>Procedure for single dose screening</i>	233
<i>Procedure for dose-response curves without illumination</i>	234
<i>Dose-response curves with illumination</i>	235
<i>Procedure for selectivity assays with illumination</i>	237
In-vivo zebrafish assays	239
<i>Fish crossing and embryo growth</i>	239
<i>Zebrafish larvae locomotion experiment</i>	240

Synthetic chemistry

Materials and methods

Chemicals and solvents

All the chemicals and solvents were obtained from commercial sources and used without purification, except the anhydrous solvents, which were treated previously through a system of solvent purification (*PureSolv*), degasified with inert gases and dried over alumina or molecular sieve (dimethyl formamide). Dry triethylamine was distilled over calcium hydride. Evonik Industries supplied the platinum-5% Iron-1% on carbon experimental catalyst.

Reaction monitoring

Reactions were monitored by thin layer chromatography (60 F, 0.2 mm, *Macherey-Nagel*) by visualisation under 254 and/or 365 nm lamp.

Purification of compounds

Flash column chromatography was performed over *Panreac* Silica Gel 60, 40-63 microns RE. *Flash* column chromatography automated with *Isolera One* with UV-Vis detection (*Biotage*) was performed with normal phase silica SNAP KP-Sil 50 microns columns (*Biotage*) or reverse-phase C18 SNAP KP-C18-HS 50 microns columns (*Biotage*).

Melting Points

Melting points were measured with *Melting Point B-545* (*Büchi*), ramp 2 °C/min with a digital temperature measurement.

Nuclear Magnetic Resonance (NMR)

Characterisation of compounds with Nuclear Magnetic Resonance spectroscopy was performed with a *Variat-Mercury 400 MHz* instrument. Chemical shifts δ are reported in parts per million (ppm) against the reference compound tetramethylsilane using the signal of the residual non-deuterated solvent (Chloroform $\delta = 7.26$ ppm (^1H), $\delta = 77.16$ ppm (^{13}C), DMSO $\delta = 2.50$ ppm (^1H) $\delta = 39.51$ ppm (^{13}C)).

High-Performance Liquid Chromatography

Purity of compounds **32b**, **83** and **84** was determined High-Performance Liquid Chromatography Alliance 2695 separation module (*Waters*) coupled to *Waters 2996*

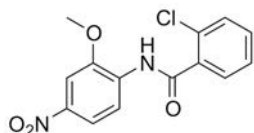
photodiode detector (PDA) (Waters), 5 μ L of sample 2.5 mM in DMSO were injected, using a Kinetex C18 2.6 μ m 4.6 x 50 mm (Phenomenex) column. The mobile phase used was a mixture of A = $\text{NaH}_2\text{PO}_4/\text{Na}_2\text{HPO}_4$ aqueous buffer 10 mM pH=7 and B = methanol, with the method described as follows: flow 1 mL/min 5%B-70%B 1 min, 70%B-80%B 1 min, 80%B-100%B 6 min, 100%B 1 min, runtime 15 min (12 min for **32b**).

Purity determination and absorption UV-Vis spectra of compounds **53**, **54**, **109b-l**, **110**, **111a-c**, **112**, **113**, **114**, **115**, **116**, **117**, **128a-b**, **129a-b**, **130a-b**, **141a-b**, **140a-c**, **141**, **142a-b** and **143** were determined with High-Performance Liquid Chromatography *Thermo Ultimate 3000SD* (Thermo Scientific Dionex) coupled to a photodiode array detector and a mass spectrometer *LTQ XL ESI-ion trap* (Thermo Scientific) (HPLC-PDA-MS); 5 μ L of sample 0.25 mM in a mixture DMSO/AcN 1:9 were injected, using a C18 column at 30°C. Four different methods have been used (methods A-D). The mobile phase used for Method A and Method B was a mixture of A = NH_4HCO_3 aqueous buffer 10 mM pH=7.4 and B = acetonitrile (MeCN), with the methods described as follows: Method A, flow 0.4 mL/min, 5%B-100%B 5 min, 100%B 4 min, total runtime 15 min (column *Acquity UPLC BEH C18* (Waters) 1,7 μ m 2,1x100 mm (SN 021532354157 76)); Method B, flow 0.3 mL/min, 5%B-100%B 3 min, 100%B 5 min, total runtime 15 min (column *Acquity UPLC BEH C18* (Waters) 1,7 μ m 2,1x100 mm (SN 021532354157 76)). The mobile phase used for Method C and Method D was a mixture of A = formic acid 0.05% in water and B = formic acid 0.05% in acetonitrile (MeCN), with the methods described as follows: Method C, flow 0.90 mL/min, 5%B-90%B 5 min, 90%B 2 min, 90%B-100%B 1 min, 100%B 2 min total runtime 15 min (column ZORBAX Eclipse Plus C18 4.6x150mm; 3.5 μ m (S.N. USUXC04483)); Method D, flow 0.6 mL/min, 5%B-100%B 3 min, 100%B 3 min, total runtime 10 min (column ZORBAX Extend-C18 2.1x50mm; 3.5 μ m (S.N. USON003324)); purity is given as % of absorbance of the *cis* and *trans* isomers at 254 nm; UV-Vis spectra were collected every 0.2 s between 650 and 275 nm and bands are % of maximal absorbance; data from mass spectra were analysed by electrospray ionization in positive and negative mode every 0.3 s between 50 and 1000 Da and peaks are given m/z (% of basis peak). High-resolution mass spectra (HRMS) and elemental composition were analysed by FIA (flux injected analysis) with Ultrahigh-Performance Liquid Chromatography (UPLC) *Aquity* (Waters) coupled to *LCT Premier Orthogonal Accelerated Time of Flight* Mass Spectrometer (TOF) (Waters). Data from mass spectra were analysed by electrospray ionization in positive and negative mode. Spectra were scanned between 50 and 1500 Da with values every 0.2 seconds and peaks are given m/z (% of basis peak).

Cis and *trans* chromatographic peaks of compounds **83** and **84** were determined with Ultrahigh-Performance Liquid Chromatography (UPLC) *Aquity* (Waters) coupled to an *Acquity TUV* UV-Vis detector (Waters) and a *LCT Premier Orthogonal Accelerated Time of Flight* Mass Spectrometer (TOF) (Waters). Chromatograms were obtained by injection of 2 μ L of sample 25 μ M in AcN/DMSO 99:1, using a *Acquity* UPLC BEH C18 1.7 μ m 2.1 x 100mm column (Waters). The mobile phase used was a mixture of A = aqueous formic acid 20 mM and B = formic acid 20 nM in acetonitrile, with the method described as follows: flow 0.3 mL/min 5%-95%B 2.69 min, 95%B 6 min, runtime 14 min. Data from mass spectra were analysed by electrospray ionization in positive and negative mode. Spectra were scanned between 50 and 1500 Da with values every 0.2 seconds and peaks are given *m/z* (% of basis peak). Data was acquired with *MassLynx* software version 4.1 (Waters) and analyses were performed at the mass spectroscopy service of IQAC-CSIC.

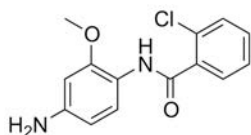
All high-resolution mass spectra (HRMS) were analysed by FIA (flux injected analysis) with Ultrahigh-Performance Liquid Chromatography (UPLC) *Aquity* (Waters) coupled a *LCT Premier Orthogonal Accelerated Time of Flight* Mass Spectrometer (TOF) (Waters). Data were obtained in the same conditions as for samples of UPLC/MS and acquired with *MassLynx* software version 4.1 (Waters). Analyses were performed at the mass spectroscopy service of IQAC-CSIC.

Synthetic procedures

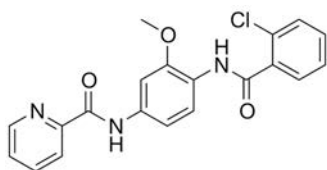


2-chloro-N-(2-methoxy-4-nitrophenyl)benzamide 88a: A mixture of 2-chlorobenzoic acid (**85a**) (1.30 g, 8.3 mmol) and thionyl chloride (6 mL, 83 mmol) was stirred at 75°C for 2 h to give the corresponding acyl chloride **86a**. The solvent was removed under vacuum and co-evaporated with toluene (2x5 mL) to give colourless oil (1.42g), which was diluted in 40 ml of DCE and DIPEA (3 mL, 17.2 mmol). Nitroaniline **87a** (1.24 g, 7.4 mmol) was added to this mixture and stirred for 2.5 h at 100°C. After cooling, the reaction mixture was poured into DCM (200 mL) and washed with an aqueous solution of Na₂CO₃ 1N (50 mL), and saturated with NaHCO₃ (50 mL), water (50 mL) and brine (50 mL). The organic layer was dried with anhydrous Na₂SO₄, filtered and the solvent removed under vacuum. The resulting solid was dissolved in EtOAc (200 mL) and washed twice with NaOH 0.75M (50 mL) and saturated with NaCl (50 mL). The organic phase was dried with anhydrous MgSO₄, filtered and the solvent removed under vacuum to give the title compound **88a**, which was previously described^{96, 217}, as a yellow solid

(2.30 g, 99% yield), which was used without further purification. ^1H NMR (400 MHz, CDCl_3) δ 8.89 (br, 1H), 8.75 (d, $J = 9.0$ Hz, 1H), 7.98 (dd, $J = 9.0, 2.3$ Hz, 1H), 7.87 – 7.80 (m, 1H), 7.79 (d, $J = 2.3$ Hz, 1H), 7.52 – 7.44 (m, 2H), 7.44 – 7.38 (m, 1H), 4.01 (s, 3H). ^{13}C NMR (101 MHz, CDCl_3) δ 164.64, 153.20, 147.97, 143.65, 134.54, 133.68, 132.43, 130.88, 130.81, 127.59, 118.95, 117.91, 105.47, 56.67. HRMS (m/z): $[\text{M}-\text{H}]^-$ calcd. for $\text{C}_{14}\text{H}_{10}\text{ClN}_2\text{O}_4$, 305.0329; found, 305.0349).

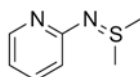


***N*-(4-amino-2-methoxyphenyl)-2-chlorobenzamide 89a**: Procedure A: Hydrochloric acid solution (13 mL, 37%, 156 mmol) was added slowly (10-15 min) to a solution of compound **88a** (0.83 g, 2.6 mmol) in THF (15 mL) stirred with dispersed tin powder (1.08 g, 9.13 mmol) at reflux temperature. The resulting turquoise solution was held at reflux temperature 30 minutes and NaOH (15 mL, 2 M) was added. The mixture was filtered through celite and the solvent was removed under vacuum. The obtained residue was dispersed in EtOAc (80 mL), filtered again through celite and washed with water (80 mL) and brine (80 mL), dried with anhydrous MgSO_4 , filtered and the solvent removed under vacuum to give a residue. The obtained brown-green residue was purified through silica *flash* column (hexanes/EtOAc 1:3 to hexanes/EtOAc 1:4) to give the title product **89a**, as sticky solid (0.68 g, 95% yield). Procedure B: Two bars of hydrogen atmosphere were applied to a suspension of **88a** (1.55 g, 4.9 mmol) and platinum-iron catalyst on carbon (5% Pt-1% Fe/C, *Evonik*) (48 mg) in ethanol (75 mL) in a standard hydrogenation reactor for 16 hours at room temperature. The reaction mixture was filtered through a Celite cake and washed with ethanol and dichloromethane. The filtrate was evaporated till dryness to afford **89a**, which was previously described^{96, 217} and used without further purification: Thick oil, 1.40 g, quant. yield. ^1H NMR (400 MHz, CDCl_3) δ 8.27 (d, $J = 8.6$ Hz, 2H), 7.76 (dd, $J = 7.2, 2.1$ Hz, 1H), 7.47 – 7.42 (m, 1H), 7.42 – 7.32 (m, 2H), 6.35 (dd, $J = 8.5, 2.3$ Hz, 1H), 6.30 (d, $J = 2.3$ Hz, 1H), 3.83 (s, 3H). ^{13}C NMR (101 MHz, CDCl_3) δ 163.79, 149.78, 143.70, 135.92, 131.40, 130.94, 130.49, 130.45, 127.25, 121.71, 119.43, 107.18, 98.61, 55.86. HRMS (m/z): $[\text{M}+\text{H}]^+$ calcd. for $\text{C}_{14}\text{H}_{14}\text{ClN}_2\text{O}_2$, 277.0744; found, 277.0718).

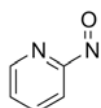


***N*-(4-(2-chlorobenzamido)-3-methoxyphenyl)picolinamide 33b**: A suspension of **89a** (100 mg, 0.361 mmol), picolinic acid (**85j**) (49 mg, 0.40 mmol), *O*-(7-azabenzotriazol-1-yl)-*N,N,N',N'*-

tetramethyluronium hexafluorophosphate (HATU) (275 mg, 0.72 mmol), diisopropylethylamine (DIPEA) (0.13 ml, 0.72 mmol) in ethyl acetate (EtOAc) (4.3 mL) was stirred for 16 hours at 40°C. It was diluted with EtOAc (100 mL) and washed with an aqueous solution of Na₂CO₃ 1N (2x 75 mL), water (75 mL) and brine (75 mL), dried with anhydrous MgSO₄, filtered off and solvent removed under vacuum to give a magenta residue, which was purified through a *flash* silica column using a *Biotage Isolera* equipment (*SNAP KP-Sil* 25g column, 45 mL/min, A = hexane B = EtOAc, 0%B 1CV, 0%B-15%B 4CV, 50%B 1CV, 50%B-100%B 9CV, 100%B 11CV). The title compound **33b**, previously described⁹⁶, was obtained (110 mg, 80% yield) as white solid. ¹H NMR (400 MHz, CDCl₃) δ 10.08 (s, 1H), 8.63 (d, J = 4.4 Hz, 1H), 8.55 (d, J = 8.5 Hz, 2H), 8.29 (d, J = 7.8 Hz, 1H), 7.97 (d, J = 1.9 Hz, 1H), 7.92 (td, J = 7.7, 1.5 Hz, 1H), 7.83 – 7.74 (m, 1H), 7.52 – 7.44 (m, 2H), 7.44 – 7.35 (m, 2H), 7.05 (dd, J = 8.7, 2.0 Hz, 1H), 3.96 (s, 3H).

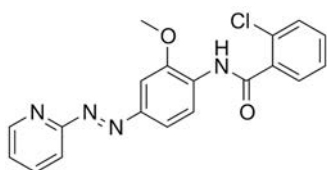


S,S-dimethyl-N-(2-pyridyl)sulphinimine 97: Dimethylsulphide (29 mL, 266 mmol) was added to a solution of 2-aminopyridine (**96**) (22.8 g, 242 mmol) in dry DCM (270 mL) at -20/-25°C. Afterwards a solution of *N*-Chlorosuccinimide (32.4 g, 243 mmol) in dry DCM (670 mL) was added over the 2-aminopyridine and dimethylsulphide at -20/-25°C in 1 hour, the temperature was left rising to r.t. and the mixture was left stirring at r.t. 1 hour. A sodium methoxide solution 25% in methanol (100 mL, 437 mmol) was added at r.t. in 20 minutes, water (270 mL) were added and the resulting mixture was left stirring at r.t. 3 hours. The layers were separated and the organic was back extracted with DCM (2x 125 mL). The combined organic layers were washed with water (125 mL), dried over anhydrous Na₂SO₄, filtered and concentrated to dryness to give orange oil that crystallises when chilled. Recrystallization from diethyl ether gave the title compound **97** as a cream-colored solid (29.8 g, 80% yield). ¹H NMR (400 MHz, CDCl₃) δ 8.03 – 7.94 (m, 1H), 7.35 – 7.28 (m, 1H), 6.67 (dt, J = 8.4, 1.0 Hz, 1H), 6.48 (ddd, J = 6.9, 5.2, 1.0 Hz, 1H), 2.73 (s, 6H). ¹H NMR chemical shifts match those described in the literature for the compound²¹⁸.

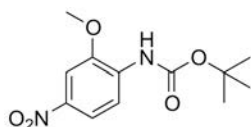


2-nitrosopyridine 90a: A solution of sulphinimine **97** (29.8 g, 193 mmol) in dry DCM (270 mL) was added over a solution of mCPBA (86 g, 347 mmol) in DCM (1.34 L) at 0/5°C, the resulting solution was stirred 90 min at 0/5°C for, dimethylsulfide was added (11.4 mL, 154 mmol) and

the resulting solution was stirred 30 additional minutes at 0/5°C. The solution was washed with sat. Na₂CO₃ (1300 mL) and the green organic layer was dried over Na₂SO₄, filtered and concentrated to dryness to give a tan solid, which was recrystallized from ethanol to give the title product **90a** as a tan crystalline solid (12.0 g, 60% yield). ¹H NMR (400 MHz, CDCl₃) δ 8.82 (dd, J = 4.8, 1.6 Hz, 1H), 8.08 (td, J = 7.7, 1.8 Hz, 1H), 7.68 (ddd, J = 7.6, 4.7, 1.1 Hz, 1H), 7.39 (dt, J = 8.0, 1.0 Hz, 1H) (monomer); ¹H NMR (400 MHz, CDCl₃) δ 8.02 (dt, J = 4.8, 1.3 Hz, 1H), 7.94 (td, J = 7.8, 1.8 Hz, 1H), 7.87 (dt, J = 8.0, 1.0 Hz, 1H), 7.31 (ddd, J = 7.4, 4.9, 1.2 Hz, 1H) (dimer). ¹H NMR chemical shifts match to the one described in the literature as a mixture of monomer and dimer²¹⁹

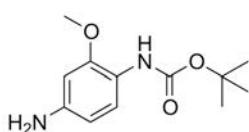


2-chloro-N-(2-methoxy-4-(pyridin-2-yl)diazenyl)phenylbenzamide 83: Glacial AcOH (1 mL) was added to a solution of **89a** (1.38 g, 4.8 mmol) and **90a** (0.80 g, 7.4 mmol) in dry DCM (75 mL), and the mixture stirred at room temperature for 75 hours. Next, the solvent was evaporated under vacuum and the residue was co-evaporated with toluene (2 x 5 mL). A dark residue (2.05 g) was obtained, which was purified through a silica flash column using *Biotage Isolera* equipment (SNAP KP-Sil 100g column, 60 mL/min, A=DCM, B=EtOAc 0%B 2CV, 0%B-1%B 2.5CV, 1%B-3%B 0.5CV, 3%B-13%B 13CV, 13%B-20% 2CV, 20%B-100%B 3CV, 100%B 5CV). The title compound **83** (1.43 g, 81% yield) was obtained as an orange solid. mp: 155-156 °C (dec.) ¹H NMR (400 MHz, CDCl₃) δ 8.83 (br, 1H), 8.79 (d, J=8.5Hz, 1H), 8.73 (dd, J=4.8, 1.0Hz, 1H), 7.93 – 7.87 (m, 1H), 7.87 – 7.82 (m, 2H), 7.80 (dd, J=7.5, 2.0Hz, 1H), 7.65 (d, J=2.0Hz, 1H), 7.52 – 7.34 (m, 4H), 3.97 (s, 3H), ¹H NMR (400 MHz, DMSO-d₆) δ 9.97 (s, 1H), 8.72 (dd, J=4.8, 1.1Hz, 1H), 8.42 (d, J=7.9 Hz, 1H), 8.10 – 8.01 (m, 1H), 7.77 – 7.68 (m, 2H), 7.63 (dd, J = 7.4, 1.4 Hz, 1H), 7.61 – 7.42 (m, 5H), 3.95 (s, 3H), ¹³C NMR (101 MHz, CDCl₃) δ 164.47, 163.17, 149.59, 148.86, 148.79, 138.46, 135.12, 132.02, 131.69, 130.94, 130.68, 130.64, 127.43, 125.14, 123.16, 119.41, 114.64, 100.71, 56.37.

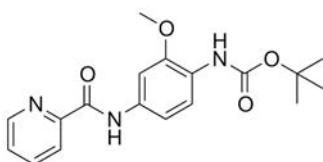


tert-butyl(2-methoxy-4-nitrophenyl)carbamate 92: Triethylamine (TEA) (0.55 mL, 6.0 mmol) was added to a solution of 2-methoxy-4-nitroaniline (**87a**) (308 mg, 1.8 mmol) and di-*tert*-butyl dicarbonate (Boc₂O, **91**) (420 mg, 2.9 mmol) in dry dichloromethane (DCM) (8 mL) and stirred

for two days at room temperature. The resulting mixture was diluted with DCM (50 mL), washed with aqueous solution of Na₂CO₃ 1N (20 mL), saturated with aqueous solution of NaHCO₃ (20 mL), water (20 mL) and brine (20 mL), dried with anhydrous Na₂SO₄, filtered off and solvent removed under vacuum to give a yellow residue, which was purified through a *flash* silica column using *Biotage Isolera* equipment (*SNAP KP-Sil* 25g column, 50 mL/min, A = hexane B = EtOAc, 13%B 5CV, 13%B-25%B 4CV, 25%B 4.5CV, 25%B-37%B 3CV, 37%B-50%B 01CV, 50%B 1.5CV, 50%B-55%B 1.5CV, 55%B-80%B 2.5CV, 80%B-100%B 3CV, 100%B 5.5CV). The title compound **92**, which was previously described²²⁰, was obtained (169 mg, 62% conversion, 56% yield) as pale yellow solid. ¹H NMR (400 MHz, CDCl₃) δ 8.26 (d, J = 9.0 Hz, 1H), 7.90 (dd, J = 9.0, 2.4 Hz, 1H), 7.72 (d, J = 2.4 Hz, 1H), 7.35 (br, 1H), 3.98 (s, 3H), 1.54 (s, 9H).

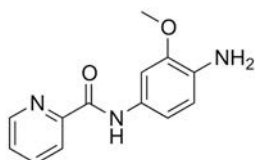


tert-butyl (4-amino-2-methoxyphenyl)carbamate 93: A mixture of **92** (148 mg, 0.55 mmol) and Pd/C (0.24 mmol) in ethanol (EtOH) under hydrogen atmosphere (2 atm) was stirred for 5 hours at room temperature. The black solid was filtered through *Celite*, washed with EtOH (2x10 mL), and the filtrates combined and solvent removed under vacuum. The title compound **93**, previously described²²⁰, was obtained (129 mg, 98% yield) as oil that was used without further purification. ¹H NMR (400 MHz, CDCl₃) δ 7.78 (br, 1H), 6.76 (br, 1H), 6.32 (dd, J = 8.5, 2.3 Hz, 1H), 6.29 (d, J = 2.3 Hz, 1H), 3.80 (s, 3H), 1.50 (s, 9H).

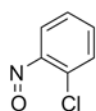


tert-butyl (2-methoxy-4-(picolinamido)phenyl)carbamate 94: A suspension of **93** (129 mg, 0.54 mmol), picolinic acid (**85j**) (75 mg, 0.61 mmol), *O*-(7-azabenzotriazol-1-yl)-*N,N,N',N'*-tetramethyluronium hexafluorophosphate (HATU) (434 mg, 1.14 mmol), diisopropylethylamine (DIPEA) (0.2 ml, 1.16 mmol) in ethyl acetate (EtOAc) (10 mL) was stirred for 16 hours at 40°C. It was next diluted with EtOAc (40 mL) and washed with an aqueous solution of Na₂CO₃ 1N (20 mL), with an aqueous saturated solution of NaHCO₃ (20 mL), water (20 mL) and brine (20 mL), dried with anhydrous MgSO₄, filtered off and solvent removed under vacuum to give a magenta residue, which was purified through a *flash* silica column using a *Biotage Isolera* equipment (*SNAP KP-Sil* 25g column, 45 mL/min, A = hexane B = EtOAc, 15%B 4CV, 15%B-18%B 3.5CV, 18%B-20%B 4.5CV, 20%B 5.5CV, 20%B-100%B 5.0CV, 100%B

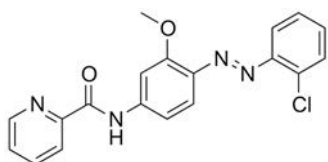
4.5CV). The title compound **94** was obtained (163 mg, 88% yield) as thick oil. ^1H NMR (400 MHz, CDCl_3) δ 9.99 (br, 1H), 8.67 – 8.55 (m, 1H), 8.28 (d, $J = 7.8$ Hz, 1H), 8.05 (d, $J = 7.8$ Hz, 1H), 7.91 (td, $J = 7.7, 1.7$ Hz, 1H), 7.86 (d, $J = 2.0$ Hz, 1H), 7.48 (ddd, $J = 7.6, 4.8, 1.2$ Hz, 1H), 7.03 (br, 1H), 7.00 (dd, $J = 8.7, 2.2$ Hz, 1H), 3.93 (s, 3H), 1.53 (s, 9H). ^{13}C NMR (101 MHz, CDCl_3) δ 161.91, 152.95, 149.99, 148.11, 147.92, 137.85, 132.97, 126.52, 124.70, 122.34, 118.27, 111.87, 102.80, 80.43, 55.95, 28.53. HRMS (m/z): $[\text{2M}+\text{H}]^+$ calcd. for $\text{C}_{36}\text{H}_{43}\text{N}_6\text{O}_8$, 687.3142; found, 687.3133,



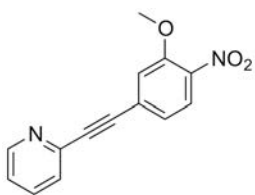
N-(4-amino-3-methoxyphenyl)picolinamide 95a: Method A: Trifluoroacetic acid (TFA) (3 mL) was added to a solution **94** (163 mg, 0.48 mmol) in DCM (9 mL) and stirred for two hours at room temperature. The solvents were removed under vacuum to give a residue, which was dissolved in EtOAc (40 mL). The solution was washed with an aqueous solution of Na_2CO_3 1N (15 mL), water (15 mL) and brine (15 mL), dried with anhydrous MgSO_4 , filtered off, and the volatiles removed under vacuum to give the title compound **95** (122 mg, quant.) as a yellow oil that was used without further purification. ^1H NMR (400 MHz, CDCl_3) δ 9.89 (br, 1H), 8.60 (d, $J = 4.7$ Hz, 1H), 8.27 (d, $J = 7.8$ Hz, 1H), 7.89 (td, $J = 7.7, 1.4$ Hz, 1H), 7.61 (s, 1H), 7.46 (dd, $J = 7.5, 4.8$ Hz, 1H), 7.00 (dd, $J = 8.3, 2.2$ Hz, 1H), 6.75 (d, $J = 8.3$ Hz, 1H), 3.91 (s, 3H). ^{13}C NMR (101 MHz, CDCl_3) δ 161.67, 150.23, 148.04, 147.64, 137.78, 132.56, 130.01, 126.33, 122.30, 115.19, 112.50, 103.78, 55.76. HRMS (m/z): $[\text{M}+\text{H}]^+$ calcd. for $\text{C}_{13}\text{H}_{14}\text{N}_3\text{O}_2$, 244.1086 ; found, 244.1087.



2-nitrosobenzene 90b: A solution of Oxone (468 mg, 0.76 mmol) in water (5.0 mL) was added to a solution of 2-chloroaniline (**98**) (49 mg, 0.38 mmol) in DCM (1.3 mL) at r.t. and the resulting mixture was stirred 2 hours at r.t. with vigorous agitation. Additional DCM was added (10 mL), the layers were separated and the organic one was washed with water (5 mL) and brine (5 mL), dried over anhydrous Na_2SO_4 and concentrated to dryness to obtain the title product **90b**, which was previously described²²¹ and was used without further purification (56 mg, quant. yield). ^1H NMR (400 MHz, CDCl_3) δ 7.79 (ddd, $J = 8.1, 1.2, 0.4$ Hz, 1H), 7.63 (ddd, $J = 8.1, 7.2, 1.7$ Hz, 1H), 7.24 (ddd, $J = 9.4, 8.1, 1.2$ Hz, 1H), 6.24 (ddd, $J = 8.1, 1.7, 0.4$ Hz, 1H).

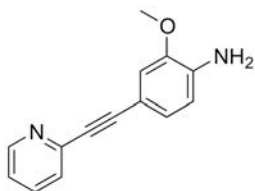


N-(4-((2-chlorophenyl)diazenyl)-3-methoxyphenyl)picolinamide 84: A drop of acetic acid (AcOH) was added to a solution of with **95** (30 mg, 0.12 mmol) and nitroso compound **90b** (17 mg, 0.12 mmol) in DCM (1.3 mL). The resulting solution was stirred in a sealed screw cap tube for three days at room temperature. The solvent was removed under vacuum and the remaining AcOH was removed by co-evaporation under vacuum with toluene (2x5 mL). The resulting dark residue was purified through a *flash* silica column using *Biotage Isolera* equipment (SNAP KP-Sil 10 g column, 25 mL/min, A = hexane B = EtOAc, 10%B 3CV, 10%B-30%B 2CV, 30%B 5.5CV, 30%B-50%B 7CV, 50%B-100%B 5CV, 100%B 4CV) to give the title compound **84** (33 mg, 75% yield) as a red solid. mp: 150-151 °C ¹H NMR (400 MHz, CDCl₃) δ 10.27 (br, 1H), 8.63 (ddd, J = 4.7, 1.6, 0.9 Hz, 1H), 8.30 (dt, J = 7.8, 1.0 Hz, 1H), 8.09 (d, J = 2.1 Hz, 1H), 7.93 (td, J = 7.7, 1.7 Hz, 1H), 7.86 – 7.82 (m, 1H), 7.71 – 7.66 (m, 1H), 7.53 – 7.49 (m, 2H), 7.36 – 7.29 (m, 2H), 7.10 (dd, J = 8.8, 2.2 Hz, 1H), 4.11 (s, 3H). ¹⁴C NMR (101 MHz, CDCl₃) δ 162.18, 158.57, 149.41, 149.25, 147.99, 142.46, 138.79, 137.89, 134.56, 130.92, 130.41, 127.27, 126.79, 122.47, 118.13, 118.10, 111.72, 103.43, 56.36. HRMS (m/z): [M+H]⁺ calcd. for C₁₉H₁₆ClN₄O₂, 367.0962; found, 367.0964. HPLC/DAD: purity (abs 254 nm) = 100%; RT = 3.86 min, 19%, λ_{max} = 193, 305, 436 nm, ((Z)-2); RT = 5.49 min, 81%, λ_{max} = 202, 383 nm ((E)-2). UPLC/MS: RT = 4.30 min, [M+H]⁺ = 367.0939 ((Z)-2); RT = 5.35 min, [M+H]⁺ = 367.0952 ((E)-2).

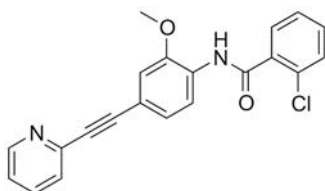


2-((3-methoxy-4-nitrophenyl)ethynyl)pyridine 103: 2-ethynylpyridine **101** (167 μL, 1.67 mmol) and dry triethylamine (0.5 ml, 3.6 mmol) were added to a suspension of 5-bromo-2-nitroanisole **102** (255 mg, 1.10 mmol), copper(I) iodide (22 mg, 0.115 mmol) and bis(triphenylphosphine) palladium (II) chloride (91 mg, 0.115 mmol) in dry dimethyl formamide (DMF) (1.5 mL) in a *Schlenk* flask under argon atmosphere at room temperature. The mixture was stirred at 50°C for 6 hours. The reaction mixture was poured into water and extracted with EtOAc (3x15 mL). The combined organic layers were washed with aqueous Na₂CO₃ 1 N (30 mL), water (30 mL) and brine (30 mL), dried over anhydrous MgSO₄, filtered and concentrated *in vacuo*. The residue was purified through automated *flash* chromatography (SNAP KP-Sil 25g,

A=DCM, B=EtOAc: 0%B 10CV, 0%B-1%B 2CV, 1%B-5%B 5CV, 5%B 6CV, 5%B-10%B 6CV, 10%B 1CV, 10%B-18%B 3CV, 18%B-100%B 3CV, 100%B 5CV giving a clear brown solid (250 mg, 89% yield). $^1\text{H NMR}$ (400 MHz, CDCl_3) δ 8.66 (ddd, $J = 4.8, 1.7, 0.9$ Hz, 1H), 7.86 (d, $J = 8.3$ Hz, 1H), 7.73 (td, $J = 7.8, 1.8$ Hz, 1H), 7.57 (dt, $J = 7.8, 1.1$ Hz, 1H), 7.35 – 7.28 (m, 2H), 7.24 (dd, $J = 8.3, 1.5$ Hz, 1H), 3.98 (s, 3H). HRMS (m/z) $[\text{M}+1]^+$ calcd. for $\text{C}_{14}\text{H}_{11}\text{N}_2\text{O}_3$ 255.0770; found, 255.0769.

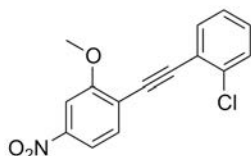


2-methoxy-4-(pyridin-2-ylethynyl)aniline 104: A mixture of nitrocompound **104** (50.0 mg, 0.20 mmol) and 6.1 mg of catalyst (5% Pt-1% Fe/C, *Evonik*, 1.6 mg) in ethanol (2 mL) was equilibrated at two bars of hydrogen atmosphere for 4 hours at room temperature in a standard hydrogenation reactor. The reaction mixture was filtered through a *Celite* cake and washed with ethanol and dichloromethane. The filtrate was evaporated to dryness to afford **104** as red oil, which was used without further purification (43 mg, 91% purity $^1\text{H NMR}$, 89% yield). $^1\text{H NMR}$ (400 MHz, CDCl_3) δ 8.58 (ddd, $J = 4.9, 1.9, 1.0$ Hz, 1H), 7.64 (td, $J = 7.7, 1.8$ Hz, 1H), 7.47 (dt, $J = 7.9, 1.1$ Hz, 1H), 7.18 (ddd, $J = 7.7, 4.9, 1.2$ Hz, 1H), 7.08 (dd, $J = 7.9, 1.7$ Hz, 1H), 7.03 (d, $J = 1.7$ Hz, 1H), 6.65 (d, $J = 8.0$ Hz, 1H), 4.03 (s, 2H), 3.86 (s, 3H). HRMS (m/z) $[\text{M}+1]^+$ calcd. for $\text{C}_{14}\text{H}_{13}\text{N}_2\text{O}$ 225.1028; found, 225.1027.

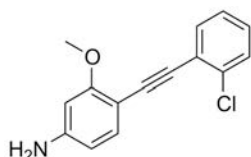


2-chloro-N-(2-methoxy-4-(pyridin-2-ylethynyl)phenyl)benzamide 99: A suspension of 2-chlorobenzoic acid (**85**) (31 mg, 0.20 mmol) in thionyl chloride (0.5 mL) was heated at reflux temperature for three hours and the solvent removed under vacuum, and the residue was co-evaporated with toluene (2x4 mL). A solution of this material and aniline **104** (43 mg, 0.17 mmol) in 1,2-dichloroethane containing DIPEA (150 μL , 0.86 mmol) was stirred at 90°C for 2 hours. The reaction mixture was concentrated under vacuum, re-dissolved in 50 mL of EtOAc and washed with Na_2CO_3 1N, saturated NaHCO_3 solution, water and brine. It was then dried with anhydrous MgSO_4 , filtered and concentrated. The residue was purified twice by *flash* chromatography (SNAP KP-Sil 10g, A=hexanes, B=EtOAc: 35%B 1CV, 35%B-45%B 2CV, 45%B-50%B 8CV, 50%B-100%B 2CV, 100%B 7CV; and SNAP KP-C18-HS 12g, A= H_2O B=MeCN: 5%B 3CV, 5%B-95%B 10CV, 95%B 3CV, 95%B-100%B 2CV, 100%B) to afford **99**: a white solid (34.3 mg,

54% yield). ^1H NMR (400 MHz, CDCl_3) δ 8.67 (s, 1H), 8.63 (s, 0H), 8.58 (d, $J = 8.3$ Hz, 1H), 7.82 – 7.75 (m, 1H), 7.68 (td, $J = 7.7, 1.8$ Hz, 1H), 7.53 (dt, $J = 7.9, 1.1$ Hz, 1H), 7.49 – 7.35 (m, 3H), 7.30 (dd, $J = 8.3, 1.7$ Hz, 1H), 7.24 (ddd, $J = 7.6, 4.9, 1.2$ Hz, 1H), 7.16 (d, $J = 1.7$ Hz, 1H), 3.91 (s, 3H). ^{13}C NMR (101 MHz, CDCl_3) δ 164.33, 150.23, 147.83, 143.61, 136.32, 135.31, 131.89, 130.93, 130.64, 130.60, 128.73, 127.40, 127.15, 125.76, 122.81, 119.71, 117.76, 113.64, 89.51, 88.38, 56.17. Mp: 136 °C - 137 °C. HPLC/PDA RT = 3.26 min purity 99.7%. HPLC/MS RT = 8.02 min, purity 100%; HRMS (m/z) $[\text{M}+1]^+$ calcd. for $\text{C}_{21}\text{H}_{16}\text{ClN}_2\text{O}_2$ 363.0900; found, 363.0906.

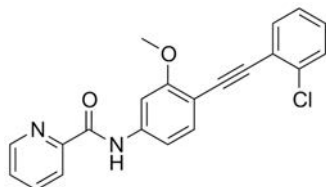


1-((2-chlorophenyl)ethynyl)-2-methoxy-4-nitrobenzene 107: 1-Chloro-2-ethynylbenzene **106** (160 μL , 1.31 mmol) and dry triethylamine (0.5 ml, 3.6 mmol) were added to a slurry of 2-bromo-5-nitroanisole **105** (203 mg, 0.87 mmol), copper(I) iodide (8.8 mg, 0.05 mmol) and bis(triphenylphosphine) palladium (II) chloride (34 mg, 0.04 mmol) in dry dimethyl formamide (DMF) (3.5 mL) in a *Schlenk* flask with argon atmosphere at room temperature. The mixture was stirred at 50°C for 2 hours. The reaction mixture was poured into water and extracted with EtOAc (3x15 mL). The combined organic layers were washed with aqueous Na_2CO_3 1 N (30 mL), water (30 mL) and brine (30 mL), dried over anhydrous MgSO_4 , filtered and concentrated *in vacuo*. The residue was purified by *flash* chromatography (SNAP KP-Sil 25g, A=hexanes B=EtOAc; 0%B 5CV, 0%B-1%B 2CV, 1%B-4%B 2.5CV, 4%B 1.5CV, 4%B-7%B 6CV, 7%B-9%B 0.5CV, 9%B-100%B 2CV, 100%B 5CV) to afford **107** as yellow solid (207 mg, 82% yield). ^1H NMR (400 MHz, CDCl_3) δ 7.84 (dd, $J = 8.4, 2.1$ Hz, 1H), 7.76 (d, $J = 2.1$ Hz, 1H), 7.65 (d, $J = 8.4$ Hz, 1H), 7.62 – 7.58 (m, 1H), 7.48 – 7.42 (m, 1H), 7.35 – 7.23 (m, 2H), 4.02 (s, 3H). ^{13}C NMR (101 MHz, CDCl_3) δ 160.46, 148.48, 136.30, 133.79, 133.63, 130.19, 126.68, 122.68, 119.39, 115.83, 105.83, 95.00, 89.22, 89.22, 56.62.

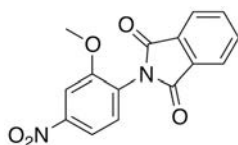


4-((2-chlorophenyl)ethynyl)-3-methoxyaniline 108: A suspension of nitrocompound **107** (31 mg, 0.11 mmol) and 1.6 mg of catalyst (5% Pt-1% Fe/C, *Evonik*) in ethanol (2 mL) was equilibrated at two bars of hydrogen atmosphere for 2.5 hours at room temperature in a standard hydrogenation reactor. The reaction mixture was filtered through a *Celite* cake and washed with ethanol and dichloromethane. The filtrate was evaporated till dryness to afford

107 as yellow oil, which was used without further purification (28 mg, 85% purity ^1H NMR, 89% yield). ^1H NMR (400 MHz, CDCl_3) δ 7.56 – 7.53 (m, 1H), 7.41 – 7.38 (m, 1H), 7.32 (d, J = 8.1 Hz, 1H), 7.26 (s, 1H), 7.21 – 7.18 (m, 2H), 6.26 (dd, J = 8.1, 2.1 Hz, 1H), 6.21 (d, J = 2.1 Hz, 1H), 3.87 (s, 5H). HRMS (m/z) [$M+1$] $^+$ calcd. for $\text{C}_{15}\text{H}_{13}\text{ClNO}$ 258.0686; found, 258.0685.

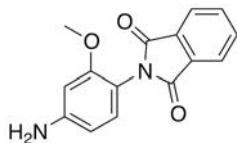


N-(4-((2-chlorophenyl)ethynyl)-3-methoxyphenyl)picolinamide 100: A suspension of picolinic acid (**85j**) (13 mg, 0.11 mmol), the aniline **108** (14 mg, 0.05 mmol) and HATU (78 mg, 0.21 mmol) in dry DMF (1 mL) with diisopropylethylamine (DIPEA) (40 μL , 0.23 mmol) was stirred at 40 $^\circ\text{C}$ for 16 hours. The resulting dark solution was diluted with EtOAc (30 mL) and washed with aqueous Na_2CO_3 1 N (15 mL), saturated aqueous NaHCO_3 (15 mL), water (15 mL) and brine (15 mL), dried over anhydrous MgSO_4 , filtered and concentrated *in vacuo*. The residue was purified by *flash* chromatography (SNAP KP-C18-HS 12g, A= H_2O B= MeCN : 5%B 3CV, 5%B-90%B 8CV, 90%B-100%B 4CV, 100%B 5CV) to afford **100** as yellow solid (13.5 mg, 81%). ^1H NMR (400 MHz, CDCl_3) δ 10.15 (s, 1H), 8.63 (dt, J = 4.6, 1.2 Hz, 1H), 8.29 (dt, J = 7.9, 1.1 Hz, 1H), 7.93 (td, J = 7.7, 1.7 Hz, 1H), 7.80 (d, J = 2.0 Hz, 1H), 7.64 – 7.56 (m, 1H), 7.53 (d, J = 8.2 Hz, 1H), 7.51 – 7.45 (m, 1H), 7.45 – 7.38 (m, 1H), 7.25 – 7.19 (m, 2H), 7.14 (dd, J = 8.3, 2.0 Hz, 1H), 3.99 (s, 3H). ^{13}C NMR (101 MHz, CDCl_3) δ 162.20, 161.02, 149.62, 148.16, 139.76, 137.96, 135.85, 134.12, 133.33, 129.35, 129.04, 126.82, 126.48, 123.81, 122.53, 111.53, 107.96, 102.51, 91.27, 90.00, 56.21. Mp: 141-142 $^\circ\text{C}$. HPLC/PDA RT = 4.18 min purity 95.4%. LC/MS RT = 9.08 min, purity 97.5%; HRMS (m/z) [$M+1$] $^+$ calcd. for $\text{C}_{21}\text{H}_{16}\text{ClN}_2\text{O}_2$ 363.0900; found, 363.0897.

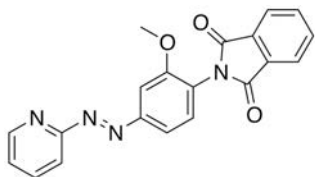


2-(2-methoxy-4-nitrophenyl)isoindoline-1,3-dione 119: A suspension of the 2-methoxy-4-nitroaniline **87a** (3.3 g, 20 mmol) and phthalic anhydride **118** (2.7 g, 18 mmol) in AcOH (120 mL) was stirred 18 hours at reflux temperature. Afterwards, it was added 100 mL of water at room temperature. A solid precipitated and, after cooling at 0-5 $^\circ\text{C}$, it was filtered off. The resulting solid was washed with cold water (5x20 mL) and it is dried under vacuum. The solid obtained was recrystallized from EtOH/EtOAc 1:1 to obtain **119** (cream solid, 2.94g, 54% yield). ^1H NMR (400 MHz, CDCl_3) δ 8.01 – 7.93 (m, 3H), 7.91 (d, J = 2.3 Hz, 1H), 7.82 (dd, J = 5.5, 3.1 Hz,

2H), 7.45 (d, J = 8.5 Hz, 1H), 3.92 (s, 3H). ¹³C NMR (101 MHz, CDCl₃) δ 166.49, 156.03, 149.22, 134.69, 132.14, 130.70, 126.61, 124.14, 116.11, 107.54, 56.69.

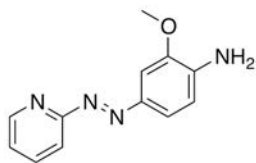


2-(4-Amino-2-methoxyphenyl)isoindoline-1,3-dione 120: To a mixture of nitrocompound **119** (0.45 g, 1.5 mmol) and 10% Pd/C (50 mg) in 1,4-dioxane (20 mL) was applied a 2 bar hydrogen atmosphere for 4-5 hours at room temperature. Afterwards, the reaction mixture was filtered through Celite, the solids washed with EtOH and 1,4-dioxane (2x5 mL each) and the filtrates were evaporated to dryness. The obtained crude was used without further purification and corresponded to the title compound **120** (yellow solid, 0.41 g, quantitative yield). ¹H NMR (400 MHz, CDCl₃) δ 7.92 (dd, J = 5.4, 3.1 Hz, 2H), 7.75 (dd, J = 5.5, 3.0 Hz, 2H), 6.99 (dd, J = 7.9, 0.7 Hz, 1H), 6.38 – 6.30 (m, 1H), 6.33 (d, J = 2.3 Hz, 1H), 3.84 (br, 2H), 3.73 (s, 3H). ¹³C NMR (101 MHz, CDCl₃) δ 168.13, 156.44, 149.13, 134.08, 132.48, 130.69, 123.66, 110.70, 107.22, 99.22, 55.79. HRMS (m/z): [M+H]⁺ calcd. for C₁₅H₁₃N₂O₃, 269.0926; found, 269.0925.

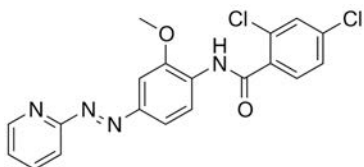


2-(2-Methoxy-4-(pyridin-2-yl diazenyl)phenyl)isoindoline-1,3-dione 112: To a solution of aniline **13** (0.26 g, 0.9 mmol) and 2-nitrosopyridine **89a** (0.11 g, 1.0 mmol) in DCM (20 mL) it was added two drops of glacial AcOH and the mixture was stirred at room temperature for 40 hours. Afterwards, the solvent was evaporated under vacuum and the AcOH was co-evaporated with toluene (2x5mL). The obtained solid was purified through silica *flash* column using *Biotage Isolera* equipment (SNAP KP-Sil 25 g; A=hexane B=EtOAc; 40%B 2CV, 40%B-44%B 2CV, 44%B 3CV, 44%B-51%B 3CV, 51%B 7CV, 51%B-60%B 7.5CV, 60%B-70%B 1.5CV, 70%B-80%B 7CV, 80%B-100%B 2.5CV, 100%B 2CV). The title product **112** was obtained (orange solid, 0.30 g, 89% yield). Mp 193.3-193.9°C. ¹H NMR (400 MHz, CDCl₃) δ 8.77 (ddd, J = 4.8, 1.9, 0.8 Hz, 1H), 7.97 (dd, J = 5.5, 3.1 Hz, 2H), 7.93 (dd, J = 7.3, 1.9 Hz, 1H), 7.87 (dt, J = 8.0, 1.1 Hz, 1H), 7.84 (dd, J = 8.2, 2.0 Hz, 1H), 7.80 (dd, J = 5.5, 3.1 Hz, 2H), 7.76 (d, J = 2.0 Hz, 1H), 7.47 (d, J = 8.2 Hz, 1H), 7.46 – 7.41 (m, 1H), 3.90 (s, 3H). ¹³C NMR (101 MHz, CDCl₃) δ 167.08, 162.86, 156.24, 153.69, 149.79, 138.59, 134.43, 132.35, 130.59, 125.72, 124.02, 123.96, 119.42, 115.64, 104.46, 56.40. HPLC-PDA-MS: method A was used; RT: 5.37 min, [M+H]⁺ 358.93, λ_{max} =

287, 430 nm (*cis*-isomer); RT: 5.67 min, $[M+H]^+$ 358.91, λ_{\max} = 319 nm (*trans*-isomer); purity 100% (254 nm). HRMS (m/z): $[M+H]^+$ calcd. for $C_{20}H_{15}N_4O_3$, 359.1144; found, 359.1150.

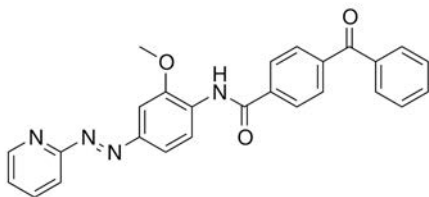


2-Methoxy-4-(pyridin-2-yl diazenyl)aniline 121: To a suspension of azocompound **112** (0.30 g, 0.8 mmol) in EtOH (10 mL), it was added 40% aqueous solution of methylamine (0.33 mL, 3.7 mmol) and the reaction mixture was stirred for two hours at 65°C and cooled to rt. It was next concentrated and the residue obtained was purified in a silica *flash* column using *Biotage Isolera* equipment (SNAP KP-Sil 25g; A=hexane B=EtOAc; 40%B 3CV, 40%B-51%B 4.5CV, 51%B 6CV, 51%B-55%B 3CV, 55%B-100%B 3CV, 100%B 4CV). The title product **121** was obtained (red solid, 0.18 g, 92% yield). 1H NMR (400 MHz, $CDCl_3$) δ 8.67 (ddd, J = 4.8, 1.9, 0.9 Hz, 1H), 7.82 (ddd, J = 8.1, 7.2, 1.9 Hz, 1H), 7.75 (dt, J = 8.1, 1.1 Hz, 1H), 7.62 (dd, J = 8.2, 2.0 Hz, 1H), 7.57 (d, J = 2.0 Hz, 1H), 7.29 (ddd, J = 7.2, 4.8, 1.2 Hz, 1H), 6.76 (d, J = 8.2 Hz, 1H), 4.42 (br, 2H), 3.91 (s, 3H). ^{13}C NMR (101 MHz, $CDCl_3$) δ 163.11, 148.66, 147.36, 145.48, 142.17, 138.91, 125.53, 124.14, 114.33, 112.95, 100.92, 55.87. HPLC-PDA-MS: method B was used, RT: 5.21 min, $[M+H]^+$ 228.92, λ_{\max} = 417 nm, (*trans*-isomer); purity 100% (254 nm). HRMS (m/z): $[M+H]^+$ calcd. for $C_{12}H_{13}N_4O$, 229.1089; found, 229.1088.

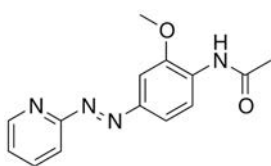


2,4-Dichloro-N-(2-methoxy-4-(pyridin-2-yl diazenyl)phenyl)benzamide 109b: A suspension of 2,4-dichlorobenzoic acid **85b** (18 mg, 0.10 mmol) in thionyl chloride (0.5 μ L) was stirred two hours at 75°C and cooled at r.t.. The solvent was removed under vacuum and the resulting residue was dissolved in DCE (1.5 mL) and azo-aniline **121** (20 mg, 0.09 mmol) and DIPEA (34 μ L, 0.19 mmol) were next added. The resulting mixture was heated at 40°C for 22 hours, cooled and diluted with EtOAc (15 mL). The solution was washed with saturated Na_2CO_3 (10 mL), $NaHCO_3$ (10 mL), water (10 mL) and brine (10 mL), dried over anhydrous $MgSO_4$, filtered and evaporated to dryness. The obtained residue was purified through C18 *flash* column using *Biotage Isolera* equipment (SNAP KP-C18-HS 12 g; A= H_2O B=MeCN; 0%B 3CV, 0%B-55%B 4CV, 55%B-80%B 8CV, 80%B-100%B 3CV, 100%B 5.5CV). The title product **109b** was obtained (red solid, 23 mg) and a fraction containing the starting aniline **15** and **109b** (1:3, orange solid, 5 mg). Mp 166.4-167.2°C. 1H NMR (400 MHz, $CDCl_3$) δ 8.85 (br, 1H), 8.76 (d, J = 8.5 Hz, 2H), 8.78

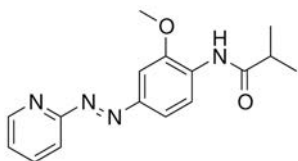
– 8.70 (m, 2H), 7.91 (ddd, $J = 8.1, 7.3, 1.8$ Hz, 1H), 7.89 – 7.80 (m, 2H), 7.79 (d, $J = 8.4$ Hz, 1H), 7.67 (d, $J = 2.1$ Hz, 1H), 7.51 (d, $J = 2.0$ Hz, 1H), 7.44 – 7.37 (m, 2H), 3.99 (s, 3H). ^{13}C NMR (101 MHz, CDCl_3) δ 163.40, 163.20, 149.68, 148.93, 148.89, 138.49, 137.66, 133.45, 131.87, 131.82, 131.47, 130.54, 127.92, 125.21, 123.14, 119.50, 114.71, 100.78, 56.44. HPLC-PDA-MS: method B was used; RT: 5.96 min, $[\text{M}+\text{H}]^+$ 400.91, $\lambda_{\text{max}} = 326, 431$ nm (*cis*-isomer); RT: 6.31 min, $[\text{M}+\text{H}]^+$ 400.90, $\lambda_{\text{max}} = 372$ nm (*trans*-isomer); purity 100% (254 nm). HRMS (m/z): $[\text{M}+\text{H}]^+$ calcd. for $\text{C}_{19}\text{H}_{15}\text{N}_4\text{O}_2\text{Cl}_2$, 401.0572; found, 401.0578.



4-Benzoyl-*N*-(2-methoxy-4-(pyridin-2-ylidiazenyl)phenyl)benzamide 109c: A suspension of 4-benzoylbenzoic acid **85c** (22 mg, 0.10 mmol) in thionyl chloride (0.5 μL) was stirred two hours at 75°C and cooled to rt. The solvent was next removed under vacuum, the residue obtained dissolved in DCE (1.5 mL) and azo-aniline **121** (20 mg, 0.09 mmol) and DIPEA (34 μL , 0.19 mmol) were added. The resulting mixture was heated at 40°C for 22 hours and was diluted in EtOAc (15 mL). The solution was washed with saturated Na_2CO_3 (10 mL), NaHCO_3 (10 mL), water (10 mL) and brine (10 mL), dried over anhydrous MgSO_4 , filtered and evaporated to dryness. The obtained residue was purified through C18 flash column using Biotage Isolera equipment (SNAP KP-C18-HS 12 g; A= H_2O B=MeCN; 0%B 3CV, 0%B-60%B 4CV, 60%B-85%B 9CV, 85%B-100%B 0.5CV, 100%B 5CV). The title product **109c** was obtained (red solid, 34 mg, 89% yield). Mp $155.1\text{--}156.4^\circ\text{C}$. ^1H NMR (400 MHz, CDCl_3) δ 8.81 (s, 1H), 8.80 (d, $J = 8.6$ Hz, 1H), 8.75 (ddd, $J = 4.8, 1.8, 0.9$ Hz, 1H), 8.03 (d, $J = 8.5$ Hz, 2H), 7.94 (d, $J = 8.5$ Hz, 2H), 7.92 – 7.89 (m, 1H), 7.88 (dd, $J = 8.5, 2.0$ Hz, 1H), 7.85 (dt, $J = 6.0, 1.1$ Hz, 2H), 7.82 (d, $J = 1.4$ Hz, 1H), 7.69 (d, $J = 2.0$ Hz, 1H), 7.64 (t, $J = 7.4$ Hz, 1H), 7.52 (t, $J = 7.5$ Hz, 2H), 7.41 (ddd, $J = 7.2, 4.8, 1.3$ Hz, 1H), 4.05 (s, 3H). ^{13}C NMR (101 MHz, CDCl_3) δ 195.86, 164.53, 163.17, 149.63, 148.81, 148.79, 140.73, 138.48, 138.05, 137.05, 133.10, 131.67, 130.49, 130.22, 128.62, 127.26, 125.18, 123.21, 119.28, 114.65, 100.70, 56.49. HPLC-PDA-MS: method B was used; RT: 6.25 min, $[\text{M}+\text{H}]^+$ 436.93, $\lambda_{\text{max}} = 380$ nm (*trans*-isomer); purity 98.5% (254 nm). HRMS (m/z): $[\text{M}+\text{H}]^+$ calcd. for $\text{C}_{26}\text{H}_{21}\text{N}_4\text{O}_3$, 437.1614; found 437.1608.

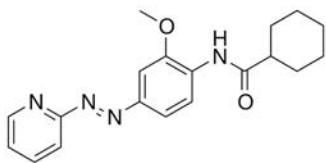


N-(2-methoxy-4-(pyridin-2-yl diazenyl)phenyl)acetamide 109d: To a suspension of azo-aniline **121** (20 mg, 0.09 mmol) and acetyl chloride **86d** (7 μ L, 0.10 mmol) in DCE (1.5 mL), DIPEA (34 μ L, 0.19 mmol) was added. The resulting mixture was heated at 40°C for 22 hours and was diluted in EtOAc (15 mL). The solution was washed with saturated Na₂CO₃ (10 mL), NaHCO₃ (10 mL), water (10 mL) and brine (10 mL), dried over anhydrous MgSO₄, filtered and evaporated to dryness. The residue was purified through C18 *flash* column using *Biotage Isolera* equipment (SNAP KP-Sil 10 g; A=hexanes B=EtOAc; 58%B-62%B 9CV, 62%B-75%B 0.5CV, 75%B-85%B 4.5CV, 85%B-100%B 1CV, 100%B 4CV). The title product **109d** was obtained (red solid, 13.2 mg, 56% yield). Mp; 126.5-128.5°C. ¹H NMR (400 MHz, CDCl₃) δ 8.72 (ddd, J = 4.8, 1.9, 0.9 Hz, 1H), 8.60 (d, J = 8.6 Hz, 1H), 7.97 (br, 1H), 7.88 (ddd, J = 8.1, 7.2, 1.8 Hz, 1H), 7.81 (dt, J = 8.2, 1.1 Hz, 1H), 7.78 (dd, J = 8.4, 1.9 Hz, 1H), 7.61 (d, J = 2.1 Hz, 1H), 7.38 (ddd, J = 7.3, 4.8, 1.2 Hz, 1H), 3.97 (s, 3H), 2.25 (s, 3H). ¹³C NMR (101 MHz, CDCl₃) δ 168.52, 163.22, 149.58, 148.36, 148.24, 138.45, 131.97, 125.06, 123.34, 118.95, 114.54, 100.43, 56.22, 25.24. HPLC-PDA-MS: method B was used; RT: 4.75 min, [M+H]⁺ 270.9, λ_{\max} = 335, 435 nm (*cis*-isomer); RT: 5.31 min, [M+H]⁺ 270.94, λ_{\max} = 374 nm (*trans*-isomer); purity 97.3% (254 nm). HRMS (m/z): [M+H]⁺ calcd. for C₁₄H₁₅N₄O₂, 271.1195; found 271.1194.

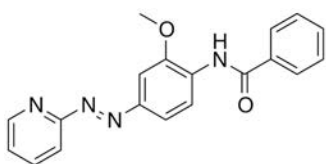


N-(2-Methoxy-4-(pyridin-2-yl diazenyl)phenyl)isobutyramide 109e: To a suspension of azo-aniline **121** (29 mg, 0.13 mmol), isobutyryl chloride **86e** (15 μ L mg, 0.14 mmol) in DCE (1.5 mL), DIPEA (49 μ L, 0.28 mmol) was added. The resulting mixture was heated at 40°C for 22 hours and diluted with EtOAc (15 mL). The solution was washed with saturated Na₂CO₃ (10 mL), NaHCO₃ (10 mL), water (10 mL) and brine (10 mL), dried over anhydrous MgSO₄, filtered and evaporated to dryness. The obtained residue was purified through C18 *flash* column using *Biotage Isolera* equipment (SNAP KP-C18-HS 12 g; A=H₂O B=MeCN; 0%B 3CV, 0%B-60%B 6CV, 60%B-80%B 4CV, 80%B-100%B 2CV, 100%B 5CV). The title product **109e** was obtained (red solid, 32 mg, 84% yield). Mp: 122.7-123.4°C. ¹H NMR (400 MHz, CDCl₃) δ 8.72 (ddd, J = 4.8, 1.9, 0.9 Hz, 1H), 8.64 (d, J = 8.6 Hz, 1H), 8.02 (br, 1H), 7.88 (ddd, J = 8.1, 7.3, 1.8 Hz, 1H), 7.80 (d, J = 7.0 Hz, 1H), 7.78 (dd, J = 8.3, 1.5 Hz, 1H), 7.61 (d, J = 2.1 Hz, 1H), 7.37 (ddd, J = 7.3, 4.8, 1.2 Hz, 1H), 3.97 (s, 3H), 2.60 (p, J = 6.9 Hz, 1H), 1.28 (d, J = 6.9 Hz, 6H). ¹³C NMR (101 MHz, CDCl₃) δ 175.49, 163.24, 149.58, 148.37, 148.26, 138.41, 132.12, 125.02, 123.39, 118.92, 114.46, 100.39, 56.26, 37.25, 19.73. HPLC-PDA-MS: method A was used; RT: 5.03 min, [M+H]⁺ 298.96,

λ_{\max} = 337, 434 nm (*cis*-isomer); RT: 5.56 min, $[M+H]^+$ 298.97, λ_{\max} = 374 nm (*trans*-isomer); purity 99.0% (254 nm). HRMS (m/z): $[M+H]^+$ calcd. for $C_{16}H_{19}N_4O_2$, 299.1508; found 299.1513.

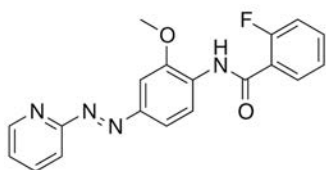


N-(2-Methoxy-4-(pyridin-2-yl-diazenyl)phenyl)cyclohexanecarboxamide 109f: To a suspension of azo-aniline **121** (29 mg, 0.13 mmol), cyclohexanecarbonyl chloride **86f** (19 μ L mg, 0.14 mmol) in DCE (1.5 mL), DIPEA (49 μ L, 0.28 mmol) was added. The resulting mixture was heated at 40°C for 16 hours and was diluted with EtOAc (15 mL). The resulting solution was washed with saturated Na_2CO_3 (10 mL), $NaHCO_3$ (10 mL), water (10 mL) and brine (10 mL), dried over anhydrous $MgSO_4$, filtered and evaporated to dryness. The obtained residue was purified through C18 *flash* column using *Biotage Isolera* equipment (SNAP KP-C18-HS 12 g; A= H_2O B=MeCN; 0%B 3CV, 0%B-50%B 5CV, 50%B-75%B 6CV, 75%B-100%B 2CV, 100%B 5CV). The title product **109f** was obtained (red solid, 38 mg, 88% yield). Mp: 106.7-107.3°C. 1H NMR (400 MHz, $CDCl_3$) δ 8.72 (ddd, J = 4.8, 1.8, 0.8 Hz, 1H), 8.65 (d, J = 8.6 Hz, 1H), 8.02 (br, 1H), 7.88 (ddd, J = 8.2, 7.2, 1.8 Hz, 1H), 7.81 (d, J = 8.9 Hz, 1H), 7.81 – 7.74 (m, 1H), 7.61 (d, J = 2.0 Hz, 1H), 7.38 (ddd, J = 7.2, 4.8, 1.2 Hz, 1H), 2.32 (tt, J = 11.7, 3.5 Hz, 1H), 1.99 (ddq, J = 12.8, 3.8, 2.1 Hz, 2H), 1.85 (dt, J = 11.8, 3.2 Hz, 2H), 1.76 – 1.65 (m, 1H), 1.56 (qd, J = 12.2, 3.3 Hz, 2H), 1.41 – 1.20 (m, 3H). ^{13}C NMR (101 MHz, $CDCl_3$) δ 174.62, 163.27, 149.59, 148.39, 148.23, 138.42, 132.20, 125.01, 123.45, 118.93, 114.46, 100.36, 56.26, 46.99, 29.79, 25.80, 25.78. HPLC-PDA-MS: method A was used; RT: 5.92 min, $[M+H]^+$ 339.23, λ_{\max} = 338, 436 nm (*cis*-isomer); RT: 6.37 min, $[M+H]^+$ 339.23, λ_{\max} = 377 nm (*trans*-isomer); purity 97.8% (254 nm). HRMS (m/z): $[M+H]^+$ calcd. for $C_{19}H_{23}N_4O_2$, 339.1821; found 339.1823.

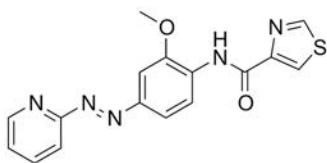


N-(2-Methoxy-4-(pyridin-2-yl-diazenyl)phenyl)benzamide 109g: To a suspension of the azo-aniline **121** (20 mg, 0.09 mmol), benzoyl chloride **86g** (15 μ L mg, 0.14 mmol) in DCE (1.5 mL), DIPEA (35 μ L, 0.19 mmol) was added. The mixture was heated at 40°C for 22 hours and was diluted in EtOAc (15 mL). The resulting solution was washed with saturated Na_2CO_3 (10 mL), $NaHCO_3$ (10 mL), water (10 mL) and brine (10 mL), dried over anhydrous $MgSO_4$, filtered and evaporated to dryness. The obtained residue was purified through C18 *flash* column using *Biotage Isolera* equipment (SNAP KP-C18-HS 12 g; A= H_2O B=MeCN; 0%B 3CV, 0%B-60%B 4CV,

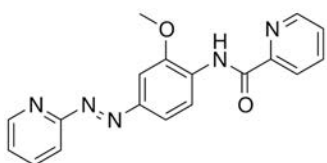
60%B-85%B 8.5CV, 85%B-100%B 0.5CV, 100%B 6.5CV). The title product **109g** was obtained (red solid, 26 mg, 89% yield). Mp: 137.2-138.5°C. ¹H NMR (400 MHz, CDCl₃) δ 8.79 (d, J = 8.6 Hz, 1H), 8.77 (br, 1H), 8.74 (ddd, J = 4.8, 1.9, 0.9 Hz, 1H), 7.92 (d, J = 6.9 Hz, 2H), 7.91 – 7.87 (m, 1H), 7.87 – 7.84 (m, 1H), 7.83 (d, J = 8.1 Hz, 1H), 7.67 (d, J = 2.1 Hz, 1H), 7.58 (t, J = 7.3 Hz, 1H), 7.52 (ddd, J = 8.6, 6.9, 1.5 Hz, 2H), 7.39 (ddd, J = 7.2, 4.8, 1.3 Hz, 1H), 4.03 (s, 3H). ¹³C NMR (101 MHz, CDCl₃) δ 165.47, 163.22, 149.60, 148.75, 148.55, 138.46, 134.95, 132.22, 132.07, 129.01, 127.26, 125.09, 123.38, 119.12, 114.56, 100.55, 56.42. HPLC-PDA-MS: method B was used; RT: 5.59 min, [M+H]⁺ 332.94, λ_{max} = 279, 331, 430 nm (*cis*-isomer); RT: 5.94 min, [M+H]⁺ 332.95, λ_{max} = 377 nm (*trans*-isomer); purity 98.1% (254 nm). HRMS (m/z): [M+H]⁺ calcd. for C₁₉H₁₇N₄O₂, 333.1352; found 333.1353



2-Fluoro-N-(2-methoxy-4-(pyridin-2-yl-diazenyl)phenyl)benzamide 109h: To a suspension of the azo-aniline **121** (29 mg, 0.13 mmol), acid 2-fluorobenzoic acid **85h** (29 mg, 0.21 mmol) and HATU (180 mg, 0.47 mmol) in DMF (1.5 mL), DIPEA (85 μL, 0.49 mmol) was added and the resulting mixture was stirred 22 h at 40°C. Afterwards, the reaction mixture was diluted with EtOAc (15 mL) and washed with 1N aq. Na₂CO₃ (10 mL), saturated aq. NaHCO₃ (10 mL), water (10 mL) and brine (10 mL), dried over anhydrous MgSO₄, filtered and evaporated to dryness. The obtained residue was purified through a silica *flash* column using the *Biotage Isolera* equipment (SNAP KP-Sil 10 g; A=DCM B=MeOH; 0%B 5CV, 0%B-0.7%B 10CV, 0.7%B 6.5CV, 0.7%B-1%B 4.5CV, 1%B 1.5CV, 1%B-10%B 2.5CV, 10%B 10CV). The title product **109h** was obtained (red solid, 23 mg, 52% yield). Mp: 160.7-161.2°C. ¹H NMR (400 MHz, CDCl₃) δ 9.47 (br, J = 15.7 Hz, 1H), 8.82 (d, J = 8.5 Hz, 1H), 8.74 (ddd, J = 4.8, 1.8, 0.9 Hz, 1H), 8.20 (td, J = 7.9, 1.9 Hz, 1H), 7.90 (ddd, J = 8.1, 7.2, 1.9 Hz, 1H), 7.87 – 7.79 (m, 2H), 7.67 (d, J = 2.0 Hz, 1H), 7.54 (dddd, J = 8.3, 7.2, 5.2, 1.9 Hz, 1H), 7.39 (ddd, J = 7.2, 4.8, 1.2 Hz, 1H), 7.33 (ddd, J = 8.3, 7.4, 1.1 Hz, 1H), 7.21 (ddd, J = 12.2, 8.3, 1.1 Hz, 1H), 4.03 (s, 3H). ¹³C NMR (101 MHz, CDCl₃) δ 163.25, 161.83, 161.39, 161.36, 159.37, 149.63, 148.91, 148.74, 138.45, 134.15, 134.06, 132.41, 132.39, 132.07, 125.24, 125.21, 125.10, 123.23, 121.54, 121.43, 119.66, 116.53, 116.28, 114.61, 56.49. HPLC-PDA-MS: method A was used; RT: 5.72 min, [M+H]⁺ 350.90, λ_{max} = 281, 332, 432 nm (*cis*-isomer); RT: 6.25 min, [M+H]⁺ 350.94, λ_{max} = 375 nm (*trans*-isomer); purity 99.5% (254 nm). HRMS (m/z): [M+H]⁺ calcd. for C₁₉H₁₆N₄O₂F, 351.1257; found 351.1260.

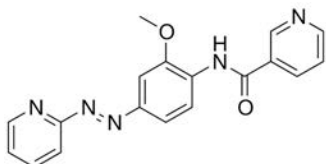


N-(2-Methoxy-4-(pyridin-2-yl-diazenyl)phenyl)thiazole-4-carboxamide 109i: To a slurry of azo-aniline **121** (29 mg, 0.13 mmol), 4-thiazolecarboxylic acid **85i** (26 mg, 0.20 mmol) and HATU (155 mg, 0.40 mmol) in DMF (1.5 mL), DIPEA (75 μ L, 0.43 mmol) was added and the resulting mixture was stirred 22 h at 40°C. Afterwards, the reaction mixture was diluted in EtOAc (15 mL) and washed with Na₂CO₃ 1N (10 mL), saturated NaHCO₃ (10 mL), water (10 mL) and brine (10 mL), dried over anhydrous MgSO₄, filtered and evaporated to dryness. The obtained residue was purified through C18 *flash* column using *Biotage Isolera* equipment (SNAP KP-C18-HS 12 g; A=H₂O B=MeCN; 5%B 3CV, 5%B-100%B 10CV, 100%B 5CV). The title product **109h** was obtained (orange solid, 29 mg, 68% yield). Mp: 181.3-182.3°C (decomp.). ¹H NMR (400 MHz, CDCl₃) δ 10.09 (br, 1H), 8.85 (d, J = 2.1 Hz, 1H), 8.79 (d, J = 8.5 Hz, 1H), 8.74 (ddd, J = 4.8, 1.9, 0.9 Hz, 1H), 8.31 (d, J = 2.1 Hz, 1H), 7.90 (ddd, J = 8.1, 7.2, 1.9 Hz, 1H), 7.84 (ddd, J = 8.5, 2.1, 0.5 Hz, 1H), 7.83 (dt, J = 8.0, 1.1 Hz, 1H), 7.67 (d, J = 2.0 Hz, 1H), 7.39 (ddd, J = 7.2, 4.8, 1.2 Hz, 1H), 4.05 (s, 3H). ¹³C NMR (101 MHz, CDCl₃) δ 163.26, 158.94, 153.05, 151.39, 149.62, 149.11, 148.75, 138.46, 131.78, 125.09, 124.44, 123.18, 119.11, 114.63, 100.73, 56.43. HPLC-PDA-MS: method A was used; RT: 5.17 min, [M+H]⁺ 339.88, λ_{\max} = 287, 334, 434 nm (*cis*-isomer); RT: 5.70 min, [M+H]⁺ 339.88, λ_{\max} = 377 nm (*trans*-isomer); purity 99.3% (254 nm). HRMS (m/z): [M+H]⁺ calcd. for C₁₆H₁₄N₅O₂S, 340.0868; found 340.9869.

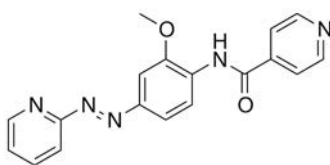


N-(2-methoxy-4-nitrophenyl)picolinamide 109j: To a suspension of azo-aniline **121** (20 mg, 0.09 mmol), picolinic acid **85j** (17 mg, 0.14 mmol) and HATU (114 mg, 0.30 mmol) in DMF (1.5 mL), DIPEA (100 μ L, 0.43 mmol) was added and the resulting mixture was stirred 22 h at 40°C. Afterwards, the mixture was diluted in EtOAc (20 mL) and washed with Na₂CO₃ 1N (10 mL), saturated NaHCO₃ (10 mL), water (10 mL) and brine (10 mL), dried over anhydrous MgSO₄, filtered and evaporated to dryness. The obtained residue was purified through C18 *flash* column using *Biotage Isolera* equipment (SNAP KP-C18-HS 12 g; A=H₂O B=MeCN; 0%B 4CV, 0%B-50%B 4CV, 50%B-66%B 6CV, 66%B-75%B 7.5CV, 75%B-100%B 1.5CV, 100%B 6CV). The title product **109j** was obtained (orange solid, 27 mg, 93% yield). Mp: 196.8-197.6°C. ¹H NMR (400 MHz, CDCl₃) δ 10.81 (br, 1H), 8.85 (d, J = 8.4 Hz, 1H), 8.74 (ddd, J = 4.8, 1.9, 0.9 Hz, 1H),

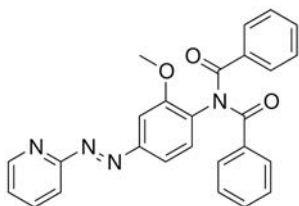
8.68 (ddd, $J = 4.7, 1.7, 0.9$ Hz, 1H), 8.31 (dt, $J = 7.8, 1.1$ Hz, 1H), 7.96 – 7.79 (m, 4H), 7.68 (d, $J = 1.9$ Hz, 1H), 7.49 (ddd, $J = 7.6, 4.7, 1.3$ Hz, 1H), 7.39 (ddd, $J = 7.3, 4.8, 1.3$ Hz, 1H), 4.07 (s, 3H). ^{13}C NMR (101 MHz, CDCl_3) δ 163.29, 162.45, 150.02, 149.61, 149.46, 148.70, 148.42, 138.43, 137.75, 131.84, 126.70, 125.04, 123.18, 122.65, 119.05, 114.59, 100.76, 56.40. HPLC-PDA-MS: method A was used; RT: 5.70 min, $[\text{M}+\text{H}]^+$ 334.17, $\lambda_{\text{max}} = 294, 339, 434$ nm (*cis*-isomer); RT: 6.16 min, $[\text{M}+\text{H}]^+$ 334.19, $\lambda_{\text{max}} = 382$ nm (*trans*-isomer); purity 98.2% (254 nm). HRMS (m/z): $[\text{M}+\text{H}]^+$ calcd. for $\text{C}_{18}\text{H}_{16}\text{N}_5\text{O}_2$, 334.1304; found 334.1308.



***N*-(2-methoxy-4-nitrophenyl)nicotinamide 109k:** To a suspension of azo-aniline **121** (20 mg, 0.09 mmol), nicotinic acid **85k** (17 mg, 0.14 mmol) and HATU (114 mg, 0.30 mmol) in DMF (1.5 mL), DIPEA (100 μL , 0.43 mmol) was added and the resulting mixture was stirred 22 h at 40°C. Afterwards, the reaction mixture was diluted in EtOAc (20 mL) and washed with Na_2CO_3 1N (10 mL), saturated NaHCO_3 (10 mL), water (10 mL) and brine (10 mL), dried over anhydrous MgSO_4 , filtered and evaporated to dryness. The obtained residue was purified once through silica *flash* column and once through C18 *flash* column using *Biotage Isolera* equipment (SNAP KP-Sil 10g; A=DCM B=MeOH; 0%B 3CV, 0%B-1.5%B 1CV, 1.5%B-2.5%B 8CV, 2.5%B-3%B 0.5CV, 3%B-4%B 10CV, 4%B-10%B 1.5CV, 10%B 6CV; and SNAP KP-C18-HS 12 g; A= H_2O B=MeOH; 0%B 5CV, 0%B-35%B 3CV, 35%B-70%B 14CV, 70%B-100%B 2CV, 100%B 5CV). The title product **109k** was obtained (orange solid, 19 mg, 65% yield). Mp: 159.0-159.7°C. ^1H NMR (400 MHz, CDCl_3) δ 9.15 (dd, $J = 2.4, 0.9$ Hz, 1H), 8.81 (dd, $J = 4.9, 1.7$ Hz, 1H), 8.79 – 8.71 (m, 3H), 8.26 (ddd, $J = 8.0, 2.4, 1.7$ Hz, 1H), 7.91 (ddd, $J = 8.1, 7.2, 1.9$ Hz, 1H), 7.88 – 7.85 (m, 1H), 7.84 (d, $J = 8.3$ Hz, 1H), 7.69 (d, $J = 2.0$ Hz, 1H), 7.48 (ddd, $J = 7.9, 4.8, 0.9$ Hz, 1H), 7.41 (ddd, $J = 7.2, 4.7, 1.2$ Hz, 1H), 4.04 (s, 3H). ^{13}C NMR (101 MHz, CDCl_3) δ 163.29, 162.45, 150.02, 149.61, 149.46, 148.70, 148.42, 138.43, 137.75, 131.84, 126.70, 125.04, 123.18, 122.65, 119.05, 114.59, 100.76, 56.40. HPLC-PDA-MS: method B was used; RT: 4.94 min, $[\text{M}+\text{H}]^+$ 333.94, $\lambda_{\text{max}} = 326, 426$ nm (*cis*-isomer); RT: 5.28 min, $[\text{M}+\text{H}]^+$ 333.94, $\lambda_{\text{max}} = 373$ nm (*trans*-isomer); purity 99.7% (254 nm). HRMS (m/z): $[\text{M}+\text{H}]^+$ calcd. for $\text{C}_{18}\text{H}_{16}\text{N}_5\text{O}_2$, 334.1304; found 334.1309.

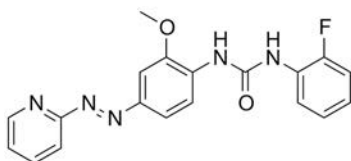


***N*-(2-methoxy-4-nitrophenyl)isoniconamide 109I**: To a suspension of the azo-aniline **121** (20 mg, 0.09 mmol), picolinic acid **85I** (17 mg, 0.14 mmol) and HATU (114 mg, 0.30 mmol) in DMF (1.5 mL), DIPEA (100 μ L, 0.43 mmol) was added and the resulting mixture was stirred 22 h at 40°C. Next the mixture was diluted in EtOAc (20 mL) and washed with Na₂CO₃ 1N (10 mL), saturated NaHCO₃ (10 mL), water (10 mL) and brine (10 mL), dried over anhydrous MgSO₄, filtered and evaporated to dryness. The obtained residue was purified through silica *flash* column and once through C18 *flash* column using *Biotage Isolera* equipment (SNAPKP-Sil 10g; A=DCM B=MeOH; 0%B 3CV, 0%B-1.5%B 1CV, 1.5%B-5%B 18.5CV, 4%B-10%B 4CV, 10%B 6CV; and SNAP KP-C18-HS 12 g; A=H₂O B=MeOH; 0%B 5CV, 0%B-35%B 2.5CV, 35%B-70%B 15CV, 70%B-100%B 2.5CV, 100%B 5CV). The title product **109I** was obtained (orange solid, 17 mg, 59% yield). Mp: 179.5-180.2°C. ¹H NMR (400 MHz, CDCl₃) δ 8.85 (d, J = 6.1 Hz, 2H), 8.84 – 8.71 (m, 3H), 7.92 (ddd, J = 8.1, 7.3, 1.9 Hz, 2H), 7.87 (dd, J = 8.8, 2.1 Hz, 2H), 7.86 (t, J = 1.0 Hz, 2H), 7.76 (d, J = 6.1 Hz, 3H), 7.69 (d, J = 2.1 Hz, 2H), 7.42 (ddd, J = 7.3, 4.8, 1.2 Hz, 2H), 4.05 (s, 7H). HPLC-PDA-MS: method B was used; RT: 4.95 min, [M+H]⁺ 333.92, λ_{\max} = 331, 432 nm (*cis*-isomer); RT: 5.30 min, [M+H]⁺ 333.95, λ_{\max} = 372 nm (*trans*-isomer); purity 99.7% (254 nm). HRMS (m/z): [M+H]⁺ calcd. for C₁₈H₁₆N₅O₂, 334.1304; found 334.1300.

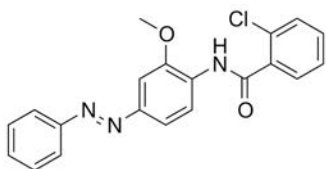


***N*-Benzoyl-*N*-(2-methoxy-4-(pyridin-2-yl)phenyl)benzamide 113**: To a suspension of azo-aniline **121** (20 mg, 0.09 mmol), benzoyl chloride **86g** (51 μ L mg, 0.44 mmol) and a crystal of DMAP in DCE (1.5 mL), DIPEA (156 μ L, 0. mmol) was added. The resulting mixture was heated at 40°C for 22 hours and was diluted in EtOAc (15 mL). The resulting solution was washed with saturated Na₂CO₃ (10 mL), NaHCO₃ (10 mL), water (10 mL) and brine (10 mL), dried over anhydrous MgSO₄, filtered and evaporated to dryness. The obtained residue was purified through C18 *flash* column using *Biotage Isolera* equipment (SNAP KP-Sil 10 g; A=DCM B=MeOH; 0%B 2.5CV, 0%B-1.2%B 9CV, 1.2%B-10%B 2CV, 10%B 3CV). The title product **113** was obtained (red solid, 34 mg, 89% yield). Mp 166.3-167.1°C. ¹H NMR (400 MHz, CDCl₃) δ 8.75 (ddd, J = 4.8, 1.9, 0.8 Hz, 1H), 7.91 (ddd, J = 8.2, 7.4, 1.9 Hz, 1H), 7.81 (dt, J = 8.0, 1.1 Hz, 1H), 7.76 (d, J = 7.0 Hz, 4H), 7.66 (dd, J = 6.5, 1.7 Hz, 1H), 7.64 (d, J = 2.0 Hz, 1H), 7.46 – 7.40 (m, 3H), 7.33 (t, J = 7.6 Hz, 4H), 7.25 (d, J = 7.3 Hz, 1H), 3.90 (s, 3H). ¹³C NMR (101 MHz, CDCl₃) δ 173.24, 162.88, 154.72, 152.78, 149.77, 138.54, 134.97, 133.16, 132.41, 129.97, 129.10, 128.56, 125.63, 120.13, 115.31, 104.31, 56.39. HPLC-PDA-MS: method B was used; RT: 5.82 min,

$[M+H]^+$ 436.91, λ_{\max} = 430 nm (*cis*-isomer); RT: 6.02 min, $[M+H]^+$ 436.94, λ_{\max} = 329 nm (*trans*-isomer); purity 98.7% (254 nm). HRMS (m/z): $[M+H]^+$ calcd. for $C_{26}H_{21}N_4O_3$, 437.1614; found 437.1615.

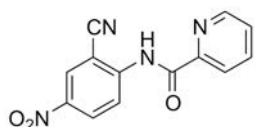


1-(2-Fluorophenyl)-3-(2-methoxy-4-(pyridin-2-yl diazenyl)phenyl)urea 114: To a slurry of aniline **121** (29 mg, 0.13 mmol) and 2-fluorophenyl isocyanate **122** (19 mg, 0.14 mmol) in THF (1.5 mL), DIPEA (24 μ L, 0.14 mmol) was added. The resulting mixture was heated at 40°C in a screw cap tube under stirring for 22 h, cooled and diluted with DCM (15 mL). The resulting solution was washed with saturated NaHCO_3 (10 mL), Na_2CO_3 (10 mL), water (10 mL) and brine (10 mL), dried over anhydrous MgSO_4 , filtered and evaporated to dryness. The obtained solid was purified twice through C18 *flash* column using *Biotage Isolera* equipment (SNAP KP-C18-HS 12 g; A = H_2O B = MeOH; 0%B 5CV, 0%B-70%B 16CV, 70%B-75%B 7.5CV, 75%B-100%B 1.5CV, 100% 5CV; and A = H_2O + 0.2% formic acid B = MeOH + 0.2% formic acid; 0%B 5CV, 0%B-40%B 3CV, 40%B-75%B 15CV, 75%B-82%B 6CV, 82%B-100%B 2CV, 100% 5CV). The title product **114** was obtained (red solid, 35 mg, 75% yield). Mp: 193.0-193.4°C. ^1H NMR (400 MHz, DMSO) δ 9.49 (br, J = 2.3 Hz, 1H), 9.20 (br, 1H), 8.70 (ddd, J = 4.8, 1.9, 0.8 Hz, 1H), 8.48 (d, J = 8.6 Hz, 1H), 8.20 (td, J = 8.3, 1.7 Hz, 1H), 8.02 (td, J = 7.7, 1.9 Hz, 1H), 7.70 (d, J = 8.1 Hz, 1H), 7.69 (dd, J = 8.6, 2.1 Hz, 1H), 7.56 (d, J = 2.2 Hz, 1H), 7.53 (ddd, J = 7.4, 4.7, 0.9 Hz, 1H), 7.26 (ddd, J = 11.6, 8.2, 1.5 Hz, 1H), 7.17 (td, J = 7.8, 1.4 Hz, 1H), 7.08 – 7.00 (m, 1H), 4.02 (s, 3H). ^{13}C NMR (101 MHz, DMSO) δ 163.02, 153.37, 151.96, 150.96, 149.27, 148.28, 146.57, 138.73, 133.41, 127.26, 127.16, 125.18, 124.53, 124.49, 122.90, 122.83, 121.28, 120.91, 120.90, 117.39, 115.17, 114.98, 112.87, 101.30, 56.05. HPLC-PDA-MS: method B was used; RT: 5.63 min, $[M+H]^+$ 365.95, λ_{\max} = 426 nm (*cis*-isomer); RT: 6.02 min, $[M+H]^+$ 365.95, λ_{\max} = 387 nm (*trans*-isomer); purity 97.1% (254 nm). HRMS (m/z): $[M+H]^+$ calcd. for $C_{19}H_{17}N_5O_2F$, 366.1366; found 366.1369.

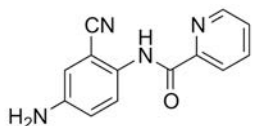


2-chloro-N-(2-methoxy-4-(phenyldiazenyl)phenyl)benzamide 110: To a solution of *N*-(4-amino-2-methoxyphenyl)-2-chlorobenzamide **89a** (25 mg, 0.09 mmol) and nitrosobenzene **90c** (14 mg, 0.13 mmol) in DCM (1 mL) it were added two drops of glacial AcOH and the mixture stirred at room temperature for 3 days. Afterwards, the solvent was evaporated under vacuum

and the AcOH was coevaporated with toluene (2x5mL). The obtained solid was purified through silica *flash* column using *Biotage Isolera* equipment (SNAP KP-Sil 10 g; A=hexane B=EtOAc; 0%B 4CV, 0%B-5%B 8CV, 5%B-10%B 2CV, 10%B 8.5CV, 10%B-26%B 7CV, 26%B-37%B 16.5CV, 37%B-100%B 5.5CV, 100%B 11CV). The title product **110** was obtained (red solid, 16 mg, 47% yield). Mp: 115.2-116.0°C. ¹H NMR (400 MHz, CDCl₃) δ 8.79 (br, 1H), 8.76 (d, J = 8.6 Hz, 1H), 7.92 (dd, J = 7.3, 1.7 Hz, 2H), 7.82 (dd, J = 7.2, 2.1 Hz, 1H), 7.73 (dd, J = 8.5, 2.0 Hz, 1H), 7.55 – 7.39 (m, 7H), 4.01 (s, 3H). ¹³C NMR (101 MHz, CDCl₃) δ 164.40, 152.78, 149.08, 148.84, 135.27, 131.95, 130.96, 130.90, 130.68, 130.67, 130.52, 129.22, 127.43, 122.89, 120.73, 119.61, 101.30, 56.23. HPLC-PDA-MS: method B was used; RT: 6.08 min, [M+H]⁺ 365.95, λ_{max} = 324, 436 nm (*cis*-isomer); RT: 6.77 min, [M+H]⁺ 365.95, λ_{max} = 366 nm (*trans*-isomer); purity 97.9% (254 nm). HRMS (m/z): [M+H]⁺ calcd. for C₂₀H₁₇N₃O₂Cl, 366.1009; found 366.1013.

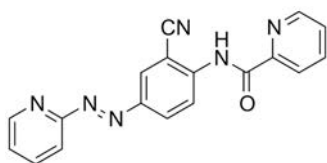


N-(2-cyano-4-nitrophenyl)picolinamide 88b: To a slurry of 2-amino-5-nitrobenzonitrile **87b** (59 mg, 0.36 mmol), picolinic acid **85j** (60 mg, 0.49 mmol) and HATU (285 mg, 1.01 mmol) in DMF (1 mL), DIPEA (200 μL, 1.15 mmol) was added and the resulting mixture was stirred a 16 h at 40°C. Afterwards, the mixture was diluted in EtOAc (30 mL) and washed with Na₂CO₃ 1N (20 mL), saturated NaHCO₃ (20 mL), water (20 mL) and brine (20 mL), dried over anhydrous MgSO₄, filtered and evaporated to dryness. The obtained solid was purified through silica *flash* column using *Biotage Isolera* equipment (SNAP KP-Sil 10 g; A=hexanes B=EtOAc; 15%B 12CV, 15%B-17%B 3CV, 17%B-21%B 8.5CV, 21%-23%B 10CV, 23%B-30%B 10.5CV, 30%B-55%B 8CV, 55%B-100%B 3CV, 100%B 4CV). The title product **88b** was obtained (white solid, 82.4 mg, 85% yield). ¹H NMR (400 MHz, CDCl₃) δ 11.25 (br, 1H), 9.02 (d, J = 9.3 Hz, 1H), 8.74 (ddd, J = 4.8, 1.7, 0.9 Hz, 1H), 8.55 (dd, J = 2.7, 0.5 Hz, 1H), 8.50 (ddd, J = 9.3, 2.6, 0.6 Hz, 1H), 8.31 (dt, J = 7.8, 1.1 Hz, 1H), 7.98 (td, J = 7.7, 1.7 Hz, 1H), 7.60 (ddd, J = 7.6, 4.8, 1.2 Hz, 1H). ¹³C NMR (101 MHz, CDCl₃) δ 162.87, 148.83, 148.10, 145.62, 142.76, 138.21, 129.64, 128.46, 127.89, 123.03, 120.14, 114.47, 102.39.

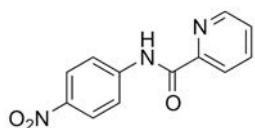


N-(4-amino-2-cyanophenyl)picolinamide 89b: To a suspension of the nitrocompound **88b** (23 mg, 0.09 mmol) and 10% Pd/C (5 mg) in ethanol/1,4-dioxane 1:1 (2 mL) was applied a hydrogen atmosphere of 2 bar for 5 hours at room temperature. Next, the black mixture was

filtered through Celite, washed with EtOH and 1,4-dioxane (2x5 mL each) and the filtrate was evaporated to dryness. The obtained crude was used without further purification and corresponded to the title compound **89b** (yellow thick oil, 20 mg, 97% yield). δ 10.49 (br, 1H), 8.67 (ddd, $J = 4.8, 1.7, 0.9$ Hz, 1H), 8.33 (d, $J = 8.9$ Hz, 1H), 8.26 (dt, $J = 7.8, 1.1$ Hz, 1H), 7.91 (td, $J = 7.7, 1.7$ Hz, 1H), 7.50 (ddd, $J = 7.6, 4.8, 1.2$ Hz, 1H), 6.95 (dd, $J = 8.9, 2.8$ Hz, 1H), 6.90 (d, $J = 2.7$ Hz, 1H), 3.81 (br, 2H). ^{13}C NMR (101 MHz, CDCl_3) δ 162.33, 149.36, 148.52, 143.24, 137.77, 132.08, 126.85, 123.04, 122.45, 120.87, 117.29, 116.62, 104.06. HRMS (m/z): $[\text{M}+\text{H}]^+$ calcd. for $\text{C}_{13}\text{H}_{11}\text{N}_4\text{O}$, 239.0933; found 239.0920.

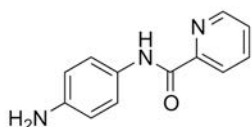


N-(2-cyano-4-(pyridin-2-ylidiazenyl)phenyl)picolinamide 111b: To a solution of the aniline **89b** (20 mg, 0.08 mmol) and 2-nitrosopyridine **90a** (11 mg, 0.10 mmol) in DCM (2 mL) it was added one drop of AcOH and was stirred at room temperature for two days. Afterwards, the solvent was evaporated under vacuum and the AcOH was coevaporated with toluene (2x5mL). The obtained solid was purified through silica *flash* column using *Biotage Isolera* equipment (SNAP KP-Sil 10 g; A=hexane B=EtOAc; 45%B 4.5CV, 50%B-55%B 5.5CV, 55%B 2CV, 55%B-75%B 2CV, 75%B-80%B 8CV, 80%B-100%B 2CV, 100%B 7CV). The title product **111b** was obtained (red solid, 16 mg, 47% yield). Mp: 204.9-205.2°C. ^1H NMR (400 MHz, CDCl_3) δ 11.10 (s, 1H), 8.96 (d, $J = 9.7$ Hz, 1H), 8.75 (dddd, $J = 14.1, 4.8, 1.8, 0.9$ Hz, 2H), 8.41 – 8.34 (m, 2H), 8.32 (dt, $J = 7.7, 1.1$ Hz, 1H), 8.00 – 7.91 (m, 2H), 7.87 (dt, $J = 8.0, 1.0$ Hz, 1H), 7.57 (ddd, $J = 7.7, 4.8, 1.2$ Hz, 1H), 7.45 (ddd, $J = 7.3, 4.8, 1.2$ Hz, 1H). ^{13}C NMR (101 MHz, CDCl_3) δ 162.74, 162.59, 149.88, 148.74, 148.67, 147.82, 143.31, 138.62, 138.03, 129.54, 128.18, 127.48, 125.86, 122.83, 120.68, 116.40, 115.68, 102.83. HPLC-PDA-MS: method A was used; RT: 5.47 min, $[\text{M}+\text{H}]^+$ 328.91, $\lambda_{\text{max}} = 317, 433$ nm (*cis*-isomer); RT: 5.87 min, $[\text{M}+\text{H}]^+$ 328.91, $\lambda_{\text{max}} = 348, 433$ nm (*trans*-isomer); purity 97.9% (254 nm). HRMS (m/z): $[\text{M}+\text{H}]^+$ calcd. for $\text{C}_{18}\text{H}_{13}\text{N}_6\text{O}$, 329.1151; found 329.1154.

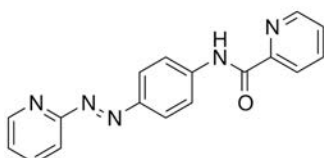


N-(4-nitrophenyl)picolinamide 88c: To a mixture of the 4-nitroaniline **87c** (65 mg, 0.47 mmol), picolinic acid **85j** (80 mg, 0.72 mmol) and HATU (573 mg, 1.51 mmol) in DMF (1.5 mL), was added DIPEA (279 μL , 1.60 mmol) and the resulting mixture was stirred a 16 h at 40°C. Afterwards, the reaction mixture was diluted in EtOAc (30 mL) and washed with Na_2CO_3 1N (20

mL), saturated NaHCO₃ (20 mL), water (20 mL) and brine (20 mL), dried over anhydrous MgSO₄, filtered and evaporated to dryness. The obtained solid was purified through silica *flash* column using *Biotage Isolera* equipment (SNAP KP-Sil 25 g; A=hexane B=EtOAc; 20%B 2CV, 20%B-27%B 13CV, 27%B-28%B 6CV, 28%-35%B 14CV, 35%B-45%B 10.5CV, 45%B-100%B 4.5CV, 100%B 6CV). The title product **88c**, previously described^{222, 223}, was obtained (white solid, 107 mg, 94% yield). ¹H NMR (400 MHz, CDCl₃) δ 10.38 (br, 1H), 8.65 (dd, J = 4.6, 1.4 Hz, 1H), 8.40 – 8.20 (m, 3H), 8.03 – 7.89 (m, 3H), 7.55 (ddd, J = 7.5, 4.8, 1.2 Hz, 1H). ¹H NMR (400 MHz, DMSO) δ 11.24 (br, 1H), 8.78 (ddd, J = 4.7, 1.7, 0.9 Hz, 1H), 8.27 (d, J = 9.4 Hz, 2H), 8.26 – 8.16 (m, 2H), 8.19 (dt, J = 7.8, 1.0 Hz, 1H), 8.10 (td, J = 7.7, 1.7 Hz, 1H), 7.72 (ddd, J = 7.5, 4.8, 1.3 Hz, 1H). ¹³C NMR (101 MHz, DMSO) δ 163.39, 149.26, 148.56, 144.65, 142.71, 138.28, 127.42, 124.69, 122.84, 120.15.

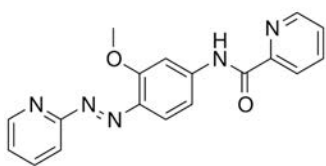


N-(4-aminophenyl)picolinamide 89c: To a suspension of the nitrocompound **88c** (65 mg, 0.24 mmol) and palladium on carbon (4 mg) in ethanol/1,4-dioxane 1:1 (6 mL) was applied a hydrogen atmosphere of 2 bar for 5 hours at room temperature. Afterwards, the black mixture was filtered through Celite, washed with EtOH and 1,4-dioxane (2x5 mL each) and the filtrate was evaporated to dryness. The obtained crude was used without further purification and corresponded to the title compound **89c**, previously described²²⁴ (yellow thick oil, 50 mg, 97% yield). ¹H NMR (400 MHz, CDCl₃) δ 9.84 (br, 1H), 8.60 (ddd, J = 4.7, 1.7, 0.9 Hz, 1H), 8.28 (dt, J = 7.9, 1.1 Hz, 1H), 7.89 (td, J = 7.7, 1.7 Hz, 1H), 7.57 (d, J = 8.7 Hz, 2H), 7.45 (ddd, J = 7.6, 4.8, 1.2 Hz, 1H), 6.72 (d, J = 8.7 Hz, 2H), 3.63 (br, 2H). ¹H NMR (400 MHz, DMSO) δ 10.21 (br, 1H), 8.70 (ddd, J = 4.7, 1.7, 0.9 Hz, 1H), 8.11 (dt, J = 7.9, 1.1 Hz, 1H), 8.04 (td, J = 7.6, 1.7 Hz, 1H), 7.63 (ddd, J = 7.5, 4.8, 1.4 Hz, 1H), 7.51 (d, J = 8.7 Hz, 2H), 6.55 (d, J = 8.7 Hz, 2H), 4.96 (br, 2H). ¹³C NMR (101 MHz, DMSO) δ 161.40, 150.31, 148.30, 145.39, 138.01, 127.38, 126.48, 121.98, 121.64, 113.72. HRMS (m/z): [M+H]⁺ calcd. for C₁₂H₁₂N₃O 214.0980; found 214.0979.

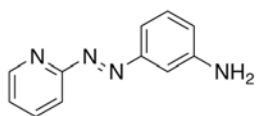


N-(4-(pyridin-2-yl)phenyl)picolinamide 111c: To solution of the aniline **89c** (50 mg, 0.23 mmol) and 2-nitrosopyridine **90a** (28 mg, 0.26 mmol) in DCM (4 mL) it was added two drops of AcOH and was stirred at room temperature for two days. Afterwards, the solvent was

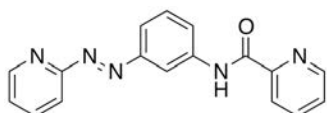
evaporated under vacuum and the AcOH was coevaporated with toluene (2x5mL). The obtained solid was purified through silica *flash* column using *Biotage Isolera* equipment (SNAP KP-Sil 10 g; A=DCM B=MeOH; 0%B 3CV, 0%B-1.1%B 8CV, 1.1%B-1.3%B 7CV, 1.3%B-1.5%B 2CV, 1.5%B-2%B 1.5CV, 2%B-5%B 3CV, 5%B-10%B 2CV, 10%B 5.5CV) and with C18 *flash* column (SNAP KP-C18-HS 12 g; A=H₂O B=MeCN; 0%B 3CV, 0%B-80%B 8CV, 80%B-100%B 5CV, 100%B 5CV). The title product **111c** was obtained (orange solid, 35 mg, 49% yield). Mp: 187.5-188.0°C. ¹H NMR (400 MHz, CDCl₃) δ 10.29 (br, 1H), 8.74 (ddd, J = 4.8, 1.9, 0.9 Hz, 1H), 8.64 (ddd, J = 4.7, 1.7, 0.9 Hz, 1H), 8.32 (dt, J = 7.8, 1.1 Hz, 1H), 8.13 (d, J = 8.9 Hz, 2H), 7.99 (d, J = 8.9 Hz, 2H), 7.93 (td, J = 7.7, 1.7 Hz, 1H), 7.91 (ddd, J = 8.0, 7.3, 1.8 Hz, 1H), 7.83 (dt, J = 8.0, 1.1 Hz, 1H), 7.51 (ddd, J = 7.6, 4.8, 1.2 Hz, 1H), 7.40 (ddd, J = 7.3, 4.8, 1.2 Hz, 1H). ¹³C NMR (101 MHz, CDCl₃) δ 163.16, 162.31, 149.65, 149.52, 149.00, 148.19, 141.51, 138.44, 137.96, 126.91, 125.20, 125.11, 122.70, 119.86, 115.47. HPLC-PDA-MS: method A was used; RT: 5.07 min, [M+H]⁺ 303.93, λ_{max} = 288, 323, 435 nm (*cis*-isomer); RT: 5.58 min, [M+H]⁺ 303.92, λ_{max} = 358 nm (*trans*-isomer); purity 99.7% (254 nm). HRMS (m/z): [M+H]⁺ calcd. for C₁₇H₁₄N₅O, 304.1198; found 304.1201.



N-(3-methoxy-4-(pyridin-2-yl-diazenyl)phenyl)picolinamide 111a: To solution of the aniline **95** (35 mg, 0.14 mmol) and 2-nitrosopyridine **90a** (16 mg, 0.14 mmol) in DCM (2.4 mL) it was added two drops of AcOH and was stirred at room temperature for 20 h. Afterwards, the solvent was evaporated under vacuum and the AcOH was coevaporated with toluene (2x5mL). The obtained solid was purified through silica *flash* column using *Biotage Isolera* equipment (SNAP KP-Sil 10 g; A=hexane B=EtOAc; 50%B 6CV, 50%B-70%B 7CV, 70%B 10CV, 70%B-100%B 5CV, 100%B 5CV). The title product **111a** was obtained (dark solid, 34 mg, 68% yield). Mp: 150.2-151.2°C. ¹H NMR (400 MHz, CDCl₃) δ 10.29 (br, 1H), 8.70 (ddd, J = 4.8, 2.0, 0.8 Hz, 1H), 8.63 (dt, J = 4.7, 1.2 Hz, 1H), 8.30 (dt, J = 7.9, 1.1 Hz, 1H), 8.09 (d, J = 2.1 Hz, 1H), 7.95 (d, J = 9.0 Hz, 1H), 7.95 – 7.90 (m, 1H), 7.90 – 7.81 (m, 1H), 7.78 (dt, J = 8.1, 1.2 Hz, 1H), 7.51 (ddd, J = 7.6, 4.8, 1.2 Hz, 1H), 7.34 (ddd, J = 7.3, 4.8, 1.2 Hz, 1H), 7.11 (dd, J = 8.8, 2.1 Hz, 1H), 4.11 (s, 3H). ¹³C NMR (101 MHz, CDCl₃) δ 163.84, 162.42, 159.29, 149.54, 149.38, 148.22, 143.31, 138.43, 138.29, 138.01, 126.98, 124.70, 122.60, 118.07, 114.72, 111.79, 103.42, 56.45. HPLC-PDA-MS: method A was used; RT: 5.13 min, [M+H]⁺ 333.90, λ_{max} = 293, 331, 443 nm (*cis*-isomer); RT: 5.58 min, [M+H]⁺ 333.94, λ_{max} = 385 nm (*trans*-isomer); purity 97.8% (254 nm). HRMS (m/z): [M+H]⁺ calcd. for C₁₈H₁₆N₅O₂, 334.1304; found 334.1306

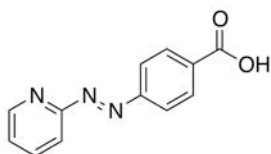


3-(pyridin-2-yl)diazenylaniline 124: To solution of the phenyldiamine **123b** (53 mg, 0.49 mmol) and 2-nitrosopyridine **90a** (68 mg, 0.63 mmol) in DCM (3 mL) it was added two drops of AcOH was stirred 30 hours at room temperature. Afterwards, the solvent was evaporated under vacuum and the AcOH was coevaporated with toluene (2x2mL). The obtained solid was purified twice by *flash* silica column (SNAP KP-Sil 25 g; A = DCM B = MeOH; 0.2%B 2CV, 0.2%B-1.5%B 3.5CV, 1.5%B-2.1%B 6.5CV, 2.1%B-2.5%B 4.5CV, 2.5%B-4%B 7.5CV, 4%B-10%B 3CV, 10%B 6CV and SNAP KP-Sil 10 g; A = hexanes B = EtOAc; 45%B 2CV, 45%B-50%B 10CV, 50%B 3CV, 50%B-54%B 3CV, 54%B 2CV, 54%B-60%B 3.5CV, 60%B-100%B 4CV, 100%B 6.5CV) to obtain **124** (17 mg, red solid) with 27% yield. ^1H NMR (400 MHz, CDCl_3) δ 8.74 (ddd, $J = 4.8, 1.9, 0.9$ Hz, 1H), 7.90 (ddd, $J = 8.1, 7.3, 1.9$ Hz, 1H), 7.80 (dt, $J = 8.1, 1.0$ Hz, 1H), 7.50 (ddd, $J = 7.8, 1.8, 1.0$ Hz, 1H), 7.40 (ddd, $J = 7.4, 4.8, 1.1$ Hz, 1H), 7.35 (t, $J = 2.1$ Hz, 1H), 7.33 (t, $J = 8.0$ Hz, 1H), 6.86 (ddd, $J = 8.0, 2.4, 1.0$ Hz, 1H), 3.84 (br, 2H). ^{13}C NMR (101 MHz, CDCl_3) δ 163.09, 153.63, 149.67, 147.36, 138.43, 130.01, 125.26, 119.14, 116.57, 115.33, 107.57. HRMS (m/z): $[\text{M}+\text{H}]^+$ calcd. for $\text{C}_{11}\text{H}_{11}\text{N}_4$, 199.0984; found 199.0984; $[\text{2M}+\text{Cu}]^+$ calcd. for $\text{C}_{22}\text{H}_{20}\text{N}_9\text{Cu}$, 459.1107; found 459.1109.

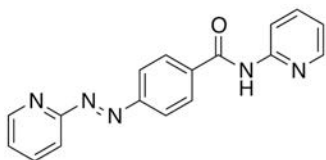


N-(3-(pyridin-2-yl)phenyl)picolinamide 115: To a suspension of the aniline **124** (17 mg, 0.09 mmol), picolinic acid **85j** (16 mg, 0.13 mmol) and HATU (99 mg, 0.26 mmol) in DMF (1 mL) it was added DIPEA (47 μL , 0.27 mmol) and the resulting mixture was stirred a temperature 16 h at 40°C. Afterwards, the mixture was diluted in EtOAc (15 mL) and washed with NaOH or Na_2CO_3 1N (10 mL), saturated NaHCO_3 (10 mL), water (10 mL) and brine (10 mL), dried over anhydrous MgSO_4 , filtered and evaporated to dryness. The obtained solid was purified through silica *flash* column (SNAP KP-Sil 10 g; A = hexanes B = EtOAc; 60%B 1CV, 60%B-65%B 2.5CV, 65%B 1.5CV, 65%B-75%B 4.5CV, 75%B-80%B 1CV, 80%B-100%B 1CV, 100%B 5CV) to obtain **115** (22 mg, orange solid) with 84% yield. Mp: 116.5-117.5°C. ^1H NMR (400 MHz, CDCl_3) δ 10.22 (br, 1H), 8.75 (ddd, $J = 4.8, 1.8, 0.9$ Hz, 1H), 8.63 (ddd, $J = 4.8, 1.7, 0.9$ Hz, 1H), 8.33 (d, $J = 1.0$ Hz, 1H), 8.31 (d, $J = 4.9$ Hz, 1H), 8.15 (ddd, $J = 8.1, 2.2, 1.0$ Hz, 1H), 7.97 – 7.83 (m, 4H), 7.57 (t, $J = 8.0$ Hz, 1H), 7.50 (ddd, $J = 7.6, 4.8, 1.2$ Hz, 1H), 7.42 (ddd, $J = 7.3, 4.8, 1.3$ Hz, 1H). ^{13}C NMR (101 MHz, CDCl_3) δ 162.90, 162.34, 153.09, 149.72, 149.65, 148.20, 138.84, 138.50, 137.87, 130.01, 126.76, 125.51, 123.26, 122.59, 120.68, 115.71, 113.61. HPLC-PDA-MS:

method B was used; RT: 5.36 min, $[M+H]^+$ 303.94, $\lambda_{\max} = 279, 429$ nm (*cis*-isomer); RT: 5.65 min, $[M+H]^+$ 303.94, $\lambda_{\max} = 309$ nm (*trans*-isomer); purity 99.8% (254 nm). HRMS (m/z): $[M+H]^+$ calcd. for $C_{17}H_{14}N_5O$, 304.1198; found 304.1200.

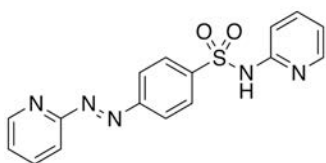


4-(pyridin-2-yl)diazenylbenzoic acid 126: To a solution of aniline **125** (44 mg, 0.32 mmol) and 2-nitrosopyridine **90a** (41 mg, 0.38 mmol) in DCM (3 mL) it was added two drops of AcOH and was stirred 48 hours at room temperature. After this period, a pink precipitate appeared. The reaction was filtered-off and the pink solid was washed with cold DCM (3x1mL) and dried under vacuum. The obtained solid **126** (40 mg, 55% yield) was used without further purification. 1H NMR (400 MHz, DMSO) δ 13.29 (br, 1H), 8.76 (ddd, $J = 4.8, 1.9, 0.8$ Hz, 1H), 8.18 (d, $J = 8.5$ Hz, 2H), 8.09 (td, $J = 7.8, 1.9$ Hz, 1H), 8.03 (d, $J = 8.5$ Hz, 2H), 7.78 (dt, $J = 8.1, 1.0$ Hz, 1H), 7.63 (ddd, $J = 7.4, 4.8, 1.1$ Hz, 1H). ^{13}C NMR (101 MHz, DMSO) δ 166.58, 162.60, 154.06, 149.53, 139.03, 133.64, 130.70, 126.29, 122.96, 113.89. HRMS (m/z): $[M+H]^+$ calcd. for $C_{12}H_{10}N_3O_2$, 228.0773; found 228.0772; $[M-H]^-$ calcd. for $C_{12}H_8N_3O_2$, 226.0617; found 226.0617.

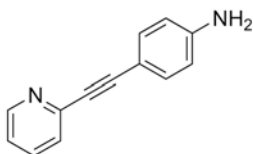


N-(pyridin-2-yl)-4-(pyridin-2-yl)diazenylbenzamide 116: A suspension of carboxylic acid **126** (22 mg, 0.09 mmol) in thionyl chloride (1 mL, 14 mmol) was stirred at 75°C for 3.5 hours. Then, the mixture was cooled and the solvent was evaporated to dryness and dissolved in DCE (2 mL) containing 2-aminopyridine **96** (19 mg, 0.20 mmol) and DIPEA (75 μ L, 0.4 mmol). The resulting solution was stirred 2 hours at 90°C and 64 hours at room temperature. Afterwards the solution was concentrated, redissolved in EtOAc (15 mL), washed with Na_2CO_3 1M (10 mL), saturated $NaHCO_3$ (10 mL), water (10 mL) and brine (10 mL), dried over anhydrous $MgSO_4$, filtered and concentrated to give a residue which was purified twice through silica *flash* column using *Biotage Isolera* equipment (SNAP KP-Sil 10 g; A = hexane B = EtOAc; 50%B 3.5CV, 50%B-67%B 1.5CV, 67%B 10CV, 67%B-74%B 1CV, 74%B-80%B 3CV, 80%B-85%B 4.5, 85%B-100%B 2.5CV, 100%B 4CV) and (SNAP KP-Sil 10 g; A = DCM B = MeOH; 0%B 1CV, 0%B-3%B 10.5CV, 3%B 8.5CV, 3%B-15%B 5CV, 15%B 8CV) to give **116** (7.6 mg, red solid) with 26% yield. Mp: 158.2-158.8°C. 1H NMR (400 MHz, $CDCl_3$) δ 8.78 (ddd, $J = 4.7, 1.9, 0.9$ Hz, 1H), 8.71 (br, 1H),

8.40 (dt, $J = 8.4, 1.0$ Hz, 1H), 8.32 (ddd, $J = 4.9, 1.9, 1.0$ Hz, 1H), 8.16 (d, $J = 8.8$ Hz, 2H), 8.11 (d, $J = 8.8$ Hz, 2H), 7.96 (ddd, $J = 8.1, 7.3, 1.9$ Hz, 1H), 7.89 (dt, $J = 8.0, 1.1$ Hz, 1H), 7.79 (ddd, $J = 8.4, 7.4, 1.9$ Hz, 1H), 7.46 (ddd, $J = 7.3, 4.8, 1.3$ Hz, 1H), 7.10 (ddd, $J = 7.4, 4.9, 1.0$ Hz, 1H). ^{13}C NMR (101 MHz, CDCl_3) δ 164.90, 162.76, 154.49, 151.47, 149.90, 148.16, 138.70, 138.63, 137.06, 128.44, 125.97, 124.01, 120.37, 116.35, 114.36. HPLC-PDA-MS: method A was used; RT: 4.86 min, $[\text{M}+\text{H}]^+$ 303.91, $\lambda_{\text{max}} = 286, 433$ nm (*cis*-isomer); RT: 5.26 min, $[\text{M}+\text{H}]^+$ 303.90, $\lambda_{\text{max}} = 326$ nm (*trans*-isomer); purity 99.8% (254 nm). HRMS (m/z): $[\text{M}+\text{H}]^+$ calcd. for $\text{C}_{17}\text{H}_{14}\text{N}_5\text{O}$, 304.1198; found 304.1195.

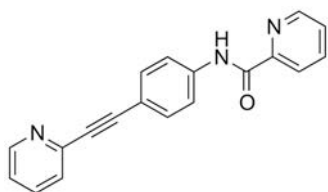


***N*-(pyridin-2-yl)-4-(pyridin-2-yl)benzenesulfonamide 117:** To solution of the sulfamide **127** (36 mg, 0.10 mmol) and 2-nitrosopyridine **89a** ((14 mg, 0.13 mmol) in DCM (1.5 mL) it was added two drops of AcOH was stirred 6 days at room temperature. Afterwards, the solvent was evaporated under vacuum and the AcOH was coevaporated with toluene (2x2mL). The obtained solid was purified twice by *flash* silica column (SNAP KP-C18-HS 12 g; A = Water + 0.2% Formic acid B = MeOH + 0.2% formic acid; 0%B 3CV, 0%B-70%B 13.5CV, 70%B-100%B 2CV, 100% 5CV; and;) to obtain **117** (32 mg, orange solid) with 90% yield. Mp: 163.3-164.0°C (decomp.). ^1H NMR (400 MHz, DMSO) δ 12.57 (br, 1H), 8.75 (dd, $J = 4.9, 1.7$ Hz, 1H), 8.12 – 8.02 (m, 5H), 7.98 (dd, $J = 6.0, 1.8$ Hz, 1H), 7.81 – 7.73 (m, 2H), 7.62 (ddd, $J = 7.4, 4.8, 1.1$ Hz, 1H), 7.24 (d, $J = 8.8$ Hz, 1H), 6.86 (t, $J = 6.2$ Hz, 1H). ^{13}C NMR (101 MHz, DMSO) δ 162.98, 153.56, 149.97, 141.91, 139.48, 128.29, 126.77, 123.76, 115.07, 114.37. HPLC-PDA-MS: method B was used; RT: 4.61 min, $[\text{M}+\text{H}]^+$ 339.88, $\lambda_{\text{max}} = 307, 430$ nm (*cis*-isomer); RT: 4.83 min, $[\text{M}+\text{H}]^+$ 339.89, $\lambda_{\text{max}} = 323$ nm (*trans*-isomer); purity 100% (254 nm). HRMS (m/z): $[\text{M}+\text{H}]^+$ calcd. for $\text{C}_{16}\text{H}_{14}\text{N}_5\text{O}_2\text{S}$, 340.0868; found 340.0869.

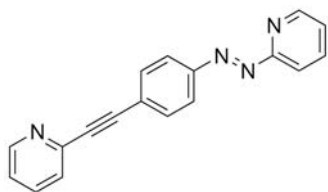


4-(pyridin-2-ylethynyl)aniline 134a: 2-chloropyridine **133** (0.13 mL, 1.37 mmol) and dry TEA (0.76 mL, 5.46 mmol) were added to a slurry of 4-ethynylaniline **132a** (249 mg, 2.05 mmol), CuI (13 mg, 0.07 mmol) and $\text{PdCl}_2(\text{PPh}_3)_2$ (48 mg, 0.07 mmol) in dry DMF (8 mL) in a *Schlenk* flask with argon atmosphere at room temperature. The mixture was stirred at 60°C for 4 hours. The reaction mixture was diluted in EtOAc (100 mL) and washed with aqueous Na_2CO_3 1 N (50 mL),

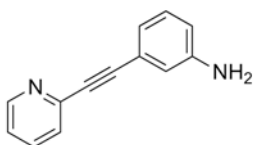
saturated NaHCO₃ (50 mL), water (50 mL) and brine (50 mL), dried over anhydrous MgSO₄, filtered and concentrated in vacuo. The residue was purified through silica flash chromatography (DCM/hexanes 9:1, DCM, DCM + 0.5% MeOH and DCM + 1% MeOH) to afford the title compound **15b** as brown thick oil (60 mg, 23% yield). ¹H NMR (400 MHz, CDCl₃) δ 8.58 (ddd, J = 4.9, 1.9, 1.0 Hz, 1H), 7.64 (td, J = 7.7, 1.8 Hz, 1H), 7.47 (dt, J = 7.9, 1.1 Hz, 1H), 7.40 (d, J = 8.7 Hz, 2H), 7.18 (ddd, J = 7.6, 4.9, 1.2 Hz, 1H), 6.63 (d, J = 8.7 Hz, 2H), 3.48 (br, 2H). ¹³C NMR (101 MHz, CDCl₃) δ 150.02, 147.46, 144.18, 136.20, 133.67, 126.88, 122.26, 114.78, 111.51, 90.69, 87.10. HRMS (m/z): [M+H]⁺ calcd. for C₁₃H₁₁N₂, 195.0922; found, 195.0923.



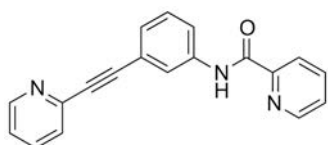
N-(4-(pyridin-2-ylethynyl)phenyl)picolinamide 128a: To a slurry of the aniline **134a** (13 mg, 0.07 mmol), picolinic acid **85j** (13 mg, 0.10 mmol) and HATU (76 mg, 0.20 mmol) in DMF (2 mL), it was added DIPEA (41 μL, 0.23 mmol) and the resulting mixture was stirred a temperature 5 h at 40°C. Afterwards, the mixture was diluted in EtOAc (40 mL) and washed with NaOH or Na₂CO₃ 1N (10 mL), saturated NaHCO₃ (10 mL), water (10 mL) and brine (10 mL), dried over anhydrous MgSO₄, filtered and evaporated to dryness. The resulting solid was purified twice through C18 *flash* column using *Biotage Isolera* equipment (SNAP KP-C18-HS 12 g; A = H₂O B = MeCN; 5%B 3CV, 5%B-60%B 5CV, 60%B-80%B 5CV, 80%B-100%B 3CV, 100%B 5CV; and SNAP KP-C18-HS 12 g; A = H₂O B = MeOH; 5%B 3CV, 5%B-50%B 3CV, 50%B-65%B 7CV, 65%B-75%B 2CV, 75%B-100%B 2CV, 100%B 4.5CV) to obtain **128a** (17 mg, orange solid) with 83% yield. Mp: 170.5-171.7 °C. ¹H NMR (400 MHz, CDCl₃) δ 10.13 (br, 1H), 8.68 – 8.57 (m, 2H), 8.29 (dt, J = 7.8, 1.1 Hz, 1H), 7.91 (td, J = 7.7, 1.7 Hz, 1H), 7.81 (d, J = 8.7 Hz, 2H), 7.68 (td, J = 7.7, 1.8 Hz, 1H), 7.63 (d, J = 8.6 Hz, 2H), 7.52 (d, J = 7.9 Hz, 1H), 7.49 (ddd, J = 7.6, 4.8, 1.3 Hz, 1H), 7.23 (ddd, J = 7.6, 4.9, 1.2 Hz, 1H). ¹³C NMR (101 MHz, CDCl₃) δ 162.16, 150.02, 149.61, 148.15, 143.55, 138.56, 137.90, 136.45, 133.20, 127.25, 126.79, 122.79, 122.61, 119.49, 117.87, 89.70, 88.42. HPLC-PDA-MS: method B was used; RT: 5.78 min, [M+H]⁺ 299.86, λ_{max} = 318 nm; purity 99.6% (254 nm). HRMS (m/z): [M+H]⁺ calcd. for C₁₉H₁₄N₃O, 300.1137; found 300.1143.



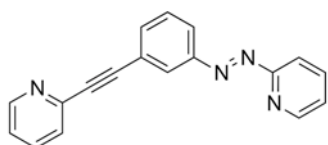
2-((4-(pyridin-2-ylidiazenyl)phenyl)ethynyl)pyridine 129a: A drop of AcOH was added to a solution of nitrosopyridine **90a** (11 mg, 0.10 mmol) and **134a** (13 mg, 0.07 mmol) in DCM (1 mL) and the mixture stirred 3 days at room temperature. Afterwards, the solvent was evaporated under vacuum and the AcOH was coevaporated with toluene (2x2mL). The obtained residue was purified by *flash* chromatography using *Biotage Isolera* equipment (SNAP KP-C18-HS 12g, A=H₂O B=MeOH; 0%B 3CV, 0%B-60%B 5CV, 60%B-85%B 8CV, 85%B-100%B 1CV, 100%B 8CV). The title product **129a** was obtained (15 mg, orange solid) with a 78% yield. Mp: 185.9-186.6°C. ¹H NMR (400 MHz, CDCl₃) δ 8.76 (ddd, J = 4.8, 1.8, 0.8 Hz, 1H), 8.65 (ddd, J = 4.9, 1.8, 0.9 Hz, 1H), 8.06 (d, J = 8.6 Hz, 2H), 7.93 (ddd, J = 8.0, 7.3, 1.9 Hz, 1H), 7.85 (dt, J = 8.0, 1.1 Hz, 1H), 7.77 (d, J = 8.6 Hz, 2H), 7.73 (dd, J = 7.7, 1.8 Hz, 1H), 7.58 (dt, J = 7.9, 1.1 Hz, 1H), 7.43 (ddd, J = 7.3, 4.7, 1.2 Hz, 1H), 7.30 (ddd, J = 7.7, 4.9, 1.2 Hz, 1H). ¹³C NMR (101 MHz, CDCl₃) δ 162.86, 152.17, 149.94, 149.76, 142.86, 138.57, 136.79, 133.14, 127.62, 126.08, 125.65, 123.79, 123.33, 116.16, 91.06, 89.43. HPLC-PDA-MS: RT = 5.48 min, 19.34% (254 nm), PDA λ_{max} = 307, 435 nm, MS (m/z) [M+H]⁺ 284.95 (*cis*-isomer); RT = 5.75 min, 80.09% (254 nm), PDA λ_{max} = 349, 443 nm, MS (m/z) [M+H]⁺ 284.96 (*trans*-isomer). HRMS (m/z): [M+H]⁺ calcd. for C₁₈H₁₃N₄, 285.1140; found, 285.1140



3-(pyridin-2-ylethynyl)aniline 134b: 2-chloropyridine **133** (0.13 mL, 1.37 mmol) and dry TEA (0.76 mL, 5.46 mmol) were added to a slurry of 3-ethynylaniline **132b** (0.25 mL, 2.13 mmol), CuI (13 mg, 0.07 mmol) and PdCl₂(PPh₃)₂ (48 mg, 0.07 mmol) in dry DMF (8 mL) in a *Schlenk* flask with argon atmosphere at room temperature. The mixture was stirred at 60°C for 4 hours. The reaction mixture was diluted in EtOAc (100 mL) and washed with aqueous Na₂CO₃ 1 N (50 mL), saturated NaHCO₃ (50 mL), water (50 mL) and brine (50 mL), dried over anhydrous MgSO₄, filtered and concentrated in vacuo. The residue was purified by silica flash chromatography (DCM and DCM + 1% MeOH) to afford the title compound **134b** as brown thick oil (80 mg, 30% yield). ¹H NMR (400 MHz, CDCl₃) δ 8.61 (ddd, J = 4.9, 1.8, 1.0 Hz, 1H), 7.67 (td, J = 7.7, 1.8 Hz, 1H), 7.50 (dt, J = 7.9, 1.1 Hz, 1H), 7.23 (ddd, J = 7.6, 4.9, 1.2 Hz, 1H), 7.14 (t, J = 7.8 Hz, 1H), 7.00 (dt, J = 7.6, 1.2 Hz, 1H), 6.91 (dd, J = 2.4, 1.5 Hz, 1H), 6.69 (ddd, J = 8.1, 2.4, 1.0 Hz, 1H), 3.13 (br, 2H). ¹³C NMR (101 MHz, CDCl₃) δ 150.11, 146.42, 143.65, 136.31, 129.45, 127.30, 123.02, 122.79, 122.62, 118.30, 116.17, 89.80, 88.09. HRMS (m/z): [M+H]⁺ calcd. for C₁₃H₁₁N₂, 195.0922; found, 195.0922.

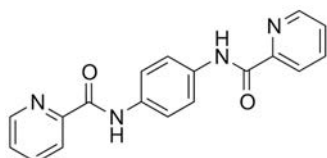


N-(3-(pyridin-2-ylethynyl)phenyl)picolinamide 128b: To a suspension of the aniline **135b** (15 mg, 0.08 mmol), picolinic acid **85j** (14 mg, 0.12 mmol) and HATU (89 mg, 0.24 mmol) in DMF (2 mL), it was added DIPEA (48 μ L, 0.27 mmol) and the resulting mixture was stirred a temperature 5 h at 40°C. Afterwards, the reaction mixture was diluted in EtOAc (40 mL) and washed with NaOH or Na₂CO₃ 1N (10 mL), saturated NaHCO₃ (10 mL), water (10 mL) and brine (10 mL), dried over anhydrous MgSO₄, filtered and evaporated to dryness. The obtained solid was purified through C18 *flash* column using *Biotage Isolera* equipment (SNAP KP-C18-HS 12 g; A = H₂O B = MeCN; 5%B 3CV, 5%B-80%B 8CV, 80%B-83%B 2CV, 83%B-100%B 1.5CV, 100%B 5CV) to obtain **128b** (18 mg, orange solid) with 78% yield. Mp: 123.5-123.8 °C. ¹H NMR (400 MHz, CDCl₃) δ 10.07 (br, 1H), 8.63 (s, 1H), 8.61 (ddd, J = 4.7, 1.7, 0.9 Hz, 1H), 8.29 (dt, J = 7.8, 1.1 Hz, 1H), 8.03 (dt, J = 2.2, 0.9 Hz, 1H), 7.91 (td, J = 7.7, 1.7 Hz, 1H), 7.83 (ddd, J = 6.2, 3.0, 2.3 Hz, 1H), 7.69 (td, J = 7.7, 1.8 Hz, 1H), 7.54 (dt, J = 7.8, 1.1 Hz, 1H), 7.49 (ddd, J = 7.6, 4.8, 1.2 Hz, 1H), 7.40 – 7.36 (m, 2H), 7.25 (ddd, J = 7.6, 4.9, 1.2 Hz, 1H). ¹³C NMR (101 MHz, CDCl₃) δ 162.21, 150.04, 149.66, 148.14, 143.38, 137.98, 137.85, 136.45, 129.33, 128.10, 127.43, 126.73, 123.15, 123.05, 122.98, 122.58, 120.50, 89.24, 88.78. HPLC-PDA-MS: method B was used; RT: 5.80 min, [M+H]⁺ 299.94, λ_{max} = 294 nm; purity 99.6% (254 nm). HRMS (m/z): [M+H]⁺ calcd. for C₁₉H₁₄N₃O, 300.1137; found 300.1120.

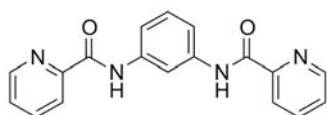


2-((3-(pyridin-2-yl)diazenyl)phenyl)ethynylpyridine 129b: A drop of AcOH was added to solution of nitrosopyridine **90a** (15 mg, 0.14 mmol) and aniline **134b** (18 mg, 0.09 mmol) in DCM (1 mL) and stirred 3 days at room temperature. Afterwards, the solvent was evaporated under vacuum and the rests of AcOH were co-evaporated with toluene (2x2mL). The obtained residue was purified by *flash* chromatography using *Biotage Isolera* equipment (SNAP KP-C18-HS 12g, A=H₂O B=MeOH; 0%B 3CV, 0%B-60%B 5CV, 60%B-85%B 8CV, 85%B-100%B 1CV, 100%B 4CV). The title product **129a** was obtained (20 mg, orange solid) with a 76% yield. Mp: 79.1-79.8 °C. ¹H NMR (400 MHz, CDCl₃) δ 8.76 (ddd, J = 4.8, 1.8, 0.9 Hz, 1H), 8.65 (ddd, J = 5.0, 1.8, 0.9 Hz, 1H), 8.31 – 8.25 (m, 1H), 8.08 (ddd, J = 8.1, 2.0, 1.2 Hz, 1H), 7.93 (ddd, J = 8.0, 7.3, 1.8 Hz, 1H), 7.85 (dt, J = 8.0, 1.1 Hz, 1H), 7.77 (dt, J = 7.7, 1.3 Hz, 1H), 7.75 (td, J = 7.7, 1.8 Hz,

1H), 7.58 (dt, $J = 7.6, 0.9$ Hz, 1H), 7.54 (t, $J = 7.9$ Hz, 1H), 7.43 (ddd, $J = 7.3, 4.8, 1.2$ Hz, 1H), 7.31 (ddd, $J = 7.6, 4.9, 1.2$ Hz, 1H). ^{13}C NMR (101 MHz, CDCl_3) δ 162.73, 152.36, 149.74, 149.67, 142.76, 138.60, 136.99, 135.45, 129.51, 127.65, 127.02, 125.70, 124.59, 123.38, 123.27, 116.09, 89.32, 88.91. HPLC-PDA-MS: RT = 5.50 min, 21.53% (254 nm), PDA $\lambda_{\text{max}} = 290, 428$ nm, MS (m/z) $[\text{M}+\text{H}]^+$ 284.96 (*cis*-isomer); RT = 5.76 min, 78.00% (254 nm), PDA $\lambda_{\text{max}} = 302, 445$ nm, MS (m/z) $[\text{M}+\text{H}]^+$ 284.95 (*trans*-isomer). HRMS (m/z): $[\text{M}+\text{H}]^+$ calcd. for $\text{C}_{18}\text{H}_{13}\text{N}_4$, 285.1140; found, 285.11405.

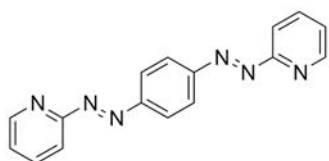


***N,N'*-(1,4-phenylene)dipicolinamide 130a:** To a suspension of *p*-phenylenediamine **123a** (26 mg, 0.24 mmol), picolinic acid **85j** (71 mg, 0.58 mmol) and HATU (440 mg, 1.2 mmol) in DMF (1.2 mL), it was added DIPEA (0.5 mL, 2.9 mmol) and the resulting mixture was stirred at room temperature for three days. Afterwards, the reaction mixture was diluted in EtOAc (40 mL), washed with Na_2CO_3 1N (10 mL), saturated NaHCO_3 (10 mL), water (10 mL) and brine (10 mL), dried over anhydrous MgSO_4 , filtered and evaporated to dryness. The obtained solid was purified through silica *flash* column using *Biotage Isolera* equipment (SNAP KP-Sil 10 g; A = DCM B = MeOH; 0%B 1CV, 0%B-0.5%B 1CV, 0.5%B 1CV, 0.5%B-1.5%B 10CV, 1.5%B-5%B 3.5CV, 5%B-10%B 2CV, 10%B 7CV) to obtain **130a** (40 mg, white solid) with 52% yield. Mp: 273.1-274.3 °C. ^1H NMR (400 MHz, CDCl_3) δ 10.06 (br, 2H), 8.63 (ddd, $J = 4.7, 1.7, 0.9$ Hz, 2H), 8.31 (dt, $J = 7.8, 1.1$ Hz, 2H), 7.92 (td, $J = 7.7, 1.7$ Hz, 2H), 7.83 (s, 4H), 7.49 (ddd, $J = 7.6, 4.8, 1.3$ Hz, 2H). ^{13}C NMR (101 MHz, CDCl_3) δ 161.96, 149.95, 148.08, 137.89, 134.31, 126.59, 122.56, 120.49. HPLC-PDA-MS: method B was used; RT: 5.57 min, $[\text{M}+\text{H}]^+$ 318.96, $\lambda_{\text{max}} = 314$ nm; purity 99.3% (254 nm). HRMS (m/z): $[\text{M}+\text{H}]^+$ calcd. for $\text{C}_{18}\text{H}_{15}\text{N}_4\text{O}_2$, 319.1195; found, 319.1210. HRMS (m/z): $[\text{2M}+\text{Na}]^+$ calcd. for $\text{C}_{36}\text{H}_{29}\text{N}_8\text{O}_4$, 637.2312; found, 637.2314.

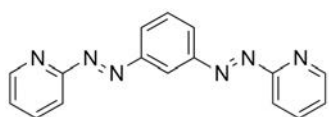


***N,N'*-(1,4-phenylene)dipicolinamide 130b:** To a suspension of the *m*-phenylenediamine **123b** (20 mg, 0.19 mmol), picolinic acid **85j** (57 mg, 0.46 mmol) and HATU (352 mg, 0.93 mmol) in DMF (2 mL), it was added DIPEA (162 μL , 0.93 mmol) and the resulting mixture was stirred 3 hours at 40°C. Afterwards, the mixture was diluted in EtOAc (30 mL), washed with Na_2CO_3 1N (10 mL), saturated NaHCO_3 (10 mL), water (10 mL) and brine (10 mL), dried over anhydrous MgSO_4 , filtered and evaporated to dryness. The obtained solid was purified through C18 *flash*

column using *Biotage Isolera* equipment (SNAP KP-C18-HS 12 g; A = H₂O B = MeCN; 5%B 3CV, 5%B-80%B 8CV, 80%B-100B 5CV, 100%B 5CV) to obtain **130b** (48 mg, white solid) with 81% yield. Mp: 146.9-147.6°C. ¹H NMR (400 MHz, CDCl₃) δ 10.12 (br, 2H), 8.61 (ddd, J = 4.7, 1.7, 0.9 Hz, 2H), 8.36 – 8.23 (m, 3H), 7.90 (td, J = 7.7, 1.7 Hz, 2H), 7.63 (dd, J = 8.1, 2.1 Hz, 2H), 7.47 (ddd, J = 7.6, 4.7, 1.2 Hz, 2H), 7.40 (t, J = 8.0, 7.5 Hz, 1H). ¹³C NMR (101 MHz, CDCl₃) δ 162.15, 149.78, 148.05, 138.57, 137.92, 129.92, 126.66, 122.60, 115.59, 110.94. HPLC-PDA-MS: method B was used; RT: 5.66 min, [M+H]⁺ 318.95, λ_{max} = 281 nm; purity 99.8% (254 nm). HRMS (m/z): [M+H]⁺ calcd. for C₁₈H₁₅N₄O₂, 319.1195; found, 319.1202. HRMS (m/z): [2M+Na]⁺ calcd. for C₃₆H₂₈N₈O₄Na, 659.2131; found, 659.2131.

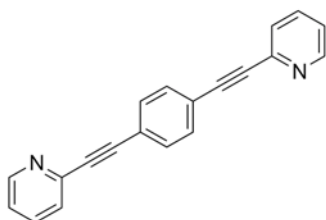


1,4-bis(pyridin-2-yl)benzene 131a: Two drops of AcOH were added to solution of nitrosopyridine **90a** (33 mg, 0.31 mmol) and *p*-phenylenediamine **123a** (15 mg, 0.14 mmol) in DCM (1 mL) and the mixture stirred 7 days at room temperature. Afterwards, the solvent was evaporated under vacuum and the rests of AcOH were co-evaporated with toluene (2x2mL). The title product **131a** (39 mg, orange solid) was afforded with a 98% yield. Mp: 211.6-212.7°C. ¹H NMR (400 MHz, CDCl₃) δ 8.78 (d, J = 3.4 Hz, 2H), 8.22 (s, 4H), 7.96 (td, J = 7.7, 1.8 Hz, 2H), 7.89 (d, J = 7.9 Hz, 2H), 7.46 (ddd, J = 7.4, 4.8, 1.3 Hz, 2H). ¹³C NMR (101 MHz, CDCl₃) δ 162.72, 154.18, 149.71, 138.73, 125.85, 124.70, 116.27. HPLC-PDA-MS: RT = 5.34 min, 5.33% (254 nm), PDA λ_{max} = 336, 437 nm, MS (m/z) [M+H]⁺ 288.89 (*cis-trans*-isomer); RT = 5.59 min, 90.61% (254 nm), PDA λ_{max} = 353, 456 nm, MS (m/z) [M+H]⁺ 288.90 (*trans-trans*-isomer), HRMS (m/z): [M+H]⁺ calcd. for C₁₅H₁₃N₆, 289.1202; found, 289.1216.

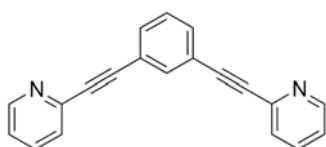


1,3-bis(pyridin-2-yl)benzene 131b: Two drops of AcOH were added to solution of nitrosopyridine **90a** (120 mg, 1.11 mmol) and *m*-phenylenediamine **123b** (40 mg, 0.37 mmol) in DCM (10 mL) and the reaction mixture was stirred for 8 days at room temperature. Afterwards, the solvent was evaporated under vacuum and the rests of AcOH were co-evaporated with toluene (2x2mL). The obtained solid was purified through silica *flash* column (hexanes/EtOAc) to give the desired product **130b** as dark solid (5 mg) with a 5% yield. Mp: 101.3-101.9°C. ¹H NMR (400 MHz, CDCl₃) δ 8.77 (ddd, J = 4.8, 1.8, 0.9 Hz, 2H), 8.70 (t, J = 2.0 Hz, 1H), 8.25 (dd, J = 7.9, 2.0 Hz, 2H), 7.95 (ddd, J = 8.0, 7.2, 1.8 Hz, 2H), 7.89 (dt, J = 8.0, 1.1 Hz,

2H), 7.73 (t, J = 7.9 Hz, 1H), 7.45 (ddd, J = 7.2, 4.8, 1.3 Hz, 2H). ^{13}C NMR (101 MHz, CDCl_3) δ 162.79, 153.33, 149.80, 138.61, 130.01, 127.09, 125.74, 118.01, 116.37. HPLC-PDA-MS: RT = 5.11 min, 3.65% (254 nm), PDA λ_{max} = 278, 428 nm, MS (m/z) $[\text{M}+\text{H}]^+$ 288.93 (*cis-cis*-isomer); RT = 5.34 min, 24.86% (254 nm), PDA λ_{max} = 314, 432 nm, MS (m/z) $[\text{M}+\text{H}]^+$ 288.95 (*cis-trans*-isomer); RT = 5.60 min, 70.71% (254 nm), PDA λ_{max} = 319, 443 nm, MS (m/z) $[\text{M}+\text{H}]^+$ 288.96 (*trans-trans*-isomer). HRMS (m/z): $[\text{M}+\text{H}]^+$ calcd. for $\text{C}_{16}\text{H}_{13}\text{N}_6$, 289.1202; found, 289.1216. HRMS (m/z): $[\text{2M}+\text{H}]^+$ calcd. for $\text{C}_{32}\text{H}_{25}\text{N}_{12}$, 577.2325; found, 577.2319.

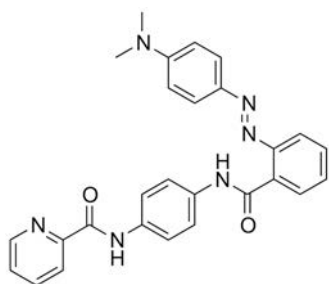


1,4-bis(pyridin-2-ylethynyl)benzene 54: 2-ethynylpyridine **101** (36 μL , 0.36 mmol) and dry diisopropylethylamine (DIPEA) (0.1 ml, 0.57 mmol) were added to a suspension of 1,3-diiodobenzene **135a** (47 mg, 0.14 mmol), CuI (2 mg, 0.01 mmol) and $\text{PdCl}_2(\text{PPh}_3)_2$ (5.4 mg, 0.01 mmol) in dry DMF (1 mL) in a *Schlenk* flask with argon atmosphere at room temperature. This mixture was stirred at 50°C for 5 hours. The reaction mixture was diluted in EtOAc (15 mL) and washed with aqueous Na_2CO_3 1 N (10 mL), saturated NaHCO_3 (10 mL), water (10 mL) and brine (10 mL), dried over anhydrous MgSO_4 , filtered and concentrated in vacuo. The residue was purified by *flash* chromatography using *Biotage Isolera* equipment (SNAP KP-C18-HS 12g, A= H_2O B=MeCN; 0%B 5CV, 0%B-1%B 2CV, 1%B-4%B 2.5CV, 4%B 1.5CV, 4%B-7%B 6CV, 7%B-9%B 0.5CV, 9%B-100%B 2CV, 100%B 5CV). The title product **54** was obtained as cream colour solid (18 mg) with a 45% yield. Mp: 187.9-188.1°C. ^1H NMR (400 MHz, CDCl_3) δ 8.65 (br, 2H), 7.72 (td, J = 7.7, 1.6 Hz, 2H), 7.60 (s, 4H), 7.56 (d, J = 8.0 Hz, 2H), 7.28 (dd, J = 6.9, 5.3 Hz, 2H). ^{13}C NMR (101 MHz, CDCl_3) δ 150.00, 143.08, 136.62, 132.18, 127.56, 123.23, 122.96, 90.55, 89.25. HPLC-PDA-MS: RT = 5.89 min, 99.72% (254 nm), PDA λ_{max} = 319 nm, MS (m/z) $[\text{M}+\text{H}]^+$ 280.91. HRMS (m/z): $[\text{M}+\text{H}]^+$ calcd. for $\text{C}_{20}\text{H}_{13}\text{N}_2$, 281.1079; found, 281.1071.



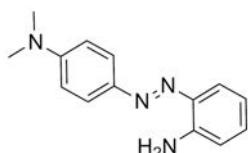
1,3-bis(pyridin-2-ylethynyl)benzene 53: 2-ethynylpyridine **101** (35 μL , 0.35 mmol) and dry diisopropylethylamine (DIPEA) (0.1 ml, 0.57 mmol) were added to a slurry of 1,3-diiodobenzene **135b** (46 mg, 0.14 mmol), CuI (2 mg, 0.01 mmol) and $\text{PdCl}_2(\text{PPh}_3)_2$ (5.4 mg, 0.01 mmol) in dry DMF (1 mL) in a *Schlenk* flask with argon atmosphere at room temperature. The

mixture was stirred at 50°C for 5 hours. The reaction mixture was diluted in EtOAc (15 mL) and washed with aqueous Na₂CO₃ 1 N (10 mL), saturated NaHCO₃ (10 mL), water (10 mL) and brine (10 mL), dried over anhydrous MgSO₄, filtered and concentrated in vacuo. The residue was purified by *flash* chromatography using *Biotage Isolera* equipment (SNAP KP-C18-HS 12g, A=H₂O B=MeCN; 0%B 5CV, 0%B-1%B 2CV, 1%B-4%B 2.5CV, 4%B 1.5CV, 4%B-7%B 6CV, 7%B-9%B 0.5CV, 9%B-100%B 2CV, 100%B 5CV). The title product **53** was obtained as brown solid (34 mg) with an 87% yield. Mp: 89.9-91.3°C. ¹H NMR (400 MHz, CDCl₃) δ 8.65 (br, 2H), 7.82 (t, J = 1.6 Hz, 1H), 7.70 (td, J = 7.7, 1.6 Hz, 2H), 7.60 (dd, J = 7.8, 1.6 Hz, 2H), 7.54 (d, J = 7.9 Hz, 2H), 7.37 (t, J = 7.7 Hz, 1H), 7.31 – 7.22 (m, 2H). ¹³C NMR (101 MHz, CDCl₃) δ 150.12, 143.22, 136.43, 135.42, 132.58, 128.76, 127.51, 123.16, 122.86, 89.33, 88.37. HPLC-PDA-MS: RT = 5.01 min, 99.87% (254 nm), PDA λ_{max} = 296 nm, MS (m/z) [M+H]⁺ 280.94. HRMS (m/z): [M+H]⁺ calcd. for C₂₀H₁₃N₂, 281.1079; found, 281.1072. HRMS (m/z): [2M+H]⁺ calcd. for C₄₀H₂₅N₄, 561.2079; found, 561.2079.

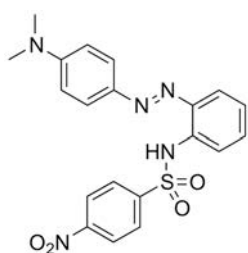


N-(4-(2-((4-(dimethylamino)phenyl)diazenyl)benzamido)phenyl) 140a: To a slurry of aniline **89c** (27 mg, 0.13 mmol), methyl red **145** (51 mg, 0.19 mmol) and HATU (145 mg, 0.38 mmol) in DMF (2 mL), it was added DIPEA (100 μL, 0.57 mmol) and the resulting mixture was stirred a temperature 14 h at 40°C. Afterwards, the reaction mixture was diluted in EtOAc (100 mL), washed with Na₂CO₃ 1N (30 mL), saturated NaHCO₃ (30 mL), water (30 mL) and brine (30 mL). The organic phase was dried over anhydrous MgSO₄, filtered and evaporated to dryness. The obtained solid was purified through silica *flash* column using *Biotage Isolera* equipment (SNAP KP-KPSil 10 g; A=DCM B=MeOH; 0%B 1CV, 0%B-3%B 5.5CV, 3%B-3.5%B 3CV, 3.5%B-5%B 2CV, 5%B-10%B 0.5CV, 10%B 4CV) and through C18 *flash* column using *Biotage Isolera* equipment (SNAP KP-C18-HS 12 g; A=H₂O B=MeOH; 0%B 3CV, 0%B-65%B 4CV, 65%B-100%B 6CV, 100%B 5CV and SNAP KP-C18-HS 12 g; A=H₂O + 0.2% formic acid B=MeCN + 0.2 % formic acid; 10%B 4CV, 10%B-100%B 10CV, 100%B 5CV) to obtain **140a** (54 mg, orange solid) with 49% yield. Mp: 193.4-194.2 °C. ¹H NMR (400 MHz, CDCl₃) δ 11.46 (br, 1H), 10.05 (br, 1H), 8.62 (d, J = 4.7 Hz, 1H), 8.49 (dd, J = 7.5, 1.9 Hz, 1H), 8.30 (d, J = 7.8 Hz, 1H), 7.95 – 7.88 (m, 1H), 7.89 (d, J = 9.3 Hz, 2H), 7.87 – 7.83 (m, 1H), 7.81 (s, 4H), 7.54 (pd, J = 7.2, 1.7 Hz, 2H), 7.48 (ddd, J = 7.6, 4.8, 1.1 Hz,

1H), 6.81 (d, J = 9.2 Hz, 2H), 3.17 (s, 6H). ¹³C NMR (101 MHz, CDCl₃) δ 164.07, 161.97, 153.53, 150.37, 149.97, 148.11, 143.54, 137.79, 135.48, 133.90, 132.22, 131.76, 129.82, 129.62, 126.53, 126.07, 122.43, 120.98, 120.39, 116.19, 111.84, 40.47. HPLC-PDA-MS: method C was used; RT: 6.72 min, [M+H]⁺ 464.96, λ_{max} = 453 nm; purity 96.05% (254 nm). HRMS (m/z): [M+H]⁺ calcd. for C₂₇H₂₅N₆O₂, 465.2039; found 465.2039.

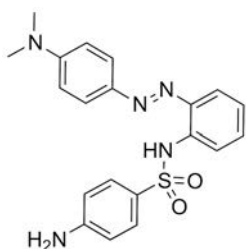


(4-((2-aminophenyl)diazenyl)-N,N-dimethylaniline 146: A solid mixture of 1,2-diaminobenzene **123c** (0,80 g, 7,4 mmol), *N,N*-dimethyl-4-nitrosoaniline **90d** (0,57 g, 3,8 mmol), and potassium hydroxide (0,62 g, 9,4 mmol) in powder was mixed thoroughly using a spatula while heating at 90 °C for 10 min. Toluene (10 ml) was added and the reaction was stirred at 90 °C for 1 hour and the resulting mixture was diluted with EtOAc (50 mL) and washed with water (30 mL), brine (2x30 mL). The organic phase was dried over anhydrous MgSO₄, filtered and evaporated to dryness. The obtained solid was purified through silica *flash* column using *Biotage Isolera* equipment (SNAP KP-Sil 50g, A=hexanes B=EtOAc; 0%B 3CV, 0%B-12%B 1CV, 12%B-20%B 8CV, 20%B-40%B 3.5CV, 40%B-100%B 1CV, 100%B 8.5CV) to afford **146** (0.52 g, red solid) with a 57% yield. ¹H NMR (400 MHz, CDCl₃) δ 7.82 (d, J = 9.0 Hz, 2H), 7.74 (dd, J = 8.0, 1.5 Hz, 1H), 7.15 (t, J = 7.6 Hz, 1H), 6.80 (t, J = 7.1 Hz, 1H), 6.77 – 6.72 (m, 3H), 5.55 (br, 2H), 3.07 (s, 6H). ¹³C NMR (101 MHz, CDCl₃) δ 151.89, 143.89, 143.05, 137.81, 130.65, 124.58, 124.16, 117.56, 116.83, 111.70, 40.36. NMR peaks match the previously reported²²⁵.

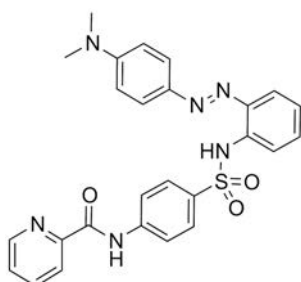


***N*-(2-((4-(dimethylamino)phenyl)diazenyl)phenyl)-4-nitrobenzenesulfonamide 148:** To a solution of azo compound **146** (134 mg, 0.56 mmol) and pyridine (49 ml, 0.61 mmol) in DCM (10 mL), it was added dropwise a solution of nosyl chloride **147** (112 mg, 0.51 mmol) in DCM (10 mL) and the resulting solution stirred 18 hours at room temperature. Afterwards, the solution was diluted in EtOAc (100 mL) and washed with HCl 1M (30 mL), saturated NaHCO₃ (30 mL), water (30 mL) and brine (30 mL), dried over anhydrous MgSO₄, filtered and evaporated to dryness to give compound **148** (155 mg, red solid, 72%), which was used

without further purification. ^1H NMR (400 MHz, CDCl_3) δ 9.87 (br, 1H), 8.08 (d, J = 8.9 Hz, 2H), 7.85 (d, J = 8.8 Hz, 2H), 7.72 – 7.66 (m, 3H), 7.64 (dd, J = 8.0, 1.4 Hz, 1H), 7.32 (td, J = 7.8, 1.5 Hz, 1H), 7.20 (td, J = 8.0, 1.2 Hz, 1H), 6.74 (d, J = 9.2 Hz, 2H), 3.14 (s, 6H). ^{13}C NMR (101 MHz, CDCl_3) δ 153.20, 150.12, 144.82, 142.74, 141.75, 132.07, 130.43, 128.43, 125.89, 125.29, 124.16, 122.45, 121.83, 111.75, 40.46. HRMS (m/z): $[\text{M}+\text{H}]^+$ calcd. for $\text{C}_{20}\text{H}_{20}\text{N}_5\text{O}_4\text{S}$, 426.1236; found 426.1223.

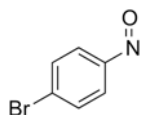


4-amino-*N*-(2-((4-(dimethylamino)phenyl)diazenyl)phenyl)benzenesulfonamide 149: A suspension of nitrocompound **148** (100 mg, 0.24 mmol) and sodium sulphide nonahydrate (124 mg, 0.52 mmol) in ethanol (8 mL) was stirred 2 h at reflux temperature. After cooling to rt the solvent was removed under vacuum and the resulting red residue was purified through silica *flash* column using *Biotage Isolera* equipment (SNAP KP-Sil 25g, A=DCM B=MeOH; 0%B 3CV, 0%B-0.5%B 4.5CV, 0.5%B-1%B 0.5CV, 0.5%B-2.7%B 11CV, 2.7%B-10%B 1.5CV, 10%B 3CV) to afford **149** (0.92 g, red solid) with a 98% yield. ^1H NMR (400 MHz, CDCl_3) δ 9.70 (br, 1H), 7.79 (d, J = 9.2 Hz, 2H), 7.66 (dd, J = 5.8, 1.5 Hz, 1H), 7.64 (dd, J = 6.1, 1.6 Hz, 1H), 7.29 – 7.23 (m, 1H), 6.75 (d, J = 9.2 Hz, 2H), 6.47 (d, J = 8.7 Hz, 2H), 3.98 (br, 2H), 3.12 (s, 6H). ^{13}C NMR (101 MHz, CDCl_3) δ 152.89, 150.70, 143.14, 140.70, 134.21, 130.48, 129.44, 127.64, 125.20, 124.09, 121.42, 120.06, 114.03, 111.66, 40.45. HRMS (m/z): $[\text{M}+\text{H}]^+$ calcd. for $\text{C}_{20}\text{H}_{22}\text{N}_5\text{O}_2\text{S}$, 396.1494; found 396.1476.

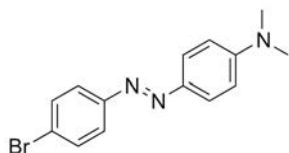


***N*-(4-(*N*-(2-((4-(dimethylamino)phenyl)diazenyl)phenyl)sulfamoyl)phenyl)picolinamide 141:** To a slurry of aniline **149** (19 mg, 0.05 mmol), picolinic acid **85j** (9 mg, 0.07 mmol) and HATU (57 mg, 0.15 mmol) in DMF (1.5 mL), it was added DIPEA (30 μL , 0.17 mmol) and the resulting mixture was stirred a temperature 18 h at 40°C. Afterwards, the suspension was diluted in EtOAc (40 mL) and washed with Na_2CO_3 1N (15 mL), saturated NaHCO_3 (15 mL), water (15 mL)

and brine (15 mL), dried over anhydrous MgSO_4 , filtered and evaporated to dryness. The obtained solid was purified twice through C18 *flash* column using *Biotage Isolera* equipment (SNAP KP-C18-HS 12 g; A= H_2O + 0.2% formic acid B= MeCN + 0.2% formic acid; 0%B 3CV, 0%B-50%B 4CV, 50%B-90%B 9CV, 90%B-100%B 1CV, 100%B 4CV; and SNAP KP-C18-HS 12 g; A= H_2O B= MeOH ; 0%B 3CV, 0%B-60%B 4CV, 60%B-100%B 8CV, 100%B 5CV) to obtain **141** (9 mg, orange solid) with 37% yield. Mp: 190.7-191.7 °C. ^1H NMR (400 MHz, CDCl_3) δ 10.11 (br, 1H), 9.83 (br, 1H), 8.58 (ddd, $J = 4.9, 1.6, 0.9$ Hz, 1H), 8.24 (dt, $J = 7.8, 1.1$ Hz, 1H), 7.90 (td, $J = 7.7, 1.7$ Hz, 1H), 7.86 – 7.71 (m, 6H), 7.68 (dd, $J = 8.3, 1.4$ Hz, 1H), 7.65 (dd, $J = 8.1, 1.5$ Hz, 1H), 7.49 (ddd, $J = 7.6, 4.7, 1.2$ Hz, 1H), 7.29 (ddd, $J = 8.8, 7.6, 1.8$ Hz, 1H), 7.12 (ddd, $J = 8.5, 7.3, 1.3$ Hz, 1H), 6.76 (d, $J = 9.2$ Hz, 2H), 3.12 (s, 6H). ^{13}C NMR (101 MHz, CDCl_3) δ 162.26, 152.83, 149.19, 148.17, 143.23, 141.90, 140.92, 137.98, 134.16, 133.57, 130.55, 128.71, 127.03, 125.25, 124.64, 122.69, 121.90, 120.56, 119.26, 111.93, 40.58. HPLC-PDA-MS: method C was used; RT: 6.54 min, $[\text{M}+\text{H}]^+$ 500.98, $\lambda_{\text{max}} = 455$ nm; purity 91.11% (254 nm). HRMS (m/z): $[\text{M}+\text{H}]^+$ calcd. for $\text{C}_{26}\text{H}_{25}\text{N}_6\text{O}_3\text{S}$, 501.1709; found 501.1705.

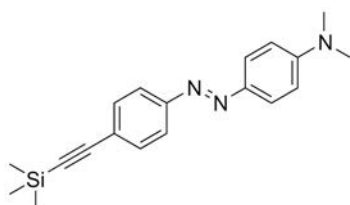


1-bromo-4-nitrosobenzene 90e: A solution of Oxone (2,9 g, 4.7 mmol) in water (28 mL) was added to a solution of 4-bromoaniline (**150**) (401 mg, 2.3 mmol) in DCM (7 mL) at r.t. and the resulting mixture was stirred 2 hours at r.t. with vigorous agitation. Additional DCM was added (30 mL), the layers were separated and the organic one was washed with water (5 mL) and brine (5 mL), dried over anhydrous Na_2SO_4 and concentrated to dryness to obtain the title product **90e**, which was previously described²²⁶, and was used without further purification (410 mg, 95%). ^1H NMR (400 MHz, CDCl_3) δ 7.78 (s, 2H), 7.78 (s, 2H). ^{13}C NMR (101 MHz, CDCl_3) δ 163.98, 132.86, 131.85, 122.28. ^1H and ^{13}C NMR chemical shifts matched to the ones described in the literature²²⁶.

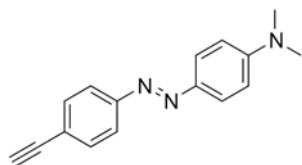


4-((4-bromophenyl)diazenyl)-N,N-dimethylaniline 152a: Two drops of AcOH were added to a solution of nitroso compound **90e** (60 mg, 0.32 mmol) and aniline **151a** (36 mg, 0.26 mmol) in DCM (2 mL) and was stirred 60 hours at room temperature. Afterwards, the solvent was evaporated under vacuum and the rests of AcOH were co-evaporated with toluene (2x3mL). The obtained residue was purified through silica *flash* chromatography using *Biotage Isolera*

equipment (SNAP KP-Sil 25g, A=hexanes B=AcOEt; 0%B 3CV, 0%B-5%B 1CV, 5%B-11%B 7CV, 11%B-100%B 3CV, 100%B 5CV). The title product **152a** was obtained (74 mg, orange solid) with a 92% yield. ^1H NMR (400 MHz, CDCl_3) δ 7.87 (d, $J = 9.2$ Hz, 2H), 7.72 (d, $J = 8.8$ Hz, 2H), 7.59 (d, $J = 8.8$ Hz, 2H), 6.75 (d, $J = 9.2$ Hz, 2H), 3.09 (s, 6H). ^{13}C NMR (101 MHz, CDCl_3) δ 152.76, 152.13, 143.63, 132.22, 125.28, 123.87, 123.40, 111.64, 40.45. HRMS (m/z): $[\text{M}+\text{H}]^+$ calcd. for $\text{C}_{14}\text{H}_{15}\text{N}_3\text{Br}$, 304.0449; found 304.0447.

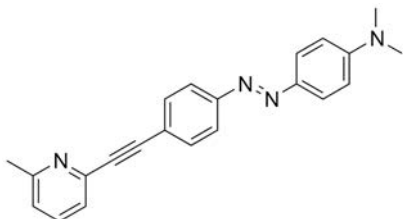


***N,N*-dimethyl-4-((4-((trimethylsilyl)ethynyl)phenyl)diazenyl)aniline 154a:** Ethynyltrimethylsilane **153** (46 μL , 0.32 mmol) and dry triethylamine (TEA) (0.1 ml, 0.72 mmol) were added to a mixture of bromocompound **152a** (49 mg, 0.16 mmol), CuI (4 mg, 0.02 mmol) and $\text{PdCl}_2(\text{PPh}_3)_2$ (15 mg, 0.02 mmol) in dry DMF (2 mL) in a *Schlenk* flask with argon atmosphere at room temperature. The reaction mixture was stirred at 50°C for 7.5 hours. The reaction mixture was diluted in EtOAc (58 mL) and washed with brine (3x30 mL), dried over anhydrous MgSO_4 , filtered and concentrated *in vacuo*. The residue was purified through silica *flash* chromatography using a *Biotage Isolera* equipment (SNAP KP-Sil 25g, A=hexanes B=EtOAc; 0%B 2CV, 0%B-7%B 10.5CV, 7%B-100%B 3CV, 100%B 6CV). The title product **154a** was obtained as an orange solid (50 mg) with a 97% yield. ^1H NMR (400 MHz, CDCl_3) δ 7.89 (d, $J = 9.1$ Hz, 2H), 7.80 (d, $J = 8.5$ Hz, 2H), 7.57 (d, $J = 8.6$ Hz, 2H), 6.96 (d, $J = 9.1$ Hz, 2H), 3.91 – 3.84 (m, 4H), 3.36 – 3.29 (m, 4H), 0.27 (s, 9H). ^{13}C NMR (101 MHz, CDCl_3) δ 153.42, 152.47, 145.82, 132.89, 124.96, 124.69, 122.47, 114.45, 105.07, 96.51, 66.79, 48.13, 0.10. $[\text{M}+\text{H}]^+$ calcd. for $\text{C}_{19}\text{H}_{24}\text{N}_3\text{Si}$, 322.1740; found 322.1743.

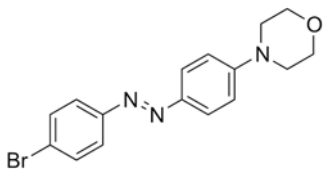


4-((4-ethynylphenyl)diazenyl)-*N,N*-dimethylaniline 155a: A mixture of azo compound **154a** (42 mg, 0.13 mmol) and K_2CO_3 (39 mg, 0.28 mmol) in a MeOH/THF 1:1 (4 mL) was stirred 2 h at r.t.. After that, it was diluted with EtOAc (50 mL), washed with water (3x30 mL), dried with MgSO_4 and concentrated *in vacuo*. The obtained residue corresponded to compound **155a** (31 mg, 95%) and was used without further purification. ^1H NMR (400 MHz, CDCl_3) δ 7.88 (d, $J = 9.2$ Hz, 2H), 7.80 (d, $J = 8.6$ Hz, 2H), 7.59 (d, $J = 8.5$ Hz, 2H), 6.75 (d, $J = 9.2$ Hz, 2H), 3.18 (s, 1H),

3.09 (s, 6H). ^{13}C NMR (101 MHz, CDCl_3) δ 153.06, 152.79, 143.79, 133.01, 125.36, 122.85, 122.29, 111.62, 83.86, 78.70, 40.43. $[\text{M}+\text{H}]^+$ calcd. for $\text{C}_{16}\text{H}_{16}\text{N}_3$, 250.1344; found 250.1345.

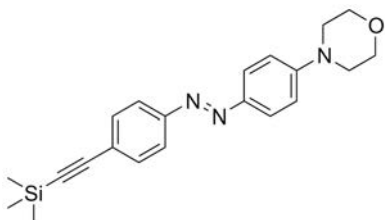


***N,N*-dimethyl-4-((4-((6-methylpyridin-2-yl)ethynyl)phenyl)diazenyl)aniline 142a:** 2-bromo-6-methylpyridine **156** (9 μL , 0.08 mmol) and dry triethylamine (TEA) (0.05 ml, 0.36 mmol) were added to a mixture of bromocompound **155a** (49 mg, 0.16 mmol), CuI (1 mg, 0.005 mmol) and $\text{PdCl}_2(\text{PPh}_3)_2$ (3.6 mg, 0.005 mmol) in dry DMF (2 mL) in a *Schlenk* flask under argon at room temperature. The mixture was stirred at 50°C for 7.5 hours. The reaction mixture was diluted in EtOAc (50 mL) and washed with 1N aq. Na_2CO_3 (30 mL), saturated aq. NaHCO_3 (30 mL), water (30 mL) and brine (30 mL). The organic phase was dried over anhydrous MgSO_4 , filtered and evaporated to dryness. The residue was purified through silica *flash* chromatography using *Biotage Isolera* equipment (SNAP KP-Sil 25g, A=DCM B=MeOH; 0%B 4CV, 0%B-1.6%B 14CV, 1.6%B-2%B 1CV, 2%B-10%B 2CV, 10%B 5CV). The title product **142a** was obtained as an orange solid (4 mg) with a 16% yield. Mp: 171.5-172.9°C (dec.). ^1H NMR (400 MHz, CDCl_3) δ 7.88 (d, J = 9.1 Hz, 2H), 7.83 (d, J = 8.5 Hz, 2H), 7.70 (d, J = 8.6 Hz, 2H), 7.58 (t, J = 7.7 Hz, 1H), 7.37 (d, J = 7.7 Hz, 1H), 7.12 (d, J = 7.8 Hz, 1H), 6.76 (d, J = 9.2 Hz, 2H), 3.10 (s, 6H), 2.60 (s, 3H). ^{13}C NMR (101 MHz, CDCl_3) δ 159.17, 153.08, 152.79, 143.87, 142.80, 136.53, 132.98, 125.38, 124.58, 123.19, 122.78, 122.36, 111.64, 90.47, 89.11, 40.44, 24.77. HPLC-PDA-MS: method C was used; RT: 7.16 min, $[\text{M}+\text{H}]^+$, 341.05, λ_{max} = 442 nm; purity 95.17% (254 nm). HRMS (m/z): $[\text{M}+\text{H}]^+$ calcd. for $\text{C}_{22}\text{H}_{21}\text{N}_4$, 341.1766; found 341.1735.

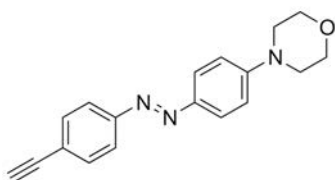


4-(4-((4-bromophenyl)diazenyl)phenyl)morpholine 152b: Two drops of AcOH were added to a solution of nitroso compound **90e** (60 mg, 0.32 mmol) and aniline **151b** (47 mg, 0.26 mmol) in DCM (2 mL) and the mixture was stirred 60 hours at room temperature. Afterwards, the solvent was evaporated under vacuum and the rests of AcOH were co-evaporated with toluene (2x3mL). The obtained residue was purified through silica *flash* chromatography using *Biotage Isolera* equipment (SNAP KP-Sil 25g, A=hexanes B=AcOEt; 0%B 1CV, 0%B-20%B 2CV,

20%B-26%B 3CV, 26%B-28%B 3CV, 28%B-35%B 2CV, 35%B-40%B 0.5CV, 40%B-100%B 1.5CV, 100%B 5CV). The title product **152b** was obtained (76 mg, orange solid) with an 83% yield. ^1H NMR (400 MHz, CDCl_3) δ 7.88 (d, $J = 9.0$ Hz, 2H), 7.74 (d, $J = 8.7$ Hz, 2H), 7.61 (d, $J = 8.7$ Hz, 2H), 6.96 (d, $J = 9.1$ Hz, 2H), 3.91 – 3.85 (m, 4H), 3.36 – 3.30 (m, 4H). ^{13}C NMR (101 MHz, CDCl_3) δ 153.45, 151.85, 145.62, 132.31, 124.94, 124.18, 124.07, 114.46, 66.78, 48.13. HRMS (m/z): $[\text{M}+\text{H}]^+$ calcd. for $\text{C}_{16}\text{H}_{17}\text{N}_3\text{OBr}$, 346.0555; found 345.0558.

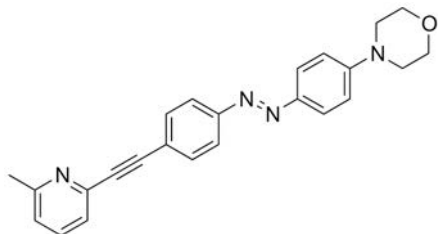


4-(4-((trimethylsilyl)ethynyl)phenyl)diazenyl)phenylmorpholine 154b: ethynyltrimethylsilane **153** (41 μL , 0.29 mmol) and dry triethylamine (TEA) (0.1 ml, 0.72 mmol) were added to a suspension of bromocompound **152b** (50 mg, 0.14 mmol), CuI (4 mg, 0.02 mmol) and $\text{PdCl}_2(\text{PPh}_3)_2$ (17 mg, 0.02 mmol) in dry DMF (2 mL) in a *Schlenk* flask under argon atmosphere at room temperature. The mixture was stirred at 50°C for 7.5 hours. The reaction mixture was diluted in EtOAc (58 mL), washed with brine (4x30 mL), dried over anhydrous MgSO_4 , filtered and concentrated *in vacuo*. The residue was purified through silica *flash* chromatography using *Biotage Isolera* equipment (SNAP KP-Sil 25g, A=hexanes B=EtOAc; 0%B 3CV, 0%B-3%B 4CV, 3%B 3CV, 3%B-6%B 3.5CV, 6%B-15%B 5CV, 15%B-100%B 3CV, 100%B 6CV). The title product **154b** was obtained as an orange solid (42 mg) with an 80% yield. ^1H NMR (400 MHz, CDCl_3) δ 7.89 (d, $J = 9.1$ Hz, 2H), 7.80 (d, $J = 8.5$ Hz, 2H), 7.57 (d, $J = 8.6$ Hz, 2H), 6.96 (d, $J = 9.1$ Hz, 2H), 3.91 – 3.84 (m, 4H), 3.36 – 3.29 (m, 4H), 0.27 (s, 9H). ^{13}C NMR (101 MHz, CDCl_3) δ 153.42, 152.47, 145.82, 132.89, 124.96, 124.69, 122.47, 114.45, 105.07, 96.51, 66.79, 48.13, 0.10. HRMS (m/z): $[\text{M}+\text{H}]^+$ calcd. for $\text{C}_{21}\text{H}_{26}\text{N}_3\text{OSi}$, 364.1845; found 364.1845.

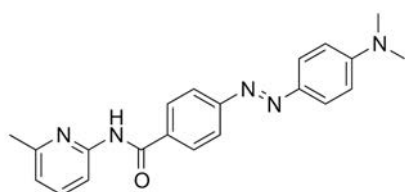


4-(4-((trimethylsilyl)ethynyl)phenyl)diazenyl)phenylmorpholine 155b: A slurry of azo compound **154b** (32 mg, 0.09 mmol) and K_2CO_3 (44 mg, 0.32 mmol) in MeOH/THF 1:1 (4 mL) was stirred 2 h at r.t.. After that, it was diluted with EtOAc (50 mL), washed with water (3x30 mL), dried with MgSO_4 and concentrated *in vacuo*. The obtained residue corresponded to compound **155b** (29 mg, 88%) and was used without further purification. ^1H NMR (400 MHz,

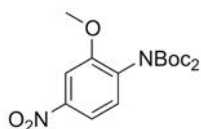
CDCl₃) δ 7.89 (d, J = 9.1 Hz, 2H), 7.82 (d, J = 8.6 Hz, 2H), 7.60 (d, J = 8.5 Hz, 2H), 6.97 (d, J = 9.1 Hz, 2H), 3.94 – 3.84 (m, 4H), 3.37 – 3.27 (m, 4H), 3.20 (s, 1H). ¹³C NMR (101 MHz, CDCl₃) δ 153.49, 152.76, 145.77, 133.05, 125.02, 123.60, 122.52, 114.44, 83.68, 79.05, 66.78, 48.12. [M+H]⁺ calcd. for C₁₈H₁₈N₃O, 292.1450; found 292.1452.



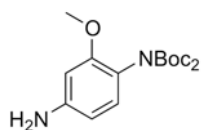
4-(4-((6-methylpyridin-2-yl)ethynyl)phenyl)diazenylphenyl)morpholine **142b:** 2-bromo-6-methylpyridine **156** (10 μL, 0.09 mmol) and dry triethylamine (TEA) (0.05 ml, 0.36 mmol) were added to a suspension of bromocompound **155b** (23 mg, 0.07 mmol), CuI (1 mg, 0.005 mmol) and PdCl₂(PPh₃)₂ (3.4 mg, 0.005 mmol) in dry DMF (1 mL) in a *Schlenk* flask filled with argon at room temperature. The mixture was stirred at 50°C for 7.5 hours. The reaction mixture was diluted in EtOAc (50 mL) and washed Na₂CO₃ 1N (30 mL), saturated NaHCO₃ (30 mL), water (30 mL) and brine (30 mL), dried over anhydrous MgSO₄, filtered and evaporated to dryness. The residue was purified by silica *flash* chromatography using *Biotage Isolera* equipment (SNAP KP-Sil 25g, A=DCM B=MeOH; 0%B 2.5CV, 0%B-1%B 1CV, 1%B-2%B 7.5CV, 2%B-10%B 2CV, 10%B 5CV) and it was additionally purified twice through C19 *flash* chromatography using *Biotage Isolera* equipment (SNAP KP-C18-HS 12 g; A=H₂O B=MeOH; 0%B 3CV, 0%B-50%B 4CV, 50%B-100%B 8CV, 100%B 8CV and SNAP KP-C18-HS 12 g; A=H₂O + 0.2% formic acid B=MeCN + 0.2% formic acid; 0%B 3CV, 0%B-55%B 4CV, 55%B-100%B 8CV, 100%B 5CV). The title product **142b** was obtained as an orange solid (10 mg) with a 38% yield. Mp: 209.3-210.8 °C. (dec.). ¹H NMR (400 MHz, CDCl₃) δ 7.90 (d, J = 9.1 Hz, 2H), 7.85 (d, J = 8.4 Hz, 2H), 7.71 (d, J = 8.5 Hz, 2H), 7.59 (t, J = 7.7 Hz, 1H), 7.38 (d, J = 7.6 Hz, 1H), 7.13 (d, J = 7.7 Hz, 1H), 6.97 (d, J = 9.1 Hz, 2H), 3.88 (dd, J = 5.9, 3.9 Hz, 4H), 3.34 (dd, J = 5.9, 3.9 Hz, 4H), 2.60 (s, 3H). ¹³C NMR (101 MHz, CDCl₃) δ 159.19, 153.47, 152.77, 145.85, 142.65, 136.62, 133.01, 125.03, 124.64, 123.91, 122.91, 122.59, 114.45, 90.68, 88.99, 66.79, 48.13, 24.72. HPLC-PDA-MS: method C was used; RT: 6.79 min, [M+H]⁺ 383.07, λ_{max} = 416 nm; purity 93.62% (254 nm). HRMS (m/z): [M+H]⁺ calcd. for C₂₄H₂₃N₄O, 383.1872; found 383.1855.



***N*-(4-(2-((4-(dimethylamino)phenyl)diazenyl)benzamido)phenyl) 143:** To a suspension of 2-amino-6-methyl pyridine **157** (20 mg, 0.19 mmol), **158** (33 mg, 0.12 mmol) and HATU (98 mg, 0.26 mmol) in DMF (1.5 mL), it was added DIPEA (45 μ L, 0.26 mmol) and the resulting mixture was stirred a temperature for 3 days at 40°C. The resulting solution was poured on 50 mL of 1N aqueous solution of Na₂CO₃ and backextracted with EtOAc (2x30 mL). The combined organic layers were washed with saturated NaHCO₃ (15 mL) and brine (15 mL), dried over anhydrous MgSO₄, filtered and evaporated to dryness. The obtained solid was purified through C18 *flash* column using *Biotage Isolera* equipment (SNAP KP-C18-HS 12 g; A=H₂O + 0.2% formic acid B=MeCN + 0.2% formic acid; 0%B 1CV, 0%B-55%B 5CV, 55%B-70%B 8CV, 70%B-100%B 3.5CV, 100%B 4CV) to obtain **143** (27 mg, orange solid) with 61% yield. Mp: 115.9-116.9°C. ¹H NMR (400 MHz, CDCl₃) δ 8.64 (br, 1H), 8.21 (d, *J* = 8.2 Hz, 1H), 8.04 (d, *J* = 8.6 Hz, 2H), 7.93 (d, *J* = 4.6 Hz, 2H), 7.91 (d, *J* = 5.0 Hz, 2H), 7.66 (t, *J* = 7.9 Hz, 1H), 6.94 (d, *J* = 7.4 Hz, 1H), 6.76 (d, *J* = 9.2 Hz, 2H), 3.11 (s, 6H), 2.49 (s, 3H). ¹³C NMR (101 MHz, CDCl₃) δ 165.30, 157.01, 155.64, 153.04, 150.97, 143.83, 138.95, 134.28, 128.31, 125.66, 122.56, 119.59, 111.61, 111.17, 40.43, 24.14. HPLC-PDA-MS: method C was used; RT: 6.65 min, [M+H]⁺ 360.05, λ_{\max} = 440 nm; purity 95.85% (254 nm). HRMS (*m/z*): [M+H]⁺ calcd. for C₂₁H₂₂N₅O, 360.1824, found 360.1823.

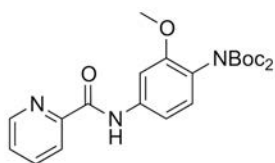


***N,N*-Di-*tert*-butoxycarbonyl-2-methoxy-4-nitroaniline 159a:** di-*tert*-butyldicarbonate (7.8 g, 36 mmol) was added to a solution of 2-methoxy-4-nitroaniline **87a** (2.0 g, 12 mmol) and DMAP (0.15 mg, 1.2 mmol) in THF (60 mL) and the resulting solution was stirred 16 h at r.t. and it was diluted in EtOAc (150 mL), washed with water (150 mL), dried over anhydrous Na₂SO₄, and concentrated to dryness. The residue was crystallised from a hexanes/diethylether to afford compound **159a**, previously described²²⁷ (yellow crystals, 3.7 g, 84% yield). ¹H NMR (400 MHz, CDCl₃) δ 7.85 (dd, *J* = 8.5, 2.4 Hz, 1H), 7.77 (d, *J* = 2.4 Hz, 1H), 7.27 (d, *J* = 8.5 Hz, 1H), 3.93 (s, 3H), 1.41 (s, 18H). ¹³C NMR (101 MHz, CDCl₃) δ 155.03, 150.81, 147.94, 134.75, 129.69, 115.94, 106.58, 83.33, 56.29, 27.99. HRMS (*m/z*): [2M+Na]⁺ calcd. for C₃₄H₄₈N₄O₁₄Na, 759.3065; found 759.3102.

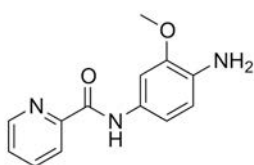


***N,N*-di-*tert*-butoxycarbonyl-3-methoxy-1,4-diaminobenzene 160a:** To a solution of the nitrocompound **159a** (2.0 g, 5.4 mmol) and 10% Pd/C (58 mg) in EtOAc (22 mL) was applied a

hydrogen atmosphere of 2 bar for 12 hours at room temperature. Afterwards, the black mixture was filtered through Celite, washed with EtOAc (2x10 mL) and the filtrate was evaporated to dryness. The crude product was used without further purification and corresponded to the title compound **160a**, previously described²²⁷ (yellow thick oil, 1.8 g, quantitative yield). ¹H NMR (400 MHz, CDCl₃) 6.83 (d, J = 8.9 Hz, 1H), 6.30 – 6.14 (m, 2H), 3.75 (s, 3H), 3.68 (br, 2H), 1.41 (s, 18H).

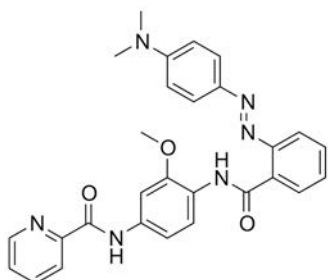


***N,N*-di-*tert*-butoxycarbonyl-2-methoxy-4-(picolinamido)aniline 161a:** To a solution of the aniline **160a** (2.1 g, 6.2 mmol) in DCM (12 mL), DIPEA (3.4 mL, 18.5 mmol) and picolinoyl chloride hydrochloride **86j** (1.3 g, 7.4 mmol) were added at 0°C and the resulting mixture was stirred during 16 h at r.t.. After that, a saturated solution of NaHCO₃ (50 mL) was added and the mixture was backextracted with DCM (3x30 mL). The combined organic layers were washed with brine (30 mL), dried over anhydrous Na₂SO₄, filtered and evaporated to dryness. The obtained orange solid corresponded to the title product **161a** (previously described⁹⁶) and was used without further purification (2.68 mg, 98% yield). ¹H NMR (400 MHz, CDCl₃) δ 10.09 (br, 1H), 8.63 (ddd, J = 4.8, 1.8, 0.9 Hz, 1H), 8.29 (d, J = 7.9 Hz, 1H), 7.92 (tt, J = 7.2, 1.0 Hz, 1H), 7.78 (s, 1H), 7.50 (ddt, J = 7.5, 4.8, 1.1 Hz, 1H), 7.13 – 7.02 (m, 2H), 3.88 (s, 3H), 1.40 (s, 18H). ¹³C NMR (101 MHz, CDCl₃) δ 162.13, 155.06, 151.92, 149.80, 148.13, 138.37, 137.91, 129.23, 126.70, 124.79, 122.47, 111.07, 103.18, 82.25, 55.76, 28.04.



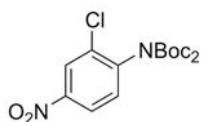
***N*-(4-amino-3-methoxyphenyl)picolinamide 95a:** Method B: Hydrochloric acid 4N in dioxane (2.0 ml, 7.9 mmol) was added dropwise to a solution compound **161a** (500 mg, 1.12 mmol) in DCM (11 mL) at 0 °C. After 15 min, the ice bath was removed and the solution was left under stirring for 3 h at rt. The orange solid in suspension obtained was filtered and diluted with EtOAc (60 mL). The resulting solution was washed with an 1N aqueous solution of Na₂CO₃ (30 mL), water (30 mL) and brine (30 mL), dried with anhydrous MgSO₄, filtered off, and solvent removed under vacuum to give the title compound **95a** (274 mg, quant.) as a cream solid that was used without further purification. ¹H NMR (400 MHz, CDCl₃) δ 9.89 (br, 1H), 8.60 (d, J = 4.7 Hz, 1H), 8.27 (d, J = 7.8 Hz, 1H), 7.89 (td, J = 7.7, 1.4 Hz, 1H), 7.61 (s, 1H), 7.46 (dd, J = 7.5, 4.8

Hz, 1H), 7.00 (dd, J = 8.3, 2.2 Hz, 1H), 6.75 (d, J = 8.3 Hz, 1H), 3.91 (s, 3H). ¹³C NMR (101 MHz, CDCl₃) δ 161.67, 150.23, 148.04, 147.64, 137.78, 132.56, 130.01, 126.33, 122.30, 115.19, 112.50, 103.78, 55.76. HRMS (m/z): [M+H]⁺ calcd. for C₁₃H₁₄N₃O₂, 244.1086 ; found, 244.1087.



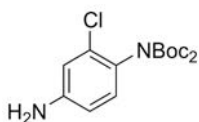
(E)-N-(4-(2-((4-(dimethylamino)phenyl)diazenyl)benzamido)-3-methoxyphenyl)picolinamide

140b: To a suspension of aniline **95a** (33 mg, 0.10 mmol), methyl red **145** (42 mg, 0.15 mmol) and HATU (118 mg, 0.31 mmol) in DMF (1 mL), it was added DIPEA (120 μL, 0.67 mmol) and the resulting mixture was stirred a temperature 14 h at 40°C. Afterwards, the reaction mixture was diluted in EtOAc (mL) and washed with Na₂CO₃ 1N (30 mL), saturated NaHCO₃ (30 mL), water (30 mL) and brine (30 mL), dried over anhydrous MgSO₄, filtered and evaporated to dryness. The obtained solid was purified through silica *flash* column using DCM as mobile phase and through a C18 *flash* column using *Biotage Isolera* equipment (SNAP KP-C18-HS 12 g; A=H₂O B=MeCN; 0%B 3CV, 0%B-65%B 4CV, 65%B-100%B 6CV, 100%B 5CV to obtain **140a** (14 mg, orange solid) with 28% yield. Mp: 189.9-190.5 °C. ¹H NMR (400 MHz, CDCl₃) δ 10.92 (br, 1H), 10.08 (br, 1H), 8.63 (ddd, J = 4.7, 1.6, 0.9 Hz, 1H), 8.60 (d, J = 8.7 Hz, 1H), 8.44 (dd, J = 7.6, 1.8 Hz, 1H), 8.29 (dt, J = 7.8, 0.9 Hz, 1H), 8.02 (d, J = 2.2 Hz, 1H), 7.97 (d, J = 9.2 Hz, 2H), 7.92 (td, J = 7.7, 1.7 Hz, 1H), 7.81 (dd, J = 7.9, 1.4 Hz, 1H), 7.58 – 7.47 (m, 3H), 7.00 (dd, J = 8.7, 2.3 Hz, 1H), 6.75 (d, J = 9.2 Hz, 2H), 3.73 (s, 3H), 3.13 (s, 6H). ¹³C NMR (101 MHz, CDCl₃) δ 164.32, 162.03, 153.22, 150.72, 149.96, 149.52, 148.18, 143.78, 137.86, 134.16, 132.00, 131.69, 130.53, 129.63, 126.59, 125.05, 122.34, 121.67, 116.30, 111.69, 111.51, 102.69, 55.73, 40.46. HPLC-PDA-MS: method D was used; RT: 4.23 min, [M+H]⁺ 494.83, λ_{max} = 460 nm; purity 98.23% (254 nm). HRMS (m/z): [M+H]⁺ calcd. for C₂₈H₂₇N₆O₃, 495.2145; found 495.2149.

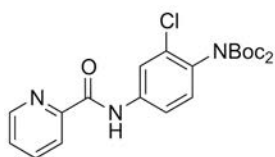


N,N-Di-tert-butoxycarbonyl-2-methoxy-4-nitroaniline 159b: di-tert-butyl dicarbonate **91** (7.6 g, 35 mmol) was added to a solution of 2-chloro-4-nitroaniline **87d** (2.0 g, 12 mmol) and DMAP (0.14 mg, 1.2 mmol) in THF (58 mL) and the resulting solution was stirred 16 h at r.t. and it was diluted in EtOAc (150 mL), washed with water (150 mL), dried over anhydrous Na₂SO₄, and

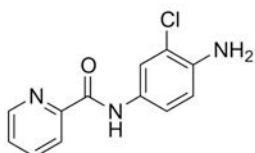
concentrated to dryness. The residue was crystallised from a hexanes/diethylether to afford compound **159b**, previously described⁹⁷ (white solid, 3.6 g, 82% yield). ¹H NMR (400 MHz, CDCl₃) δ 8.33 (d, J = 2.5 Hz, 1H), 8.15 (dd, J = 8.7, 2.5 Hz, 1H), 7.41 (d, J = 8.7 Hz, 1H), 1.41 (s, 18H). ¹³C NMR (101 MHz, CDCl₃) δ 149.69, 147.35, 143.15, 134.21, 130.73, 125.06, 122.46, 84.15, 27.90.



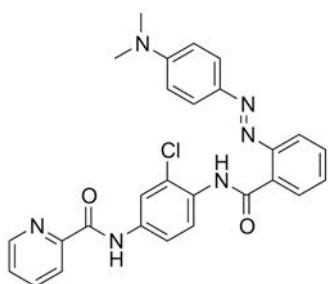
***N,N*-Di-*tert*-butoxycarbonyl-3-chloro-1,4-diaminobenzene 160b:** To a mixture of nitrocompound **159b** (3.2 g, 8.6 mmol) and 10% Pd/C (46 mg) in EtOAc (34 mL) was applied a hydrogen atmosphere of 2 bar for 12 hours at room temperature. Afterwards, the black dispersion was filtered through Celite, washed with EtOAc (2x10 mL) and the filtrate was evaporated to dryness. The obtained crude was used without further purification and corresponded to the title compound **161a**, previously described^{96,97} (transparent thick oil, 2.9 g, quantitative yield). ¹H NMR (400 MHz, CDCl₃) δ 6.94 (d, J = 8.5 Hz, 1H), 6.72 (d, J = 2.6 Hz, 1H), 6.53 (dd, J = 8.5, 2.6 Hz, 1H), 3.75 (br, 2H), 1.41 (s, 18H).



***N,N*-di-*tert*-butoxycarbonyl-2-methoxy-4-(picolinamido)aniline 161b:** To a solution of the aniline **160b** (2.8 g, 8.2 mmol) in DCM (12 mL) at 0°C, DIPEA (4.3 mL, 24.8 mmol) and picolinoyl chloride hydrochloride **86j** (1.8 g, 9.9 mmol) were added and the resulting mixture was stirred 16 h at r.t.. After that, a saturated solution of NaHCO₃ (50 mL) was added and the mixture was backextracted with DCM (3x30 mL). The combined organic layers were washed with brine (30 mL), dried over anhydrous Na₂SO₄, filtered and evaporated to dryness. The obtained orange solid corresponded to the title product **161b** (previously described^{96,97}) and was used without further purification (2.9 mg, 79% yield). ¹H NMR (400 MHz, CDCl₃) δ 10.11 (br, 1H), 8.62 (ddd, J = 4.8, 1.7, 0.9 Hz, 1H), 8.29 (d, J = 7.8 Hz, 1H), 8.03 (d, J = 2.4 Hz, 1H), 7.93 (td, J = 7.7, 1.7 Hz, 1H), 7.64 (dd, J = 8.6, 2.4 Hz, 1H), 7.51 (ddd, J = 7.6, 4.8, 1.2 Hz, 1H), 7.20 (d, J = 8.6 Hz, 1H), 1.40 (s, 18H).



***N*-(4-amino-3-chlorophenyl)picolinamide 95b**: 4N Hydrochloric acid in dioxane (2.0 ml, 7.8 mmol) was added dropwise to a solution compound **161b** (500 mg, 1.12 mmol) in DCM (11 mL) at 0 °C. After 15 min, the ice bath was removed and the solution was left stirring for 3 h at r.t. The orange solid in suspension obtained was filtered and diluted in EtOAc (60 mL). The resulting solution was washed with a 1N aqueous solution of Na₂CO₃ (30 mL), water (30 mL) and brine (30 mL), dried with anhydrous MgSO₄, filtered off, and solvent removed under vacuum to give the title compound **95b** (270 mg, 98% yield) as a cream solid that was used without further purification that was used without further purification. ¹H NMR (400 MHz, CDCl₃) δ 9.84 (br, 1H), 8.59 (ddd, J = 4.7, 1.7, 0.9 Hz, 1H), 8.27 (dt, J = 7.8, 1.1 Hz, 1H), 7.90 (td, J = 7.7, 1.7 Hz, 1H), 7.83 (d, J = 2.4 Hz, 1H), 7.46 (ddd, J = 7.6, 4.7, 1.2 Hz, 1H), 7.43 (dd, J = 8.6, 2.4 Hz, 1H), 6.78 (d, J = 8.6 Hz, 1H), 3.99 (br, 2H). ¹³C NMR (101 MHz, CDCl₃) δ 161.78, 149.94, 148.07, 139.90, 137.80, 129.72, 126.48, 122.42, 121.38, 119.90, 119.53, 116.09. HRMS (m/z): [M+H]⁺ calcd. for C₁₃H₁₄N₃O₂Cl, 248.0591 ; found, 248.0549.



***(E)*-*N*-(3-chloro-4-(2-((4-(dimethylamino)phenyl)diazenyl)benzamido)phenyl)picolinamide**

140c: To a suspension of aniline **95b** (23 mg, 0.09 mmol), methyl red **145** (38 mg, 0.14 mmol) and HATU (107 mg, 0.28 mmol) in DMF (1 mL), it was added DIPEA (100 μL, 0.6 mmol) and the resulting mixture was stirred a temperature 4 days at 40°C. Afterwards, the reaction mixture was diluted in EtOAc (100 mL) and washed with 1N aq. Na₂CO₃ (30 mL), saturated NaHCO₃ (30 mL), water (30 mL) and brine (30 mL), dried over anhydrous MgSO₄, filtered and evaporated to dryness. The obtained solid was purified through silica *flash* column using dichloromethane as mobile phase and through and through C18 *flash* column using *Biotage Isolera* equipment (SNAP KP-C18-HS 12 g; A=H₂O B=MeCN; 0%B 3CV, 0%B-65%B 4CV, 65%B-100%B 6CV, 100%B 5CV) to obtain **140c** (9 mg, orange solid) with 19% yield. Mp: 179.9-180.7 °C. ¹H NMR (400 MHz, CDCl₃) δ 11.05 (br, 1H), 10.06 (br, 1H), 8.62 (dd, J = 4.7, 0.5 Hz, 1H), 8.44 (dd, J = 7.7, 1.6 Hz, 1H), 8.43 (d, J = 8.8 Hz, 1H), 8.29 (d, J = 7.8 Hz, 1H), 8.25 (d, J = 2.4 Hz, 1H), 7.96 – 7.91 (m, 1H), 7.90 (d, J = 9.2 Hz, 2H), 7.83 (dd, J = 8.0, 1.2 Hz, 1H), 7.58 (td, J = 7.7, 1.7 Hz, 1H), 7.55 – 7.50 (m, 1H), 7.50 (ddd, J = 7.5, 4.9, 1.2 Hz, 1H), 7.46 (dd, J = 8.9, 2.5 Hz, 1H), 6.75 (d, J = 9.2 Hz, 2H), 3.13 (s, 6H). ¹³C NMR (101 MHz, CDCl₃) δ 164.84, 162.14, 153.47, 150.98, 149.60, 148.18,

143.46, 137.92, 134.60, 132.48, 131.99, 131.75, 129.56, 129.47, 126.78, 125.54, 124.63, 122.58, 120.56, 118.63, 116.63, 111.54, 40.44. HPLC-PDA-MS: method D was used; RT: 4.35 min, $[M+H]^+$ 498.84, λ_{\max} = 460 nm; purity 95.34% (254 nm). HRMS (m/z): $[M+H]^+$ calcd. for $C_{27}H_{24}N_6O_2Cl$, 499.1649; found 499.1650.

Photochemical characterisation

Materials and methods

Light source

As light sources, we used single or dual wavelength LED plates (*FCTecnics*) at a distance of 2-3 cm or a monochromator *Polychrome V* (*Till Photonics*), the potency was set at 100% and a bandwidth of 15 nm, coupled to an optic fibre placed at a distance of 5 cm from the sample. To evaluate the isomerisation of the samples spectrophotometrically, we applied continuous illumination for a minimum of two minutes on the sample solutions, placed in 10-mm Quartz *Suprasil* cells (*Hellma Analytics*).

UV-Visible absorption spectra

The absorption spectra of the photoisomerisable compounds were obtained with 25 μ M solutions in DMSO or MeCN using a *Varian Cary 300* UV-Vis spectrophotometer scanning between 650 nm and 300 nm with an average time of 33 ms at 5-nm intervals for full absorption spectra. To achieve UV-Vis spectra after illumination, we performed the measure immediately after illuminating for a minimum of two minutes.

Determination of optimal wavelengths for alloswitch-1 (83)

To determine the optimal illumination wavelengths to photoisomerise from *trans* to *cis* configuration, we recorded UV-Vis spectra with a *Varian Cary 300* UV-Vis spectrophotometer after illumination at defined wavelengths, extracted the maximal absorbance values around 380 nm and plotted them versus the illumination wavelength. For the reverse isomerisation, from *cis* to *trans* isomers, we recorded UV-Vis spectra after illumination at defined wavelengths and plotted them versus the last illumination wavelength. In all cases samples were solutions 25 μ M of alloswitch-1 (**83**) in DMSO/PBS 3:1.

Stability of the photoisomerisation

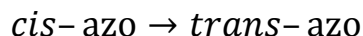
To examine the stability of the photoisomerisation, we evaluated the effect of repeated light cycles to sample of 25 μM of our compounds in DMSO, to affording *cis* and *trans* isomers and reading absorbance at a determined single wavelength after every illumination with a *Varian Cary 300* UV-Vis spectrophotometer.

Thermal relaxation of *cis* isomers

To determine the thermal relaxation rate of the *cis* isomers of our compounds, 25 μM solutions in PBS solution adjusted to pH = 7.4 with 1% DMSO (for compounds **83**, **84**, **109-115**) or in DMSO 100% (for compounds **140-143**) were prepared and illuminated with the a determined wavelength for minimum of two minutes. Absorbance was measured at a defined wavelength and with a specific frequency depending on the compound with a *Varian Cary 300* UV-Vis spectrophotometer. We calculated the relaxation half-life ($t_{1/2}$) by plotting absorbance readings versus time and by fitting the obtained curve to an exponential decay function, corresponding to a first-order reaction (*formulae 1*), with *GraphPad Prism 6* software.

Compound	λ of read (nm)	Frequency of read (s)	Compound	λ of read (nm)	Frequency of read (s)
83/109a	360	2	109l	360	5
84	395	0.2	112	330	5
109b	360	5	113	360	5
109c	380	5	114	395	5
109d	360	5	115	330	5
109e	360	5	140a	430	0.5
109f	360	5	140b	475	0.5
190g	360	5	140c	460	0.5
109h	360	5	141	435	0.5
109i	360	5	142a	460	0.5
109j	360	5	142b	430	0.5
109k	360	5	143	450	0.5

Table 21: Conditions used for the determination of thermal relaxation of *cis* isomers



$$A = A_0 \cdot e^{-kt} \quad k = \frac{1}{\tau} = \frac{\ln 2}{t_{1/2}}$$

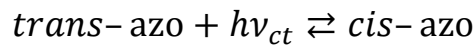
Formulae 1: Formulae for the thermal relaxation from *cis*- to *trans*-isomers corresponding to a direct first-order reaction.

Nuclear magnetic resonance (NMR)

To quantify the amount of *trans* and *cis* isomer of alloswitch-1 (**83**) we prepared a 250 μM solution in deuterated DMSO ($(\text{CD}_3)_2\text{SO}$) and placed 700 μL in a *Wilmad* screw-cap NMR tube, then we inserted an optical fibre inside the NMR tube through a septum cap till it slightly immersed into the solution, we closed the tube and it was introduced it into the NMR magnet probe of a *Variant-Innova 500 MHz* instrument. The optical fibre was coupled to an external monochromator *Polychrome V (Till Photonics)*. We performed ^1H NMR experiments with a single acquisition in dark conditions and 6 consecutive acquisitions under continuous illumination at 380 nm. Acquisitions consisted in 512 scans with a collecting time of 25 min 41 s. The obtained spectra from each acquisition were processed equally, integrating the region from 4.90 to 4.00 ppm, which corresponded to the methoxide protons of the *trans*-isomer, and the region from 3.59 to 3.69 ppm, corresponding to the same peak for the *cis* isomer. The area relations were converted to a molar percentage of *cis* isomer and this percentages were plotted versus time and the obtained curve was fitted to an exponential decay function, corresponding to a first-order equilibrium reaction (*formulae 2*), with *GraphPad Prism 6* software. The concentration of *cis*-**83**, corresponding to the plateau or the span values, is 80%.

Acquisition	Time means (min)	Area <i>trans</i> - 83	Area <i>cis</i> - 83	% <i>cis</i> - 83
dark	0	1.00	0.00	0%
1st	13	1.00	0.18	15%
2nd	39	1.00	0.54	35%
3rd	65	1.00	0.93	48%
4th	91	1.00	1.42	59%
5th	117	1.00	1.90	66%
6th	143	1.00	2.34	70%

Table 22: Quantification of amount of *trans*- and *cis*- **83** upon time of illumination on photoisomerisation assays with NMR detection.



$$[cis\text{-azo}] = [cis\text{-azo}]_{\infty} + [cis\text{-azo}]_{\infty} \cdot e^{-(k'_d+k_i)\cdot t}$$

concerning compound **83**:

$$[cis\text{-azo}] = 80.4 - 79.9e^{-0.0144t}$$

Formulae 2: Formulae for bidirectional reaction of *trans*- to *cis*-isomers to reach the photostationary equilibrium corresponding to a pseudo-first-order reaction, as light intensity remains constant.

Pharmacological characterisation

Functional cell-based assays

Cell culture and transfection

Materials and methods

HEK293 cells were cultured and transfected by electroporation for expression of all rat mGlu receptors as explained in the procedure section. Cultures were performed in Dulbecco's modified Eagle's medium (*Gibco* DMEM; *Thermo Fisher Scientific*) supplemented with 10% fetal calf serum (DMEM, *Thermo Fisher Scientific*). For those mGlu receptors that are not naturally linked to the phospholipase C (PLC) signalling pathway (all except mGlu_{1/5}), we co-transfected a chimeric G_{q/i}-protein (G_q top) to couple receptor activation to the PLC pathway and obtain IP production²²⁸. To maintain ambient glutamate at minimal concentrations, we co-transfected the excitatory amino acid transporter 1 (EAAC1). All receptors contained an HA tag in their *N*-terminus to monitor their cell surface expression by ELISA. Once transfected, cells were seeded in black clear-bottom 96-well plates at a concentration of 1.5 × 10⁵ cells/well. At least 6 h later, we changed the medium to glutamate-free DMEM *GlutaMAX-1* (*Thermo Fisher Scientific*).

Procedure

First of all, we prepared the two DNA mixes in different eppendorf tubes, as the following table shows for each one of the mGlu receptors corresponding a 20 million cells. The plasmid solution concentration was generally 1 µg/µL.

After that, the black 96-well plates with opaque-bottom (for classic IP accumulation experiment) or with transparent bottom (for IP accumulation with illumination) were filled with 50 µL of poly-L-ornithine 1x (PLO), and they were left in the incubator at 37°C and 5% CO₂

for 30 minutes minimum. We selected dishes with HEK293 cells with a 70% of confluence and removed the medium of the dishes. Then the cells were washed with 3-5 mL of PBS and 3 mL of trypsin were added in each dish and then were left in the incubator at 37°C and 5% CO₂ for 5-10 minutes.

	mGlu ₁	mGlu ₅	mGlu ₂	mGlu ₃
mGlu	4 µL (4 µg)	1.2 µL (1.2 µg)	8 µL (8 µg)	8 µL (8 µg)
EAAC1	4 µL (4 µg)	4 µL (4 µg)	4 µL (4 µg)	4 µL (4 µg)
Gq top	0 µL	0 µL	4 µL (4 µg)	4 µL (4 µg)
H2O	296 µL	298.8 µL	288 µL	288 µL
EB5x	80 µL	80 µL	80 µL	80 µL
MgSO4	16 µL	16 µL	16 µL	16 µL
	mGlu ₄	mGlu ₆	mGlu ₇	mGlu ₈
mGlu	7 µL (7 µg)	12 µL (12 µg)	10 µL (10 µg)	6 µL (6 µg)
EAAC1	4 µL (4 µg)	4 µL (4 µg)	4 µL (4 µg)	3 µL (3 µg)
Gq top	4 µL (4 µg)	4 µL (4 µg)	6 µL (4 µg)	3 µL (4 µg)
H2O	289 µL	284 µL	284 µL	292 µL
EB5x	80 µL	80 µL	80 µL	80 µL
MgSO4	16 µL	16 µL	16 µL	16 µL

Table 23: Amounts of DNA solutions and buffers used in transfection of HEK293 cells per mGlu receptor subtype.

Afterwards, we added 7 mL of DMEM to each dish with trypsin, homogenised the cell suspensions and placed in two *falcon* tubes. Then we counted the amount of cells in the suspension taking a 20 µL with the aid of a Malasez chamber.

We centrifuged the *falcon* tube with the cell suspension is 5 minutes at 1000 rpm. After that, the supernatant was aspired and we added the corresponding volume of electroporation buffer (EB1x) to obtain a cell suspension of 10 million cells per 100 µL.

We added 200 µL of a freshly prepared cell suspension to each *ependorf* tube with the corresponding DNA mix and we placed the obtained suspensions in an electroporation cuvette and were electroporated with the programme of 10 million cells. The obtained Tc should be between 16 and 24 ms.

Then, we placed the living cells of each cuvette in a falcon tube with 19-20 mL of DMEM. The tubes with the same transfected cells were joined and homogenised.

Afterwards, the PLO solution was aspirated from the plates washed every well with 100 μL of PBS and 150 μL of each cell solution was added to every well of the corresponding plate. Then the plates were kept in the incubator at 37°C and 5% CO_2 . Between 4 hours later and 4 hours before the experiment, we removed the medium and added 100 μL of *Glutamax* medium and the plates were kept in the incubator at 37°C and 5% CO_2 .

IP accumulation assays

General materials and methods

We estimated IP accumulation using the *IP-One HTRF* kit (*Cisbio Bioassays*) according to the manufacturer's instructions. Cells were stimulated to induce IP accumulation while being treated with test compounds for 30 min, at 37 °C and 5% CO_2 . For experiments with illumination, the plates placed over an LED plate (*FCTecnics*) at a distance of 2–3 cm with continuous illumination during the stimulation with the compounds. To allow stimulation in both dark conditions and violet light illumination, one-half of the 96-well plate bottom was covered with aluminium foil. To avoid effects derived from the fast relaxation of photoisomerisable compounds in aqueous solution after the 30-min stimulation, we washed cells once in stimulation buffer alone before continuing with the lysis step of the assay protocol. For fluorescence readings with a *RUBYstar HTRF HTS* microplate reader (*BMG Labtech*), we transferred cell lysates to a black opaque-bottom 96-well plate only for plates cells stimulated under illumination. The fluorescence of the non-illuminated plates was read directly. Data was analysed, dose-response curves were fitted to the corresponding sigmoidal curve and variance analysis was done with *GraphPad Prism 6*.

HTRF IP-One basis

The IP accumulation assay that we used is based in a time resolved FRET^a, using a terbium cryptate donor, which emits fluorescence at 620 nm, and an acceptor that emits at 665 upon Förster resonance energy transfer. Additionally, this fluorescence is characteristically long-lived and introducing a time delay of approximately 50 to 150 μs between the system excitation and fluorescence measurement allows the signal to be cleared of all non-specific short-lived emissions. Particularly, in HTRF IP-One assay we used a specific inositol phosphate (IP) antibody labelled with the terbium cryptate (FRET donor) and IP labelled with the FRET acceptor (d2).

^a Förster resonance energy transfer

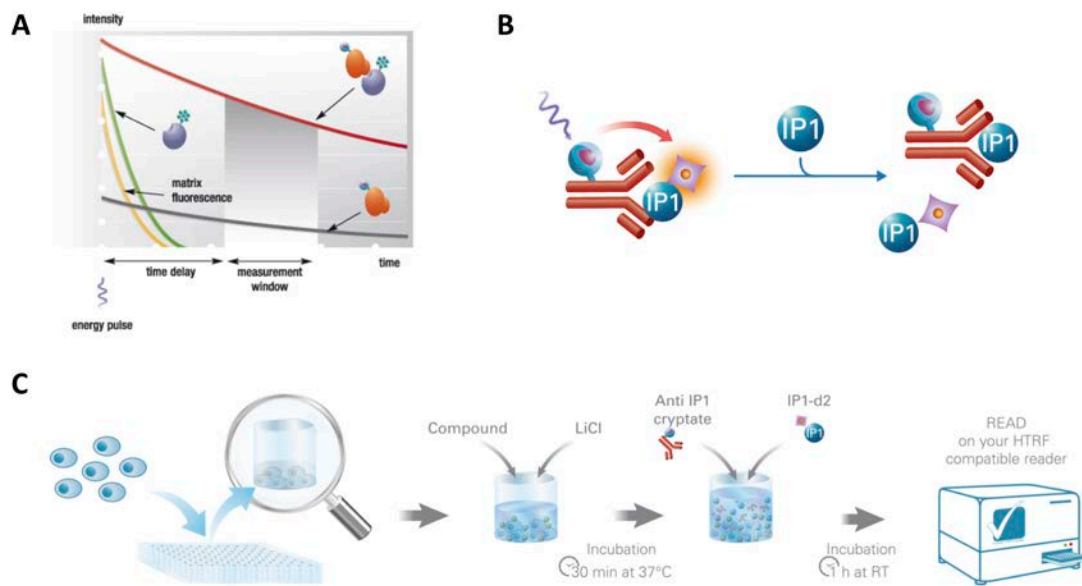


Figure 88: Basis of IP-One HTRF assay. (A) HTRF emission is time-delayed and avoids interferences with conventional fluorescence at the measurement point. (B) A terbium-cryptate-labelled antibody and a d2-labelled IP are used, which produce FRET upon recognition. Cell-production of IP induces a competition with the introduced d2-labelled IP for the recognition of the antibody, leading a single donor emission or FRET emission. (C) Diagram of the procedure of *IP-One* assay.

The procedure of the assay begins with 30 minutes of incubation of the compounds to be tested dissolved IP-One HTRF stimulation buffer (*Cisbio Bioassays*) in cells previously cultured and overexpressing the receptor we want stimulate. This buffer contains lithium chloride, that inhibits the degradation of intracellular inositol phosphate (IP) to *myo*-inositol, leading to a IP accumulation in the cytosol. Subsequent addition of the labelled antibody and d2-IP in a lysis buffer, produces rupture of the membranes of the cells and a competition of the introduced d2-labelled IP and the cell-produced IP for the recognition of the antibody, leading to FRET emission or a single donor emission respectively. Therefore, the fluorescence emissions could be read to obtain the results as a ratio of fluorescence detection at 665 nm and 620 nm. Afterwards we normalised the top and the bottom values between 0 and 100% of receptor activation with the values of a control compound with well-defined standardised pharmacology.

Procedure for single dose screening

First of all the solution of the compounds to be tested were prepared as depicted in *table 24* in IP-One stimulation buffer. We removed the medium from the black 96-well plate with transfected HEK293 cells, and added 70 μ L of the corresponding solution in every well. Every compound was tested with 3 replicates inside the plate. Then the plates were left incubating the compounds at 37°C and 5% CO₂ for 30 minutes. After that, we removed the cellular

medium with the compounds and added 70 μL of stimulation buffer per well and 15 μL of solution of d2 and 15 μL of solution of terbium cryptate in HTRS lysis buffer (*Cisbio Bioassays*). We left the plates protected from light incubating a minimum of 1 hour at room temperature and the fluorescence was read with a *RUBYstar HTRF HTS* microplate reader (*BMG Labtech*).

	Chapter 3		Chapter 5	
	mGlu ₄	mGlu ₅	mGlu ₄	mGlu ₅
Compound to test	30 μM	30 μM	50 μM	50 μM
Orthosteric agonist	50 nM (L-AP ₄)	30 nM	3 nM (for PAM) 300 nM (for NAM)	1 nM (for PAM) 100 nM (for NAM)

Table 24: Concentrations used of compounds to test and orthosteric agonists for single-dose screenings.

Procedure for dose-response curves without illumination

First we prepared eight intermediate solutions of each compound to be tested with *IP-One stimulation buffer* (*Cisbio Bioassays*) and we added another solution of the corresponding orthosteric agonist (L-AP₄ 10 nM for mGlu₄ PAM evaluation, quisqualate 300 nM for mGlu₅ NAM evaluation), also in the same buffer, obtain a constant dilution for all the points of the dose-response curve.

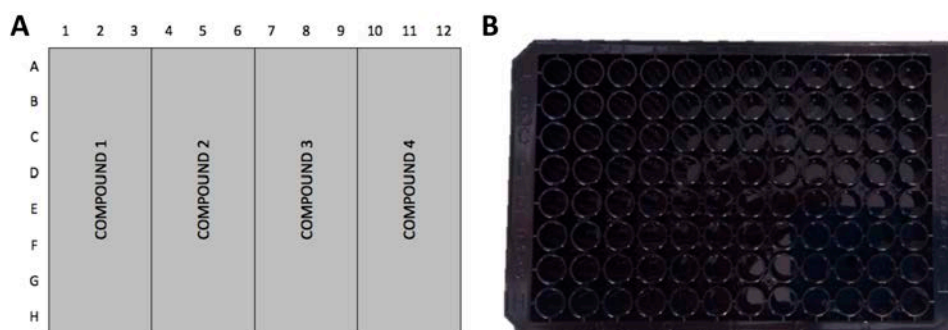


Figure 89: Plates used for dose-response curves without illumination. (A) Disposition of the compounds on the plates with three replicates per point of the resulting curve. (B) Black bottom 96-well plate used in these experiments.

We removed the medium in a dark opaque-bottom 96-well plate with HEK293 cells expressing the corresponding receptor and added 70 μL of the corresponding solution in every well. For each compound, we generated a dose response curve with eight points with three replicates per point. Then the plates were left incubating the compounds at 37°C and 5% CO₂ for 30 minutes. After that, we removed the cellular medium with the compounds and added 70 μL of stimulation buffer per well and 15 μL of solution of d2 and 15 μL of solution of terbium cryptate in *HTRF lysis buffer* (*Cisbio Bioassays*). The plates were protected from light and

incubated a minimum of 1 hour at room temperature and the fluorescence was read *with a RUBYstar HTRF HTS microplate reader (BMG Labtech)*.

Dose-response curves with illumination

The procedure was the same for the dose-response curves without illumination with little variations to be able to evaluate photoswitching properties of azocompounds. We generated eight-point-dose-response curves, corresponding to eight concentrations of compound tested. We removed the medium from the black 96-well plate with transfected HEK293 cells, and added 70 μ L of the corresponding solution in every well. We located two of the replicates in the six first columns of the plate and the two resting on the six last columns (*figure 90A*) and we covered the bottom part of the six first columns with aluminium foil and paper strips to affix it (*figure 90BC*).

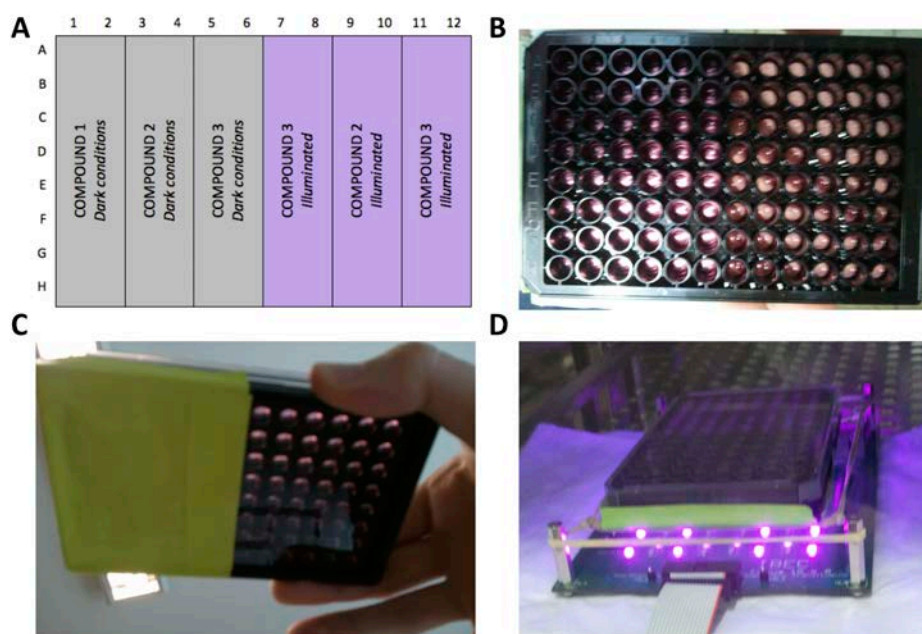


Figure 90: Plates used for dose-response curves with illumination. (A) Arrangement of the compounds on the plates with two replicates per point of the resulting curve. Violet background corresponds to the solutions illuminated during the incubation of the compounds and grey background to those compounds protected from light. (B) Transparent bottom 96-well plate used in these experiments from the top. (C) Transparent bottom 96-well plate used in these experiments from the bottom. Half of the bottom of the plate was covered with aluminium foil and strips to protect the cells and compounds solutions from light. (D) Incubation of the compounds with the cells with illumination from the bottom with a LED-plate with half of the plate protected from light.

For the stimulation, we placed the plate over a LED-plate with the desired photoswitching wavelength (*figure 90D*) and we stimulated the cells with the compounds at 37°C and 5% CO₂ for 30 minutes in dark conditions (located in the covered half of the plate) and under illumination (located in the uncovered half of the plate) in parallel. After the incubation, we

removed the cellular medium with the compounds and added 70 μL of stimulation buffer per well and 15 μL of solution of d2 and 15 μL of solution of terbium cryptate in HTRS lysis buffer (*Cisbio Bioassays*). We left the plates protected from light incubating a minimum of 1 hour at room temperature and the fluorescence was read with a *RUBYstar HTRF HTS* microplate reader (*BMG Labtech*).

However, as it is described in *chapter 3*, we obtained some biphasic curves probably due to unspecific adhesion of compounds to the end of the pipette tips, and the subsequent release in next wells, leading to increased concentrations. In fact, during experiments it was possible to observe a slight coloration of the tips (*figure 91*).



Figure 91: Orange-reddish dyed pipette tip after performing dilutions without changing the tips.

To prove that hypothesis, we introduced two modifications on the procedure, while preparing the eight concentrations of compound tested, to generate the dose-response curve:

- 1) The compound solutions of the orthosteric agonists were added without mixing the resulting solution. They were mixed just before adding them to each well of the plate where the cells were placed.
- 2) The pipette tips were changed after every dilution, so as not to retain and release undesired amounts of compounds into the most diluted dissolutions.

The rest of the protocol was exactly the same than explained above. We removed the medium from the black 96-well plate with transfected HEK293 cells, and added 70 μL of the corresponding solution in every well. We located two of the replicates in the six first columns of the plate and the two resting on the six last columns and we covered the bottom part of the six first columns with aluminium foil and paper strips to affix it. For the stimulation, we placed the plate over a LED-plate with the desired photoswitching wavelength and we stimulated the cells with the compounds at 37°C and 5% CO_2 for 30 minutes in dark conditions (located in the

covered half of the plate) or under illumination (located in the uncovered half of the plate) in parallel. After the incubation, we removed the cellular medium with the compounds and added 70 μ L of stimulation buffer per well and 15 μ L of solution of d2 and 15 μ L of solution of terbium cryptate in HTRS lysis buffer (*Cisbio Bioassays*). We left the plates protected from light incubating a minimum of 1 hour at room temperature and the fluorescence was read with a *RUBYstar HTRF HTS* microplate reader (*BMG Labtech*).

After validating the “changing tip” protocol, the dilutions for dose response curves were performed with this improved protocol.

Procedure for selectivity assays with illumination

The selectivity assays procedure is very similar to the single-dose screening. We used it to test a single dose of a compound on the eight subtypes of mGlu receptors, as PAMs are NAMs. To do that we used two black plates with transparent bottom with HEK293 cells overexpressing a single mGlu subtype every two rows (*figure 92A*).

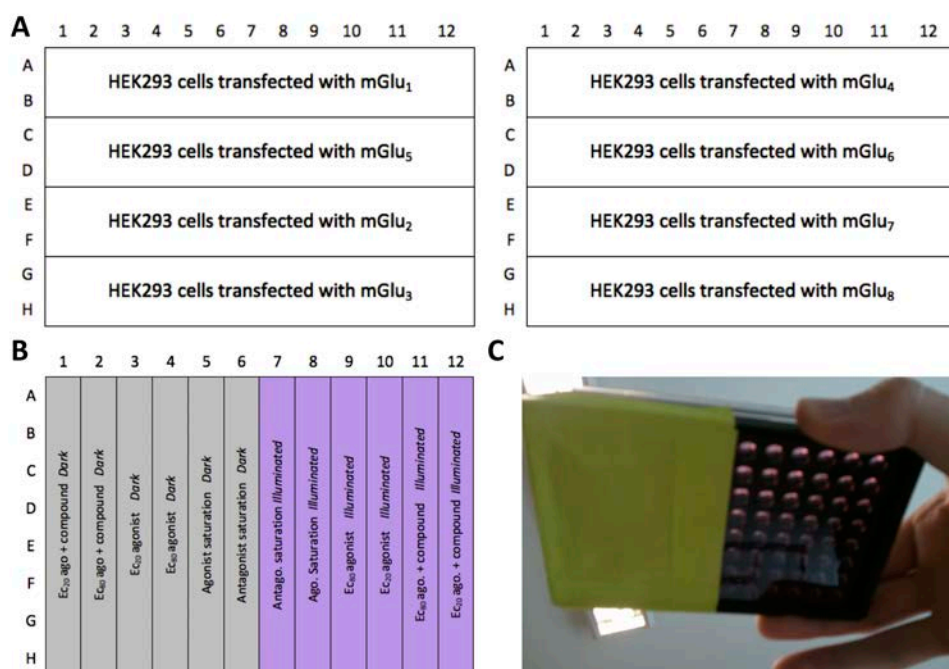


Figure 92: Plates used for selectivity assays under illumination. (A) Disposition of the different HEK293 cells transfected with different mGlu subtypes on two 96-well plates (B) Disposition of the compounds on the plates with two replicates per point of the resulting curve. Violet background corresponds to the solutions illuminated on the incubation of the compounds and grey background to those compounds protected from illumination. (C) Transparent bottom 96-well plate used in these experiments from the bottom. Half of the bottom of the plate was covered with aluminium foil and strips to protect the cells and compounds solutions from light.

The solutions to stimulate the cells were prepared with *HTRF IP-One stimulation buffer (Cisbio Assays)*, with the corresponding orthosteric agonists specific for each mGlu subtype, as depicted in *table 25*, and with the testing concentration of the photochromic compound under evaluation. We did four replicates for each dilution: two for evaluation in dark conditions and two for evaluation under illumination (*figure 92B*).

We removed the medium from the black 96-well plate with transfected HEK293 cells, and added 70 μL of the corresponding solution in every well. We located two of the replicates in the six first columns of the plate and the two resting on the six last columns and we covered the bottom part of the six first columns with aluminium foil and paper strips to affix it. For the stimulation, we placed the plate over a LED-plate with the desired photoswitching wavelength (and we stimulated the cells with the compounds at 37°C and 5% CO_2 for 30 minutes in dark conditions (located in the covered half of the plate) or under illumination (located in the uncovered half of the plate) in parallel. After the incubation, we removed the cellular medium with the compounds and added 70 μL of stimulation buffer per well and 15 μL of solution of d2 and 15 μL of solution of terbium cryptate in HTRS lysis buffer (*Cisbio Bioassays*). We left the plates protected from light incubating a minimum of 1 hour at room temperature and the fluorescence was read with a *RUBYstar HTRF HTS microplate reader (BMG Labtech)*.

Group	Subtype	Orth. ago	Low dose ($\approx\text{EC}_{20}$)	High dose ($\approx\text{EC}_{80}$)	Saturating dose
I	mGlu ₁	Quisqualic acid (2)	20 nM	2 μM	200 μM
	mGlu ₅		0.5 nM	100 nM	10 μM^+
II	mGlu ₂	LY 354740 (3)	1 nM	100 nM	10 μM
	mGlu ₃		2 nM*	200 nM	20 μM
III	mGlu ₄	L-AP4 (4)	3 nM ⁺	300 nM ⁺	30 μM^+
	mGlu ₇		100 nM	10 μM	1 mM
	mGlu ₈		5 μM	500 μM	10 mM
	mGlu ₆		10 nM	1 μM	100 μM

Table 25: Doses used for every receptor for the study of the selectivity. Low doses were used to evaluate PAM effects, high doses to evaluate NAM effects, saturating doses as an agonist control and a concentration of LY341495 200 μM for every subtype as an antagonist control. *An additional 100 nM of LY341495 was added to the low dose and the high doses for mGlu₃ to decrease its constitutive activity. ⁺For evaluating compound **83** saturating dose of quisqualate was 5 μM for mGlu₅ and, for mGlu₄, low dose of L-AP₄ 5 nM, high dose 500 nM and saturating dose 50 μM .

In-vivo zebrafish assays

Fish crossing and embryo growth

We performed the *in-vivo* locomotion experiments with TL zebrafish larvae (*danio rerio*) 7 days after fertilisation of the eggs.

To obtain fertilised eggs we used a small fish tank with a porous bottom placed inside another tank, with a solid bottom, full of water. Inside the fish tank there is a mobile plastic barrier that separates the tank in two chambers. One of these chambers contained a plastic plant inside. We selected one male and one female individual and put the female in the chamber with the plastic plant and the male in the other chamber (*figure 93A*). They were covered from light during 16 hours. After that we uncovered the fish, removed the barrier that separated the tank and inclined the internal tank between 30 and 45°. Then the fish crossed producing a considerable amount of fertilized eggs (*figure 93B*).

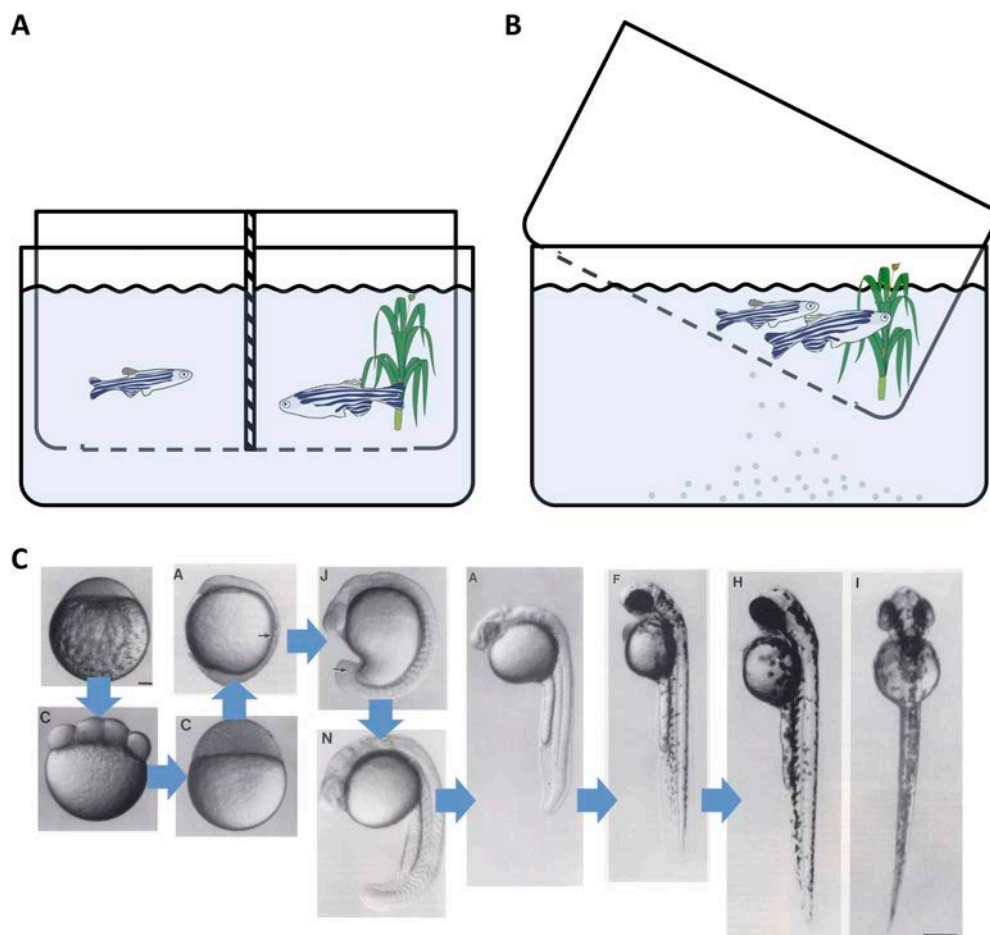


Figure 93: Fish-crossing methodology and zebrafish embryo and larvae growth. (A) Arrangement of the zebrafish male (left) and female (right) in a reproduction tank 12 hours before crossing. (B) Configuration of the zebrafish

male and female in a reproduction tank during crossing time. Fertilised eggs fell through the porous bottom of the tank. (C) Evolution from a fertilised egg, to an embryo stage and a larva stage after 4 days approximately.

We collected the eggs, and removed the non-fertilised ones and the impurities from the medium. After that, we left the eggs in an incubator at 18 °C during 7 days to allow the embryos grow, hatching out and growing as larvae (*figure 93C*). During these days we cleaned the water regularly and removed the dead eggs or the embryos and larvae with malformations or strange behaviour. After these 7 days the zebrafish embryos are ready for the experiment.

Zebrafish larvae locomotion experiment

General materials and methods

Fish locomotion was measured with an IR camera in a *Zebrabox* prototype (*ViewPoint*), which recorded all movement of the fish (*figure 94A*). This *Zebrabox* is also equipped with two LED plates over the emplacement of the fish and a white light lamp from the bottom to illuminate the animal containers (*figure 94B*). We used 7-day-after-fertilization zebrafish larvae and recorded the locomotion during 30 minutes after the application of the compounds (10 µM). Using the same animal individuals, the photoswitching experiment was next performed. This consisted in maintaining the fish 1 minute in the dark and after applying 6 cycles of 1 minute with illumination with violet light (380 nm), 5 seconds with white light and 55 seconds in the dark. Data and parameters obtained from *Zebralab* software (*ViewPoint*) were analysed with *Microsoft Excel 2011* and *GraphPad Prism 6*.

Procedure

We first placed one zebrafish larva per well in a transparent 96-well plate (*Corning Costar*) with the aid of a pipette (100µL of total volume) (*figure 94C*) and put the plate inside the *Zebrabox* (*figure 94A*) during 30 minutes, so as the fish to acclimatise to the environment and temperature of the instrument. After that we applied 100 µL of a 20 µM solution of the testing compound with a 0.2% of DMSO (to a final concentration of 10 µM with a 0.1% DMSO) and place again the plate inside the *Zebrabox*. Then we started the first experiment of 30 minutes in dark conditions, in which the movement of the fish in every well was monitored and integrated in periods of 5 minutes. *Zebralab* software analysed individually the track of every fish, and differentiate the swimming distances lower than 2 mm and the larger than 2 mm (green and red tracks respectively on *figure 94D*) and also proportionated several variables to analyse properly the animal behaviour, like long and short swimming distance, time of mobility, times in which the fish are moving, etc. For our application the sum of the short and large swimming distance provided the most helpful results.

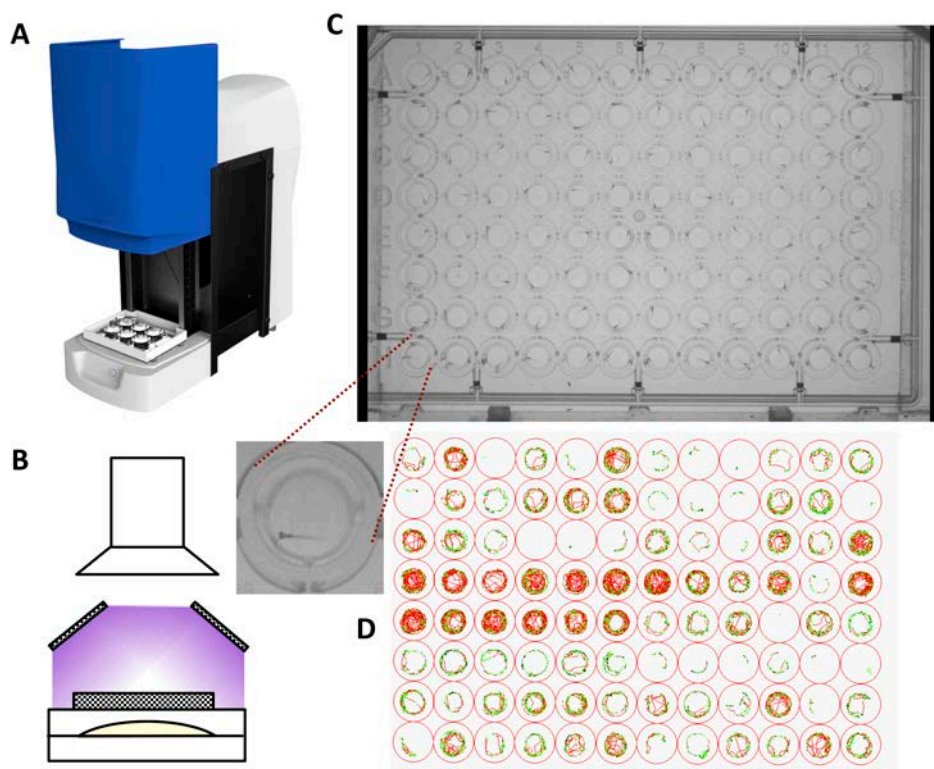


Figure 94: Zebrafish embryos locomotion materials and instruments. (A) *Zebabox* prototype. (B) Diagram of the *Zebabox* functioning: an IR camera on the top with two LED plates for illuminating the samples from the top in diagonal and a white lamp to illuminate the samples from the bottom. (C) We used transparent 96-well plates with one larva in each well. (D) Output form *ZebraLab* software showing the swimming tracks lower than 2 mm in green and the larger than 2 mm in red.

After the first experiment, we performed a new one of 12 minutes with illumination cycles and with the integration of the movement of the fish every minute. *ZebraLab* software also gave the corresponding track for each period and other variables were also recorded and processed to properly analyse the animal behaviour. Among those, the sum of the short and large swimming provided us the best useful results and was used to analyse the effect of the compounds both in the dark and under light conditions.

Resum en català

Continguts del resum en català

Introducció	247
Glutamat i els seus receptors homònims	247
Control de funcions de proteïnes amb llum.....	261
Resultats i Discussió.....	267
Capítol 1: l'alloswitch-1 i l'optogluram: una prova de concepte	267
Capítol 2: els bioisòsters no fotocommutables de l'alloswitch-1 i l'optogluram i la confirmació del commutació molecular doble	273
Capítol 3: Una nova sèrie de fenilazopiridines per controlar finament la funció del mGlu ₅ amb llum	276
Capítol 4: La busca de PAMs de mGlu ₄ PAMs i NAMs de mGlu ₅ duals: Azologització i amidació del 2-BisPEB	287
Capítol 5: Una aproximació més adequada: PAMs mGlu ₄ i NAMs de mGlu ₅ fotocommutable cis-on	295
Resum de conclusions.....	303

Introducció

Glutamat i els seus receptors homònims

L'àcid glutàmic o l'àcid (S)-2-aminopentanedioic o glutamat, com a base conjugada, és un aminoàcid no essencial i els codons de DNA corresponents per a la seva translació són GAA i GGA. La cadena lateral del glutamat correspon to a un àcid propiònic amb un $pK_a=4.1$, que provoca una desprotonació a pH fisiològic ($pH\approx 7.4$) i, per tant, es considera un aminoàcid polar.

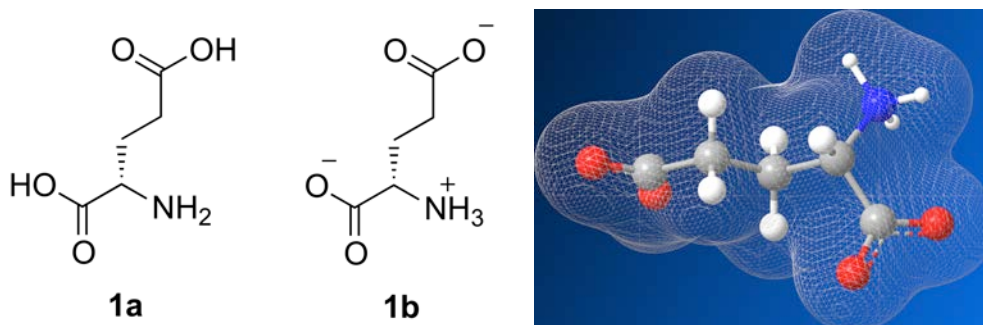


Figura 1: Estructura química de l'àcid glutàmic com a base lliure **1a**, la corresponent forma zwitteriònica **1b** amb l'àcid carboxílic de la cadena desprotonat i l'estructura 3D en forma de boles amb una superfície de densitat de càrrega com a malla.

Les funcions biològiques en que el glutamat està involucrat són nombroses, ja que no només és un aminoàcid proteínogènic. El glutamat també és el responsable de l gust "umami"; un dels cinc gustos bàsics i està relacionat amb uns GPCRs de classe C anomenats TAS1R1+3, que naturalment s'uneixen a glutamat i aspartat com a lligands. El glutamat també és el precursor de síntesi del transmissor inhibitori àcid gamma amino butíric, en les neurones GABA-èrgiques, a través de la catàlisi de la descarboxilasa de glutamat. A més a més, el glutamat és el neurotransmissor excitatori més important en els sistemes nerviosos dels vertebrats i la seva senyalització i així mateix és crític pel processament sensorial i les funcions cognitives⁴⁰.

En la sinapsis glutamatèrgica, el glutamat s'emmagatzema en vesícules en els compartiments presinàptics a través de transportadors de glutamat vesiculars (VGLUT) i, en una entrada massiva de calci desencadenada per potencials d'acció; aquestes vesícules ràpidament alliberen el neurotransmissor des del terminal nerviós. Així mateix, la maquinària de recaptació de glutamat en ambdós terminals presinàptics i als astròcits adjacents controlen la concentració de glutamat en l'espai sinàptic. Un cop el glutamat arriba al terminal postsinàptic d'una cèl·lula nova, en el costat oposat del terminal presinàptic, activa la maquinària de la

densitat postsinàptica (PSD)^a, on es trobem receptors de glutamat i la cascada de senyalització continua (figura 2).

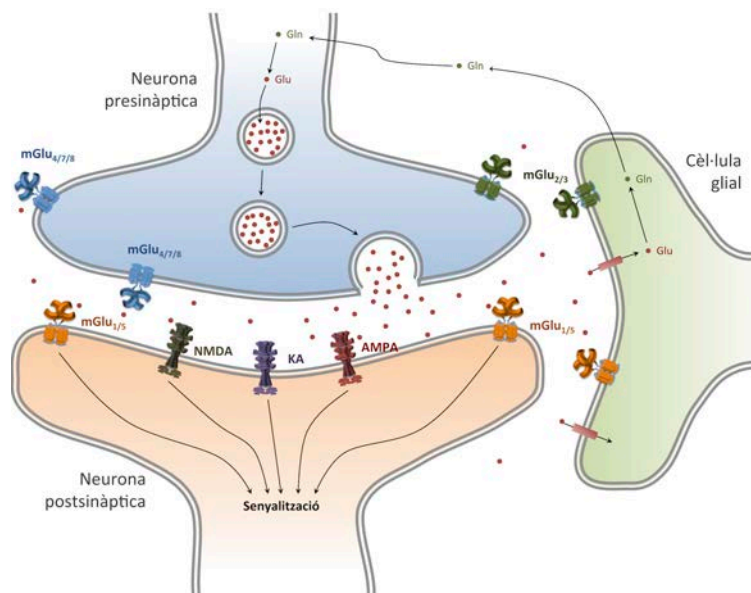


Figura 2: La sinapsi de glutamat El glutamat (Glu) s'acumula a en vesícules als terminals presinàptics a través dels receptors de glutamat vesiculars (VGLUT). En la sinapsi, aquestes vesícules es fonen amb la membrana neuronal, alliberant glutamat. Llavors, aquest glutamat activa els receptors iGlu (AMPA, NMDA i KA) i els mGlu₁ i mGlu₅, que es troben al terminal postsinàptic d'una nova neurona i desencadenen una cascada de senyalització. Les cèl·lules glials realitzen la recaptació de glutamat a través dels transportadors de glutamat (EAAC), i allà es converteix a glutamina (Gln) i novament s'allibera per entrar finalment a la neurona presinàptica, on es converteix amb glutamat i s'emmagatzema a les vesícules de glutamat,

Els receptors ionotròpics de glutamat (iGluRs)

Els receptors ionotròpics de glutamat són canals catiónics sensibles a lligands que controlen la neurotransmissió, que és una transmissió crucial pel desenvolupament i funcions cerebrals. En unir-s'hi, el glutamat provoca una obertura d'un porus selectiu per cations. Estan dividits en tres subfamílies principals, anomenats segons el lligand sintètic preferit per cada subgrup: receptor α -amino-3-hidroxi-5-metil-4-isoxazolepropionic (AMPA), receptor kainat (KA) i receptors *N*-Metil-D-aspartat (NMDA). Hi ha una subfamília addicional, anomenada delta (GluD) que és homòloga estructuralment però no s'activa amb glutamat.

Tots ells són receptors proteics tetramèrics. Cada subunitat conté 4 dominis: Un domini *N*-terminal (NTD), que regula la composició de la subunitat i on, en els receptors NMDA, es poden unir alguns moduladors; un domini d'unió del lligands (LBD), on el glutamat o la glicina

^a La densitat postsinàptica (PSD) és una xarxa de proteïnes estructurals, receptors i molècules de senyalització, entre les quals s'inclouen els receptor ionotròpics i metabotròpic de glutamat, que es troben als terminals postsinàptics de les neurones, en la cara oposada a la zona activa presinàptica.

s'uneixen; un domini transmembrana (TMD), i un domini C-terminal (CTD) on es troben els llocs de fosforilació i on interaccionen les proteïnes estructurals.

Família	Gen / nom de la subunitat
AMPA	GRIA1/GluA1, GRIA2/GluA2, GRIA3/GluA3 and GRIA4/GluA4
Kainat	GRIK1/GluK1, GRIK2/GluK2, GRIK3/GluK3, GRIK4/GluK4 and GRIK5/GluK5
NMDA	GRIN1/GluN1, GRIN2/GluN2A, GRIN2B/GluN2B, GRIN2C/GluN2C, GRIN2D/GluN2D, GRIN3A/GluN3A and GRIN3B/GluN3B,
Orfes	GRID1/GluD1, GRID2/GluD2

Taula 1: Classificació dels iGluR amb la nomenclatura de subunitats i gens humans recomanada per la IUPHAR⁴¹

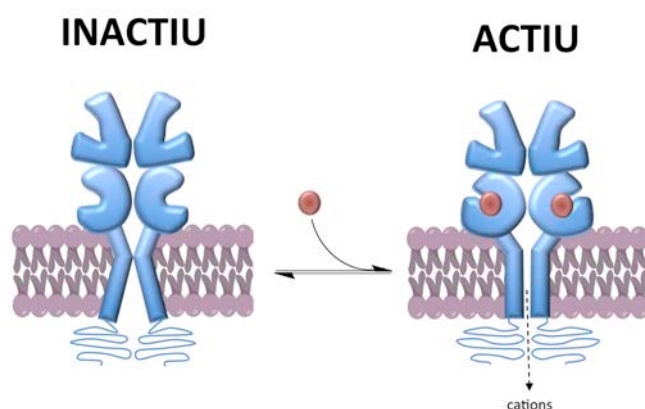


Figura 3: Topologia d'un receptor iGlu (amb dues subunitats per una visualització correcta, haurien de ser quatre subunitats) i el model general d'unió de glutamat en el LBD amb la corresponent obertura del canal catiònic.

A grans trets, els receptors ionotròpics d'AMPA són els responsables de una part important del potencial excitatori postsinàptic, ja que estan en major nombre i estan localitzats en la zona activa de la PSD. El canal s'obre quan s'ocupen dos dels quatre llocs d'unió amb un agonista i el corrent s'incrementa amb la posterior ocupació dels demés lloc d'unió. La alta EC_{50} pel glutamat (100-50 μ M) dóna evidència que l'activació del receptor només té lloc en l'alliberament sinàptic de glutamat i mostra unes velocitats grans d'activació i desactivació, així com una dessensibilització ràpida i severa⁴³.

Els receptors de kainat tenen propietats semblants als receptors d'AMPA, però només són responsables d'una mínima part dels corrents postsinàptics. De fet, tenen un paper neuromodulador. Una diferència substancial entre els receptors d'AMPA i kainat és que els darrers necessiten Na^+ and Cl^- per activar-se i que es poden modular amb subunitats auxiliars (proteïnes Neto). També els receptors de kainat dessensibilitzen més ràpid que els AMPA a concentracions baixes de agonista^{40, 44}.

Els receptors ionotròpic de NMDA són heterotetramèrics i, depenent de les subunitats, es pot unir glutamat o glicina, actuant com a coagonistes. Són un tipus singular de receptors

ionotròpics, ja que no només necessiten dos agonistes diferents per ser activats, sinó que també és necessària una despolarització forta per treure un ió de magnesi (Mg^{2+}) que bloqueja el porus. Es creu que les principals funcions que tenen són reguladores i s'ha descrit que tenen un paper important en el control de la plasticitat sinàptica^a i la funció de memòria⁴⁵.

Els receptors metabotròpics de glutamat (mGluRs)

Els receptors metabotròpics de glutamat (mGluRs) pertanyen a la classe C de proteïnes G, abundants i amplament distribuïts pel sistema nerviós central i perifèric (CNS i PNS). S'activen amb glutamat i poden regular diverses funcions neuronals i gials. D'aquesta manera, tenen un rol important en la excitabilitat neuronal i la transmissió sinàptica.

Topologia i mecanismes d'activació dels receptors mGlu.

Com a GPCRs de classe C, els receptors mGlu són obligatòriament dímers i cada protòmer està format per tres dominis: Un domini transmembrana (TMD), un domini ric en cisteïna (CRD) i una dionea ("Venus flytrap", VFT).

El VFT és un domini gran, format per dos lòbuls que defineixen una escletxa on s'uneix el glutamat. S'han resolt estructures cristal·lines dels VFT dels receptor mGlu₁ en la seva conformació oberta i tancada amb i sense glutamat^{26,27}. Més tard, es van resoldre també les estructures cristal·lines d'altres dominis VFT d'altres receptors mGlu^{28,29}. Aquestes estructures donen suport a la teoria que el glutamat estabilitza la conformació tancada dels dos lòbuls, ja que es formen contactes més estables amb el lligand que en la conformació oberta. A més a més, s'ha observat que els antagonistes impedeixen el tancament dels lòbuls, i que si es bloqueja el tancament dels lòbuls amb un pont disulfur, es provoca una activació constant del receptor³⁰. Els VFTs formen dímers estables que experimenten canvis d'orientació considerables en l'activació del receptor⁴⁶.

El CRD és el domini que enllaça el VFT amb el TMD, format per 70 residus, incloent 7 cisteïnes altament conservades que formen quatre ponts disulfur i la novena cisteïna s'uneix al VFT també formant un pont disulfur²⁹. En l'estat inactiu, els dos CRDs s'associen i estan pràcticament en contacte²⁴. Es creu que el seu rol és crucial i s'ha descrit com una associació precisa entre ambdós és suficient per l'activació del receptor mGlu²⁴.

^a La plasticitat és la qualitat de ser fàcilment soldejat. En biologia es refereix a la adaptabilitat d'un organisme als canvis en el medi o diferències en diversos hàbitats. En neurociències, la plasticitat sinàptica és l'habilitat de enfortir o afeblir sinapsis en el temps en resposta a augments o davallades d'activitat (New Oxford American dictionary).

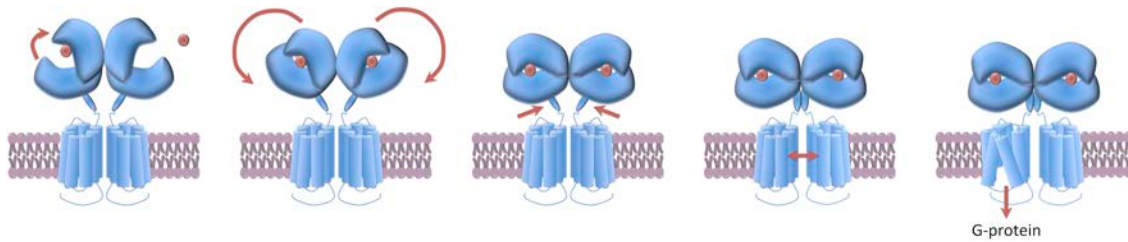


Figura 4: Passos esquemàtics de l'activació dels mGluRs. Adaptat de Rondard i Pin⁴⁷.

El TMD, també anomenat 7TM, consisteix en set hèlix transmembrana formant un manat que es el responsable de l'activació de la proteïna G, com la resta de GPCRs. En l'activació del receptor, només el TMD d'un protòmer adopta una conformació activa, mentre que l'altre es manté en conformació inactiva. El que està en conformació inactiva és el responsable de la transducció del senyal d'activació per glutamat en el VFT a la proteïna G corresponent⁴⁸.

Recentment, es van resoldre les primeres estructures cristal·lines del TMD del mGlu₁ i mGlu₅ en conformació inactiva^{31, 32, 51}, amb un plegament semblant als GPCRs de classe A, tot i la baixa homologia de seqüència. De moment no s'ha descrit cap estructura cristal·lina d'un TMD de receptor mGlu en conformació activa, però s'han descrit models d'homologia⁵², amb plegaments semblants a GPCRs de classe A amb propostes de llocs d'unió de PAM⁵⁰.

La figura 4 representa un resum dels principals passos del mecanisme d'activació explicat anteriorment, començant dels de la unió de glutamat al VFT, amb la seva corresponent reorientació, seguit de l'associació dels CRDs en un total de ~30 ms. Seguidament a aquest canvi conformacional, el TMD d'una de les dues subunitats s'activa en ~50 ms, i propicia l'activació de la proteïna G⁵³.

Classificació dels mGluRs, anatomia funcional i principals rols biològics

Els receptors mGlu consten de 8 subtipus diferents, classificats en tres grups diferents, en base a similituds en la seqüència primària, farmacologia d'agonistes i acoblament de proteïna G. Els subtipus del grup I (mGlu₁ i mGlu₅) són principalment presinàptics^a ai s'uneixen a la subunitat G_qα, mentre que els del grup II (mGlu₂ i mGlu₃) i grup III (mGlu₄, mGlu₆, mGlu₇ i mGlu₈) són majoritàriament postsinàptics i s'uneixen a la subunitat G_{i/o}α (taula 2).^b

Els receptors mGlu₁ and mGlu₅ estan expressats extensivament en el CNS, en neurones i també en cel·lules glials. Es troben principalment en regions postsinàptiques, on sembla estar

^a Presinàptic: relaciona o denota una cèl·lula nerviosa que segrega un neurotransmissor a una sinàpsi durant la transmissió d'un impuls (New Oxford American Dictionary).

^b Postsinàptic: Localitzat a la banda distal de una sinapsi (Collins English Dictionary)

concentrat en ares perisinàptiques^a i extrasinàptiques^b D'aquesta manera, els receptors mGlu s'activen amb grans concentracions de glutamat que s'escapen dels mecanismes de recaptació i que s'escampen pels costats de l'espai sinàptic^{55, 56}.

Grup	Subtipus	Gen	Glu EC ₅₀	ago. ort.	EC ₅₀	Prot. G senyalització princ.
I	mGlu ₁	GRM1	9-13	Àcid quisquàlic (2)	0.1-1.0	G _q (↑IP ₃ , ↑Ca ²⁺ intracel·lular, ↑DAG, activació PKC)
	mGlu ₅	GRM5	3-10		0.03-0.3	
II	mGlu ₂	GRM2	4-20	LY 354740 (3)	0.005	G _{i/o} (↓cAMP, inhibeix canals de Ca ²⁺ sensibles a voltatge, activa canals de K ⁺ , activa les vies de MAPK i PtdIns-3-K)
	mGlu ₃	GRM3	4-5		0.0034	
III	mGlu ₄	GRM4	3-20	L-AP4 (4)	0.2-1.2	G _{i/o} (↓cAMP, inhibeix canals de Ca ²⁺ sensibles a voltatge, activa canals de K ⁺ , activa les vies de MAPK i PtdIns-3-K)
	mGlu ₇	GRM7	1000		0.9	
	mGlu ₈	GRM8	16		160-500	G _o (inhibeix canal TrpM1 de Ca ²⁺)
	mGlu ₆	GRM6	2.5-11		0.06-0.60	

Taula 2: Classificació dels receptors mGlu en grups, amb la potència de glutamat per cada subtipus EC₅₀ en unitats μM⁵⁴, els agonistes utilitzats per cada grup més comuns (figura 5), amb la seva potència com EC₅₀ en unitats μM⁵⁴ amb les corresponents proteïnes G i les principals vies de senyalització que activen⁵⁵.

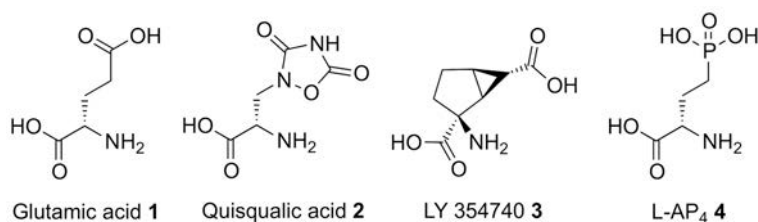


Figura 5: Estructura dels agonistes ortoestèrics selectius de grup més comuns i l'antagonista no selectiu LY 341495.

Els receptors mGlu₂ and mGlu₃ estan expressats amplament en el CNS i també en el PNS. Generalment es troben en neurones presinàptiques, lluny de la zona d'alliberament de neurotransmissor, on s'activen per un excés de glutamat sinàptic o per glutamat alliberat des d'astròcits. El mGlu₃ es pot trobar també en cel·lules glials i regions postsinàptiques on poden induir hiperpolarització. La principal funció d'aquests dos receptors als terminals presinàptics és inhibir l'alliberació de neurotransmissor^{55, 56}.

Els receptors mGlu de grup III estan distribuïts amplament en el CNS en regions presinàptiques de neurones, excepte el mGlu₆ que està expressat quasi exclusivament en la retina. L'activació d'aquests receptors regula negativament l'alliberament de neurotransmissor. El glutamat s'uneix a mGlu₄ i mGlu₈ amb una afinitat relativament alta, però mostra una afinitat molt baixa

^a Perisinàptic correspon a prop de l'espai sinàptic

^b Extrasinàptic correspon a l'exterior de l'espai sinàptic

pel mGlu₇ (*taula 2*). A més a més, el receptor mGlu₇ està localitzat a les zones més actives de la sinapsi. Per això s'ha proposat que té un rol de prevenció de sobreestimulació per glutamat, per la seva localització i les altes concentracions de glutamat necessàries per activar-lo. El receptor mGlu₆, involucrat en la percepció visual, s'expressa postsinàpticament a les dendrites de les cel·lules bipolars ON de la retina i respon al glutamat alliberat pels fotoreceptors bastons i cons a les fosques^{55,56}.

Modificació de la funció dels mGluR: lligands ortoestèrics i al·lostèrics

Les aproximacions clàssiques per modular la funció dels receptors mGlu són l'ús molècules petites com a lligands que s'uneixen al receptor, de manera que estabilitza la conformació activa o inactiva.

Les molècules petites que s'utilitzen com a lligands que actuen en mGluRs es poden classificar en dos grups principals: Lligands que s'uneixen al VFT, que normalment són lligands ortoestèrics o competitiu amb el glutamat, i lligands que s'uneixen al TMD, que són lligands al·lostèrics o no competitiu.

El lligand endogen dels receptors mGlu, el glutamat, s'uneix a l'esclatxa dins el VFT. En base a l'estructura del glutamat i en estudis estructurals del VFT, molts compostos s'han dissenyat i assajat⁵⁸. Consisteixen en agonistes, agonistes parcials, antagonistes o agonistes inversos i són tots competitiu amb el glutamat⁵⁴. No obstant això, aconseguir una bona selectivitat per un determinat subtipus de mGlu suposa una feina àrdua, ja que el lloc d'unió del glutamat està altament conservat. En els primers anys, els esforços en farmacologia molecular només van aportar agonistes selectius de grup (*figura 7*) com el quisqualat pel grup I (**2**), LY 354740 (**3**) pel grup II i el L-AP4 (**4**) pel grup III (*taula 2, figura 5*). A més, es van descobrir alguns antagonistes com el LY 341495, que és actiu en els vuit receptors mGlu però té una lleu selectivitat pel grup II (*figura 6*).

Més recentment, s'han descobert nous agonistes de grup III amb cadenes més llargues, com el LSP4-2022 (**6**)⁵⁹ (*figura 6*), que s'uneix al lloc d'unió del glutamat però també a una altra lloc proper. Aquesta cavitat addicional sembla ser un lloc d'unió de clorur (Cl⁻), per no es coneixia cap rellevància farmacològica d'aquest ió pels receptors mGlu⁶⁰. De fet, molt recentment, s'ha descrit que l'ió clorur actua com a modulador al·lostèric positiu, unint-se a un mínim de dos llocs diferents del VFT⁶¹. Per tant, aquest descobriment permet dissenyar agonistes llargs que simultàniament s'uneixi al lloc ortoestèric i també als llocs al·lostèrics extracel·lulars (edAM) del clorur, com el LSP4-2022(**6**) en mGlu₄.

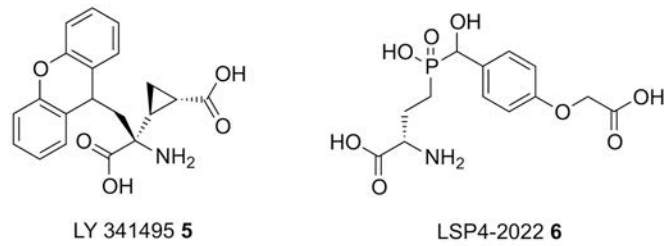


Figura 6: Estructures de l'antagonista ortostèric LY 341495 i l'agonista selectiu en mGlu₄ LSP4-2022.

Tot i que esta descrit que el clorur modula al·lostèricament l'activitat del glutamat a través d'un lloc d'unió que es troba en el TMD, la majoria dels moduladors al·lostèrics de receptors mGlu s'uneixen a un lloc d'unió que es troba dins el TMD i dona a aquests moduladors propietats molt diferents als que s'uneixen al VFT. Poden incrementar (moduladors al·lostèrics positius, PAMs, *figura 7E*) o inhibir (moduladors al·lostèrics negatius, NAMs, *figura 7F*) l'activitat del receptor, modulant l'afinitat del agonista ortostèric i afectant a l'eficàcia intrínseca d'aquest agonista per desencadenar la resposta de senyalització⁶². S'uneixen a un lloc similar als lligands de classe A, on els NAMs estableixen la conformació inactiva d'ambdós TMDs i els PAMs, la conformació activa de un dels TMDs. Així mateix, també existeix un nou tipus de modulador al·lostèric anomenat modulador al·lostèric silenciós (SAM). Aquests lligands al·lostèrics s'uneixen al TMD, però no estableixen cap conformació del receptor en concret, de manera que provoquen cap canvi en la funcionalitat del receptor⁶³.

Com hem mencionat anteriorment, el TMD es troba en la membrana cel·lular, en un ambient hidrofòbic. A més a més, com que els GPCRs de classe C no tenen moduladors al·lostèrics endògens, el lloc d'unió al·lostèric s'ha mantingut més hidrofòbic que els GPCRs de classe A o B. Per això, la polaritat d'aquests moduladors al·lostèrics ha de ser suficientment baixa per poder unir-se a un entorn tant hidrofòbic, molt més baixa que els lligands ortostèrics, que normalment són derivats d'aminoàcids que s'uneixen al VFT altament hidròfil. Aquesta alta lipofília ofereix diverses avantatges i desavantatges als moduladors al·lostèrics respecte els lligands ortostèrics. Per exemple, la solubilitat en aigua d'aquests compostos és baixa i això suposo una desavantatge important que pot ser compensada amb una alta potència farmacològica, que permeti l'ús de dosis molt petites, que no necessitin una alta concentració en plasma per ser actives. Cal dir també que l'absorció de molècules lipofíliques quan són administrades oralment és adequada i tendeixen a travessar la barrera hematoencefàlica, mentre que l'absorció dels lligands ortostèrics necessiten un disseny de profàrmacs i només poden creuar la barrera hematoencefàlica mitjançant transport actiu d'aminoàcids⁵⁸.

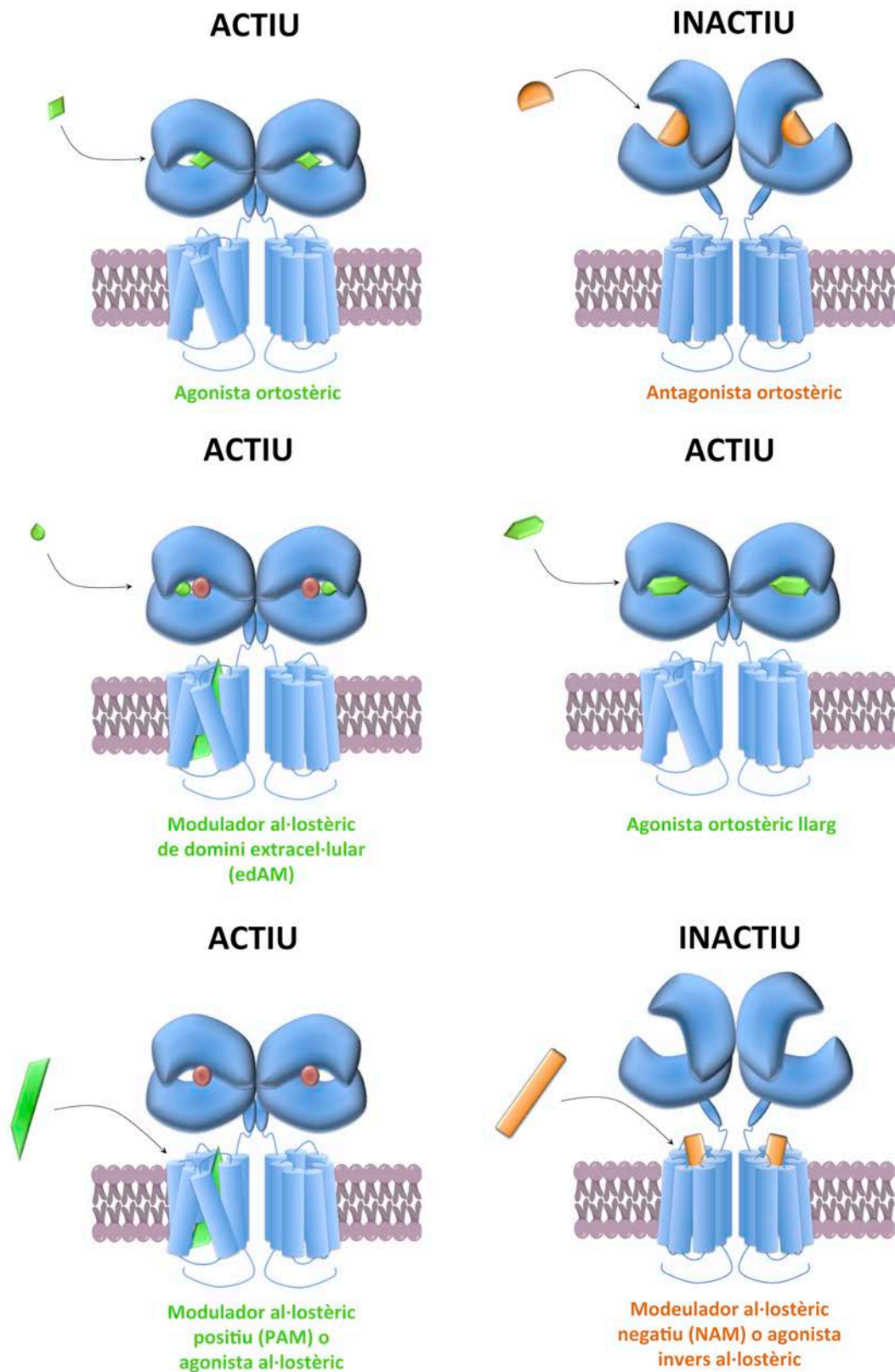


Figura 7: Topologia dels receptors mGlu i model general d'unió de: A) agonistes ortostèrics, B) antagonistes ortostèrics, C) moduladors al·lostèrics de domini extracel·lular (edAM), D) agonistes ortostèrics llargs, E) moduladors al·lostèrics positius (PAM) i F) moduladors al·lostèrics negatius o agonistes inversos al·lostèrics (adaptat de Rondard³⁰ i Kniazeff²³)

A part d'això, els moduladors al·lostèrics de mGlu ofereixen altres avantatges, Per exemple, hi ha més possibilitats d'aconseguir una bona selectivitat sobre els diferents subtipus de mGlu amb molècules que s'uneixen al TMD, ja que el seu lloc actiu té una pressió evolutiva menor en comparació al lloc d'unió ortostèric del VFT, que és altament conservat⁵⁸. Tot i les possibilitats de descobrir agonistes ortostèrics a través de l'ocupació d'un lloc edAM, només el LSP4-2022 i (S)-DCPG són els únics lligands ortostèrics selectius que actuen en els mGlu^{59, 76}. En canvi, hi ha nombrosos exemples de moduladors al·lostèrics amb bons perfils de selectivitat.

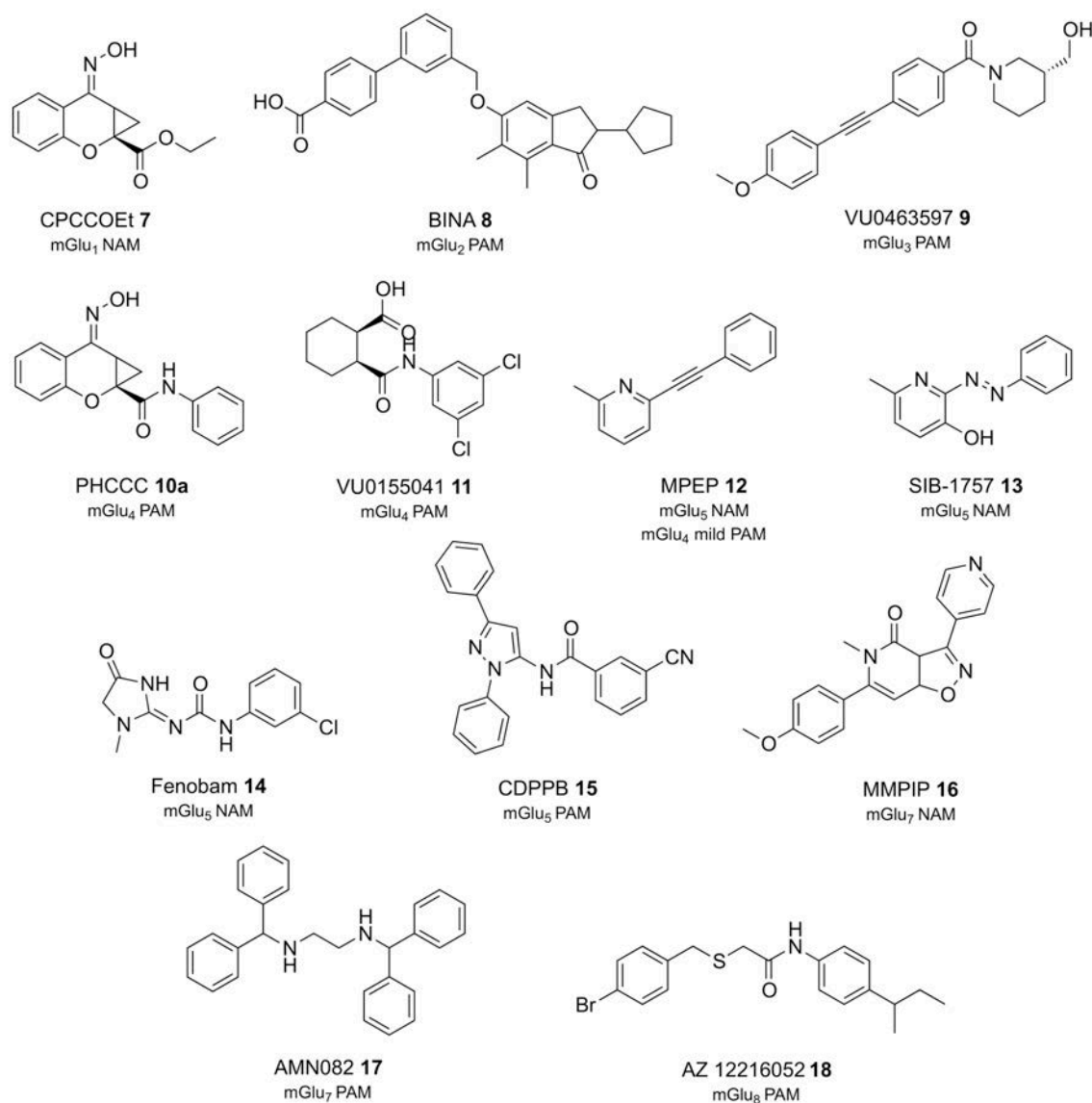


Figura 8: Exemples de moduladors al·lostèrics selectius per un subtipus de mGlu concret. No hi ha exemples de moduladors al·lostèrics per mGlu₆ degut a la falta de farmacologia específica, ja que la seva reduïda aplicabilitat no interessa als programes de descobriment de fàrmacs.

Una altra avantatge potencial és que els moduladors al·lostèrics que no mostren agonisme són completament inactius sense la presència de lligands ortostèrics i només potencien o

inhibeixen la resposta del receptor a la presència d'un agonista ortostèric alliberat en la sinapsi. Al contrari, els agonistes i antagonistes ortostèrics fan el seu efecte contínuament, independentment de l'alliberament de neurotransmissor. D'altra banda, també hi ha la possibilitat d'obtenir antagonistes parcials, que redueixen la resposta del mGlu a un nivell més baix, però sense suprimir-la completament. En resum, aquests moduladors al·lostèrics ofereixen una aproximació de "ajustament fi", que es creu millor i més controlable des d'un punt de vista terapèutic^{10, 63}.

Un fenomen comú: la commutació molecular

Tot i la selectivitat de subtipus d'un modulador al·lostèric o el rol concret com a PAM, NAM o SAM modificacions subtils en l'estructura química poden propiciar canvis en la seva farmacologia, modes d'unió o selectivitat de subtipus. Aquest fenomen s'anomena "commutació molecular" o "commutació química" i és freqüent entre moduladors al·lostèrics dels receptors mGlu.

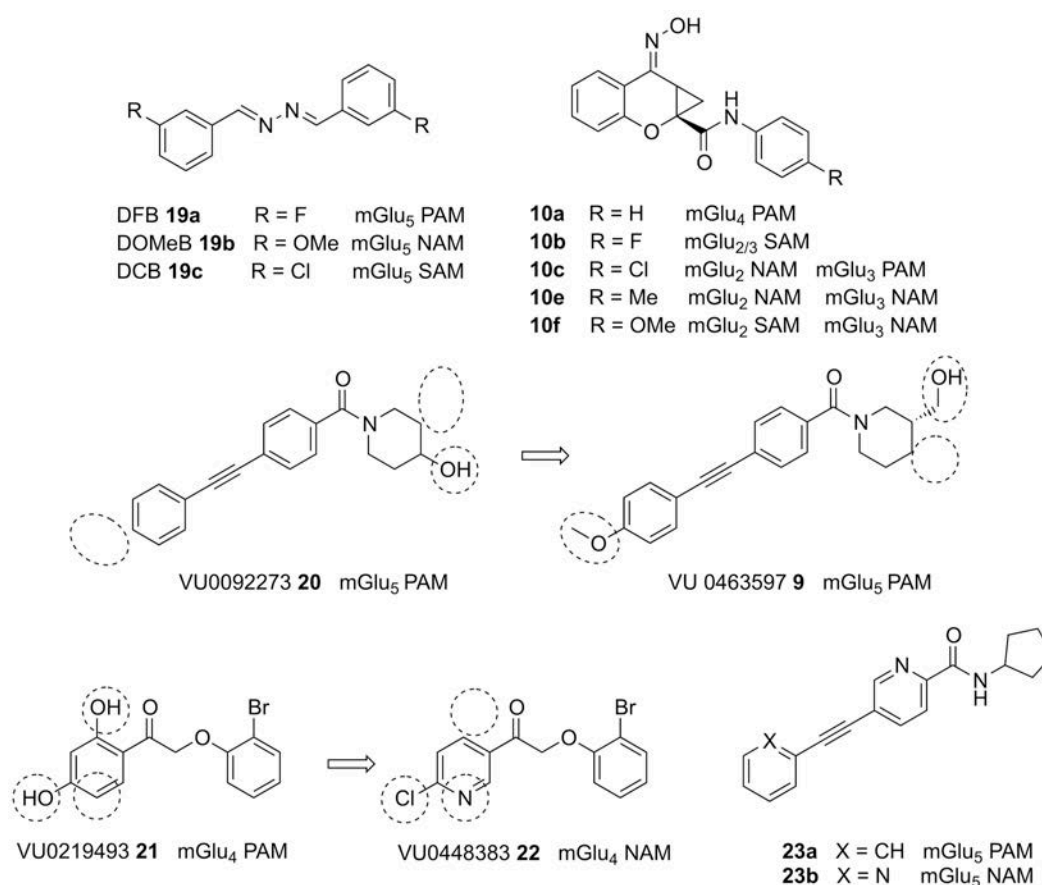


Figura 9: Exemples de commutadors moleculars de moduladors al·lostèrics receptors mGlu

El primer exemple de commutador molecular en receptors mGlu va ser el DFB (**19**), que amb canvis subtils canviava la seva activitat en mGlu₅ de PAM a NAM o SAM⁷⁸ (figura 9). Altres

exemples estan contemplats a la (**figura 16**), com el PHCCC que amb canvis subtils pot canviar de subtipus de mGlu i de tipus de modulació⁷⁹ (*figura 9*). Altres exemples poden ser també el VU0092273(**20**)⁵⁶, VU0219493 (**21**)⁸⁰ o el CPPhENA (**23a**)⁸¹.

Receptors mGlu com a diana per tractar trastorns humans

Com s'ha comentat abans, els receptors mGlu estan amplament distribuïts pel sistema nerviós central i perifèric i cada un dels subtipus tenen rols concrets que es poden modular amb agonistes, antagonistes o moduladors al·lostèrics. Per aquest motiu es pensa que els receptors mGlu són una diana terapèutica excel·lent per tractar una gran varietat de trastorns del sistema nerviós central. No obstant això, encara no es troben lligands de mGlu al mercat o fins en vistes d'aprovació per les agències reguladores. De totes maneres, encara hi ha espè⁸⁴rança per utilitzar-los com a diana per tractar trastorns neurològics i psiquiàtrics.

Dolor

El dolor crònic és una condició que implica que afecta seriosament la qualitat de vida de més del 19% de la societat europea i els seus tractaments no ofereixen un alleugeriment significatiu. Una estratègia raonable podria ser bloquejar l'activitat glutamatèrgica associada al dolor, però és necessari seleccionar les dianes terapèutiques adequades^{10, 83}. Aquestes dianes poden ser els diferents receptors mGlu, ja que regulen processos nociceptius^{a84}.

Un exemple seria el mGlu₁, que està expressat en regions del CNS essencials pels processos nociceptius. El mGlu₅ també constitueix una possible diana ja que en assajos preclínics i clínics ha mostrat efectes analgèsics amb NAMs.

L'activació de receptors mGlu de grup II pot resultar també en efectes analgèsics. De fet, alguns agonistes de mGlu_{2/3} han tenir efectes analgèsic en models de dolor inflamatori i neuropàtic, tot i que també es va observar tolerància després d'un tractament crònic^{10, 84}.

Els mGlu de grup III també són abundants en les vies nociceptives, particularment el mGlu₄ i mGlu₇. S'ha demostrat també en assajos preclínics que els agonistes de mGlu₄ ajuden a reduir hipersensibilitat associada estímuls mecànics i juguen un paper com a neuroprotectors en processos inflamatoris^{10, 83, 84, 88}.

^a Relacionat als processos neurals de codificació d'estímuls noxiousos (events d'actual o potencial dany en teixits) (Associació Internacional de l'estudi del dolor <http://www.iasp-pain.org/Taxonomy?navItemNumber=576>)

Subtipus	MdA*	Aplicacions en malalties del CNS
mGlu ₁	PAM	N/A
	NAM	Dolor neuropàtic, síndrome X fràgil, trastorns de ansietat/estrès, addicció
mGlu ₅	PAM	Trastorns d'ansietat, malaltia de Huntington, esquizofrènia, complex d'esclerosi tuberosa
	NAM	Trastorns d'ansietat, trastorns de ansietat, dolor crònic, síndrome X fràgil, migranya, malaltia de Parkinson, discinèsia induïda per L-DOPA.
mGlu ₂	PAM	Addicció, trastorns d'ansietat, depressió, esquizofrènia
	NAM	Depressió
mGlu ₃	NAM	Depressió
mGlu ₄	PAM	Dolor Neuropàtic, neuroinflamació, neuroprotecció, malaltia de Parkinson, esquizofrènia
mGlu ₇	Agonista	Ansietat, depressió, malaltia de Parkinson
	NAM	Ansietat, depressió
mGlu ₈	Agonista	Malaltia de Parkinson, ansietat

Taula 3: Aplicació potencial de moduladors al·lostèrics de mGlu en malalties del CNS (adaptat de Nickols¹⁰) *Mode d'acció

Malaltia de Parkinson

La malaltia de Parkinson (PD) és una malaltia neurodegenerativa amb una incidència alta en població més gran de 55 anys. El tractament actual consisteix en la substitució de dopamina i inicialment es efectiva, però cause efectes secundaris no desitjats i la seva eficàcia disminueix a mesura que la malaltia avança. Els receptors mGlu de grup III són una diana prometedora per tractar el PD, ja que estan expressats presinàpticament en diferents sinapsis glutamatèrgiques que controlen la funció motora, i que està alterades en pacients de PD. De fet, s'ha descobert que el L-AP₄ i PAMs de mGlu₄ reverteixen els símptomes motors en models animals de PD, entre altres característiques de PD^{10, 88}.

Els tractaments actuals provoquen el desenvolupament progressiu de discinèsia induïda per L-DOPA. En models animals experimentals i fases clíniques, s'ha demostrat que els NAMs de mGlu₅ redueixen aquesta discinèsia, així com els símptomes motors de PD. A més a més, s'ha observat que aquestes molècules tenen propietats neuroprotectores en rosegadors i primats⁸².

Síndrome X fràgil i trastorns de l'espectre autista

La síndrome X fràgil (FXS) és la forma més comuna de discapacitat intel·lectual humana i la major causa d'autisme heretat. Està causat per una mutació al gen FMR1, que resulta en una falta d'expressió d'una proteïna que es troba a la regió postsinàptica glutamatèrgica que provoca un augment de la senyalització constitutiva de mGlu₅ de manera que es desregula la

funció sinàptica. Per tant, l'agonisme invers que poden fer NAMs de mGlu₅ beneficiós pels pacients amb FXS¹⁰, com van demostrar alguns estudis clínics⁸². També s'ha descrit que els NAMs de mGlu₁ són ser eficaços en models animals o que el tractament amb el PAM de mGlu₄ VU0155041 (**11**) era eficient en alleugerir dèficits de conducta⁸⁹.

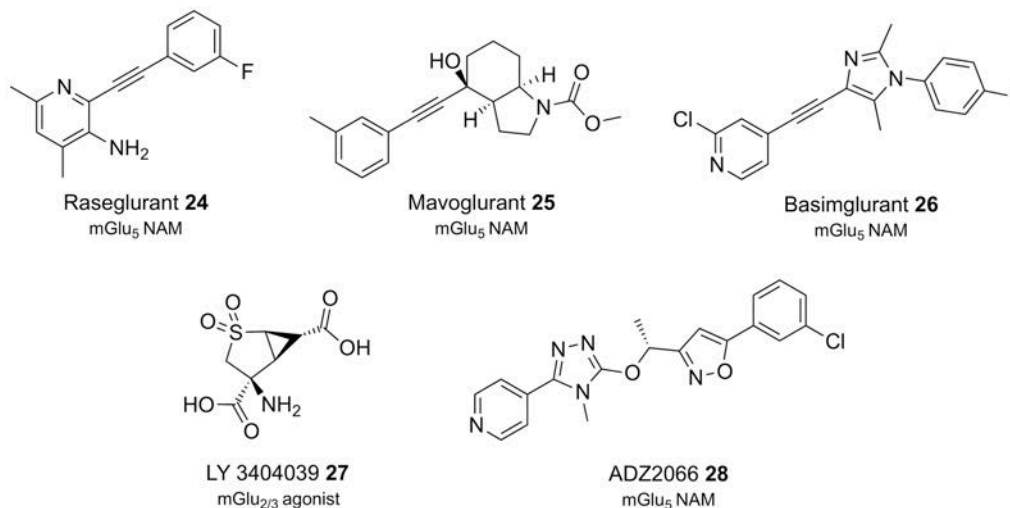


Figura 10: Exemples de lligands de mGlu assajats en fases clíniques

Esquizofrènia i trastorns d'ansietat

L'esquizofrènia és el major trastorn psiquiàtric que afecta a una fracció considerable de la població en tot el món. Es creu que està basada en una hipofunció dels receptors NMDA i anormalitats entre la comunicació entre mGlu₂ i 5-HT_{2A}. Els agonistes de grup II són eficaços en models preclínics de psicosis, ansietat altres models d'esquizofrènia. De fet un profàrmac d'un agonista de mGlu_{2/3}, LY404039 (**27**) ha estat assajat en fases clíniques i, també, PAMs de mGlu₅ són eficients en models d'activitat antipsicòtica i s'estan provant en fases clíniques. A més a més, l'activació de mGlu₄ també té efectes antipsicòtics i es creu que el mGlu₁ també està involucrat en esquizofrènia degut a una mutació en el gen GRM1 que provoca una pèrdua de funció del receptor^{82, 88}.

Depressió

El trastorn major depressiu (MDD) és una malaltia mental molt comuna que afecta entre el 2% i el 16% de la població, depèn de la regió. Els antidepressius actuals tenen poca eficàcia en molts pacients i el seu inici d'acció és lent, arribant a 3 o 4 setmanes a manifestar-se millores.

Els antagonistes de NMDA, com la ketamina, són antidepressius eficaços. Per tant, els NAMs de mGlu₅ podrien esdevindre alternatives a la ketamina, més segures i amb menor potencial d'addicció. Actualment el basimglurant (**26**) i AZD2066 (**28**) estan sota desenvolupament clínic per depressió. A més a més estudis preclínics amb PAMs de mGlu₂ mostren activitat

antidepressiva, tot i que alguns antagonistes també la mostren^{10, 82, 88}. També NAMs de mGlu₇ han mostrat eficàcia en tractaments d'ansietat i depressió en models animals.

Drogoaddicció

Es pensa que la transmissió glutamatèrgica és clau per l'establiment i manteniment de la drogoaddicció. Els NAMs dels mGlu de grup I constitueixen agents terapèutics potencials per a tractar les addiccions. De fet, NAMs de mGlu₅ i antagonistes de mGlu₁ mostren eficàcia en models d'addicció a la cocaïna. A més a més, la inhibició de Glu₅ disminueix els efectes satisfactoris de altres drogues d'abús com l'amfetamina, morfina o alcohol^{10, 82, 88}.

Altres trastorns

Tot i que els principals trastorns que es poden tractar amb moduladors de mGlu s'han explicat anteriorment, També s'han proposat com a dianes farmacològiques potencials per altres trastorns relacionats amb el CNS, com la potenciació del mGlu_{2/3} o NAMs de mGlu₅ per ansietat, NAMs de mGlu₅ per trastorns astrocítics, distonia iatrogènica o reflux gastroesofagal o potenciació de mGlu₇ o mGlu₈ per estrès i ansietat⁸⁸.

Control de funcions de proteïnes amb llum

Els fàrmacs normalment són substàncies químiques, normalment molècules petites, que tenen activitat biològica, moltes vegades a través d'un canvi de les funcions normals de proteïnes i normalment són el principi actiu dels medicaments.

La farmacologia és la branca del coneixement que estudia aquestes substàncies des del punt de vista bioquímic i fisiològic. Pel que fa als fàrmacs que canvien les activitats funcionals de proteïnes, la farmacologia és la disciplina encarregada de trobar les interaccions d'aquests fàrmacs (l·ligands) amb les proteïnes diana, els seus canvis funcionals i la seva resposta terapèutica. Tot i això, un cop el fàrmac és introduït al cos, es reparteix per l'organisme i el control de la substància. De manera lenta i imprecisa, acaben unint-se a la seva proteïna diana, on estigui localitzada, sense tenir en compte el tipus de cèl·lula, teixit o sistema on estigui expressada¹³⁵. Així mateix, una selectivitat pobre pot provocar diversos efectes secundaris indesitjats que poden incrementar el límit de toxicitat i obligar així a disminuir la dosi i, per tant, a perdre part del potencial del fàrmac^{136, 137}.

La optofarmacologia, també coneguda com a fotofarmacologia, consisteix en l'ús de llum per regular l'activitat d'un fàrmac fotosensible en el seu receptor i combina òptica i química per controlar la funció de proteïnes clau amb llum, a través de commutadors fotoreversibles o

gàbies fotolàbils, també anomenats compostos químics fotocromics¹³⁵. Normalment la llum no interfereix al sistema viu que es vol estudiar i es pot utilitzar de forma remota i no invasiva. La llum es pot manipular amb alta resolució tant temporalment com espacialment, de manera fa possible l'estudi de processos ràpids confinats en compartiments específics cel·lulars o grups específics de cèl·lules¹³⁸. A més a més, la llum també es pot regular de forma qualitativa i quantitativa, amb l'ajust de la longitud d'ona i la intensitat¹³⁷. Per tant, l'optofarmacologia pot aportar avantatges i una aproximació més precisa a les teràpies amb fàrmacs convencionals.

Azobenzè

Els derivats d'azobenzè, incloses les fenilazopiridines i azopiridines, són els fotocommutadors més utilitzats en aplicacions biològiques. L'estructura de l'azobenzè consisteix en dos anells de fenil units per un grup -N=N-, també anomenat enllaç azo, o pont azo. L'isòmer *trans* té una geometria planar amb un angle diedre de 180°, una deslocalització estesa dels electrons π en els anells aromàtics i l'enllaç azo i un moment dipolar negligible. En canvi, l'isòmer *cis* té una geometria angular, 3 Å més curta que el *trans*, amb els anells de fenil estan torçats en 55° fora del pla, l'angle diedre de l'enllaç azo és de 11° i té un moment dipolar de 3.7 Debye^a. Aquesta geometria provoca una ruptura de la deslocalització dels electrons π a l'enllaç azo. Els espectres de l'azobenzè *trans* i *cis* són diferents però se sobreposen. L'azobenzè *Trans* mostra una banda molt feble $n-\pi^*$ a prop dels 400 nm, prohibida per simetria, i una transició intensa $\pi-\pi^*$ a prop dels 320 nm. Alternativament, l'azobenzè *cis* mostra una banda $n-\pi^*$ més intensa també prop de 440 nm i bandes $\pi-\pi^*$ més petites a 280 i 250 nm L'isòmer *trans* de l'azobenzè és 10-12 kcal/mol més estable que el *cis*, de manera que resulta en una forta predominança de l'isòmer *trans* en l'equilibri a les fosques¹³⁹.

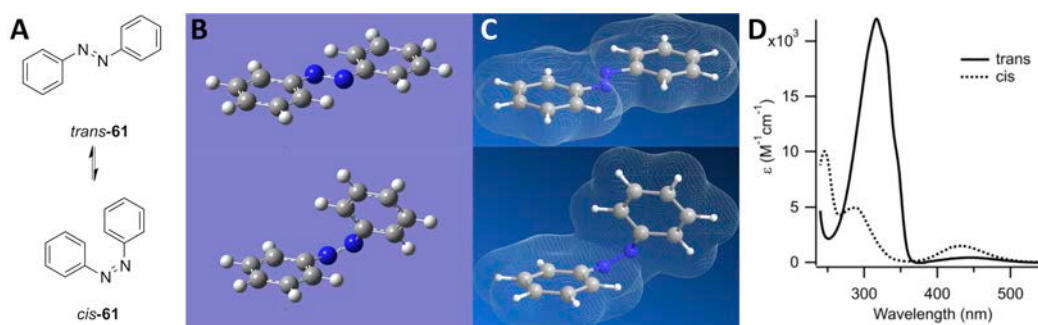


Figura 11: Estructura dels isòmers *trans/cis* i l'espectre d'absorció UV-Vis. A) estructura 2D; B) estructura 3D després de minimitzar l'energia dels dos isòmers amb Gaussian 03 (B3LYP restringit, 6-31G); estructura 3D amb una superfície de densitat electrònica total; D) espectre d'absorció UV-Vis d'ambós isòmers.

^a Dades mesurades després de realitzar minimitzacions DFT dels dos isòmers amb Gaussian 03 (B3LYP restringit, 6-31G)

L'isòmer *cis* es pot obtenir amb il·luminació amb llum ultraviolada (≈ 340 nm), i és possible tornar a l'estat inicial tant tèrmicament com amb il·luminació amb llum visible (>450 nm). Les condicions per isomeritzar de l'isòmer *trans* al *cis* no són adequades per aplicacions biològiques, ja que la llum UV pot ser nociva per teixits i cèl·lules^{148, 149}. De totes maneres, si substituïm els anells de fenil amb grups adequats podem desplaçar aquesta longitud d'ona a rangs amb longituds d'ona més ampla més biocompatibles i, addicionalment, també es pot modificar el temps de relaxació¹⁵⁰. Una prova d'aquest fet és l'amplia varietat de pigments azobenzenics presents a la literatura¹⁵¹, però en la major part dels casos, els seves propietats fotoisomeritzables no estan descrites.

Aproximacions optofarmacològiques

Les maneres més comuns actualment per controlar la funció d'una proteïna o d'una via de senyalització amb llum, es resumeixen en 4 aproximacions: Optogenètica, farmacologia optogenètica, optofarmacologia amb compostos gàbia, i optofarmacologia amb compostos fotoisomeritzables.

L'optogenètica està basada en cromòfors fotoisomeritzables que es troben en la natura i poden commutar la funció de la proteïna amb llum, com pot ser el retinal en les opsines o canalrodopsines o bacteriopsines. Hi ha publicacions on aquestes opsines es transfecten genèticament en cèl·lules cultivades o fins i tot *in vivo* i la seva funció es pot controlar amb llum (*figura 12A*)^{164, 165}.

La farmacologia optogenètica és una aproximació que es basa en l'ús de lligands fotocommutables ancorats (PTLs), que consisteixen en un lligand terminal unit a un fotocommutador intermedi, que alhora està unit en l'extrem oposat a un grup reactiu amb cisteïnes (*figura 12B*). D'aquesta manera, els PTL es poden unir covalentment a una proteïna amb una cisteïna de la superfície, que normalment s'introdueix per mutagènesi^{135, 138}.

L'optogenètica i la farmacologia optogenètica permet el control de les funcions de la proteïna amb precisió i eficiència, però és necessari introduir-hi una modificació genètica, fet que les exclou com a tècniques terapèutiques per humans. La optofarmacologia amb compostos gàbia o compostos fotoisomeritzables són una alternativa valuosa ja que no necessiten manipulació genètica i tenen propietats moleculars que els permetrien ser candidats a fàrmac.

Els compostos gàbia està basat en l'ús de grups protectors fotolàbils que estan enllaçats covalentment a la molècula bioactiva, però sota l'exposició de llum, aquest enllaç es trenca, alliberant així el compost bioactiu de forma irreversible. Aquesta aproximació permet el control espaciotemporal de l'alliberament dels compostos, però un cop s'han alliberat, el seu

control es perd, com en els fàrmacs convencionals. A més a més, alguns productes secundaris de les "gàbies" poden tenir activitats indesitjables o poden ser tòxics. Per aquesta raó el control amb llum per activar i inactivar podria ser una eina interessant¹⁷⁶.

Els lligands fotoisomeritzables poden ser una solució per aquest problema, ja que el fotocommutador (normalment azobenzè) està inclòs en l'estructura o es troba a prop dels grups que interaccionen amb la proteïna. D'aquesta manera s'aconsegueix un canvi destacable en la configuració en l'espai de la molècula sota il·luminació, que pot ser restaurat amb il·luminació amb una segona longitud d'ona per recuperar l'estat inicial (*figura 12D*).

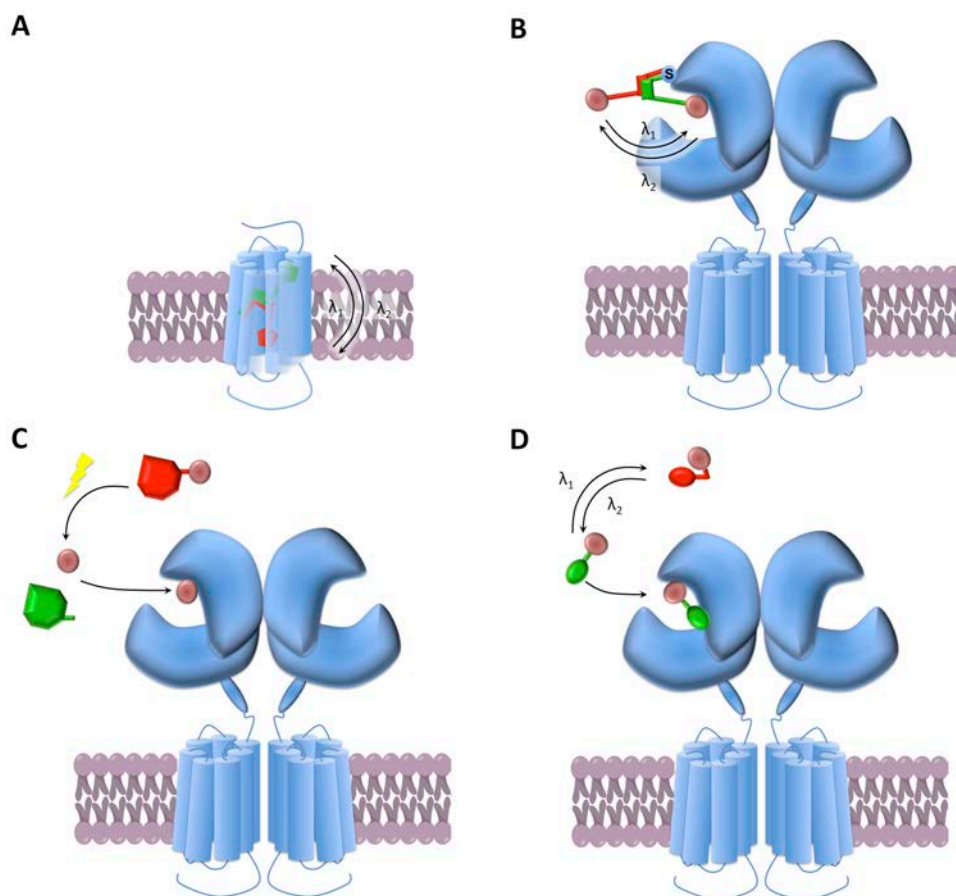


Figura 12: Les quatre principals aproximacions per controlar l'activitat d'una proteïna amb llum: (A) Optogenètica, (B) farmacologia optogenètica, (C) optofarmacologia amb compostos gàbia, (D) optofarmacologia amb compostos fotoisomeritzables. Adaptat de Kramer¹³⁵.

Hi ha dos aproximacions de lligands fotoisomeritzables: (A) Lligands fotoisomeritzables *trans*-on (*figura 13A*), que s'uneixen a la proteïna diana en configuració *trans*, mentre que el *cis* no s'uneix; i (B) lligands fotoisomeritzables *cis*-on, que funcionen de manera oposada: s'uneixen a la proteïna diana en configuració *cis* mentre que en *trans* no s'uneixen (*figura 13B*). Des del punt de vista terapèutic, l'aproximació *cis*-on amb un isòmer *trans* inactiu seria una

aproximació òptima, ja que podríem activar aquest lligand en el lloc d'acció amb un control espaciotemporal complet mentre, fora de lloc d'il·luminació el compost es mantindria inactiu.

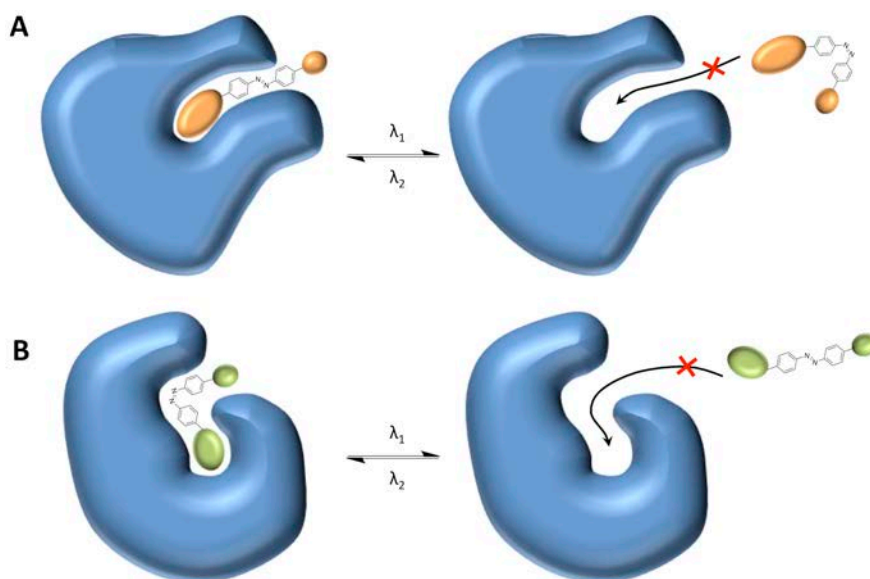


Figura 13: Representació dels modes d'unió dels lligands fotoisomeritzables. (A) aproximació *trans-on*, (B) aproximació *cis-on*

El primer compost fotoisomeritzable amb activitat biològica va ser el bisQ (**72**), que en disposició *trans* obria el porus dels canals nicotínics d'acetilcolina¹⁶⁸. Un altre exemple clàssic és el gluazo (**74**), que és un agonista de GluK1 en disposició *trans*, o la família de bloquejadors de ions potassi AAQ, BzAQ, PrAQ, DENAQ, PhENAQ or QAQ (**73a-f**)¹⁸²⁻¹⁸⁶.

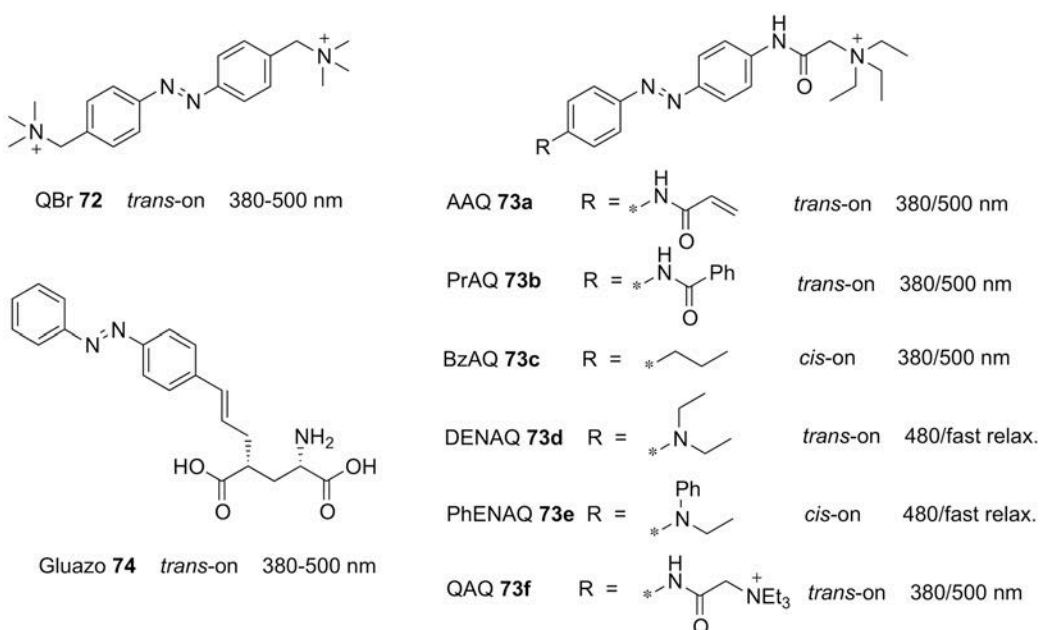


Figura 14: Compostos clàssics fotoisomeritzables amb activitat al CNS

Per obtenir compostos fotocommutables es poden fer servir també fàrmacs o molècules bioactives conegudes. Segons una revisió recent de Trauner¹⁸⁷, hi ha dues aproximacions: "Azo-extensió" i "azologització". L'azo-extensió es pot obtenir amb l'extensió amb un azobenzè d'un anell aromàtic preexistent en un fàrmac o compost bioactiu, sense abolir la seva activitat biològica. Alguns exemples es poden observar a la *figura 15*, com l'azopropofol (**75b**), un derivat d'azobenzè *trans*-on del propofol (potenciador de GABA_A) (**75a**)¹⁹⁰, la quinolona-2 antibacteriana *cis*-on (**76b**), derivada de la ciprofloxacina (**76a**)¹⁸⁹, el AC4, també *cis*-on (**77b**), derivat de la capsazepina (antagonista de TRPV1) (**77a**)¹⁸⁸, o el derivat de l'agonista del GPCR_o opioide μ fentanyl (**78a**), fotofentanyl (**78b**)¹⁹¹.

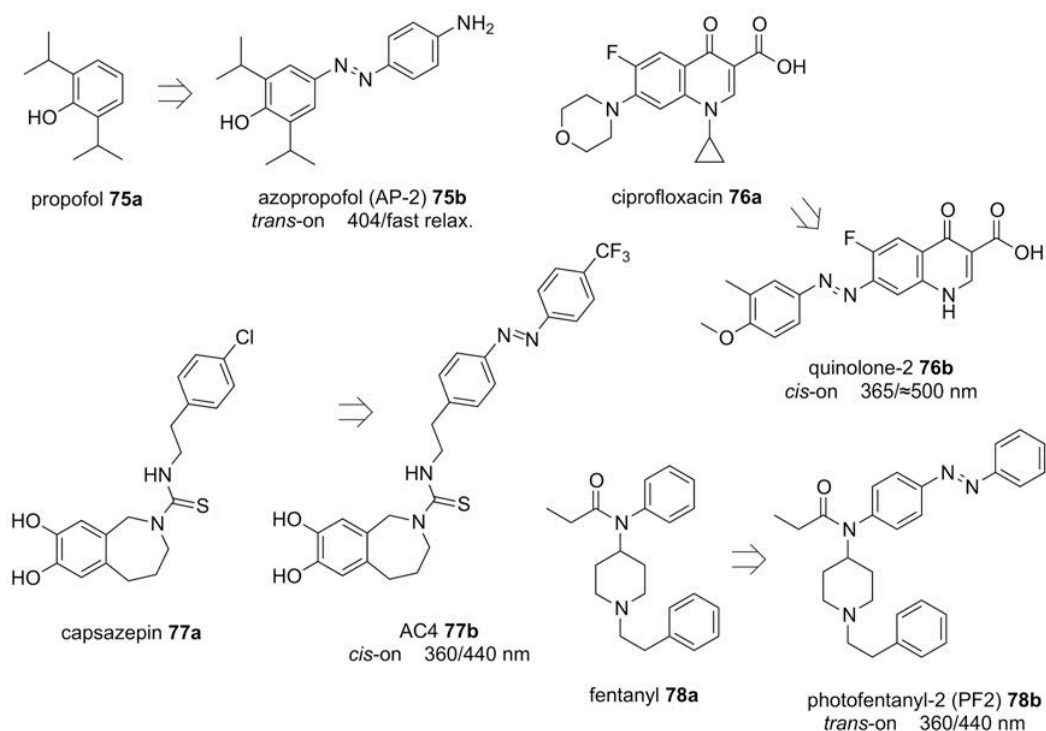


Figura 15: Exemples de l'aproximació azo-extensió per obtenir compostos bioactius fotoisomeritzables

D'altra banda, l'azologització està basada en la substitució d'un pont entre dos anells aromàtics, com un etilè, amida, o metilè èter entre d'altres, per un enllaç azo. Es poden trobar diversos exemples a la literatura, i aquí n'exemplifiquem una petita selecció (*figura 16*): La fotocaina (**79b**) és un derivat *trans*-on de l'anestèsic local fomocaina (**79a**)¹⁹²; el JB253 (**80b**), és un derivat *cis* glimepirida, un inhibidor de canals de K⁺ sensible a ATP¹⁹³; el lípid fotocommutable AzCA4 (**81b**), que és un derivat de la capsaicina, activa els canals TRPV1 en configuració *cis*¹⁹⁴; i, el PST-1 (**82b**), és un inhibidor de microtúbuls *cis*-on amb propietats antimitòtiques i proapoptòtiques, derivat de la combretastatina A-4 (**82a**)¹⁹⁵.

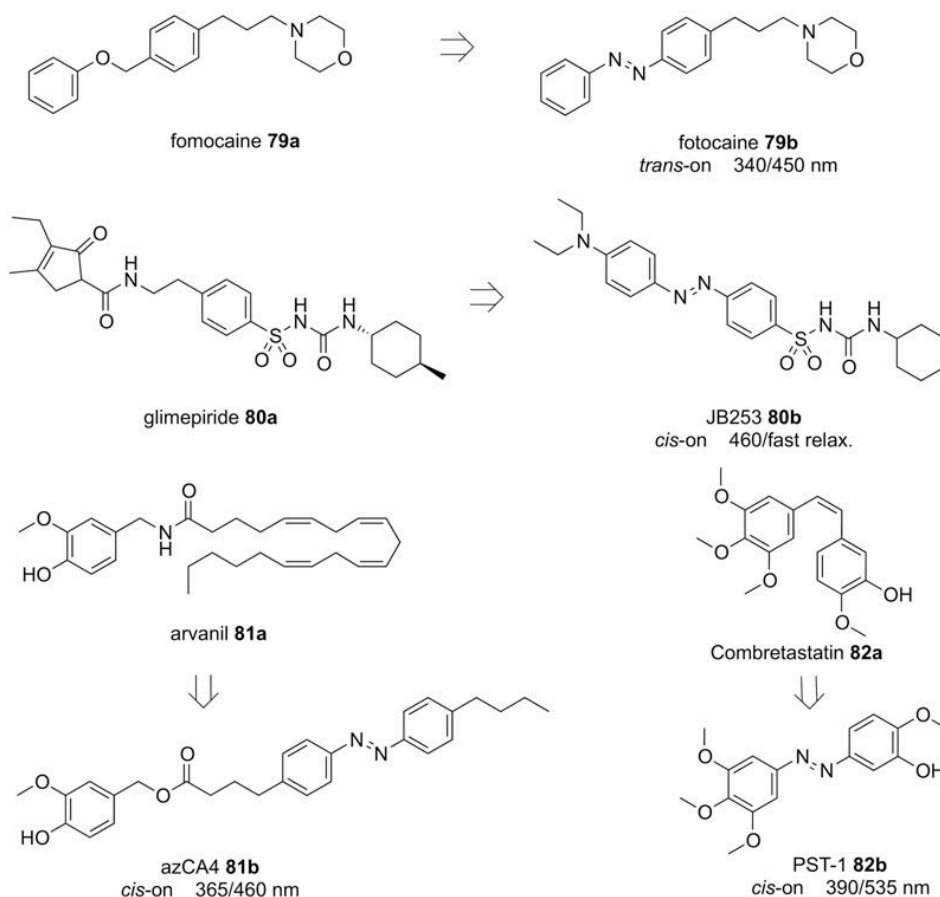


Figura 16: Exemples de l'aproximació de l'azologització per obtenir compostos bioactius fotoisomeritzables.

Aquestes aproximacions, especialment les *cis-on*, obren noves perspectives a la farmacologia, ja que la llum aporta un control espaciotemporal fi, que no s'obté amb farmacologia clàssica. Aquest tipus de molècules poden millorar radicalment la selectivitat, no només d'un subtipus de proteïna, sinó també per una proteïna expressada en una localització concreta de l'organisme i que la seva activitat es pot suprimir un cop s'hagi aconseguit l'efecte terapèutic. D'aquesta manera, podem estar començant a veure la llum d'una revolució farmacològica.

Resultats i Discussió

Capítol 1: l'alloswitch-1 i l'optogluram: una prova de concepte

Disseny de la primera sèrie de compostos fotocommutables

Al principi del projecte en que aquesta tesi està inclosa, vam decidir de dissenyar un modulador al·lostèric positiu (PAM) fotoisomeritzable de mGlu₄, a través de l'azologització¹⁸⁷ d'un PAM de mGlu₄ prèviament conegut. aquesta activitat.

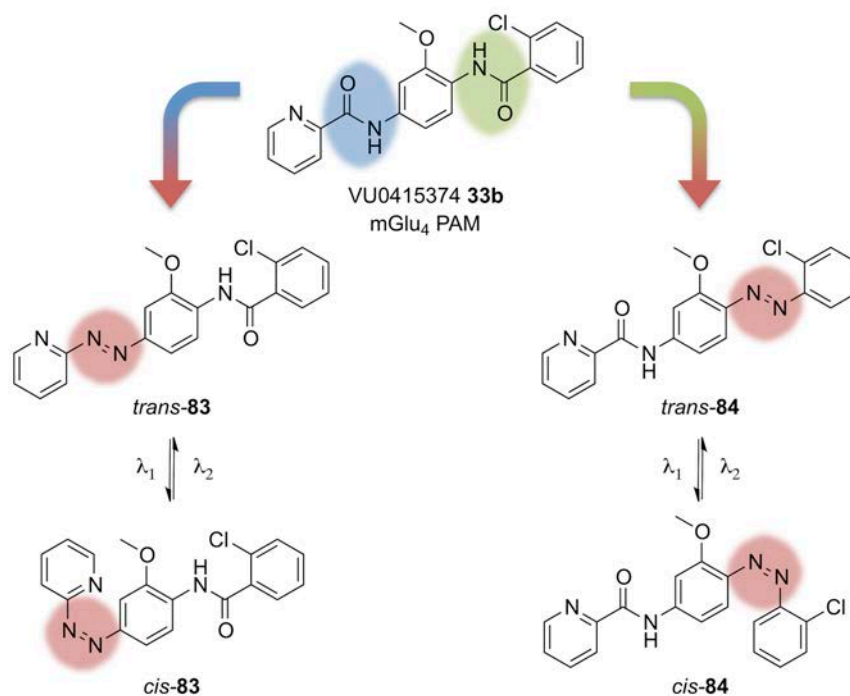
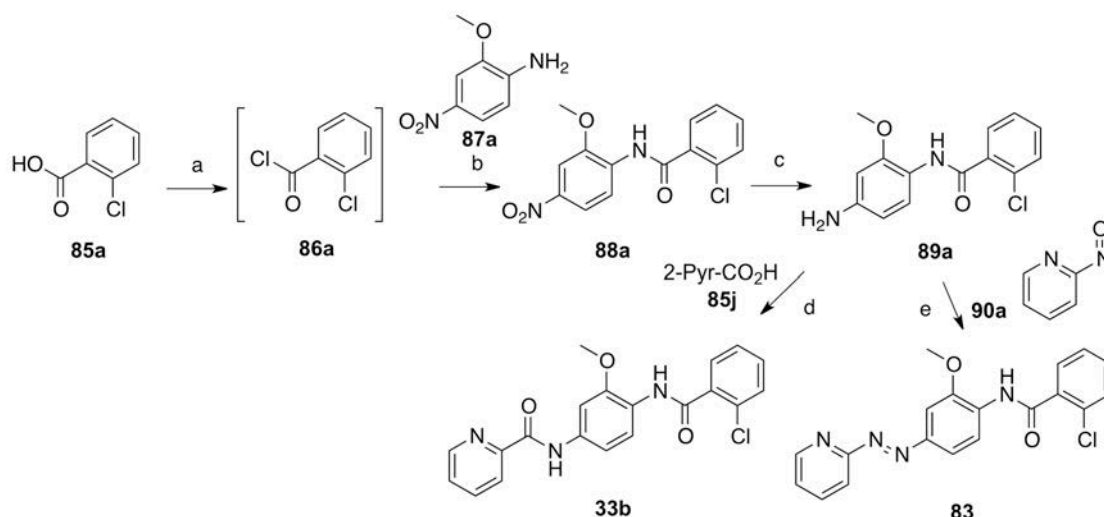


Figura 17: Aproximació d'azologització de VU0415374 (34b) per obtenir els compostos fotoisomeritzables teòrics *trans*-on **83** i **84**.

Per tant, vam buscar a la literatura PAMs de mGlu₄ i vam optar finalment per VU0415374 (**33b**)⁹⁶ per tres raons: (a) era molt potent (EC₅₀ de 99.5 nM); (b) la síntesi aparentment no era difícil; i (c) contenia dues amides entre anells aromàtics, susceptibles de ser substituïdes per un grup azo. Les amides aromàtiques tenen una estructura planar degut a la deslocalització electrònica, de manera semblant als azobenzens, per tant la aproximació utilitzada podria ser correcta. A través de l'azologització, vam substituir l'amida picolínica del compost **33b** per obtenir el compost **83**, mentre que substituint la amida 2-clorofenílica vam obtenir el compost **84** (figura 17). Amb aquesta aproximació, degut a similituds estructurals, els isòmers *trans* haurien de tenir una activitat semblant a la del compost **33b**, mentre que sota il·luminació, els isòmers *cis* no s'haurien d'unir i perdrien la activitat en el receptor.

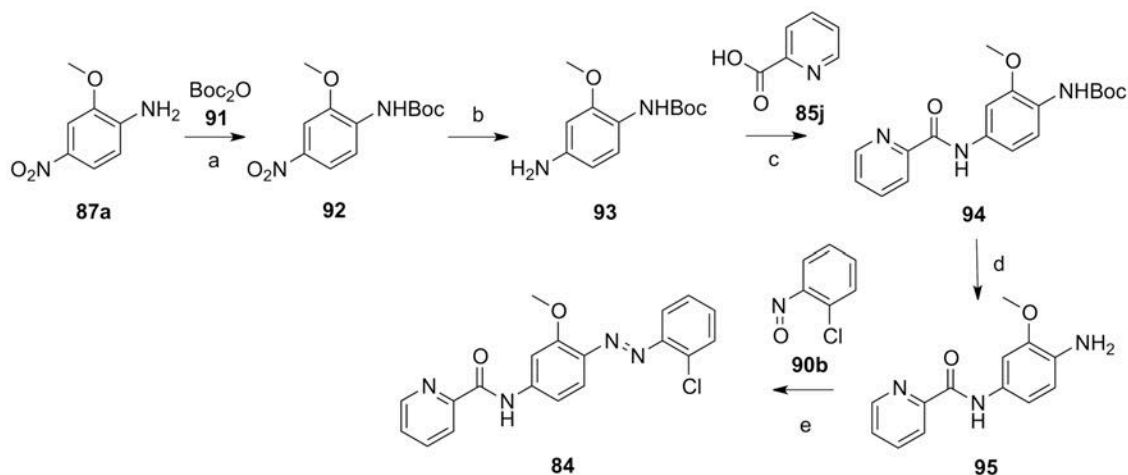
Síntesi dels compostos **33b**, **83** i **84**

Vam sintetitzar el compost **33b** seguint un procediment semblant al descrit prèviament⁹⁶, utilitzant l'anilina **89a** com a intermedi comú **83**. Les dues rutes sintètiques estan representades al *Esquema 1*. La síntesi es va basar en la acilació de la nitroanilina **87a** amb clorur d'àcid 2-chlorobenzoic, la reducció del grup nitro, per donar l'anilina **89a** i la posterior acilació amb àcid picolínic per donar el PAM de mGlu₄ VU0415474 (**33b**). D'altra banda, es va preparar la fenilazopiridina **83** fent reaccionar l'anilina **89a** amb la 2-nitrosopiridina **90** en medi àcid.



Esquema 16: Síntesi dels compostos **33b** i **83**: (a) SOCl_2 , 2h, reflux, quant. (b) DIPEA, DCE, 100°C , 2.5h, 99%; (c) Sn, HCl (aq), THF, reflux, 30 min min, 95%; or H_2 (2 atm), Pt-Fe/C, EtOH, r.t, 15h, quant.; (d) HATU, DIPEA, EtOAc, 40°C , 80%; (e) EtOAc cat., DCM, r.t, 75 hours, 81%

L'azocompost **84** es va preparar segons la següent estratègia sintètica que es mostra en l'esquema 2. Es pot resumir com la protecció del grup amina del compost **87a**, la posterior reducció del grup nitro, l'acilació de l'anilina **93** amb àcid picolínic (**85j**), desprotecció de l'amina amb medi àcid i formació de l'enllaç azo amb 2-cloronitrosobenzè i medi àcid.



Esquema 17: Síntesi del compost **84**: (a) Boc_2O , DCM, r.t., 48 h, 56% (62% conv.); (b) H_2 (2 atm), Pd/C, EtOH, r.t., 5h, 98%; (c) HATU, DIPEA, EtOH, AcOEt, 40°C , 16 h, 88%; (d) TFA, DMF, r.t., 2h, quant.; (e) AcOH cat., DCM, r.t, 3 d, 75%.

Caracterització fotoquímica dels compostos **83** i **84**

Primer es van mesurar l'espectre d'absorció UV-Vis dels dos azocompostos en solució $25 \mu\text{M}$ en DMSO a les fosques. Tots dos espectres tenien la típica banda de transició $\pi-\pi^*$ a 370-390 nm. Després d'il·luminar les mostres dos minuts amb llum amb $\lambda = 380 \text{ nm}$ vam obtenir uns

espectres amb un aspecte diferent. En canvi, després d'il·luminar les mostres a 500 nm vam obtenir pràcticament els mateixos espectres que en condicions a les fosques.

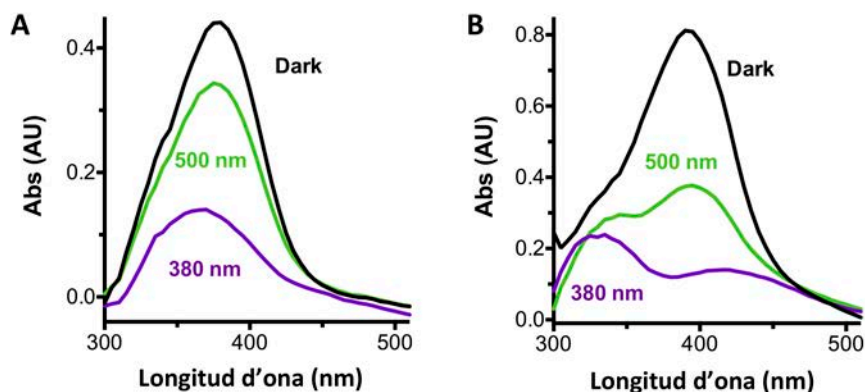


Figura 18: Propietats fotoquímiques de **83** i **84** (1): Espectre d'absorció UV-Vis dels compostos **83** (A) i **84** (B) a les fosques (dark, línia negra), sota il·luminació a 380 nm (línia violeta) i sota il·luminació a 500 nm (línia verda).

Avaluació biològica in-vitro dels compostos **83** i **84**

Corbes dosi-resposta preliminars; X. Rovira, IGF, Montpeller

Primer, els compostos **33b**, **83** i **84** es van avaluar *in-vitro* a les fosques amb un assaig d'acumulació d'inositol fosfat (IP-One) en cèl·lules HEK293 transfectades amb mGlu₄ i G_q-top, que permet l'acoblament amb tots els receptors mGlu. Desafortunadament, el compost **83** no va mostrar activitat en mGlu₄ i l'azobenzè **84** era actiu, però amb una potència molt menor que la diamida **33b**. No obstant això, ja que el compost **83** està relacionat estructuralment amb els NAMs de mGlu5 MPEP (**12**)⁶⁹ or SIB-1757 (**13**)⁷⁵, vam assajar els compostos **83** i **84** en mGlu₅ amb el mateix assaig. Amb aquest nous experiments vam descobrir que el compost **83** era un NAM de mGlu₅ excel·lent amb una potència (IC₅₀) en el rang nanomolar. Degut a les seves excel·lents propietats el vam anomenar alloswitch-1, com el primer modulador al·lostèric capaç de modular la funció d'un GPCR i vam seguir caracteritzant la seva activitat en el receptor mGlu₅.

Caracterització farmacològica in-vitro del compost 83: alloswitch-1; S. Pittolo, IBEC, Barcelona - IGF, Montpeller

Per a caracteritzar farmacològicament l'alloswitch-1 (**83**) i comprovar si la seva fotoisomerització pot alterar l'activitat farmacològica en mGlu₅, es van realitzar assajos IP-One simultàniament a les fosques i sota il·luminació amb 380 nm de longitud d'ona. Amb els resultats de l'experiment, es van generar corbes dosi-resposta a les fosques i amb il·luminació. De fet la potència a les fosques va resultar similar a la dels assajos preliminars (IC₅₀=25±19 nM),

però la potencia pels compostos il·luminats era 100 vegades inferior, el que indica una fotocommutació de l'activitat del mGlu₅ molt consistent.

Per demostrar la reversibilitat de la fotocommutació de l'activitat en mGlu₅, també es va fer un assaig amb alloswitch-1 (**83**), monitoritzant el calci intracel·lular en cèl·lules HEK293 sobreexpressant receptor mGlu₅ (*figura 19B*). En aquest, experiment, l'aplicació del agonista ortostèric quisqualat (**2**) va produir oscil·lacions de calci com a resposta a l'activació de mGlu₅¹⁹⁹. Amb la posterior aplicació de alloswitch-1 (**83**), aquestes oscil·lacions van desaparèixer, però en il·luminació amb llum violeta es van recuperar, indicant que l'activitat del mGlu₅ es reprenia. Seguidament, es va il·luminar la mostra amb llum verda, i les oscil·lacions de calci es van inhibir novament, tancant un procés reversible que es pot repetir diverses vegades de manera efectiva i consistent.

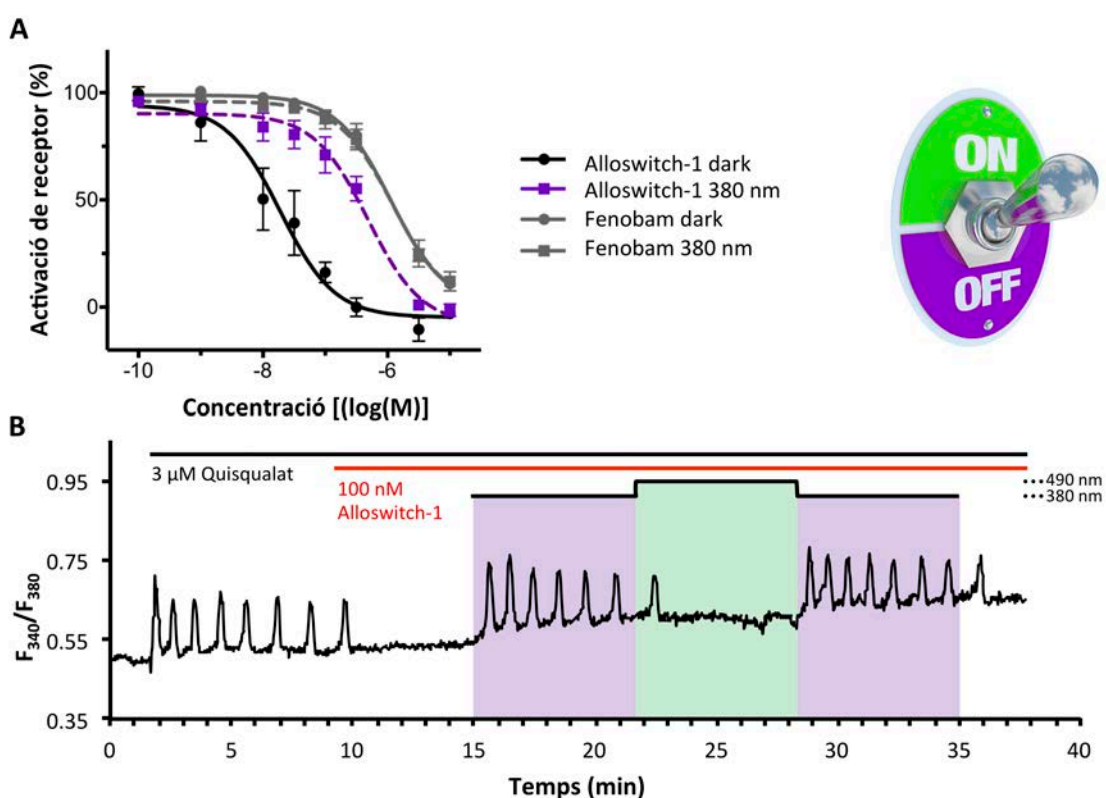


Figura 19: Caracterització farmacològica de l'alloswitch-1 (**83**). (A) Corbes dosi-resposta de l'alloswitch-1 (**83**) amb una concentració constant de quisqualat 100 nM en cèl·lules HEK293 sobreexpressant mGlu₅ en condicions diferents: A les fosques (punts rodons i línia contínua negra), o sota il·luminació a 380 nm (punts quadrats i discontinua negra) El fenobam es va utilitzar com a NAM de mGlu₅ control (línies grises) a les fosques punts rodons i línia contínua), o sota il·luminació a 380 nm (punts quadrats i discontinua) (B) Imatge de calci a temps real amb cèl·lules HEK293 sobreexpressant mGlu₅. Relació de fluorescència de l'indicador de calci (F_{340}/F_{380}) en el temps en cèl·lules individuals tractades amb agonista (3 μ M quisqualat) i alloswitch-1 (**83**). Els quadres corresponen a il·luminació violeta o verda.

Caracterització farmacològica In-vitro del compost 84: optogluram

El compost **84**, tot i tenir una potència menor que VU0415374 (**33b**)⁹⁶, era un bon candidat com a modulador al·lostèric positiu fotocommutable per mGlu₄. Així doncs, li el vam anomenar optogluram i el vam caracteritzar farmacològicament.

Primer vam generar corbes dosi-resposta amb il·luminació utilitzant assajos IP-One amb les mateixes condicions que amb l'alloswitch-1 (**83**), però utilitzant cèl·lules que sobreexpressen mGlu₄. A les fosques, vam obtenir una EC₅₀ de 385±41 nM a les fosques, molt més baixa que el valor obtingut amb les corbes-dosi resposta sense il·luminació preliminar. Una possible explicació d'aquest fet és que en els assajos preliminars, les mostres no es va protegir de la llum ambiental, amb el que hi podria haver una quantitat força gran de isòmer *cis* residual, que fos inactiu.

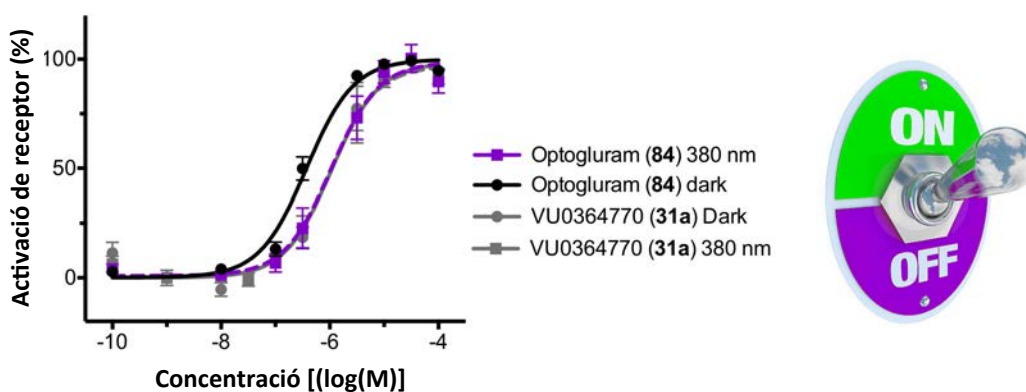


Figura 20: Caracterització farmacològica del optogluram (**84**). (A) Corbes dosi-resposta de l'optogluram (**84**) amb una concentració constant de L-AP₄ (**4**) 3 nM en cèl·lules HEK293 sobreexpressant mGlu₄ en condicions diferents: A les fosques (punts rodons i línia continua negra), o sota il·luminació a 380 nm (punts quadrats i discontinua negra). El VU0364770 (**31a**) es va utilitzar com a NAM de mGlu₅ control (línies grises a les fosques punts rodons i línia continua), o sota il·luminació a 380 nm (punts quadrats i discontinua).

En quant a la isomerització, amb il·luminació amb llum violeta vam obtenir una disminució de 3,5 respecte a la obtinguda a les fosques. Tot i ser una disminució baixa, no vam considerar insatisfactòria, ja que en solució ens va donar satisfactòria i tenia marge de millor si es feien assajos *in-vivo* amb il·luminació més directa.

Capítol 2: els bioisòsters no fotocommutables de l'alloswitch-1 i l'optogluram i la confirmació del commutació molecular doble

Disseny dels bioisòsters de l'alloswitch-1 i l'optogluram

En el capítol anterior havíem descrit una aproximació molecular, on es substituïa una fenil picolinamida del PAM de mGlu₄ VU0415374 (**33b**)⁹⁶ per un grup fenilazopiridina. La nova molècula aconseguida (alloswitch-1) va resultar ser NAM de mGlu₅. Paral·lelament el NAM de mGlu₅ SIB-1757 (**13**)⁷⁵ també conté aquesta estructura de fenilazopiridina i molts altres NAMs contenen una feniletinilpiridina, com l'MPEP (**12**)⁶⁹.

Degut a les semblances electròniques i geomètriques d'aquests dos grups, va, pensar que la substitució de les amides del VU0415374 (**33b**) o de l'enllaç azo de l'alloswitch-1 (**83**) o l'optogluram (**84**), podríem obtenir bioisòsters no fotocommutables d'aquests dos darrers compostos.

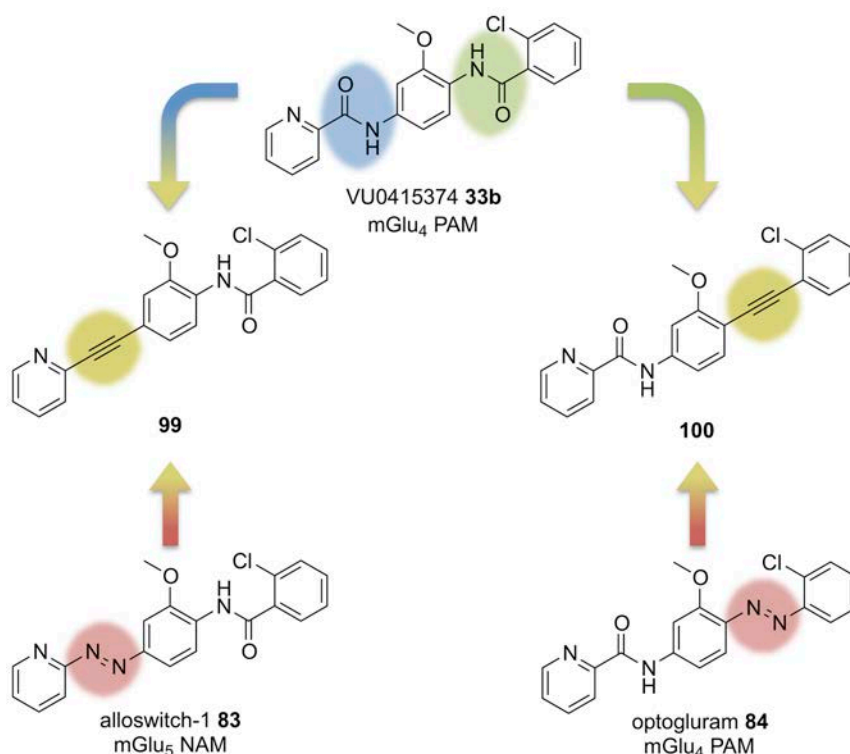
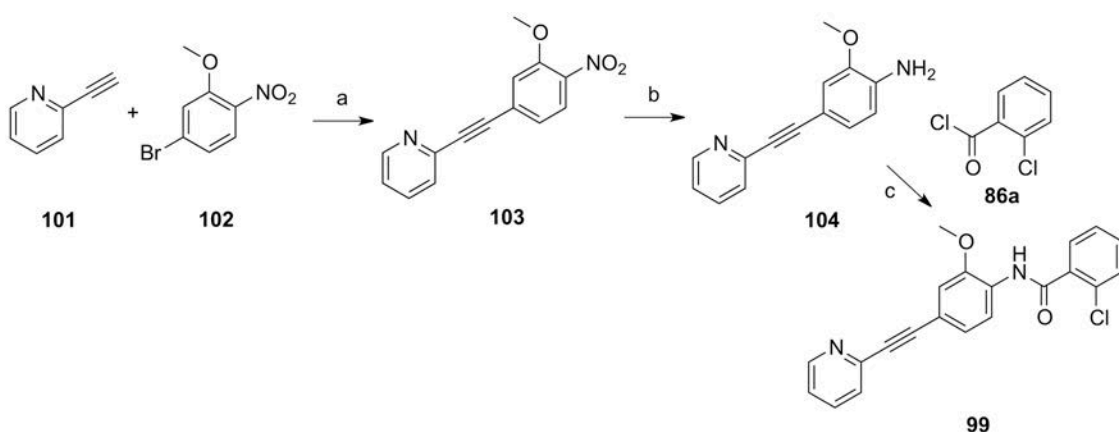


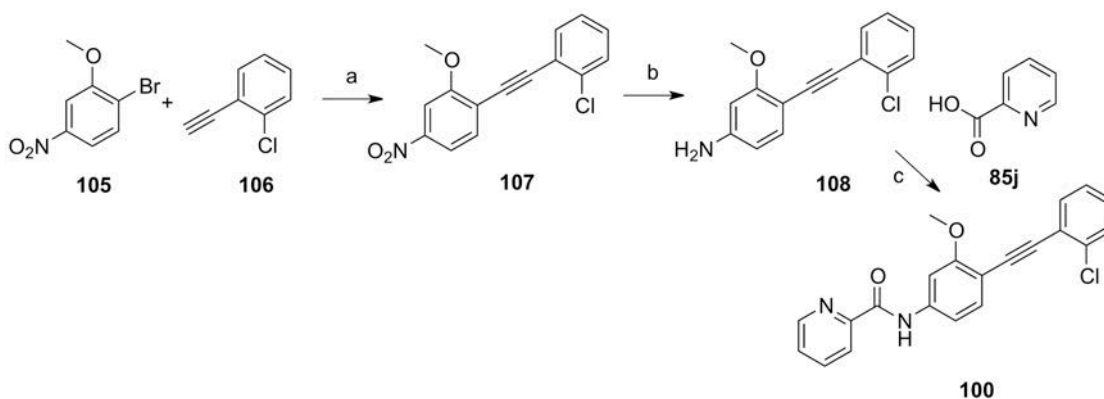
Figura 21: Disseny del compost **99** i **100**, com a bioisòsters de VU0415374 (**33b**), alloswitch-1 (**83**) i optogluram (**84**).

Síntesi dels compostos **99** i **100**

El compostos **99** i **100** es van sintetitzar segons les estratègies sintètiques presentades en l'esquema 3 i l'esquema 4 respectivament. Es pot resumir en un acoblament de Sonogashira dels compostos **101** i **102** o (**105**) i (**106**) seguit per una reducció selectiva del grup nitro i una acilació de l'anilina resultant amb clorur de clorobenzoïl (**86a**) o àcid picòlic (**85j**).



Esquema 18: Preparació de **99**. Reactius i condicions: (a) CuI 2.5 %mol, Pd(PPh₃)₂Cl₂ 2.5 %mol, TEA, DMF, 50°C, 89%. (b) H₂, Pt-Fe/C cat., EtOH, r.t., 89%. (c) i) àcid 2-clorobenzoic, SOCl₂, reflux, 3h, ii) DIPEA, DCE, 90°C, 54%.



Esquema 19: Preparació de **100**. Reactius i condicions: (a) CuI 5 %mol, Pd(PPh₃)₂Cl₂ 5 %mol, TEA, DMF, 50°C, 82%. (b) H₂, Pt-Fe/C cat., EtOH, r.t., 85% (c) àcid picolínic, HATU, DIPEA, DMF, 40°C, 81%.

Caracterització farmacològica dels compostos **99** i **100**

L'activitat funcional dels compostos **33b**, **99** i **100** es va determinar en paral·lel en els receptors mGlu₄ i mGlu₅ amb una assaig d'acumulació de IP (*IP-One*) Els tres compostos van resultar PAMs de mGlu₄ amb potències molt diferents. El compost **33b** va resultar tenir una potència nanomolar (EC₅₀ = 104 nM), mentre que el compost **100** la va disminuir fins al rang micromolar (EC₅₀ = 4 μM) i el compost **99** va realitzar un efecte molt feble.

Pel que fa a mGlu₅, el compost **33b** va resultar ser un NAM molt feble (IC₅₀ = 103 μM) i el **100** va resultar inactiu, però el compost **99** va resultar un NAM molt potent (IC₅₀ = 24 nM), 4 vegades més potent que el MPEP (IC₅₀ = 89 nM), que vam utilitzar com a control de NAM de mGlu₅. Aquests resultats indiquen que la substitució dels enllaços amide per grups etnil no afavoreix l'activitat PAM en mGlu₄ dels nostres compostos, però la substitució de l'amida picolínica per aquest grup és essencial per generar un NAM potent de mGlu₅.

Compost	PAM mGlu ₄		NAM mGlu ₅	
	EC ₅₀ (μM)	SEM	IC ₅₀ (μM)	SEM
33b	0.104	0.017	> 30	
99	> 30		0.024	0.005
100	4.1	0.2	n.a. ^a	
84			0.024	0.019
85	0.39	0.04	n.a. ^a	

Taula 4: Potències dels compostos **33b**, **99** i **100**, obtingudes a partir de les corbes-dosi resposta (figura 22) en mGlu₄ i mGlu₅. Les dades es mostren com a mitjana ± SEM de un mínim de tres replicats independents realitzats per triplicat.

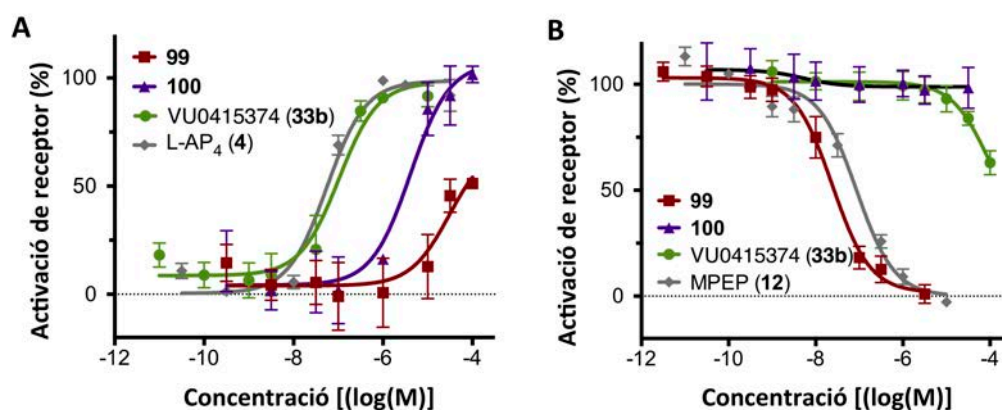


Figura 22: Corbes dosi-resposta dels compostos **33b**, **99** i **100** corresponents a l'assaig IP-One en (A) cèl·lules HEK293 sobreexpressant mGlu₄ amb una concentració constant 10 nM de L-AP₄ (4) i (B) cèl·lules HEK293 sobreexpressant mGlu₅ amb una concentració constant 300 nM de quisqualat (2).

Els resultats obtinguts, afegits als obtinguts en el primer capítol, descriuen un commutador molecular^{77, 78, 81} de doble efecte en el rang nanomolar de potència, en el que modificacions mínimes en l'estructura del lligand han provocat un canvi radical del mode de farmacologia i la selectivitat de subtipus. En aquest cas, un PAM de mGlu₄ molt potent s'ha commutat a NAM mGlu₅, també amb una gran potència. Aquesta alta activitat dels compostos **33b** i **99**, juntament amb els compostos **83** i **84**, que resulten bioisòmers fotoisomeritzables, suggereix una similitud estructural entre els llocs d'unió al·lostèrics de PAMs de mGlu₄ i de NAMs de mGlu₅, ja que són capaços de reconèixer compostos que únicament es diferencien en la funcionalitat de pont entre dos anells aromàtics.

^a No actiu

Capítol 3: Una nova sèrie de fenilazopiridines per controlar finament la funció del mGlu₅ amb llum

Consideracions inicials per dissenyar una sèrie de fenilazopiridines

El disseny una sèrie de compostos fotocromics capaços de induir una fotocommutació farmacològica en l'activitat d'un receptor determinat no és senzill, ja que s'han de tenir en compte diversos factors que es poden resumir en tres condicions:

- d) **Longituds d'ona d'il·luminació biocompatibles**, preferentment en el rang visible, ja que se sap que la llum UV pot ser nociva per cèl·lules i teixits. Amb una longitud d'ona al rang visible, els lligands fotocommutables es poden fer servir durant períodes de temps llargs sense toxicitat.
- e) **Una clara diferència entre les poblacions relatives d'ambdós isòmers entre condicions a les fosques i sota il·luminació, o bé sota dues condicions d'il·luminació.** Aquest fet es pot donar amb una correcta selecció de les longituds d'il·luminació òptimes i una velocitat de relaxació de l'isòmer *cis* adequada (desenes de segons). Al contrari, si els temps de relaxació són massa ràpids, per aconseguir una població *cis* alta, es necessitarien intensitats de llum molt altes, que podrien ser nocives per sistemes biològics.
- f) **Una diferència considerable d'activitat funcional entre dos fotoisòmers per la proteïnes diana.** Un dels isòmers s'ha d'unir al receptor amb una afinitat alta per induir l'activitat funcional desitjada, però l'altre ha de ser completament inactiu o bé tenir una activitat funcional molt menor a l'altre.

L'alloswitch-1 (**83**) ja va complir raonablement aquestes tres condicions, però el SIB-1757 (**13**)⁷⁵, també una fenilazopiridina amb activitat NAM nanomolar en mGlu₅, no les compleix. Això és degut a l'hidroxil de la seva estructura que pot induir un equilibri azo-hidrazona, que provoca una isomerització molt ràpida de l'isòmer *cis* al *trans*¹⁵³, que no ens permet observar isòmer *cis* sota il·luminació.

Per crear una llibreria de derivats de l'alloswitch-1 (**83**), vam decidir no introduir canvis radicals en l'estructura, sinó petites modificacions que puguin alterar pels propietats de l'alloswitch-1, tant de fotoisomerització com biològiques (*figura 23*).

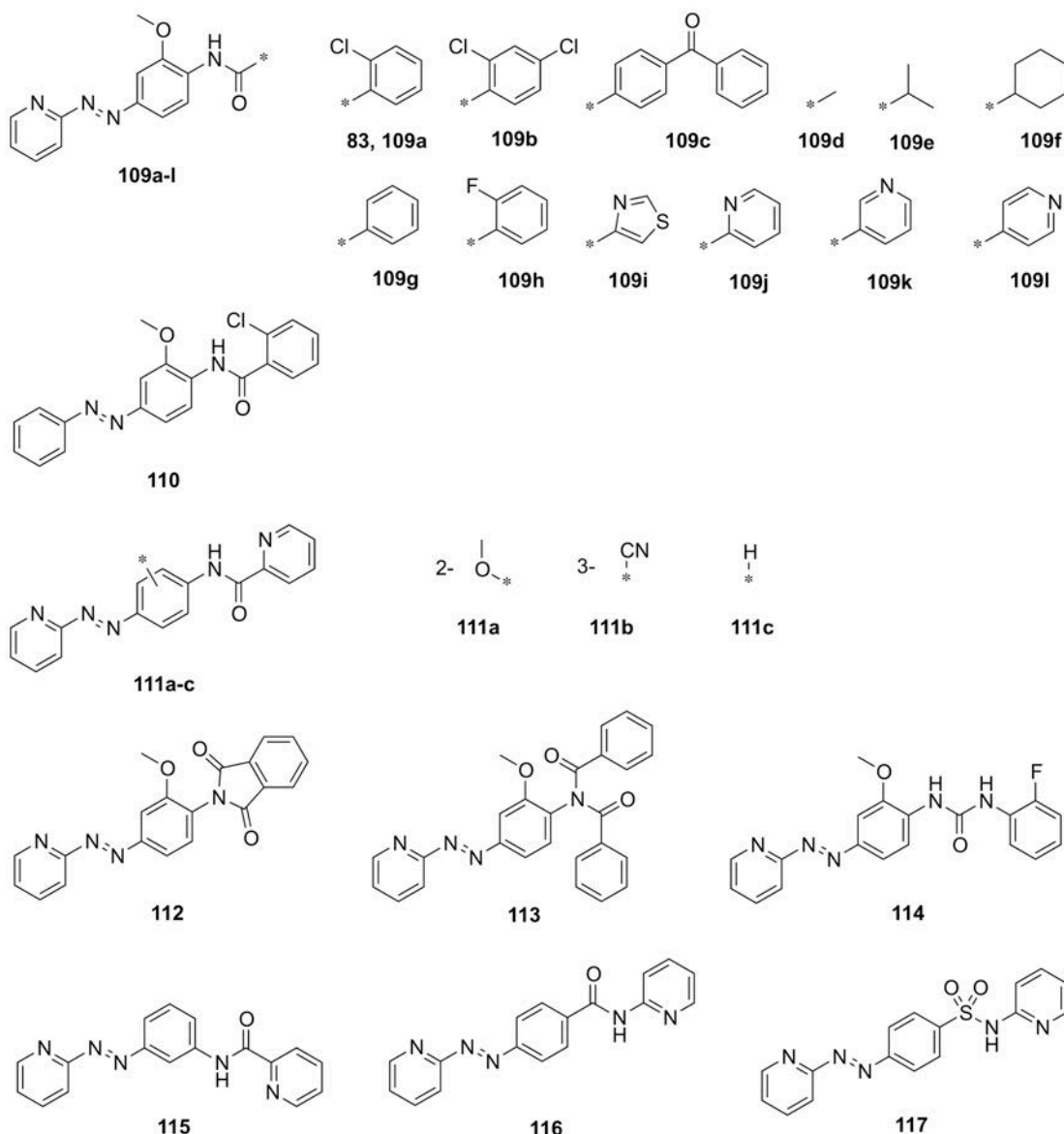


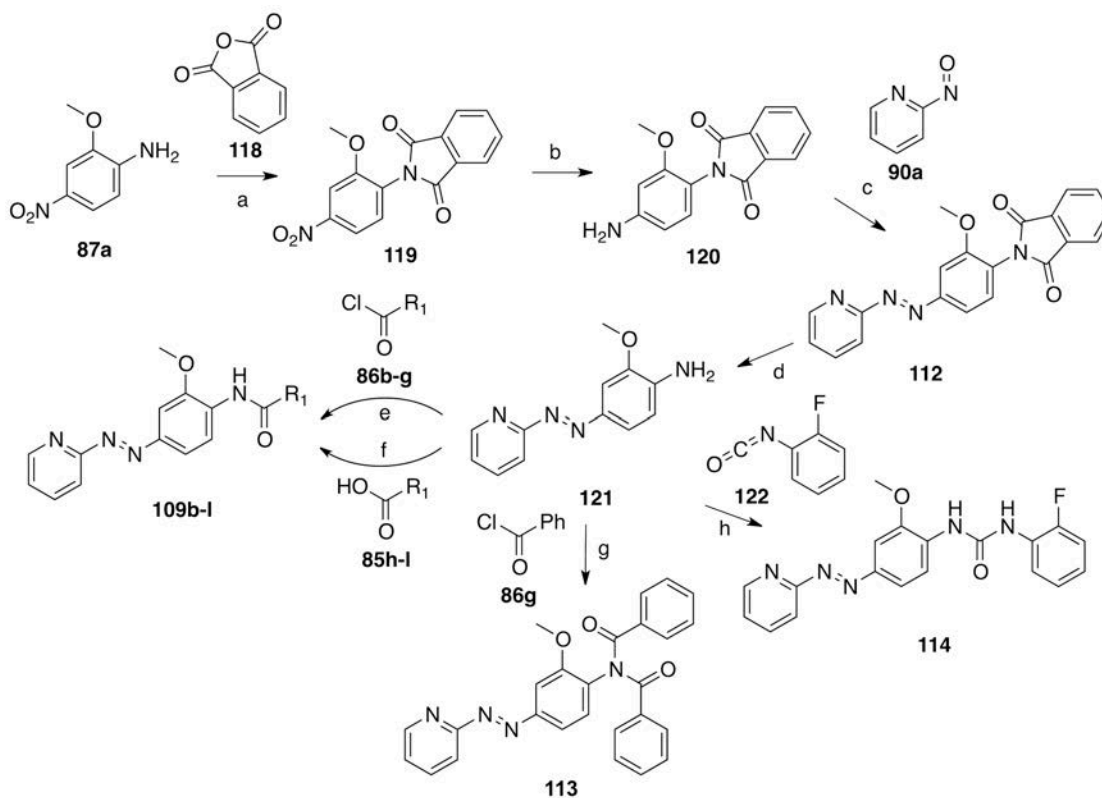
Figura 23: Estructures dels compostos de la nova sèrie de anàlegs del alloswitch-1 ((109-117))

Síntesi

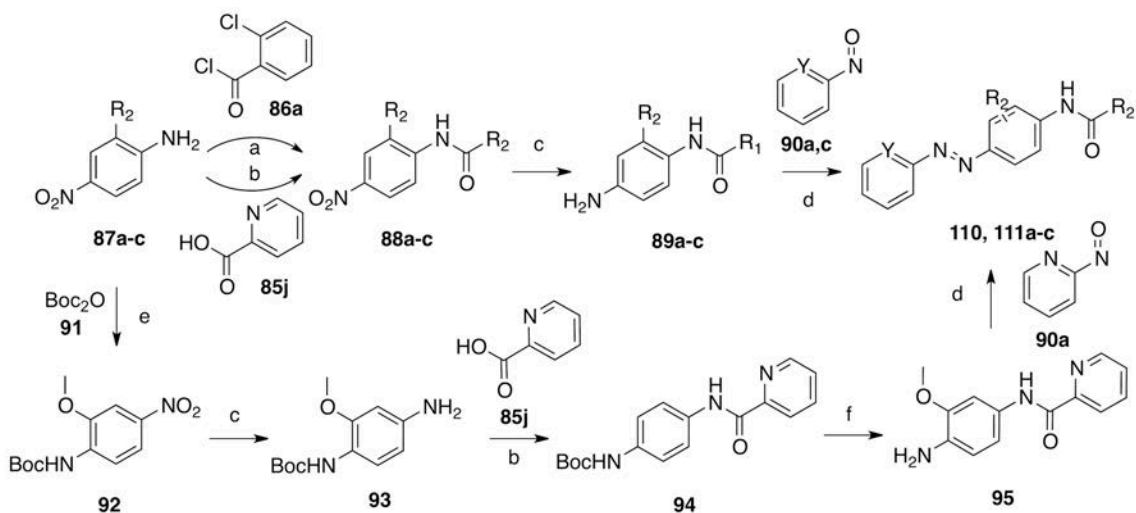
Els compostos **109b-l** i **113-114** es van preparar segons l'estratègia sintètica mostrada en l'*esquema 5*. En resum al síntesi es basa en la protecció de la nitroanilina **87a** amb anhídrid ftàlic, la posterior reducció del grup amino, la formació de l'enllaç azo amb 2-nitrosopiridina **90a**, la desprotecció de la primera amina i com a darrer pas l'acilació d'aquesta amb els corresponents grups acilants, o bé la formació d'urea amb l'isocianat **122**.

Els compostos **110** i **111a-c** es van preparar seguint la estratègia sintètica mostrada en l'*esquema 6*. Pels compostos **110** i **111b-c** primer es va acilar la nitroanilina **87b-c** amb els corresponents àcids carboxílics, es va reduir el grup nitro, i l'anilina resultant es va acilar amb els nitrosoarils **90a-b** corresponents en medi àcid. Pel compost **111a**, totes les etapes

sintètiques les mateixes que per sintetitzar els compostos **33b** i **83** excepte la darrera etapa que es forma l'enllaç azo nitrosobenzè **90b** en medi àcid.

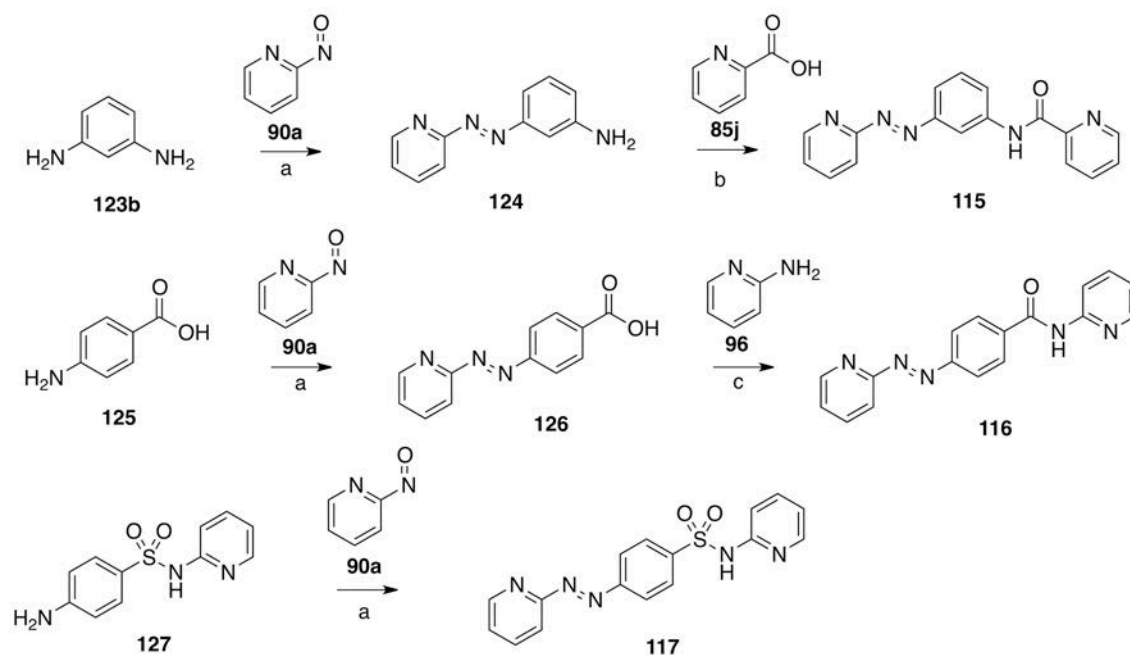


Esquema 20: Síntesi de **109b-l**, **113-114**. Reactius i condicions: (a) AcOH, reflux, 18 h; 54%; (b) H₂ (2 bar), Pd/C cat., 1-4-dioxà, r.t., 5 h, quant.; (c) AcOH cat., DCM, r.t., 40h, 89%; (d) MeNH₂ 40% (aq.), EtOH, 65°C, 2 h, 92%; (e) DCE, DIPEA, 40°C, 22 h 86-89%; (f) HATU, DIPEA, DMF, 40°C, 22h, 52-93%; (g) DCE, DIPEA, DMAP cat. 40°C, 22h, 89%; (h) DIPEA, THF, 40°C, 22h, 75%.



Esquema 21: Síntesi de **100**, i **111a-c**. Reactius i condicions: (a) DCE, DIPEA, 100°C, 2.5 h or HATU, DIPEA, DMF or EtOAc, 40°C, 22h (85-99%); (b) H₂ (2 bar), Pt+Fe/C or Pd/C, EtOH/1,4-dioxà r.t. 5 h, 97-100% (c) AcOH cat., DCM, r.t., 20-72h, 47-68%; (d) DCM, r.t., 48 h, 62% conv., 54%; (e) TFA, DCM, r.t., 2h, quant.

L'azocompost **115** es va preparar segons la següent estratègia sintètica que es mostra en l'*esquema 7*. Resumidament, es va formar l'azocompost **124** amb la *m*-fenilendiamina **123b** i 2-nitrosoanilina **90a** en medi àcid i posteriorment es va acilar amb àcid picolínic. El compost **116** es va preparar segons la estratègia sintètica que es mostra també en l'*esquema 3*, per l'acoblament de l'àcid 4-aminobenzoic **125** i la 2-nitrosoanilina **90a** i seva posterior acilació amb la 2-aminopiridina **126**. El compost **117** es va preparar amb l'acoblament de la sulfapiridina **127** i la 2-nitrosoanilina **90a** en medi àcid, com es mostra en l'*esquema 7*.



Esquema 22: Síntesi of **7-9**. Reactius i condicions: (a) AcOH cat., DCM, r.t., 1-6 dies, 27%; (b) HATU, DIPEA, DMF, 40°C, 84%; (c) i) SOCl₂, 75°C, 3.5h, ii) DIPEA; DCE, 90°C, 2h, r.t., 64h, 26%.

Caracterització fotoquímica dels compostos 109-117

Espectroscòpia d'Absorció UV-Vis dels isòmers cis i trans

Vam poder mesurar l'espectre de absorció UV-Vis d'ambdós isòmers de tots els compostos mitjançant separació cromatogràfica amb per HPLC acoblat a un detector de sèrie de fotodíodes (PDA) i a espectròmetre de masses (MS). D'aquesta manera, el PDA ens proporcionava l'espectre d'absorció i podíem corroborar la massa del pic que ens donava el MS. Els isòmers *trans* presentaven una banda π - π^* en el rang entre 310-400 nm, tot i que la major part de fenilazopiridines tenien aquest màxim al voltant dels 380 nm (*figura 24D*). Els isòmers *cis* tenien la banda típica n - π^* amb el màxim al rang 420-450 nm (*Figura 24D*).

La situació d'aquestes bandes depèn de la naturalesa dels substituents dels anells aromàtics dels azocompostos¹⁵². Per exemple, el compost **117**, que té una sulfonamida, desplaça el

màxim que en l'alloswich-1 (**83**) es troba a 370 nm fins a 310 nm, degut a la sulfonamida que és electron-atraient, fent-lo inviable per aplicacions biològics. En canvi, el compost amb urea **114** desplaça aquest màxim a 387 nm, o l'intermedi **121**, amb una simple amina, el desplaça fins a 417 nm, degut a que tenen grups electron-donadors.

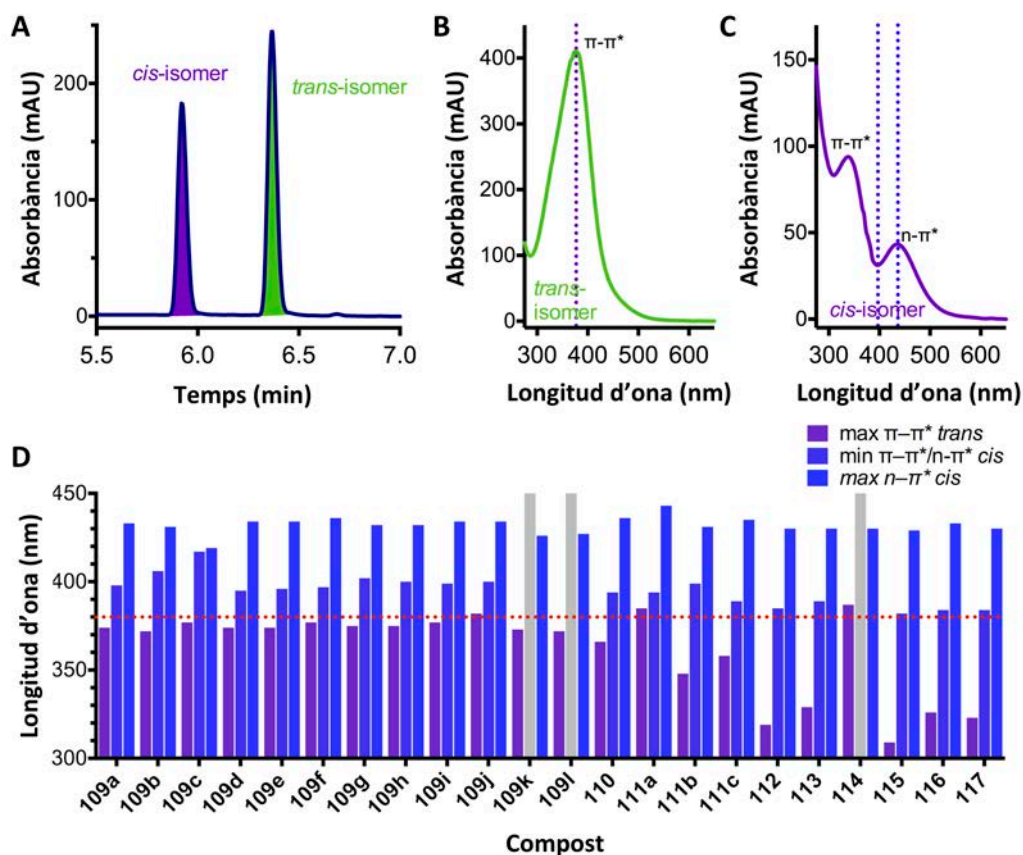


Figura 24: Espectre d'absorció de UV-Vis extret de l'anàlisi per HPLC-PDA-MS d'una mescla de fenilazopiridines *cis* i *trans*. (A) Ampliació del cromatograma del compost **109f** entre 5,5 i 7,0 minuts amb detecció a 254 nm, just on tant l'isòmer *cis* com el *trans* s'elueixen. El primer pic correspon al isòmer *cis*, ja que l'espectre de masses correspon al **109f** i l'espectre UV-Vis a perfil de azobenzè *cis*, amb les bandes de transició $\pi\text{-}\pi^*$ i $n\text{-}\pi^*$ típiques (C). El segon pic correspon a l'isòmer *trans*, tenint en compte l'espectre de masses amb una sola banda de transició $\pi\text{-}\pi^*$ (B). (D) Longituds d'ona d'absorbància màxima de les bandes $\pi\text{-}\pi^*$ de l'isòmer *trans* (barres violetes), mínima del isòmer *cis* entre les bandes de transició $\pi\text{-}\pi^*$ i $n\text{-}\pi^*$ (barres liles) i longituds d'ona del màxim de l'isòmer *cis*, corresponent a la transició $n\text{-}\pi^*$ (barres blaves). Les barres grises corresponen als mínims d'absorció de l'isòmer entre les bandes de transició $\pi\text{-}\pi^*$ i $n\text{-}\pi^*$ que no es poden mesurar. Pràcticament en tots els compostos, els 380 nm es troben entre el màxim de l'isòmer *trans* i el mínim de l'isòmer *cis*, pel que 380 nm és una bona longitud d'ona per il·luminar.

Fotoisomerització dels compostos **109-117** amb espectroscòpia d'absorció UV-Vis

Per mesurar el grau d'isomerització, vam preparar mostres dels compostos en DMSO amb concentració 25 μM i escollir 380 nm com a longitud d'ona per il·luminar ja que es trobaria a prop de la longitud d'ona òptima per la major part dels compostos i, així, maximitzar la

quantitat de isòmer *cis* obtingut en il·luminar. Per realitzar la isomerització inversa, vam escollir 500 nm ja que està a prop de la transició n- π^* de l'isòmer *cis*.

Com amb els compostos **83** i **84** (*capítol 1*), les fosques només van detectar isòmer *trans*, mentre que sota il·luminació a 380 nm, vam obtenir diferents quantitats d'isòmer *cis* que tornarien a *trans* en il·luminar a 500 nm.

Compost	$t_{1/2}$ (s)	$\lambda_{\text{illum.}}$ (nm)	PIS _{f-v}	PIS _{v-v}
109a	54	380	5	3
109b	25	380	4	3
109c	19	380	3	2
109d	489	380	4	4
109e	556	380	4	3
109f	353	380	5	3
109g	71	380	4	3
109h	65	380	3	2
109i	41	380	4	3
109j	134	380	4	4
109k	15	380	1	1
109l	13	380	1	0
110	187	380	5	4
111a	75	380	5	4
111b	25	380	4	0
111c	322	380	5	4
112	245	380	3	2
113	46	380	3	2
114	10	380 400	2 5	1 4
115	62	380	2	1
116	-	380	1	0
117	-	380	1	0

Taula 5: Dades de fotoisomerització pels compostos **109-117**

Amb la informació obtinguda dels espectes vam proposar un "graü fotoisomerització" (PIS) com un index per mesurar l'efectivitat de la fotocommutació (entre 0-5; 0 no isomerització, 5 isomerització màxima). La majoria de compostos tenen un perfil de fotoisomerització semblant

a l'alloswitch-1 (**83**), amb algunes excepcions, com podrien ser els compostos que tenen el màxim d'absorbència desplaçat al UV, o amb una velocitat de relaxació més gran.

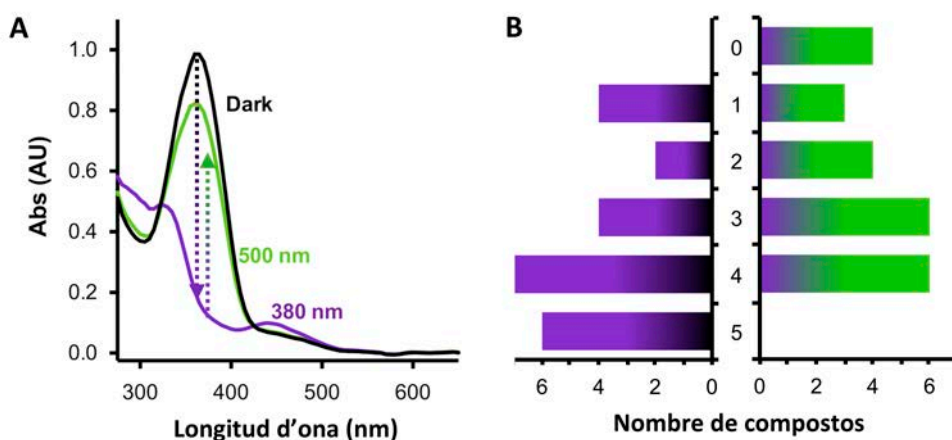


Figura 25: Fotoisomerització dels compostos **109-117**. (A) Espectre d'absorció UV-Vis del compost **111c** en solució 25 µM en DMSO. La línia negra correspon a l'espectre a les fosques, al violeta, després d'il·luminar a 380 nm, i la verda després d'il·luminar amb 500 nm (B) Relació de nombre de compostos amb el grau fotoisomerització amb il·luminació a 380 nm (barres violetes) i sota il·luminació a 400 nm (barres verdes)

Avaluació biològica in-vitro dels compostos 109-117

Per avaluar l'activitat farmacològica de totes les fenilazopiridines primer vam realitzar un experiment a dosi simple amb un assaig d'acumulació d'IP (IP-One) en mGlu₅ com a NAMs. Pràcticament tots els compostos de la sèrie van donar actius com a antagonistes de mGlu₅, excepte el **117**.

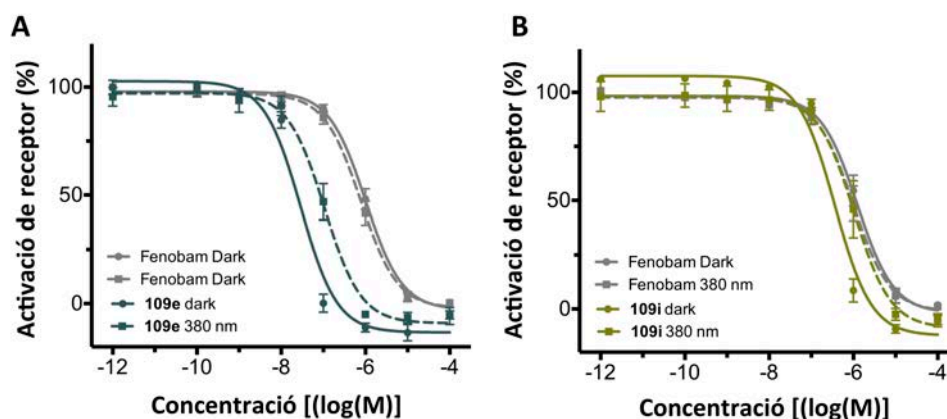


Figura 26: Corbes dosi-resposta generades a partir dels experiments en que s'utilitzava l'assaig IP-One en cèl·lules sobrexpressant el receptor mGlu₅ amb una concentració constant de quisqualat (**2**) 100 nM. Les línies contínues corresponen a les mostres incubades a les fosques (dark) i les discontinúes, a les il·luminades amb 380 nm. Cada punt correspon a la mitjana de un mínim de tres replicats independents amb la corresponent SEM com a barres d'error.

Per tant vàrem haver d'estudiar tots els compostos actius amb corbes dosi-resposta. Vam generar corbes dosi-resposta utilitzant l'assaig d'acumulació de IP IP-One, amb il·luminació com havíem utilitzat per l'alloswitch-1 (83). Les diferents IC₅₀ que vam obtenir estaven entre el rang del baix nanomolar fins al micromolar, amb alguns compostos més i menys potents que l'alloswitch-1 (83).

Compostos	λ d'illuminació	IC ₅₀ (nM)	SEM (nM)	PPS
109a	380 nm	297	77	5.1
109b	380 nm	904	82	7.1
109c	380 nm	1884	44	1.7
109d	380 nm	183	36	3.7
109e	380 nm	30	4	3.7
109f	380 nm	76	12	4.8
109g	380 nm	180	28	4.1
109h	380 nm	308	43	4.1
109i	380 nm	328	18	2.5
109j	380 nm	309	5	2.9
109k	380 nm	356	57	1.3
109l	380 nm	1025	257	1.2
110	380 nm	4667	392	2.5
111a	380 nm	31661	3601	>13
111b	380 nm	2002	334	3.6
111c	380 nm	3209	269	>13
112	380 nm	2496	32	3.2
113	380 nm	1477	265	3.3
114	380 nm	1204	220	4.4
115	380 nm	14029	1826	1.5
116	380 nm	7785	640	2.1
Fenobam (14)	380 nm	1603	269	0.9

Taula 6: IC₅₀ i desplaçament de potencia fotoinduït (PPS) obtingut de les corbes dosi-resposta (mínim 3 replicats independents) *n.t. no assajat,

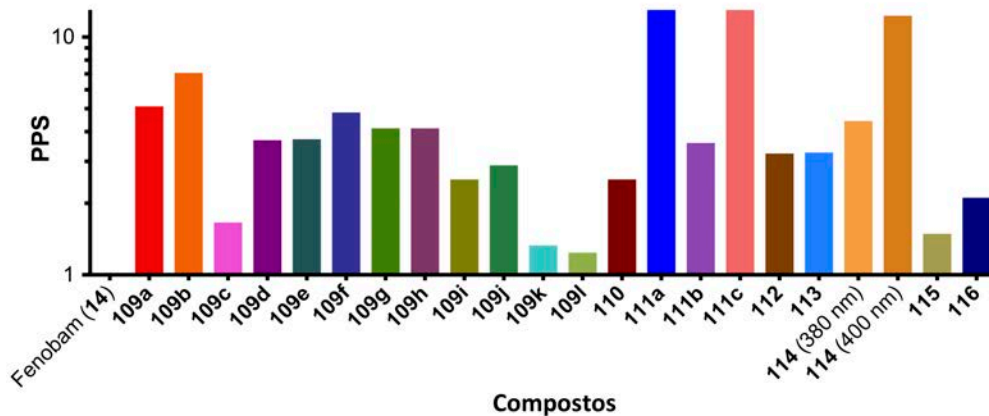


Figura 27: Propietats de fotocommutació en assajos cèl·lules en mGlu₅. Desplaçament de potència fotoinduït (PPS) de cada compost extret de les corbes dosi-resposta en mGlu₅.

Pel que fa a les propietats de fotocommutació, vam obtenir uns desplaçaments de potència fotoinduïts (PPSs, quocient entre IC₅₀ sota il·luminació i IC₅₀ a les fosques) que no depèn de la potència de cada compost però sí que depèn del grau de fotoisomerització (PIS) calculat a partir dels espectres UV-Vis. Aquest fet valida la hipòtesi central de l'optofarmacologia per aquesta família de compostos.

Avaluació biològica *in-vivo* dels compostos 109-115

Assajos In-vivo amb peixos zebra a dosi simple a les fosques

Vam seleccionar les fenilazopiridines amb una millor eficàcia en els assajos d'acumulació de IP per assajar-los amb assajos de comportament de larves de peixos zebra. En un primer punt, l'activitat de tots els compostos es va avaluar monitoritzant la locomoció dels peixos a les fosques. D'aquesta manera, es van administrar de 10 µM de cada compost al medi dels peixos, i es va gravar el seu recorregut i la distància nedada per cada un d'ells es va integrar cada 5 minuts (*figura 28A*).

Pràcticament totes les fenilazopiridines de la sèrie van induir inhibició de la motilitat dels peixos zebra amb diferents mesures, excepte el compost **115**, que va induir un petit augment de la motilitat dels animals (*figura 28B*), si es compara amb l'efecte del vehicle. Les raons per aquest comportament anormal són desconegudes. Vam utilitzar el darrer període de 25-30 min per avaluar l'efecte farmacològic *in-vivo* de cada compost (*figura 28C*) i vam observar que el grau d'inhibició de la motilitat de la major part de compostos era comparable a les potències obtingudes als assajos cel·lulars.

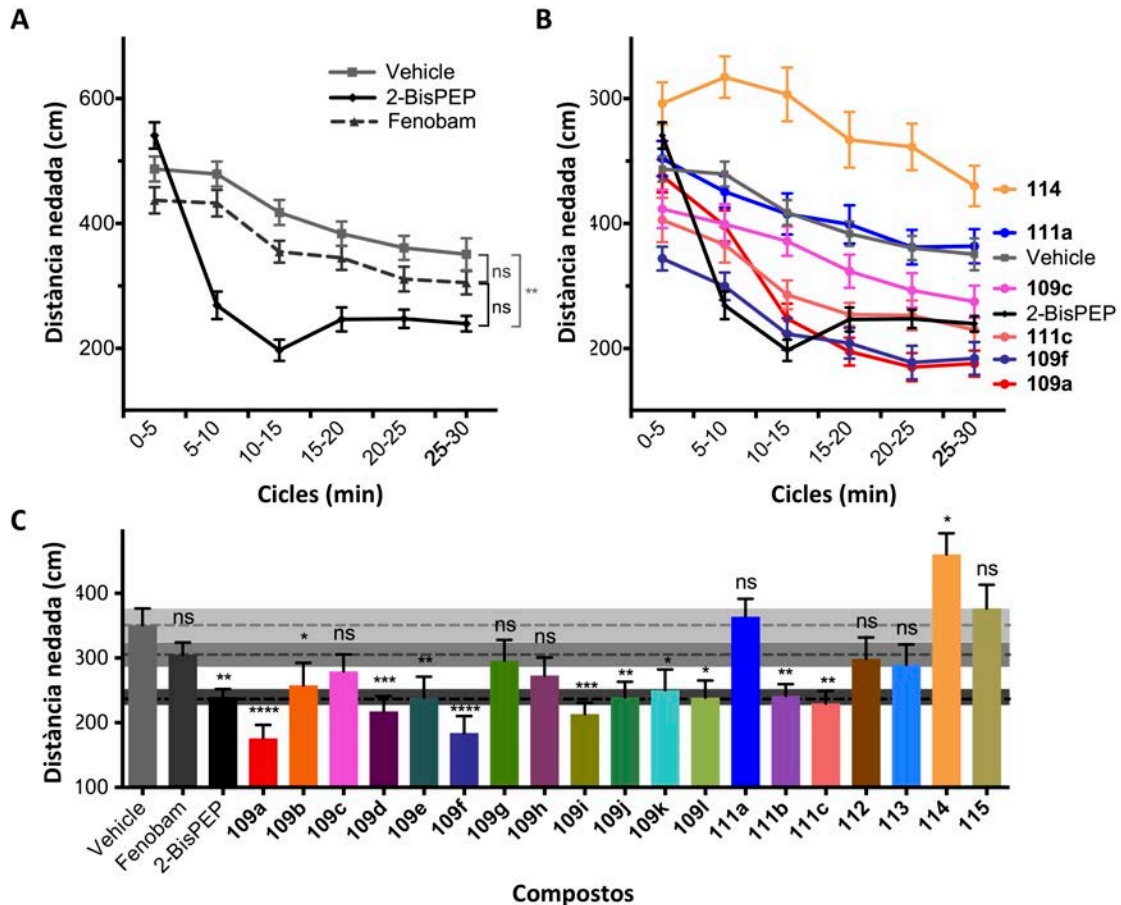


Figura 28: Assaig in-vivo amb larves de peixos zebra de 7 dies en condicions de foscor. (A,B) Integració de la distància nedada total per cada 5 minuts després de l'aplicació de 10 μ M de les solucions de control (A) o els compostos diferents (B) Els valors corresponen a la mitjana i la SEM a les barres d'error d'un mínim de 30 animals. L'anàlisi de variància (ANOVA de dos vies (compost, temps) amb el temps com a mesura repetida i incloent la correcció de Šidák; * $p < 0.05$, ** $p < 0.01$, *** $p < 0.001$, **** $p < 0.0001$) va mostrar diferències significatives en la resposta d'alguns compostos amb la del vehicle (només es mostra el període 25-30 min). El fenobam (14) no va mostrar un efecte significat quan es compara amb el vehicle, però sí que ho fa el 2-BisPEP (53). (C) Integració de la distància nedada total durant 5 minuts, 25 minuts després de l'administració dels compostos. Els valors corresponen a la mitjana i la SEM a les barres d'error d'un mínim de 30 animals.

Assajos In-vivo amb peixos zebra a dosi simple amb llum

Per avaluar les propietats de fotocommutació fisiològica *in-vivo*, vam fer un nou assaig amb exactament els mateixos animals després de fer l'experiment a les fosques. Amb aquest segon experiment, es mesurava la motilitat dels peixos amb una integració de la distància nedada cada 60 s. Vam aplicar sis cicles repetitius que consistien en un minut a les fosques i un minut sota il·luminació amb llum violeta ($\lambda = 380$ nm). Entre els cicles amb llum violeta i a les fosques, s'il·luminava també durant 5 s amb llum visible per accelerar la relaxació de les fenilazopiridines de la configuració *cis* a la *trans*. Tots els cicles amb llum violeta van provocar

un augment de la motilitat dels peixos, incloent els tractats amb vehicle i 2-BisPEB. No obstant això, els tractats amb 2-BisPEB mostraven una inhibició sostinguda de la seva mobilitat independentment de les condicions de llum, quan es compara amb el vehicle (*figura 29A*).

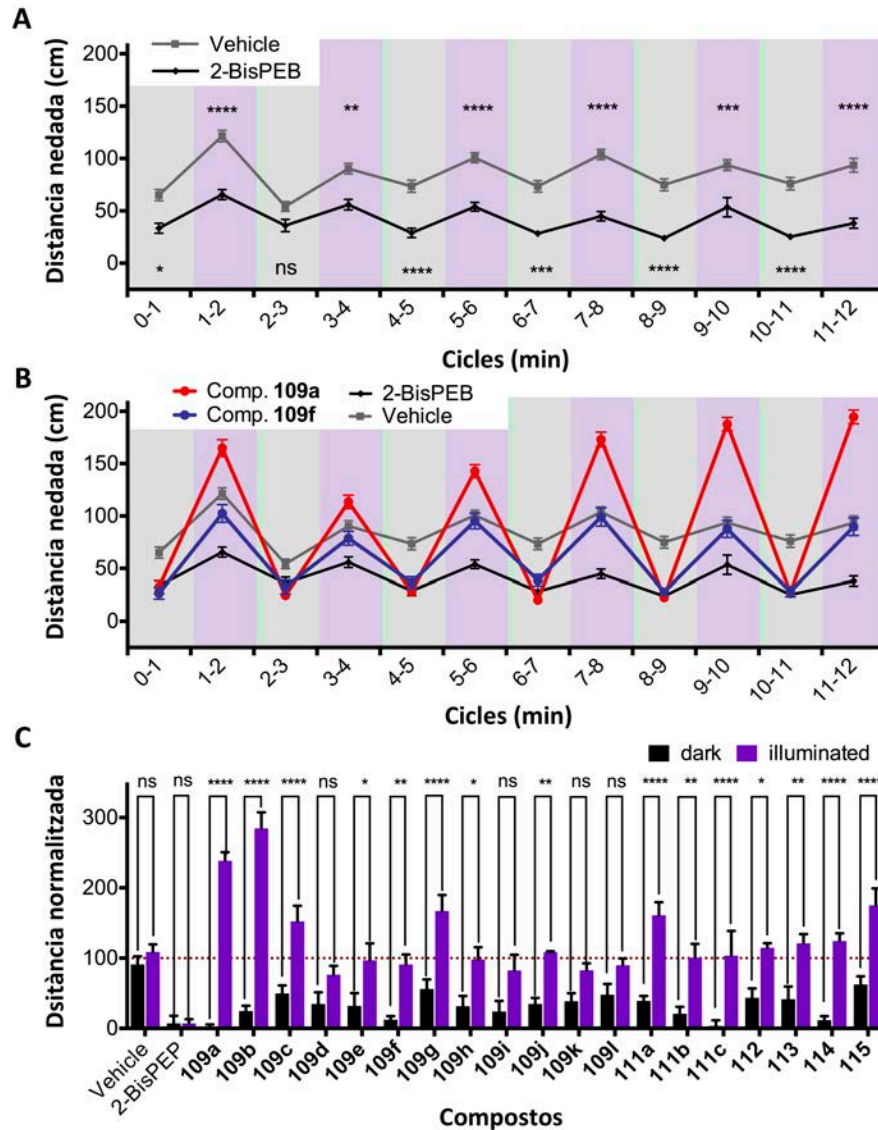


Figura 29: Assaig in-vivo amb larves de peixos zebra de 7 dies amb llum. (A-C) Integració de la distància nedada total per cada minut. 5 minuts, 25 minuts després de l'administració dels compostos. Vam aplicar repetitivament el següent cicle: 1 min a les fosques i 1 min amb il·luminació violeta. Entre les dues condicions cam il·luminar els animals 5 s amb llum blanca. Anàlisi variància (ANOVA de dos vies (compost, temps) amb el temps com a mesura repetida i incloent la correcció de Šidák; * $p < 0.05$, ** $p < 0.01$, *** $p < 0.001$, **** $p < 0.0001$). El vehicle i el 2-BisPEB mostren diferències significatives (A) i el compost **109a** i **109f** a una concentració $10 \mu\text{M}$ inhibeixen la motilitat animal de manera similar al 2-BisPEB a les fosques (fons gris), mentre que sota llum violeta (fons violeta), els peixos tractats amb **109f** recuperen el comportament normal i els tractats amb **109a** experimenten un augment de la seva motilitat (B). Els valors corresponen a la mitjana i la SEM a les barres d'error d'un mínim de 24 animals (A-B). (C) Eficàcia de fotocommutació in-vivo dels compostos **109a-l**, **111b,c** i **112-115** amb l'anàlisi de variància corresponent. Cada barra correspon a la mitjana (amb la SEM com a barres d'error) de la suma dels punts de les distàncies

nedades a les fosques i sota il·luminació violeta per cada experiment (6 animals per experiment, 4 experiments), restant l'efecte corresponent al 2-BisPEB (**53**) i normalitzant les distàncies per l'efecte més baix i l'efecte del vehicle per minimitzar l'efecte de la llum no corresponent a l'efecte dels compostos administrats. Anàlisi variància (ANOVA de dos vies (compost, condicions de llum) amb les condicions de llum com a mesura repetida i incloent la correcció de Šidák; * $p < 0.05$, ** $p < 0.01$, *** $p < 0.001$, **** $p < 0.0001$) .

En general, per totes les fenilazopiridines de la sèrie, l'efecte inhibitori a les fosques desapareixia amb llum a 380 nm, i es recuperava al següent període d'il·luminació de forma reversible (*figura 29BC*). No obstant això, vam trobar dos comportaments diferents sota il·luminació a 380 nm:

- c) Un grup de compostos que causen una motilitat en línia a la del vehicle (com el compost **109f**)
- d) Un grup de compostos que indueixen una sobreactivació de la motilitat dels animals, sobrepassant els nivells que mostren els peixos tractats amb el vehicle (com el compost **109a**)

Les sobreactivacions de la motilitat dels peixos, observades per algun dels compostos, són un efecte atípic que només es pot observar utilitzant compostos fotocommutables i seran subjecte d'estudis futurs per poder donar-hi explicacions moleculars. Tots els compostos indueixen una regulació de la motilitat dels peixos zebra que depèn de la llum (*figura 29D*) amb diferents graus. Com és evident, els compostos que provoquen sobreactivacions sota il·luminació violeta mostren diferències significatives més grans en la seva fotocommutació. Tot i això, les diferències per quasi tota la resta de compostos encara era significatives. De fet, la diferència de entre els valors de llum i a les fosques de cada compost de la *figura 29D* correlacionen amb el grau de fotoisomerització (PIS) (coeficient de Pearson $r = 0.70$, $P = 0.025$) i amb el logaritme del desplaçament de potència fotoinduït (PPS) (coeficient de Pearson $r = 0.83$, $P = 0.0031$). Tots aquests resultats mostren una alta robustesa dels nostres compostos fotoisomeritzables a través de diversos assajos, des de compostos en solució fins a assajos de comportament *in-vivo*, passant per assajos cel·lulars *in-vitro*.

Capítol 4: La busca de PAMs de mGlu₄ PAMs i NAMs de mGlu₅ duals: Azoligització i amidació del 2-BisPEB

Consideracions inicials i disseny dels compostos 128-133

Com hem explicat en el *capítol 1 i 2*, entre els llocs d'unió al·lostèrics de PAM de mGlu₄ i NAM mGlu₅ poden tenir un grau de similitud molt gran, ja que poden reconèixer compostos que

només difereixen en funcionalitats molt concretes. Per tant, seria plausible dissenyar i sintetitzar compostos amb les dues activitats farmacològiques: PAM de mGlu₄ i NAM mGlu₅.

Un exemple addicional d'aquesta dualitat seria el cas dels compostos **109j** i **111a**, del capítol 3. El compost **109j** va resultar un NAM potent de Glu₅ en assajos cel·lulars (figura 30), mentre que el compost **111a**, que només difereix en la posició del grup metoxi, és un PAM de mGlu₄ (figura 30) i no té una activitat negligible en mGlu₅.

Com el nostre objectiu en aquest capítol era aconseguir les dues activitats en un sol compost, vam decidir prescindir del grup metoxi. Aquest fet, ens podria fer perdre potència, però els possibles efectes sinèrgics a la sinapsi, podria compensar aquesta petita pèrdua d'activitat.

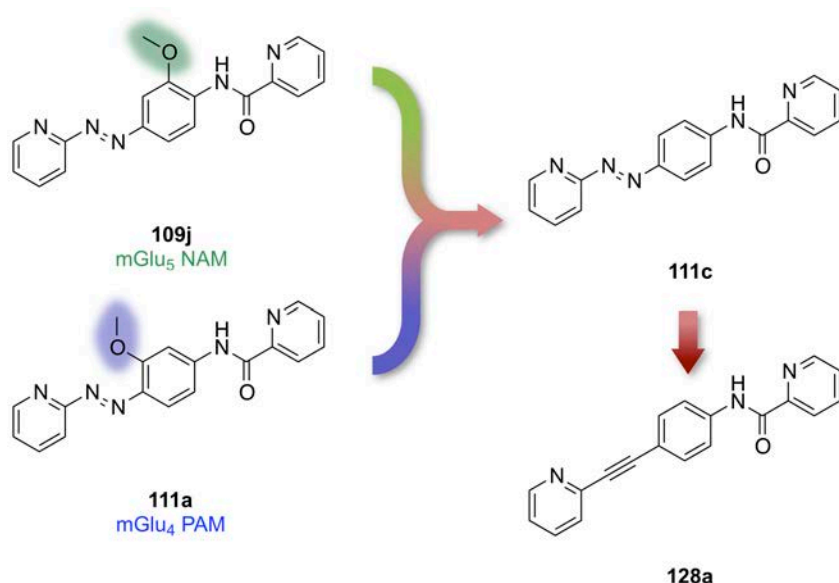


Figura 30: Disseny dels compostos duals PAM de mGlu₄ i NAM de mGlu₅. Si es treu el grup metoxi dels compostos **109j** i **111a** s'arriba al compost **111c** que pot tenir activitat dual com PAM de mGlu₄ i NAM de mGlu₅. LA "desazologització" del compost **111c** donaria el compost no fotocommutable **128a** amb una possible activitat dual.

De fet aquest compost ja es va sintetitzar (**111c**) en la sèrie anterior i era un NAM Glu₅ al rang micromolar baix (IC₅₀ = 3.2 μM), però quedava pendent l'assaig en mGlu₄. A més a més, ja que el compost **111c** conté una fenilazopiridina va considerar la seva "desazologització", substituint l'enllaç azo per un acetilè i aconseguir un bioisòmer no fotoisomeritzable.

Ja que el **111c** i **128a** comprenen un anell de fenil unit en posició 1,4 a dues piridines amb tres possibles ponts: azo, acetilè o *N*-àmida, vam decidir cobrir totes les possibles combinacions i estudiar com poden afectar a l'activitat PAM₄ i NAM de mGlu₅. També vam cobrir la substitució 1,3, ja que el 2-BisPEB^{124, 209} estaria inclòs dins aquestes combinacions en posició 1,3 i és un NAM de mGlu₅ molt potent.

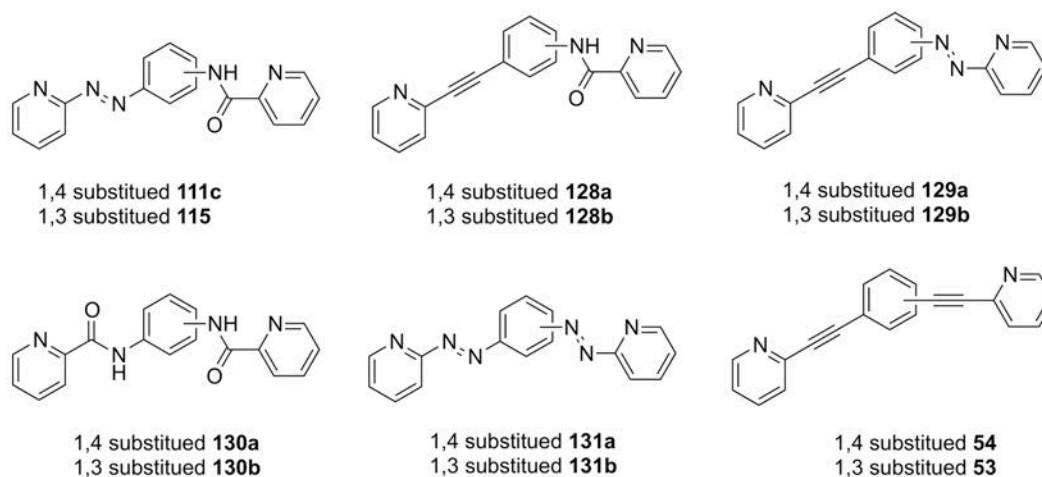
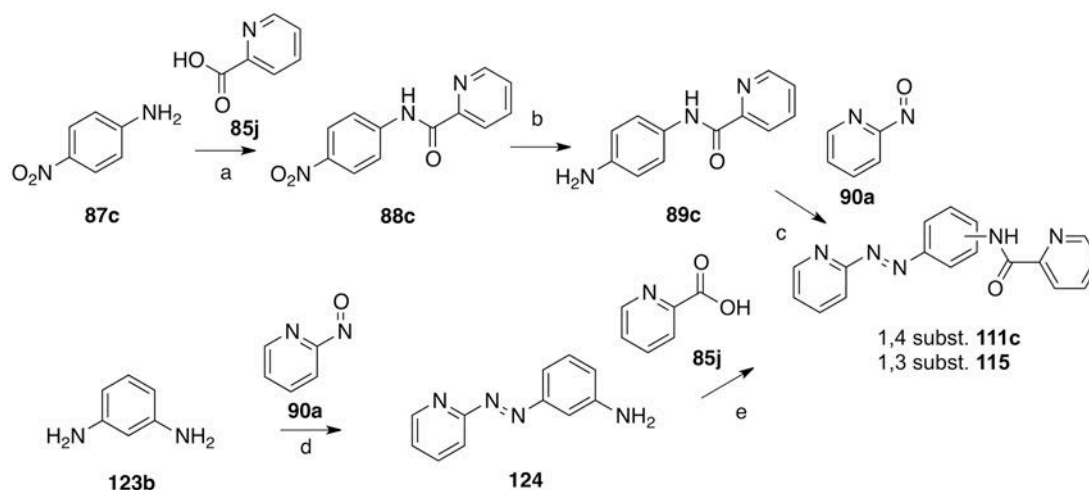


Figura 31: Noves series de compostos **128-132**

Síntesi dels compostos **111c**, **115**, **128-131**, **53**, **54**

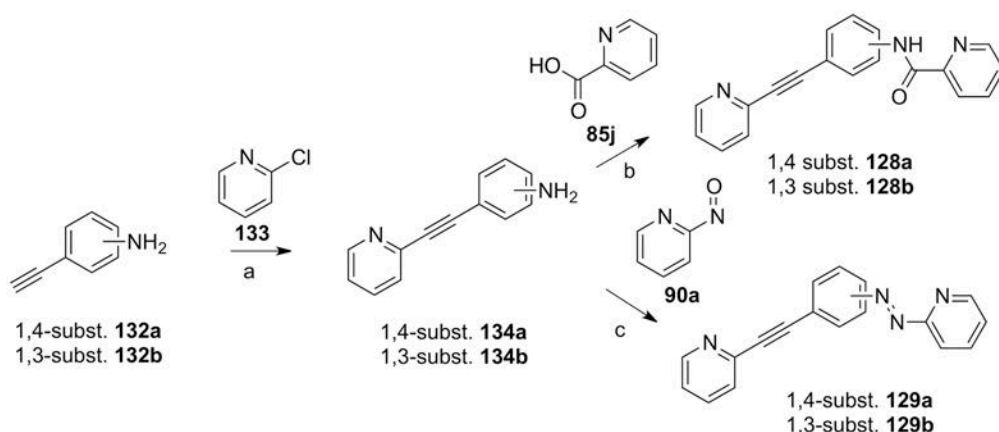
Els compostos **111c** i **115** es van preparar segons la següent estratègia sintètica que es mostra en l'*esquema 8*. Les estratègies sintètiques estan descrites en el *capítol 3*.



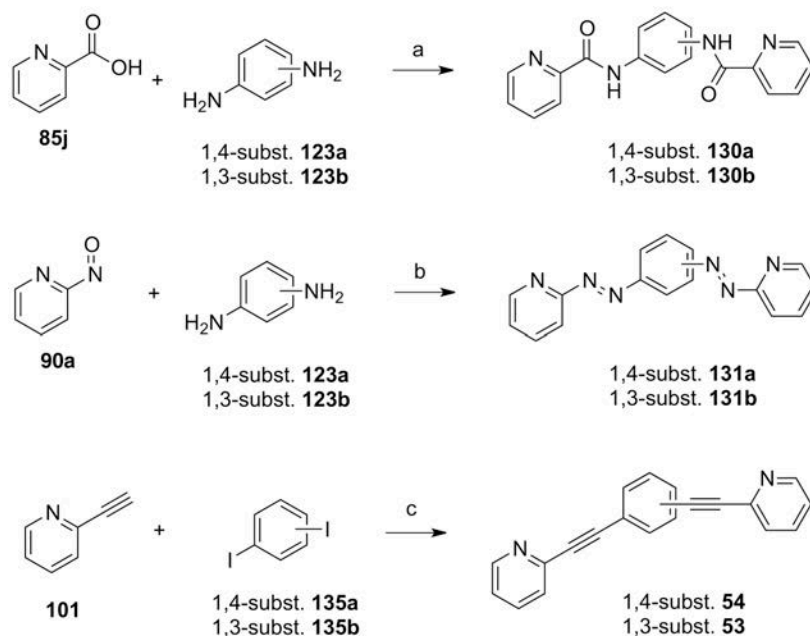
Esquema 8 Síntesi de **111c** i **115**. Reactius i condicions: (a) HATU, DIPEA, DMF, 40°C, 22h (94%); (b) H₂ (2 bar), Pd/C, EtOH/1,4-dioxà r.t. 5 h, 97% (c) AcOH cat., DCM, r.t., 20-72h, 49%;

Els compostos **128a-b** i **129a-b** es van preparar seguint la estratègia sintètica que es mostra en l'*esquema 9*. En resum, es parteix d'un acoblament de Sonogashira de les etilamines **133a** o **133b** amb la 2-cloropiridina (**134**) i les anilines resultants s'acilen amb àcid picolínic (**85j**) o es formen el corresponents azoderivats fent-les reaccionar amb la 2-nitrosopiridina (**90a**).

Els compostos simètrics **130-132** es van preparar en una sola etapa, com es mostra en l'*esquema 10*: amb l'acilació de les fenilendiamines **122a** i **122b** amb l'àcid picolínic, o la l'acoblament amb 2-nitrosopiridina **90a**, o bé amb un acoblament de Sonogashira dels diiodobenzens **136a** i **136b** amb 2-etilpiridina **101**.



Esquema 24: Síntesi de **128a-b** i **129a-b**. Reactius i condicions: (a) PdCl₂(PPh₃)₂, CuI, Et₃N, DMF, 60°C (**135a** 23%, **135b** 30%); (b) HATU, DIPEA, DMF, 40°C (**128a** 83%, **128b** 78%); (c) AcOH cat., DCM, r.t., 49% (**129a** 78%, **128b** 76%)



Esquema 25: Síntesi de **130a-b**, **131a-b**, **54** i **53**. Reactius i condicions: (a) HATU, DIPEA, DMF, 40°C (**130a** 52%, **130b** 81%); (b) AcOH cat., DCM, r.t., 49% (**131a** 98%, **131b** 5%); (c) PdCl₂(PPh₃)₂, CuI, Et₃N, DMF, 60°C (**54** 45%, **53** 87%)

Avaluació fotoquímica dels compostos **111c**, **115**, **128-131**, **53**, **54**

Vam mesurar els espectres d'absorció UV-Vis dels compostos **111c**, **115**, **129a-b** i **131a-b** a les fosques i després d'il·luminar amb llum violeta ($\lambda = 380$ nm) i després amb llum blava ($\lambda = 430$ nm) en solució d'acetonitril. a les fosques, pràcticament només vam detectar l'isòmer *trans* i vam poder detectar una fotoisomerització completa pels compostos **111c** i **129a** (figura 32A).

Pels demés compostos vam poder detectar només fotoisomerització parcial (figura 32B). Possiblement, per aconseguir una fotoisomerització acceptable pels compostos amb substitució 1,3, necessàriem longituds d'ona més baixes, que serien nocives per sistemes biològics. Però també la fotoisomerització pobra observada podria ser per una diferència

d'absorció insuficient entre isòmers *trans* i *cis*. Però, com ja havíem avançant en el capítol anterior, no tots els azocompostos mostres una fotoisomerització adequada per obtenir una commutació on/off.

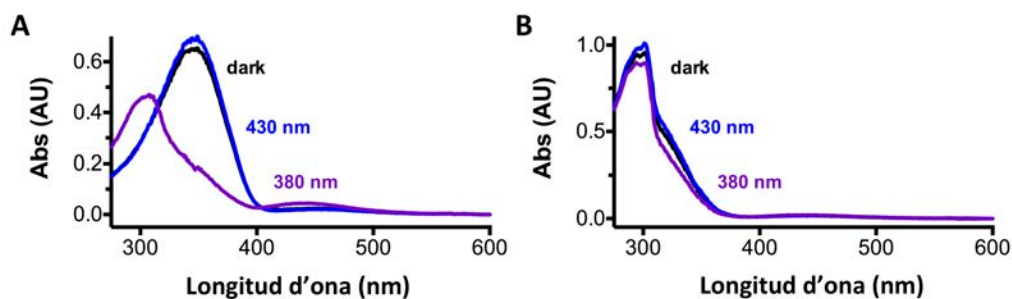


Figura 32: Propietats de fotoisomerització dels compostos: espectres de absorció de UV-Vis del compost **129a** (A) i **129b** (B) 25 μM in acetonitril a les fosques (dark, línia fosca), després d'il·luminar a 380 nm (línia violeta) i després d'il·luminar amb llum a 430 nm (línia blava).

Avaluació farmacològica in-vitro dels compostos 127-133

Dualitat PAM *mGlu₄* i NAM *mGlu₅*: Corbes dosi-resposta

Per avaluar els perfils farmacològic d'aquesta sèrie de compostos vam generar corbes dosi-resposta amb el mateix assaig d'acumulació de IP, utilitzat en els capítols 1-4 amb cèl·lules HEK293 sobreexpressant *mGlu₄* o *mGlu₅*. Basant-nos en el coneixement adquirit en els treballs previs, vam esperar que els compostos amb els grups piridina-amida-fenil mostrarien activitat PAM en *mGlu₄*, i que els que tenen els grups piridina-azo-fenil o piridina-etinil-fenil mostrarien activitat NAM en *mGlu₅*. Per tant els compostos **111c**, **115** i **128a-b**, amb les dues característiques alhora, haurien de tenir activitat dual.

No obstant això, finalment només els compostos **111c** i **128a** van mostrar activitat PAM en *mGlu₄* clara (taula 7), i que alhora també la van mostrar com a NAMs de *mGlu₅*. No obstant això, pràcticament tots els compostos amb grups piridina-azo-fenil o piridina-etinil-fenil van mostrar activitat NAM en *mGlu₅*. En resum, vam obtenir dos compostos amb activitat dual PAM en *mGlu₄* i NAM en *mGlu₅* amb potències en el rang micromolar.

Compost	<i>mGlu₄</i> PAM			<i>mGlu₅</i> NAM		
	EC_{50} (μM)	SEM (μM)	PPS	EC_{50} (μM)	SEM (μM)	PPS
111c	8.9	1.3	2.8	3.21	0.33	>13
115	>25		-	14.03	2.24	1.5
128a	9.94	3.45		0.84	0.28	
128b	>25			0.84	0.38	

129a	>25		-	3.09	0.27	2.9
129b	>25		-	0.96	0.24	1.2
130a	>25			n.a.		
130b	n.a.			n.a.		
131a	>25		-	6.13	0.16	1.2
131b	n.a.		-	4.92	1.10	2.0
54	>25			1.21	0.46	
53	18.00	2.44		0.43	0.10	
VU0364770	1.17	0.32	1.0			
Fenobam				2.30	0.25	1.0

Taula 7: Valors extrets de les corbes dosi-resposta corresponents a les EC₅₀ com a PAMS de mGlu₄ PAMs i IC₅₀ com a NAMs de mGlu₅, com a mitjanes de tres replicats independents amb la SEM corresponent.

Selectivitat dels compostos 111c i 128a

Un cop caracteritzada l'activitat dual dels compostos **111c** i **128a**, vam avaluar la possible activitat dels compostos en la resta de subtipus de receptor mGlu per determinar la selectivitat. Vam assajar la possible activitat PAM i NAM amb una dosi simple de 100 µM en cèl·lules HEK293 sobreexpressant els receptor corresponent.

Desafortunadament, vam obtenir efectes parcials en mGlu₂ i els subtipus de mGlu de grup-III mGlu (mGlu₆₋₈). Aquests resultats de selectivitat no defineixen aquests dos compostos com a compostos clau per estudiar la hipòtesi dels compostos duals.

En conclusió, els dos compostos **111c** i **128a** tenen activitat dual com a PAM de mGlu₄ PAM i NAM de mGlu₅, però al seva selectivitat no és òptima i no es poden considerar compostos duals purs. No obstant això, els efectes observats coincidirien amb els d'un compost amb propietats neuroprotectores⁸². Tot i això, podem aconseguir noves molècules duals amb una potència superior i un perfil de selectivitat millor, optimitzant la substitució d'aquests dos compostos.

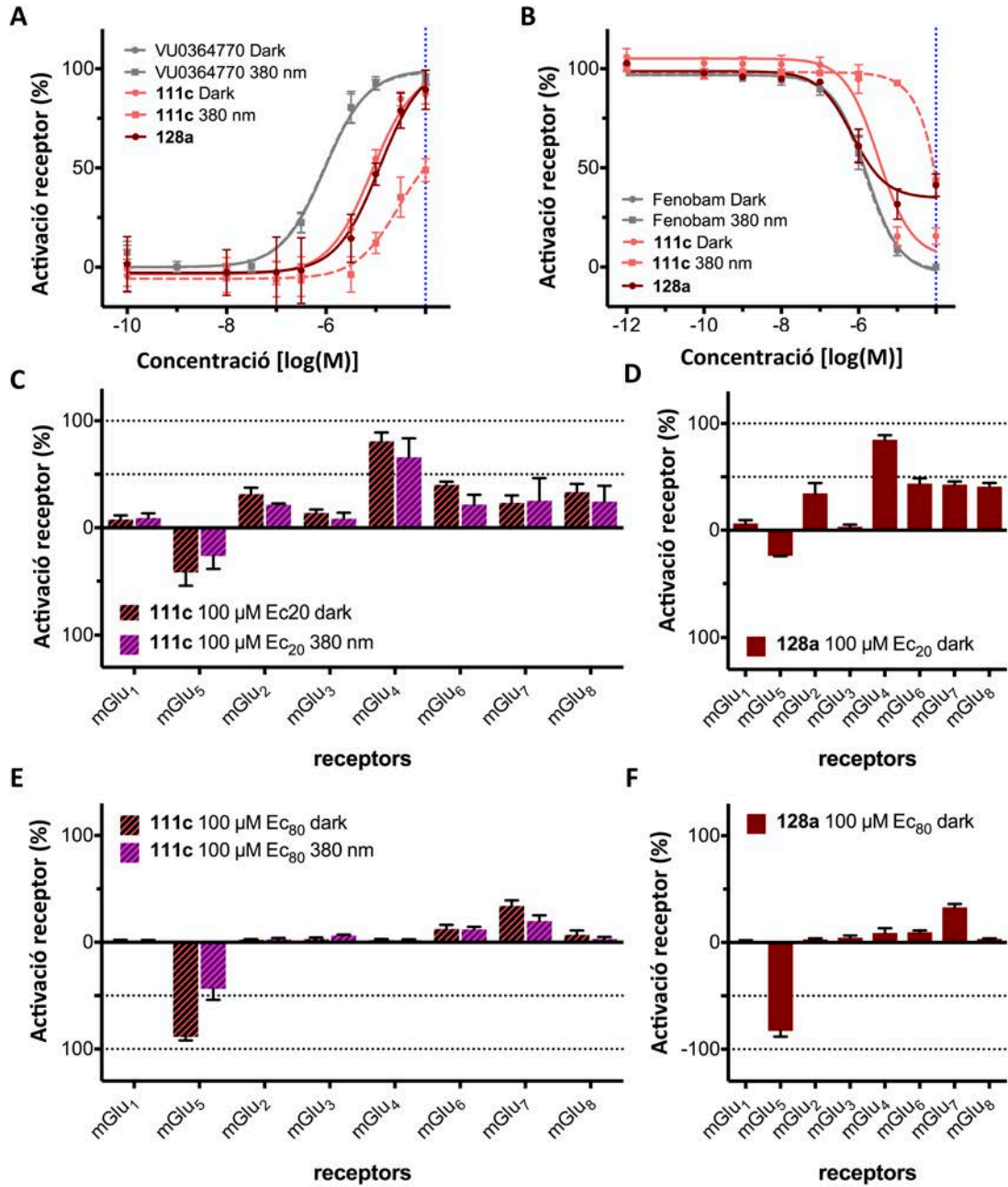


Figura 33: Selectivitat dels compostos **111c** i **128a** a concentració 100 µM utilitzant l'assaig IP-One en cèl·lules sobreexpressant els corresponents subtipus de mGlu. (A-B) Corbes dosi-resposta dels compostos **111c** i **128a** en mGlu₄ amb una concentració constant de 3 nM de L-AP₄ (A) i en mGlu₄ amb concentració constant de 100 nM de quisqualat. La dosi utilitzada per assajos de selectivitat (100 µM) està marcada amb una línia blava discontinua. (C-F) Perfils de selectivitat en els 8 subtipus de mGlu del compost **111c** com a PAM (C) o com a NAM (E) i del compost **128a** com a PAM (D) o com a NAM (F) a una concentració de 100 µM. Els valors per l'avaluació PAM estan normalitzats entre la EC₂₀ i la saturació dels agonistes ortostèrics corresponents, i els valors per l'avaluació NAM estan normalitzats entre la he EC₈₀ dels agonistes ortostèrics corresponents i la saturació d'un antagonista. Cada punt de cada gràfic correspon a la mitjana d'un mínim de 3 experiments independents amb la SEM corresponent com a barres d'error.

Un efecte inesperat en mGlu₅: Isòmers posicionals que porten a diferents eficàcies

En les corbes dosi-resposta fetes en mGlu₅ vam poder observar una clara diferència d'eficàcia en tots els bioisòmers de **111c** i **115**. De fet, els compostos amb substitució 1,3 van resultar ser agonistes inversos (**128b**, **129b** i **131b**), de manera similar al fenobam (**14**), així com el compost **53** (2-BisPEB), que ja s'havia descrit anteriorment^{124, 209}. Per altra banda, els corresponents isòmers posicionals 1,4 substituïts (**128a**, **129a**, **131a** i **54**) també tenien un efecte antagonístic, però amb una eficàcia menor que el fenobam, es a dir parcial. A més a més, la potència (IC₅₀) dels isòmers 1,4 no es va alterar significativament respecte la dels isòmers 1,3, excepte per la parella de compostos **111c/115** (taula 8, figura 34).

Compost	EC ₅₀ (μM)	SEM (μM)	PPS	Eficàcia (%)	SEM (%)
111c	3.21	0.33	>13	92	6
115	14.03	2.24	1.5	90	5
128a	0.84	0.28		67	9
128b	0.84	0.38		120	1
129a	3.09	0.27	2.9	35	4
129b	0.96	0.24	1.2	115	4
131a	6.13	0.16	1.2	19	4
131b	4.92	1.10	2.0	114	3
54	1.21	0.46		42	4
53	0.43	0.10		120	1
Fenobam	2.30	0.25	1.0	100	0

Taula 8: Valors extrets de les corbes dosi-resposta (IP-One) corresponents a la IC₅₀ com a NAM de mGlu₅, com a mitjanes de tres replicats independents amb la SEM corresponent com a barres d'error. L'eficàcia es va mesurar des de la base de la corba dosi-resposta, normalitzada per la resposta màxima del fenobam, entre 0% i 100%.

Aquesta diferència d'eficàcia dels isòmers posicionals, sense alterar significativament la potència, es podria explicar com a diferents modes d'unió al domini transmembrana. A més a més, la rigidesa dels grups azo i etinil fa que els compostos siguin molt rígids en forma lineal i angular. D'aquesta manera, en unir-se al receptor, seria el mateix receptor el que s'adaptaria als compostos de dues maneres clarament diferents, que podria donar a lloc a dues conformacions possibles que podrien donar respostes funcionals diferents.

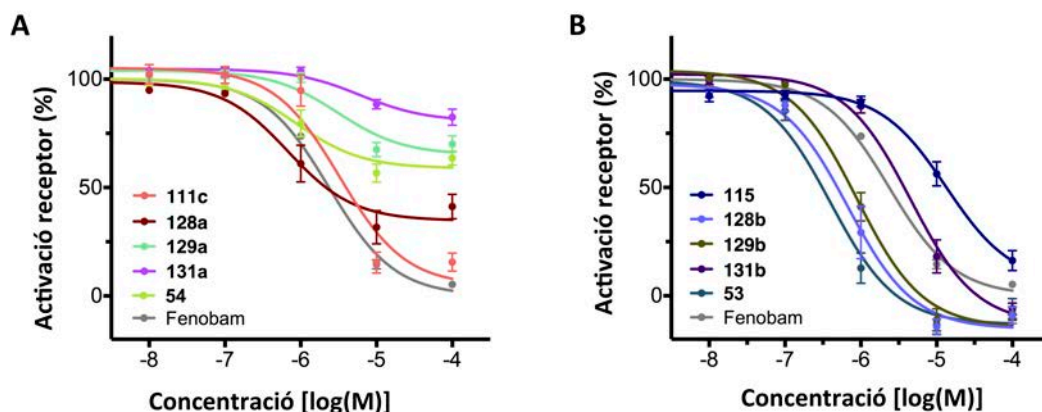


Figura 34: Corbes dosi-resposta obtingudes amb els assajos IP-One en cèl·lules HEK293 transfectades amb receptor mGlu₅. (A-B) Ampliació de les corbes dels compostos amb substitució 1,4 amb antagonisme parcial (A) i amb substitució 1,3 amb agonisme invers amb alta eficàcia (B).

Capítol 5: Una aproximació més adequada: PAMs mGlu₄ i NAMs de mGlu₅ fotocommutable cis-on

Els compostos fotocommutables que mostrats en els *capítols 1, 2 i 4*, són compostos que en la seva configuració *trans*, que és la més estable tèrmicament, són actius. Sota il·luminació amb llum violeta, fotoisomeritzen i l'isòmer *cis* format és inactiu, o menys actiu.

Des d'un punt de vista terapèutic, no és la aproximació més prometedora, ja que desactivar un fàrmac actiu amb precisió espacial i temporal té unes aplicacions terapèutiques molt limitades.

La possibilitat de obtenir un compost fotoisomeritzable inactiu en la seva configuració termodinàmicament estable *trans*, que en isomeritzar a *cis* sota il·luminació, tingui una activitat biològica, és de molt gran interès des del punt de vista terapèutic. En aquesta aproximació, el control amb alta precisió espaciotemporal que ofereix la llum, té molt més sentit i la relaxació dels isòmers *cis* contribueix a la desactivació del compost quan difon a altres parts de l'organisme.

Disseny dels compostos 140a-c, 141, 142, 143 i 144

Abans de començar a treballar experimentalment vam fer una busca bibliogràfica exhaustiva en PAMs de mGlu₄ PAMs i NAMs de mGlu₅, centrant-nos en molècules grans que s'unissin al lloc al·lostèric amb una postura angular. La nostra intenció era mimetitzar la postura angular amb un enllaç azo *cis*, de manera que en geometria *trans trans*, adoptés una disposició allargada que no cabés en la butxaca al·lostèrica, de manera que s'abolís l'efecte en el receptor.

En buscar PAMs de mGlu₄ a la literatura vam trobar que la *N*-fenilpicolinamida era un fragment molt comú en diversos moduladors al·lostèrics positius, com el VU364439 (**32b**)⁹⁵ o el

VU415374 (**33b**)⁹⁶ entre d'altres^{90, 97, 98}, que tenien una llargada superior amb una certa geometria angular. A més a més quan en l'anell de fenil tenien una substitució cloro o metoxi en posició 3, la seva potència augmentava. Per tant, vam decidir sintetitzar compostos amb la *N*-fenilpicolinamida, amb H, Cl i OMe en posició 3 del fenil i amb una azo-extensió en un tercer anell enllaçat en forma de *N*-amida (**140a-c**) i també un altre compost amb la mateixa azo-extensió, però enllaçada amb un grup sulfonamida (**141**).

Pel que fa a NAMs de mGlu₅, els seus moduladors al·lostèrics acostumen a tenir un grup acetilè, que acostuma a fer de pont entre una 2-piridina (o 5-metil-2-piridina) i un fenil, com el 2-BisPEB (**53**)^{124, 209} o el MPEP (**12**)⁶⁹. En algun cas aquest 1,2-etindiil està substituït per una *N*-amida¹²³. A més a més, com hem vist en el capítol 4, els NAMs de mGlu₅ amb una alta eficàcia semblen tenir una geometria angular. Per tant, vam dissenyar compostos fotoisomeritzables que tinguessin el fragment 2-feniletinilpiridina amb una azo-extensió que en disposició *trans* tinguessin una geometria linear i en *cis* angular (**142a-b**). A més a més, van dissenyar també l'isòmer amb una *N*-amida en comptes de l'etnil (**143**).

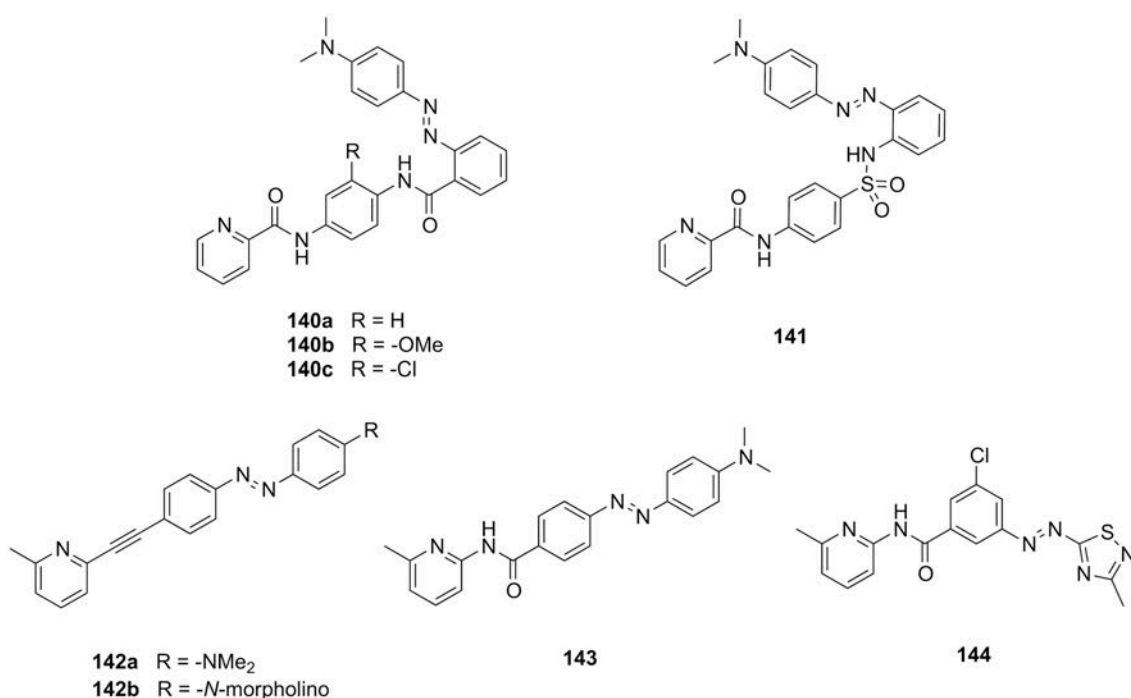


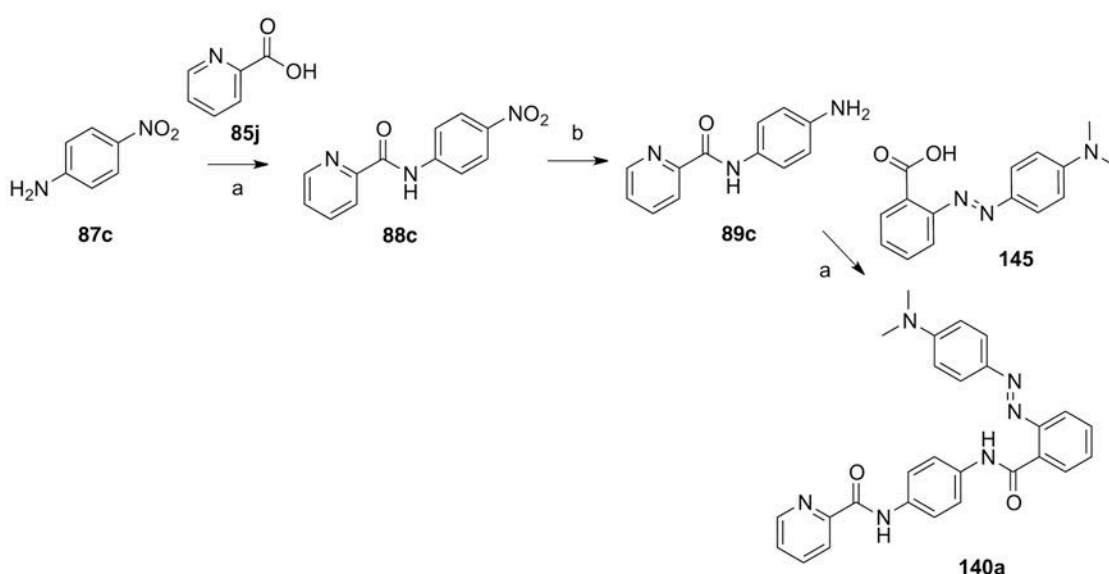
Figura 35: Compostos dissenyats com a suposats moduladors al·lostèrics *cis*-on de mGlu. (A) Els compostos **140a-c** i **141** es van dissenyar per tenir activitat PAM *cis*-on en mGlu₄. (B) Els compostos **142a-b** i **143** es van dissenyar per tenir activitat NAM *cis*-on mGlu₅.

Adicionalment, com que la llum visible ofereix diversos avantatges sobre la llum UV en que normalment isomeritzen els azobenzens, vam voler desplaçar la longitud d'ona d'il·luminació a rangs visibles. Per a tal vam introduir grups electrodonadors (NMe₂ i N-morfolino) en posició

para, tenint en compte que en podíem obtenir compostos "push-pull", que es caracteritzen per la alta velocitat de relaxació de l'isòmer *cis*. En tot cas, com que tenim una aproximació *cis-on*, un temps de relaxació ràpid pot ser avantatjós, ja que tan aviat com el compost difon i surt de la zona d'il·luminació, isomeritza a la disposició *trans* inactiva.

Síntesi dels compostos 140-144

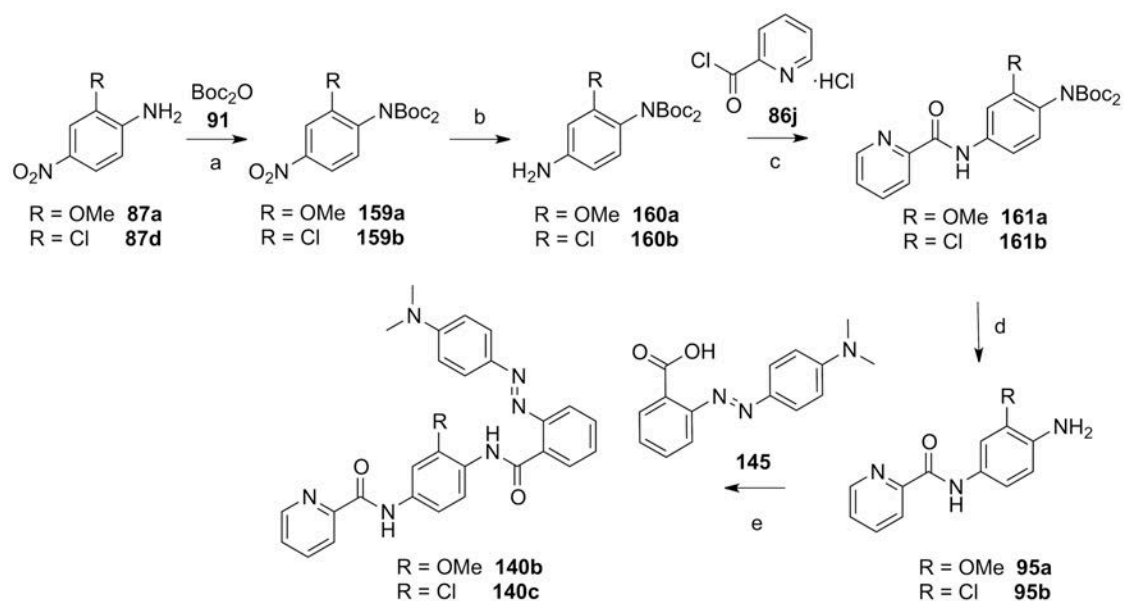
El compost **140a** es va preparar segons la següent estratègia sintètica que es mostra en l'*esquema 11*. En resum es basa en l'acilació de la 4-nitroanilina **87a-c** amb àcid picolínic (**85j**), seguida per la reducció del grup nitro i l'acilació de l'anilina resultant amb vermell de metil **140a**



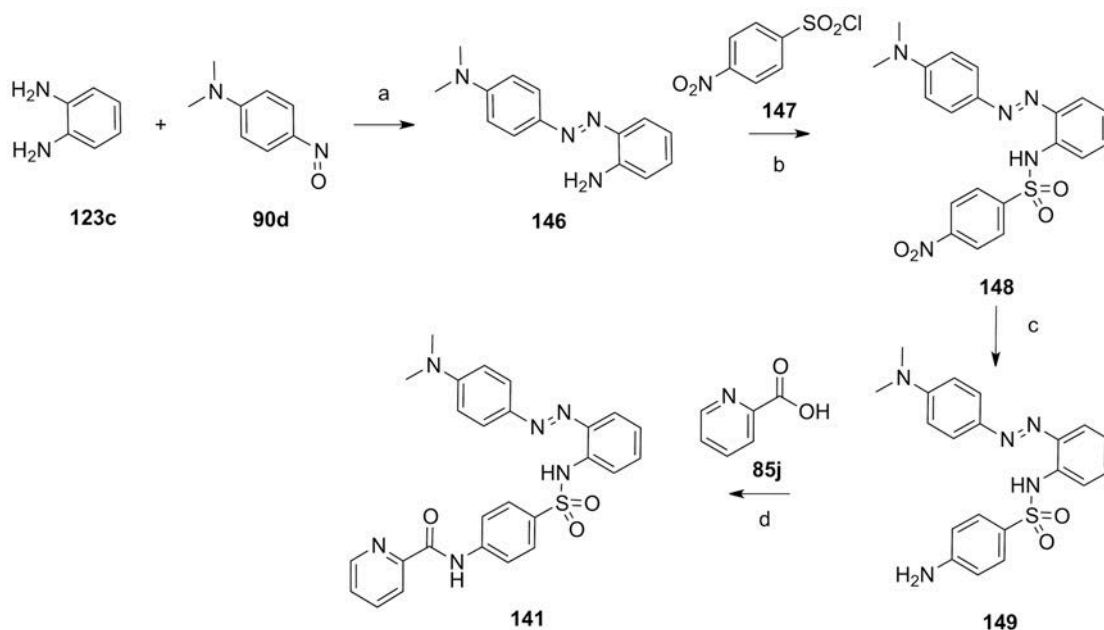
esquema 26: Síntesi del **140a**. Reactius i condicions: (a) HATU, DIPEA, DMF 40°C, 14-22h, 94%- 49%; (b) H₂ (2 bar), Pd/C, EtOH/1,4-dioxà r.t. 5 h, 97%.

Els compostos **140b-c** es van preparar seguint l'estratègia sintètica que es mostra a l'*esquema 14*. En resum, es va protegir les nitrosoanilines **87a,d**, es va reduir el grup nitro, l'anilina resultant es va acilar amb clorur de picolinoil(**86j**), es va desprotegir la primera anilina per acilar-la amb vermell de metil **145**).

El compost **141** es va sintetitzar segons el procediment representat a l'*esquema 12*. En resum, la *o*-fenilendiamina **123c** es fa fer reaccionar amb the nitrosoanilina **90d** amb hidròxid de potassi, es va *p*-nosilar, després vam reduir el grup nitro per acilar la anilina resultant amb àcid picolínic.

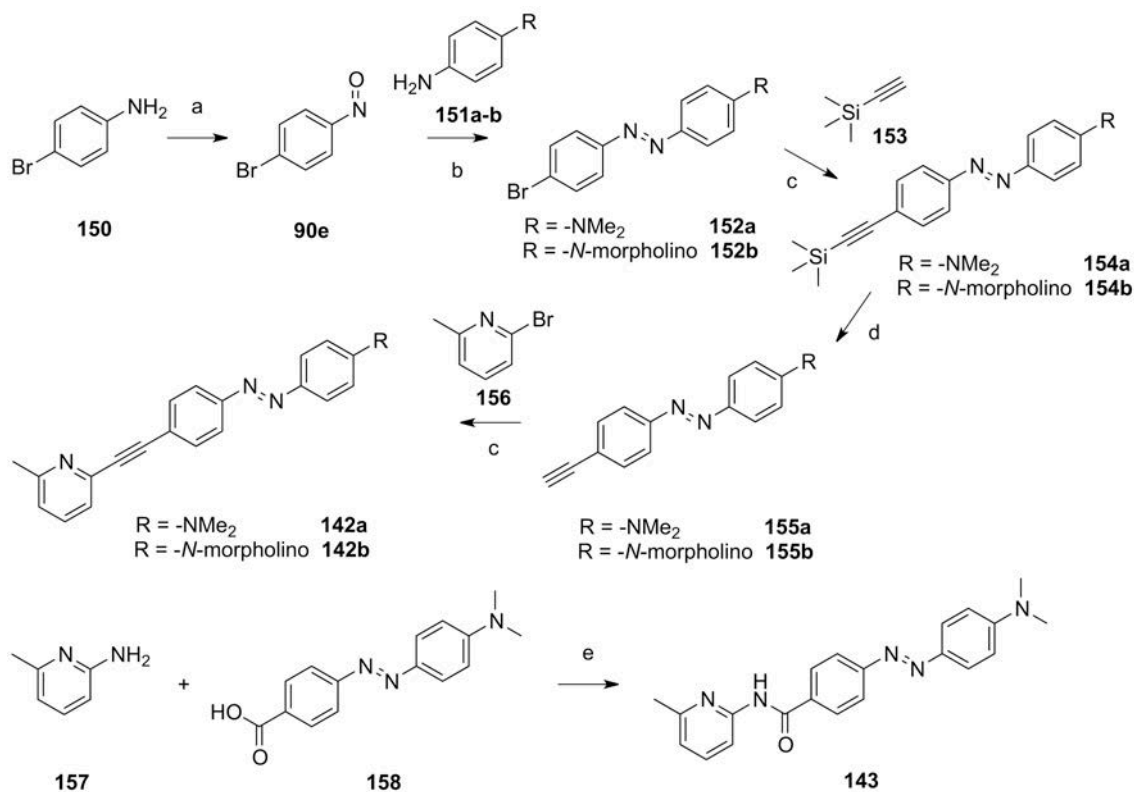


Esquema 27: a) DMAP cat., THF, r.t., 16 h 82-84%; b) H₂ (2 bar), Pd/C, AcOEt, r.t., 16h 98-100%; c) DIPEA, DCM, 0°C to r.t., 16h, 79-98%; d) HCl 4N in 1,4-dioxane, r.t. 3h 98-100%; e) HATU, DIPEA; DMF, 40 °C, 4d 19-25%



Esquema 28: Síntesi de **141**. Reactius i condicions: (a) (i) KOH (sense dissolvent); (ii) toluè 90°C 1h, 57%; (b) piridina, DCM, r.t., 18h, 72%; (c) NaS·9H₂O, EtOH, reflux, 2h, 98% (d) HATU, DIPEA, DMF, 40°C, 18 h, 37%.

Els compostos **142a-b** i **143** es van sintetitzar segons el procediment representat a l'esquema 13. Resumidament, les anilines **151a** o **151b** es van fer reaccionar 4-bromo-nitrosobenzè **90e**, se li va fer un acoblament de Sonogashira amb etiltrimetilsilà, l'alquí terminal es va alliberar amb carbonat de sodi i es va fer un nou acoblament de Sonogashira amb metil-2-bromopiridina (**156**) El compost **143** es va sintetitzar en una sola etapa d'acilació de la 2-amino-6-metil-piridina (**157**) amb l'àcid dimetilaminoazobenzoic **158**.



Esquema 29: Síntesi de **142a-b** i **143**. Reactius i condicions: (a) Oxone, DCM/H₂O, 2 h, r.t. 95%; (b) AcOH, DCM, r.t., 60 h, 92%; (c) CuI 7-13% mol, Pd(PPh₃)₂Cl₂ 7-13% mol, TEA, DMF, 50°C, 7,5 h, 16-97%; (e) K₂CO₃, MeOH/THF, 2 h, r.t., 88-95% (f) HATU, DIPEA, DMF, 40°C, 3 d, 61%

Propietats de fotoisomerització dels compostos 140-143

Vam assajar la fotoisomerització dels compostos d'aquesta sèrie amb una solució (DMSO, 25 μM) sota diferents condicions de llum. L'espectre adquirit a les fosques, corresponent a l'isòmer *trans* van resultar tenint el màxim corresponent a la transició π-π* entre 420 i 470 nm, ja que els azobenzens presents eren més rics electrònicament que els que havíem vist anteriorment i alguns amb efecte "push-pull". Vam adquirir els espectres després de 2 minuts d'il·luminació contínua amb 460, 430, 420, 400 o 380 nm, obtenint així mescles de isòmers *cis-trans* i per cada longitud d'ona d'il·luminació. El decreixement de l'alçada de la banda de transició π-π* de l'isòmer *trans* ens va donar una idea qualitativa del grau de fotoisomerització. Tots els compostos de la sèrie van presentar unes propietats de fotoisomerització molt semblants sota il·luminació a 460, 430 o 420 nm, mentre sota il·luminació a 380 nm es recuperava una fracció considerable de l'isòmer *trans* (figura 36). Per tant, vam escollir 430 or 460 nm com a longituds d'ona per il·luminar en els assajos cel·lulars, que estan en el rang blau de l'espectre.

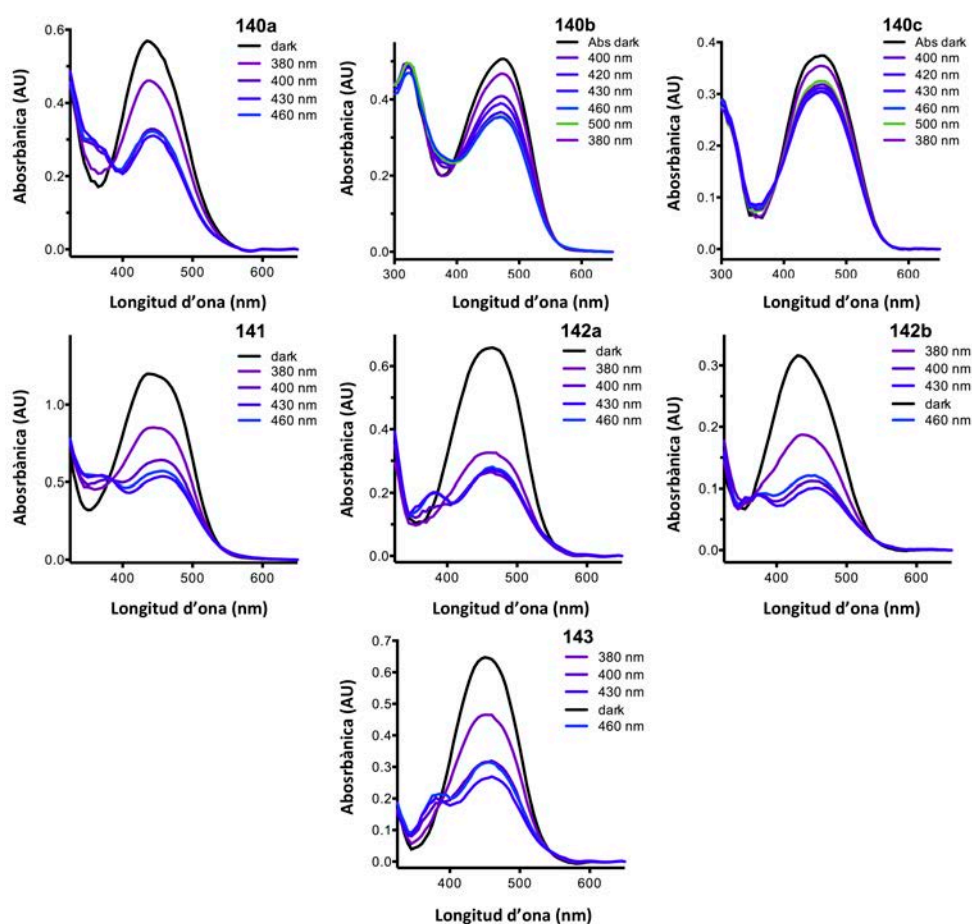


Figura 36: Espectres d'absorció UV-Vis dels compostos **140a-c**, **141**, **142a-b** i **143** a les fosques (dark) i amb il·luminació amb diferents longituds d'ona. La il·luminació amb 420, 430 i 460 nm dona perfils molt similars.

Caracterització farmacològica dels compostos 140-143

Assajos a dosi simple - Joan Font, IGF-CNRS, Montpeller

Per avaluar l'activitat farmacològica dels suposats PAMs de mGlu₄ o NAMs de mGlu₅ *cis-on*, primer vam realitzar assajos a dosi única amb cèl·lules HEK293 sobreexpressant mGlu₄ o mGlu₅ amb l'assaig IP-One. Vam assajar tots els compostos com a PAMs i NAMs de mGlu₄ PAMs i mGlu₅, independentment del propòsit en el disseny i amb cada mesura feta simultàniament a les fosques i amb il·luminació amb llum blava ($\lambda = 460$ nm). Tot i els esforços en el disseny dels compostos, no vam trobar cap efecte considerable sota il·luminació amb llum blava ni cap diferència d'activitat entre les mostres il·luminades i les mantingudes en condicions de fosc (figura 37). Només vam poder detectar efectes *cis-on* molt febles com a PAMs de mGlu₄ pel compost **140a** i mínimament pels compostos **141** i **143**. Tot i això aquests efectes són insuficients. Addicionalment el compost **142b** també va mostrar un efecte parcial com a PAM de mGlu₄ independentment de les condicions de llum/fosc. Per tant, vam decidir estudiar amb corbes dosi resposta els efectes PAM en mGlu₄ dels compostos **140a-c**, **141**, **142b** i **143**.

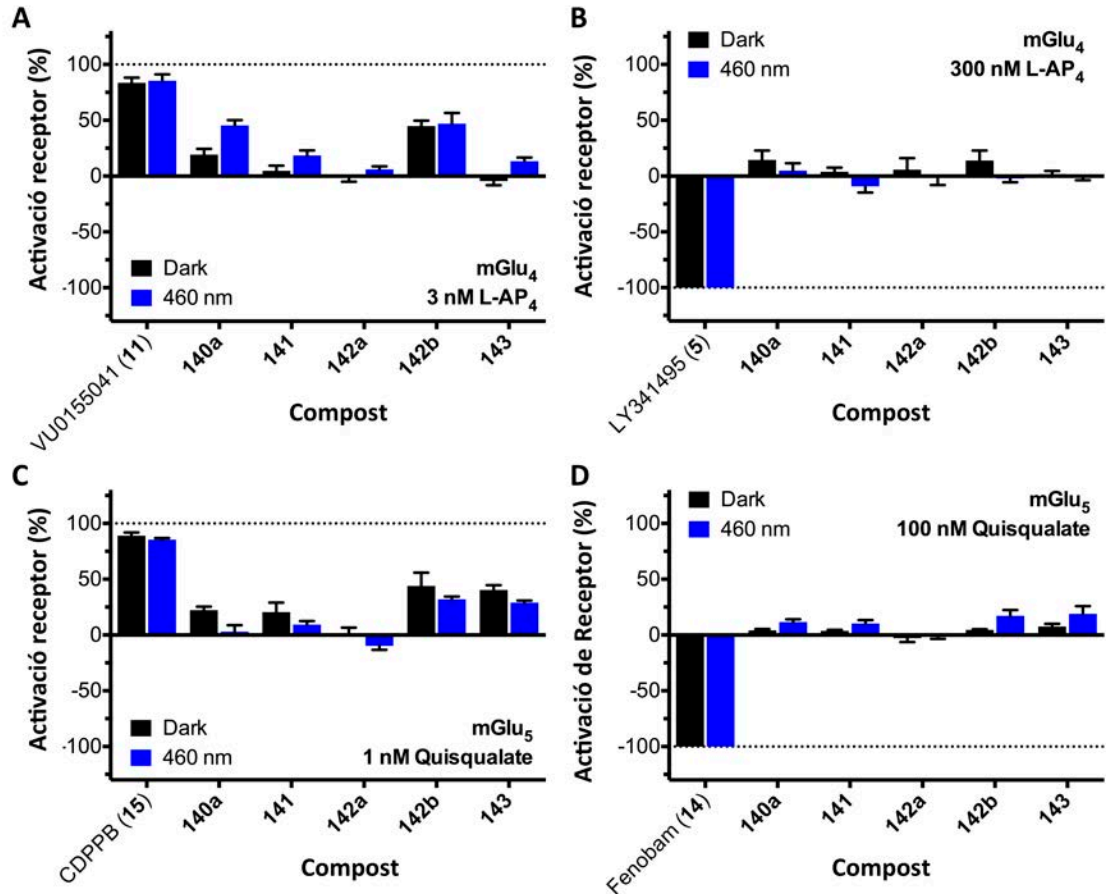


Figura 37: Experiments de dosi simple dels compostos **140a**, **141**, **142b** i **143**, com (A) a PAMs de mGlu₄, (B) NAMs mGlu₄, (C) PAMs de mGlu₅ i (D) NAMs de mGlu₅. La resposta FRET es va normalitzar a 0%-100% entre l'efecte a concentració baixa d'agonista (EC₂₀) i l'efecte de saturació d'agonista per l'avaluació efecte PAM. Per l'avaluació NAM, la resposta FRET es va normalitzar a -100%-0% entre l'efecte de saturació de l'antagonista amb la concentració alta d'antagonista (EC₈₀). Cada barra correspon a la mitjana d'un mínim de dos replicats independents amb la SEM corresponent cm a barres d'error.

Corbes dosi-resposta - en col·laboració amb Joan Font i Xavier Rovira, IGF-CNRS Montpellier

Per avaluar millor el mínim efecte *cis-on* com a PAMs de mGlu₄ dels compostos **140a-c**, **141**, **142b** i **143**, vam generar corbes dosi-resposta amb cèl·lules HEK293 sobreexpressant el receptor mGlu₄ amb l'assaig IP-One amb il·luminació a 460 nm.

Desafortunadament, a les corbes dosi-resposta no vam trobar cap perfil *cis-on*, excepte els compostos **140b** i **140c**. Aquests resultats no eren concordants amb els experiments a dosi simple, ja que havíem trobat alguns petits efectes *cis-on*. Pel que fa el compost **140b**, a les fosques va resultar tenir una potència micromolar com a PAM de mGlu₄ i sota il·luminació blava, va disminuir la seva IC₅₀, però insuficientment com per obtenir una fotocommutació adequada (figura 38). D'altra banda, el compost **140c** va mostrar només una modulació molt

feble de l'activitat de mGlu₄ a les fosques, mentre que sota llum blava va mostrar un efecte PAM considerable en el rang micromolar.

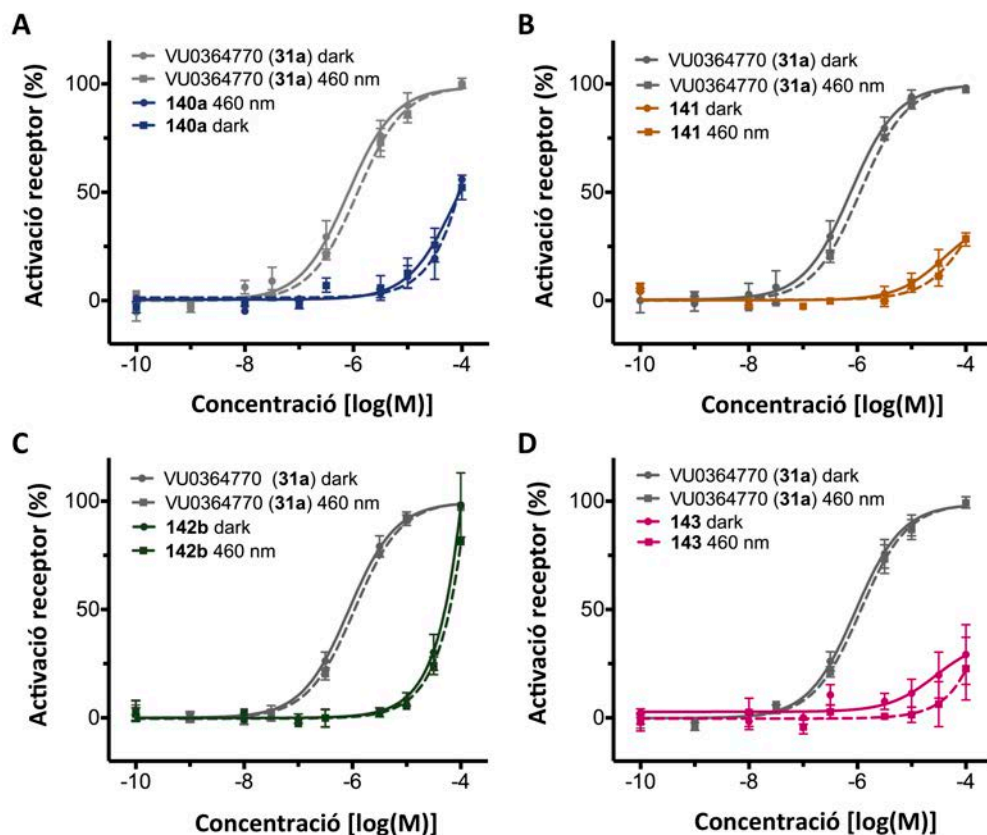


Figura 38: Corbes dosi-resposta estretes dels experiments fets amb l'assaig IP-One amb cèl·lules HEK293 sobreexpressant el receptor mGlu₄ receptor amb una concentració constant de L-AP₄ (**4**) 3 nM. Les línies contínues corresponen a les mostres incubades a la foscor mentre que les discontinües sota il·luminació a 460 nm. Cada punt correspon a la mitjana de tres replicats independents amb la SEM corresponent com a barres d'error.

Per confirmar aquests resultats, finalment vam realitzar dos experiments amb els compostos **140b** i **140c** per excloure efectes no específics. L'experiment va ser amb il·luminació contínua a 460 nm amb cèl·lules HEK293 transfectades amb el receptor mGlu₄ i amb cèl·lules HEK293 transfectades amb un plàsmid de DNA buit que no codifica el receptor mGlu₄ (cèl·lules mock) en paral·lel. Malauradament, tots dos compostos va mostrar un efecte en les cèl·lules mock, semblant a l'observat en cèl·lules transfectades amb mGlu₄ i no observat amb el control PAM de mGlu₄ VU0364770 (**31a**) (figura 39). Aquests resultats indiquen que l'efecte *cis-on* observat és un artefacte, que podria ser un resultat d'un efecte *cis-on* induït en receptors endògens desconeguts o en proteïnes dianes constitutivament presents en les cèl·lules HEK293, i que probablement estan involucrats en la producció de IP.

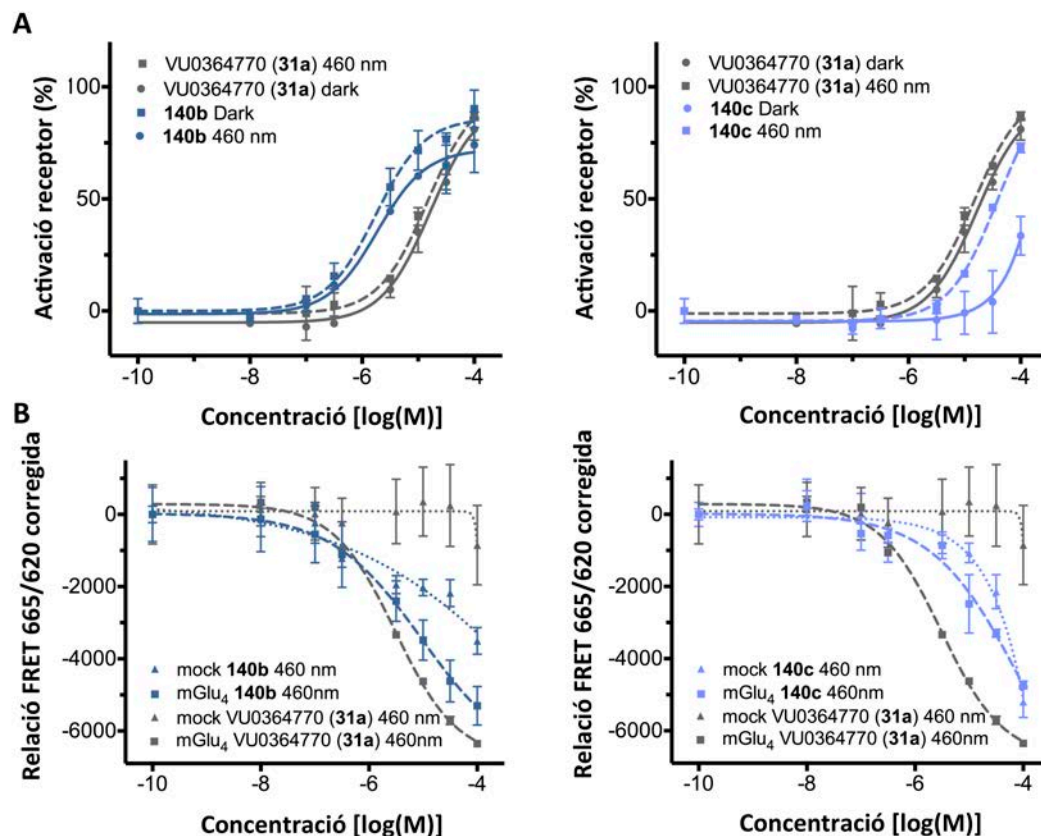


Figura 39: Corbes dosi-resposta amb l'assaig IP-One en cèl·lules HEK293 amb els compostos **140b** and **140c** utilitzant el VU0364770 (**31a**) com a control de PAM de mGlu₄ (A) Cèl·lules HEK293 que sobreexpressen el receptor mGlu₄ amb una concentració constant de L-AP₄ (**4**) 3 nM. Les línies contínues corresponen a les mostres incubades a les fosques i les discontinües sota llum a 460 nm. Cada punt correspon a la mitjana d'un mínim de tres punts amb la SEM corresponent com a barres d'error. (B) Les línies discontinües gruixudes corresponen a cèl·lules HEK293 que sobreexpressen el receptor mGlu₄ i les de punts a cèl·lules HEK293 sense expressió de mGlu₄. Ambdues condicions es van assajar amb una concentració constant de L-AP₄ (**4**) 3 nM i sota il·luminació a 460 nm. Cada punt correspon a la mitjana d'un mínim de dos punts amb la SEM corresponent com a barres d'error.

Resum de conclusions

El reemplaçament de les amides del compost VU0416374 (**33b**) per grups azo va tenir èxit per obtenir moduladors al·lostèrics de receptors mGlu. Vam dissenyar i sintetitzar l'alloswitch-1 (**83**), un modulador al·lostèric negatiu de mGlu₅ potent i selectiu fotocommutable amb llum violeta i verda, amb potencial *in-vivo*. Vam dissenyar i sintetitzar també l'optogluram (**84**), un modulador al·lostèric positiu de mGlu₄ potent fotocommutable amb llum violeta i verda, amb potencial *in-vivo*.

Vam obtenir també dos bioisòsters no fotocommutables dels compostos **83** i **84** (**99** i **100** respectivament), confirmant una doble commutació molecular entre PAMs de mGlu₄ i NAMs mGlu₅, i la viabilitat del reemplaçament-azo dels diarilacetilens.

Vam sintetitzar una sèrie de NAMs fotocommutables de mGlu₅ *trans-on* basats en l'estructura de la fenilazopiridina, amb una SAR robusta, que eren capaços de inhibir la motilitat de peixos zebra amb control òptic amb llum violeta o llum visible.

Vam sintetitzar també 12 compostos, dels quals dos (**111c** i **128a**) tenien tanta activitat PAM de mGlu₄ com NAM de mGlu₅, amb potències similars. No obstant la seva selectivitat front la resta de subtipus de mGlu no era òptima, però el seu ús com a agent neuroprotector encara és possible.

D'aquesta sèrie vam descobrir que els compostos amb substitució 1,3 eren agonistes inversos, mentre els que tenien substitució 1,4 eren agonistes parcials, fet que pot ser de gran interès per dissenyar NAMs de mGlu₅ més segurs des del punt de vista terapèutic.

El disseny utilitzat per obtenir PAMs de mGlu₄ i NAMs de mGlu₅ *cis-on* no va tenir èxit, ja que no vam obtenir cap compost amb una fotocommutació de l'activitat dels receptors acceptable i sense efectes inespecífics.

Bibliographic references

1. Fredriksson, R., et al. The G-protein-coupled receptors in the human genome form five main families. Phylogenetic analysis, paralogon groups, and fingerprints. *Mol Pharmacol* **2003**, 63, 1256-72.
2. Lagerstrom, M. C.; Schioth, H. B. Structural diversity of G protein-coupled receptors and significance for drug discovery. *Nat Rev Drug Discov* **2008**, 7, 339-57.
3. Gloriam, D. E., et al. The G protein-coupled receptor subset of the rat genome. *BMC Genomics* **2007**, 8, 338.
4. Bjarnadottir, T. K., et al. Comprehensive repertoire and phylogenetic analysis of the G protein-coupled receptors in human and mouse. *Genomics* **2006**, 88, 263-73.
5. The Nobel Prize in Chemistry 2012. http://www.nobelprize.org/nobel_prizes/chemistry/laureates/2012/index.html
6. Overington, J. P., et al. How many drug targets are there? *Nat Rev Drug Discov* **2006**, 5, 993-6.
7. Garland, S. L. Are GPCRs still a source of new targets? *J Biomol Screen* **2013**, 18, 947-66.
8. Rask-Andersen, M., et al. The druggable genome: Evaluation of drug targets in clinical trials suggests major shifts in molecular class and indication. *Annu Rev Pharmacol Toxicol* **2014**, 54, 9-26.
9. Katritch, V., et al. Structure-function of the G protein-coupled receptor superfamily. *Annu Rev Pharmacol Toxicol* **2013**, 53, 531-56.
10. Nickols, H. H.; Conn, P. J. Development of allosteric modulators of GPCRs for treatment of CNS disorders. *Neurobiol Dis* **2014**, 61, 55-71.
11. van der Westhuizen, E. T., et al. Endogenous allosteric modulators of G protein-coupled receptors. *J Pharmacol Exp Ther* **2015**, 353, 246-60.
12. Shonberg, J., et al. GPCR crystal structures: Medicinal chemistry in the pocket. *Bioorg Med Chem* **2015**, 23, 3880-906.
13. Bockaert, J.; Pin, J. P. Molecular tinkering of G protein-coupled receptors: an evolutionary success. *EMBO J* **1999**, 18, 1723-9.
14. Milligan, G.; Kostenis, E. Heterotrimeric G-proteins: a short history. *Br J Pharmacol* **2006**, 147 Suppl 1, S46-55.
15. Foord, S. M., et al. International Union of Pharmacology. XLVI. G protein-coupled receptor list. *Pharmacol Rev* **2005**, 57, 279-88.
16. Davenport, A. P., et al. International Union of Basic and Clinical Pharmacology. LXXXVIII. G protein-coupled receptor list: recommendations for new pairings with cognate ligands. *Pharmacol Rev* **2013**, 65, 967-86.
17. G protein-coupled receptors | IUPHAR/BPS Guide to PHARMACOLOGY. <http://www.guidetopharmacology.org/GRAC/FamilyDisplayForward?familyId=694&familyType=GPCR>
18. Palczewski, K., et al. Crystal structure of rhodopsin: A G protein-coupled receptor. *Science* **2000**, 289, 739-45.
19. Cherezov, V., et al. High-resolution crystal structure of an engineered human beta2-adrenergic G protein-coupled receptor. *Science* **2007**, 318, 1258-65.
20. Rasmussen, S. G., et al. Crystal structure of the human beta2 adrenergic G-protein-coupled receptor. *Nature* **2007**, 450, 383-7.

21. Hoare, S. R. Mechanisms of peptide and nonpeptide ligand binding to Class B G-protein-coupled receptors. *Drug Discov Today* **2005**, 10, 417-27.
22. Bortolato, A., et al. Structure of Class B GPCRs: new horizons for drug discovery. *Br J Pharmacol* **2014**, 171, 3132-45.
23. Kniazeff, J., et al. Dimers and beyond: The functional puzzles of class C GPCRs. *Pharmacol Ther* **2011**, 130, 9-25.
24. Huang, S., et al. Interdomain movements in metabotropic glutamate receptor activation. *Proc Natl Acad Sci U S A* **2011**, 108, 15480-5.
25. Geng, Y., et al. Structural mechanism of ligand activation in human GABA(B) receptor. *Nature* **2013**, 504, 254-9.
26. Kunishima, N., et al. Structural basis of glutamate recognition by a dimeric metabotropic glutamate receptor. *Nature* **2000**, 407, 971-7.
27. Tsuchiya, D., et al. Structural views of the ligand-binding cores of a metabotropic glutamate receptor complexed with an antagonist and both glutamate and Gd³⁺. *Proc Natl Acad Sci U S A* **2002**, 99, 2660-5.
28. Monn, J. A., et al. Synthesis and pharmacological characterization of C4-disubstituted analogs of 1S,2S,5R,6S-2-aminobicyclo[3.1.0]hexane-2,6-dicarboxylate: identification of a potent, selective metabotropic glutamate receptor agonist and determination of agonist-bound human mGlu2 and mGlu3 amino terminal domain structures. *J Med Chem* **2015**, 58, 1776-94.
29. Muto, T., et al. Structures of the extracellular regions of the group II/III metabotropic glutamate receptors. *Proc Natl Acad Sci U S A* **2007**, 104, 3759-64.
30. Rondard, P., et al. The complexity of their activation mechanism opens new possibilities for the modulation of mGlu and GABAB class C G protein-coupled receptors. *Neuropharmacology* **2011**, 60, 82-92.
31. Wu, H., et al. Structure of a class C GPCR metabotropic glutamate receptor 1 bound to an allosteric modulator. *Science* **2014**, 344, 58-64.
32. Dore, A. S., et al. Structure of class C GPCR metabotropic glutamate receptor 5 transmembrane domain. *Nature* **2014**, 511, 557-62.
33. Dijksterhuis, J. P., et al. WNT/Frizzled signalling: receptor–ligand selectivity with focus on FZD-G protein signalling and its physiological relevance: IUPHAR Review 3. *Br J Pharmacol* **2014**, 171, 1195-1209.
34. Wang, C., et al. Structure of the human smoothed receptor bound to an antitumour agent. *Nature* **2013**, 497, 338-43.
35. Janda, C. Y., et al. Structural basis of Wnt recognition by Frizzled. *Science* **2012**, 337, 59-64.
36. Koval, A., et al. Yellow submarine of the Wnt/Frizzled signaling: submerging from the G protein harbor to the targets. *Biochem Pharmacol* **2011**, 82, 1311-9.
37. Wang, C., et al. Structural basis for Smoothed receptor modulation and chemoresistance to anticancer drugs. *Nat Commun* **2014**, 5, 4355.
38. Simundza, J.; Cowin, P. Adhesion G-protein-coupled receptors: elusive hybrids come of age. *Cell Commun Adhes* **2013**, 20, 213-26.
39. Hamann, J., et al. International Union of Basic and Clinical Pharmacology. XCIV. Adhesion G protein-coupled receptors. *Pharmacol Rev* **2015**, 67, 338-67.

40. Volk, L., et al. Glutamate Synapses in Human Cognitive Disorders. *Annu Rev Neurosci* **2015**.
41. Collingridge, G. L., et al. A nomenclature for ligand-gated ion channels. *Neuropharmacology* **2009**, 56, 2-5.
42. Jackson, A. C.; Nicoll, R. A. The expanding social network of ionotropic glutamate receptors: TARPs and other transmembrane auxiliary subunits. *Neuron* **2011**, 70, 178-99.
43. Traynelis, S. F., et al. Glutamate receptor ion channels: structure, regulation, and function. *Pharmacol Rev* **2010**, 62, 405-96.
44. Perrais, D., et al. Gating and permeation of kainate receptors: differences unveiled. *Trends in Pharmacological Sciences* 31, 516-522.
45. Li, F.; Tsien, J. Z. Memory and the NMDA receptors. *N Engl J Med* **2009**, 361, 302-3.
46. Doumazane, E., et al. Illuminating the activation mechanisms and allosteric properties of metabotropic glutamate receptors. *Proc Natl Acad Sci U S A* **2013**, 110, E1416-25.
47. Rondard, P.; Pin, J. P. Dynamics and modulation of metabotropic glutamate receptors. *Curr Opin Pharmacol* **2015**, 20, 95-101.
48. Hlavackova, V., et al. Evidence for a single heptahelical domain being turned on upon activation of a dimeric GPCR. *EMBO J* **2005**, 24, 499-509.
49. El Moustaine, D., et al. Distinct roles of metabotropic glutamate receptor dimerization in agonist activation and G-protein coupling. *Proc Natl Acad Sci U S A* **2012**, 109, 16342-7.
50. Xue, L., et al. Major ligand-induced rearrangement of the heptahelical domain interface in a GPCR dimer. *Nat Chem Biol* **2015**, 11, 134-40.
51. Christopher, J. A., et al. Fragment and Structure-Based Drug Discovery for a Class C GPCR: Discovery of the mGlu5 Negative Allosteric Modulator HTL14242 (3-Chloro-5-[6-(5-fluoropyridin-2-yl)pyrimidin-4-yl]benzotrile). *J Med Chem* **2015**, 58, 6653-64.
52. Rovira, X., et al. Overlapping binding sites drive allosteric agonism and positive cooperativity in type 4 metabotropic glutamate receptors. *FASEB J* **2015**, 29, 116-30.
53. Hlavackova, V., et al. Sequential inter- and intrasubunit rearrangements during activation of dimeric metabotropic glutamate receptor 1. *Sci Signal* **2012**, 5, ra59.
54. Pin, J. P., et al. New perspectives for the development of selective metabotropic glutamate receptor ligands. *Eur J Pharmacol* **1999**, 375, 277-94.
55. Nicoletti, F., et al. Metabotropic glutamate receptors: from the workbench to the bedside. *Neuropharmacology* **2011**, 60, 1017-41.
56. Sheffler, D. J., et al. Allosteric modulation of metabotropic glutamate receptors. *Adv Pharmacol* **2011**, 62, 37-77.
57. D'Antoni, S., et al. Dysregulation of group-I metabotropic glutamate (mGlu) receptor mediated signalling in disorders associated with Intellectual Disability and Autism. *Neurosci Biobehav Rev* **2014**, 46 Pt 2, 228-41.
58. Flor, P. J.; Acher, F. C. Orthosteric versus allosteric GPCR activation: the great challenge of group-III mGluRs. *Biochem Pharmacol* **2012**, 84, 414-24.
59. Goudet, C., et al. A novel selective metabotropic glutamate receptor 4 agonist reveals new possibilities for developing subtype selective ligands with therapeutic potential. *FASEB J* **2012**, 26, 1682-93.

60. Acher, F. C., et al. A critical pocket close to the glutamate binding site of mGlu receptors opens new possibilities for agonist design. *Neuropharmacology* **2011**, 60, 102-7.
61. Tora, A. S., et al. Allosteric modulation of metabotropic glutamate receptors by chloride ions. *FASEB J* **2015**.
62. Conn, P. J., et al. Opportunities and challenges in the discovery of allosteric modulators of GPCRs for treating CNS disorders. *Nat Rev Drug Discov* **2014**, 13, 692-708.
63. Conn, P. J., et al. Allosteric modulators of GPCRs: a novel approach for the treatment of CNS disorders. *Nat Rev Drug Discov* **2009**, 8, 41-54.
64. Litschig, S., et al. CPCCOEt, a noncompetitive metabotropic glutamate receptor 1 antagonist, inhibits receptor signaling without affecting glutamate binding. *Mol Pharmacol* **1999**, 55, 453-61.
65. Galici, R., et al. A selective allosteric potentiator of metabotropic glutamate (mGlu) 2 receptors has effects similar to an orthosteric mGlu2/3 receptor agonist in mouse models predictive of antipsychotic activity. *J Pharmacol Exp Ther* **2005**, 315, 1181-7.
66. Sheffler, D. J., et al. Development of a novel, CNS-penetrant, metabotropic glutamate receptor 3 (mGlu3) NAM probe (ML289) derived from a closely related mGlu5 PAM. *Bioorg Med Chem Lett* **2012**, 22, 3921-5.
67. Maj, M., et al. (-)-PHCCC, a positive allosteric modulator of mGluR4: characterization, mechanism of action, and neuroprotection. *Neuropharmacology* **2003**, 45, 895-906.
68. Niswender, C. M., et al. Discovery, characterization, and antiparkinsonian effect of novel positive allosteric modulators of metabotropic glutamate receptor 4. *Mol Pharmacol* **2008**, 74, 1345-58.
69. Gasparini, F., et al. 2-Methyl-6-(phenylethynyl)-pyridine (MPEP), a potent, selective and systemically active mGlu5 receptor antagonist. *Neuropharmacology* **1999**, 38, 1493-503.
70. Mathiesen, J. M., et al. Positive allosteric modulation of the human metabotropic glutamate receptor 4 (hmGluR4) by SIB-1893 and MPEP. *Br J Pharmacol* **2003**, 138, 1026-30.
71. Porter, R. H., et al. Fenobam: a clinically validated nonbenzodiazepine anxiolytic is a potent, selective, and noncompetitive mGlu5 receptor antagonist with inverse agonist activity. *J Pharmacol Exp Ther* **2005**, 315, 711-21.
72. Kinney, G. G., et al. A novel selective positive allosteric modulator of metabotropic glutamate receptor subtype 5 has in vivo activity and antipsychotic-like effects in rat behavioral models. *J Pharmacol Exp Ther* **2005**, 313, 199-206.
73. Suzuki, G., et al. In vitro pharmacological characterization of novel isoxazolopyridone derivatives as allosteric metabotropic glutamate receptor 7 antagonists. *J Pharmacol Exp Ther* **2007**, 323, 147-56.
74. Duvoisin, R. M., et al. Acute pharmacological modulation of mGluR8 reduces measures of anxiety. *Behav Brain Res* **2010**, 212, 168-73.
75. Varney, M. A., et al. SIB-1757 and SIB-1893: Selective, Noncompetitive Antagonists of Metabotropic Glutamate Receptor Type 5. *Journal of Pharmacology and Experimental Therapeutics* **1999**, 290, 170-181.
76. Thomas, N. K., et al. (S)-3,4-DCPG, a potent and selective mGlu8a receptor agonist, activates metabotropic glutamate receptors on primary afferent terminals in the neonatal rat spinal cord. *Neuropharmacology* **2001**, 40, 311-8.

77. Wood, M. R., et al. "Molecular switches" on mGluR allosteric ligands that modulate modes of pharmacology. *Biochemistry* **2011**, 50, 2403-10.
78. O'Brien, J. A., et al. A family of highly selective allosteric modulators of the metabotropic glutamate receptor subtype 5. *Mol Pharmacol* **2003**, 64, 731-40.
79. Schann, S., et al. Chemical switch of a metabotropic glutamate receptor 2 silent allosteric modulator into dual metabotropic glutamate receptor 2/3 negative/positive allosteric modulators. *J Med Chem* **2010**, 53, 8775-9.
80. Utley, T., et al. Synthesis and SAR of a novel metabotropic glutamate receptor 4 (mGlu4) antagonist: unexpected 'molecular switch' from a closely related mGlu4 positive allosteric modulator. *Bioorg Med Chem Lett* **2011**, 21, 6955-9.
81. Sams, A. G., et al. Efficacy switching SAR of mGluR5 allosteric modulators: highly potent positive and negative modulators from one chemotype. *Bioorg Med Chem Lett* **2011**, 21, 3407-10.
82. Nicoletti, F., et al. Metabotropic glutamate receptors as drug targets: what's new? *Curr Opin Pharmacol* **2015**, 20, 89-94.
83. Vilar, B., et al. Alleviating pain hypersensitivity through activation of type 4 metabotropic glutamate receptor. *J Neurosci* **2013**, 33, 18951-65.
84. Goudet, C., et al. Metabotropic receptors for glutamate and GABA in pain. *Brain Res Rev* **2009**, 60, 43-56.
85. Marin, J. C.; Goadsby, P. J. Glutamatergic fine tuning with ADX-10059: a novel therapeutic approach for migraine? *Expert Opin Investig Drugs* **2010**, 19, 555-61.
86. Cavallone, L. Fenobam on Heat/Capsaicin Induced Hyperalgesia in Healthy Volunteers. <https://clinicaltrials.gov/ct2/show/NCT01981395>
87. Sukoff Rizzo, S. J., et al. The metabotropic glutamate receptor 7 allosteric modulator AMN082: a monoaminergic agent in disguise? *J Pharmacol Exp Ther* **2011**, 338, 345-52.
88. Gregory, K. J., et al. Pharmacology of metabotropic glutamate receptor allosteric modulators: structural basis and therapeutic potential for CNS disorders. *Prog Mol Biol Transl Sci* **2013**, 115, 61-121.
89. Becker, J. A., et al. Autistic-like syndrome in mu opioid receptor null mice is relieved by facilitated mGluR4 activity. *Neuropsychopharmacology* **2014**, 39, 2049-60.
90. Robichaud, A. J., et al. Recent progress on the identification of metabotropic glutamate 4 receptor ligands and their potential utility as CNS therapeutics. *ACS Chem Neurosci* **2011**, 2, 433-49.
91. Christov, C., et al. Integrated synthetic, pharmacological, and computational investigation of cis-2-(3,5-dichlorophenylcarbamoyl)cyclohexanecarboxylic acid enantiomers as positive allosteric modulators of metabotropic glutamate receptor subtype 4. *ChemMedChem* **2011**, 6, 131-40.
92. Bennouar, K. E., et al. Synergy between L-DOPA and a novel positive allosteric modulator of metabotropic glutamate receptor 4: implications for Parkinson's disease treatment and dyskinesia. *Neuropharmacology* **2013**, 66, 158-69.
93. East, S. P., et al. An orally bioavailable positive allosteric modulator of the mGlu4 receptor with efficacy in an animal model of motor dysfunction. *Bioorg Med Chem Lett* **2010**, 20, 4901-5.

94. Engers, D. W., et al. Synthesis and evaluation of a series of heterobiaryl amides that are centrally penetrant metabotropic glutamate receptor 4 (mGluR4) positive allosteric modulators (PAMs). *J Med Chem* **2009**, 52, 4115-8.
95. Engers, D. W., et al. Synthesis and SAR of novel, 4-(phenylsulfamoyl)phenylacetamide mGlu4 positive allosteric modulators (PAMs) identified by functional high-throughput screening (HTS). *Bioorg Med Chem Lett* **2010**, 20, 5175-8.
96. Engers, D. W., et al. Discovery, synthesis, and structure-activity relationship development of a series of N-(4-acetamido)phenylpicolinamides as positive allosteric modulators of metabotropic glutamate receptor 4 (mGlu(4)) with CNS exposure in rats. *J Med Chem* **2011**, 54, 1106-10.
97. Jones, C. K., et al. Discovery, synthesis, and structure-activity relationship development of a series of N-4-(2,5-dioxopyrrolidin-1-yl)phenylpicolinamides (VU0400195, ML182): characterization of a novel positive allosteric modulator of the metabotropic glutamate receptor 4 (mGlu(4)) with oral efficacy in an antiparkinsonian animal model. *J Med Chem* **2011**, 54, 7639-47.
98. McCauley, J. A., et al. Sulfonamide derivative metabotropic glutamate r4 ligands. In Patent WO 2010/033350: 2010.
99. McCauley, J. A., et al. Phthalimide derivative metabotropic glutamate r4 ligands. In Patent WO 2010/033349: 2010.
100. Conn, P. J., et al. Benzoimidazolesulfonamides substitués et indolesulfonamides substitués en tant que potentialisateurs de mglur4. In Patent WO 2011/011722: 2011.
101. Liverton, N., et al. Allosteric modulators of metabotropic glutamate receptors. In Patents WO 2013/060029: 2013.
102. Liverton, N., et al. Allosteric modulators of metabotropic glutamate receptors. In Patents WO 2013/063100: 2013.
103. Hong, S. P., et al. Tricyclic thiazolopyrazole derivatives as metabotropic glutamate receptor 4 positive allosteric modulators. *J Med Chem* **2011**, 54, 5070-81.
104. Bolea, C.; Celanire, S. Pyrazole derivatives as modulators of metabotropic glutamate receptors. In Patent WO 2009/010455: 2009.
105. Le Poul, E., et al. A potent and selective metabotropic glutamate receptor 4 positive allosteric modulator improves movement in rodent models of Parkinson's disease. *J Pharmacol Exp Ther* **2012**, 343, 167-77.
106. Jimenez, H. N., et al. 4-(1-Phenyl-1H-pyrazol-4-yl)quinolines as novel, selective and brain penetrant metabotropic glutamate receptor 4 positive allosteric modulators. *Bioorg Med Chem Lett* **2012**, 22, 3235-9.
107. Jalan-Sakrikar, N., et al. Identification of positive allosteric modulators VU0155094 (ML397) and VU0422288 (ML396) reveals new insights into the biology of metabotropic glutamate receptor 7. *ACS Chem Neurosci* **2014**, 5, 1221-37.
108. Roppe, J., et al. Discovery of novel heteroarylazoles that are metabotropic glutamate subtype 5 receptor antagonists with anxiolytic activity. *J Med Chem* **2004**, 47, 4645-8.
109. Roppe, J. R., et al. 5-[(2-Methyl-1,3-thiazol-4-yl)ethynyl]-2,3'-bipyridine: a highly potent, orally active metabotropic glutamate subtype 5 (mGlu5) receptor antagonist with anxiolytic activity. *Bioorg Med Chem Lett* **2004**, 14, 3993-6.

110. Huang, D., et al. 2-(2-[3-(pyridin-3-yloxy)phenyl]-2H-tetrazol-5-yl) pyridine: a highly potent, orally active, metabotropic glutamate subtype 5 (mGlu5) receptor antagonist. *Bioorg Med Chem Lett* **2004**, 14, 5473-6.
111. Eastman, B., et al. Expedited SAR study of an mGluR5 antagonists: generation of a focused library using a solution-phase Suzuki coupling methodology. *Bioorg Med Chem Lett* **2004**, 14, 5485-8.
112. Alagille, D., et al. Functionalization at position 3 of the phenyl ring of the potent mGluR5 noncompetitive antagonists MPEP. *Bioorg Med Chem Lett* **2005**, 15, 945-9.
113. Bonnefous, C., et al. Dipyrindyl amides: potent metabotropic glutamate subtype 5 (mGlu5) receptor antagonists. *Bioorg Med Chem Lett* **2005**, 15, 1197-200.
114. Chua, P. C., et al. Cyclohexenyl- and dehydropiperidinyl-alkynyl pyridines as potent metabotropic glutamate subtype 5 (mGlu5) receptor antagonists. *Bioorg Med Chem Lett* **2005**, 15, 4589-93.
115. Tehrani, L. R., et al. 3-[Substituted]-5-(5-pyridin-2-yl-2H-tetrazol-2-yl)benzonnitriles: identification of highly potent and selective metabotropic glutamate subtype 5 receptor antagonists. *Bioorg Med Chem Lett* **2005**, 15, 5061-4.
116. Iso, Y., et al. Synthesis and structure-activity relationships of 3-[(2-methyl-1,3-thiazol-4-yl)ethynyl]pyridine analogues as potent, noncompetitive metabotropic glutamate receptor subtype 5 antagonists; search for cocaine medications. *J Med Chem* **2006**, 49, 1080-100.
117. Kulkarni, S. S., et al. Structure-activity relationships comparing N-(6-methylpyridin-yl)-substituted aryl amides to 2-methyl-6-(substituted-arylethynyl)pyridines or 2-methyl-4-(substituted-arylethynyl)thiazoles as novel metabotropic glutamate receptor subtype 5 antagonists. *J Med Chem* **2009**, 52, 3563-75.
118. Simeon, F. G., et al. Synthesis and simple ¹⁸F-labeling of 3-fluoro-5-(2-(2-(fluoromethyl)thiazol-4-yl)ethynyl)benzonnitrile as a high affinity radioligand for imaging monkey brain metabotropic glutamate subtype-5 receptors with positron emission tomography. *J Med Chem* **2007**, 50, 3256-66.
119. Milbank, J. B., et al. Rational design of 7-arylquinolines as non-competitive metabotropic glutamate receptor subtype 5 antagonists. *Bioorg Med Chem Lett* **2007**, 17, 4415-8.
120. Wendt, J. A., et al. Synthesis and SAR of 2-aryl pyrido[2,3-d]pyrimidines as potent mGlu5 receptor antagonists. *Bioorg Med Chem Lett* **2007**, 17, 5396-9.
121. Galatsis, P., et al. Synthesis and SAR comparison of regioisomeric aryl naphthyridines as potent mGlu5 receptor antagonists. *Bioorg Med Chem Lett* **2007**, 17, 6525-8.
122. Raboisson, P., et al. Discovery and characterization of AZD9272 and AZD6538-Two novel mGluR5 negative allosteric modulators selected for clinical development. *Bioorg Med Chem Lett* **2012**, 22, 6974-9.
123. Felts, A. S., et al. Discovery of VU0409106: A negative allosteric modulator of mGlu5 with activity in a mouse model of anxiety. *Bioorg Med Chem Lett* **2013**, 23, 5779-85.
124. Kaae, B. H., et al. Structure-activity relationships for negative allosteric mGluR5 modulators. *ChemMedChem* **2012**, 7, 440-51.
125. Zhou, H., et al. Discovery and structure-activity relationship of 1,3-cyclohexyl amide derivatives as novel mGluR5 negative allosteric modulators. *Bioorg Med Chem Lett* **2013**, 23, 1398-406.

126. Zhang, L., et al. Discovery and preclinical characterization of 1-methyl-3-(4-methylpyridin-3-yl)-6-(pyridin-2-ylmethoxy)-1H-pyrazolo-[3,4-b]pyrazine (PF470): a highly potent, selective, and efficacious metabotropic glutamate receptor 5 (mGluR5) negative allosteric modulator. *J Med Chem* **2014**, 57, 861-77.
127. Jaeschke, G., et al. Synthesis and biological evaluation of fenobam analogs as mGluR5 receptor antagonists. *Bioorg Med Chem Lett* **2007**, 17, 1307-11.
128. Gichinga, M. G., et al. Synthesis and Evaluation of Metabotropic Glutamate Receptor Subtype 5 Antagonists Based on Fenobam(). *ACS Med Chem Lett* **2011**, 2, 882-884.
129. Burdi, D. F., et al. Design, synthesis, and structure-activity relationships of novel bicyclic azole-amines as negative allosteric modulators of metabotropic glutamate receptor 5. *J Med Chem* **2010**, 53, 7107-18.
130. Pilla, M., et al. The identification of novel orally active mGluR5 antagonist GSK2210875. *Bioorg Med Chem Lett* **2010**, 20, 7521-4.
131. Carcache, D., et al. Benzimidazoles as Potent and Orally Active mGluR5 Receptor Antagonists with an Improved PK Profile. *ACS Med Chem Lett* **2011**, 2, 58-62.
132. Weiss, J. M., et al. 6-Aryl-3-pyrrolidinylpyridines as mGluR5 receptor negative allosteric modulators. *Bioorg Med Chem Lett* **2011**, 21, 4891-9.
133. Hao, J., et al. Discovery of (1R,2R)-N-(4-(6-isopropylpyridin-2-yl)-3-(2-methyl-2H-indazol-5-yl)isothiazol-5-yl)-2-methylcyclopropanecarboxamide, a potent and orally efficacious mGluR5 receptor negative allosteric modulator. *Bioorg Med Chem Lett* **2013**, 23, 1249-52.
134. Danysz, W., et al. Pyrazolopyrimidines, a process for their preparation and the use as a medicine. In Patent WO 2008/015271: 2008.
135. Kramer, R. H., et al. Optogenetic pharmacology for control of native neuronal signaling proteins. *Nat Neurosci* **2013**, 16, 816-23.
136. Lehar, J., et al. Synergistic drug combinations tend to improve therapeutically relevant selectivity. *Nat Biotechnol* **2009**, 27, 659-66.
137. Velema, W. A., et al. Photopharmacology: beyond proof of principle. *J Am Chem Soc* **2014**, 136, 2178-91.
138. Gorostiza, P.; Isacoff, E. Y. Optical switches for remote and noninvasive control of cell signaling. *Science* **2008**, 322, 395-9.
139. Szymanski, W., et al. Reversible photocontrol of biological systems by the incorporation of molecular photoswitches. *Chem Rev* **2013**, 113, 6114-78.
140. Volgraf, M., et al. Switchable Proteins and Channels. In *Molecular Switches*, Wiley-VCH Verlag GmbH & Co. KGaA: 2011; pp 563-593.
141. Banghart, M. R., et al. Engineering light-gated ion channels. *Biochemistry* **2006**, 45, 15129-41.
142. Noble, A. III. Zur Geschichte des Azobenzols und des Benzidins. *Justus Liebigs Annalen der Chemie* **1856**, 98, 253-256.
143. Griffiths, J. II. Photochemistry of azobenzene and its derivatives. *Chemical Society Reviews* **1972**, 1, 481-493.
144. Merino, E. Synthesis of azobenzenes: the coloured pieces of molecular materials. *Chem Soc Rev* **2011**, 40, 3835-53.

145. Wagner, G., et al. Controllable selective functionalization of a cavitand via solid state photolysis of an encapsulated phenyl azide. *Org Lett* **2009**, 11, 3056-8.
146. Chiba, S., et al. Copper-catalyzed synthesis of azaspirocyclohexadienones from alpha-azido-N-arylamides under an oxygen atmosphere. *J Am Chem Soc* **2010**, 132, 7266-7.
147. Hartley, G. S. The Cis-form of Azobenzene. *Nature* **1937**, 140, 281-281.
148. Dong, Q., et al. Photobiological effects of UVA and UVB light in zebrafish embryos: evidence for a competent photorepair system. *J Photochem Photobiol B* **2007**, 88, 137-46.
149. Forman, J., et al. Photobiological and thermal effects of photoactivating UVA light doses on cell cultures. *Photochem Photobiol Sci* **2007**, 6, 649-58.
150. Beharry, A. A., et al. Azobenzene photoswitching without ultraviolet light. *J Am Chem Soc* **2011**, 133, 19684-7.
151. Venkataraman, K. *The chemistry of synthetic dyes*. Academic Press: New York, 1956.
152. Bandara, H. M. D.; Burdette, S. C. Photoisomerization in different classes of azobenzene. *Chemical Society Reviews* **2012**, 41, 1809-1825.
153. Garcia-Amoros, J.; Velasco, D. Recent advances towards azobenzene-based light-driven real-time information-transmitting materials. *Beilstein J Org Chem* **2012**, 8, 1003-17.
154. Asano, T.; Okada, T. Thermal Z-E isomerization of azobenzenes. The pressure, solvent, and substituent effects. *The Journal of Organic Chemistry* **1984**, 49, 4387-4391.
155. Brown, E. V.; Granneman, G. R. Cis-trans isomerism in the pyridyl analogs of azobenzene. Kinetic and molecular orbital analysis. *J Am Chem Soc* **1975**, 97, 621-627.
156. Sueyoshi, T., et al. FURTHER EVIDENCE OF INVERSION MECHANISM FOR THE CIS-TO-TRANS THERMAL ISOMERIZATION OF 4-DIMETHYLAMINOAZOBENZENE DERIVATIVES. ADDITIVITY RULE OF SUBSTITUENT CONSTANTS. *Chemistry Letters* **1974**, 3, 1131-1134.
157. Nishimura, N., et al. Thermal *Cis*-to-*Trans* Isomerization of Substituted Azobenzenes II. Substituent and Solvent Effects. *Bulletin of the Chemical Society of Japan* **1976**, 49, 1381-1387.
158. Nishimura, N., et al. The Thermal Isomerization of Azobenzenes. III. Substituent, Solvent, and Pressure Effects on the Thermal Isomerization of Push-pull Azobenzenes. *Bulletin of the Chemical Society of Japan* **1984**, 57, 1617-1625.
159. Pozhidaeva, N., et al. Reversible photocontrol of peptide helix content: adjusting thermal stability of the cis state. *Bioconjug Chem* **2004**, 15, 1297-303.
160. Sadvovskii, O., et al. Spectral tuning of azobenzene photoswitches for biological applications. *Angew Chem Int Ed Engl* **2009**, 48, 1484-6.
161. Samanta, S., et al. Photoswitching azo compounds in vivo with red light. *J Am Chem Soc* **2013**, 135, 9777-84.
162. Siewertsen, R., et al. Highly efficient reversible Z-E photoisomerization of a bridged azobenzene with visible light through resolved S(1)(n pi*) absorption bands. *J Am Chem Soc* **2009**, 131, 15594-5.
163. Fenno, L., et al. The development and application of optogenetics. *Annu Rev Neurosci* **2011**, 34, 389-412.
164. Boyden, E. S., et al. Millisecond-timescale, genetically targeted optical control of neural activity. *Nat Neurosci* **2005**, 8, 1263-8.

165. Kleinlogel, S., et al. A gene-fusion strategy for stoichiometric and co-localized expression of light-gated membrane proteins. *Nat Methods* **2011**, 8, 1083-8.
166. Wietek, J., et al. Conversion of channelrhodopsin into a light-gated chloride channel. *Science* **2014**, 344, 409-12.
167. Zhang, Y., et al. Channelrhodopsin-2-expressed dorsal root ganglion neurons activates calcium channel currents and increases action potential in spinal cord. *Spine (Phila Pa 1976)* **2014**, 39, E865-9.
168. Bartels, E., et al. Photochromic activators of the acetylcholine receptor. *Proc Natl Acad Sci U S A* **1971**, 68, 1820-3.
169. Banghart, M., et al. Light-activated ion channels for remote control of neuronal firing. *Nat Neurosci* **2004**, 7, 1381-6.
170. Chambers, J. J., et al. Light-induced depolarization of neurons using a modified Shaker K(+) channel and a molecular photoswitch. *J Neurophysiol* **2006**, 96, 2792-6.
171. Fortin, D. L., et al. Optogenetic photochemical control of designer K⁺ channels in mammalian neurons. *J Neurophysiol* **2011**, 106, 488-96.
172. Sandoz, G., et al. Optical control of endogenous proteins with a photoswitchable conditional subunit reveals a role for TREK1 in GABA(B) signaling. *Neuron* **2012**, 74, 1005-14.
173. Volgraf, M., et al. Allosteric control of an ionotropic glutamate receptor with an optical switch. *Nat Chem Biol* **2006**, 2, 47-52.
174. Levitz, J., et al. Optical control of metabotropic glutamate receptors. *Nat Neurosci* **2013**, 16, 507-16.
175. Izquierdo-Serra, M., et al. Two-photon neuronal and astrocytic stimulation with azobenzene-based photoswitches. *J Am Chem Soc* **2014**, 136, 8693-701.
176. Klan, P., et al. Photoremovable protecting groups in chemistry and biology: reaction mechanisms and efficacy. *Chem Rev* **2013**, 113, 119-91.
177. Callaway, E. M.; Katz, L. C. Photostimulation using caged glutamate reveals functional circuitry in living brain slices. *Proc Natl Acad Sci U S A* **1993**, 90, 7661-5.
178. Canepari, M., et al. Photochemical and pharmacological evaluation of 7-nitroindolyl- and 4-methoxy-7-nitroindolyl-amino acids as novel, fast caged neurotransmitters. *J Neurosci Methods* **2001**, 112, 29-42.
179. Fino, E., et al. RuBi-Glutamate: Two-Photon and Visible-Light Photoactivation of Neurons and Dendritic spines. *Front Neural Circuits* **2009**, 3, 2.
180. Rial Verde, E. M., et al. Photorelease of GABA with Visible Light Using an Inorganic Caging Group. *Front Neural Circuits* **2008**, 2, 2.
181. Donato, L., et al. Water-soluble, donor-acceptor biphenyl derivatives in the 2-(o-nitrophenyl)propyl series: highly efficient two-photon uncaging of the neurotransmitter gamma-aminobutyric acid at lambda = 800 nm. *Angew Chem Int Ed Engl* **2012**, 51, 1840-3.
182. Banghart, M. R.; Sabatini, B. L. Photoactivatable neuropeptides for spatiotemporally precise delivery of opioids in neural tissue. *Neuron* **2012**, 73, 249-59.
183. Fortin, D. L., et al. Photochemical control of endogenous ion channels and cellular excitability. *Nat Methods* **2008**, 5, 331-8.
184. Banghart, M. R., et al. Photochromic blockers of voltage-gated potassium channels. *Angew Chem Int Ed Engl* **2009**, 48, 9097-101.

185. Mouroto, A., et al. Tuning photochromic ion channel blockers. *ACS Chem Neurosci* **2011**, 2, 536-43.
186. Mouroto, A., et al. Rapid optical control of nociception with an ion-channel photoswitch. *Nat Methods* **2012**, 9, 396-402.
187. Broichhagen, J., et al. A Roadmap to Success in Photopharmacology. *Acc Chem Res* **2015**, 48, 1947-60.
188. Stein, M., et al. Azo-propofols: photochromic potentiators of GABA(A) receptors. *Angew Chem Int Ed Engl* **2012**, 51, 10500-4.
189. Velema, W. A., et al. Optical control of antibacterial activity. *Nat Chem* **2013**, 5, 924-8.
190. Stein, M., et al. Optical control of TRPV1 channels. *Angew Chem Int Ed Engl* **2013**, 52, 9845-8.
191. Schonberger, M.; Trauner, D. A photochromic agonist for mu-opioid receptors. *Angew Chem Int Ed Engl* **2014**, 53, 3264-7.
192. Schoenberger, M., et al. Development of a new photochromic ion channel blocker via azologization of fomicaine. *ACS Chem Neurosci* **2014**, 5, 514-8.
193. Broichhagen, J., et al. Optical control of insulin release using a photoswitchable sulfonyleurea. *Nat Commun* **2014**, 5, 5116.
194. Frank, J. A., et al. Photoswitchable fatty acids enable optical control of TRPV1. *Nat Commun* **2015**, 6, 7118.
195. Borowiak, M., et al. Photoswitchable Inhibitors of Microtubule Dynamics Optically Control Mitosis and Cell Death. *Cell* **2015**, 162, 403-11.
196. Taylor, E. C., et al. Conversion of a primary amino group into a nitroso group. Synthesis of nitroso-substituted heterocycles. *The Journal of Organic Chemistry* **1982**, 47, 552-555.
197. Priewisch, B.; Rück-Braun, K. Efficient Preparation of Nitrosoarenes for the Synthesis of Azobenzenes†. *The Journal of Organic Chemistry* **2005**, 70, 2350-2352.
198. Banghart, M. R.; Trauner, D. A ¹H NMR assay for measuring the photostationary States of photoswitchable ligands. *Methods Mol Biol* **2013**, 995, 107-20.
199. Nash, M. S., et al. Determinants of metabotropic glutamate receptor-5-mediated Ca²⁺ and inositol 1,4,5-trisphosphate oscillation frequency. Receptor density versus agonist concentration. *J Biol Chem* **2002**, 277, 35947-60.
200. Sali, A.; Blundell, T. L. Comparative protein modelling by satisfaction of spatial restraints. *J Mol Biol* **1993**, 234, 779-815.
201. Pettersen, E. F., et al. UCSF Chimera--a visualization system for exploratory research and analysis. *J Comput Chem* **2004**, 25, 1605-12.
202. Morris, G. M., et al. AutoDock4 and AutoDockTools4: Automated docking with selective receptor flexibility. *J Comput Chem* **2009**, 30, 2785-91.
203. Bennett, K. A., et al. Structures of mGluRs shed light on the challenges of drug development of allosteric modulators. *Curr Opin Pharmacol* **2015**, 20, 1-7.
204. Kolber, B. J., et al. Activation of metabotropic glutamate receptor 5 in the amygdala modulates pain-like behavior. *J Neurosci* **2010**, 30, 8203-13.
205. Runtsch, L. S., et al. Azobenzene-based inhibitors of human carbonic anhydrase II. *Beilstein J Org Chem* **2015**, 11, 1129-1135.

206. Christopoulos, A.; Kenakin, T. G protein-coupled receptor allosterism and complexing. *Pharmacol Rev* **2002**, 54, 323-74.
207. Sun, Y., et al. Dosage-dependent switch from G protein-coupled to G protein-independent signaling by a GPCR. *EMBO J* **2007**, 26, 53-64.
208. Strachan, R. T., et al. Divergent Transducer-specific Molecular Efficacies Generate Biased Agonism at a G Protein-coupled Receptor (GPCR). *Journal of Biological Chemistry* **2014**, 289, 14211-14224.
209. Molck, C., et al. Pharmacological characterization and modeling of the binding sites of novel 1,3-bis(pyridinylethynyl)benzenes as metabotropic glutamate receptor 5-selective negative allosteric modulators. *Mol Pharmacol* **2012**, 82, 929-37.
210. Dalton, J. A., et al. Shining Light On An mGlu5 Photoswitchable NAM: A Theoretical Perspective. *Curr Neuropharmacol* **2015**.
211. Gould, R. W., et al. Partial mGlu Negative Allosteric Modulators Attenuate Cocaine-Mediated Behaviors and Lack Psychotomimetic-Like Effects. *Neuropsychopharmacology* **2015**.
212. Nickols, H. H., et al. VU0477573: Partial Negative Allosteric Modulator of the Subtype 5 Metabotropic Glutamate Receptor with In Vivo Efficacy. *J Pharmacol Exp Ther* **2016**, 356, 123-36.
213. Abou Farha, K., et al. Metabotropic glutamate receptor 5 negative modulation in phase I clinical trial: potential impact of circadian rhythm on the neuropsychiatric adverse reactions-do hallucinations matter? *ISRN Psychiatry* **2014**, 2014, 652750.
214. Campbell, U. C., et al. The mGluR5 antagonist 2-methyl-6-(phenylethynyl)-pyridine (MPEP) potentiates PCP-induced cognitive deficits in rats. *Psychopharmacology (Berl)* **2004**, 175, 310-8.
215. Conn, P. J., et al. Mglur4 allosteric potentiators, compositions, and methods of treating neurological dysfunction. In Patent WO 2011/029104: 2011.
216. Dalton, J. A., et al. Shining Light On An mGlu5 Photoswitchable NAM: A Theoretical Perspective. *Curr Neuropharmacol* **2015**.
217. Burgeson, J. R., et al. SAR analysis of a series of acylthiourea derivatives possessing broad-spectrum antiviral activity. *Bioorg Med Chem Lett* **2012**, 22, 4263-72.
218. Claus, P. K., et al. N-aryl sulfimides. *Tetrahedron* **1975**, 31, 505-510.
219. Gowenlock, B. G., et al. The solid- and solution-state structures of 2-nitrosopyridine and its 3- and 4-methyl derivatives. *Journal of the Chemical Society, Perkin Transactions 2* **2000**, 2280-2286.
220. Kim, H. M., et al. Two-photon fluorescent probes for acidic vesicles in live cells and tissue. *Angew Chem Int Ed Engl* **2008**, 47, 2231-4.
221. Jankowiak, A., et al. Synthesis and structural, spectroscopic, and electrochemical characterization of benzo[c]quinolinium and its 5-aza-, 6-aza, and 5,6-diaza analogues. *Tetrahedron* **2011**, 67, 3317-3327.
222. Broxton, T. J., et al. Intramolecular catalysis in the basic methanolysis of N-2-pyridinylbenzamide and related compounds. *J Am Chem Soc* **1977**, 99, 2268-2271.
223. Damkaci, F., et al. N-picolinamides as ligands for Ullmann-type homocoupling reactions. *Tetrahedron Letters* **2014**, 55, 690-693.
224. Bloom, J. D., et al. Thiourea inhibitors of herpes viruses. Part 1: bis-(aryl)thiourea inhibitors of CMV. *Bioorg Med Chem Lett* **2003**, 13, 2929-32.

225. Tamagnan, G., et al. Compounds and amyloid probes thereof for therapeutic and imaging uses. In Patent US 2007/0258887 A1: 2007.
226. Molander, G. A.; Cavalcanti, L. N. Nitrosation of Aryl and Heteroaryltrifluoroborates with Nitrosonium Tetrafluoroborate. *The Journal of Organic Chemistry* **2012**, *77*, 4402-4413.
227. Garcia-Barrantes, P. M., et al. Lead optimization of the VU0486321 series of mGlu1 PAMs. Part 1: SAR of modifications to the central aryl core. *Bioorg Med Chem Lett* **2015**, *25*, 5107-10.
228. Gomeza, J., et al. Coupling of metabotropic glutamate receptors 2 and 4 to G alpha 15, G alpha 16, and chimeric G alpha q/i proteins: characterization of new antagonists. *Mol Pharmacol* **1996**, *50*, 923-30.